CUKUROVA UNIVERSITY
INSTITUTE OF NATURAL AND APPLIED SCIENCES

MSc THESIS

Cascade Sliding Mode Control with Applications

Rıdvan TOKYÜREK

Department of Electrical and Electronics Engineering

November, 2025

CUKUROVA UNIVERSITY
INSTITUTE OF NATURAL AND APPLIED SCIENCES

MSc THESIS APPROVAL

Cascade Sliding Mode Control with Applications

Rıdvan TOKYÜREK

Department of Electrical and Electronics Engineering

This Master's Thesis was evaluated by the following Jury Members on 18/11/2025 and was approved by unanimity / majority of votes.

Jury : Prof. Dr. İlyas EKER (Advisor) …………

: Assoc. Prof. Dr. Necdet Sinan ÖZBEK …………

: Asst. Prof. Dr. Oğuzhan TİMUR …………

This Thesis was written in the Department of Electrical and Electronics Engineering Institute of Natural and Applied Sciences.
Thesis Number:

Prof. Dr. Sadık DİNÇER
Director
Institute of Natural and Applied Sciences

This work was supported by Cukurova University Scientific Research Projects Unit.
Project ID: FYL-2024-16865

CONTENTS

CUKUROVA UNIVERSITY
INSTITUTE OF NATURAL AND APPLIED SCIENCES

MSc THESIS

Cascade Sliding Mode Control with Applications

Rıdvan TOKYÜREK

Advisor: Prof. Dr. İlyas EKER

Department of Electrical and Electronics Engineering

ABSTRACT

This study has comprehensively investigated the applicability and performance of the Sliding Mode Control (SMC) method within a cascade control structure. The primary objective of the present study is to evaluate the viability of SMC-based controllers as a reliable and robust alternative to conventional proportional–integral–derivative (PID) controllers in nonlinear and time-varying systems. In order to this end, single-loop P, PI and PID controllers, as well as SMC-1 (First-Order Sliding Mode Control) and SMC-2 (Second-Order Sliding Mode Control) controllers were designed. Various cascade and hybrid SMC-based control structures incorporating different outer-loop and inner-loop combinations were also developed. These were then subjected to comparative performance analyses.

A fundamental objective of the study was to mitigate the inherent oscillations (chattering) observed in SMC systems. In order to achieve this objective, a hyperbolic tangent (tanh) function within a boundary layer approach was utilised as an alternative to the classical sgn function. This modification has been shown to reduce switching noise, ensure smoother control signals, and improve the robustness and stability of the system against disturbances and model uncertainties. The control algorithms were implemented on a DC motor system using the DIGIAC 1750 training set with experimentally determined parameters, and were validated through simulation and real-time testing in MATLAB/Simulink. The system's responses were evaluated using standard performance criteria, including rise time, settling time, overshoot and delay. The findings indicate that Cascade Sliding Mode Control (CSMC) structures, particularly those employing an SMC-2 controller in the outer-loop, exhibit a faster transient response, reduced overshoot, diminished steady-state error, and enhanced disturbance rejection capability. Consequently, CSMC can be regarded as a reliable and effective alternative to conventional PID-based control methods.

Keywords: Sliding Mode Control (SMC), Cascade Control, DC Motor, Nonlinear Control, MATLAB/Simulink.

ÇUKUROVA ÜNİVERSİTESİ
FEN BİLİMLERİ ENSTİTÜSÜ

YÜKSEK LİSANS TEZİ

Uygulamalı Ardışık Kayan Kipli Kontrol

Rıdvan TOKYÜREK

Danışman: Prof. Dr. İlyas EKER

Elektrik ve Elektronik Mühendisliği Anabilim Dalı

ÖZ

Bu çalışma, kademeli kontrol yapısı içinde Kayan Kipli Kontrol (SMC) yönteminin uygulanabilirliğini ve performansını kapsamlı bir şekilde araştırmıştır. Çalışmanın ana amacı, SMC tabanlı kontrolörlerin doğrusal olmayan ve zamanla değişen sistemlerde geleneksel oransal-bütünsel-türevsel (PID) kontrolörlere güvenilir ve sağlam bir alternatif olup olmadığını değerlendirmektir. Bu amaçla tek döngülü P, PI ve PID kontrolörlerin yanı sıra SMC-1 (Birinci Dereceden Kayan Kipli Kontrol) ve SMC-2 (İkinci Dereceden Kayan Kipli Kontrol) kontrolörler, farklı dış-iç döngü kombinasyonlarını içeren çeşitli kademeli ve hibrit SMC tabanlı kontrol yapıları ile birlikte tasarlanmış ve tümü karşılaştırmalı performans analizlerine tabi tutulmuştur.

Çalışmanın ana odak noktası, kayma modu kontrol sistemlerinde gözlemlenen doğal salınımları (titreme) azaltmaktı. Bu amaçla, klasik işaret sgn fonksiyonu yerine sınır tabakası yaklaşımı içinde hiperbolik tanjant (tanh) fonksiyonu kullanıldı. Bu değişiklik, anahtarlama gürültüsünü etkili bir şekilde azaltır, daha düzgün kontrol sinyalleri sağlar ve sistemin bozulmalara ve model belirsizliklerine karşı sağlamlığını ve kararlılığını artırır. Kontrol algoritmaları, deneysel olarak belirlenen parametrelerle DIGIAC 1750 eğitim seti kullanılarak bir DC motor sisteminde uygulandı ve MATLAB/Simulink'te simülasyon ve gerçek zamanlı testlerle doğrulandı. Sistemin tepkileri, yükselme süresi, yerleşme süresi, aşma ve gecikme gibi performans endeksleri kullanılarak değerlendirildi. Sonuçlar, Kaskad Kayan Kipli Kontrol (CSMC) yapılarının, özellikle dış döngüde SMC-2 kontrolörü kullananların, daha hızlı geçici tepki, daha düşük aşma, daha küçük kararlı durum hatası ve daha büyük bozulma reddetme kabiliyeti sağladığını göstermektedir. Sonuç olarak, CSMC geleneksel PID tabanlı kontrol yöntemlerine etkili ve güvenilir bir alternatif olarak düşünülebilir.

Anahtar Kelimeler: Kayan Kipli Kontrol (SMC), Ardışık Kontrol, Doğru Akım Motoru, Doğrusal Olmayan Kontrol, Matlab/Simulink.

GENİŞLETİLMİŞ ÖZET

Bu tez çalışmasında, Kayan Kipli Kontrol (Sliding Mode Control, SMC) metodunun ardışık kontrol sistemlerinde uygulamalı performansları kapsamlı bir biçimde incelenmiş ve elde edilen sonuçlar hem simülasyon hem de deneysel düzeyde karşılaştırmalı olarak değerlendirilmiştir. Endüstriyel otomasyon sistemlerinde motor kontrolü, sistemin genel performansını doğrudan etkileyen temel bir parametre olduğundan, kullanılan kontrol algoritmalarının etkinliği büyük önem taşımaktadır. Bu çalışmada özellikle SMC yöntemlerinin, klasik kontrolörlere kıyasla kararlılık, hızlı yanıt süresi ve bozucu etkilere karşı dayanıklılık açısından ne derece üstün performans sergilediği araştırılmıştır. Çalışmanın temel amacı, farklı kontrol yapılarının sistem yanıtı üzerindeki etkilerini incelemek hem geçici hem de kararlı rejim davranışlarını ortaya koymak ve SMC tabanlı kontrolörlerin üstün yönlerini sayısal olarak göstermektir.

Günümüzde motor kontrolü uygulamaları, sanayi robotlarından elektrikli araçlara, üretim hatlarından hassas pozisyonlama sistemlerine kadar çok geniş bir alanda kullanılmaktadır. Bu sistemlerde hızın kararlı biçimde kontrol edilmesi, enerji verimliliği, güvenlik ve sistem ömrü açısından kritik bir öneme sahiptir. Klasik kontrol yöntemleri (P, PI, PID gibi) uzun yıllardır yaygın olarak kullanılsa da sistem parametrelerinde meydana gelen belirsizlikler, dış bozucular ve doğrusal olmayan dinamikler bu kontrolörlerin performansını sınırlamaktadır. Bu bağlamda, sistem dinamiklerini doğrudan göz önünde bulunduran ve doğrusal olmayan yapısıyla sistemin kararlılığını artıran SMC yöntemi alternatif bir çözüm olarak öne çıkmaktadır. SMC, sistemin belirli bir yüzey üzerinde kaymasını sağlayarak, hata dinamiklerini kararlı hâle getiren dayanıklı bir kontrol yaklaşımıdır. Bu yöntem hem model belirsizliklerine hem de dış bozuculara karşı yüksek düzeyde direnç gösterdiğinden, motor hız kontrolü gibi hassas uygulamalarda oldukça etkili sonuçlar vermektedir.

Çalışmada kullanılan DC motor modeli, armatür ve alan sargılarının dinamik etkileri dikkate alınarak matematiksel olarak modellenmiş ve MATLAB/Simulink ortamında gerçekleştirilmiştir. Motor modeli; moment denklemleri, gerilim-akım ilişkileri ve elektromanyetik kuvvet parametreleri ile tanımlanmış, böylece hem elektriksel hem de mekanik alt sistemlerin birlikte analiz edilmesine olanak sağlanmıştır. Model üzerinde farklı kontrol yapıları uygulanarak motor hızının referans değere ulaşma süresi, aşım miktarı, kararlı durum hatası ve kontrol sinyali davranışları detaylı şekilde gözlemlenmiştir.

Klasik kontrolör tasarımlarında oransal (P), oransal-integral (PI) ve oransal-integral-türevsel (PID) kontrolörler kullanılmıştır. Bu kontrolörler, temel parametre ayarları yapıldıktan sonra sistemin adım tepkisi üzerinden değerlendirilmiştir. Tek döngülü SMC yapılarında ise SMC-1 ve SMC-2 olarak adlandırılan iki farklı yapı uygulanmıştır. Bu iki yapının farkı, anahtarlama yüzeyi tanımı ve kazanç katsayılarının belirlenme yönteminden kaynaklanmaktadır. SMC-1 yapısı daha sade bir yüzey tanımı ile daha düşük anahtarlama frekansına sahipken, SMC-2 daha agresif bir kontrol yasası ile bozucu etkilere karşı daha güçlü bir kararlılık sunmuştur.

Ayrıca bu çalışmada, iç ve dış döngüden oluşan ardışık kontrol yapıları oluşturulmuştur. Bu yapılarda iç döngü genellikle akım veya moment kontrolü sağlarken, dış döngü hız kontrolünü üstlenmektedir. Bu sayede sistem hem düşük seviyeli kontrol değişkenlerinde hem de yüksek seviyeli çıkış değişkenlerinde daha kararlı bir performans elde etmektedir. Özellikle iç döngü PI veya SMC-1, dış döngü ise SMC-2 olarak seçildiğinde, sistem hem hızlı bir geçici yanıt hem de minimum kalıcı hata ile optimum bir kontrol başarımı göstermiştir. Ardışık yapılar sayesinde klasik kontrolörlerin yaşadığı aşım, yavaş yerleşme veya kararsızlık problemleri büyük oranda giderilmiştir.

Simülasyon çalışmaları, birim basamak girişine karşılık sistem tepkilerinin incelenmesiyle yürütülmüş ve performans değerlendirmesi için ITAE (Integral of Time-weighted Absolute Error), ISE (Integral of Squared Error), IAE (Integral of Absolute Error), ITSE (Integral of Time-weighted Squared Error), ISCI (Integral of Squared Control Input) ve ISTE (Integral of Squared Tracking Error) gibi performans indeksleri kullanılmıştır. Klasik kontrolörler hızlı yükselme süresi sağlamasına rağmen, kararlı duruma ulaşma süreleri uzun olmuş ve belirli bir kalıcı hata gözlemlenmiştir. Örneğin, tek döngülü PI kontrolör ±7 rpm hata ile çalışırken PID kontrolör ±6 rpm düzeyinde kalıcı hata göstermiştir. Tek döngülü SMC kontrolörlerde ise aşım değeri neredeyse sıfıra inmesine rağmen yerleşme süresi klasik kontrolörlere göre bir miktar uzun bulunmuştur. Ancak ardışık yapılar, özellikle dış döngüde SMC-2 kontrolörü kullanıldığında bu dezavantaj ortadan kalkmış ve hem aşım hem kalıcı hata minimuma inmiştir. Dış döngü SMC-2/iç döngü PI (SMC-2/PI) kontrol yapısı ±3 rpm kalıcı hata ile en başarılı sonucu vermiştir.

Performans indeksleri açısından da SMC tabanlı kontrolörler açık bir üstünlük göstermiştir. ITAE ve IAE değerlerinin düşük çıkması, sistem hatasının hem anlık hem de toplamda minimuma indirildiğini göstermektedir. ISCI indeksinin yüksek olması ise kontrol sinyallerinin kararlı ve güçlü bir etki sağladığını, sistemin bozulmalara karşı dayanıklı olduğunu ortaya koymuştur. Bu sonuçlar, SMC'lerin klasik kontrolörlere göre daha az hata ile daha kararlı bir dinamik yanıt sunduğunu doğrulamaktadır.

Deneysel doğrulama aşamasında, simülasyon ortamında elde edilen kontrol algoritmaları gerçek bir DC motor sürücü sistemi üzerinde uygulanmıştır. Deney düzeneği; kontrol kartı, sürücü devresi, motor, hız sensörü ve veri toplama biriminden oluşmaktadır. Elde edilen gerçek zamanlı veriler, simülasyon sonuçlarıyla oldukça yüksek oranda uyum göstermiştir. Tek döngülü SMC kontrolörler, aşım değerini neredeyse sıfıra indirirken klasik kontrolörlere kıyasla daha kısa sürede kararlı duruma ulaşmıştır. Ardışık SMC tabanlı kontrol yapılarında ise geçici rejim süresinin belirgin biçimde azaldığı, sistemin referans değişimlerine daha hızlı uyum sağladığı ve bozulmalara karşı daha az hassasiyet gösterdiği gözlenmiştir. Özellikle SMC-2/PI kontrolöründe ±5 rpm kalıcı hata ile en düşük hata değeri elde edilmiştir. Ayrıca SMC-2/SMC-1 ardışık kontrol yapısında ISTE değeri 0.0005'e kadar düşerek sistemin hatayı en küçük düzeyde tuttuğu belirlenmiştir.

Tüm bu sonuçlar, SMC'nin klasik kontrolörlere kıyasla açık bir performans üstünlüğü sergilediğini göstermektedir. Klasik kontrolörler basit yapılarına rağmen parametre değişimlerinden ciddi biçimde etkilenirken, SMC tabanlı kontrolörler sistem belirsizliklerine rağmen kararlılığını koruyabilmiştir. Bu da SMC'nin özellikle değişken yük, sürtünme veya gerilim dalgalanması gibi bozulmaların bulunduğu sistemlerde etkin bir çözüm sunduğunu kanıtlamaktadır. Ayrıca ardışık yapılar, sistemin hem içsel dinamiklerini hem de çıkış davranışını dengelediğinden, kararlı ve düzgün bir hız yanıtı elde edilmiştir.

Sonuç olarak, bu tez çalışması SMC tabanlı ardışık kontrol yapılarının DC motor hız kontrolü uygulamalarında klasik kontrolörlere göre daha yüksek doğruluk, daha hızlı tepki süresi ve daha güçlü dayanıklılık sağladığını ortaya koymuştur. Elde edilen hem simülasyon hem de deneysel sonuçlar, SMC endüstriyel uygulamalarda kullanılabilirliğini açık biçimde göstermektedir. Bu doğrultuda, ilerleyen çalışmalarda farklı motor tipleri, değişken yük koşulları ve adaptif SMC algoritmalarının incelenmesi önerilmektedir. Ayrıca gerçek zamanlı uygulamalar için kontrol algoritmalarının DSP veya FPGA tabanlı sistemlerde uygulanması, enerji tüketimi, anahtarlama frekansı ve kontrol sinyali yoğunluğu açısından optimizasyon yapılması da gelecekteki araştırmalar için önemli bir yol haritası sunmaktadır.

Bu kapsamlı çalışma, kontrol mühendisliği alanında hem teorik hem de uygulamalı olarak önemli katkılar sunmaktadır. Elde edilen sonuçlar, sadece DC motor hız kontrolü özelinde değil, aynı zamanda benzer yapıya sahip elektromekanik sistemlerin kontrol stratejilerinin geliştirilmesinde de yol gösterici niteliktedir. SMC'nin ardışık yapılarla birleştirilmesi, sistem kararlılığını artırmakla kalmayıp, aynı zamanda kontrol sinyalinin sürekliliğini ve sistem yanıtının hassasiyetini de iyileştirmiştir. Bu yönüyle çalışma, klasik kontrol yöntemlerinin ötesine geçerek modern kontrol stratejilerinin pratikteki etkinliğini ortaya koymaktadır.

Gelecekte yapılacak araştırmaların, SMC'nin yapay zekâ, bulanık mantık (fuzzy logic) ve adaptif kontrol algoritmaları ile birleştirilmesi üzerine yoğunlaşması, kontrol sistemlerinin hem esnekliğini hem de öğrenme kabiliyetini artıracaktır. Özellikle öğrenen ve kendini uyarlayabilen kontrolörler, endüstriyel otomasyon sistemlerinde enerji verimliliği ve güvenlik açısından yeni bir dönemin kapısını aralayacaktır. Ayrıca, IoT (Nesnelerin İnterneti) tabanlı akıllı motor sürücü sistemleriyle SMC'nin entegre edilmesi, uzaktan izleme, hata teşhisi ve öngörücü bakım uygulamalarında yüksek potansiyel taşımaktadır.

Sonuç olarak bu tez, yalnızca mevcut kontrol yöntemlerini karşılaştırmakla kalmamış, aynı zamanda geleceğin akıllı ve dayanıklı kontrol sistemlerinin temelini oluşturabilecek bir araştırma perspektifi sunmuştur. Elde edilen bulguların hem akademik literatüre hem de endüstriyel uygulamalara katkı sağlayacağı düşünülmektedir.

ACKNOWLEDGEMENTS

First of all, I would like to express my sincere gratitude to my advisor Prof. Dr. İlyas EKER for his valuable guidance, encouragement, and support throughout the preparation of this thesis. His knowledge, experience, and patience have greatly contributed to the completion of this work.

I would like to sincerely thank Assoc. Prof. Dr. Necdet Sinan ÖZBEK, from whom I benefited greatly through his courses and knowledge during my master’s studies, and Asst. Prof. Dr. Oğuzhan TİMUR, for their valuable contributions as members of my thesis jury.

I would like to express my heartfelt thanks to my mother Leman TOKYÜREK, my sisters Zehra TUNA and Emine TOKYÜREK, for their endless love, understanding, and support during every stage of my life.

I would like to express my deepest gratitude to my late father Sıtdık TOKYÜREK, whose memory, values, and sacrifices have always been my greatest source of strength and motivation.

Finally, I would like to extend my special thanks to my fiancée Ayşenur GENÇOĞLU, for her patience, understanding, and constant support throughout this challenging journey.

LIST OF TABLES

LIST OF FIGURES

SYMBOLS AND ABBREVIATIONS

A, b, B, b, C, c	: Nominal System Parameters
BLDC	: Brushless Direct Current Motor
D(t)	: Lumped Uncertainty
CSMC	: Cascade Sliding Mode Control
DAQ	: Data Acquisition Card
DC	: Direct Current
$d(t)$	: External Disturbance
$d_{\max}$	: Upper Bound of Uncertainty
DSP	: Digital Signal Processing
$e(t)$	: Tracking Error
e_a	: Applied Armature Voltage
e_b	: Back Electromotive Force
f	: Viscous Friction Coefficient of the Motor and Load
FL	: Fuzzy Logic
FOPDT	: First-Order Plus Dead-Time
$G(s)$	: Approximate Model of the System
HOSMC	: Higher-Order Sliding Mode Control
IAE	: Integral Absolute Error
ISCI	: Integral Squared Control Input
ISE	: Integral Squared Error
I-SMC	: Integral Sliding-Mode Control
ISSF	: Integral Squared Sliding Function
ISTE	: Integral Squared Time Error
ITAE	: Integral Time Absolute Error
ITSE	: Integral Time Squared Error
i_a	: Armature Winding Current
i_f	: Field Current
J	: Moment of Inertia of the Motor and Load
K	: Gain
K_f	: Torque Constant
K_m	: Motor Gain Constant
L_a	: Armature Winding Inductance

λ_c	: Positive Design Parameters
MIMO	: Multi-Input Multi-Output
n	: The Order of the System
PCCS	: Parallel Cascade Control Structure
PI/P	: Outer-Loop PI/Inner-Loop P
PI/PI	: Outer-Loop PI/Inner-Loop PI
PID	: Proportional, Integral and Derivative
PID/PI	: Outer -Loop PID/Inner-Loop PI
$\mathbb{R}$	: Set of Real Numbers
$\mathbb{R}+$	: Set of Positive Real Numbers
R_a	: Armature Winding Resistance
rpm	: Revolution per Minute
$r(t)$	: Set Point
sat	: Saturation Function
SCCS	: Series Cascade Control Structure
SD	: Standard Deviation
sgn	: Signum Function
SISO	: Single-Input Single-Output
SMC	: Sliding Mode Control
SMC-1	: First-Order Sliding Mode Control
SMC-1/P	: Outer-Loop SMC-1/Inner-Loop P
SMC-1/PI	: Outer-Loop SMC-1/Inner-Loop PI
SMC-1/PID	: Outer-Loop SMC-1/Inner-Loop PID
SMC-1/SMC-1	: Outer-Loop SMC-1/Inner-Loop SMC-1
SMC-2	: Second-Order Sliding Mode Control
SMC-2/P	: Outer-Loop SMC-2/Inner-Loop P
SMC-2/PI	: Outer-Loop SMC-2/Inner-Loop PI
SMC-2/PID	: Outer-Loop SMC-2/Inner-Loop PID
SMC-2/SMC-1	: Outer-Loop SMC-2/Inner-Loop SMC-1
$\sigma(t)$	: Sliding Manifold
STA	: Super-Twisting Algorithm
T	: Torque Produced by the Motor
T_m	: Motor Time Constant
t_d	: Time Delay
t_p	: Time Constant

$tanh$: Tangent Hyperbolic Function

TV : Total Variance

$u(t)$: Control Input

$u_{eq}(t)$: Equivalent Input

u_{max} : Maximum Control Input

$u_{sw}(t)$: Switching Input

$V(t)$: Lyapunov Function

V_b : Back Electromotive Force

V : Input Voltage

VSC : Variable Structure Control

VSS : Variable Structure Systems

$y(t)$: Measured Output

Z-N : Ziegler–Nichols

θ : Angular Displacement of the Motor Shaft

1. INTRODUCTION

The continuous advancement of automation and control technologies has led to an increased demand for control systems that are capable of functioning reliably under uncertain and nonlinear conditions. It is evident that traditional linear control methods frequently encounter difficulties in sustaining adequate performance when confronted with model inaccuracies, external disturbances and parameter variations. In order to surmount these challenges, researchers have turned to robust nonlinear control strategies. Among these, Sliding Mode Control (SMC) is distinguished by its inherent robustness and simplicity (Kuo et al., 2008).

SMC is a variable structure control method that forces the system state trajectory to reach and then remain on a predefined sliding surface, thereby ensuring robustness against uncertainties and disturbances (Lee, 2010). This property renders SMC particularly appealing for systems where exact modelling is difficult or impossible. Notwithstanding its numerous advantages, the conventional SMC approach is subject to the so-called "chattering" phenomenon, whereby high-frequency oscillations in the control input are caused by discontinuous switching. Chattering has been demonstrated to degrade system performance and cause mechanical wear in electromechanical devices. Consequently, significant research has been undertaken to mitigate this effect.

A methodology that has been proven to enhance control performance and reduce chattering is the utilisation of cascade control structures (Srinivasarao et al., 2022). Cascade control is comprised of multiple feedback loops which are nested. Typically, there is an outer-loop which is responsible for the main system variable, and an inner-loop which controls a faster subsystem variable. This configuration facilitates expedited disturbance rejection and enhanced dynamic response by managing system dynamics in a hierarchical manner. The integration of cascade control with SMC unites the robustness of SMC with the adaptability of multi-loop architectures (Torga et al., 2022).

The application of CSMC has been demonstrated in various fields, including robotics, aerospace, marine systems, and electrical drives (Wul et al., 2024). Among these, DC motors are particularly prevalent in industrial applications due to their ease of control, reliability, and widespread availability. Accurate control of DC motor speed and current is imperative for ensuring system efficiency, reducing energy consumption, and extending equipment lifespan. Consequently, DC motors are regarded as suitable platform for the development and validation of advanced control algorithms.

The central objective of this thesis is to develop, simulate and experimentally verify cascade SMC (CSMC) strategies applied to DC motor speed and current regulation. The research is structured in such a manner as to first create detailed models in the MATLAB/Simulink programming language. The purpose of these models is to facilitate analysis of control system performance under a variety of operating conditions, including those that involve parameter uncertainties and external disturbances. These simulations offer insights into controller tuning, stability and robustness characteristics.

Subsequent to the simulation studies, a comprehensive experimental setup is established for the implementation of the proposed control schemes in real hardware. The experimental validation of controllers is of critical importance in order to verify their practical applicability. This is because experimental validation exposes the system to real-world nonlinearities, sensor noise and unmodeled dynamics that are difficult to capture in simulations. The experimental results are then analysed in order to assess controller performance metrics such as tracking accuracy, disturbance rejection, response time and chattering magnitude.

The main contributions of this work include:

- Design and implementation of CSMC tailored for DC motor applications, emphasizing robustness and reduced chattering.
- Comparative analysis of different controller configurations and parameter sets through both simulation and experimental studies.
- Development of a reliable experimental platform that facilitates rigorous testing and evaluation of nonlinear control algorithms.

Insights into the practical challenges and solutions associated with deploying CSMC in electromechanical systems.

By bridging the gap between theoretical control design and practical implementation, this thesis offers valuable contributions to the field of robust control. It provides researchers and practitioners with effective methods for applying advanced SMC techniques in real-world industrial environments, enhancing system performance and reliability.

1.1. Thesis Topic

The central objective of this thesis is to undertake a comprehensive investigation into the dynamics of CSMC through the utilisation of simulation software and experimental studies conducted within a laboratory setting. In order to evaluate and optimise the performance of CSMC, both simulation tools and experimental setups will be utilised. SMC techniques, which are utilised extensively in contemporary control systems, enhance system robustness against external disturbances and parameter variations. However, conventional SMC methods frequently encounter limitations in practical applications due to specific drawbacks, notably the chattering phenomenon (Eghbal and Seyedeh-Solmaz, 2024).

In this context, CSMC have been developed to overcome the shortcomings of traditional approaches and to provide a more stable and efficient control strategy. In the context of this study, the theoretical underpinnings of the controller will be meticulously examined, existing methods in the extant literature will be analysed, and appropriate mathematical models will be formulated.

In addition to theoretical work, the performance of the CSMC will be evaluated through experimentation. This evaluation will be conducted on a system using simulation tools. These simulations will be conducted in MATLAB/Simulink, and the results will be evaluated in detail. Moreover, the theoretical analyses and simulation results will be validated through experimental studies carried out in a laboratory environment. During the experimental phase, the performance of the CSMC on real systems will be tested using suitable hardware and software tools. Optimization studies will be carried out based on the obtained data.

This thesis aims to contribute to the field by exploring the effectiveness, stability and practical applicability of CSMC. As a result of the conducted studies, the development of a more efficient and reliable control strategy is targeted, both in terms of academic and industrial applications.

The main objective of this study is to investigate the design of a CSMC through both simulation tools and experimental work conducted in a laboratory environment and to evaluate its performance. CSMC offer an effective control strategy, particularly for nonlinear systems and dynamic systems with high levels of uncertainty (Fan and Wu, 2023). Due to their high robustness against parameter variations and external influences, this control method is frequently preferred in both industrial applications and academic research (Fan and Wu, 2023).

Within the scope of the study, the theory of CSMC will first be examined in detail and the mathematical foundations of this method will be established. Subsequently, to analyze the performance of this controller, various simulation environments (e.g., MATLAB/Simulink) will be used to conduct tests on virtual models. During the simulation phase, the controller's behavior under different system dynamics and various disturbances will be examined. Performance criteria such as system stability, speed and sensitivity will be evaluated.

Following the simulation studies, experimental work will be carried out in a laboratory environment to test the practical validity of the findings. At this stage, real-time control systems and microcontroller-based platforms will be used to observe the effectiveness of the controller on a physical system. During the experimental studies, performance-related data will be collected and compared with the simulation results. This comparison will enable an understanding of the consistency and possible deviations between the theoretical model and the actual system.

Another important aspect of the present study is to highlight the advantages and disadvantages of the CSMC in comparison to conventional SMC methods. In this context, a comprehensive analysis will be conducted in terms of parameters such as controller complexity, ease of implementation, energy efficiency and system stability. Furthermore, the potential applications of this control method in fields such as industrial automation, robotics, electric vehicles and energy systems will also be discussed.

In conclusion, the aim is to present a comprehensive evaluation of the effectiveness and applicability of the CSMC by combining its theoretical foundations with simulation and experimental results. The findings are expected to contribute to the academic literature and provide practical solutions applicable in industrial settings.

1.2. Objective of the Thesis

The SMC method is particularly used for the control of complex and uncertain systems. The primary objective of the CSMC approach is to improve the performance of a two-loop system compared to a single-loop system, while also ensuring greater robustness against uncertainties, external disturbances, or modeling errors (Bartolini et al., 2008).
For comparison purposes, the effectiveness of the system will be demonstrated by applying the SMC method to both single-loop and two-loop PID controllers. In the SMC method, a solution is obtained by considering a sliding surface. The aim of solution is to minimize disturbances, errors and uncertainties in both loops of the system (Bartolini et al., 2008). Figure 1.1 shows the feedback control system, Figure 1.2 illustrates the cascade control system and Figure 1.3 depicts the CSMC system.

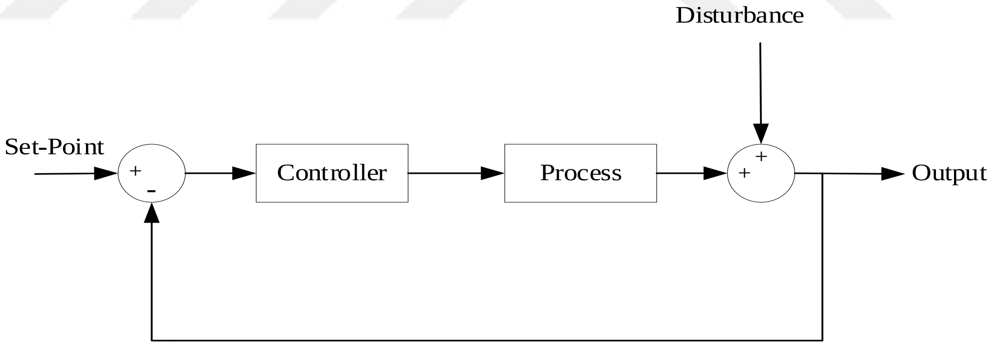

Figure 1.1. Feedback control system

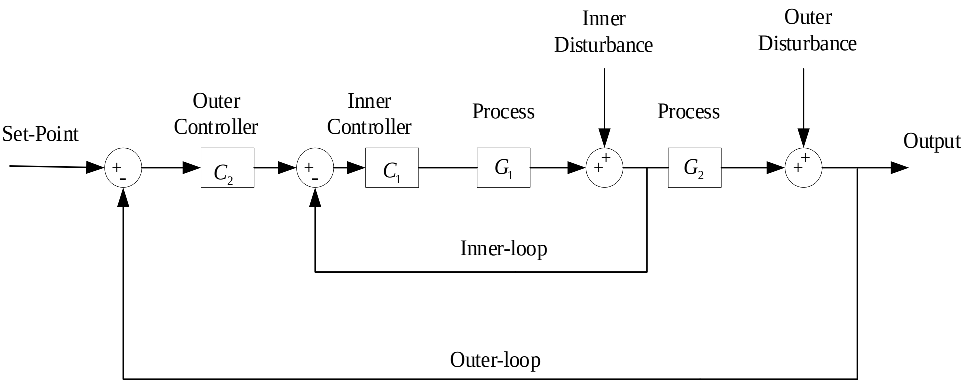

Figure 1.2. Cascade control system

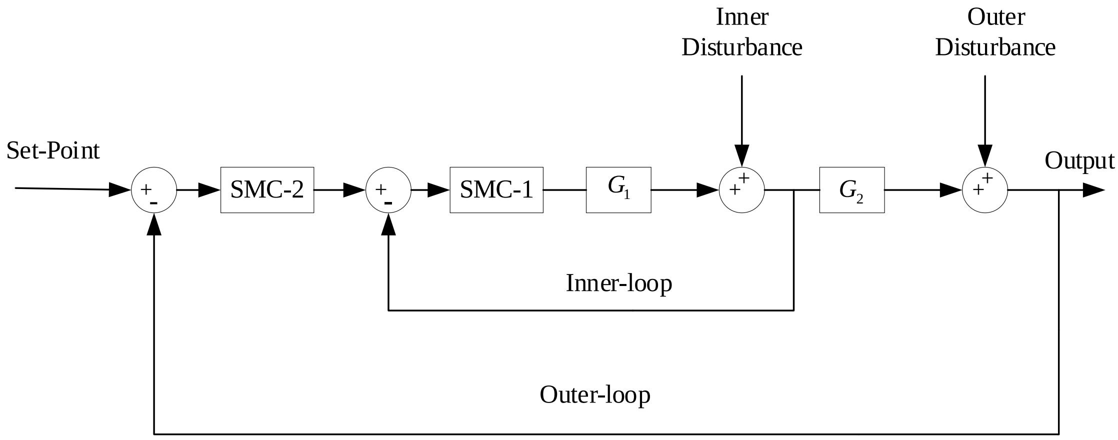

Figure 1.3. Cascade sliding mode control system

Including a second inner-loop control structure (cascade) into a conventional closed-loop feedback system enhances the system's efficiency, flexibility and reliability. Due to the presence of multiple sensors in a cascade control system, it has been observed to deliver better performance than traditional single-loop control (Goswami and Khairnar, 2017). The cascade control structure is especially known to improve system performance in scenarios involving disturbances (Laware et al., 2016).

Various cascade control strategies have been briefly reviewed in the literature for stable, integrating, unstable process models and appropriate tuning strategies have been proposed: (i) In most tuning strategies, the closed-loop time constants are typically selected from a predefined range, which ensures a balance between performance and robustness. This often involves a trial-and-error approach. (ii) Only a limited number of tuning strategies have been reported for integrating and unstable process models. (iii) Cascade control strategies have shown the potential to improve closed-loop performance in such processes. (iv) For unstable process models, cascade control strategies in both primary and secondary loops have not received sufficient research attention. (v) Most cascade control strategies require tuning of several controller and filter parameters. However, in practical applications, a simpler control structure with fewer controllers is preferred. Therefore, there is a need for simple cascade control strategies that involve a limited number of tuning parameters (Raja and Ali, 2017). This study aims to explore the design and application of CSMC systems, supported by simulation and experimental results using the mentioned method.

To better understand the control scenario, highlight its essential characteristics and explore different solutions, simulations and laboratory experiments will be conducted as a case study focusing on the CSMC.

1.3. Cascade Control

Cascade control generally consists of two nested loops: an inner (secondary) loop and an outer (primary) loop, also referred to as the slave and master loops, respectively. Although it is theoretically possible to design an infinite number of nested loops, industrial applications typically utilize a two-loop structure: one inner and one outer-loop (Çakıroğlu et al., 2015). The reasons for the widespread use of cascade control in industry include:

i) Rapid suppression of disturbances affecting the system to enhance dynamic performance,

ii) Increasing system speed to mitigate the adverse effects of time delays,

iii) Eliminating disturbances occurring in the inner-loop before they affect the system output.

According to the literature, cascade control structures can be classified into two types: parallel cascade control and series cascade control.

1.3.1. Series Cascade Control Structure (SCCS)

To mitigate the effects of disturbances acting on the system, control engineers employ the series cascade control structure (SCCS), which utilizes an intermediate sensor or controller. First to implement the SCCS using the ITAE performance criterion in chemical reactors (Franks and Worley, 1956). In the conventional SCCS, there are two nested control loops, each with its respective controller. Figure 1.4 illustrates the conventional SCCS structure (Raja and Ali, 2017).

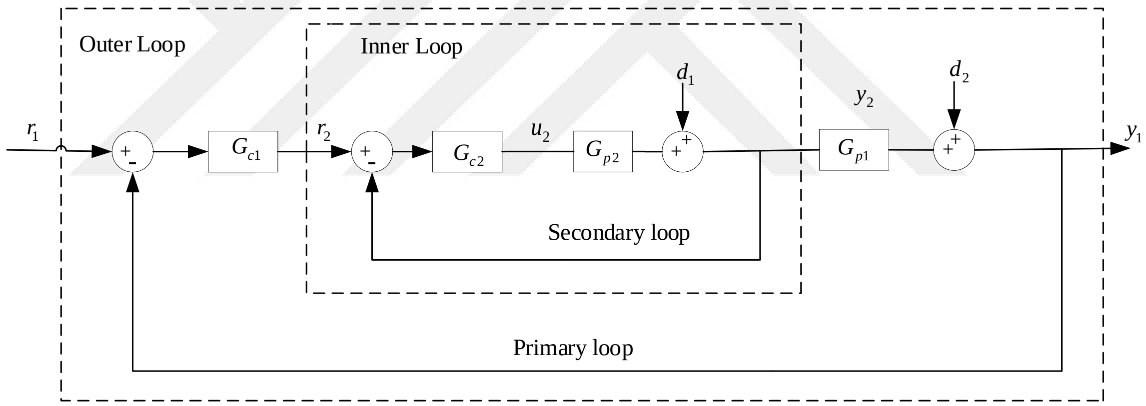

Figure 1.4. Conventional series cascade control structure

In Figure 1.4, G_{p1} and G_{p2} and represent the process model of the primary and secondary systems, respectively. G_{c1} and G_{c2} denote the controllers for the primary and secondary systems. Disturbances d_1 and d_2 refer to the disturbances acting at the input and output of the secondary system. The reference input of the primary system is denoted by r_1, while the output r_2 of the primary system's controller G_{c1} becomes the reference input for the secondary system (Raja and Ali, 2017).

In a cascade control structure, the controller G_{c2} is used to ensure stability in the inner-loop, while the controller G_{c1} is responsible for maintaining stability in the outer-loop (Nalbantoğlu and Güler, 2017). One of the reasons for preferring cascade control is its superior disturbance rejection performance. For effective disturbance suppression, the inner-loop is expected to be faster than the outer-loop. This allows the inner-loop to suppress disturbances rapidly, thereby reducing the steady-state error in the main system (Raja and Ali, 2017):

- The inner measurement is intended to suppress the impact of disturbances introduced in the outer process.
- The outer process measurement is used to control the quality of the system's final output.

Cascade control is mainly employed to ensure rapid rejection of disturbances before they propagate to other parts of the system.

1.3.2. Parallel Cascade Control Structure (PCCS)

As an alternative to the SCCS, the parallel cascade control structure (PCCS) was first studied by Luyben, who investigated the differences between SCCS and PCCS (Luyben, 1973). Unlike SCCS, in PCCS the control signal u_2, generated by the controller G_{c2} in the secondary loop and the disturbances simultaneously affect both the primary and secondary system outputs. The PCCS is illustrated in Figure 1.5 (Raja and Ali, 2015).

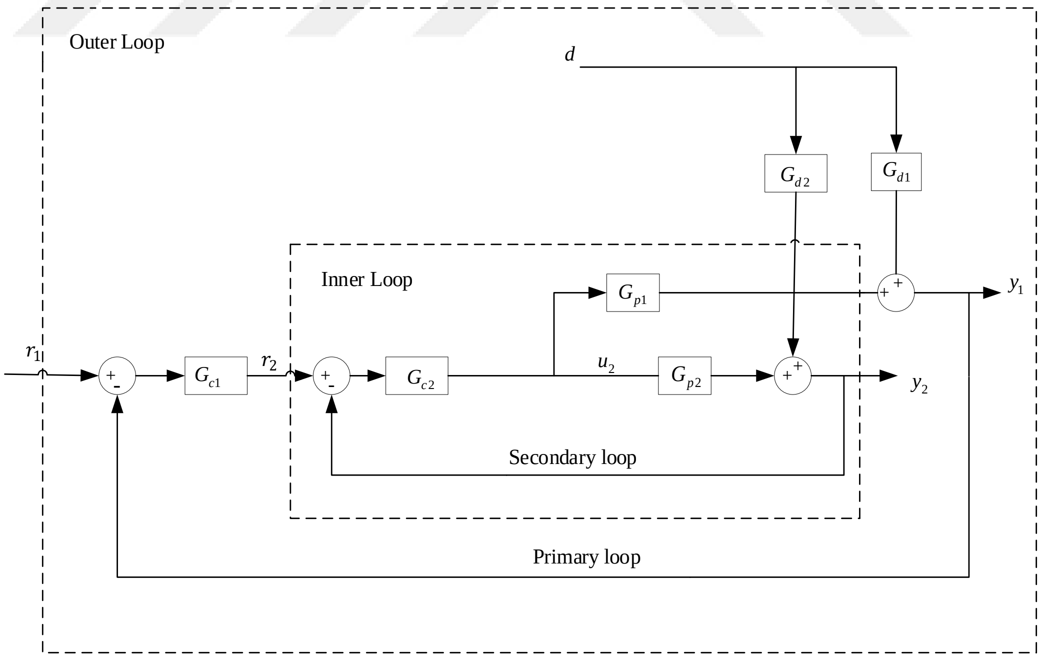

Figure 1.5. Parallel cascade control structure

1.4. Sliding Mode Control

In control theory, SMC is a special type of variable structure control (Tang et al., 2007). This method is a robust control approach based on altering the structure of the controller in response to changes in the system state to achieve the desired output. The robustness of a control system refers to its ability to maintain performance in the presence of uncertainties and external disturbances. In SMC, high-speed switching control actions are employed to drive the system trajectory toward a sliding manifold defined by the user and to keep it on that manifold (Franks and Worley, 1956).

SMC has been extensively studied for over 50 years (Eker, 2006; Eker and Akınal, 2008). The first major publication in this field was by Vadim I. Utkin in 1977 (Utkin, 1977). Since then, SMC has become a major area of interest for the global control research community (Xinghou and Kaynak, 2009). Thanks to its flexible yet simple design process, SMC has proven to be one of the most powerful solutions for many practical control problems (Utkin and Chang, 2002) This has led to its successful application in various fields such as automotive systems, induction motors, automotive climate control, diesel engines, alternators (Utkin and Chang, 2002), DC motors (Eker, 2006; Eker and Akınal, 2008), submarines (Walcko et al, 2003), electric drives (Akpolat and Gökbulut, 2003; Lin et al., 1998), stepper motors (Zribi et al., 2001) and missile attitude control (Huang and Way, 2001).

Control techniques can generally be classified as model-based and model-free approaches. Model-based control techniques follow a systematic structure and are applicable to a wide range of scenarios. Features such as robustness and tracking accuracy can be predefined and various optimization criteria can also be satisfied. However, real-world systems often contain unpredictable parameters and disturbances that are difficult to model. Therefore, model-free control techniques are commonly used in practice due to their simplicity and low computational burden. Nevertheless, such methods offer limited performance and robustness guarantees and their non-systematic design process makes them challenging to apply to complex systems (Cavallo and Natale, 2004).

SMC, on the other hand is a control method that delivers strong performance in the face of external disturbances and unexpected parameter variations, without requiring a complete model of the system (Zhou et al., 2024). For this reason, SMC is recognized as a successful control method for nonlinear systems (Tai and Ahn, 2010).

1.4.1. Fundamentals of Sliding Mode Control

One of the most significant advantages of SMC is their robustness and systematic design procedure (Eker, 2006). Traditionally, SMC methods have been designed for systems with a relative degree of one (Janardhanan, 2006). In such systems, the control input appears in the first derivative of the sliding function and the relative degree with respect to control is one. This type of SMC method is referred to as classical SMC or first-order SMC.

1.4.2. Classical Sliding Mode Control Design Procedure

The classical SMC design process consists of two main phases (Xinghou and Kaynak, 2009):

i) Reaching Phase: The system state is directed to reach the defined switching manifold from any initial condition within a finite time.

ii) Sliding Mode Phase: The system is forced to slide along the switching manifold.

These two phases correspond to the following design steps:

- Selection of the Switching Manifold: A set of switching manifolds with the desired dynamic properties is chosen.
- Design of Discontinuous Control: A discontinuous control strategy is designed to ensure finite-time reachability of the switching manifold.

1.4.3. Structure of Classical Sliding Mode Control

A classical SMC consists of two different control laws: switching control and equivalent control. The most critical task is designing the switching control law that forces the system to the user-defined sliding surface and maintains the system state on that surface (Figure 1.6).

In Figure 1.6, e denotes the error between set-point and the output, $\dot{e}$ is the derivative of error.

The system's dynamic performance depends on the appropriate selection of this switching control law. The Lyapunov approach is commonly used to determine the equivalent control law without needing to solve the state equations (Eker and Akınal, 2008). The equivalent control is applied when the system is operating in sliding mode.

The first step in designing a classical SMC is to define the sliding manifold, $s(t)$ (also referred to as the sliding surface or sliding function). This function is expressed using the tracking error, $e(t)$ (the difference between the setpoint and the output measurement) and its derivatives $\dot{e}(t) = \dfrac{de(t)}{dt}$ (Janardhanan, 2006):

$$s(t) = \left(\lambda + \frac{d}{dt}\right)^{n-1} e(t) \tag{1.1}$$

where n denotes order of the system and λ is a design parameter.

When the system is in sliding mode, both the error and its derivative are equal to zero $s(t) = 0, \dot{s}(t) = 0$:

$$
\begin{cases}
s(t) = \lambda e(t) + \dfrac{d}{dt} e(t) \\
s(t) = \lambda e(t) + \dot{e}(t) = 0 \\
\dot{s}(t) = \lambda \dot{e}(t) + \ddot{e}(t) = 0
\end{cases}
\tag{1.2}
$$

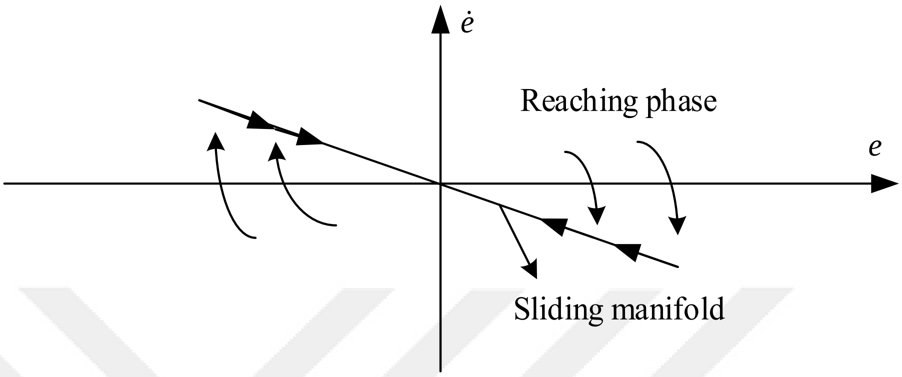

Figure 1.6. Sliding surface

The objective here is to define a control law that ensures the convergence of the tracking error and its derivative to zero within a finite time, regardless of the initial condition. This control law consists of two components: switching (discontinuous, $u_{sw}(t)$) and equivalent (continuous, $u_{eq}(t)$) control.

$$
u(t) = u_{eq}(t) + u_{sw}(t) \tag{1.3}
$$

If the system trajectory is not initially on the sliding surface, the equivalent control component directs the error toward the sliding surface. This stage is referred to as the reaching phase. However, equivalent control alone may not be sufficient; therefore, an additional control component is included. The switching control is typically designed based on a relay-like function, as this structure allows for instantaneous changes in the system dynamics (Camacho et al., 2007):

$$
u_{sw}(t) = -ksgn(s(t)) \tag{1.4}
$$

In the literature, the switching part of the control law is chosen such that k is a positive real $k \in \mathbb{R}+$, where $\mathbb{R}+$ denotes set of the positive real numbers. This constant must be large enough to suppress all bounded uncertainties and unpredictable system dynamics (Bartolini et al., 2008). The switching function also defined using a signum function $sgn(.)$ as illustrated in Figure 1.7, as:

$$\mathrm{sgn}(s) = \begin{cases} -1 \; if \;\; s < 0 \\ 0 \; if \;\; s = 0 \\ 1 \; if \;\; s > 0 \end{cases} \tag{1.5}$$

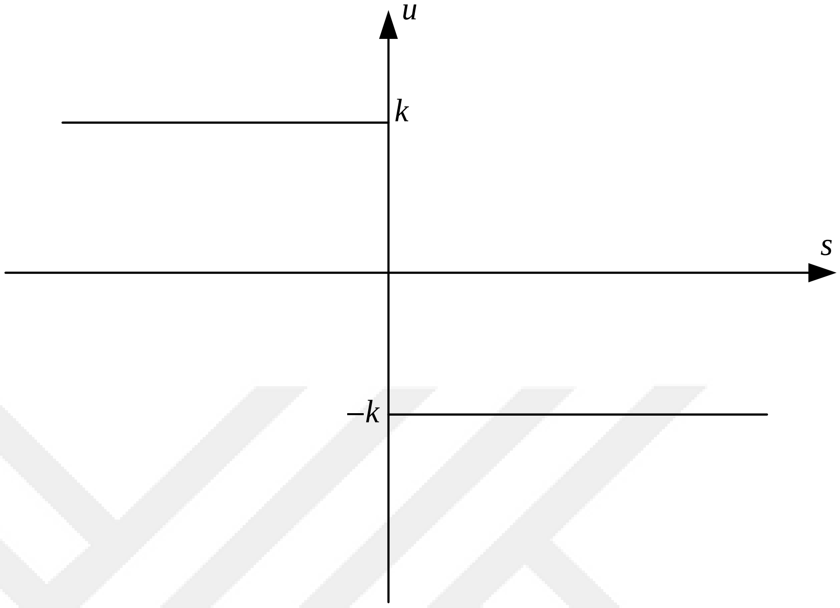

Figure 1.7. Signum function

Figure 1.8 presents a block diagram illustrating the operating principle of SMC applied to a system.

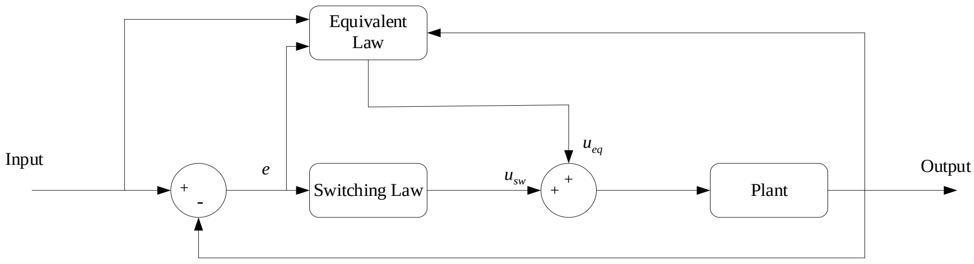

Figure 1.8. Classical sliding mode control structure

1.5. Lyapunov Stability Theory and Design

Various classical SMC methods exist in the literature. The stability of classical SMC is generally guaranteed by Lyapunov stability theory. In this theory, stability is ensured by showing that the Lyapunov function around the equilibrium point is positive definite and its derivative is negative definite (Janardhanan, 2006; Alwi and Edwards, 2008; Barambones and Alkorta, 2011; Roopaei and Jahromi, 2009).

According to Lyapunov theory, a positive definite Lyapunov function based on the error dynamics is selected. Then, it is shown that the derivative of this function is negative definite (Walcko et al., 2003).

If the Lyapunov function $V(t)$ is positive definite, $V(t) > 0$ for $t > 0$ and its derivative $\dot{V}(t)$ is negative definite, the equilibrium point at the origin is globally stable. Furthermore, all trajectories starting outside the sliding surface asymptotically reach the surface $s(t) = 0$ and remain on it. In this case, the error $e(t)$, converges to zero as time $t \to \infty$. This special behavior exhibited by the system when it reaches the sliding surface is commonly referred to as the sliding mode (Barambones and Alkorta, 2011).

To derive the SMC law that forces the system states to move along the sliding surface $s = 0$, a positive definite Lyapunov function is defined as follows (Eker, 2006):

$$V(t) = \frac{1}{2}s^2(t) \tag{1.6}$$

If the derivative $\dot{V}(t)$ is negative definite, $\dot{V}(t) < 0$ the system is stable and the system trajectories approach the sliding surface and move toward the origin. This property is well known as the sliding mode condition:

$$\dot{V}(t) = s(t)\dot{s}(t) < 0,\ s(t) \neq 0,\ \dot{s}(t) \neq 0 \tag{1.7}$$

1.5.1. Chattering Phenomenon

In the design of classical SMC, an appropriate sliding surface must be determined to reduce tracking errors and output deviations to a satisfactory level. Despite its simplicity and robustness advantages, classical SMC often suffers from a well-known problem called chattering. Chattering is characterized by high-frequency oscillations of the sliding variable around the sliding manifold, as illustrated in Figure 1.9 (Janardhanan, 2006; Tan, 2024; Huang and Way, 2001; Barambones and Alkorta, 2001).

There are two possible mechanisms that cause chattering (Xinghou and Kaynak, 2009):

i) Lack of Switching Imperfections: The absence of switching imperfections, such as delays, means the switching device ideally switches at infinite frequency (Young et al., 1999). Execution delays required for control signal computation or, more recently, transmission delays in networked control systems can also lead to chattering.

ii) Presence of Parasitic Dynamics: Parasitic dynamics connected in series with the plant cause small amplitude, high-frequency oscillations near the sliding manifold.

Mathematically, it is impossible to perfectly model a practical system and some unpredictable dynamics always exist. These parasitic dynamics generally represent fast actuator and sensor dynamics that are neglected during controller design (Xinghou and Kaynak, 2009).

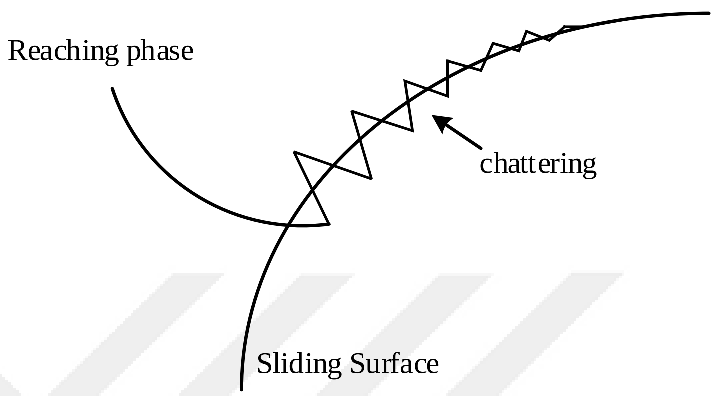

Figure 1.9. Chattering phenomenon in sliding mode control

The chattering caused by the discontinuous part of the control signal is highly undesirable for real systems and actuators because it can lead to actuator failure and unnecessarily large control signals. In practice, the presence of time delays (such as time lag, transport delay, dead time and physical constraints) in many industrial processes and actuators prevents infinite-frequency switching along the sliding surface as required by the theory of classical SMC algorithms (Nalbantoğlu and Güler, 2017; Cavallo and Natale, 2004).

Various techniques have been proposed in classical SMC algorithms to overcome the chattering phenomenon. Chattering can be reduced by smoothing the control discontinuities and ensuring exponential stability. Commonly preferred methods include replacing the relay control with saturation functions, sigmoid functions, hyperbolic functions and hysteresis saturation functions (Bishop and Dorf, 2017).

One solution to reduce chattering, instead of using the sgn function, is to employ the saturation function shown in Figure 1.10. This is expressed for the switching control law in Equation (1.8):

$$u_{sw} = -k sat\left(\frac{s}{\Omega}\right) \tag{1.8}$$

Which defines the thickness of the boundary layer around the switching surface, is defined as shown in Figure 1.11 and mathematically described as:

$$sat\left(\frac{s}{\Omega}\right)=\begin{Bmatrix} \frac{s}{\Omega}\ if\ \left|\frac{s}{\Omega}\right|\le 1 \\ sgn\left(\frac{s}{\Omega}\right)\ if\ \left|\frac{s}{\Omega}\right|\ge 1 \end{Bmatrix} \tag{1.9}$$

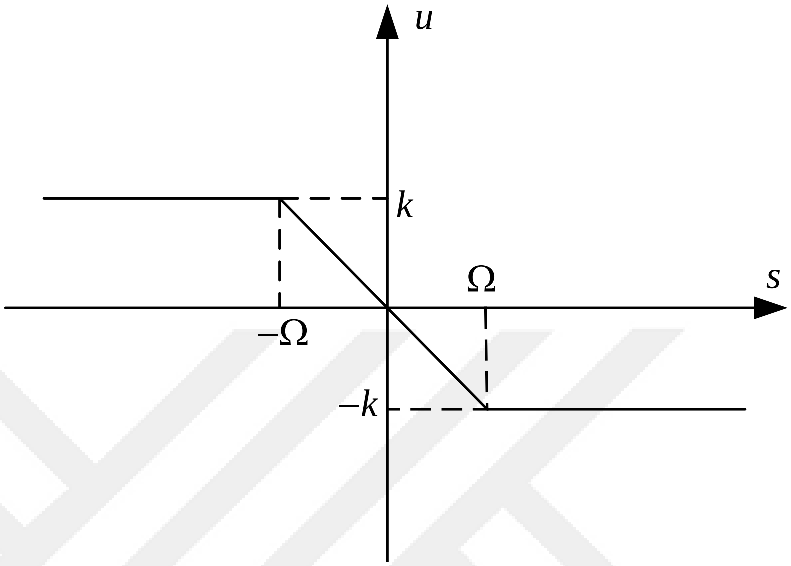

Figure 1.10. Saturation function

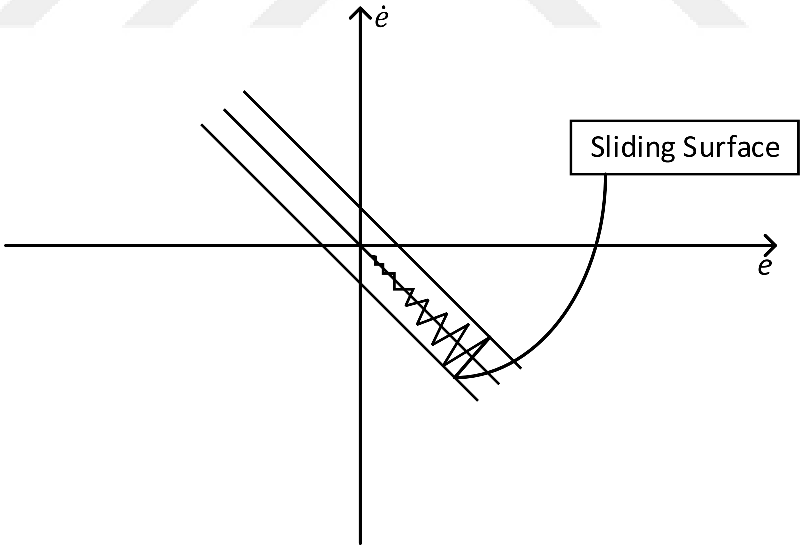

Figure 1.11. Boundary layer

1.6. Sliding Mode Control and Other Control Methods

In practice, an ideal SMC does not exist because physical systems are nonlinear and cannot be perfectly modeled with mathematical expressions capturing all dynamics (Xinghou and Kaynak, 2009). There are always unmodeled dynamics. Therefore, to improve the performance of classical SMC and reduce chattering effects, other control methods have been integrated.

An integral SMC method has been proposed in the literature (Eker and Akınal, 2008) and the sliding surface is selected as:

$$s(t) = \left(\lambda + \frac{d}{dt} \right)^{n-1} e(t) + k_i \int_0^t e(\tau) d\tau \qquad (1.10)$$

The proposed method using Figure (1.10) was applied to an electromechanical system, demonstrating that the SMC + I approach outperforms the classical SMC.

To enhance the robustness of classical SMC, a PID (Proportional-Integral-Derivative) based SMC was proposed (Eker, 2006):

$$s(t) = k_1 e(t) + k_2 \int_0^t e(\tau) d\tau + k_3 \frac{de(t)}{dt} \qquad (1.11)$$

where k_1, k_2, k_3 are positive constants. The goal of this control law is to drive the error $e(t)$ to the sliding surface and maintain the system state on this surface to reach the equilibrium point. To ensure stability, the commonly used Lyapunov function from Equation 1.8 is selected. The saturation function from Equation 1.9 is used for the discontinuous control part to define a thin boundary layer. Therefore, a PI-PD sliding function based SMC was proposed (Kaya, 2007):

$$s(t) = k_1 e(t) + k_2 \int_0^t e(\tau) d\tau - k_3 y(t) - k_4 \frac{dy(t)}{dt} \qquad (1.12)$$

where $e(t)$ is the tracking error, $y(t)$ is the system output and k_1, k_2, k_3, k_4 are tuning parameters that determine the performance of the sliding mode system. To reduce chattering, the hyperbolic tangent function from Equation 1.11 is used in the discontinuous control part.

A different approach for designing SMC based on dead-time process models was presented (Camacho and Smith, 2000). The aim was to develop an SMC suitable for self-regulating chemical processes. The sliding surface was chosen as an integral-derivative Equation affecting the tracking error e(t):

$$s(t) = \left(\lambda + \frac{d}{dt} \right)^{n} \int_0^t e(t) dt \qquad (1.13)$$

Chattering reduction is achieved through the control signal (Camacho and Cruz, 2004):

$$U_D(t) = K_D \frac{S(t)}{S(t)+\delta} \quad (1.14)$$

where K_D is the access mode parameter and δ is a tuning parameter for chattering reduction.

For processes with large dead-time constants, a method combining the internal model approach and SMC was proposed (Camacho et al., 2003). Stability was ensured via a Lyapunov function and the discontinuous part of the control signal was selected as defined in Equation 1.14

A fuzzy sliding surface method combining SMC with fuzzy logic was proposed (Yorgancıoğlu and Kömürcügil, 2008). Stability analysis was performed using a Lyapunov function. The proposed method was tested through computer simulations of an inverted pendulum system. Simulation results showed faster error convergence and reduced settling time.

Based on the combination of sliding mode and fuzzy control, a fuzzy SMC was developed for nonlinear Multi-Input Multi-Output (MIMO) systems with uncertainties and external disturbances (Roopaei and Jahromi, 2009). Stability was guaranteed by a Lyapunov function and the chattering phenomenon was eliminated by designing an appropriate switching control law using a fuzzy logic control scheme. Simulation results demonstrated that chattering was eliminated without compromising system robustness.

An adaptive wavelet SMC algorithm for continuous-time unknown nonlinear systems was presented (Yau and Chen, 2006). The proposed algorithm integrates wavelet transform properties, feedback linearization techniques, adaptive control schemes and SMC to address tracking control problems in nonlinear systems with uncertain or unknown parameters and external disturbances. Daubechies wavelet, considered the most suitable wavelet basis for practical applications, was preferred in controller design. The closed-loop system was found to be Lyapunov stable. The controller was generally simulated on an inverted pendulum and simulation results demonstrated the achievement of the desired performance.

1.6.1. Summary of Classical Sliding Mode Control Methods

Various classical SMC exist in the literature. Early studies focused on Single-Input Single-Output (SISO) systems and developed different approaches. However, recent research predominantly addresses MIMO systems. Due to its simplicity and robustness against parameter variations and matched disturbances, SMC remains popular within the control community (Xinghou and Kaynak, 2009).

Traditionally, SMC methods have been designed for systems with relative degree one (Janardhanan, 2006). Most of these methods are relay-based, where the control signal switches between two structures depending on the sgn of the sliding function. However, these control structures can cause a severe issue called chattering, which is problematic in practical applications.

Classical SMC methods generally suffer from this well-known problem. If the control signal cannot adapt to uncertainties while in sliding mode, the known robustness condition of SMC cannot be satisfied.

Several methods have been developed to reduce chattering in the control signal. Although a few techniques have been proposed in the literature to eliminate chattering, most have been tested only through model-based computer simulations (Alwi and Edwards, 2008; Ngo and Mahony, 2007). Since practical systems always contain unmodeled dynamics, an ideal SMC does not exist in practice. However, if partial knowledge of uncertainties and unmodeled dynamics can be identified using learning mechanisms such as artificial neural networks and fuzzy systems, this partial information may assist in providing an appropriate switching input signal (Xinghou and Kaynak, 2009).

1.7. Cascade Sliding Mode Control

Cascade Sliding Mode Control (CSMC) is a extension of SMC, particularly used in multi-layered (hierarchical) systems. This method decomposes the system dynamics into multiple subsystems and designs a separate sliding surface for each subsystem. As a result, the overall control performance improves and controllability becomes easier. CSMC is especially preferred in the following cases: when system dynamics are complex and nonlinear, when uncertainties or external disturbances exist in the system and in applications requiring high precision and robustness (Eker, 2006).

The behavior of variable structure control systems is defined by a certain feedback control strategy and a decision-making mechanism. The switching function, which acts as the decision-making mechanism for the system, selects the function that determines the system's operating mode. In the SMC approach, the states of the variable structure control system are designed to lie on a surface in the phase space called the "sliding surface." The goal of this control method is to ensure that the system states reach and remain on this sliding surface (Kjaer, 2004).

1.7.1. Basic Principles of Cascade Sliding Mode Control

CSMC controls the system dynamics progressively. Each stage uses the output of the previous stage as its reference and constructs its own sliding surface. The procedure steps are as follows:

- Decomposition of System Dynamics: The system is divided into multiple subsystems (stages). For example, in a two-stage system:
  First stage: outer-loop,
  Second stage: inner-loop.

- Design of Sliding Surfaces: A distinct sliding surface is designed for each stage. The sliding surface defines the desired behavior of the system.
  Example:
  First stage sliding surface:

$$S_1 = x_1 - x_{1d} \tag{1.15}$$

where x_1 is the state variable of the outer-loop and x_{1d} is desired/reference value for x_1.

Second stage sliding surface:

$$S_2 = x_2 - x_{2d} \tag{1.16}$$

where x_2 is the state variable of the outer-loop and x_{2d} is desired/reference value for x_2.

- Determination of Control Law: A separate control law is designed for each stage. This law ensures that the system reaches and stays on the sliding surface.
  The control law is generally expressed as:

$$u(t) = u_{eq}(t) + u_{sw}(t) \tag{1.17}$$

where u_{eq} is the equivalent control, u_{sw} is the switching control.

- Inter-Stage Interaction**:** Each stage determines the reference for the next stage. Thus, the overall system dynamics are controlled in a coordinated manner.

Advantages:

- Robustness: Exhibits high resistance against system uncertainties and external disturbances.
- Fast Response Time: SMC enables rapid convergence to the desired state.
- Effectiveness in Complex Systems: Easily applicable to multi-layered systems.

Disadvantages:

- Chattering Problem: A well-known drawback of SMC is the high-frequency oscillations (chattering) in the control signal, which can negatively impact system performance.
- Design Complexity: Designing separate sliding surfaces and control laws for each stage can be complex in multi-stage systems.

SMC inherently exhibits a discontinuous nature. In this control method, when the system states reach the sliding surface and tend to leave it, a sudden control signal is generated to bring the states back to the surface. This process causes the system to switch directions many times in a very short period. The infinite-frequency, abrupt switching control signal used to maintain system states on the sliding surface is called "chattering." Chattering may cause various problems in practical applications; especially in fast-moving mechanical systems, such control can damage moving parts. Therefore, SMC is generally not recommended for systems with fast dynamics. Various methods such as filtering, discontinuous approximation, saturation functions, or fuzzy control can be used to reduce chattering. However, these methods tend to reduce the robustness feature of SMC (Eker, 2006).

There are two main phases in SMC: reaching phase and sliding phase.

The fundamental rules for the reaching phase are (Latosiński, 2017):

- Constant Variable Reaching Law (Latosiński, 2017):

$$\dot{s}(t) = \rho sgn(s(t)) \tag{1.18}$$

- Constant-Proportional Variable Reaching Law (Latosiński, 2017):

$$\dot{s}(t) = \rho sgn(s(t)) - Ks(t) \tag{1.19}$$

- Exponential Variable Reaching Law (Latosiński, 2017):

$$\dot{s}(t) = -\rho \left| s(t) \right|^{a} \operatorname{sgn}(s(t)) \tag{1.20}$$

where a is the exponential power determining approach smoothness, ρ is the reaching speed and K is the control gain adjusting the convergence rate.

The motion of the sliding surface occurs along the directions indicated by arrows in Figure 1.12 shows the phase plane of the sliding surface s and its derivative $\dot{s}$. The horizontal axis represents the error e. The vertical axis represents the derivative of the error $\dot{e}$. The line labeled $s=0$ corresponds to the sliding surface, where the system reaches the desired trajectory. The arrows indicate the direction of system motion when $s \neq 0$, showing how the system state moves toward the sliding surface. The dashed lines show an initial state $(e, \dot{e})$ and the trajectory converging toward $s=0$. Interpretation: The system starts away from the sliding surface $(s \neq 0)$ and moves along the trajectories toward the sliding manifold, illustrating the reaching phase of SMC.

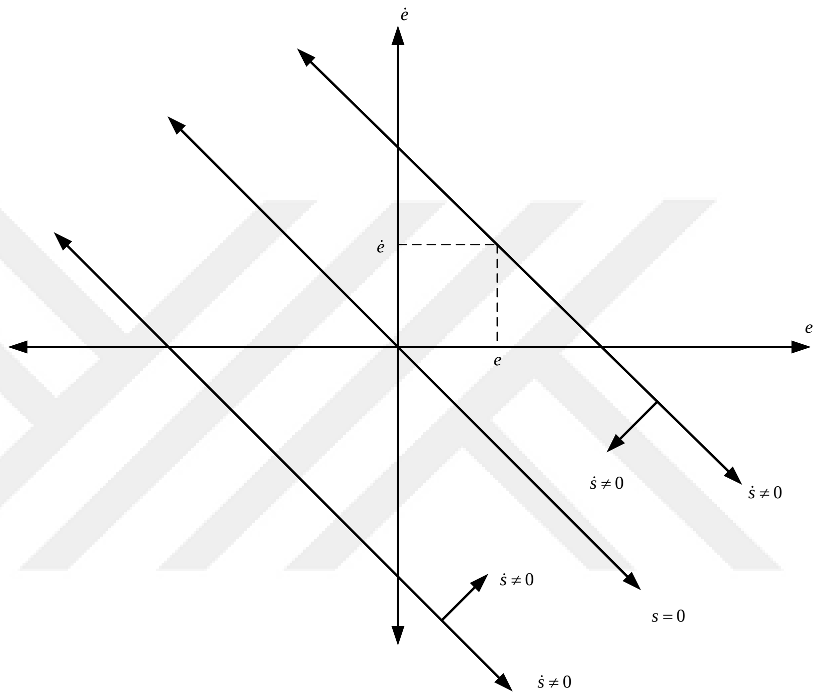

Figure 1.12. Sliding surface

The inner-loop affects the outer-loop; therefore, it is essential to understand how the secondary controller influences the primary process. Otherwise, the primary controller may lose control over its own process. The inner-loop is more sensitive than the outer-loop, so the secondary process controller must respond at least 3 times faster to the efforts of the primary process than the primary process reacts to its own efforts (Eker, 2006).

Disturbances in the inner-loop are significantly less severe than those generated by the outer-loop. Otherwise, the secondary controller would be occupied with correcting its disturbances rather than applying corrective efforts to the primary process.

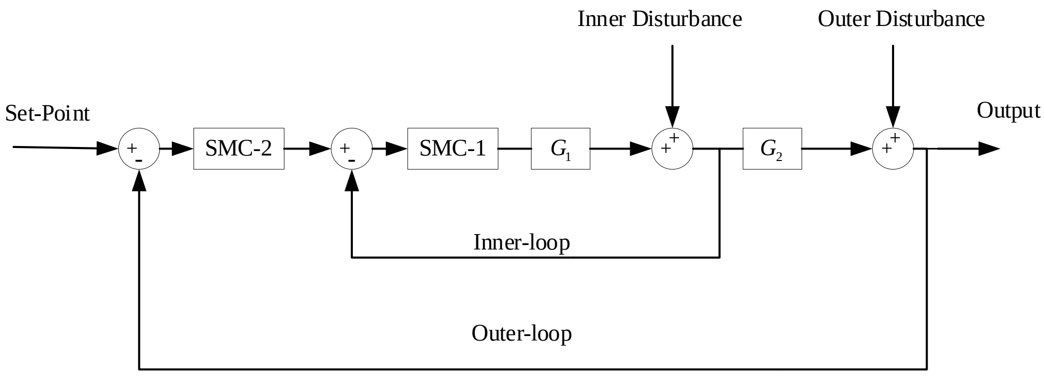

Figure 1.13. Cascade sliding mode control system

2. PRELIMINARY WORK

2.1. Historical Development and Fundamentals of Sliding Mode Control

SMC is a robust control technique derived from Variable Structure Systems (VSS) theory, widely used for nonlinear system control. Initially introduced by Soviet researchers in the 1950s, the method gained international recognition following Utkin's seminal work in 1977 (Utkin, 1977). Utkin formulated the control law based on the system state "sliding" along a predefined sliding surface, ensuring robustness against disturbances and parameter uncertainties. This approach offers fast transient response and high resilience to modeling errors.

One of the main advantages of SMC is its low computational demand coupled with strong stability properties. However, the sharp switching action inherent to SMC causes undesired high-frequency oscillations, known as "chattering," which can lead to mechanical wear and energy inefficiency. Therefore, various strategies have been proposed to mitigate chattering effects (Chalanga and Bandyopadhyay, 2023).

The fundamental advantage of SMC remains its robustness against disturbances and parameter uncertainties, offering fast transient response. However, the classic challenge of "chattering" persists, driving contemporary research towards innovative solutions that are computationally efficient and practical for modern digital implementation (Pham et al., 2024; Li et al., 2023).

2.2. Fundamentals of Cascade Control Structures

Cascade control is a widely adopted multi-loop feedback configuration in which two or more control loops are nested to enhance system performance. Typically, the outer-loop regulates the main process variable, while the inner-loop governs a faster subsystem. This arrangement allows the inner-loop to rapidly suppress disturbances, thereby reducing the burden on the outer-loop and improving dynamic response (Aström and Murray, 2008). Cascade control has proven effective in diverse applications such as robotics, motor drives and process industries. Åström and Murray demonstrated that cascade control significantly improves disturbance rejection and system responsiveness, especially in systems with tightly coupled dynamics. For example, in DC motor control, the outer-loop regulates speed, while the inner-loop manages current or torque, ensuring high precision. Contemporary studies continue to validate the efficacy of this structure in complex electromechanical systems, where it provides a solid foundation for integrating advanced robust controllers such as SMC in the outer-loop (Li et al., 2023; Preindl and Bolognani, 2013).

2.3. Integration of SMC with Cascade Control: Applications and Advances

Recent research has increasingly focused on embedding SMC within cascade control frameworks to combine their complementary strengths. In most implementations, SMC is placed in the outer-loop, while classical controllers such as PI or PID regulate the inner-loop. For instance, Alwi and Edwards employed dual-loop SMC in flight control systems, achieving robustness against aerodynamic uncertainties (Alwi and Edwards, 2008). Similarly, Song et al. integrated SMC in the outer-loop with PI control in the inner-loop for DC motor speed regulation, yielding improved transient performance and reduced chattering (Tan, 2024). Khan et al. further optimized equivalent and switching control signals in CSMC to mitigate high-frequency oscillations (Wang et al., 2023). Beyond motor drives, CSMC has been applied successfully to robotic manipulators (Chalanga and Bandyopadyay, 2023), unmanned aerial vehicles (Ngo and Mahony, 2007), marine systems (Castillo et al., 2005) and power electronics (Shtessel et al., 2012). A notable recent trend is replacing inner-loop PI controllers with Finite Control Set Model Predictive Control (FCS-MPC), which provides faster transient dynamics, while the outer-loop employs SMC for robust regulation (Liu et al., 2024). Additionally, the integration of SMC with deep learning for automatic parameter tuning represents a promising direction, enabling improved adaptability and performance without manual intervention (Zhao et al., 2023). Recent applications include precision motion control in robotics (Zeinali and Notash, 2010) and disturbance rejection in aerospace systems (Shtessel et al., 2023), highlighting the versatility and continuing evolution of CSMC.

Recent advances in motor control emphasize the extension of cascade and sliding mode approaches to BLDC and multi-motor systems. For example, an observer-based order-reduction speed control method with current-loop adaptation has been proposed for converter-fed BLDC motors, enhancing robustness to parameter uncertainties (Gong et al., 2024). In DC motors with DC/DC converters, an inverse optimal control–based adaptive speed control scheme has been experimentally demonstrated, showing faster dynamics compared to cascaded PI approaches (Hussein and Yasin, 2023). Furthermore, comparative studies between traditional PI controllers and sliding mode with metaheuristic tuning (e.g. Salp Swarm) for dual BLDC motors illustrate the superiority of SMC in demanding reference tracking tasks (Montoya-Acevedo et al., 2024). Lastly, comprehensive reviews on multi-motor drives discuss structural diversity, control coordination and evolving challenges, positioning CSMC as a promising candidate for future high-performance motor drive systems (Kim et al., 2023).

2.4. Chattering Issue and Mitigation Techniques

One of the principal drawbacks of SMC is the chattering phenomenon, characterized by high frequency switching in the control signal (Liu et al., 2021; Pan et al., 2025). This effect can degrade system performance, increase energy consumption and accelerate mechanical wear. In CSMC architectures, the chattering problem becomes even more critical due to the interaction of multiple control loops. Modern research has progressed beyond traditional boundary layer approaches, introducing more advanced methods. A prominent solution is the Super-Twisting Algorithm (STA), a second-order SMC scheme that suppresses chattering while preserving robustness (Liu et al., 2021;

Pan et al., 2025). Adaptive SMC strategies have also gained popularity, dynamically adjusting switching gains to the minimum level required for stability, thus reducing oscillations under varying conditions (Bagheri et al., 2023; El-Sousy et al., 2022). Levant's Higher-Order SMC (HOSMC) further addresses this issue by employing derivatives of sliding surfaces to smooth control actions (Levant, 2003). Similarly, adaptive gain controllers proposed by Shtessel et al. regulate switching intensity based on system states, effectively mitigating high-frequency oscillations (Chalanga and Bandyopadhyay, 2023). Other promising approaches include replacing discontinuous switching with continuous approximations via boundary layers, as well as employing neuro-adaptive filters to directly estimate and cancel chattering components (Wang et al., 2024). Collectively, these methods illustrate the extensive ongoing efforts to overcome chattering while preserving the robustness that defines SMC.

2.5. Research Gap and Contribution of This Thesis

Although extensive research has been conducted on CSMC, notable gaps remain in its experimental validation and comparative assessment. Modern chattering-reduction techniques - such as the Super-Twisting Algorithm (STA) and adaptive-gain strategies - have largely been examined only through simulations or on highly specialized systems (Khan et al., 2022). Moreover, the integration of data - driven and learning-based methods for auto-tuning CSMC loops represents an emerging yet underexplored field with considerable practical potential (Zhou et al., 2024). Existing studies are often limited to simulations or application-specific scenarios, while experimental investigations of CSMC in DC motor speed and current control remain scarce. Similarly, practical chattering mitigation approaches still lack comprehensive empirical evaluation.

This thesis seeks to address these gaps by conducting an experimental comparison of modern cascade configurations. Furthermore, it proposes and validates a practical framework for adaptive gain tuning (Zhou et al., 2024), thereby contributing both to the academic body of knowledge and to real-world engineering applications.

2.6. Cascade Sliding Mode Control DC Motors

The practical implementation of CSMC requires real-time capable digital platforms that support robust control algorithms. Various digital platforms, including microcontrollers, DSP boards and training kits, have been widely used in literature for experimental validation of SMC schemes (Utkin et al., 2009; Kuo, 1995). These platforms allow hands-on experimentation, verification of simulation results and observation of control phenomena such as transient response, robustness against disturbances and chattering. The DIGIAC 1750 training system is a modular educational platform specifically designed for control experiments on DC motors and other electromechanical systems. It integrates power electronics, speed and current sensors and digital controllers, providing a realistic environment to test CSMC algorithms. In cascade configurations, the inner-loop typically regulates motor current or torque, while the outer-loop controls speed, allowing precise study of the controller's performance (Feedback Instruments, 2009; Hacettepe University, 2018). Experiments on the DIGIAC 1750 include step and ramp speed reference tracking, evaluation of inner-loop controllers (classical PI vs. SMC) and analysis of chattering phenomena. Advanced chattering mitigation strategies, such as boundary layers, super-twisting algorithms and adaptive-gain tuning, can be implemented and assessed in this setup. This integrated approach bridges theoretical analysis and practical implementation, offering both educational and research benefits and provides experimental validation for modern CSMC configurations in real-time digital environments.

2.7. Experimental Studies Using DIGIAC 1750 for DC Motor Speed Control

The experimental validation of CSMC is a crucial step to assess the real-time performance of the proposed control strategies. In this study, the DIGIAC 1750 educational platform was employed to perform DC motor speed control experiments. The platform provides a versatile interface for implementing both classical and modern control algorithms, allowing real-time observation of motor response under varying load conditions (Feedback Instruments, 2009; Hacettepe University, 2018). In the experimental setup, the DC motor speed was regulated using a CSMC structure, with the outer-loop controlling motor speed and the inner-loop regulating armature current. Different chattering reduction techniques, including super-twisting and adaptive-gain methods, were implemented to evaluate their effectiveness in practical scenarios. The experiments demonstrated that the SMC-based cascade controller achieved fast transient response, robust performance under parameter uncertainties and effective disturbance rejection, consistent with simulation results. Moreover, the DIGIAC 1750 allowed for systematic comparison of various controller configurations, highlighting the practical advantages and limitations of each approach. The experimental results provide empirical evidence supporting the theoretical analysis and validate the applicability of CSMC in real-world DC motor applications (Utkin et al., 2009; Kuo, 1995; Feedback Instruments, 2009; Hacettepe University, 2018).

3. MODELLING OF THE DC MOTOR

DC motors are a type of DC shunt motor specially designed for low inertia, symmetric rotation and smooth low-speed characteristics. The DC motor is a closed-loop feedback system in which the motor position is fed back to the control circuit to determine how the motor should rotate to reach the desired position.

SMC is robust against system uncertainties and insensitive to external disturbances. This control method is frequently used to achieve good dynamic performance in controllable systems. However, the phenomenon of chattering, caused by finite switching speeds of the actuators, can significantly affect system behavior. Moreover, sliding control requires knowledge of the system’s mathematical model and bounded uncertainties (Haque and Rahman, 2001).

Chattering can be reduced without sacrificing robust performance by combining the attractive features of fuzzy logic (FL) with SMC. Fuzzy logic is a powerful tool for controlling systems with undefined or variable parameters. By generalizing fuzzy rules, FL controllers can provide robustness against modeling errors. Additionally, fuzzy logic can prevent heavy computational loads with well-tuned expressions (Attaianese et al., 1999).

DC motors are commonly controlled by conventional PID controllers because they are easy to design and implement, cost-effective, require low maintenance and offer effective performance. However, tuning PID parameters requires knowledge of the system's mathematical model or experimental trials. Moreover, it is well-known that conventional PID controllers often perform poorly in nonlinear applications and especially in complex systems lacking precise mathematical models (Rahman et al., 2004).

To overcome these challenges, modified PID controllers such as auto tuning and adaptive PID have been developed. Additionally, FL can be used for such problems. Compared to conventional controllers, the primary advantage of FL is that it does not require mathematical modeling (Abdel Ghany and Bensenouci, 2004). In this study, a robust and effective controller has been designed and implemented using the proposed approach. A PID outer-loop is employed in the control law and the gains of the sliding term and PID term are tuned online via a fuzzy system (Ramesh, 2013).

Computer simulations have been conducted to validate the proposed system. The results obtained by the modified SMC are compared with those of the conventional PID controller and fuzzy SMC. The advantages and limitations of each method are discussed.

DC motors consist of four main components: a DC motor, a position sensing device (e.g., potentiometer), a gear reduction section and a control unit. These components work together so that the motor accepts control signals representing the desired output of the motor shaft and drives the shaft until it reaches the correct position. Unlike standard DC motors, the shaft in DC motors does not rotate freely; it can only rotate approximately 200 degrees in either direction. The position sensing device in the DC motor determines the shaft rotation and thus controls the motor's movement.

3.1. Modeling and System Description

A DC motor is used in control systems when significant shaft power is required. DC motors is be armature-controlled with a fixed field or field-controlled with a fixed armature current. The DC motors used in measuring devices have a permanent magnet field and the control signal is applied to the armature terminals.

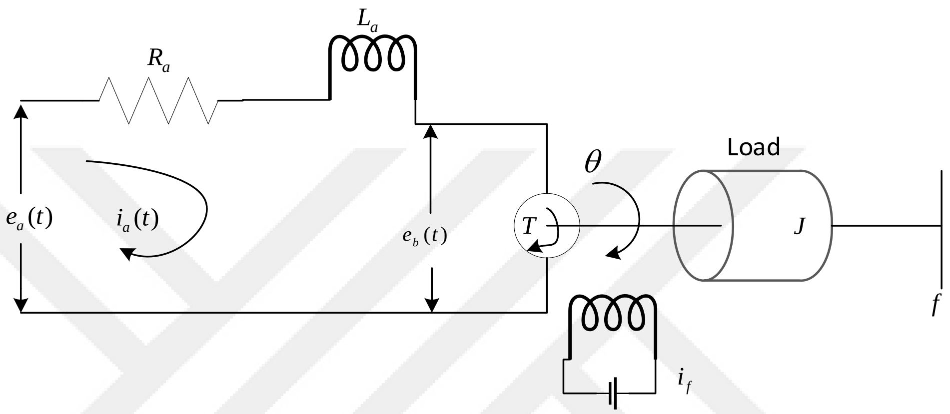

Figure 3.1. Schematic diagram of armature-controlled gear DC motor

To model the DC motor shown in Figure 3.1, the following parameters and variables are defined:

- R_a : Armature winding resistance (ohms)
- L_a : Armature winding inductance (henry)
- i_a : Armature winding current (amperes)
- i_f : Field current (amperes)
- e_a : Applied armature voltage (volts)
- e_b : Back electromotive force (back EMF) (volts)
- θ : Angular displacement of the motor shaft (radians)
- T : Torque produced by the motor (lb-ft)
- J : Moment of inertia of the motor and load (referenced to the motor shaft) (slug-ft²)
- f : Viscous friction coefficient of the motor and load (referenced to the motor shaft) (lb-ft/rad/s)

The torque T produced by the motor is proportional to the product of the armature current i_a and the air-gap flux φ. The air-gap flux φ, is directly proportional to the field current i_f :

$$\varphi = K_f i_f \tag{3.1}$$

where K_f is a constant. The torque can thus be expressed as:

$$T(t) = K_f i_f(t) K_a i_a(t) \tag{3.2}$$

where K_a is another constant. Therefore, the torque is directly proportional to the armature current and the motor torque constant K is defined as:

$$T(t) = K i_a(t) \tag{3.3}$$

The back EMF is proportional to the angular velocity $\frac{d\theta(t)}{dt}$, where K_b back EMF constant.

$$e_b(t) = K_b \frac{d\theta(t)}{dt} \tag{3.4}$$

The speed of an armature-controlled DC servo motor is controlled by the armature voltage e_a supplied by the power source. The differential Equation for the armature circuit is:

$$e_a(t) = L_a(t) \frac{di_a(t)}{dt} + R_a i_a(t) + e_b(t) \tag{3.5}$$

The armature current produces torque, which acts against inertia and friction:

$$T = K i_a(t) = J \frac{d^2\theta(t)}{dt^2} + f \frac{d\theta(t)}{dt} \tag{3.6}$$

Assuming zero initial conditions and applying Laplace transforms to the above three differential Equations, the following Equations in Laplace domain are obtained:

$$E_b(s) = K_b s\theta(s) \tag{3.7}$$

$$E_a(s) = (L_a s + R_a) I_a(s) \tag{3.8}$$

$$KI_a(s) = (Js^2 + fs)\theta(s) \tag{3.9}$$

Considering $E_a(s)$ as the input and $\theta(s)$ as the output, the block diagram can be constructed based on these three Equations. The effect of the back electromotive force is represented as a feedback signal proportional to the motor speed. This back EMF increases the effective damping of the system.

$$\frac{\theta(s)}{E_a(s)} = \frac{K}{JL_a s^3 + (JR_a + fL_a)s^2 + (R_a f + KK_b)s} \tag{3.10}$$

The armature circuit inductance L_a is usually small and can be neglected. If L_a is neglected, the transfer function simplifies to:

$$\frac{\theta(s)}{E_a(s)} = \frac{K}{JR_a s^2 + (R_a f + KK_b)s} = \frac{K_m}{s(T_m s + 1)} \tag{3.11}$$

where K_m is the motor gain constant and τ_m is the motor time constant. The Equations are given in Equations (3.12) and (3.13).

$$K_m = \frac{K}{R_a f + KK_b} \tag{3.12}$$

$$T_m = \frac{JR_a}{R_a f + KK_b} \tag{3.13}$$

This shows how the difference between the input voltage $V_i(s)$ and the back EMF $V_b(s)$ affects the armature current $I_a(s)$. The input voltage $U(s)$, is applied to the armature circuit after subtracting the back EMF $V_b(s)$

$$I_a(s) = \frac{V_i(s) - V_b(s)}{L_a s + R_a} \tag{3.14}$$

$$V_b(s) = K_b \omega(s) \tag{3.15}$$

$$\omega(s) = \frac{1}{J_m s + B_m} T_m(s) = \frac{1}{J_m s + B_m} K_i I_a(s) \tag{3.16}$$

$$I_a(s) = \frac{V_i(s) - K_b \dfrac{1}{J_m s + B_m} K_i I_a}{L_a s + R_a} \tag{3.17}$$

$$I_a(s)(L_a s + R_a) + \left(\frac{K_b K_i}{J_m s + B_m} \right) I_a(s) = V_i(s) \tag{3.18}$$

$$V_i(s) = I_a(s) \left[L_a s + R_a + \frac{K_b K_i}{J_m s + B_m} \right] \tag{3.19}$$

$$\frac{I_a(s)}{V_i(s)} = \frac{J_m s + B_m}{(L_a s + R_a)(J_m s + B_m) + K_b K_i} \tag{3.20}$$

3.2. DC Motor Open-Loop Test Results: Experimental and Simulation Results

In this study, an armature-controlled DC motor was employed as the experimental system. Data acquisition and signal exchange were performed using the NI PCI-6229 DAQ card, a multifunction data acquisition device by National Instruments designed for high-precision, real-time measurement and control applications. It features 32 single-ended or 16 differential analog input channels with 16-bit resolution and a maximum sampling rate of 250 kS/s, offering programmable input ranges of ±0.2 V, ±1 V, ±5 V, and ±10 V. The card includes four 16-bit analog output channels with an update rate up to 833 kS/s and ±10 V output range. In addition, it provides 48 bidirectional digital I/O lines (5 V TTL compatible) and two 32-bit counters capable of operating up to 80 MHz for pulse, frequency, and PWM measurements. With a timing resolution of 50 ns, ±50 ppm clock accuracy, ±25 V overvoltage protection, and a 4095-sample FIFO buffer, the NI 6229 ensures reliable high-speed data transfer and control. The control algorithms and system modeling were implemented within the MATLAB/Simulink environment, where the control structure was designed with an inner-loop dedicated to current control and an outer-loop for speed control. Each control loop was equipped with a specifically designed sliding surface, thereby improving overall system performance and robustness.

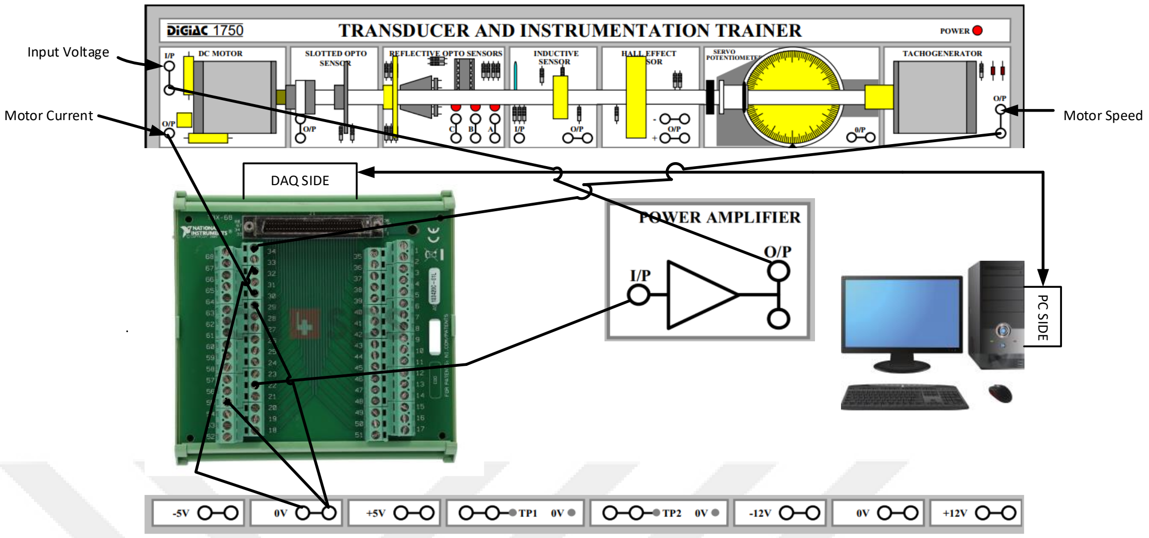

Figure 3.2. Physical view of the experimental test setup

3.2.1. Experimental Test

A step input voltage $V_i = 3.81$ volt that correspond to then 1000 rpm operating speed is applied from the motor input, the motor armature current $i_a(t)$ the output speed $\omega_m(t)$, speed are measured.

Figures 3.3 and 3.4 illustrate the current and speed responses of the DC motor obtained from the experimental system over a duration of 1 second.

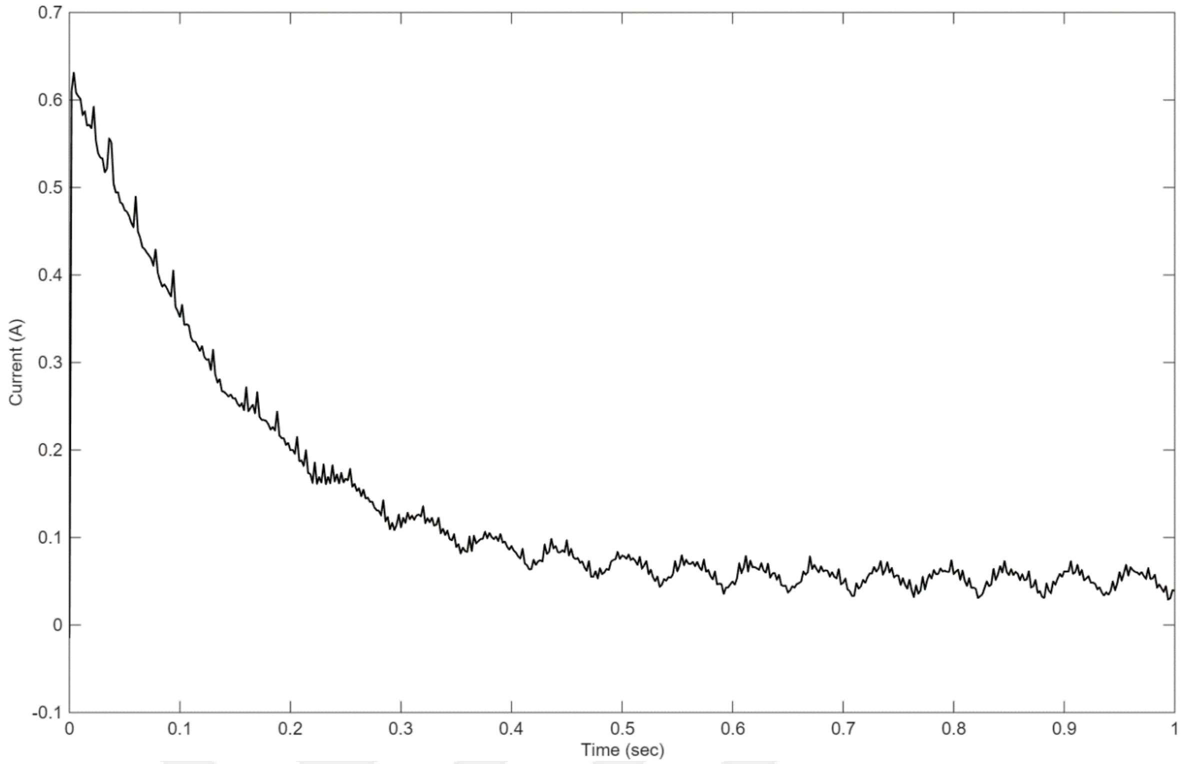

Figure 3.3. Measured current (A), $i_a(t)$

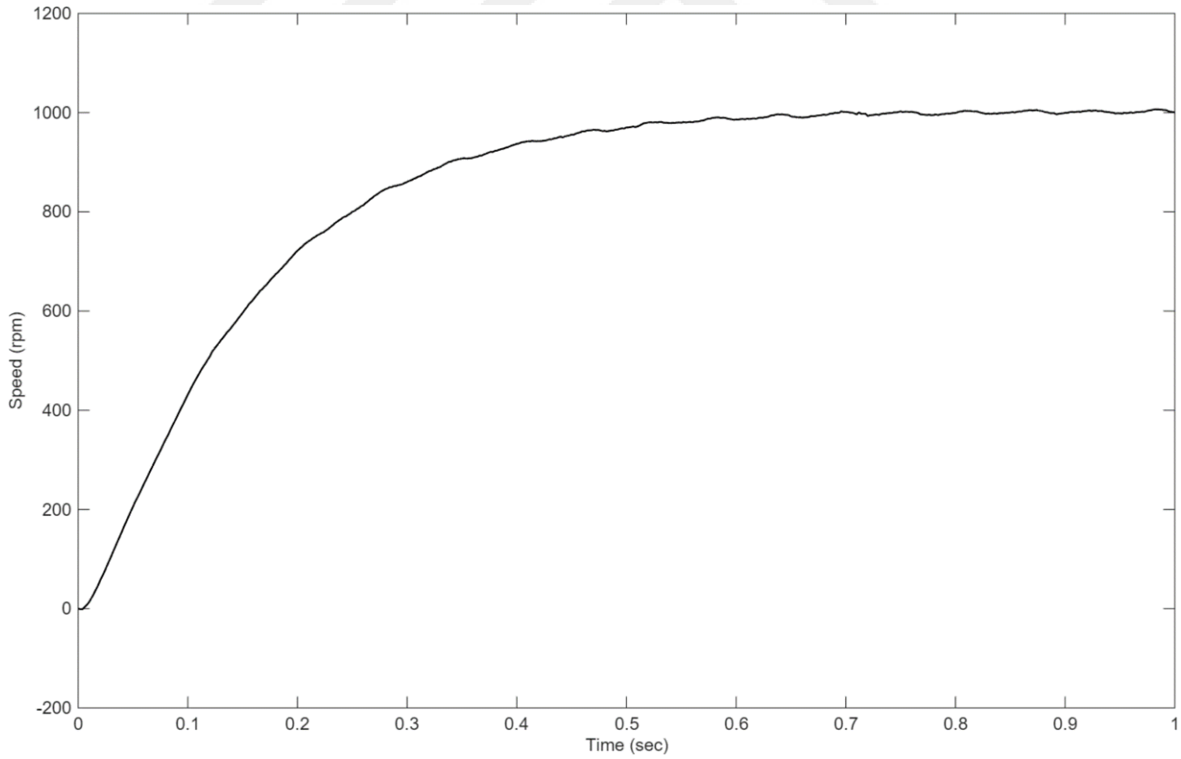

Figure 3.4. Measured motor speed (rpm), $\omega_m(t)$

3.2.2. Simulation Results

Figure 3.5 shows the DC motor circuit, indicating where the current is measured and where the voltage is taken in the MATLAB/Simulink model.

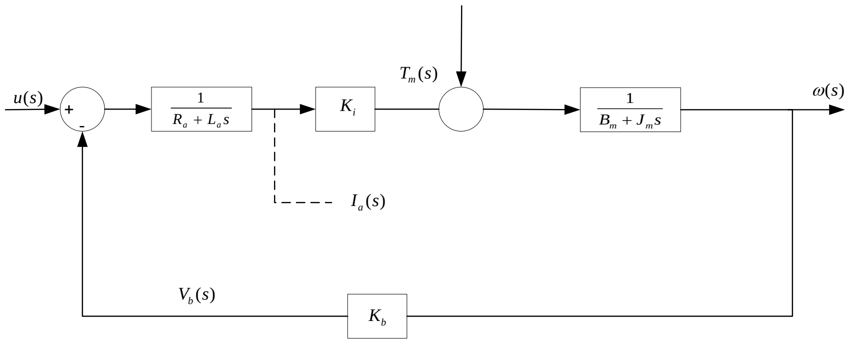

Figure 3.5. Simplified Model

Figure 3.6. Shows the simplified MATLAB/Simulink model of the DC motor used in this study

$$\frac{\omega(s)}{u(s)} = \frac{K_i}{L_a J_m s^2 + (R_a J_m + L_a B_m)s + R_a B_m + K_b K_i} \tag{3.21}$$

$$\frac{\omega(s)}{u(s)} = \frac{457.235}{s^2 + 83.916s + 537.9} \tag{3.22}$$

$$\frac{I_a(s)}{u(s)} = \frac{13.468s + 5.579}{s^2 + 83.916s + 537.9} \tag{3.23}$$

By dividing both the numerator and the denominator by $L_a J_m$ the transfer function can be rewritten as:

$$\frac{\omega(s)}{u(s)} = \frac{\frac{K_i}{L_a J_m}}{s^2 + s\frac{(R_a J_m + L_a B_m)}{L_a J_m} + \frac{R_a B_m + K_b K_i}{L_a J_m}} \tag{3.24}$$

$$J_m = \frac{K_i}{L_a \times 457.235} \tag{3.25}$$

$$B_m = \frac{83.916 \times K_i L_a - R_a K_i}{L_a^{\ 2} \times 457.235} \tag{3.26}$$

$$K_b = \frac{537.9 \times K_i L_a^{\ 2} + R_a^{\ 2} K_i - R_a \times 83.916 \times L_a K_i}{L_a^{\ 2} K_i \times 457.235} \tag{3.27}$$

In this simulation, the parameters $K_i = 0.035$, $R_a = 6.2\ \Omega$, $L_a = 0.07425\ H$ were used, with an initial and final value of 4.48 output that corresponds to 1000 rpm speed, a step time of 1 s and a sample time of 0.002 s.

The system's speed output is represented by a dynamic system with the transfer function $\dfrac{457.235}{s^2 + 83.916s + 537.9}$.

The system's current output is represented by a dynamic system with the transfer function $\dfrac{13.468s + 5.579}{s^2 + 83.916s + 537.9}$.

A current model close to the real system was designed in the MATLAB/Simulink environment and a graph showing the 1-second behavior of this model was obtained (Figure 3.6).

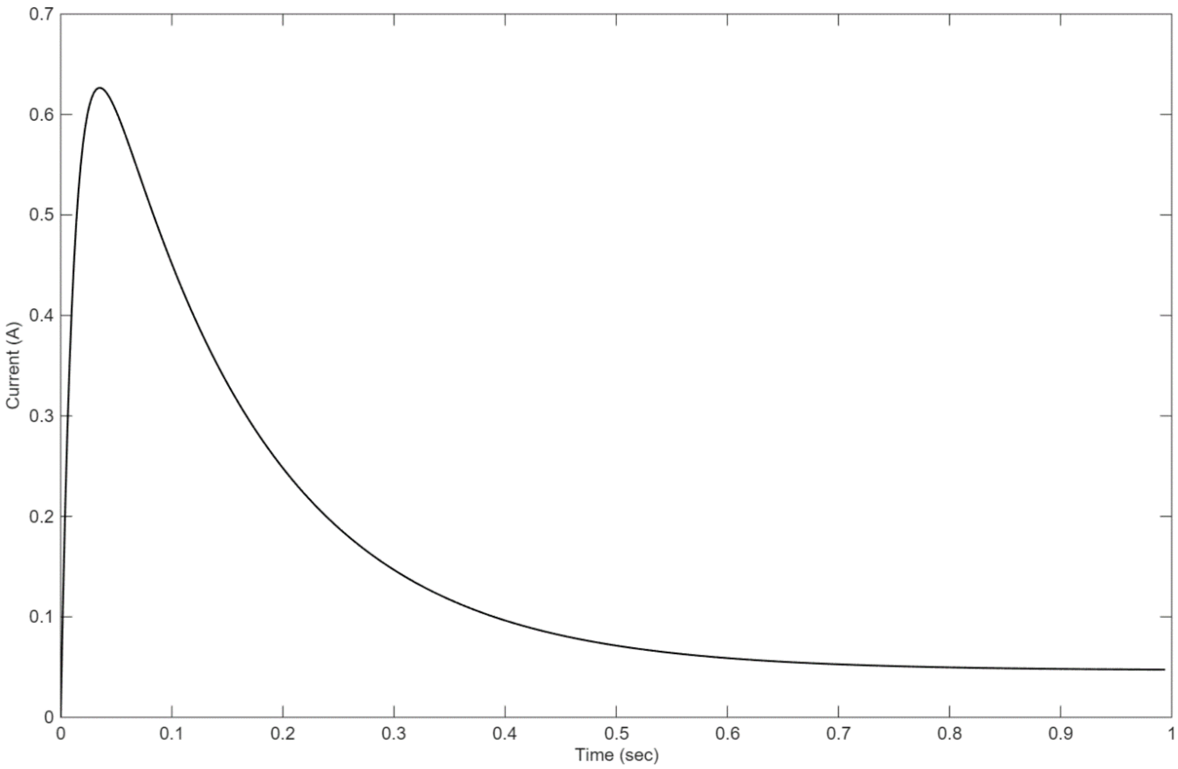

Figure 3.6. MATLAB/Simulink model current

A speed model closely representing the real system was developed in the MATLAB/Simulink environment and its 1-second dynamic behavior was obtained (Figure 3.7).

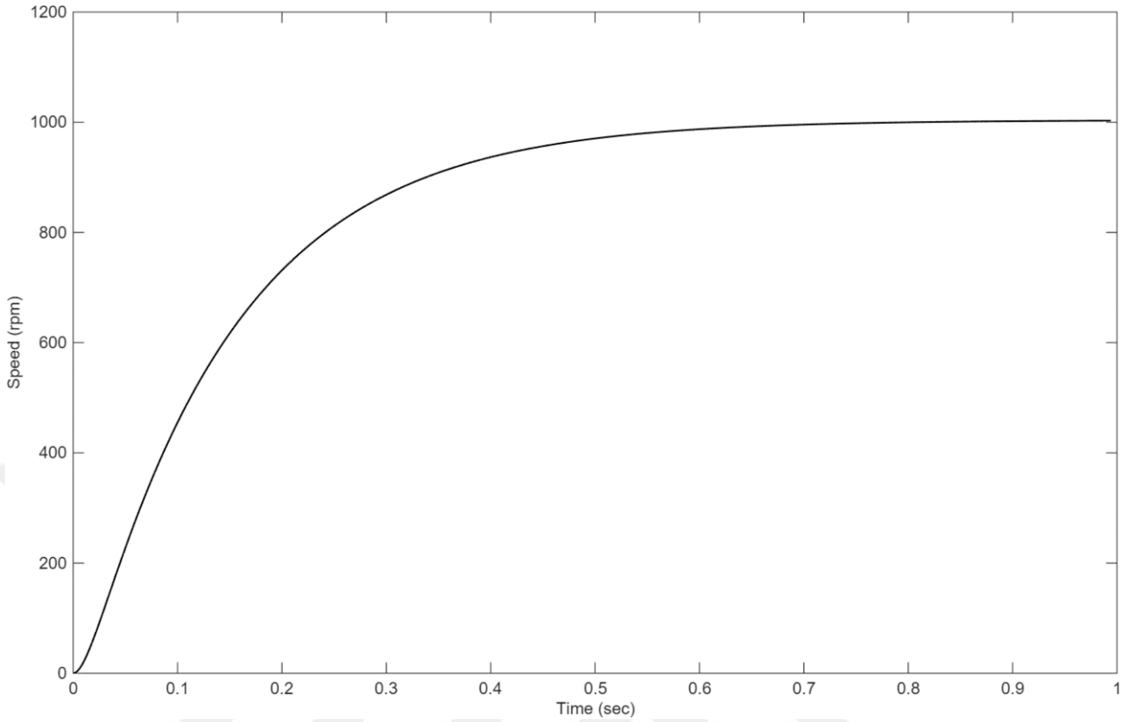

Figure 3.7. MATLAB/Simulink speed model (rpm)

3.2.3. Comparison of Experimental and Simulation Data

The superimposed comparison of the measured and simulated current (Figure 3.8) and measured and simulated motor speed (rpm) (Figure 3.9) is presented.

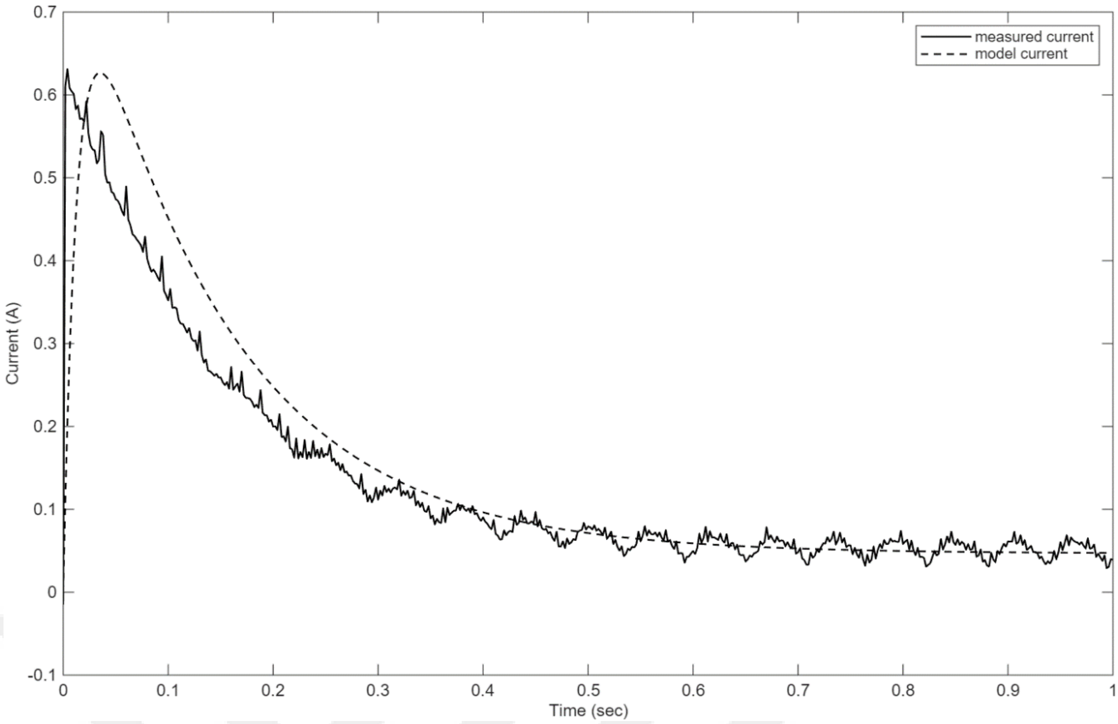

Figure 3.8. Model and measured currents

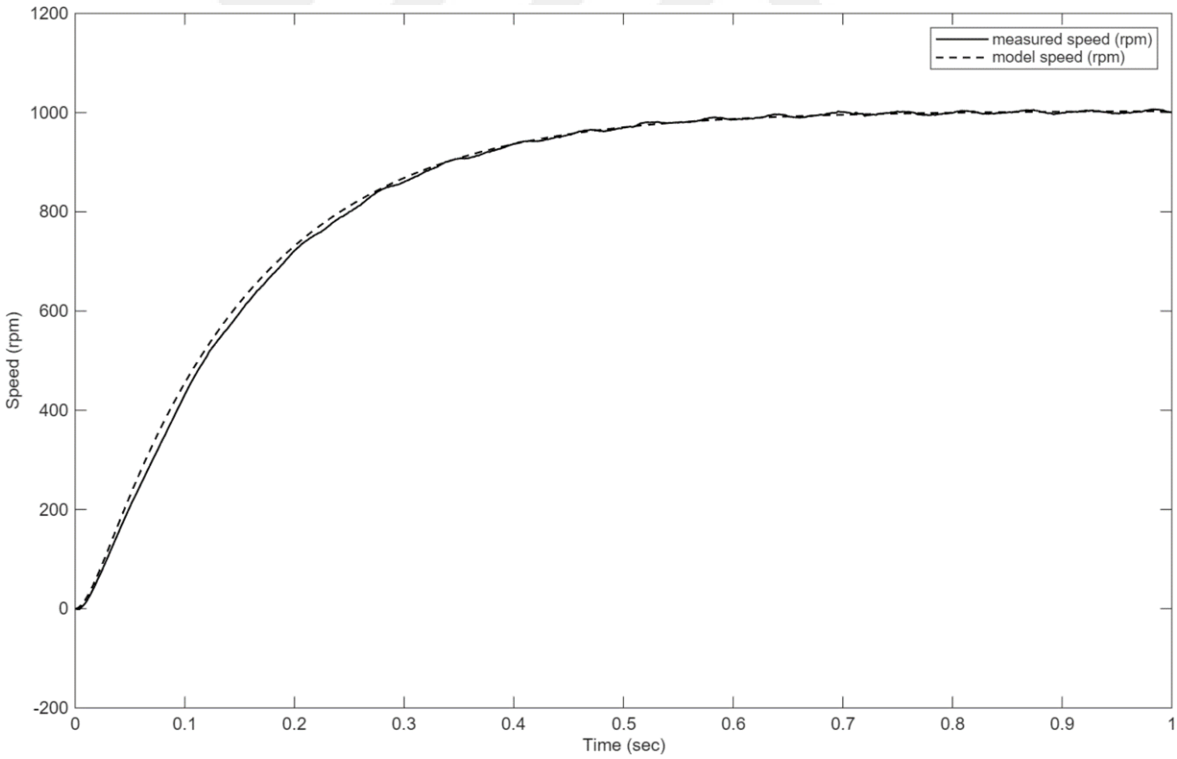

Figure 3.9. Model and measured speeds (rpm)

3.2.4. Error Analysis

Figure 3.10 illustrates the error between the measured current and the model current, showing an approximate deviation of 5%.

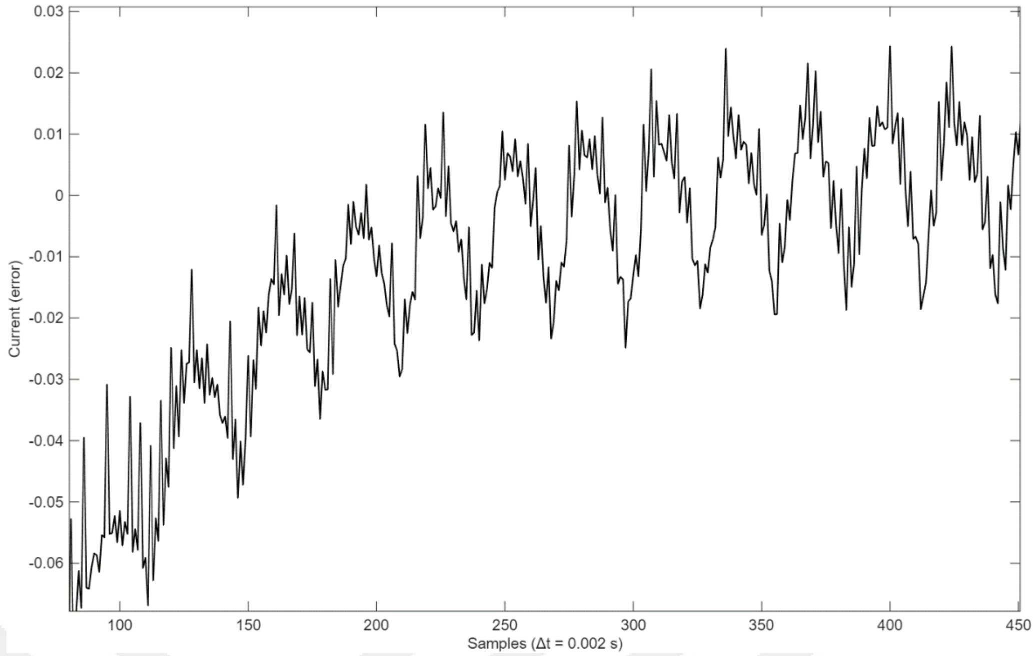

Figure 3.10. Model and measured error

Figure 3.11 illustrates the error between the measured speed and the model speed, showing an approximate deviation of 5%.

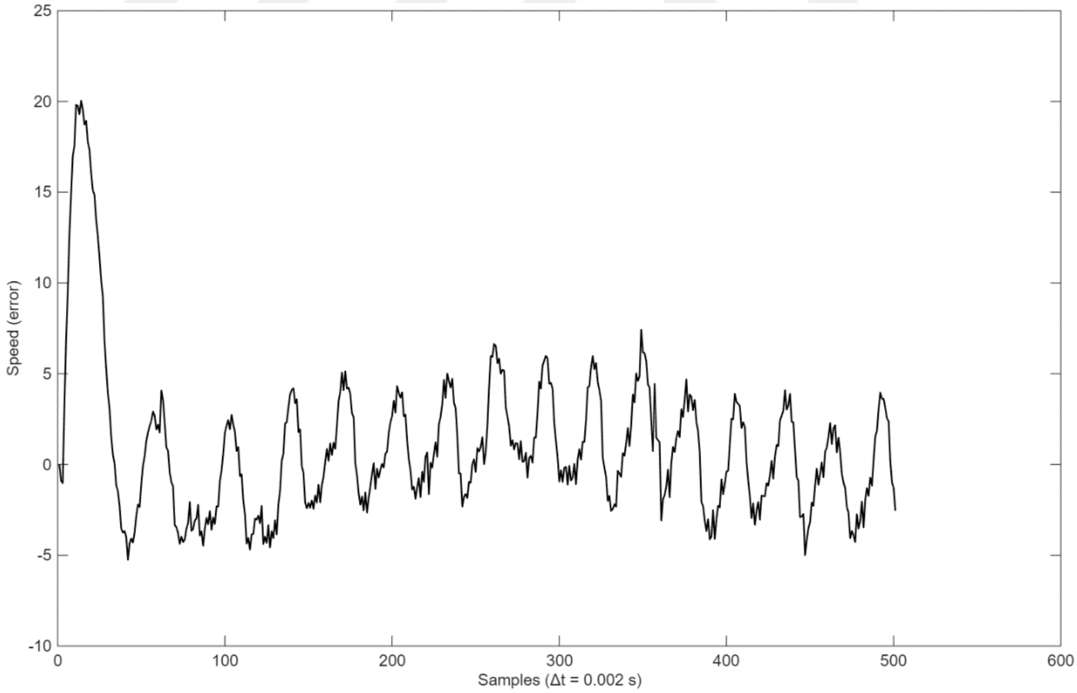

Figure 3.11. Model and measured speed error

3.3. Ziegler Nichols (Z-N) Process Reaction Curve PID Method

This method is based on the step response of a system. The system's response to a unit step input is analyzed and the process model is approximated as a first-order system with dead time, as expressed in Equation (3.26) some parameters obtained from this response are used to calculate the PID controller parameters K_p (proportional gain), T_i (integral time) and T_D (derivative time).

Steps of the Method:

- Obtain the Unit Step Response of the System:

A unit step input is applied to the system.
The system's output (process reaction curve) is recorded.

- Determine Parameters from the Response Curve:

K : System gain (steady-state output change / input change).

T_D : Dead time, i.e., the time delay before the system starts responding after the input is applied.

T : Time constant, i.e., the time at which the system output reaches 63.2% of its final value.

PID parameters are calculated using the Ziegler-Nichols method (Luyben, 1973):

- P (Proportional) Controller:

$$K_p = \frac{T}{Kt_d} \tag{3.28}$$

- PI (Proportional-Integral) Controller:

$$K_P = \frac{0.9T}{Kt_d}, T_i = 3.33t_d \tag{3.29}$$

- PID (Proportional-Integral-Derivative) Controller:

$$K_p = \frac{1.2T}{Kt_d}, T_i = 2t_d, T_D = 0.5t_d \tag{3.30}$$

Advantages of the method:

- Quick implementation: PID parameters can be quickly tuned based on experimental model data.

- Wide applicability: Commonly used in industrial processes and control systems.

Disadvantages of the method:

- Aggressive response**:** Especially for PID controllers, it can cause overshoot and oscillations.
- Limited accuracy: May not perform well if the system dynamics are complex.
- Requires experimental data: The system's step response must be obtained.

Applications:

- Industrial automation: control of temperature, pressure, flow, etc.
- Motor control: speed and position control.
- Chemical industry: reactor temperature and pressure control.

$$G(s) = \frac{0.85e^{-0.013s}}{0.143s+1} \cong \frac{0.85}{(0.143s+1)(0.013s+1)}$$
$$K = 0.85,\ t_d = 0.0133,\ T = 0.143$$
(3.31)

P controller;

$$K_p = \frac{T}{Kt_d} = \frac{0.143}{0.85 \times 0.013} = 12.941 \tag{3.32}$$

PI controller:

$$K_p = \frac{0.9T}{Kt_d} = \frac{0.9 \times 0.143}{0.85 \times 0.013} = 11.647,\ T_i = 3.33t_d = 3.33 \times 0.013 = 0.04329 \tag{3.33}$$

PID controller:

$$\begin{pmatrix} K_p = \dfrac{1.2T}{Kt_d} = \dfrac{1.2 \times 0.143}{0.85 \times 0.013} = 15.529 \\ T_i = 2t_d = 2 \times 0.013 = 0.026 \\ T_D = 0.5t_d = 0.5 \times 0.013 = 0.006 \end{pmatrix} \tag{3.34}$$

The controller calculated parameters are summarized in Table 3.1.

Table 3.1. Ziegler-Nichols paramaters

Controllers	K	T_i	T_D
P Controller	12.941	-	-
PI Controller	11.647	0.043	-
PID Controller	15.529	0.026	0.0065

Controller parameters calculated using the open-loop Ziegler–Nichols method (Haugen, 2010). A saturation block (0–10 V) is applied since, during the experimental test, the data acquisition card operated within a 0–10 V input–output range. All controller parameters calculated using the Ziegler-Nichols method are presented in Table 3.3. Utilizing these parameters, the output speed responses of the P, PI and PID controllers are plotted on a single graph (Figure 3.12). Similarly, the control input signals of these controllers are illustrated in Figure 3.13, while the error signals are comparatively presented on a single graph in Figure 3.14.

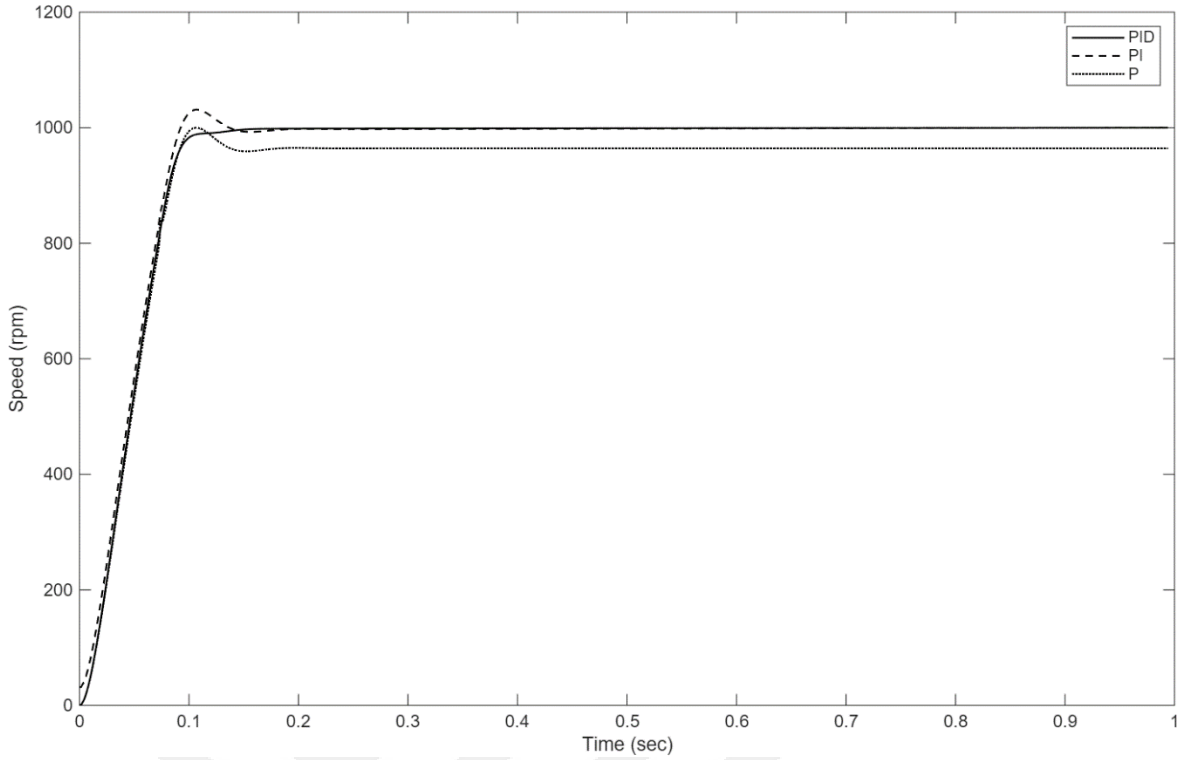

Figure 3.12. Output speed (rpm) (P, PI, and PID)

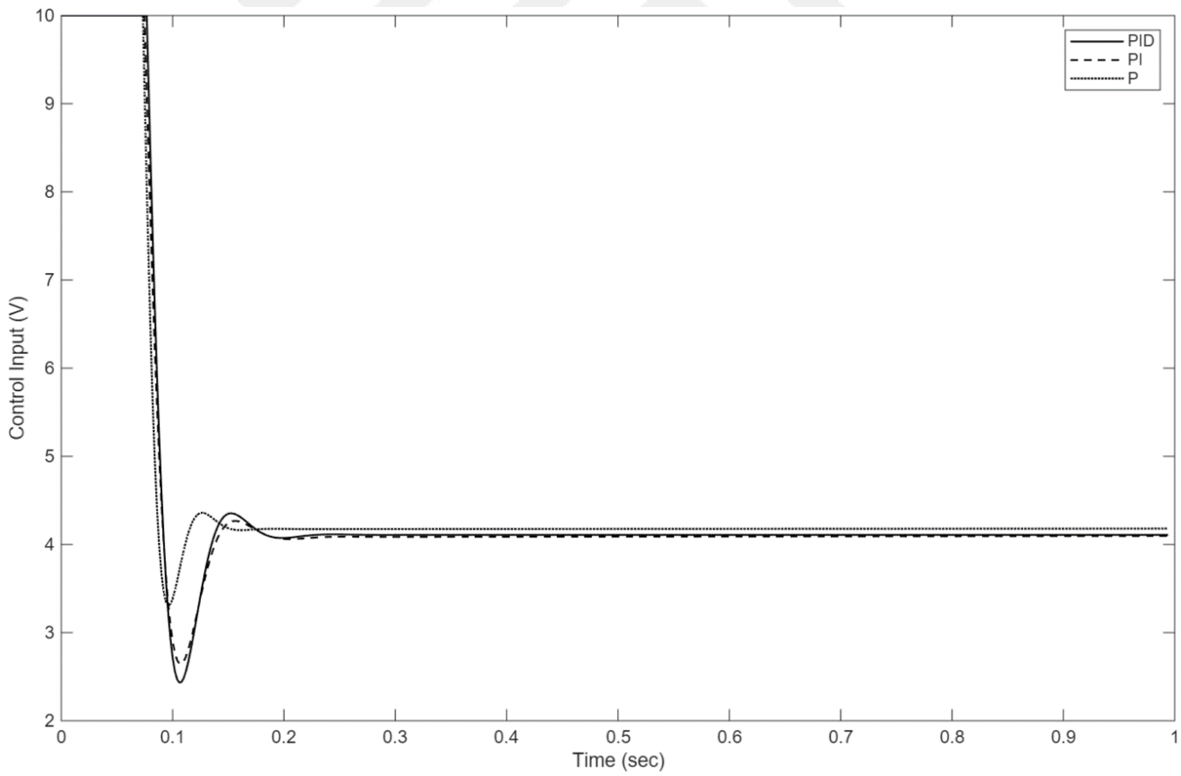

Figure 3.13. Control input voltage, $u(t)$ (P, PI, and PID)

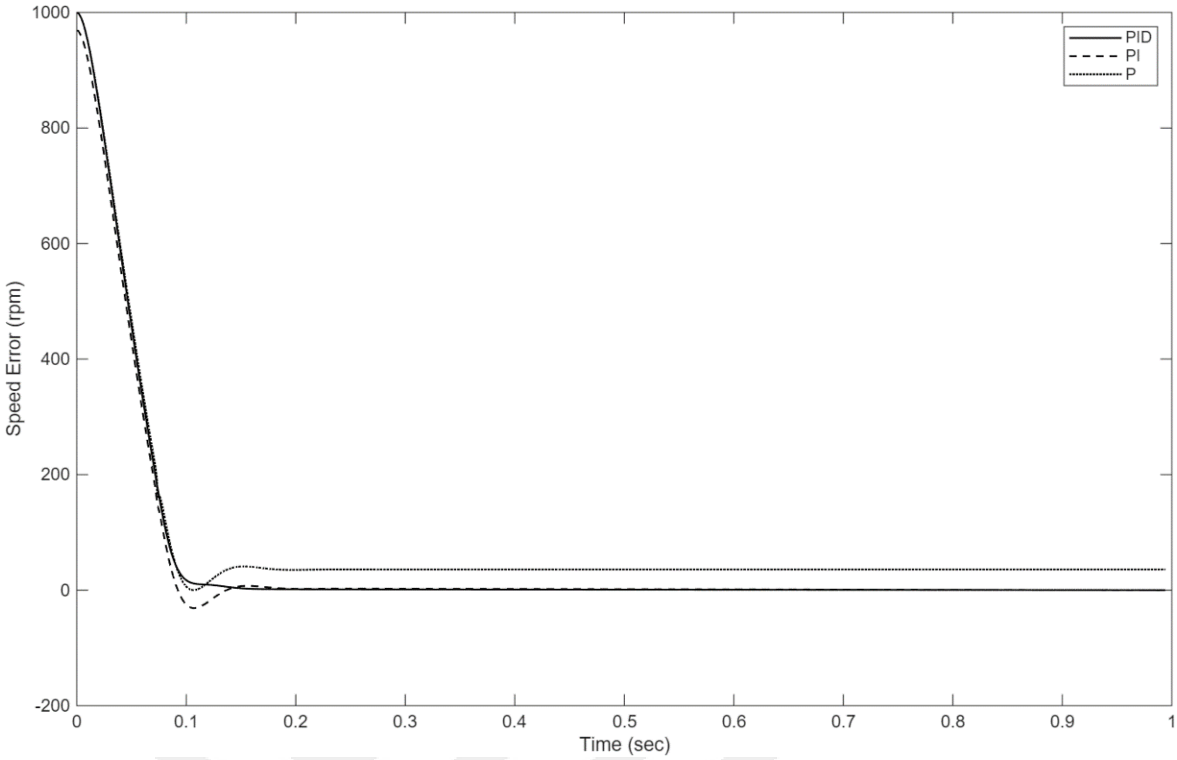

Figure 3.14. Speed error (rpm) (P, PI, and PID)

The performance of the evaluated controllers can also be measured using indices based on output parameters. Typically, the tracking error over the evaluation period is used. Some commonly used error-based performance indices are formulated as follows (Eker, 2006):

ISCI (Integral Squared Control Input) = $\int_0^t |u(t)|^2 dt$ (3.35)

IAE (Integral Absolute Error) = $\int_0^t |e(t)| dt$ (3.36)

ITAE (Integral Time Absolute Error) = $\int_0^t t\,|e(t)| dt$ (3.37)

ISE (Integral Squared Error) = $\int_0^t e^2(t) dt$ (3.38)

ITSE (Integral Time Squared Error) = $\int_0^t te^2(t) dt$ (3.39)

ISTE (Integral Squared Time Error) = $\int_0^t t^2 e(t) dt$ (3.40)

As demonstrated in Table 3.2, the PID-Ziegler Nichols controller attains a settling time of 0.0982 s, which is more rapid than both the P controller (0.122 s) and the PI controller (0.1205 s). Furthermore, the PID controller provides 0% overshoot, whereas the P and PI controllers yield overshoots of 3.70% and 3.21%, respectively. Despite the rise times being almost identical across all controllers (approximately 0.064–0.066 s), the PID controller exhibits a more balanced transient behaviour by attenuating oscillatory tendencies. As illustrated in Table 3.3, the PID controller demonstrates superiority over competing controllers in terms of error-based performance indices, exhibiting minimal values for ITAE (0.1338), IAE (0.430) and ITSE (0.0456). While the PI controller demonstrates marginal enhancements in comparison to the P controller, particularly with ISCI (23.12) the PID controller attains the optimal ISTE value (0.0850). The PID design is the most effective approach in this regard, as it simultaneously minimises error indices and enhances transient response performance.

Table 3.2. Time domain results (P, PI and PID–Z-N)

Controller	Rise Time (s)	Settling time (s)	Overshoot (%)	Delay time (s)
P-Ziegler Nichols	0.0646	0.122	3.7087	0.016
PI-Ziegler Nichols	0.0644	0.1205	3.2086	0.016
PID-Ziegler Nichols	0.0665	0.0982	0	0.016

Table 3.3. Performance indices (P, PI and PID–Z-N)

Controller	ITAE	ISE	IAE	ITSE	ISCI	ISTE
P-Ziegler Nichols	0.1613	0.606	0.476	0.0615	23.37	0.1041
PI-Ziegler Nichols	0.1697	0.617	0.493	0.0670	23.12	0.1094
PID-Ziegler Nichols	0.1338	0.580	0.430	0.0456	23.72	0.0850

3.4. Single-Loop P, PI and PID Controllers Design

This section presents the design and analysis of single-loop P, PI and PID controllers for the system under consideration. Conventional PID controller parameters are determined using the Ziegler-Nichols sustained oscillation method. For each controller type, a MATLAB/Simulink model was designed and its dynamic response characteristics were investigated. The resulting system output, control, current and error signals were analysed to evaluate the transient and steady-state performance of each controller. The utilisation of comparative assessments, founded upon these signals, engenders a comprehensive understanding of the relative merits and constraints inherent to the P, PI and PID control approaches. In addition, the domain performance specifications metrics and output performance indices obtained from these controllers are presented in and provide quantitative evidence for the performance evaluation.

3.4.1. Single-Loop P controller

Figure 3.15 shows the single-loop Simulink model. Through this model, with $k_p = 150$, the dynamic characteristics of the system were analyzed, and various performance-related signals were obtained. The system output speed response is illustrated in Figure 3.16, while the corresponding control signal is depicted in Figure 3.17. The motor current signal, representing the electrical behaviour of the system, is presented in Figure 3.18. Additionally, the error signal, which indicates the deviation from the reference value, is shown in Figure 3.19. Furthermore, Figure 3.20 provides a comparative representation of the error signal and its derivative, offering insight into the transient response and error variation behaviour of the P controller.

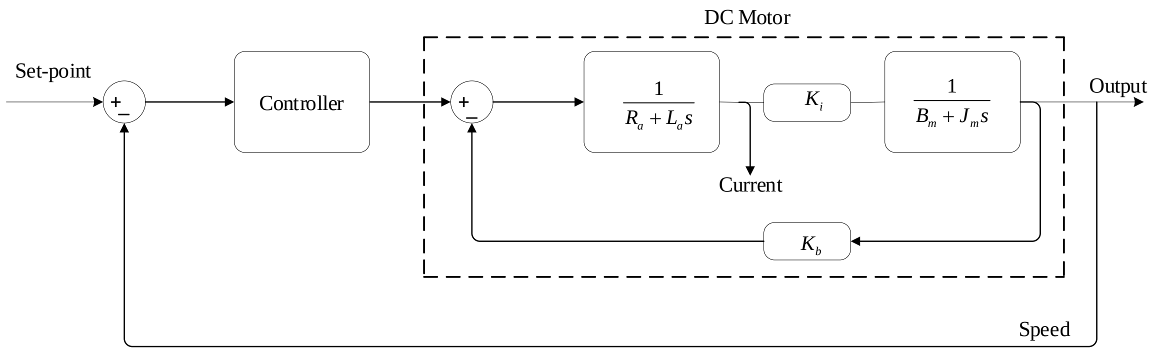

Figure 3.15. Single-loop Simulink model

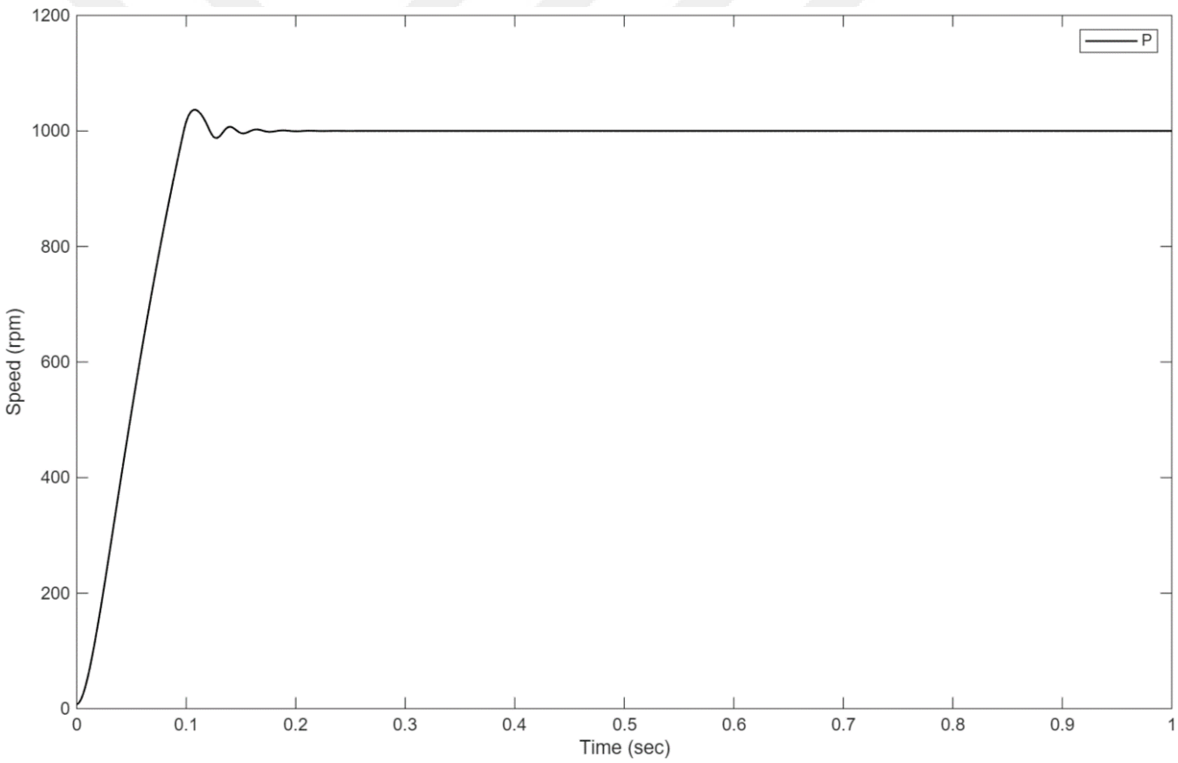

Figure 3.16. Output speed signal (rpm) (P)

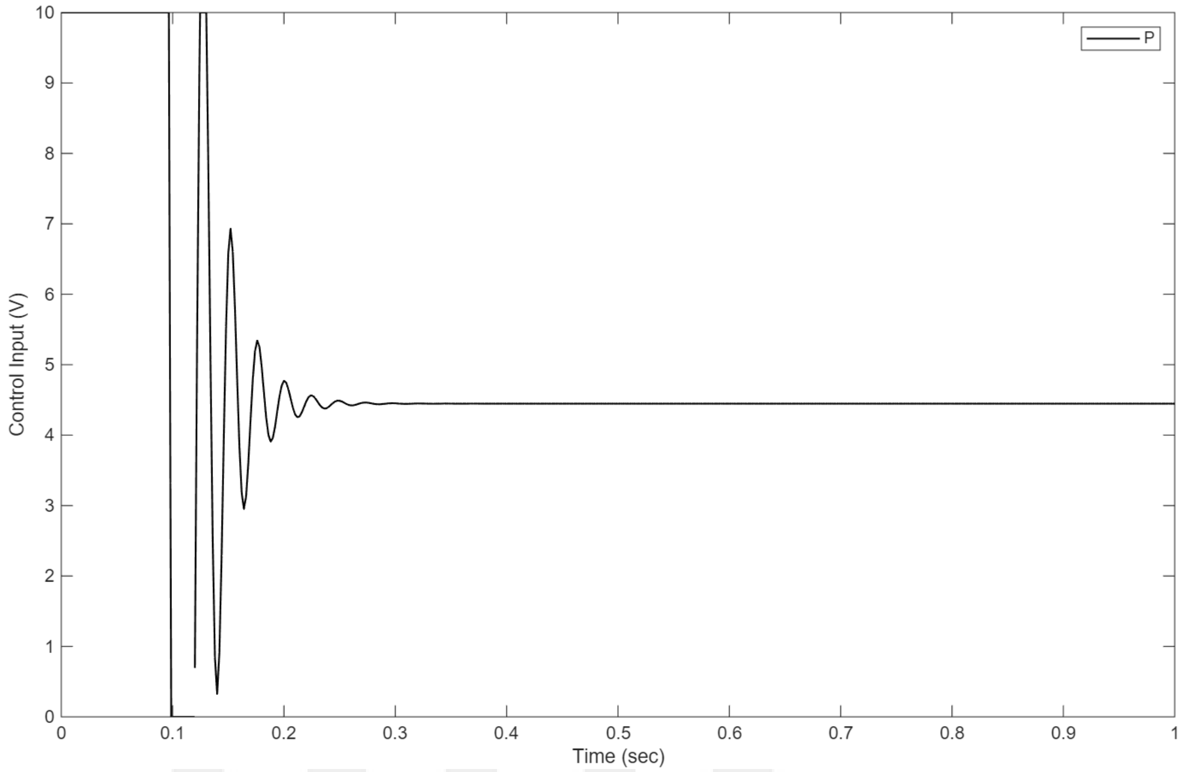

Figure 3.17. Control input voltage signal, $u(t)$ (P)

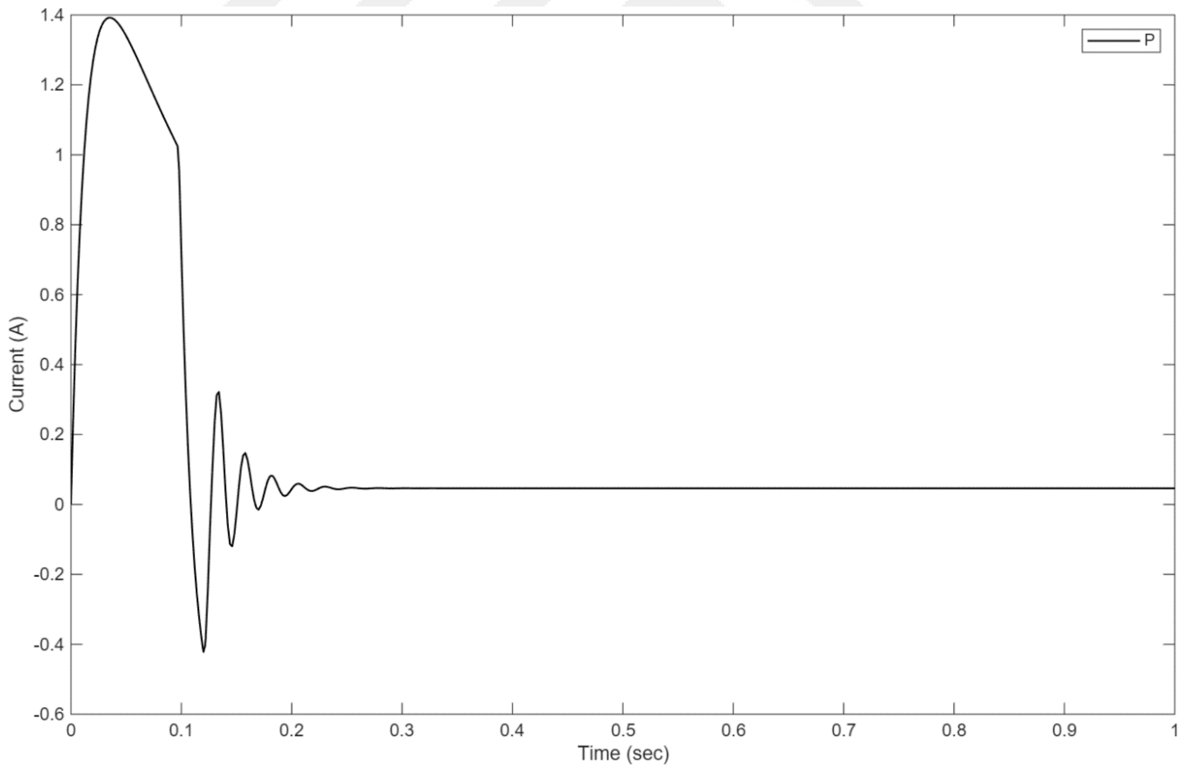

Figure 3.18. Armature current signal, $i_a(t)$ (P)

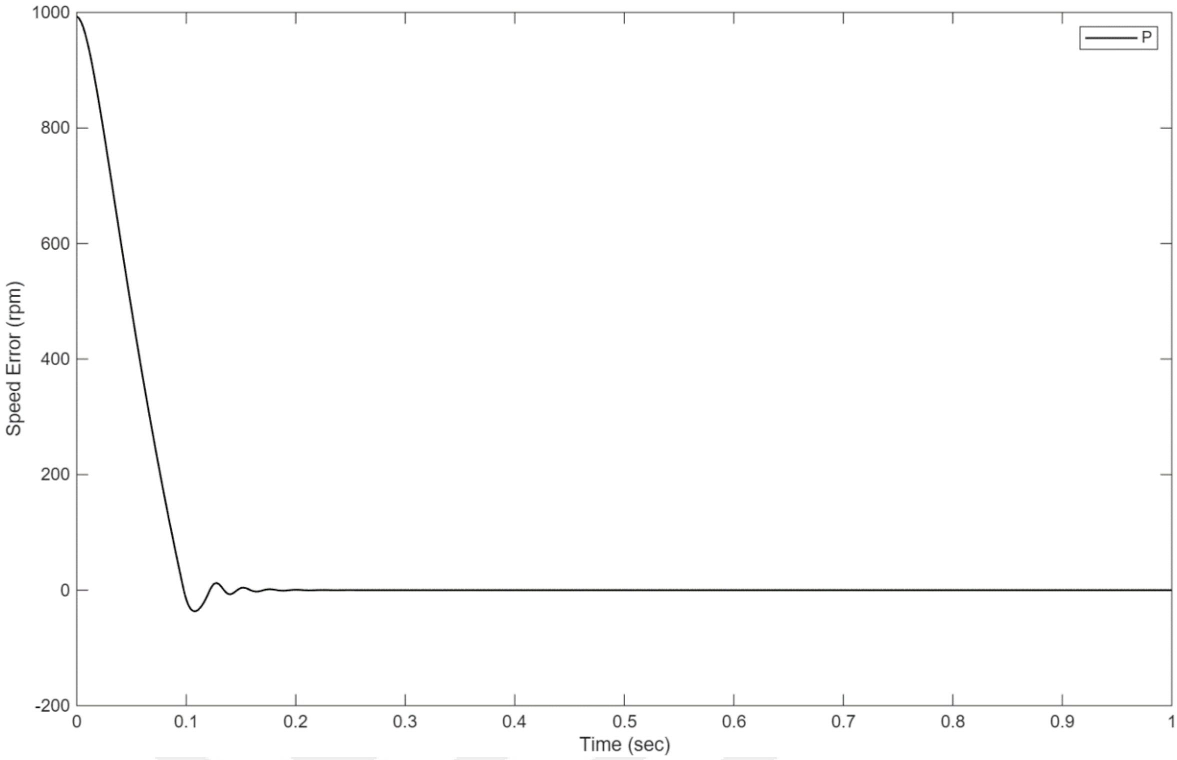

Figure 3.19. Speed error signal (rpm) (P)

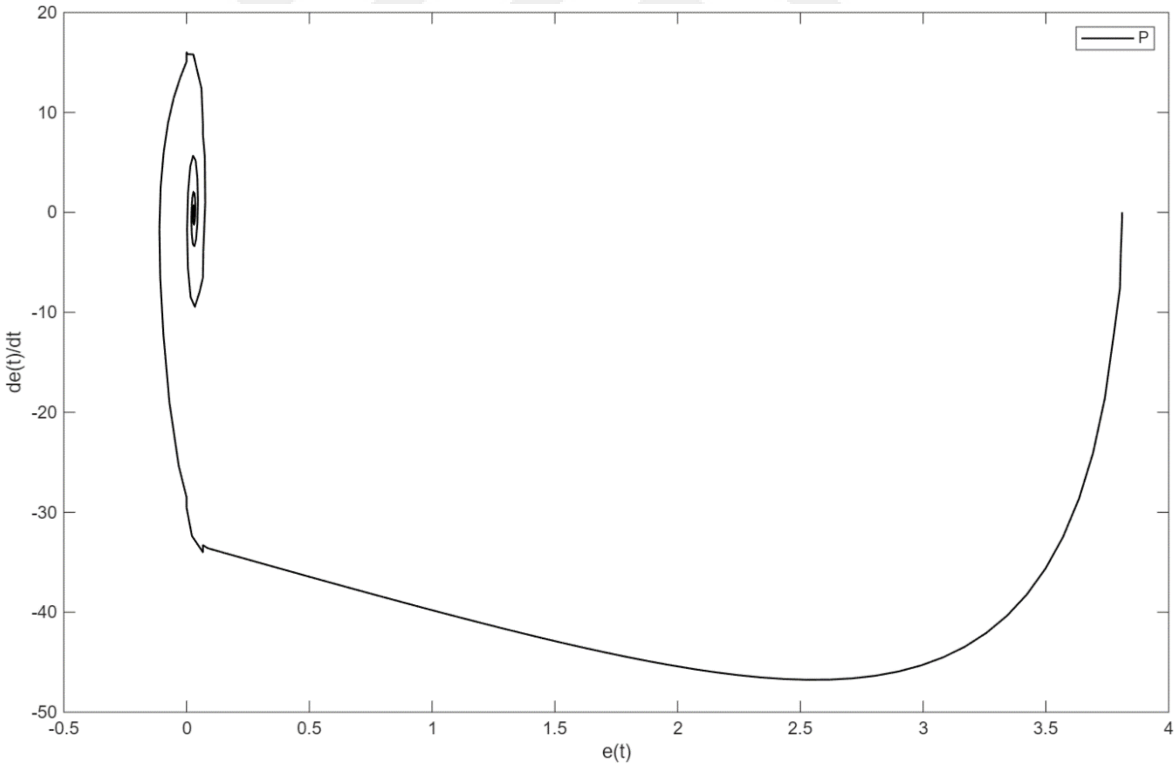

Figure 3.20. Phase plane of $e(t)$ and $de(t)/dt$ signal (P)

As demonstrated in Table 3.4, the time domain results of the single-loop P controller demonstrates a rise time of 0.071 s and a settling time of 0.1165 s. The 3.71% overshoot indicates that the controller rapidly reaches the setpoint without generating excessive response. The system delay of 0.05 s demonstrates that the system responds promptly to the control input. As demonstrated in Table 3.5, the performance indices ITAE = 0.0209, ISE = 0.5174 and IAE = 0.2205 indicate that both the magnitude of the error and its time-weighted effect are constrained. The ITSE value of 0.0127 indicates low squared error energy, thus confirming efficient utilisation of control effort. The control signal indicator, ISCI = 27.83 confirm that the intensity and continuity of the control input remain within acceptable limits. In conclusion, the single-loop P controller provides a rapid transient response, low overshoot and balanced error performance, thus making it a reliable baseline control strategy under experimental conditions.

Table 3.4. Time domain results (P)

Controller	Rise Time (s)	Settling time (s)	Overshoot (%)	Delay time (s)
P	0.0710	0.1165	3.71	0.050

Table 3.5. Performance indices (P)

Controller	ITAE	ISE	IAE	ITSE	ISCI	ISTE
P	0.0209	0.5174	0.2205	0.0127	27.83	0.0101

3.4.2. Single-Loop PI Controller:

Based on this model, with the controller parameters PI = $40\left(1+\frac{1}{2.67s}\right)$, the dynamic behaviour of the system was analysed, and the corresponding signals were obtained. The system output speed response is illustrated in Figure 3.21, while the corresponding control input signal is depicted in Figure 3.22. The motor current signal is presented in Figure 3.23, and the system error response is shown in Figure 3.24. Furthermore, Figure 3.25 provides a comparative visualisation of the error signal and its derivative, thereby highlighting the transient performance and error variation characteristics of the designed controller.

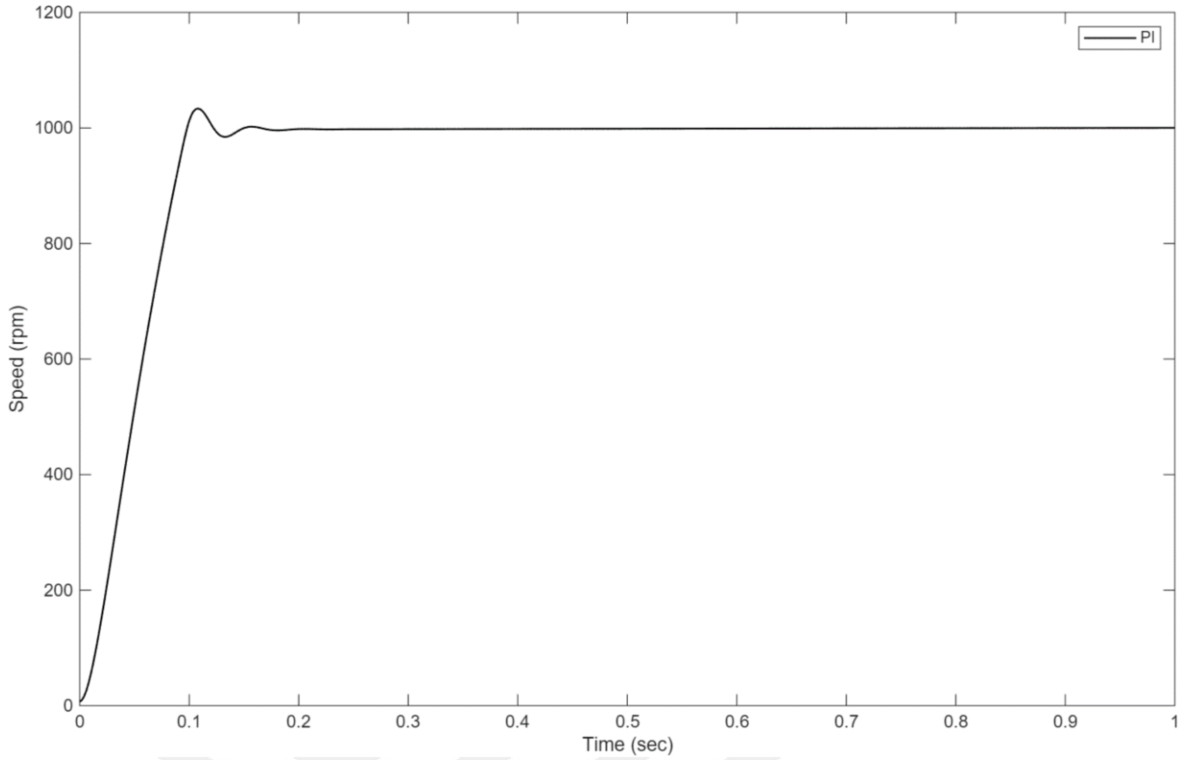

Figure 3.21. Output speed signal (rpm) (PI)

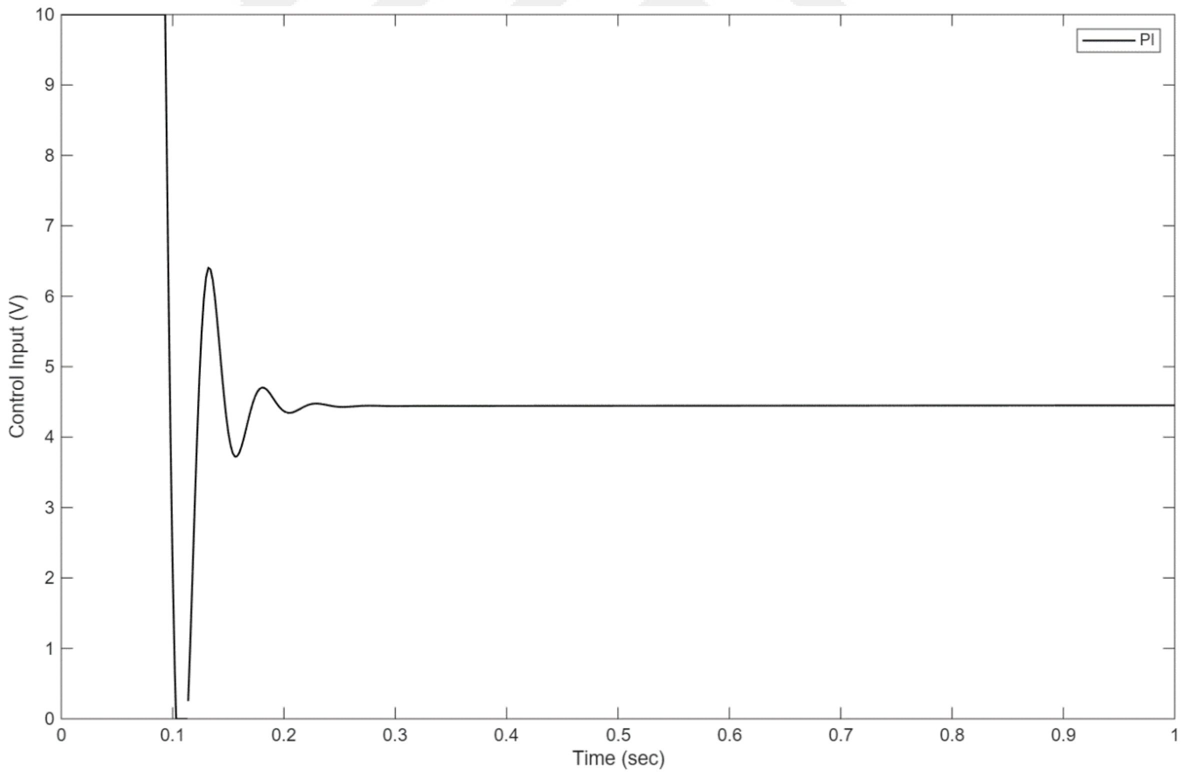

Figure 3.22. Control input voltage signal, $u(t)$ (PI)

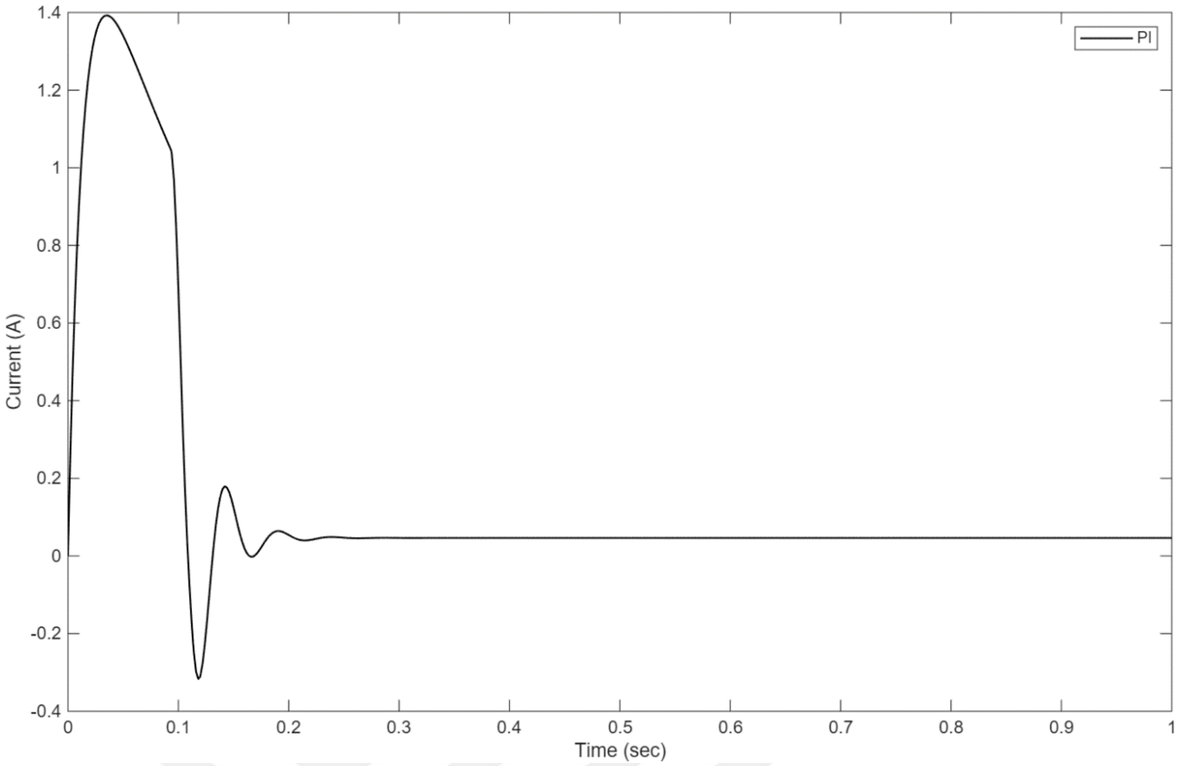

Figure 3.23. Armature current signal, $i_a(t)$ (PI)

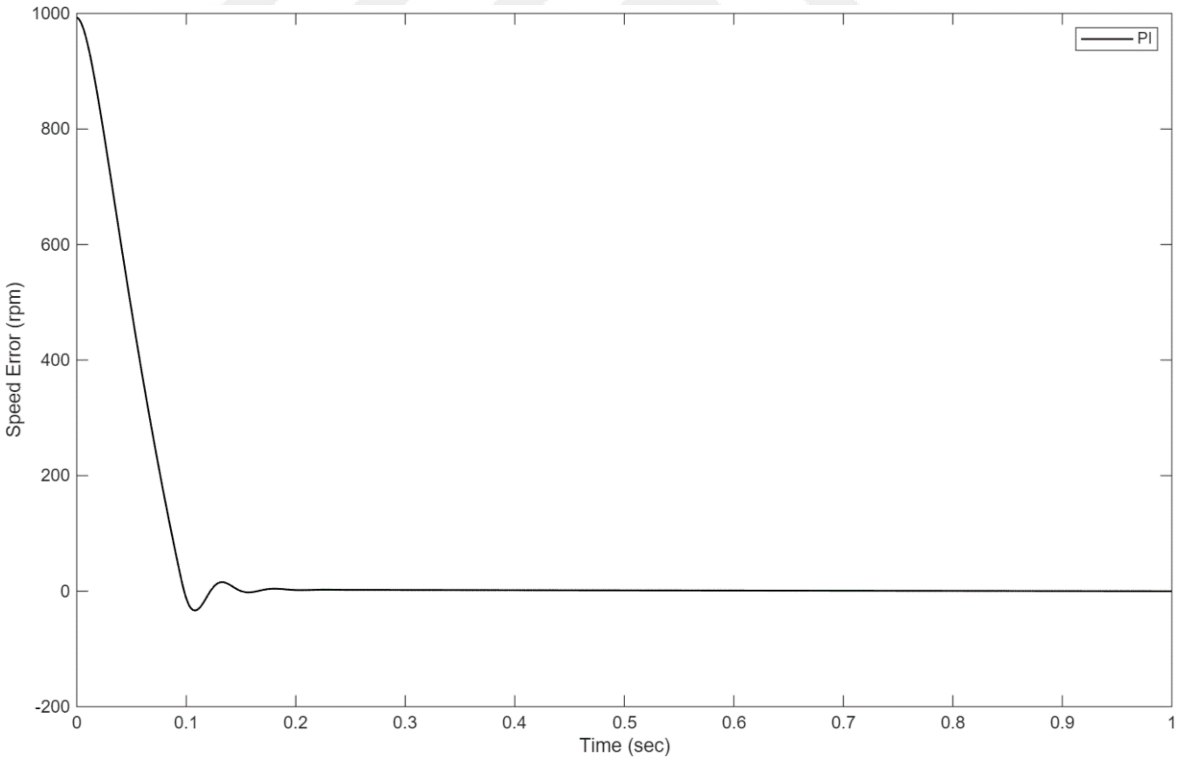

Figure 3.24. Speed error signal (rpm) (PI)

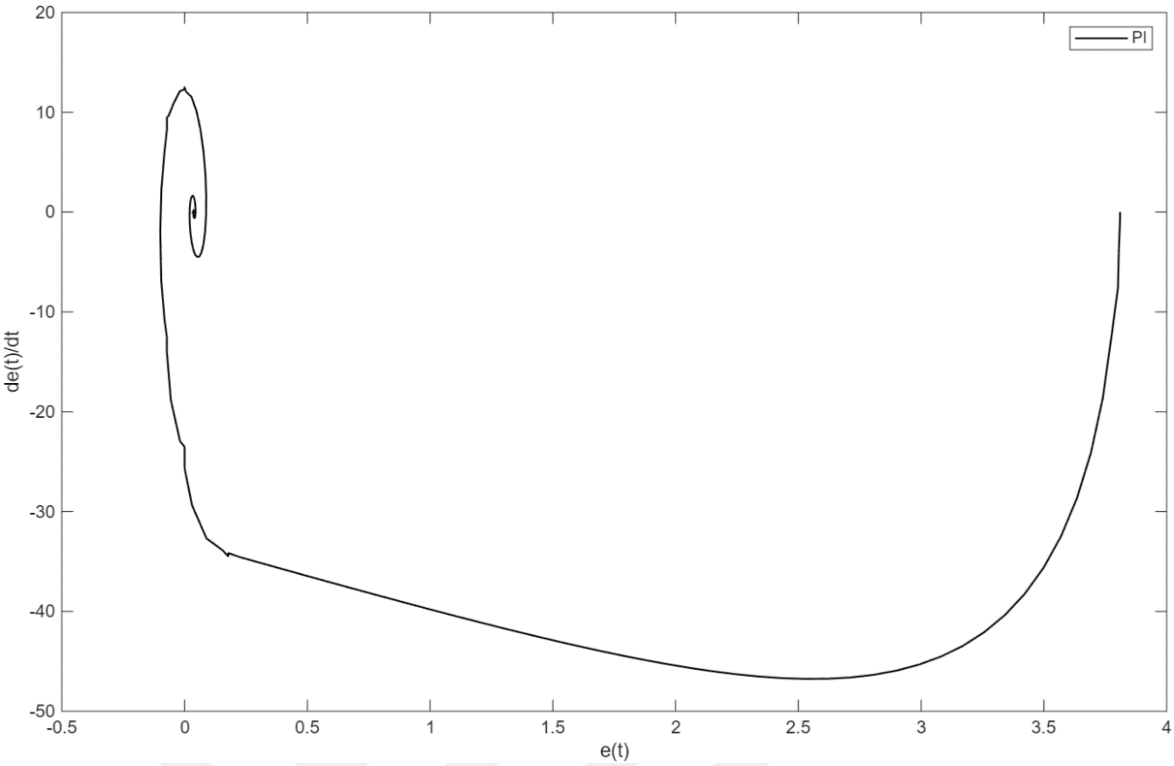

Figure 3.25. Phase plane of $e(t)$ and $de(t)/dt$ signal (PI)

As demonstrated in Table 3.6, the time domain results of the single-loop PI controller exhibits a rise time of 0.071 s and a settling time of 0.1157 s. The 3.37% overshoot indicates that the controller delivers a swift response while concurrently attenuating oscillations. The system delay of 0.05 s confirms a prompt and effective response to the control input. As demonstrated in Table 3.7, the performance indices ITAE = 0.0221, ISE = 0.5176 and IAE = 0.2238 indicate that the magnitude of error and its time-weighted effects are constrained. The ITSE value of 0.0128 confirms efficient operation in terms of squared error, while the control signal indicator ISCI = 27.23 indicate that the control efforts are balanced and sustainable. In conclusion, the single-loop PI controller has been demonstrated to provide a rapid and balanced response, minimal overshoot, and consistent error performance. These properties combine to establish the controller as a reliable control strategy in experimental settings.

Table 3.6. Time domain results (PI)

Controller	Rise Time (s)	Settling time (s)	Overshoot (%)	Delay time (s)
PI	0.0710	0.1157	3.37	0.050

Table 3.7. Performance indices (PI)

Controller	ITAE	ISE	IAE	ITSE	ISCI	ISTE
PI	0.0221	0.5176	0.2238	0.0128	27.23	0.0106

3.4.3. Single-Loop PID Controller:

With the PID = $30\left(1+\frac{1}{2.14s}+0.05s\right)$, the dynamic characteristics of the system were investigated, and various performance-related signals were obtained. The system output speed response is illustrated in Figure 3.26, while the corresponding control input signal is shown in Figure 3.27. The motor current signal, which reflects the electrical behaviour of the system, is presented in Figure 3.28, and the error signal, which indicates the deviation from the reference value, is given in Figure 3.29. Furthermore, Figure 3.30 provides a comparative representation of the error signal and its derivative, thereby offering insight into the transient response and error variation behaviour of the PID controller.

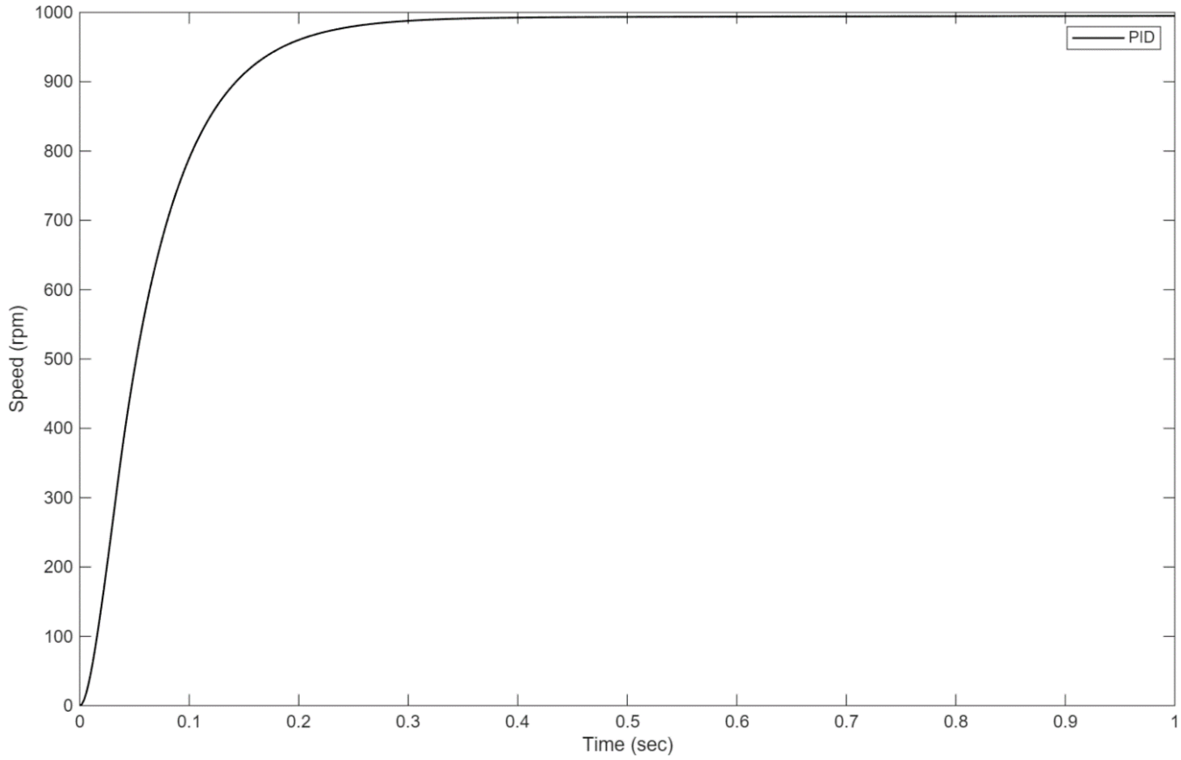

Figure 3.26. Output speed signal (rpm) (PID)

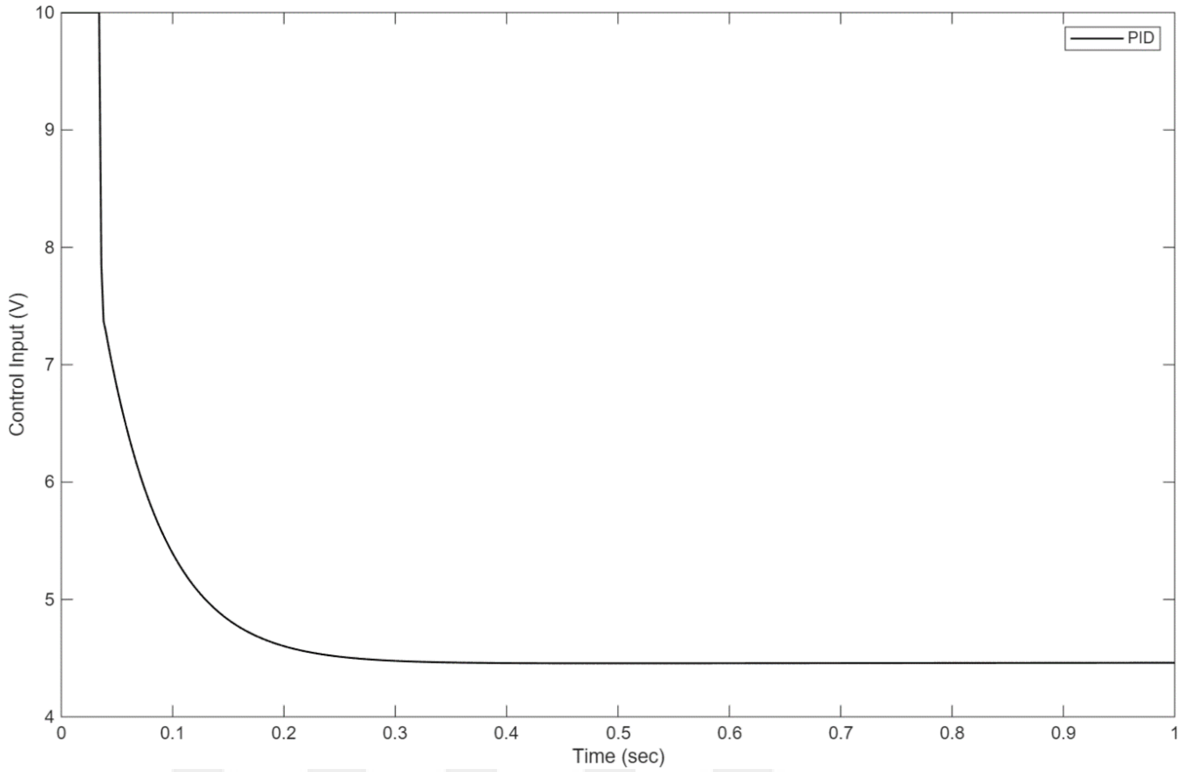

Figure 3.27. Control input voltage signal, $u(t)$ (PID)

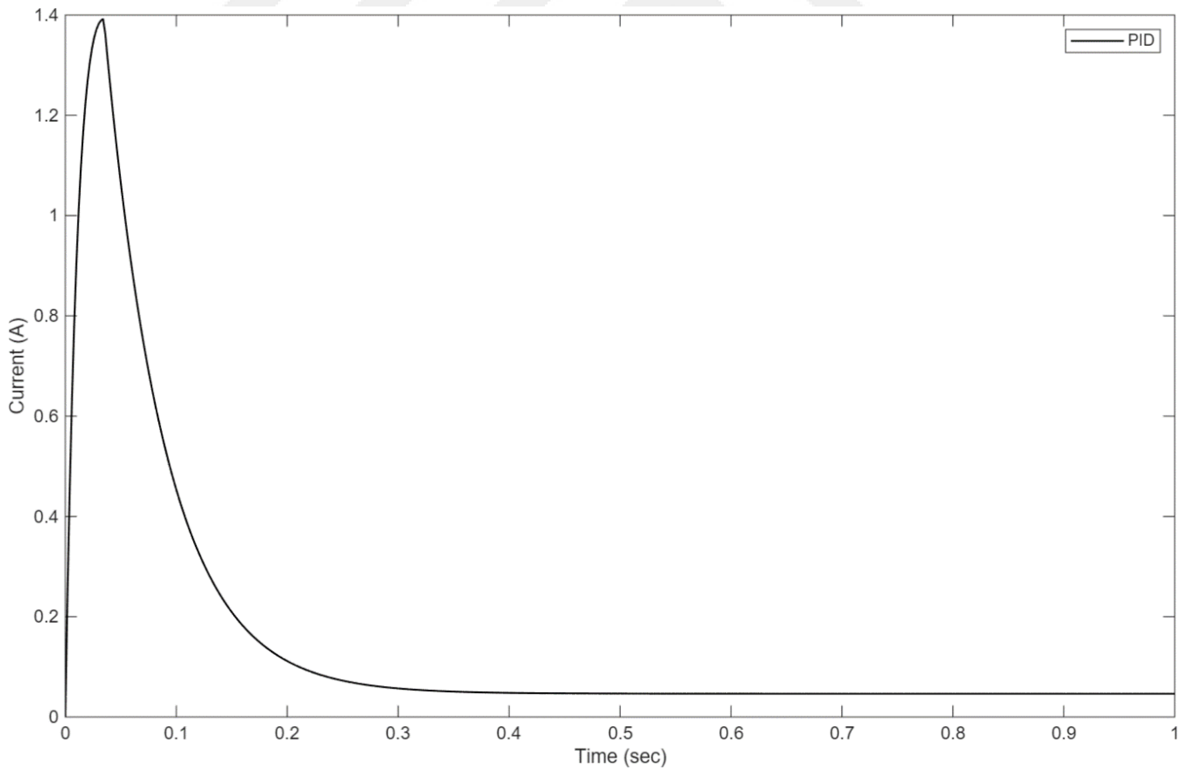

Figure 3.28. Armature current signal, $i_a(t)$ (PID)

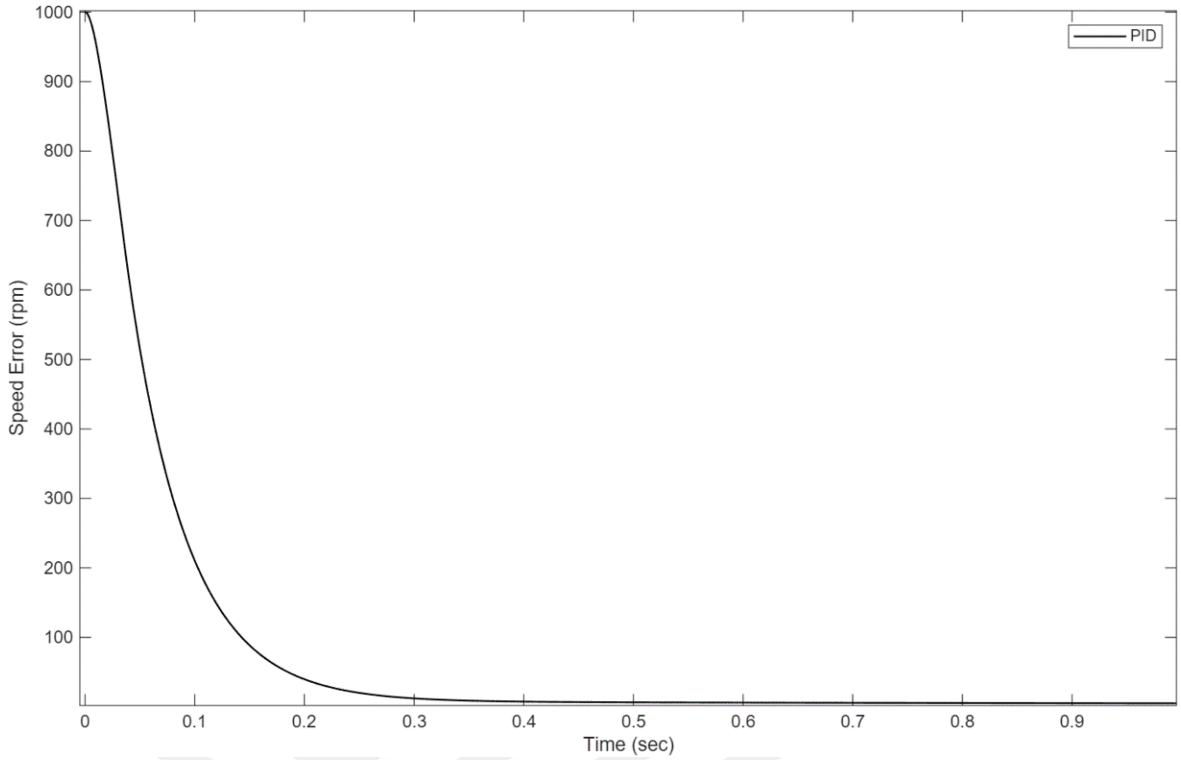

Figure 3.29. Speed error signal (rpm) (PID)

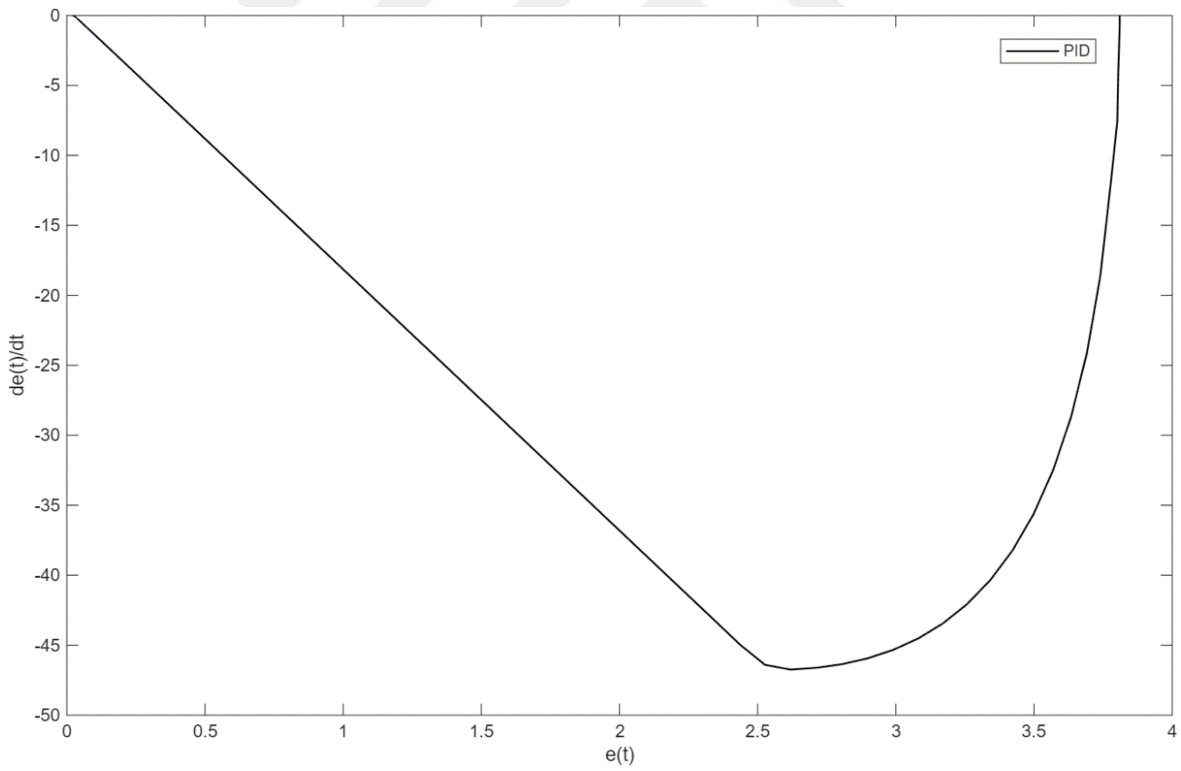

Figure 3.30. Phase plane of $e(t)$ and $de(t)/dt$ signal (PID)

As demonstrated in Table 3.8, the time domain results of the single-loop PID controller exhibits a rise time of 0.1244 s and a settling time of 0.2328 s. The absence of any overshoot, indicated by 0% overshoot, signifies that the controller delivers a highly stable response, attaining the setpoint without any overshoot. The system delay of 0.052 s confirms a prompt and effective response to the control input. As illustrated in Table 3.9, the performance indices demonstrate that the error magnitude and its time-weighted effects remain within limited levels, as indicated by the values ITAE = 0.0256, ISE = 0.5735 and IAE = 0.2780. The ITSE value of 0.0178 confirms efficient operation regarding squared error, while the control signal indicator ISCI = 24.80 confirm that the control input remains balanced and continuous. In conclusion, the single-loop PID controller provides stable performance, non-excessive response and reliable error management under experimental conditions.

Table 3.8. Time domain results (PID)

Controller	Rise Time (s)	Settling time (s)	Overshoot (%)	Delay time (s)
PID	0.1244	0.2328	0.00	0.0520

Table 3.9. Performance indices (PID)

Controller	ITAE	ISE	IAE	ITSE	ISCI	ISTE
PID	0.0256	0.5735	0.2780	0.0178	24.80	0.0088

3.5. Cascade Control

The present section is devoted to an examination of the design and analysis of cascade control structures, which have been demonstrated to offer enhanced dynamic performance in comparison with conventional single-loop controllers. In the context of this study, three cascade configurations were examined: The following designs are to be considered: outer-loop PID/inner-loop PI (PID/PI), outer-loop PI/inner-loop PI (PI/PI), and outer-loop PI/inner-loop PI (PI/P). The inner and outer control loops for each configuration were designed using appropriate tuning methods, and their dynamic characteristics were evaluated through MATLAB/Simulink models. The resulting output, control, current and error signals were analysed to assess transient and steady-state performance. A comparative analysis of the various cascade designs has been undertaken in order to provide insight into their relative advantages and limitations in terms of response speed, overshoot and steady-state error. Furthermore, the controller parameter combinations utilised for each cascade structure are outlined in Table 3.10, thereby providing a reference point for the applied tuning strategy.

Table 3.10. Comparison of cascaded controllers structures

Combination	Outer-Loop	Inner-Loop
PI/P	$k_p = 10, t_i = 200$	$k_p = 30$
PI/PI	$k_p = 5, t_i = 2.5$	$k_p = 20, t_i = 4$
PID/PI	$k_p = 60, t_i = 10, t_d = 0.067$	$k_p = 7, t_i = 3.5$

3.5.1. Cascade Controller: Outer-Loop PI/Inner-Loop P (PI/P)

Figure 3.31 shows the cascade-loop Simulink model. Within the scope of the cascade control design for the PI/P configuration, the outer-loop controller parameters were set as PI = $10\left(1+\frac{1}{200s}\right)$, while the inner loop employed a proportional controller with $k_p = 30$. Following the implementation of the aforementioned control scheme, an analysis of the system's behaviour was conducted. The dynamic responses obtained from this model include the output speed signal (Figure 3.32), current signal (Figure 3.33), control input signal (Figure 3.34), speed error signal (Figure 3.35), and the error signal alongside its derivative (Figure 3.36).

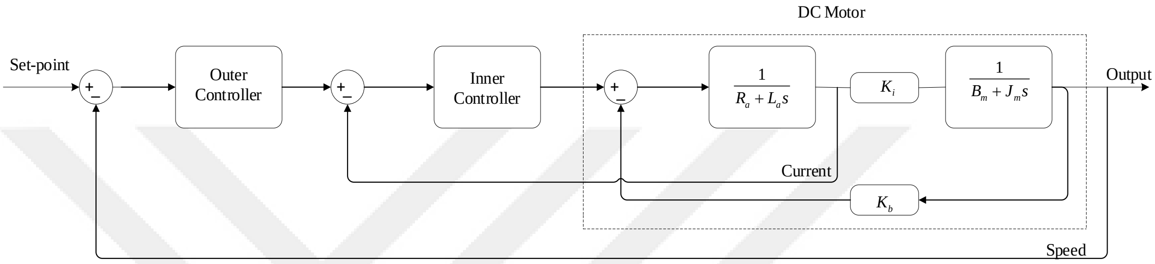

Figure 3.31. Cascade-loop Simulink model

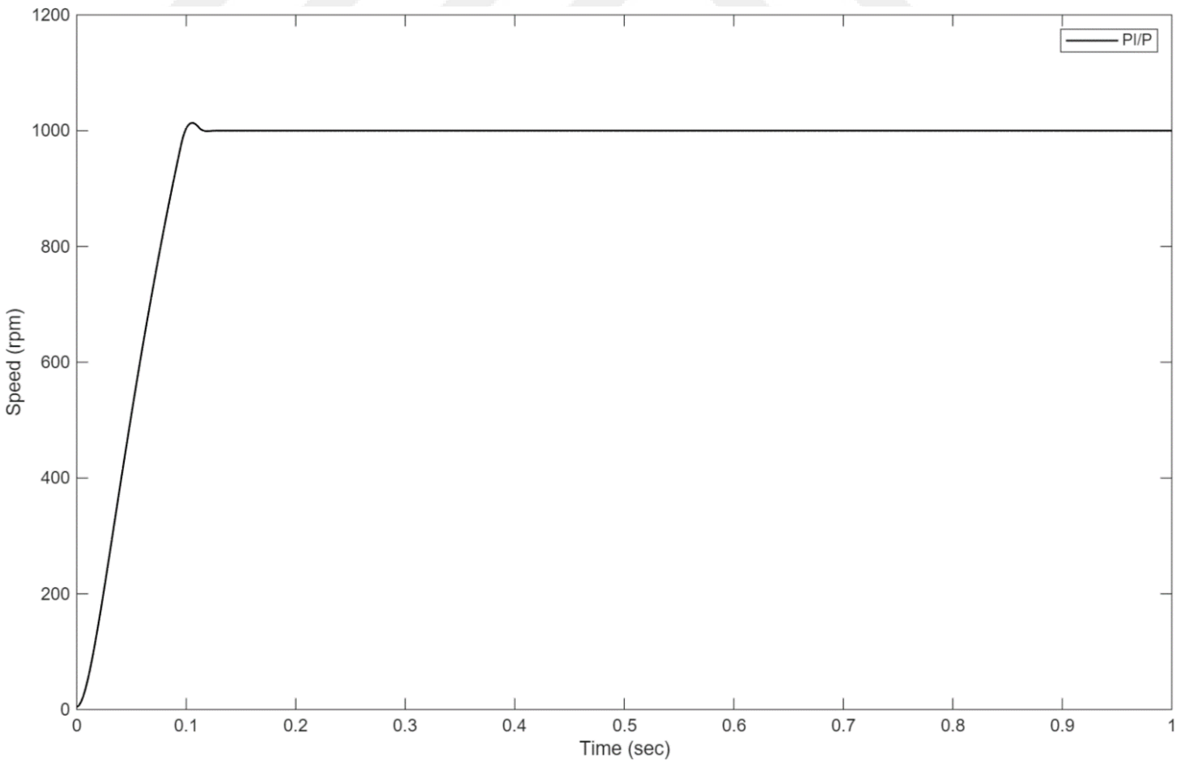

Figure 3.32. Output speed signal (rpm) (PI/P)

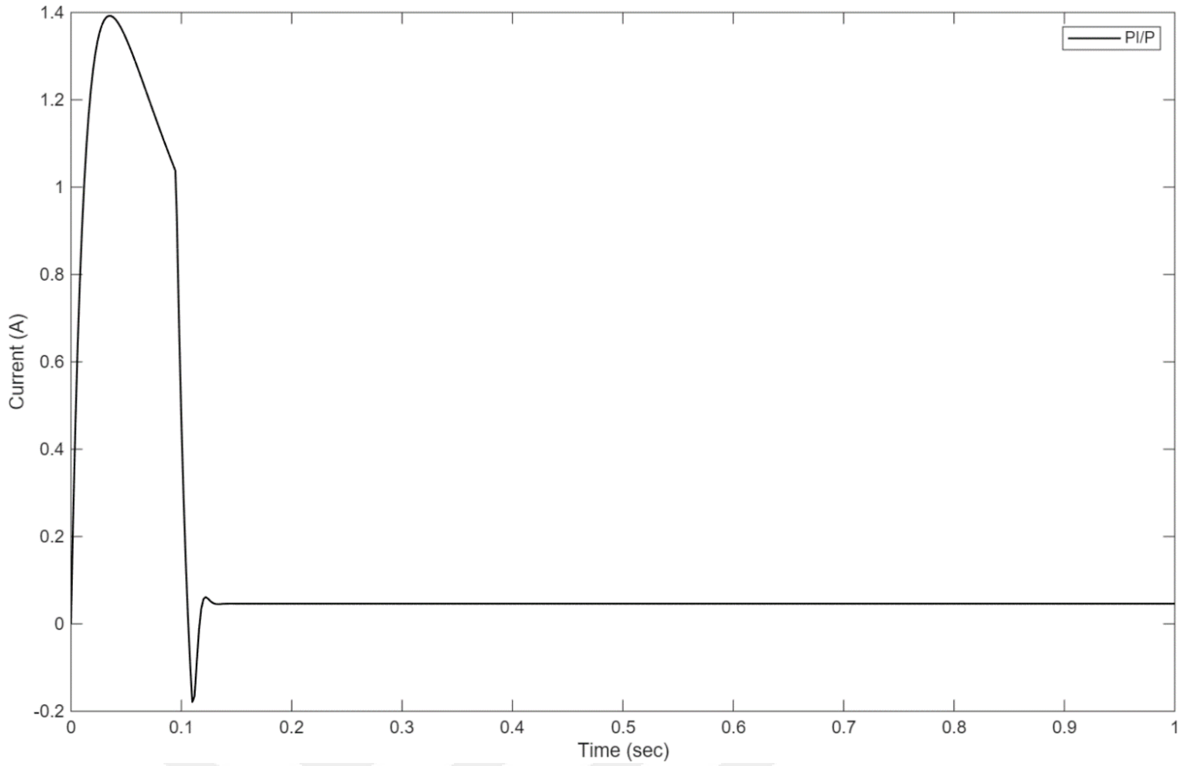

Figure 3.33. Armature current signal, $i_a(t)$ (PI/P)

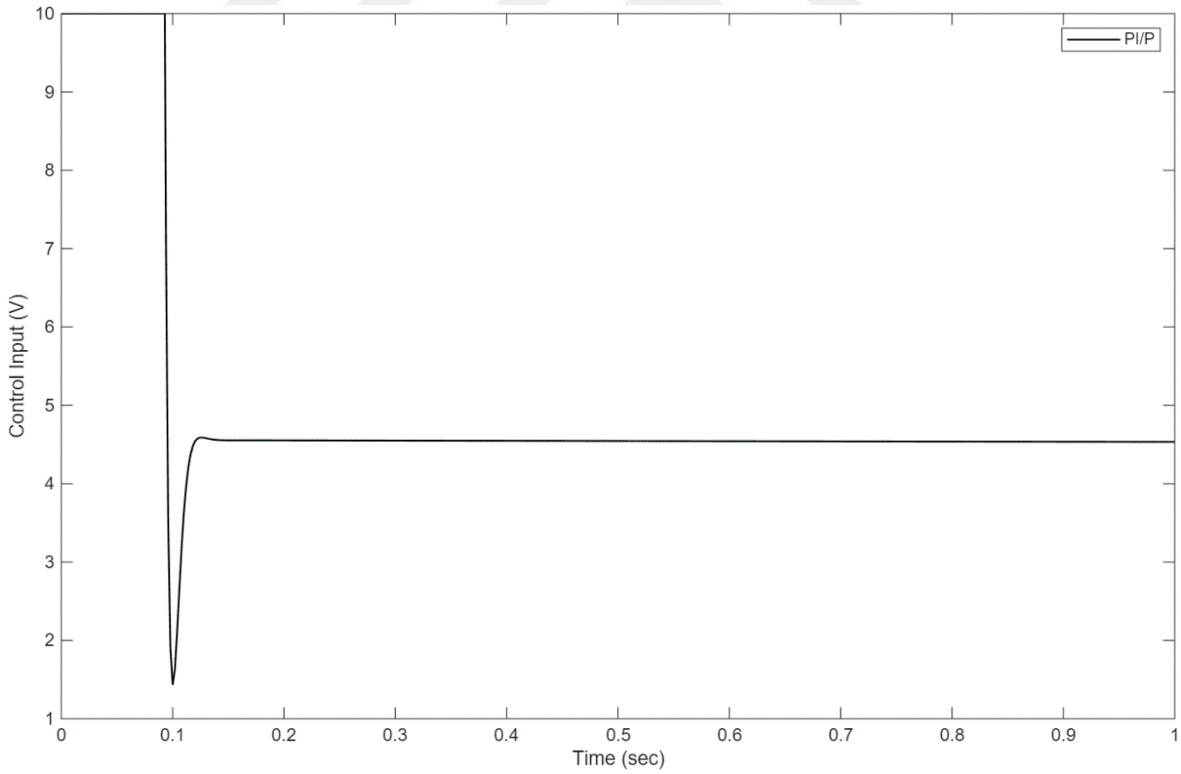

Figure 3.34. Control input voltage signal, $u(t)$ (PI/P)

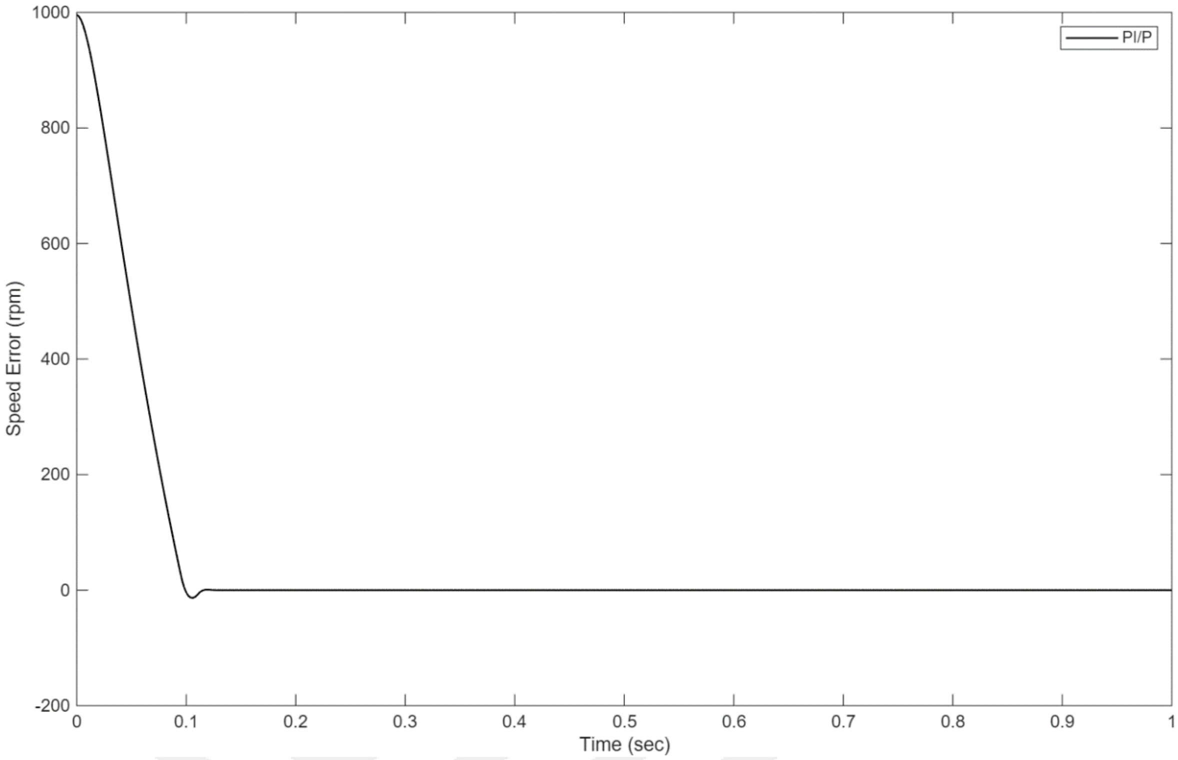

Figure 3.35. Speed error signal (rpm) (PI/P)

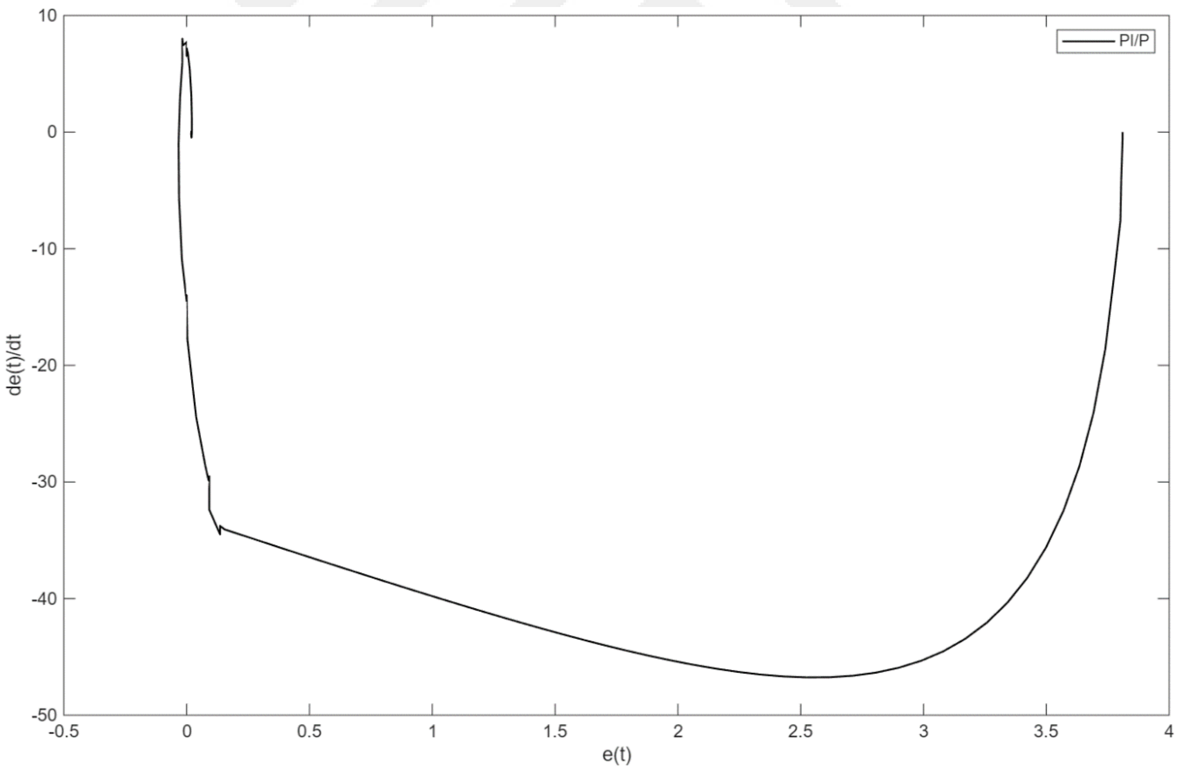

Figure 3.36. Phase plane of $e(t)$ and $de(t)/dt$ signal (PI/P)

The time domain results of the controller is summarised in Table 3.11, which demonstrates a fast and stable response. The rise time is 0.0712 s, the settling time is 0.0958 s, the overshoot is 2.35% and the delay time is 0.005 s. In addition, the output performance indices presented in Table

3.12 indicate favourable dynamic characteristics, with an ITAE of 0.015, an ISE of 0.516 and a low steady-state error index (ISTE) of 0.006. This confirms the effectiveness of the cascade PI/P controller configuration.

Table 3.11. Time domain results (PI/P)

Controller	Rise Time (s)	Settling time (s)	Overshoot (%)	Delay time (s)
Cascade Outer-Loop PI/Inner-Loop P	0.0712	0.0958	2.35	0.005

Table 3.12. Performance indices (PI/P)

Controller	ITAE	ISE	IAE	ITSE	ISCI	ISTE
Cascade Outer-Loop PI/Inner-Loop P	0.015	0.516	0.209	0.012	27.32	0.006

3.5.2. Cascade Controller: Outer-Loop PI/Inner-Loop PI (PI/PI)

Within the scope of the cascade control design for the PI/PI configuration, the outer-loop controller parameters were selected as PI = $5\left(1+\frac{1}{2.5s}\right)$, while the inner-loop employed a PI controller with gain PI = $20\left(1+\frac{1}{4s}\right)$. The main system signals obtained from the experiments are as follows: output speed response (Figure 3.37), current signal (Figure 3.38), control input signal (Figure 3.39), speed error signal (Figure 3.40), and the error signal with its derivative (Figure 3.41).

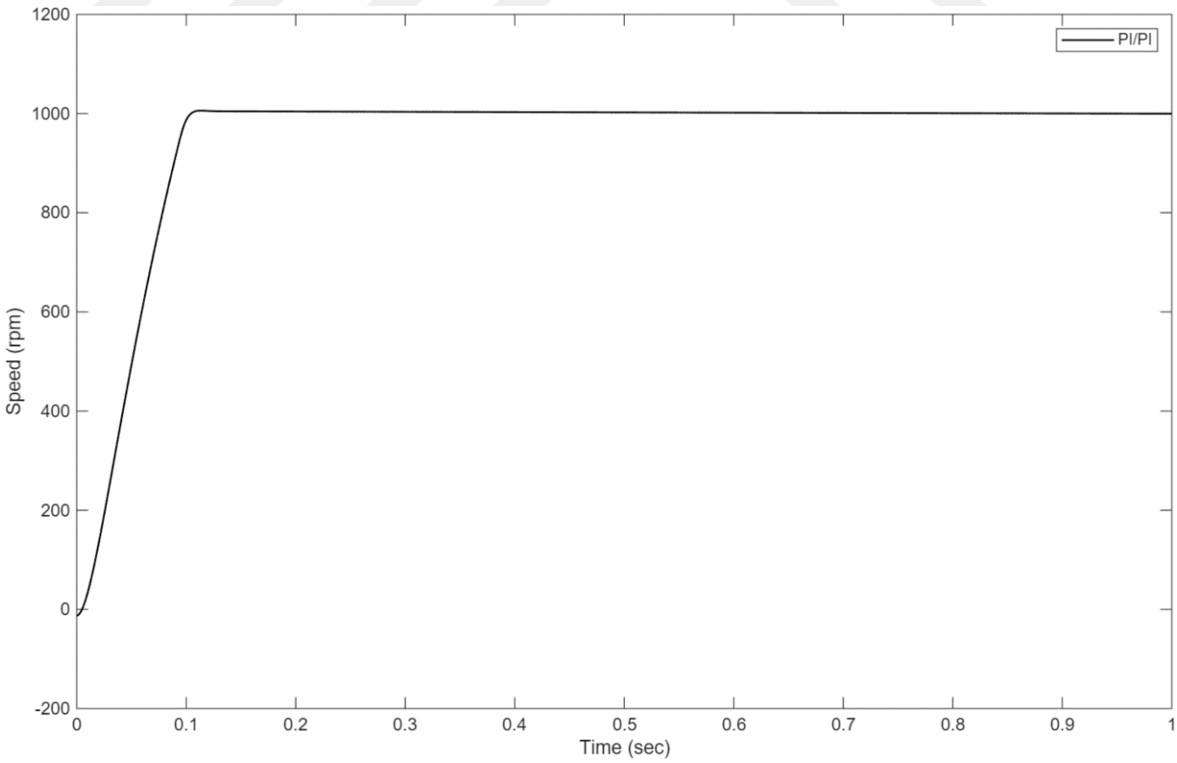

Figure 3.37. Output speed signal (rpm) (PI/PI)

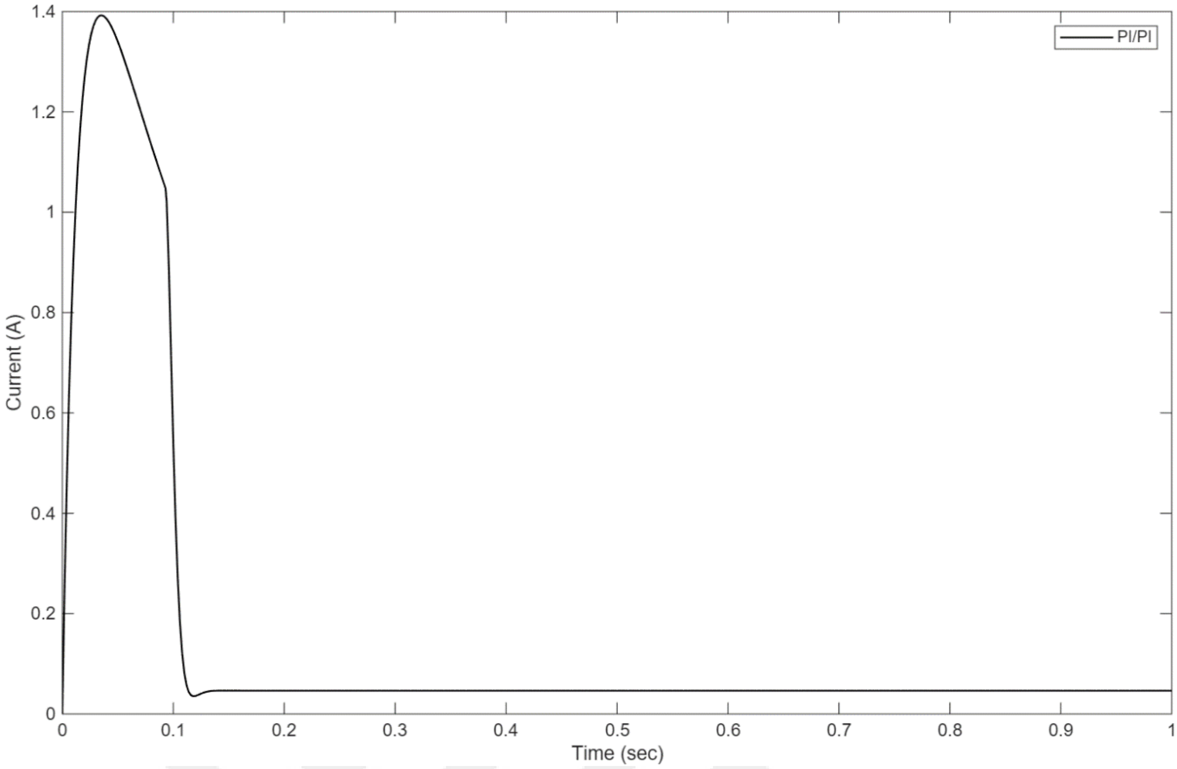

Figure 3.38. Armature current signal, $i_a(t)$ (PI/PI)

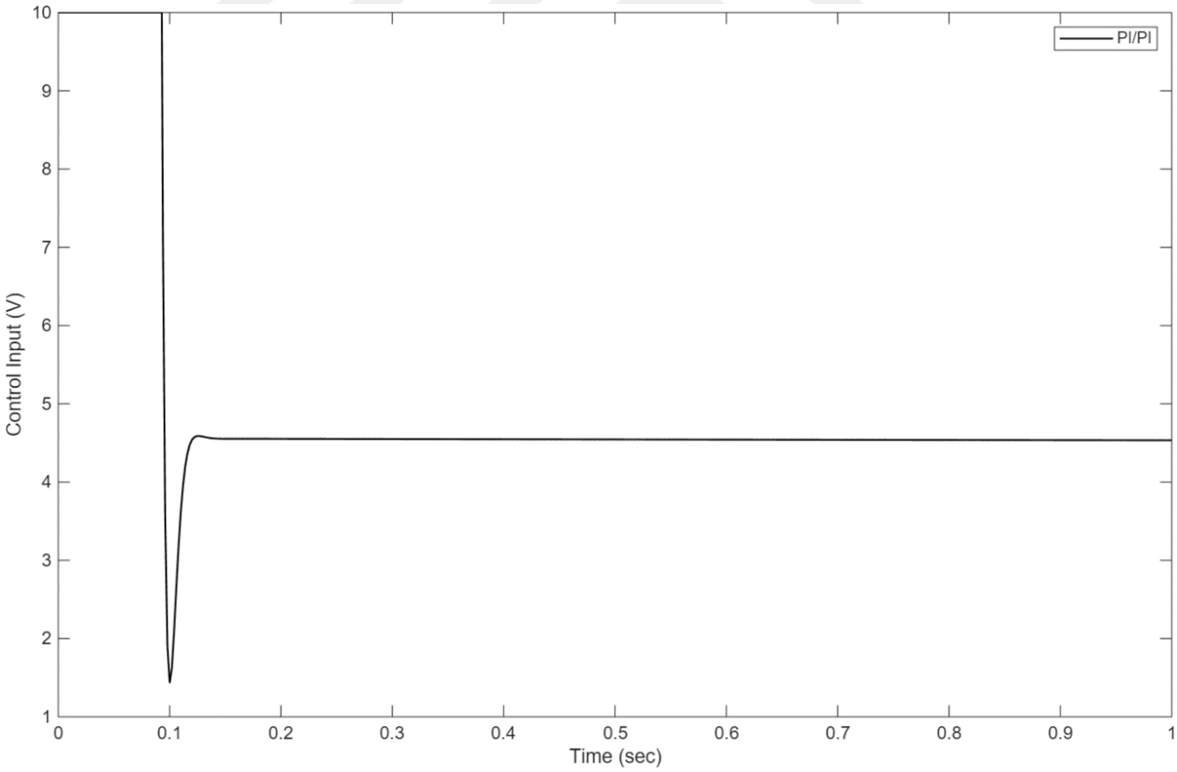

Figure 3.39. Control input voltage signal, $u(t)$ (PI/PI)

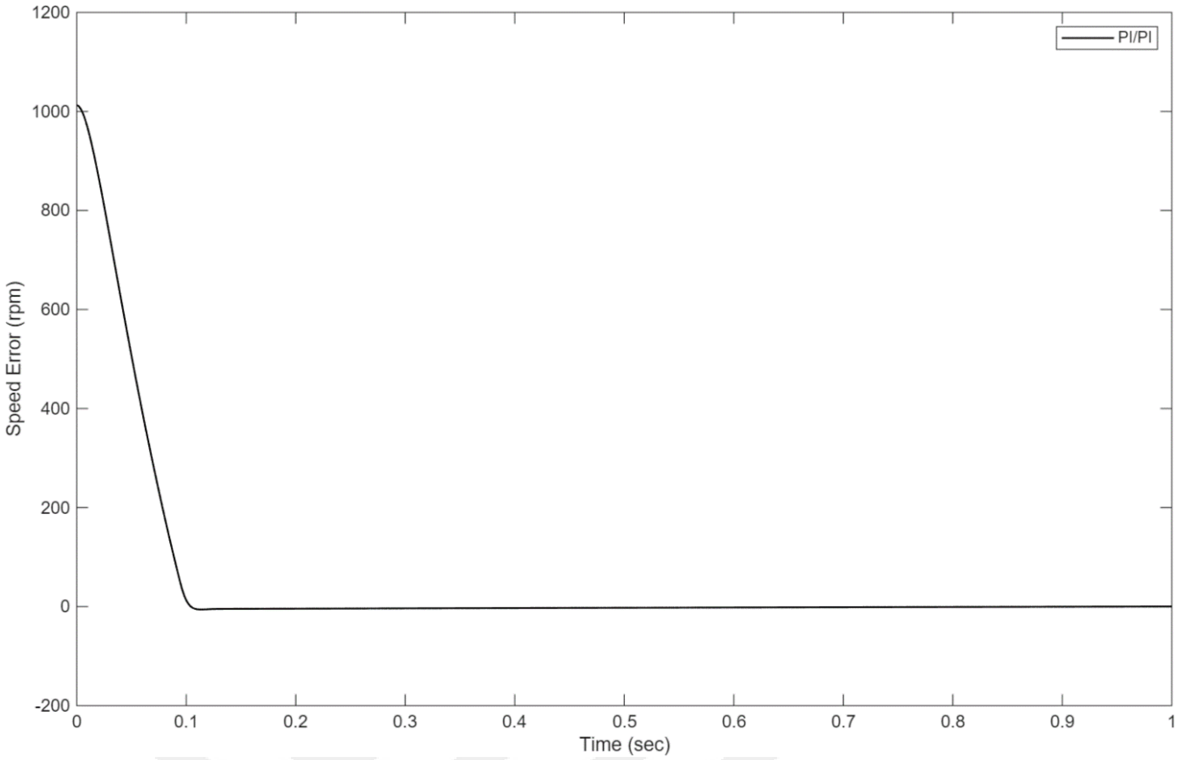

Figure 3.40. Speed error signal (rpm) (PI/PI)

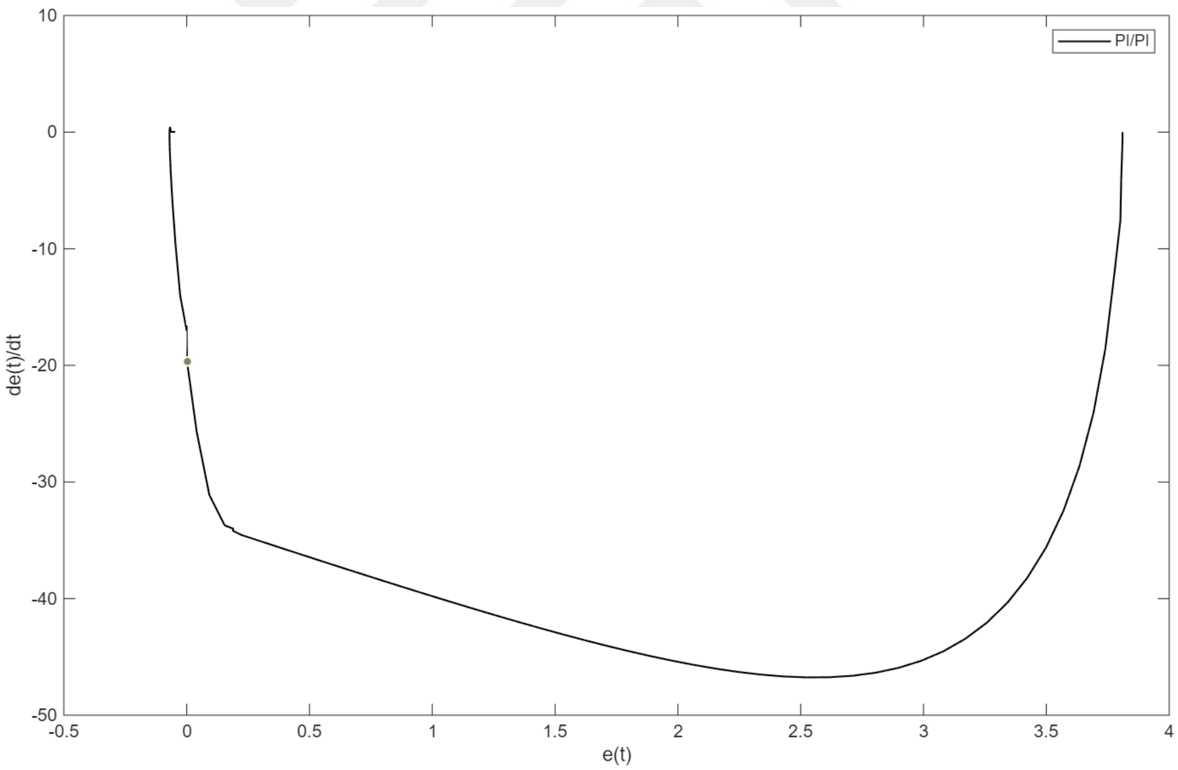

Figure 3.41. Phase plane of $e(t)$ and $de(t)/dt$ signal (PI/PI)

As demonstrated in Table 3.13, the cascade PI/PI controller attains a rise time of 0.0727 s and a settling time of 0.0985 s, signifying that the system furnishes a relatively expeditious transient response. Furthermore, the overshoot is limited to 0.60%, which confirms that the cascade structure enhances system stability by effectively suppressing undesired oscillations. The system's responsiveness to input changes is indicated by the delay time of 0.052 s. As illustrated by the performance indices enumerated in Table 3.14, the controller attains modest values, including ITAE = 0.032, IAE = 0.242, and ITSE = 0.013. These results imply that both the magnitude of the error and its time-weighted influence have been minimised effectively. Furthermore, the ISTE value of 0.0168 indicates that long-term error components are also maintained at a minimal level. The cascade PI/PI structure has been shown to provide significant improvements by offering a fast transient response with minimal overshoot, while simultaneously optimizing error-based performance measures to enhance system stability.

Table 3.13. Time domain results (PI/PI)

Controller	Rise Time (s)	Settling time (s)	Overshoot (%)	Delay time (s)
Cascade Outer-Loop PI/Inner-Loop PI	0.0727	0.0985	0.60	0.0520

Table 3.14. Performance indices (PI/PI)

Controller	ITAE	ISE	IAE	ITSE	ISCI	ISTE
Cascade Outer- Loop PI/Inner-Loop PI	0.032	0.519	0.242	0.013	27.86	0.0168

3.5.3. Cascade Control: Outer-Loop PID/Inner-Loop PI (PID/PI)

Within the cascade control framework, the PID/PI configuration was implemented with outer-loop controller gains set to PID = $60\left(1+\frac{1}{10s}+0.067s\right)$, while the inner-loop utilized a controller with parameters PI = $7\left(1+\frac{1}{3.5s}\right)$. The main system’s signals, including the output speed response (Figure 3.42), current signal (Figure 3.43), control input signal (Figure 3.44), speed error signal (Figure 3.45) and the error and its derivative (Figure 3.46), were examined to evaluate controller performance.

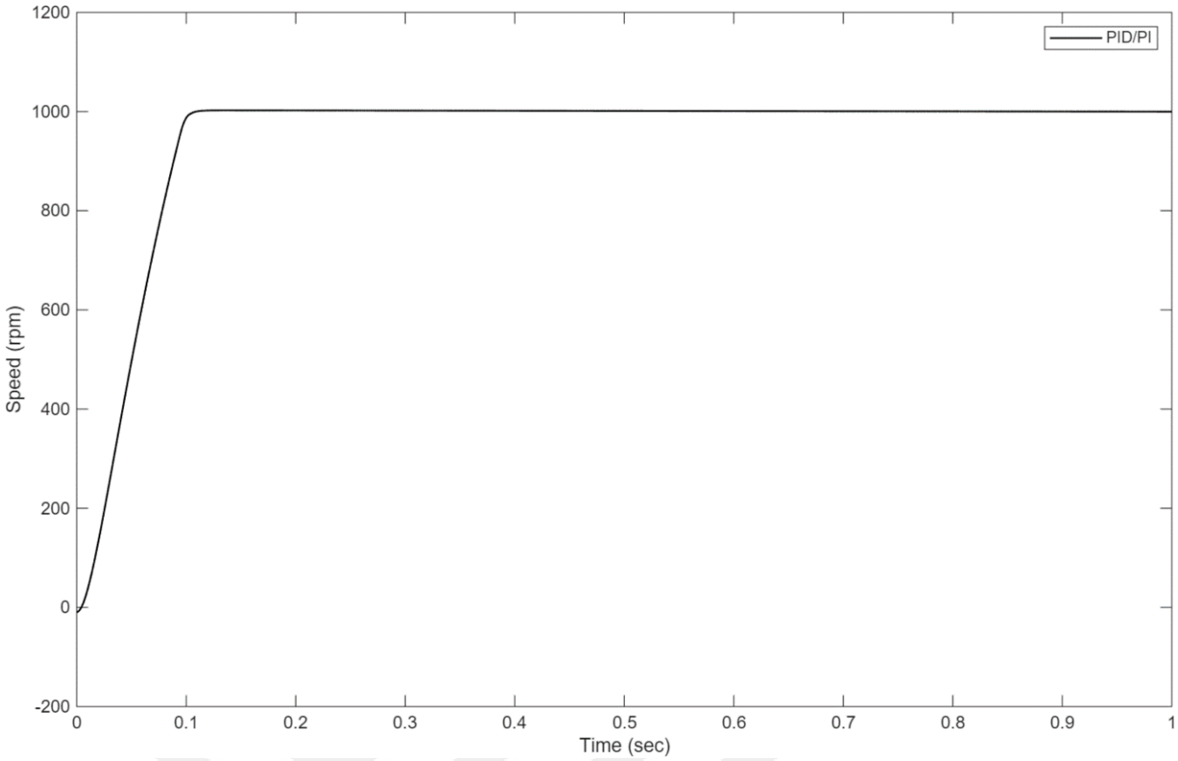

Figure 3.42. Output speed signal (rpm) (PID/PI)

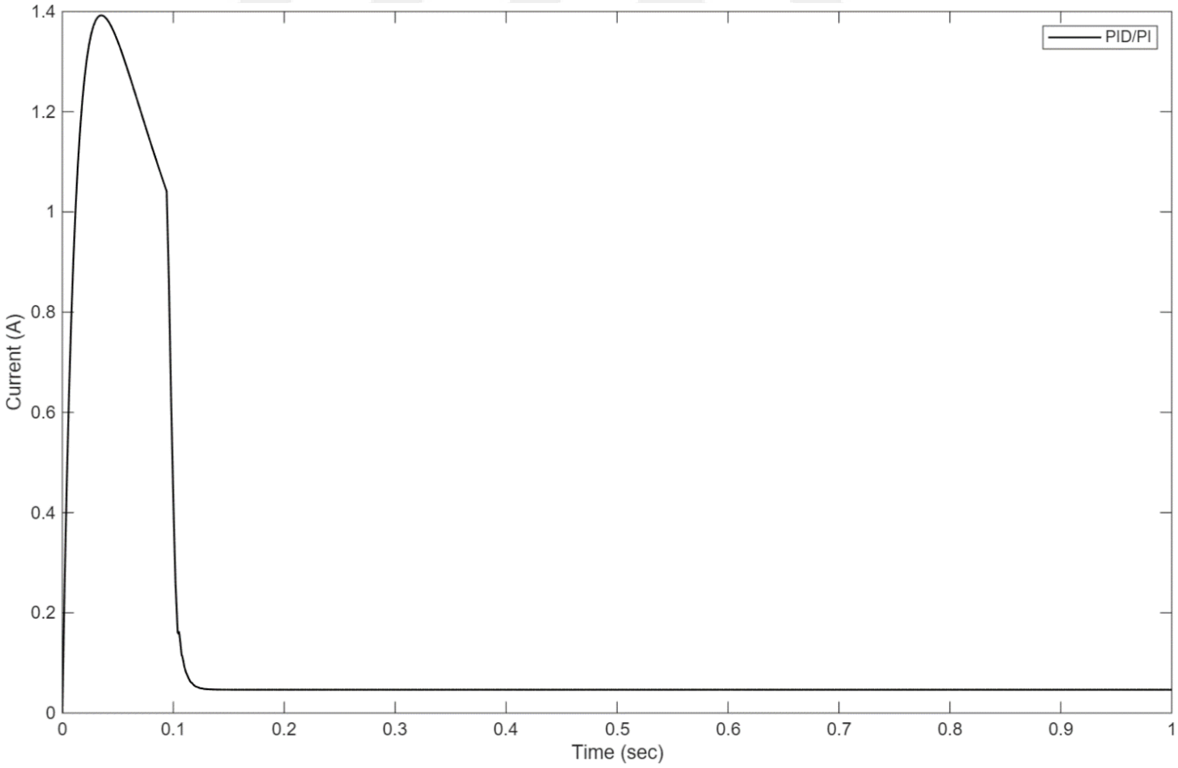

Figure 3.43. Armature current signal, $i_a(t)$ (PID/PI)

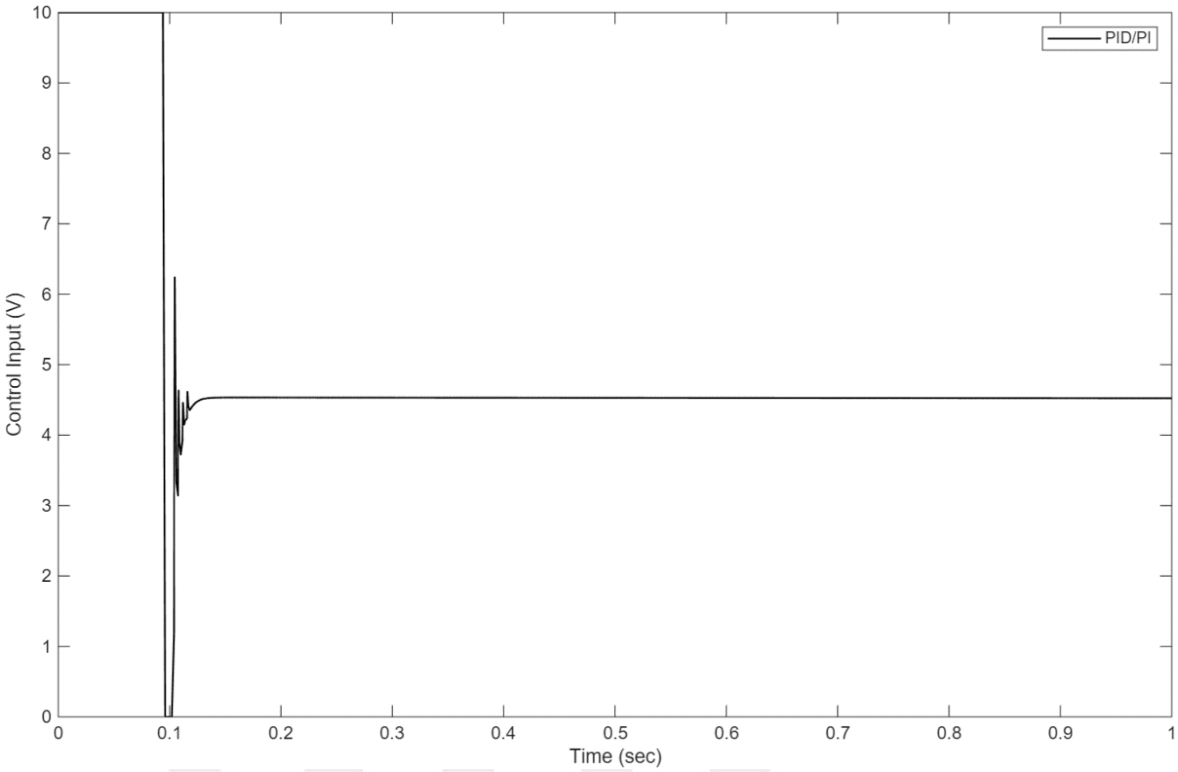

Figure 3.44. Control input voltage signal, $u(t)$ (PID/PI)

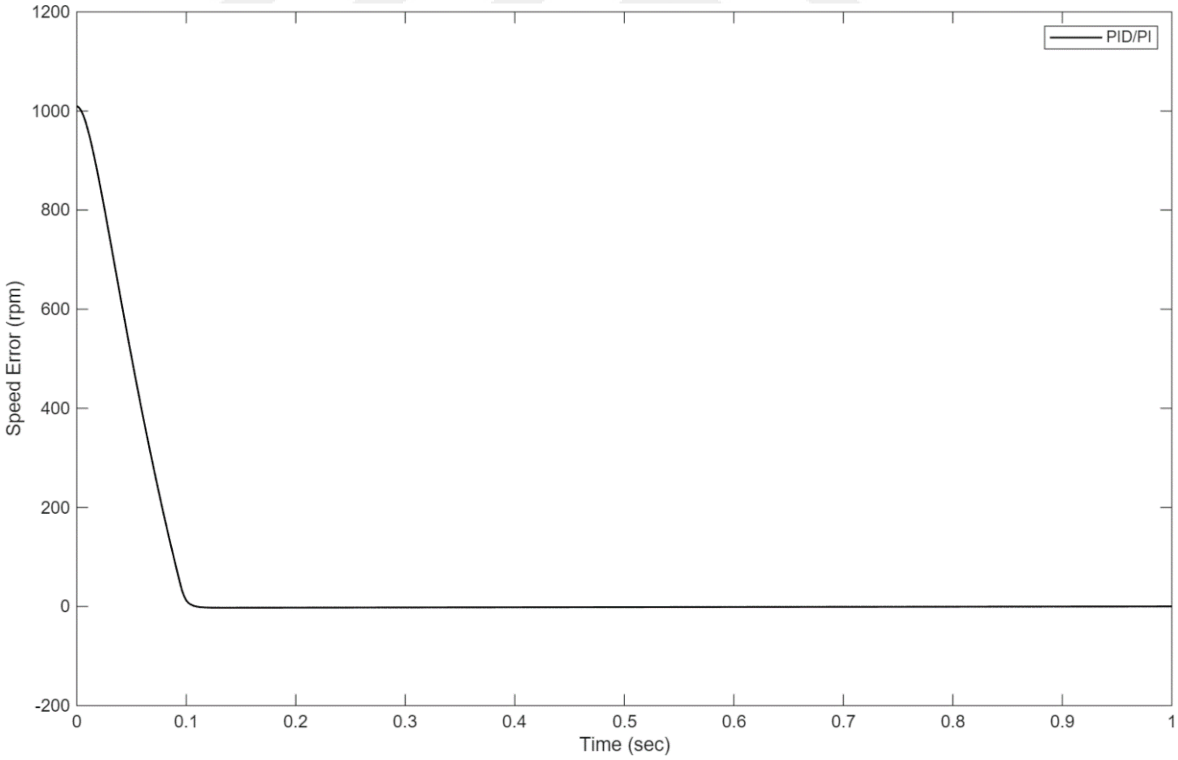

Figure 3.45. Speed error signal (rpm) (PID/PI)

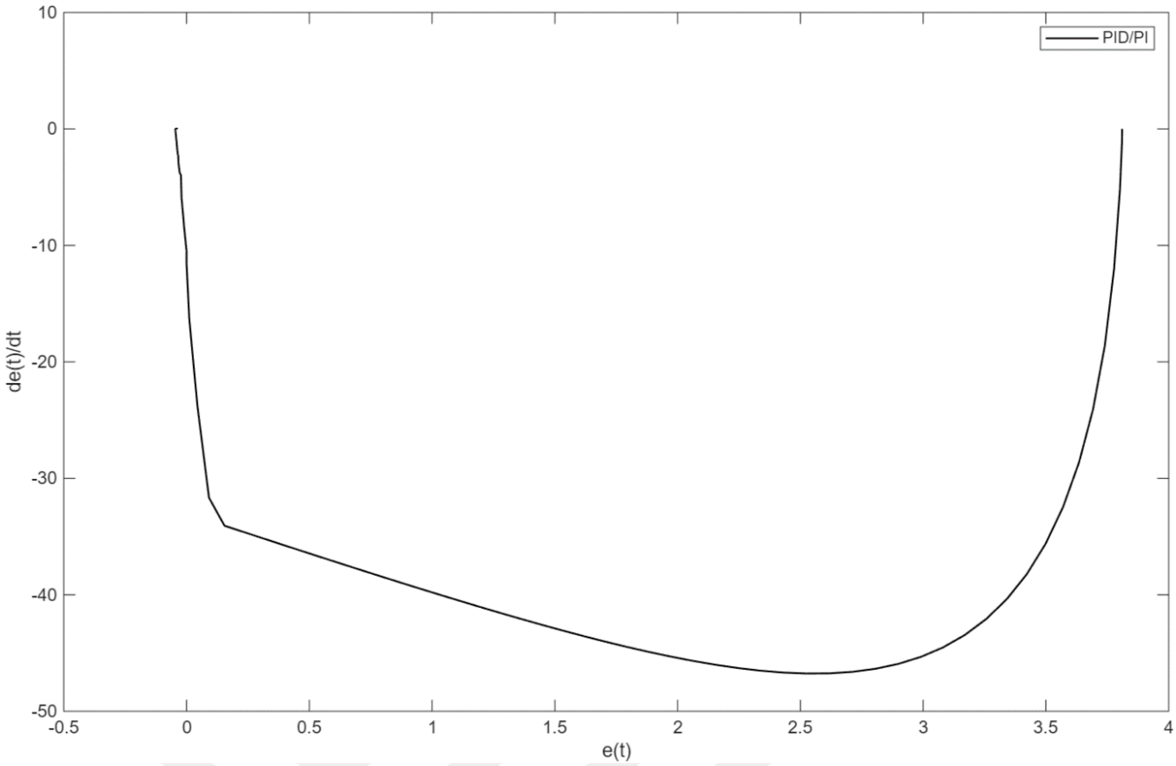

Figure 3.46. Phase plane of $e(t)$ and $de(t)/dt$ signal (PID/PI)

As demonstrated in Table 3.15 time domain results, the PID-PI cascade controller attains a rise time of 0.0725 s, a settling time of 0.0982 s, a minimal overshoot of 0.26%, and a delay time of 0.05 s. These metrics signify the controller's capacity to exhibit a swift and effectively dampened transient response. Furthermore, the performance indices presented in Table 3.16, including an ITAE of 0.025, an ISE of 0.5179, and a low steady-state error index (ISTE) of 0.012, suggest that the PID-PI cascade configuration offers enhanced control accuracy and stability in comparison to other configurations examined.

Table 3.15. Time domain results (PID/PI)

Controller	Rise Time (s)	Settling time (s)	Overshoot (%)	Delay time (s)
Cascade Outer-Loop PID/Inner-Loop PI	0.0725	0.0982	0.26	0.05

Table 3.16. Performance indices (PID/PI)

Controller	ITAE	ISE	IAE	ITSE	ISCI	ISTE
Cascade Outer-Loop PID/Inner-Loop PI	0.025	0.5179	0.229	0.013	27.81	0.012

4. SLIDING MODE CONTROL (SMC)

The development of control methodologies that are resilient to model uncertainties and external disturbances in linear and nonlinear systems constitutes a fundamental research area in contemporary control theory. In this context, SMC is a notable solution due to its high robustness and fast dynamic response advantages. In this study, the focus is on the control of a second-order system using the SMC approach. This is achieved through a combination of theoretical background and simulation analysis.

4.1. System Definition of Sliding Mode Control

The corresponding control law is given in Equation 3.27. This transfer function practically models the dynamic behavior of a DC motor or an electromechanical actuator. The system parameters is given in Equation 3.26. Accordingly, the system is approximated by a second-order model.

4.1.2. First-OrderSliding Mode Control (SMC-1)

SMC is a widely used robust control method for nonlinear systems, known for its resistance to parameter uncertainties and external disturbances. The fundamental principle of SMC is to drive the system states onto a predefined "sliding surface" and maintain them on this surface. The second order system dynamics can be expressed as (Eker, 2006):

$$\ddot{y}(t) = -a\dot{y}(t) - by(t) + cu(t) + d(t) \tag{4.1}$$

where

$y(t)$: System Output,

$u(t)$: Control Input,

$d(t)$: External disturbance $\left(|d(t)| < d_{max}\right)$

a, b, c : System Parameters

d_{max} : Upper bound of uncertainty

PID sliding surface dynamics (Eker, 2006):

$$s(t) = k_p e(t) + k_i \int_0^t e(t)\,dt + k_d \frac{de(t)}{dt} \tag{4.2}$$

$$s(t) = k_p \dot{e}(t) + k_i e(t) + k_d\left(y_r(t) + a\dot{y}(t) + by(t) - cu(t) - d(t)\right) \tag{4.3}$$

The equivalent $u_{eq}(t)$ is obtain where $s(t)=0,\ \dot{s}(t)=0,\ d(t)=0$

$$u_{eq}(t)=\frac{1}{k_d c}\left(k_p\dot{e}(t)+k_i e(t)+k_d y_r(t)+k_d a\dot{y}(t)+k_d b y(t)\right) \tag{4.4}$$

The switching signal is given (Eker, 2006):

$$u_{sw}(t)=k_c sgn(s(t))\cong k_c tanh\left(\frac{s(t)}{\Omega}\right) \tag{4.5}$$

To prove the stability of the system, the Lyapunov function is used:

$$V(t)=\frac{1}{2}s^2(t) \tag{4.6}$$

If the Lyapunov function is differentiated with respect to time, we get:

$$\begin{aligned}\dot{V}(t)&=s(t)\dot{s}(t)=s(t)(k_p\dot{e}(t)+k_i e(t)+k_d y_r(t)+k_d a\dot{y}(t)+k_d b y(t)-\\&k_d c(u_{eq}(t)+u_{sw}(t))-k_d d(t))\end{aligned} \tag{4.7}$$

$$\begin{aligned}\dot{s}(t)&=k_p\dot{e}(t)+k_i e(t)+k_d y_r(t)+k_d a\dot{y}(t)+k_d b y(t)-\\&k_d c(u_{sw}(t)+\frac{1}{k_d c}\left(k_p\dot{e}(t)+k_i e(t)+k_d y_r(t)+k_d a\dot{y}(t)+k_d b y(t)\right))\\&=-k_d c u_{sw}(t)-k_d d(t)\end{aligned} \tag{4.8}$$

Equation 4.7 is simplified as:

$$\dot{V}(t)=\left(\begin{aligned}&s\dot{s}=s\left(-k_d c u_{sw}-k_d d(t)\right) \qquad |d(t)|<d_{max}\\&=-sk_d c u_{sw}+sk_d d_{max}\\&=-sk_d ck_c sgn(s)+sk_d d_{max}\\&=-k_d ck_c s\frac{|s|}{s}+sk_d d_{max}\\&=-k_d ck_c|s|+sk_d d_{max}\\&\le -k_d ck_c|s|+|s|k_d d_{max}\\&=|s|\left(-k_d ck_c+k_d d_{max}\right)\\&=-|s|\left(k_d ck_c-k_d d_{max}\right)\end{aligned}\right) \tag{4.9}$$

The closed loop system is stable if:

$$\dot{V}(t) < 0 \;\; if \;\; k_c > \frac{d_{max}}{c} \tag{4.10}$$

4.1.3. Second-Order Sliding Mode Control (SMC-2)

In this section, the Second-Order Sliding Mode Control (SMC-2) method is discussed, along with its theoretical background and experimental implementation (Eker, 2010).
The second-order plant model:

$$\ddot{y}(t) = -a\dot{y}(t) - by(t) + cu(t) + d(t) \tag{4.11}$$

$$e(t) = y_r(t) - y(t) \tag{4.12}$$

$$\dot{e}(t) = \dot{y}_r(t) - \dot{y}(t) \tag{4.13}$$

$$\ddot{e}(t) = \ddot{y}_r(t) - \ddot{y}(t) \tag{4.14}$$

$$\ddot{e}(t) = \ddot{y}_r(t) - \left(-a\dot{y}(t) - by(t) + cu(t) + d(t)\right) \tag{4.15}$$

The sliding surface is given (Eker, 2010):

$$s(t) = \dot{s}(t) = \dots s^{(r-1)}(t) = 0 \tag{4.16}$$

$$\dot{s}(t) + \beta s(t) = k_p e(t) + k_i \int_0^t e(t)dt + k_d \dot{e}(t) \tag{4.17}$$

The second time derivative of the sliding surface, given in

$$\ddot{s}(t) + \beta \dot{s}(t) = k_p \dot{e}(t) + k_i e(t) + k_d \ddot{e}(t) \tag{4.18}$$

The equivalent control is found by recognizing that $\ddot{s}(t) = 0$ is a necessary condition for the error to stay on the sliding surface $s(t)$ and $d(t)$ is not considered for the equivalent control since the nominal plant parameters are assumed known (Kaya, 2007; Attaianes et al., 1999; Rahman et al., 2004). Then, the equivalent control for the nominal plant $d(t)=0$.

$$\beta\dot{s}(t)=k_p\dot{e}(t)+k_i e(t)+k_d\ddot{e}(t) \tag{4.19}$$

$$\beta\dot{s}(t)=k_p\dot{e}(t)+k_i e(t)+k_d(\ddot{y}_r(t)-\ddot{y}(t)) \tag{4.20}$$

$$\beta\dot{s}(t)=k_p\dot{e}(t)+k_i e(t)+k_d(\ddot{y}_r(t)-(-a\dot{y}(t)-by(t)+cu(t)+d(t))) \tag{4.21}$$

$$k_d cu(t)=k_p\dot{e}(t)+k_i e(t)+k_d(\ddot{y}_r(t)+a\dot{y}(t)+by(t))-\beta\dot{s}(t) \tag{4.22}$$

$$u_{eq}(t)=\frac{1}{k_d c}\left(k_p\dot{e}(t)+k_i e(t)+k_d(\ddot{y}_r(t)+a\dot{y}(t)+by(t))-\beta\dot{s}(t)\right) \tag{4.23}$$

Switching Control:

$$u_{sw}(t)=\lambda_1 s(t)+k_s tanh\left(\frac{\dot{s}(t)}{\Omega}\right) \tag{4.24}$$

4.2. Single-Loop SMC-1 Controller System

The transfer function was obtained in Equations 3.21. In the simulation model, the SMC-1 controller was designed with the following parameters:

- Control coefficients: $k_d = 0.4$, $k_p = 25$, $k_i = 5$, $k_s = 4.5$
- Smoothing parameter: $\Omega = 8$

These parameters were selected considering the Lyapunov stability criterion and the system's stability has been mathematically proven.

The implementation and analysis of the SMC-1 strategy was conducted. The system output speed response (Figure 4.1) demonstrates the evolution of the output speed over time, thus revealing the efficacy of the SMC-1 controller in effectively regulating the system dynamics. In a similar manner, the present current response (Figure 4.2) is indicative of the system's electrical behaviour and its interaction with the control action, while the control input signal (Figure 4.3) illustrates the requisite control effort for optimal performance. Moreover, the equivalent input (Figure 4.4), switching input (Figure 4.5), sliding surface signal (Figure 4.6), speed error signal (Figure 4.7), error and error derivative signal (Figure 4.8) offer a comprehensive insight into the system's sliding mode behaviour and its robustness properties.

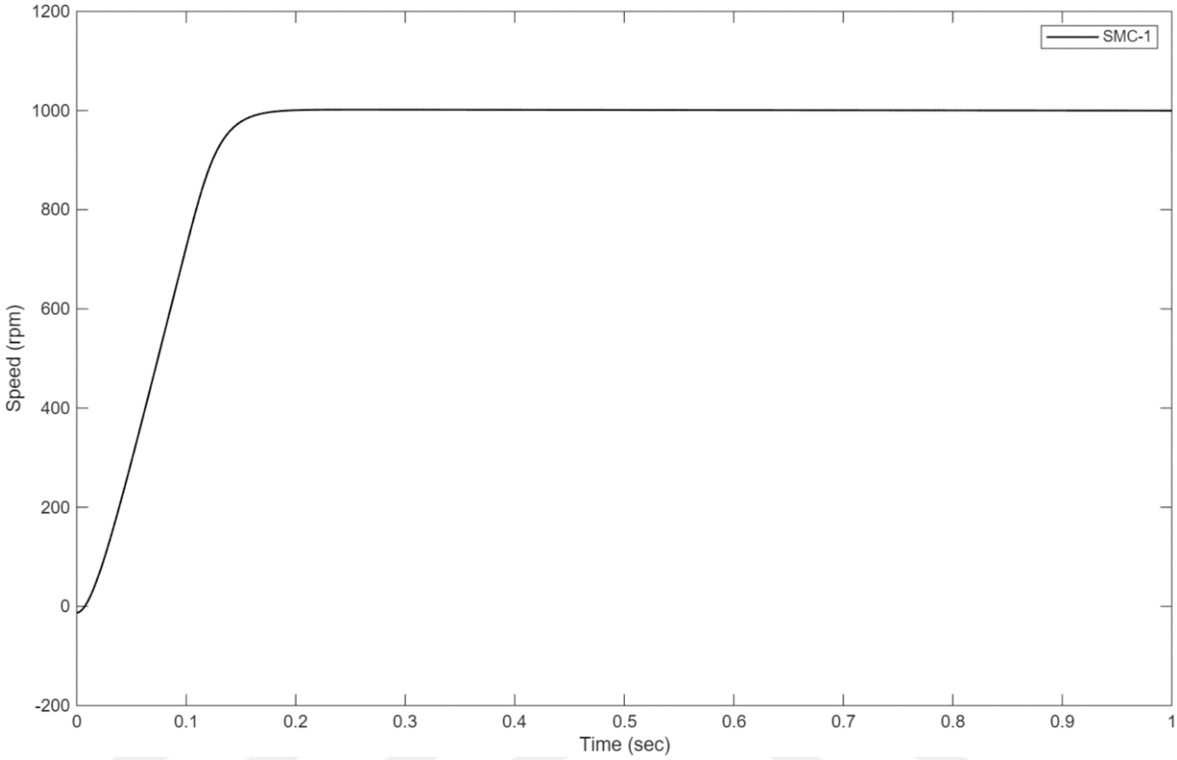

Figure 4.1. Output speed signal (rpm) (SMC-1)

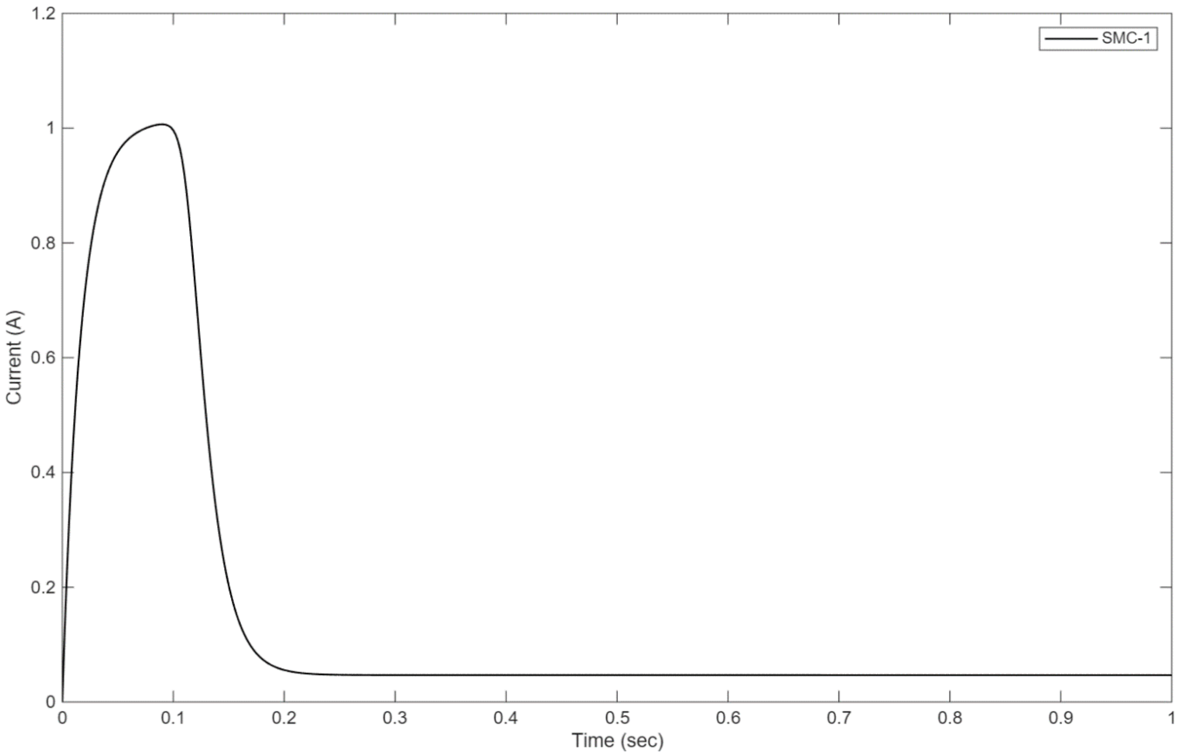

Figure 4.2. Armature current signal, $i_a(t)$ (SMC-1)

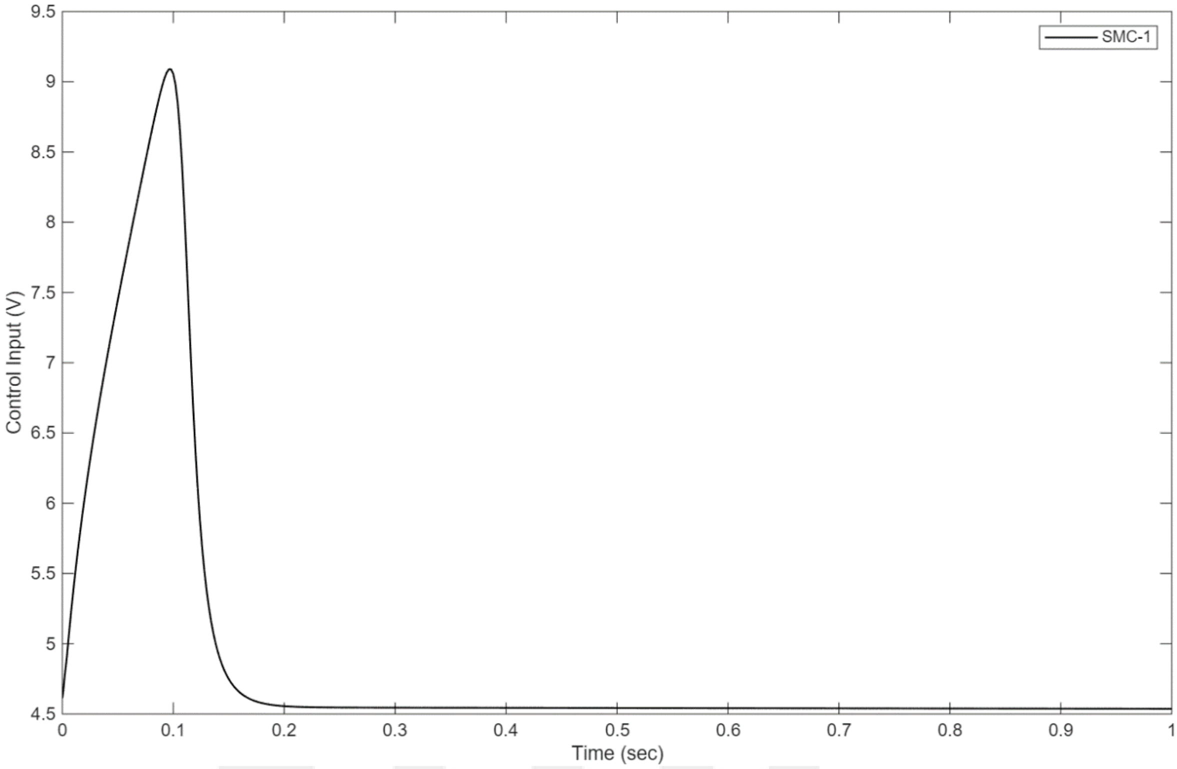

Figure 4.3. Control input voltage signal, $u(t)$ (SMC-1)

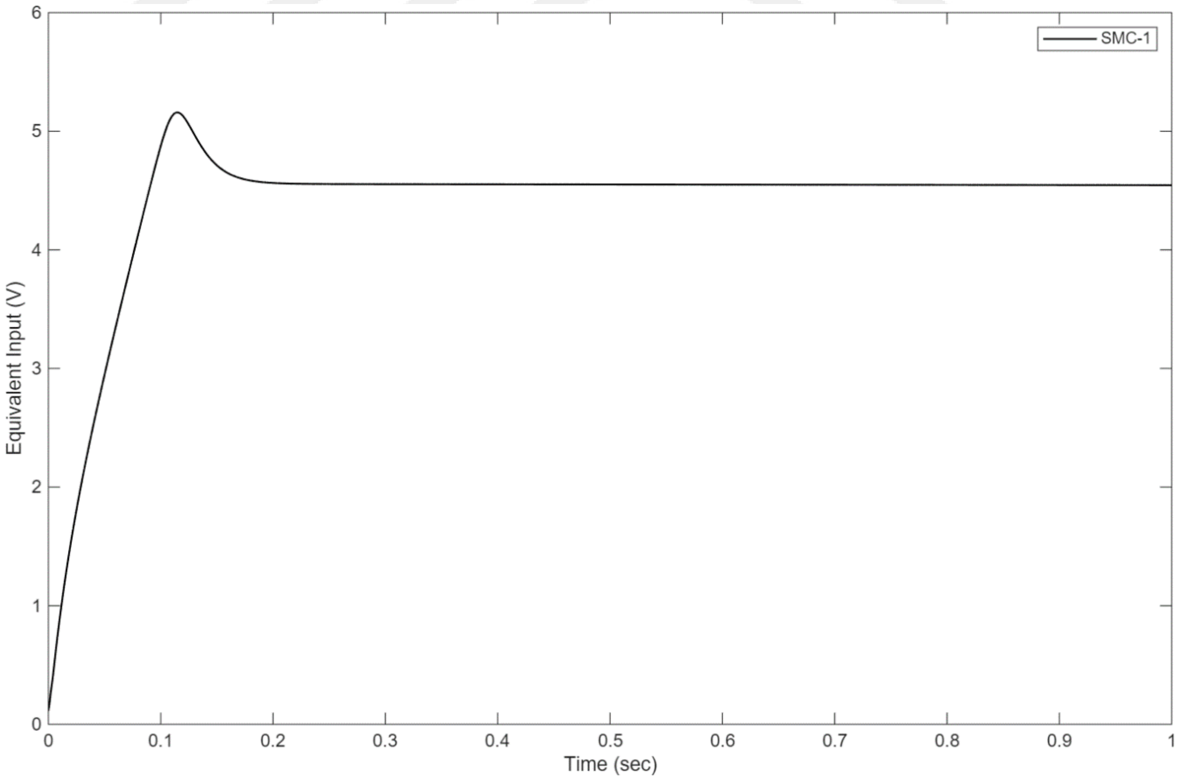

Figure 4.4. Equivalent input signal, $u_{eq}(t)$ (SMC-1)

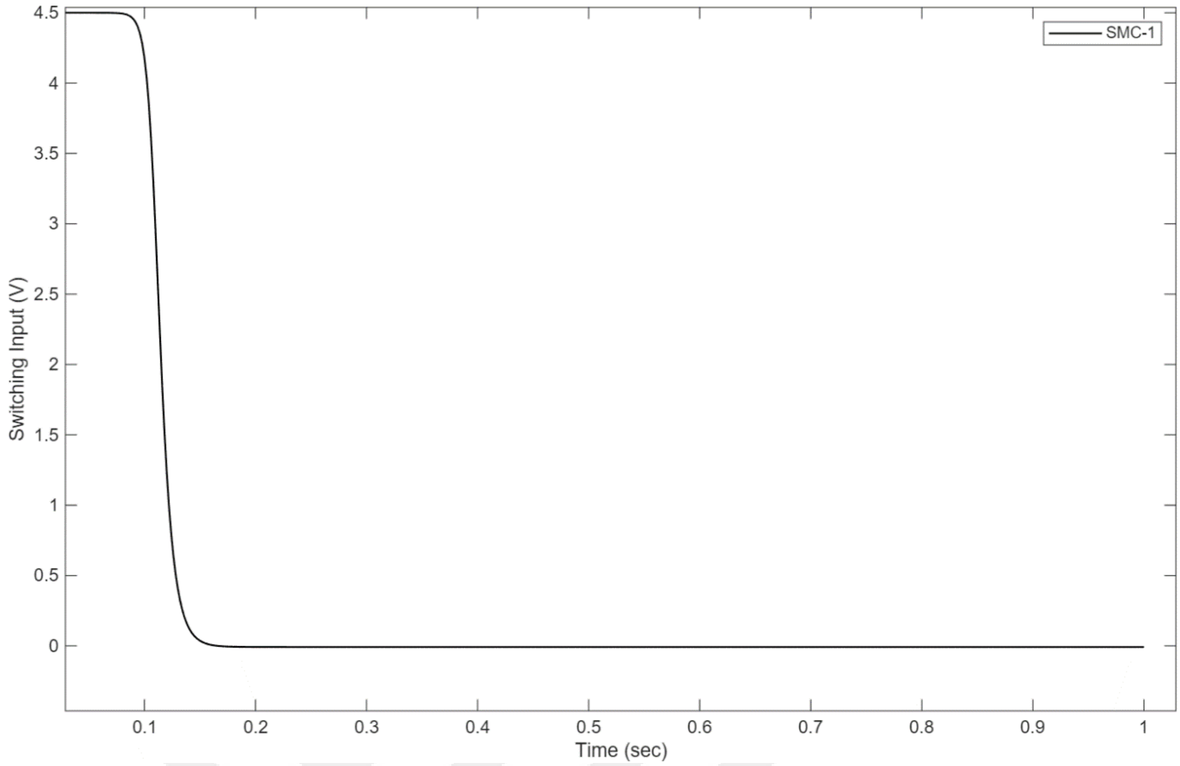

Figure 4.5. Switching input signal, $u_{sw}(t)$ (SMC-1)

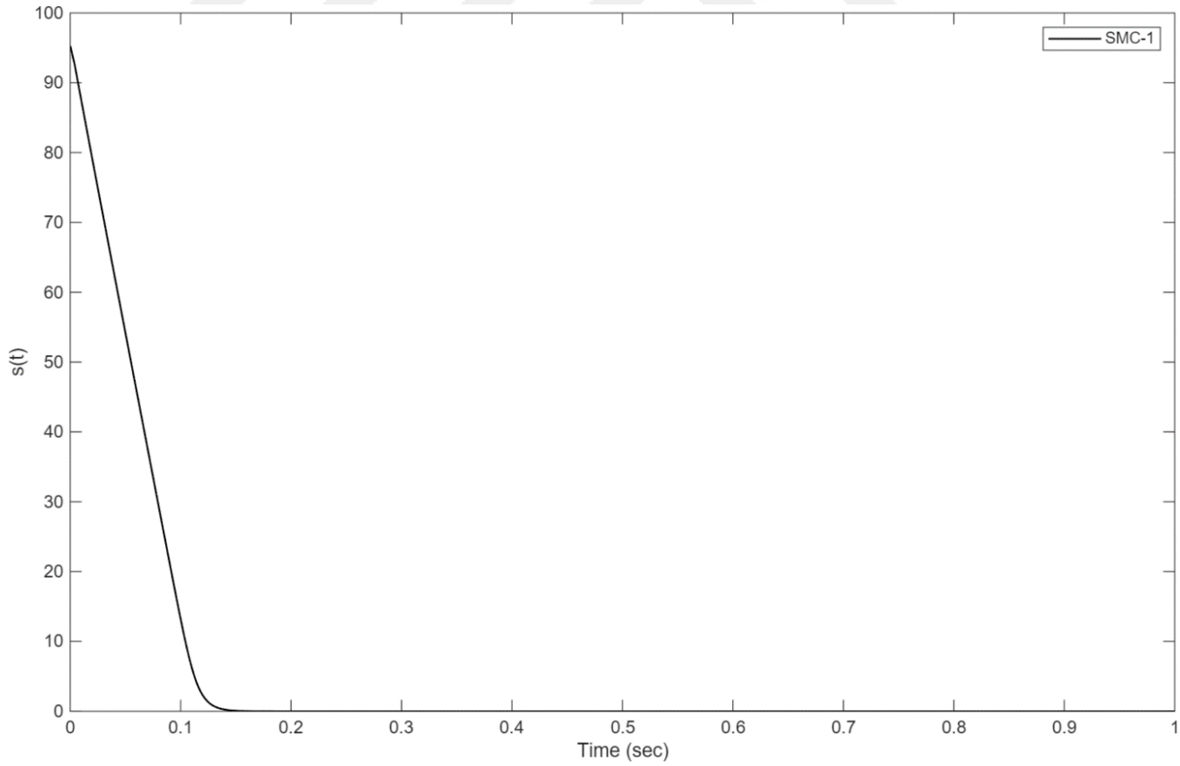

Figure 4.6. Sliding surface signal, $s(t)$ (SMC-1)

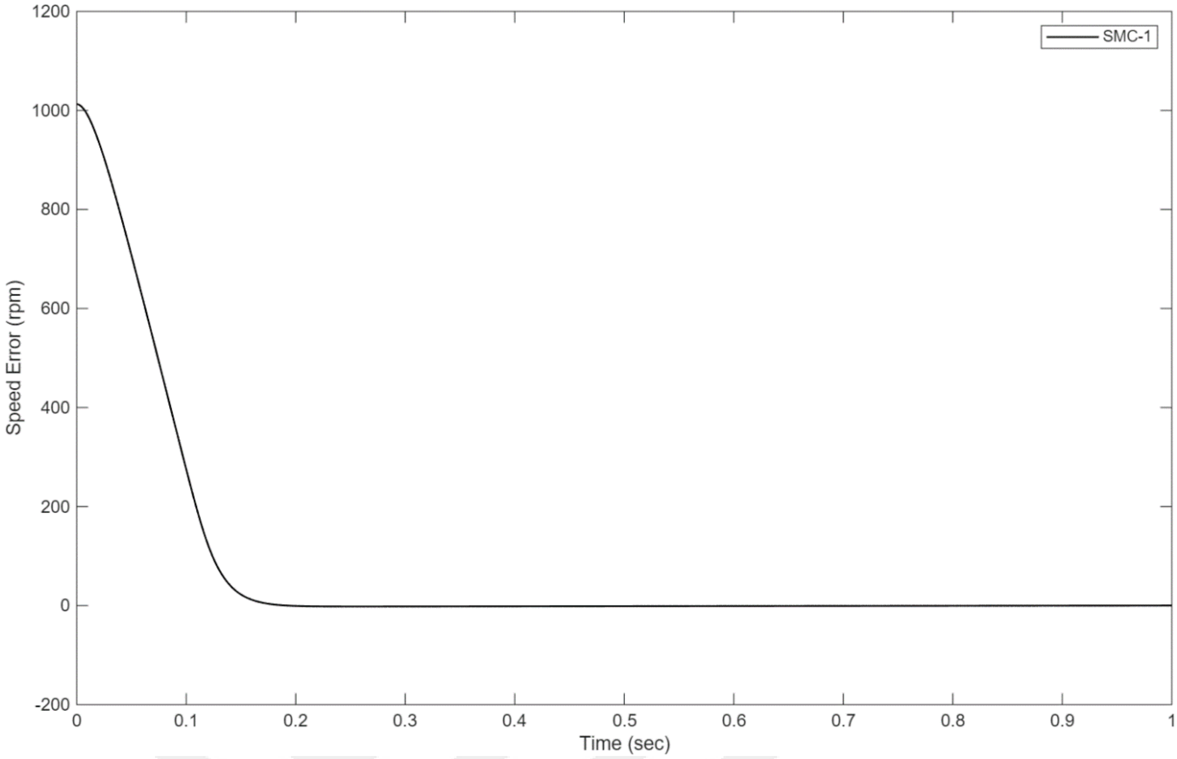

Figure 4.7. Speed error signal (rpm) (SMC-1)

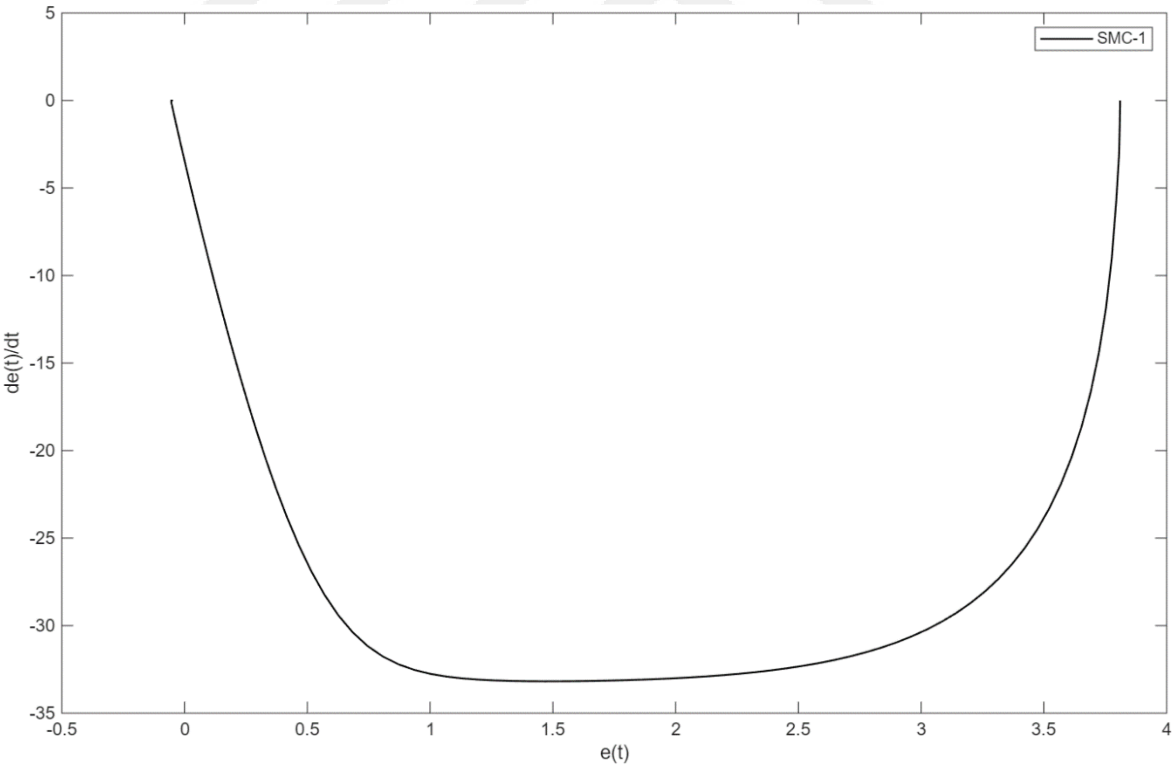

Figure 4.8. Phase plane of $e(t)$ and $de(t)/dt$ signal (SMC-1)

As demonstrated in Table 4.1 time domain results, the single-loop SMC-1 controller attains a rise time of 0.0998 s and a settling time of 0.1516 s, signifying that the system responds with a relatively expeditious transient behaviour. Furthermore, the overshoot is limited to 0.19%, which demonstrates that the SMC-1 controller ensures a highly stable response by almost eliminating oscillations. The delay time of 0.074 s further corroborates the system's capacity to respond expeditiously to input alterations. As demonstrated in Table 4.2, the controller exhibits low values for performance indices such as ITAE = 0.0373, IAE = 0.417, and notably ISTE = 0.0048, thereby underscoring its efficacy in mitigating both short-term and long-term error contributions. Conversely, the relatively higher values of ISE = 1.067 and ITSE = 0.0534 suggest that the squared error criteria are not minimised to the same extent. The SMC-1 controller has been demonstrated to offer a balanced performance, characterised by a stable response with negligible overshoot. In addition, the controller has been shown to enhance error-based indices, thereby improving system robustness.

Table 4.1. Time domain results (SMC-1)

Controller	Rise Time (s)	Settling time (s)	Overshoot (%)	Delay time (s)
SMC-1	0.0998	0.1516	0.19	0.0740

Table 4.2. Performance indices (SMC-1)

Controller	ITAE	ISE	IAE	ITSE	ISCI	ISTE
SMC-1	0.0373	1.067	0.417	0.0534	22.89	0.0048

4.3. Single-Loop SMC-2 Controller Method

The SMC-2 method has been modeled in the MATLAB/Simulink environment using the transfer function given in Equations (3.21).

The values are determined as follows.

Selected parameters for the SMC-2 controller are:

- Switching gain: $k_{sc} = 3$
- Control gains: $k_d = 1.5,\ k_p = 40,\ k_i = 5$
- Smoothing parameter: $\Omega_c = 10$
- Sliding surface gains: $\beta = 150,\ \lambda_1 = 50$

In the block diagram, saturation limits were applied at the system input to ensure the control algorithm operates within hardware limits (0-10, +10 volt).

The SMC-2 strategy was implemented and analyzed. The system output speed response (Figure 4.9) demonstrates how effectively SMC-2 regulates the output dynamics, while the output current response (Figure 4.10) highlights the stable electrical behavior of the system. The control input signal output (Figure 4.11) indicates the required control effort, the switching input (Figure 4.12), equivalent input (Figure 4.13), sliding surface signal (Figure 4.14), error signal (Figure 4.15), error and error derivative signal (Figure 4.16) provide a comprehensive view of the sliding mode behavior and robustness of the system.

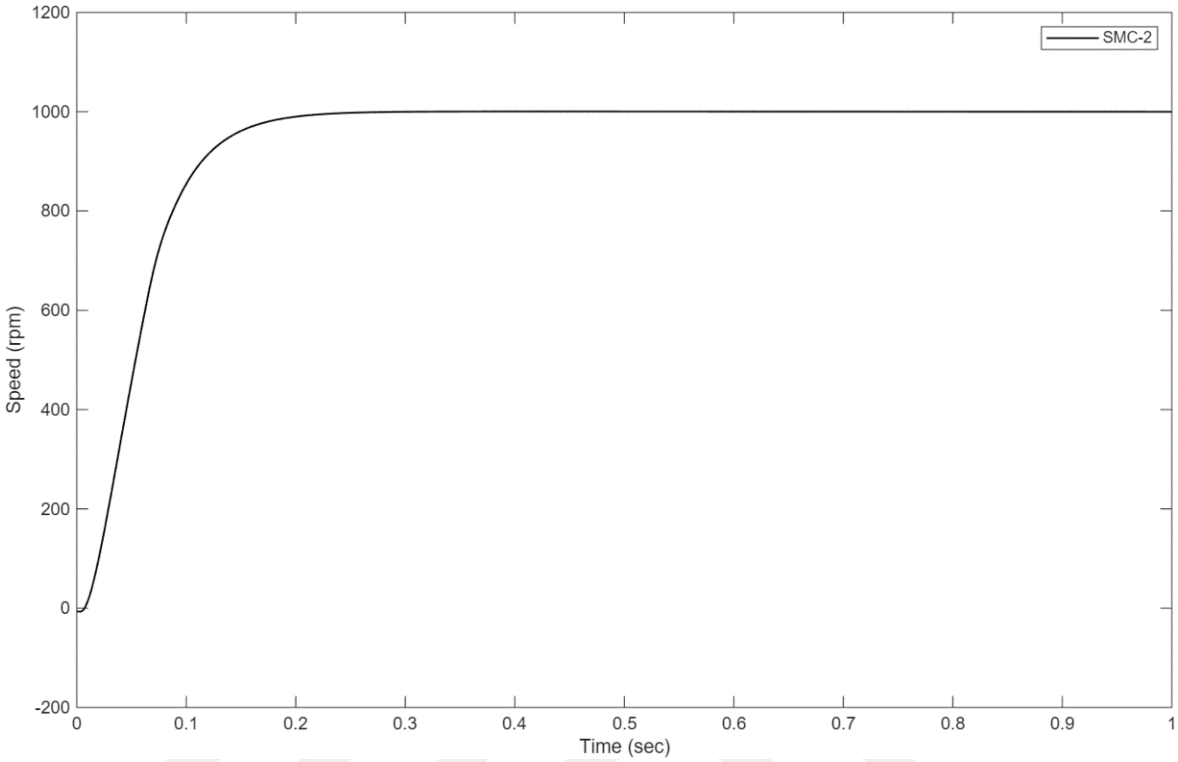

Figure 4.9. Output speed signal (rpm) (SMC-2)

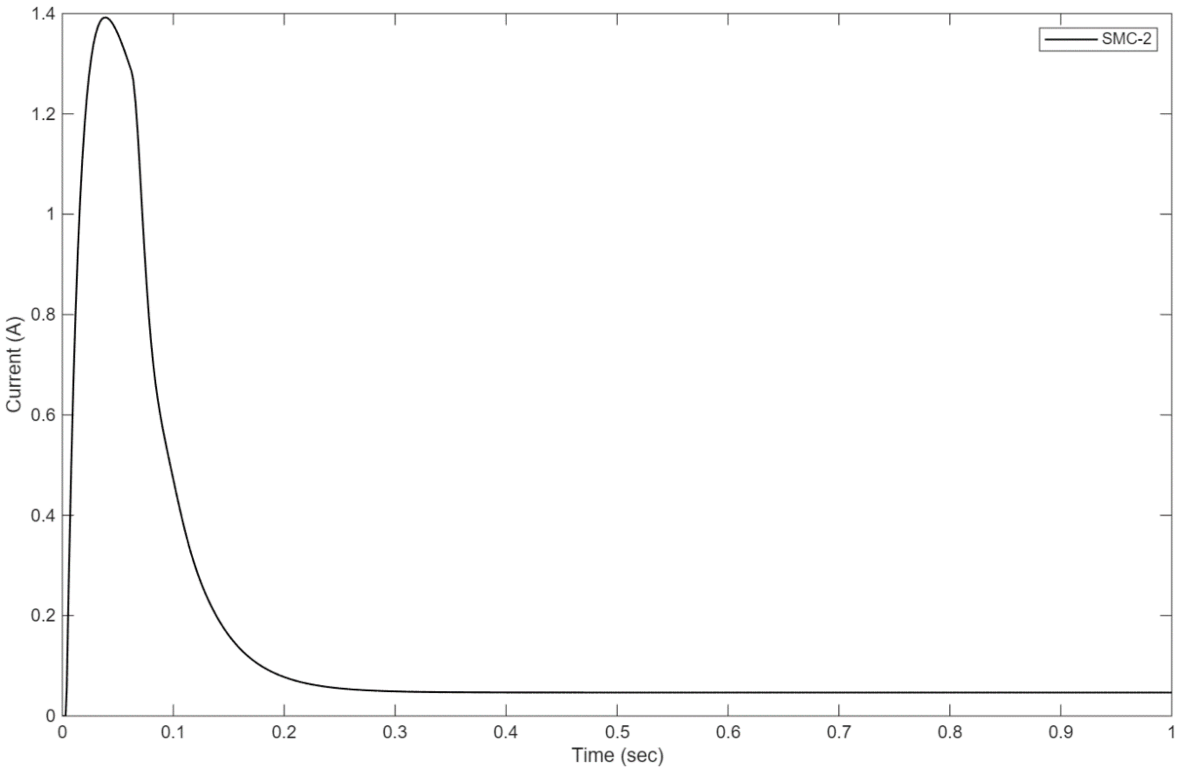

Figure 4.10. Armature current signal, $i_a(t)$ (SMC-2)

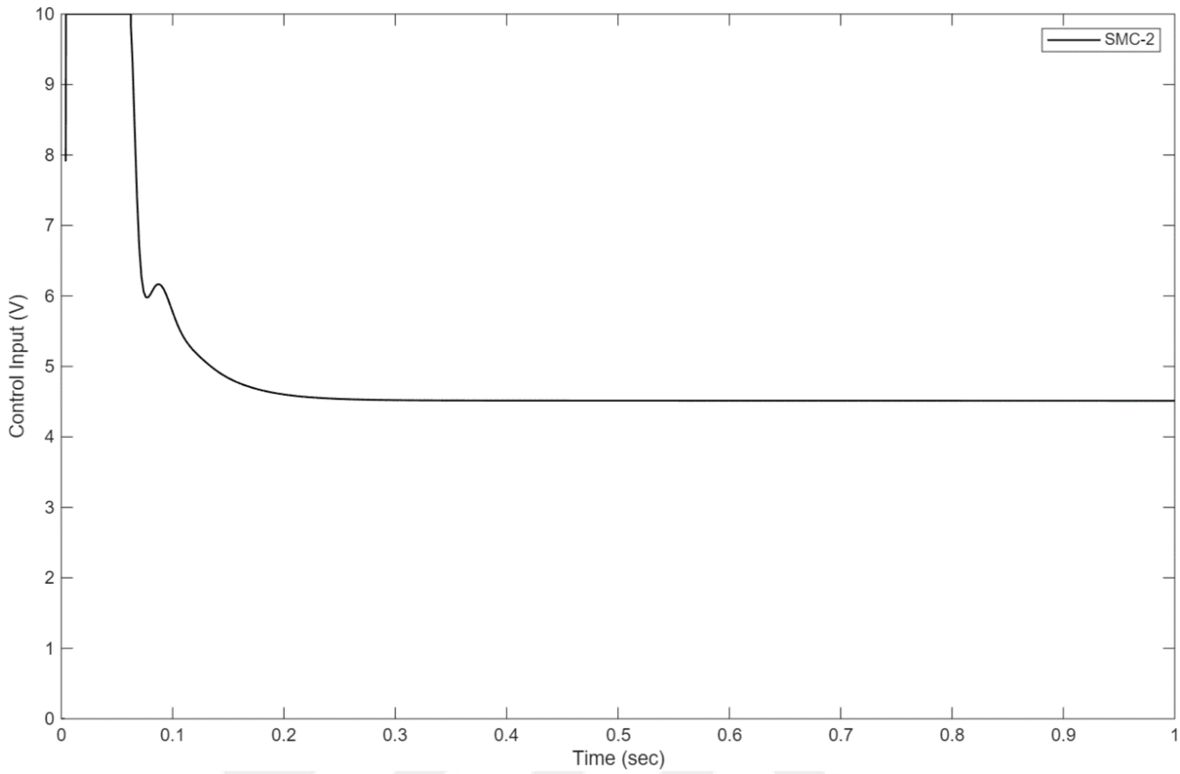

Figure 4.11. Control input voltage signal, $u(t)$ (SMC-2)

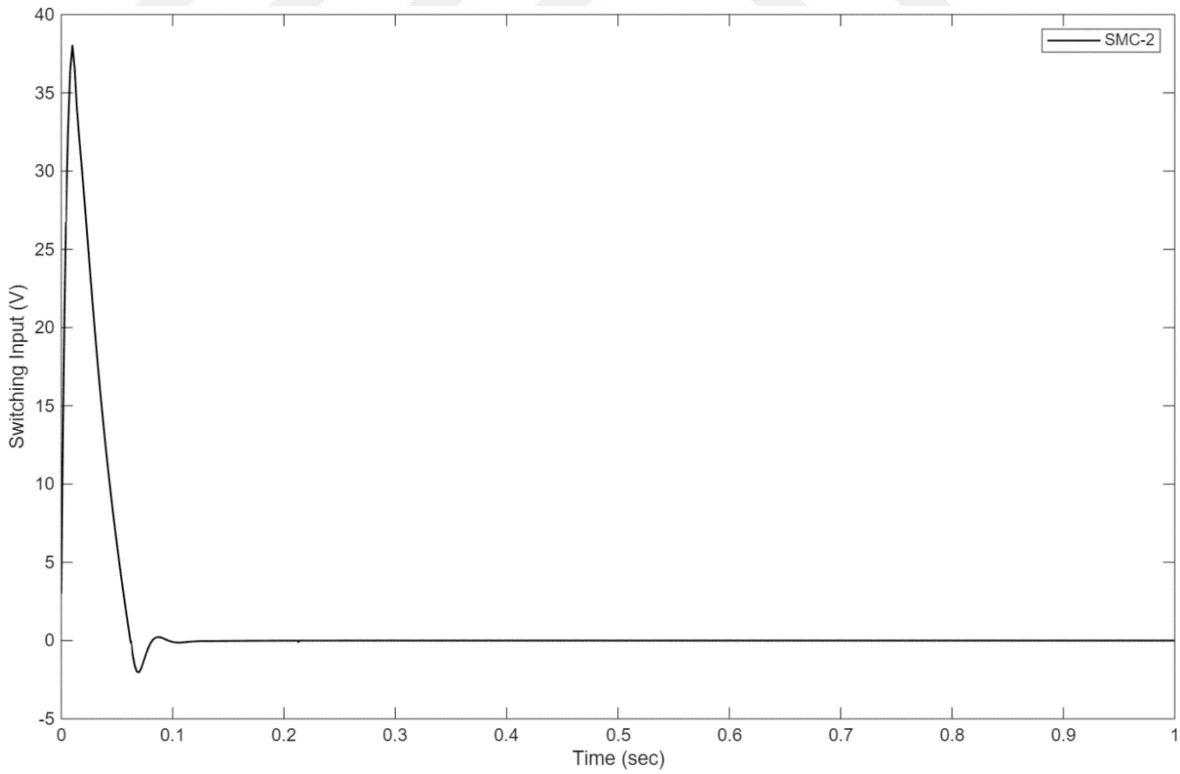

Figure 4.12. Switching input signal, $u_{sw}(t)$ (SMC-2)

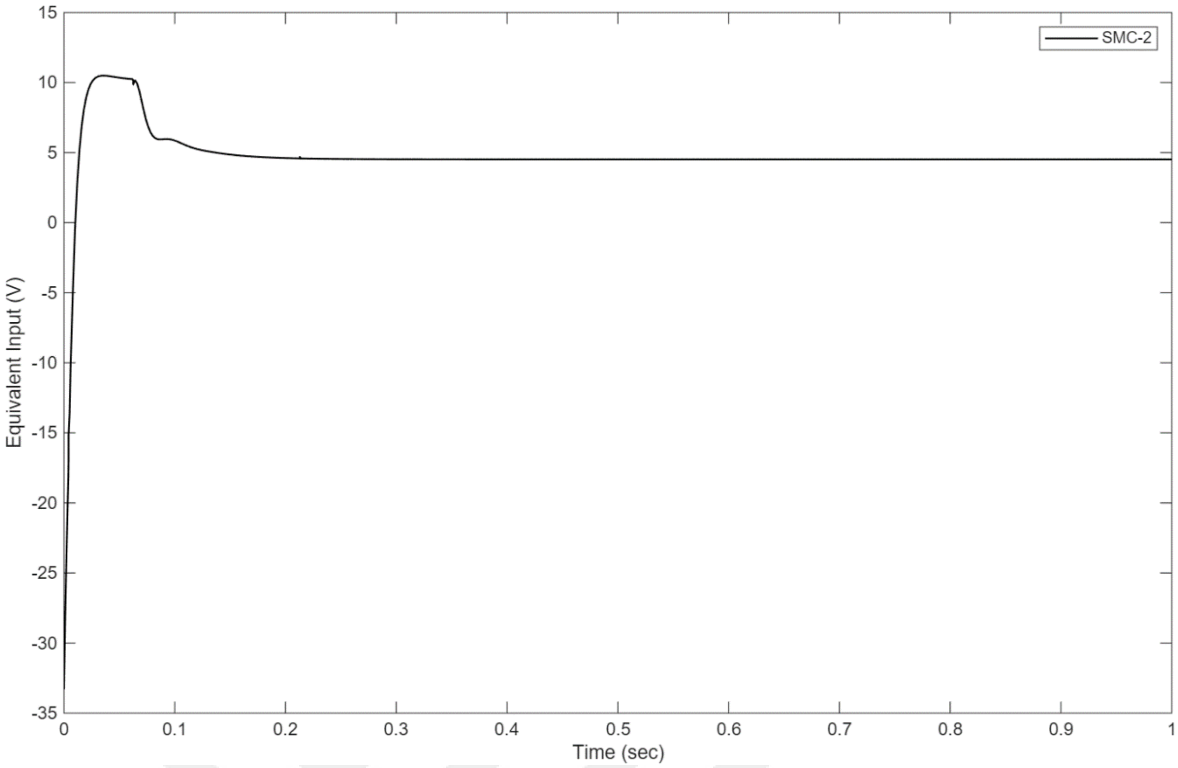

Figure 4.13. Equivalent input signal, $u_{eq}(t)$ (SMC-2)

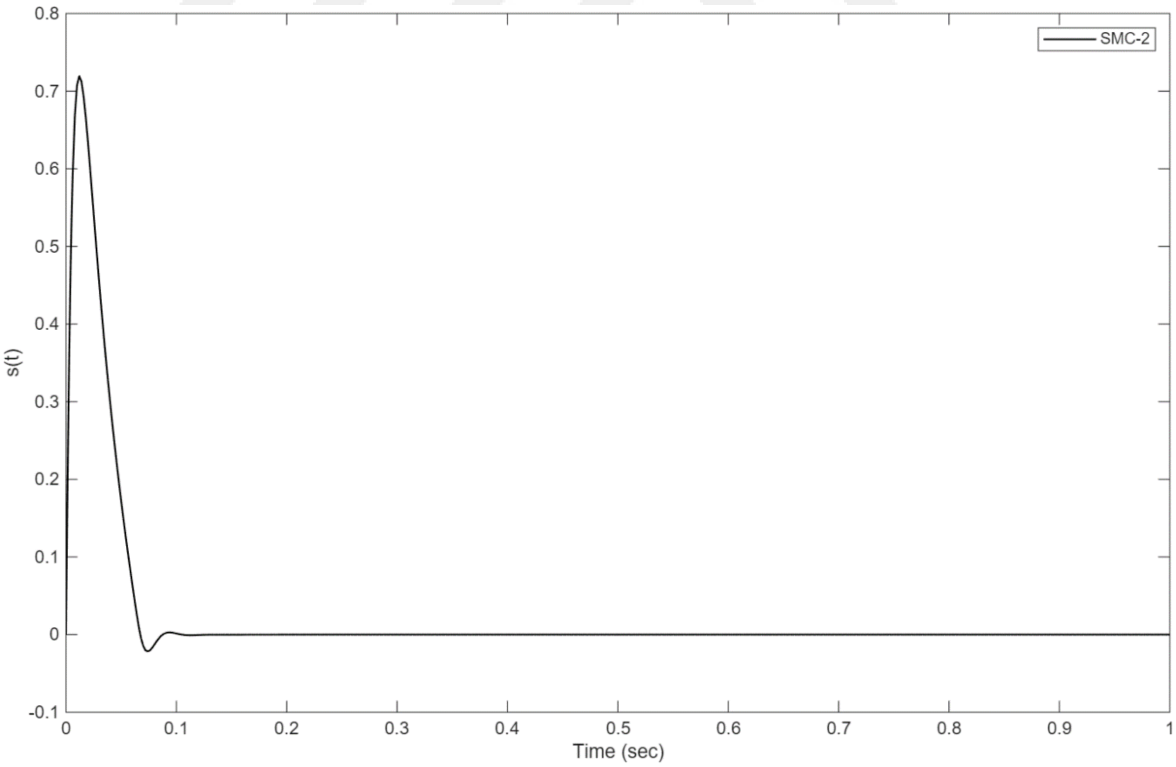

Figure 4.14. Sliding surface signal, $s(t)$ (SMC-2)

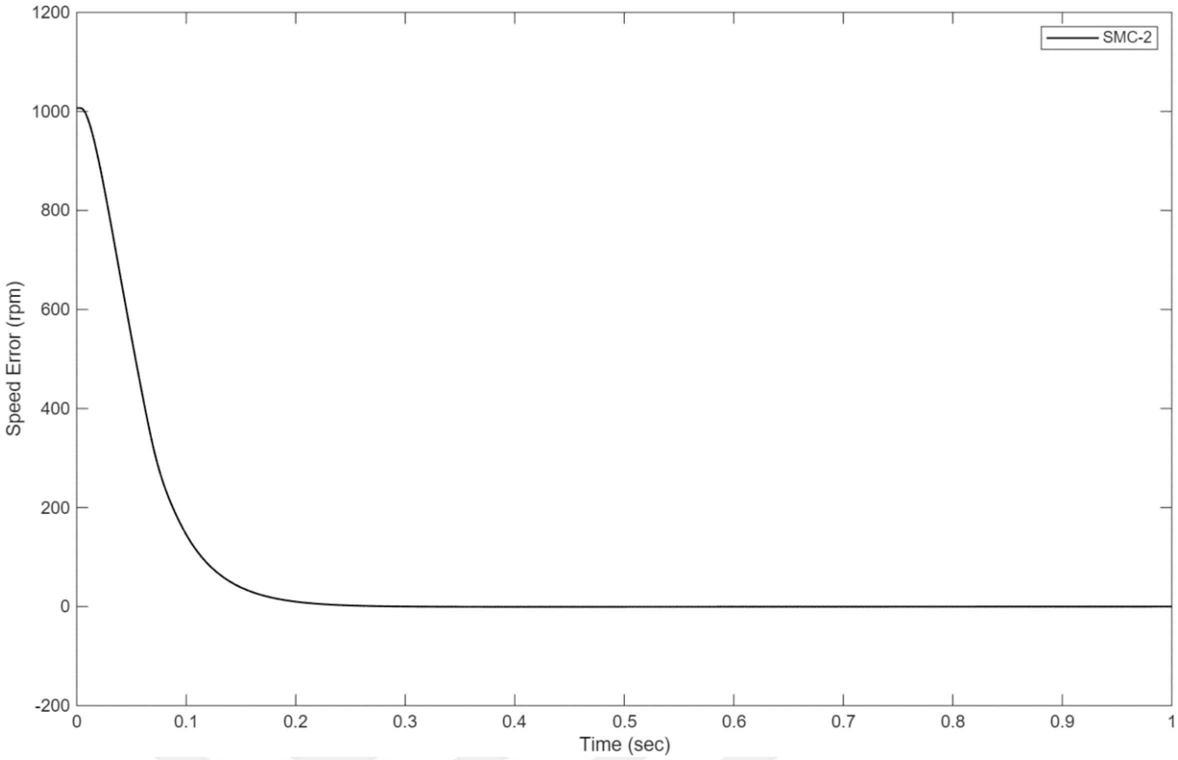

Figure 4.15. Speed error signal (rpm) (SMC-2)

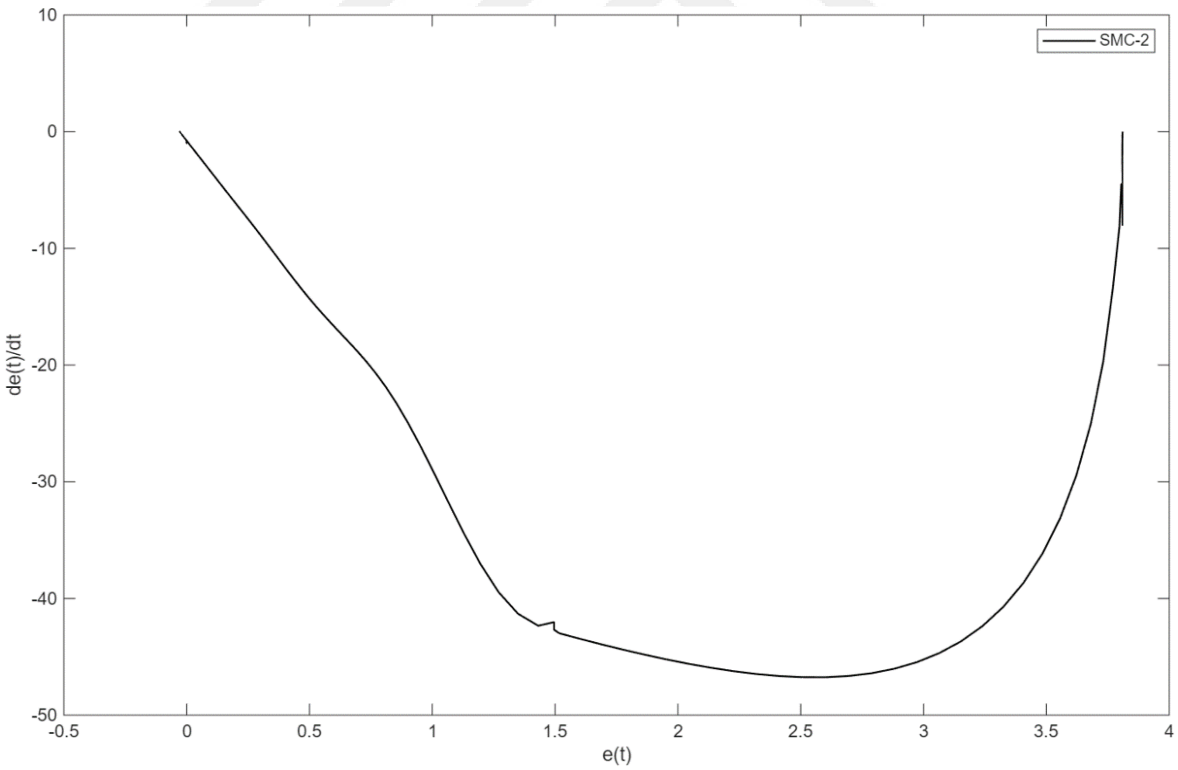

Figure 4.16. Phase plane of $e(t)$ and $de(t)/dt$ signal (SMC-2)

The time domain results, as outlined in Table 4.3, demonstrate a rise time of 0.0944 s, a settling time of 0.1744 s, an exceedingly minimal overshoot of 0.05%, and a delay time of 0.0540 s.

Moreover, the performance indices enumerated in Table 4.4, incorporating an ITAE of 0.04004, an ISE of 0.8056, and an ISTE of 0.0173, signify enhanced transient performance and diminished steady-state error in comparison to the single-loop SMC-1 controller. The findings indicate that the SMC-2 design attains smoother control actions, enhanced dynamic performance and superior robustness under varying operating conditions, thereby demonstrating clear superiority over the single-loop SMC-1 configuration.

Table 4.3. Time domain results (SMC-2)

Controller	Rise Time (s)	Settling time (s)	Overshoot (%)	Delay time (s)
SMC-2	0.0944	0.1744	0.05	0.0540

Table 4.4. Performance indices (SMC-2)

Controller	ITAE	ISE	IAE	ITSE	ISCI	ISTE
SMC-2	0.0400	0.805	0.3333	0.028	25.52	0.017

4.4. Simulation Results of Cascade Sliding Mode Controllers: (1) Outer-Loop SMC-1/Inner-Loop P (SMC-1/P), (2) Outer-Loop SMC-1/Inner-Loop PI (SMC-1/PI) and (3) Outer-Loop SMC-1/Inner-Loop PID (SMC-1/PID)

In this section, the simulation outcomes of the cascade control strategy are presented for the case where the outer-loop is controlled by SMC-1 and the inner-loop is regulated using three different classical controllers (P, PI and PID). The proportional controller in the inner-loop provides a simple but limited regulation capability; while the SMC-1 ensures robustness in the outer-loop, the lack of integral action results in a small but noticeable steady-state error and the system exhibits relatively fast dynamics with moderate oscillations near the settling period. When the inner-loop is equipped with a PI controller, the steady-state error is eliminated and the dynamic response is shown to improve in comparison to the P controller case, as the integral term complements the robustness of the SMC-1 outer-loop, thereby providing more accurate tracking. However, the presence of integral action has been demonstrated to slightly increase the settling time. The PID-controlled inner-loop serves to enhance the system by balancing proportional, integral, and derivative effects. The derivative action of the PID controller functions to suppress oscillations, whilst the integral term ensures that zero steady-state error is achieved. This results in a smoother response with less overshoot and faster stabilisation when compared to the PI configuration. Consequently, within the three cases, the SMC-1/PID combination provides the most effective control.

4.4.1. Cascade Sliding Mode Control: Outer-Loop SMC-1/Inner-Loop P (SMC-1/P)

This section presents and analyzes the simulation results of the cascade control structure, including the output speed signal (Figure 4.17), armature current signal (Figure 4.18), control input voltage (Figure 4.19), equivalent input (Figure 4.20), switching input (Figure 4.21), sliding surface

(Figure 4.22), phase plane of the sliding surface signal (Figure 4.23), speed error signal (Figure 4.24), and the phase plane of the error and its derivative (Figure 4.25). The outer SMC-1 controller is adjusted with the parameters $k_d = 0.4,\ k_p = 25,\ k_i = 5,\ k_s = 4.5,\ \Omega = 8$ while the inner-loop P controller is tuned with $k_p = 0.8$. The obtained voltage and current responses demonstrate that the SMC-1/P configuration provides rapid transient performance along with satisfactory steady-state accuracy. The control signal illustrates a balanced interaction between the robustness of the outer-loop SMC-1 and the fast response of the inner-loop P. As a result, overshoot and oscillations are significantly reduced and the chattering effect, typically observed in SMC, is mitigated.

The tracking error and its derivative indicate accurate reference following, confirming stable system behavior and enhanced disturbance rejection capability. Moreover, the sliding surface and its derivative show that the trajectory of the system remains close to the designed sliding manifold, validating the effectiveness of the proposed control strategy.

Overall, the simulation outcomes verify that the SMC-1/P cascade controller achieves superior performance compared to a standalone proportional controller, as it successfully merges the resilience of SMC with the simplicity and fast dynamics of proportional action.

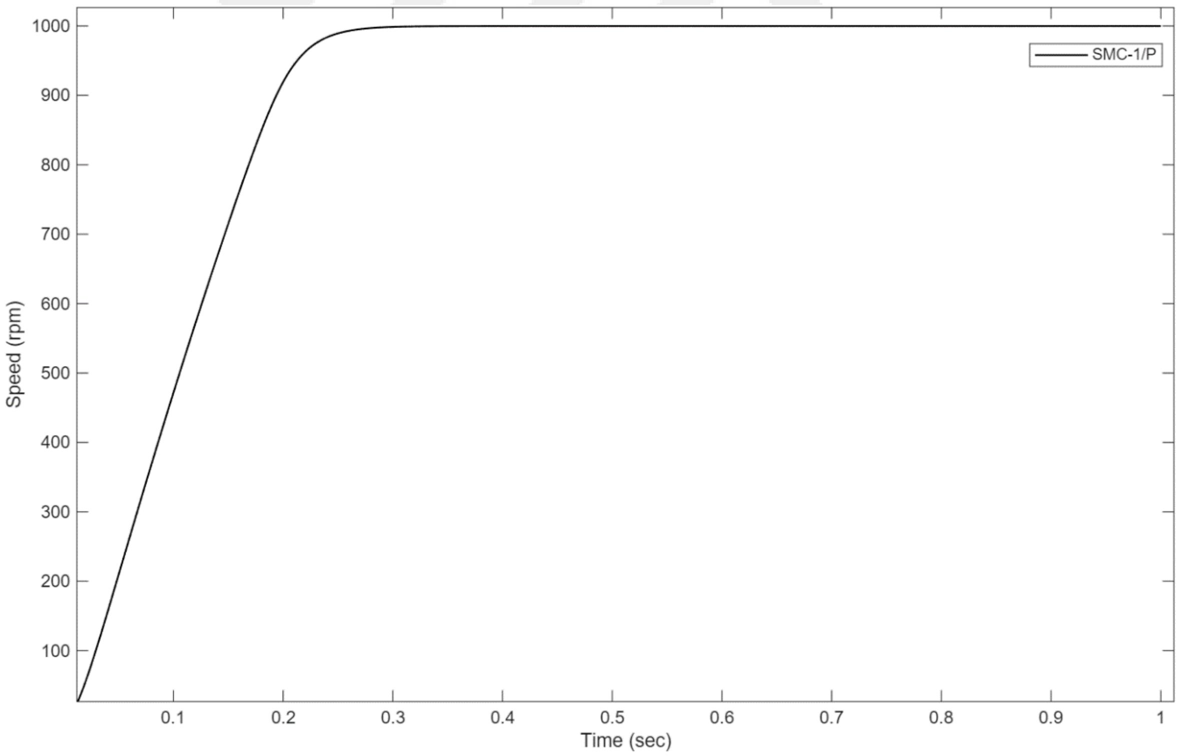

Figure 4.17. Output speed signal (rpm) (SMC-1/P)

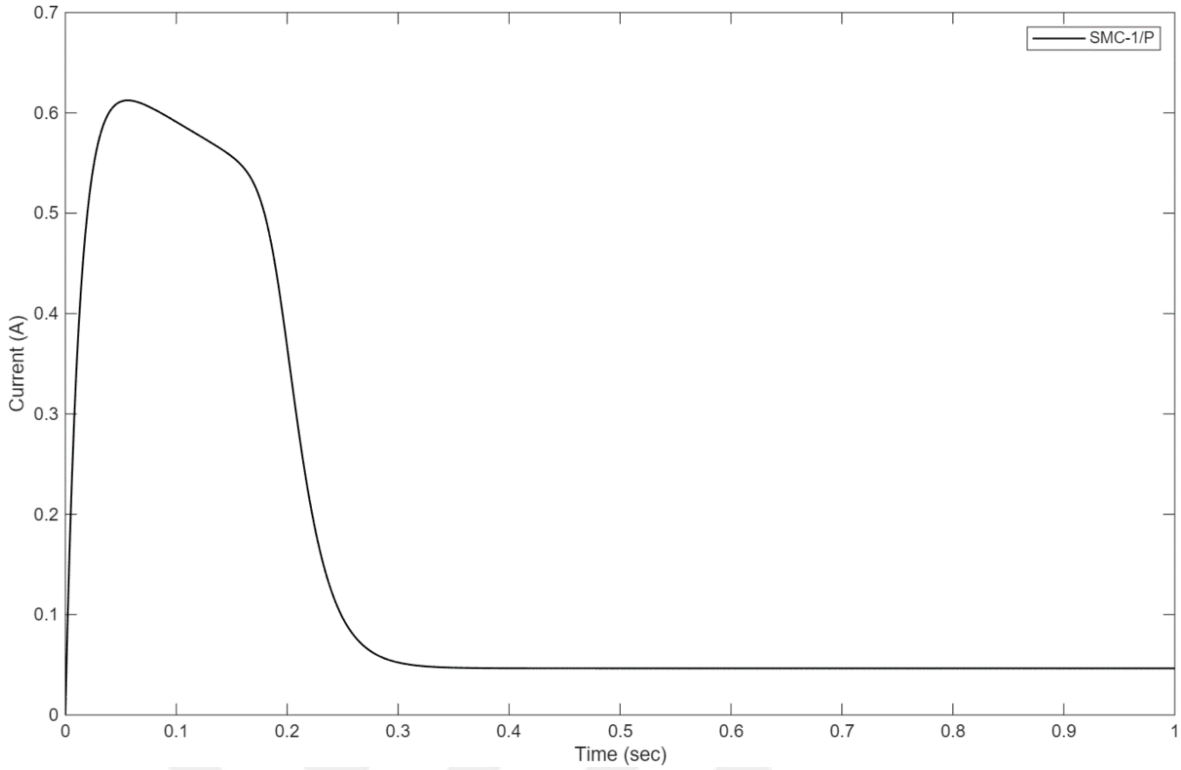

Figure 4.18. Armature current signal, $i_a(t)$ (SMC-1/P)

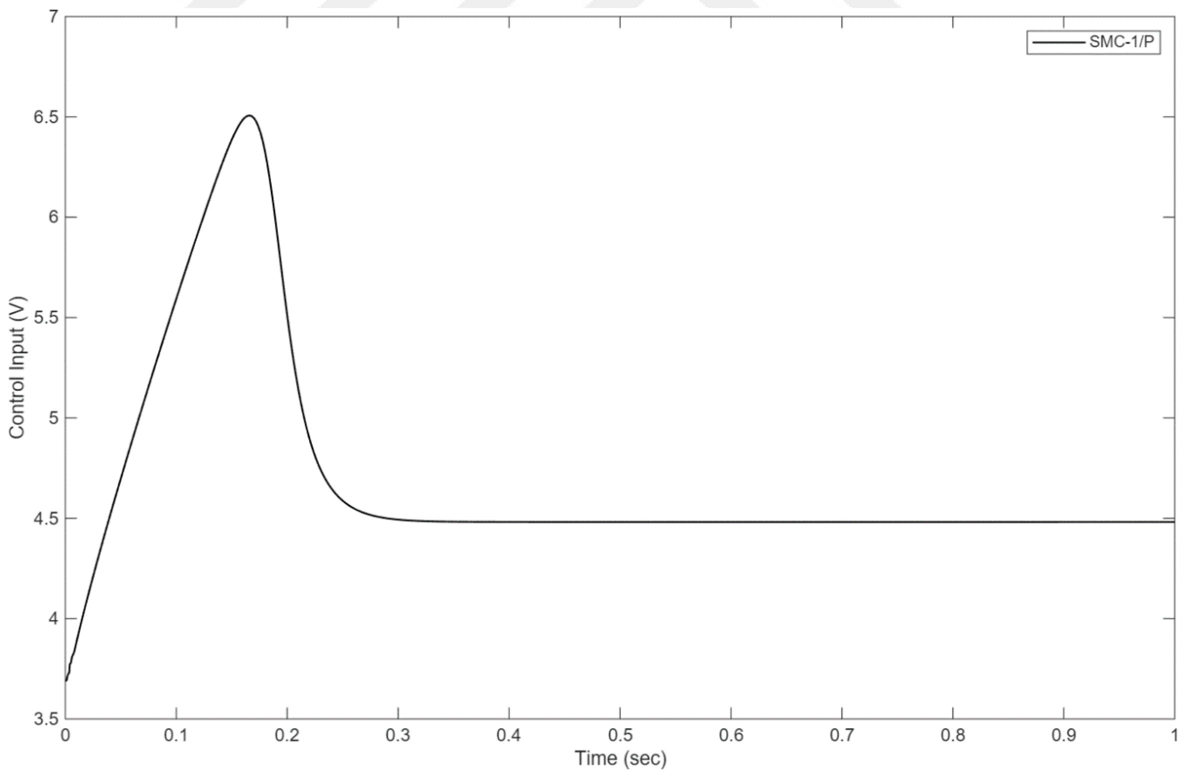

Figure 4.19. Control input voltage signal, $u(t)$ (SMC-1/P)

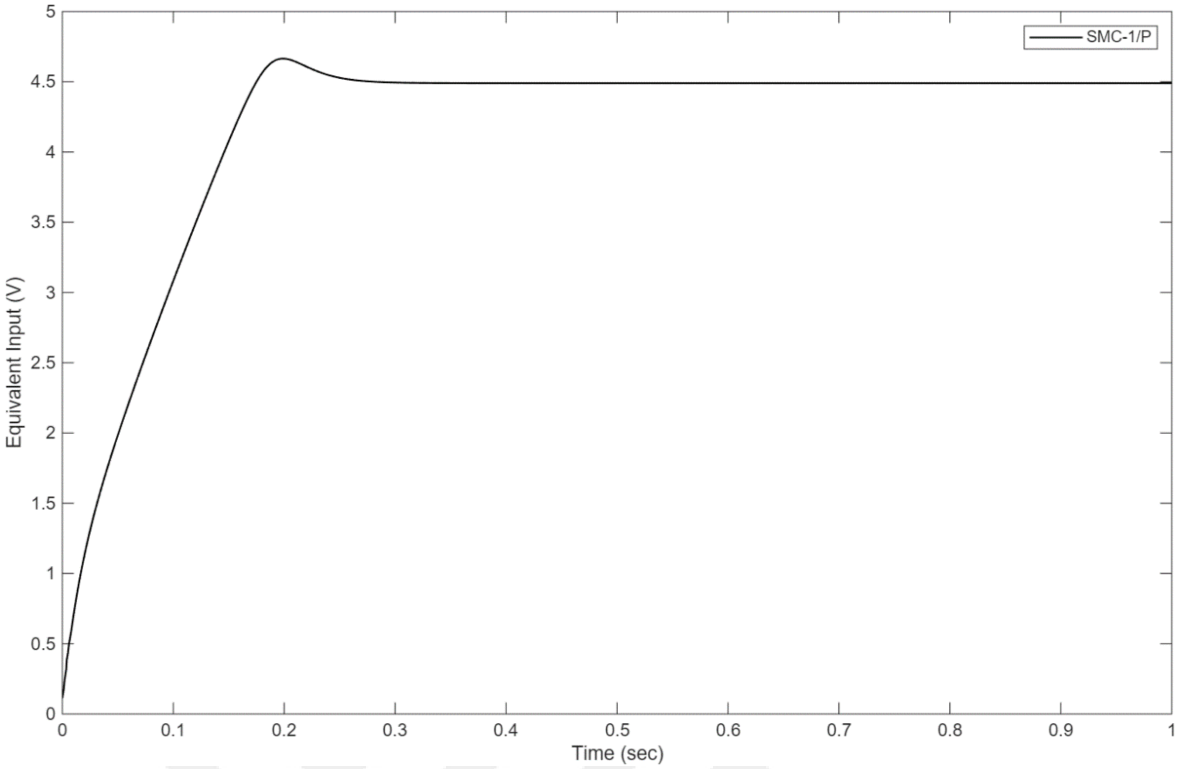

Figure 4.20. Equivalent input signal, $u_{eq}(t)$ (SMC-1/P)

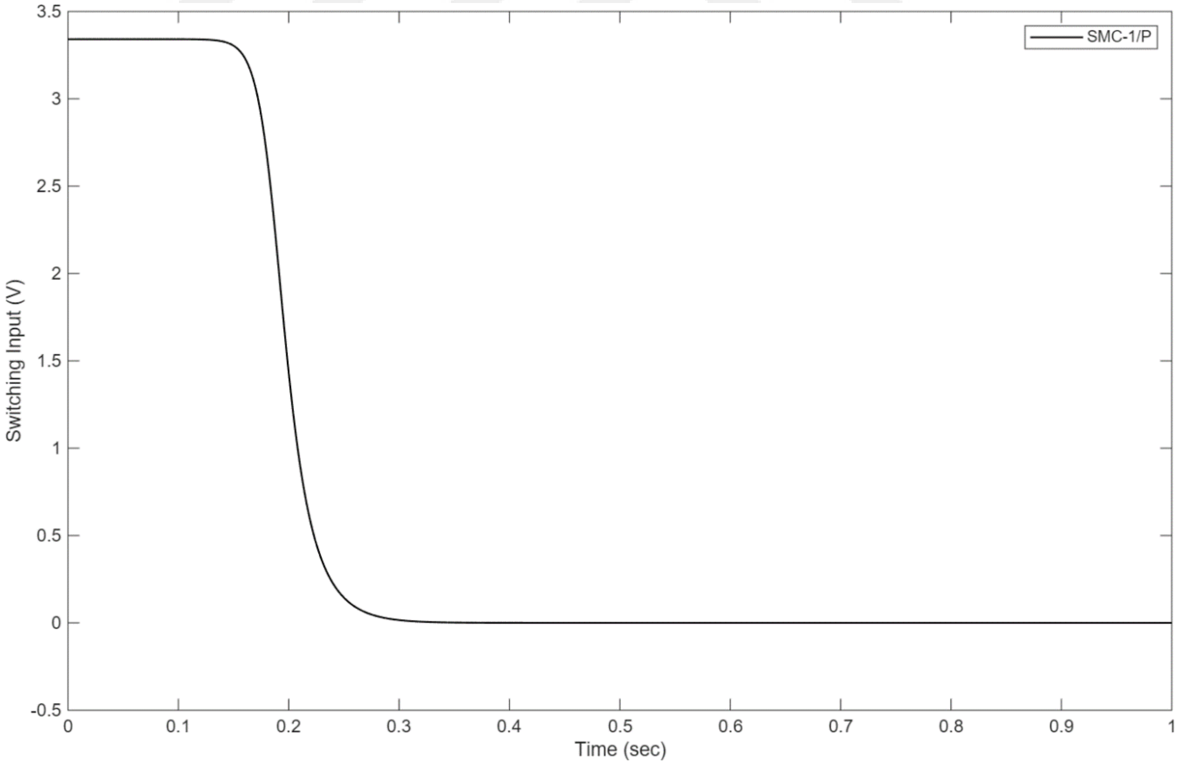

Figure 4.21. Switching input signal, $u_{sw}(t)$ (SMC-1/P)

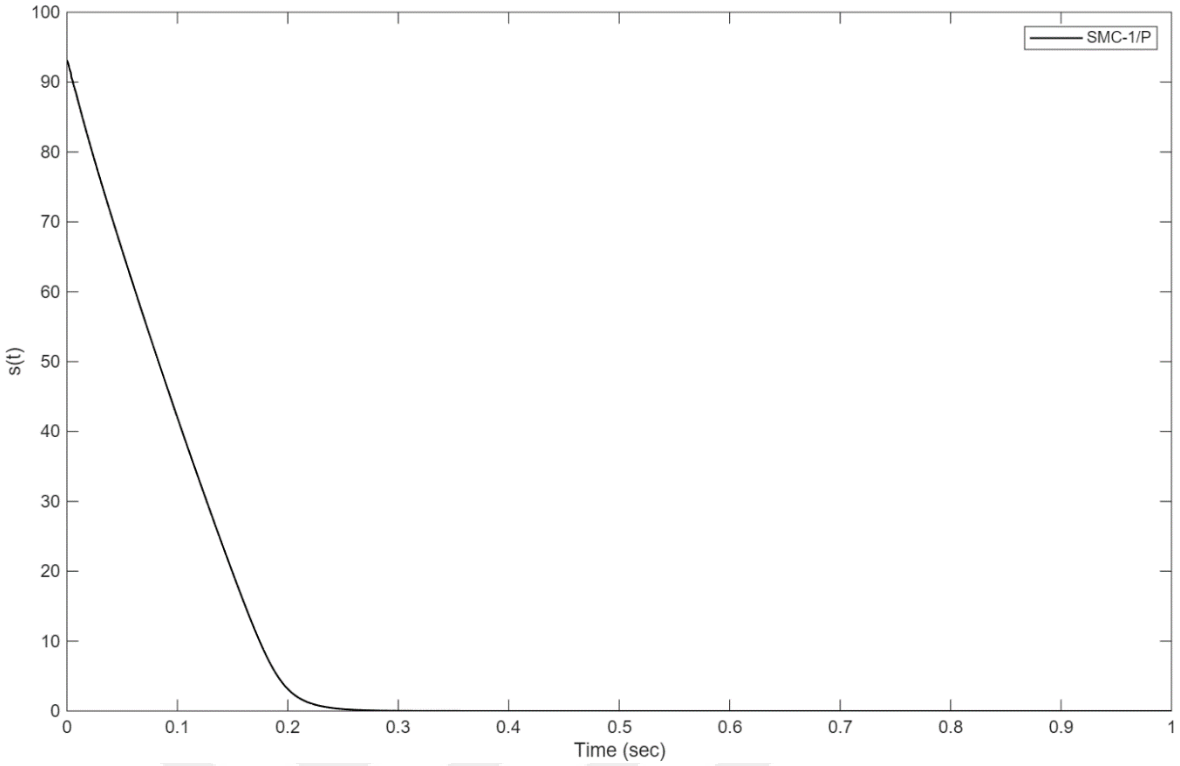

Figure 4.22. Sliding surface signal, $s(t)$ (SMC-1/P)

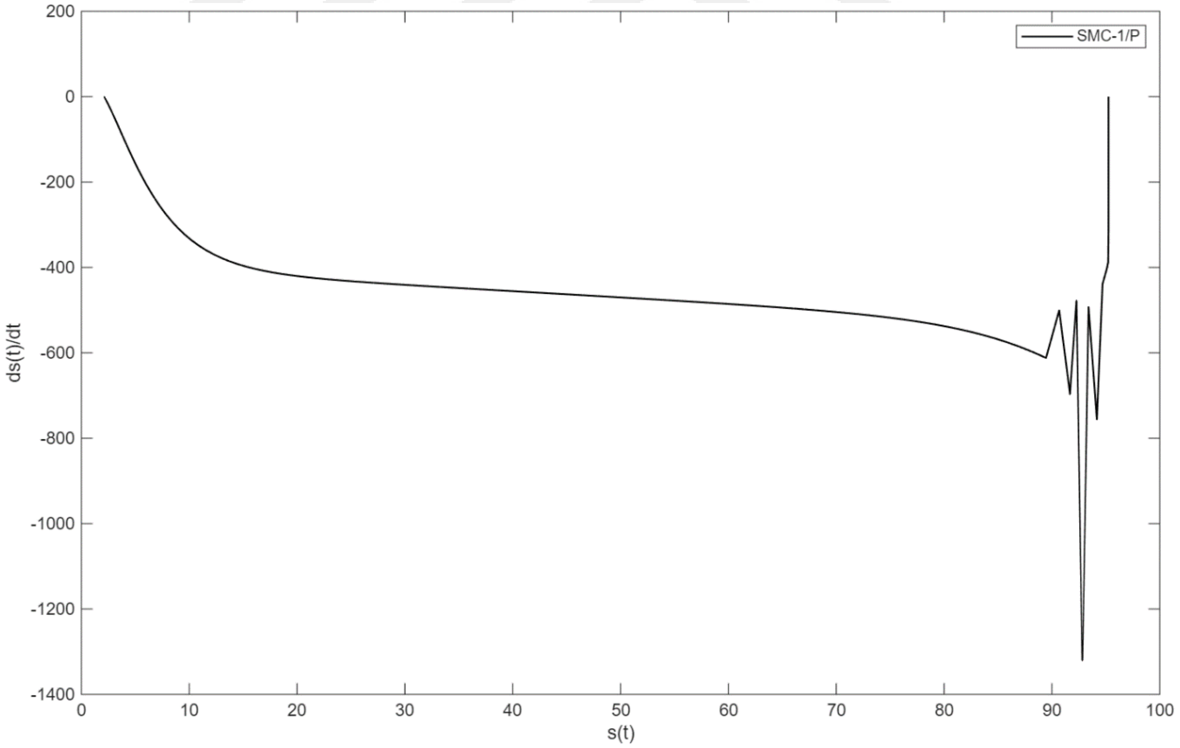

Figure 4.23. Phase plane of $s(t)$ and $ds(t)/dt$ signal (SMC-1/P)

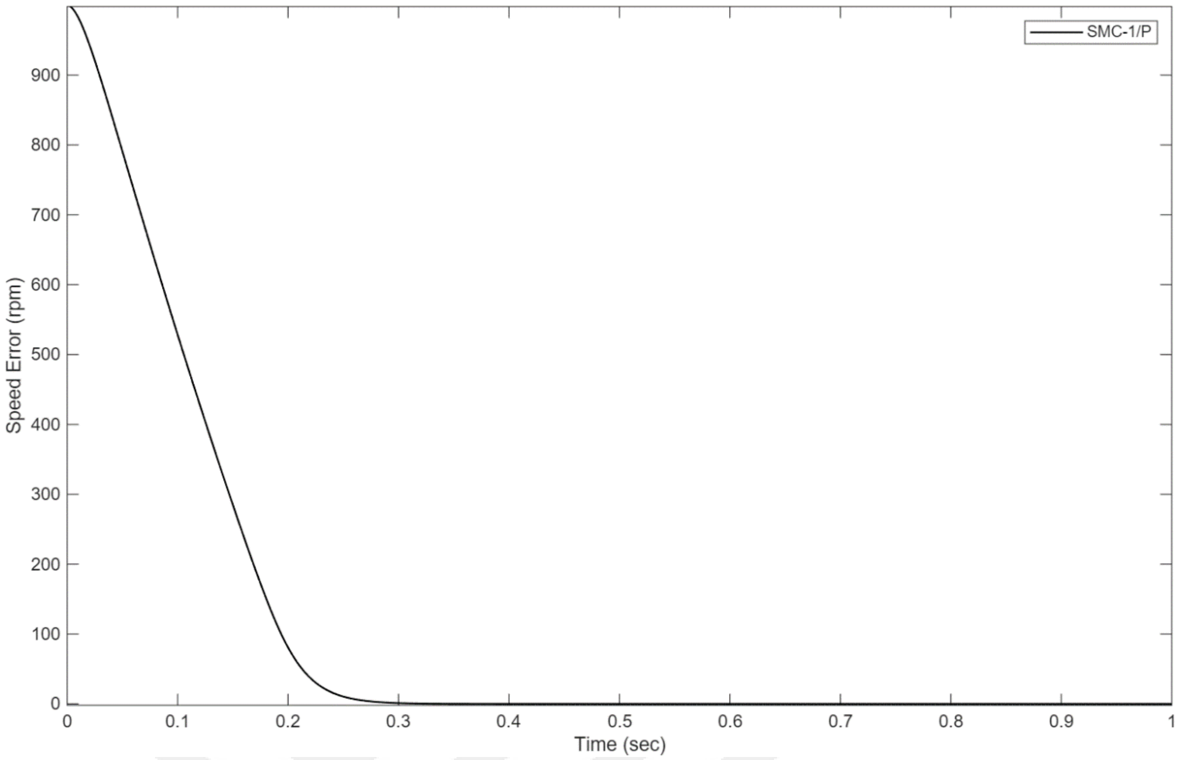

Figure 4.24. Speed error signal (rpm) (SMC-1/P)

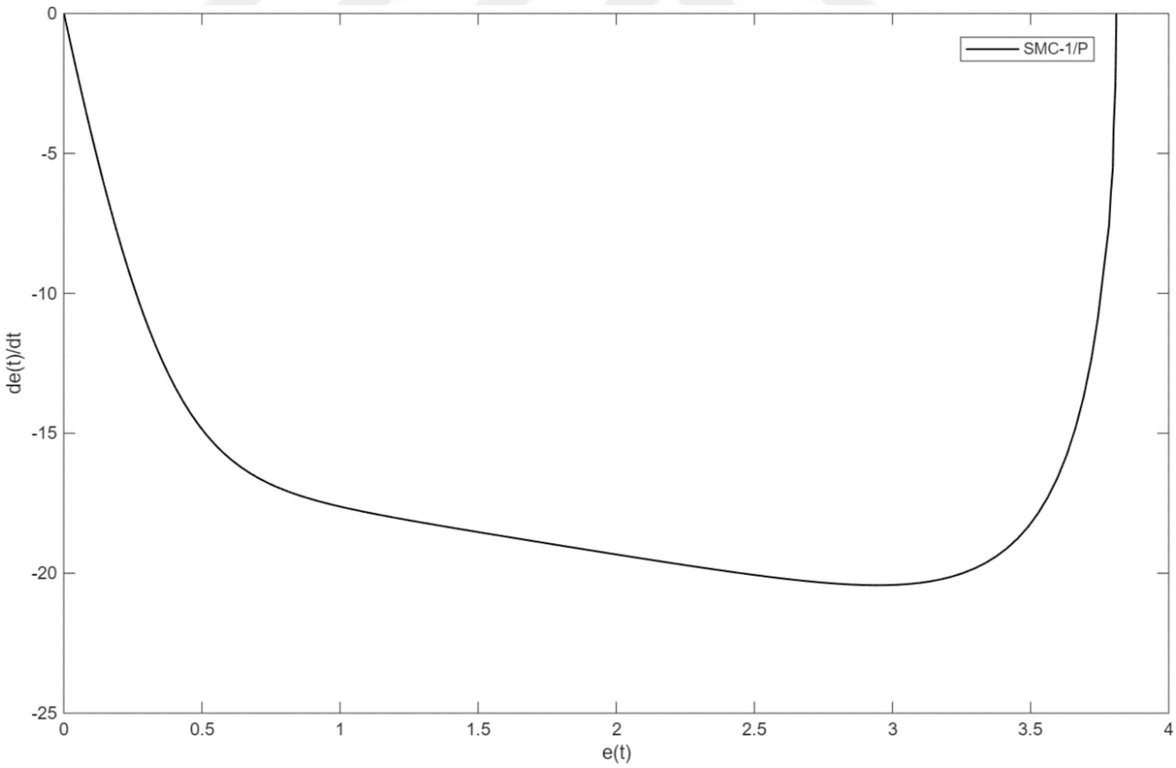

Figure 4.25. Phase plane of $e(t)$ and $de(t)/dt$ signal (SMC-1/P)

As presented in Table 4.5, the cascade SMC-1/P controller results in a rise time of 0.1645 s and a settling time of 0.2350 s, indicating a slower transient response compared to single-loop configurations. However, the controller achieves 0% overshoot, which confirms that the system exhibits fully stable behavior by eliminating oscillations. The delay time of 0.106 s also suggests that the cascade structure introduces an additional response delay in the control process. According to the performance indices in Table 4.6, relatively low error values such as ITAE = 0.0305 and IAE = 0.4184 are achieved, which indicates that both the magnitude of the error and its time-weighted impact are effectively reduced. Moreover, the ISTE value of 0.003 highlights the ability of the controller to minimize long-term error components. On the other hand, the relatively higher values of ISE = 1.077 and ITSE = 0.056 imply that the squared error measures are not reduced to the same extent. In summary, the cascade SMC-1/P controller provides a highly stable system response by eliminating overshoot while balancing error performance at the cost of a slower response time.

Table 4.5. Time domain results (SMC-1/P)

Controller	Rise Time (s)	Settling time (s)	Overshoot (%)	Delay time (s)
Cascade Outer-Loop SMC-1/Inner-Loop P	0.1645	0.2350	0	0.1060

Table 4.6. Performance indices (SMC-1/P)

Controller	ITAE	ISE	IAE	ITSE	ISCI	ISTE
Cascade Outer-Loop SMC-1/ Inner-Loop P	0.0305	1.077	0.4184	0.056	22.27	0.003

4.4.2. Cascade Sliding Mode Control: Outer-Loop SMC-1/Inner-Loop PI (SMC-1/PI)

This subsection presents and analyzes the simulation results of the cascade configuration where the outer-loop employs an SMC-1 controller and the inner-loop is regulated by a PI controller, including the output speed signal (Figure 4.26), armature current signal (Figure 4.27), control input voltage signal (Figure 4.28), equivalent input signal (Figure 4.29), switching input signal (Figure 4.30), sliding surface signal (Figure 4.31), speed error signal (Figure 4.32), and the phase plane of the error and its derivative (Figure 4.33). The outer-loop controller is designed with the parameters $k_d = 0.3,\ k_p = 10,\ k_i = 0.5,\ k_s = 5,\ \Omega = 3$, while the inner-loop PI controller is tuned with PI $= 0.85\left(1 + \frac{1}{8.5s}\right)$. The voltage and current responses indicate that the SMC-1/PI cascade control structure ensures faster convergence with smoother transient dynamics compared to the SMC-1/P configuration. The inclusion of the integral action in the inner-loop enhances steady-state accuracy, effectively eliminating residual steady-state errors. The interaction between the outer sliding mode loop and the inner-loop PI controller contributes to improved robustness against disturbances while maintaining good dynamic performance.

The error signal and its derivative demonstrate precise reference tracking. Additionally, the sliding surface plots confirm that the system trajectory remains consistently close to the designed manifold, signifying strong stability and reliable convergence.

In conclusion, the simulation outcomes confirm that the SMC-1/PI hybrid structure provides a more refined performance than both the single PI controller and the SMC-1/P configuration. By combining the robustness of SMC with the steady-state accuracy of the PI regulator, the cascade system achieves a balanced and efficient control strategy.

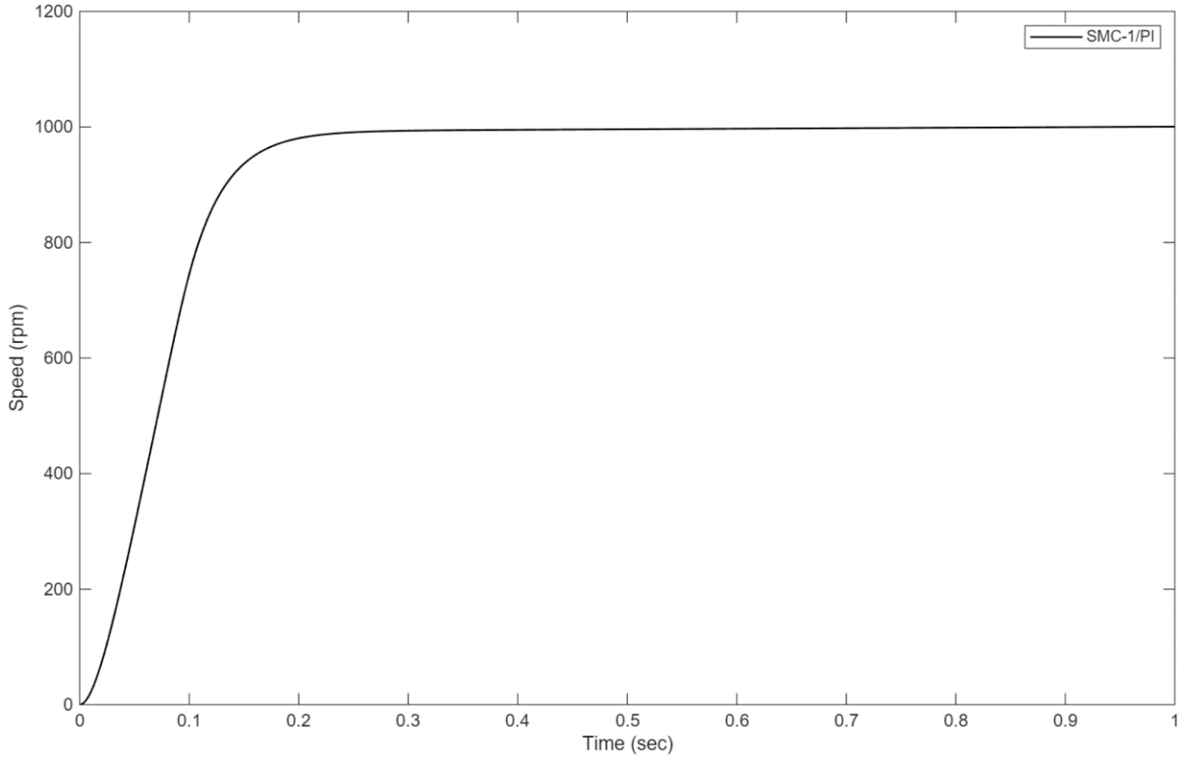

Figure 4.26. Output speed signal (rpm) (SMC-1/PI)

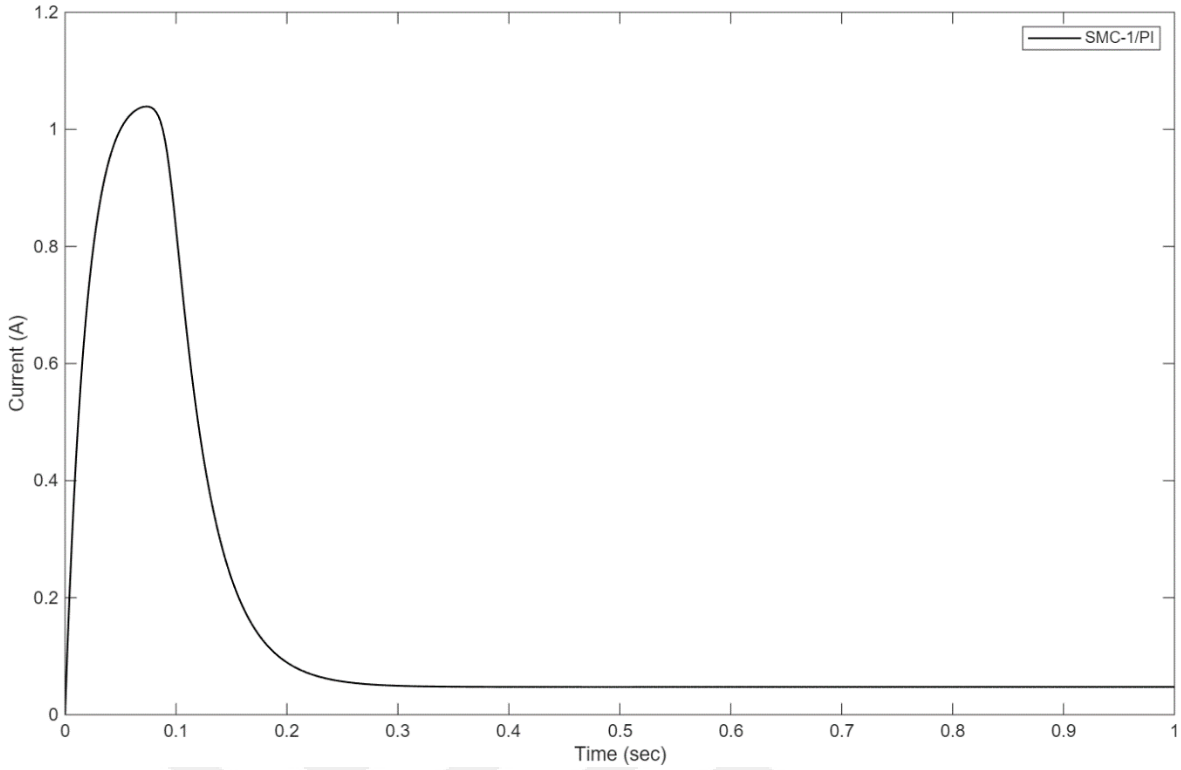

Figure 4.27. Armature current signal, $i_a(t)$ (SMC-1/PI)

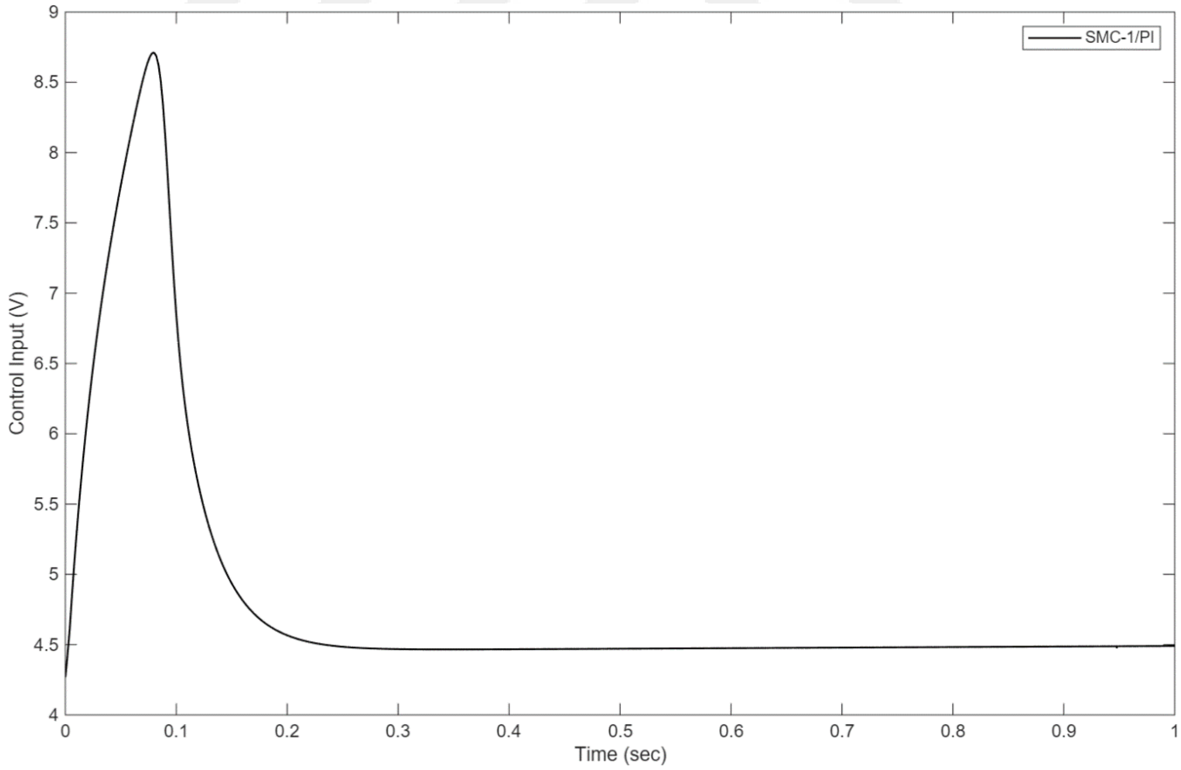

Figure 4.28. Control input voltage signal, $u(t)$ (SMC-1/PI)

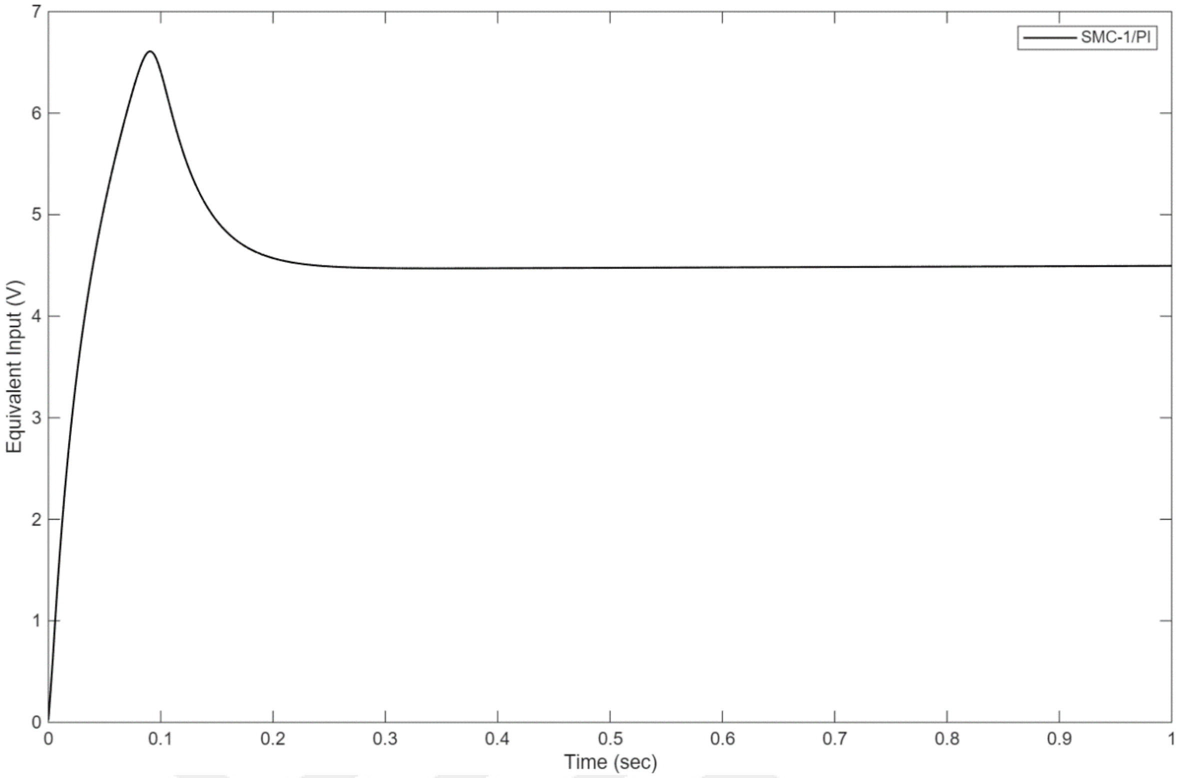

Figure 4.29. Equivalent input signal, $u_{eq}(t)$ (SMC-1/PI)

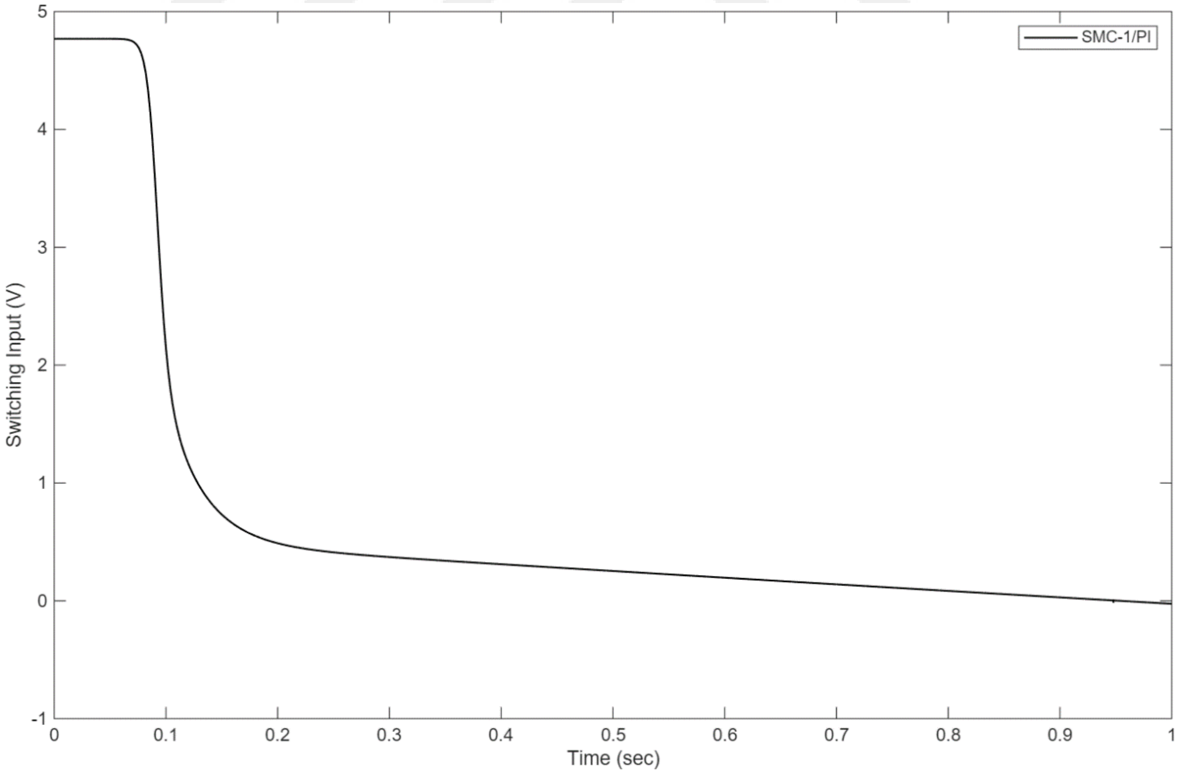

Figure 4.30. Switching input signal, $u_{sw}(t)$ (SMC-1/PI)

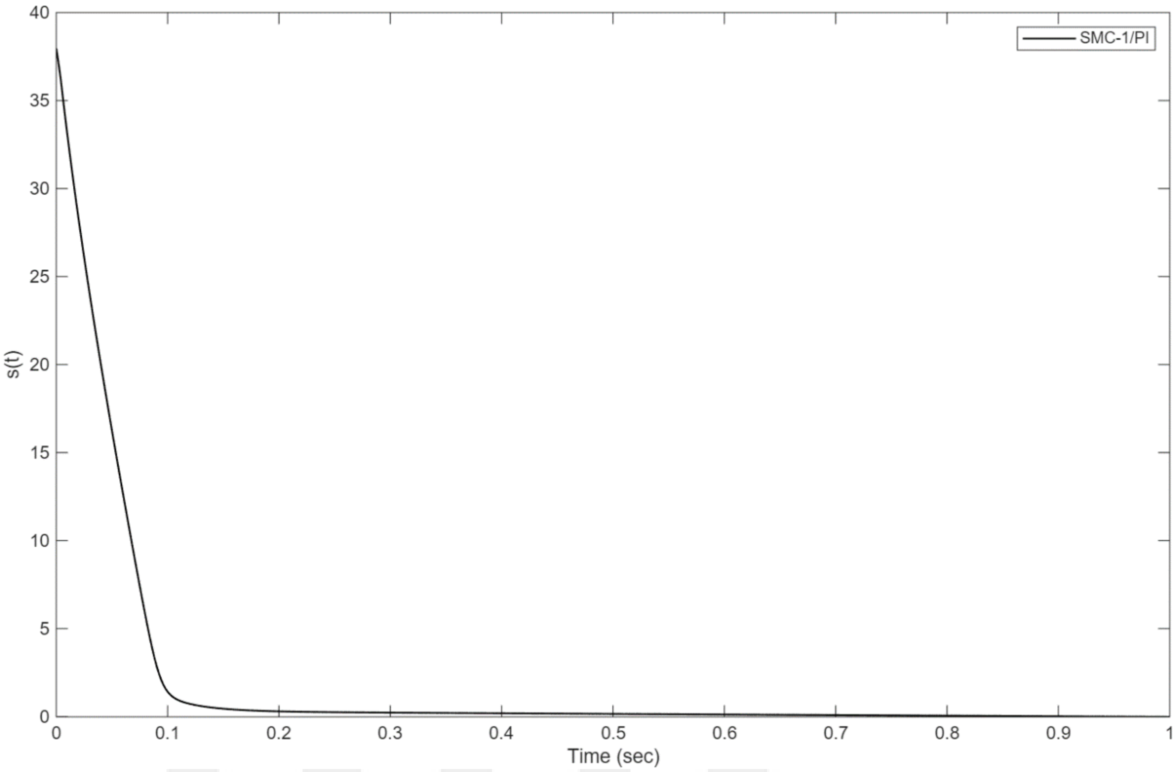

Figure 4.31. Sliding surface signal, $s(t)$ (SMC-1/PI)

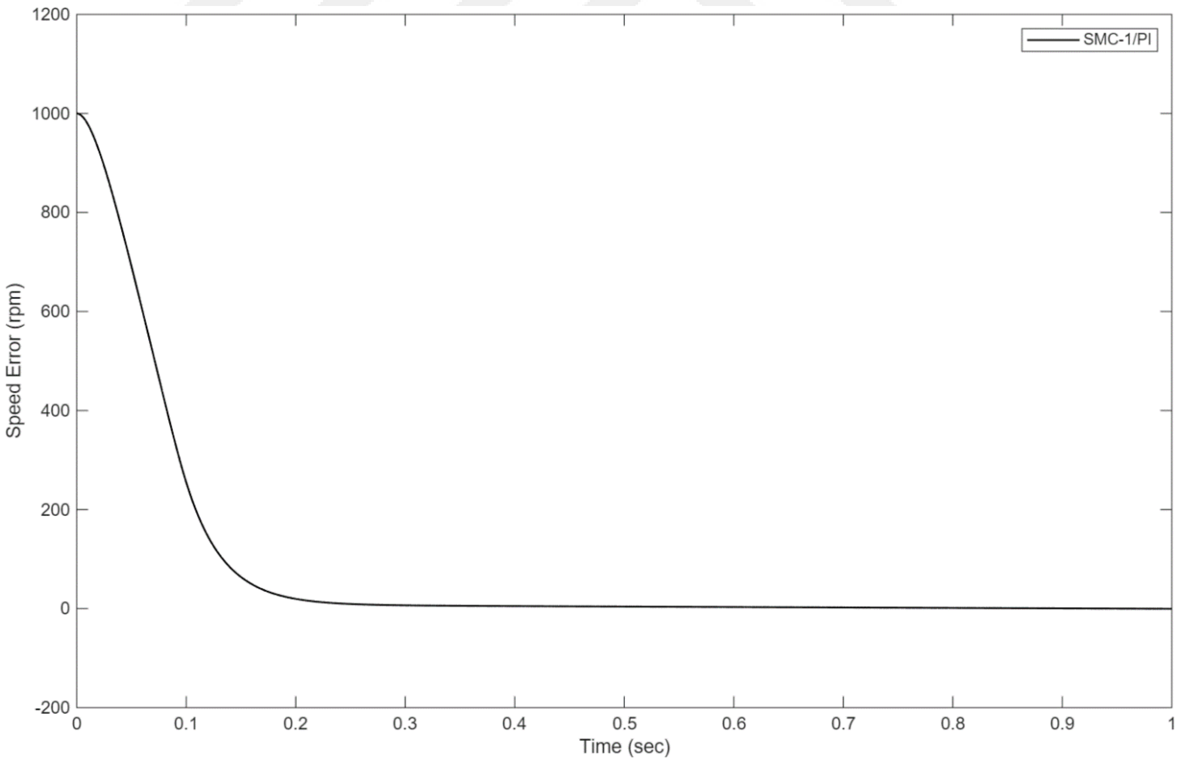

Figure 4.32. Speed error signal (rpm) (SMC-1/PI)

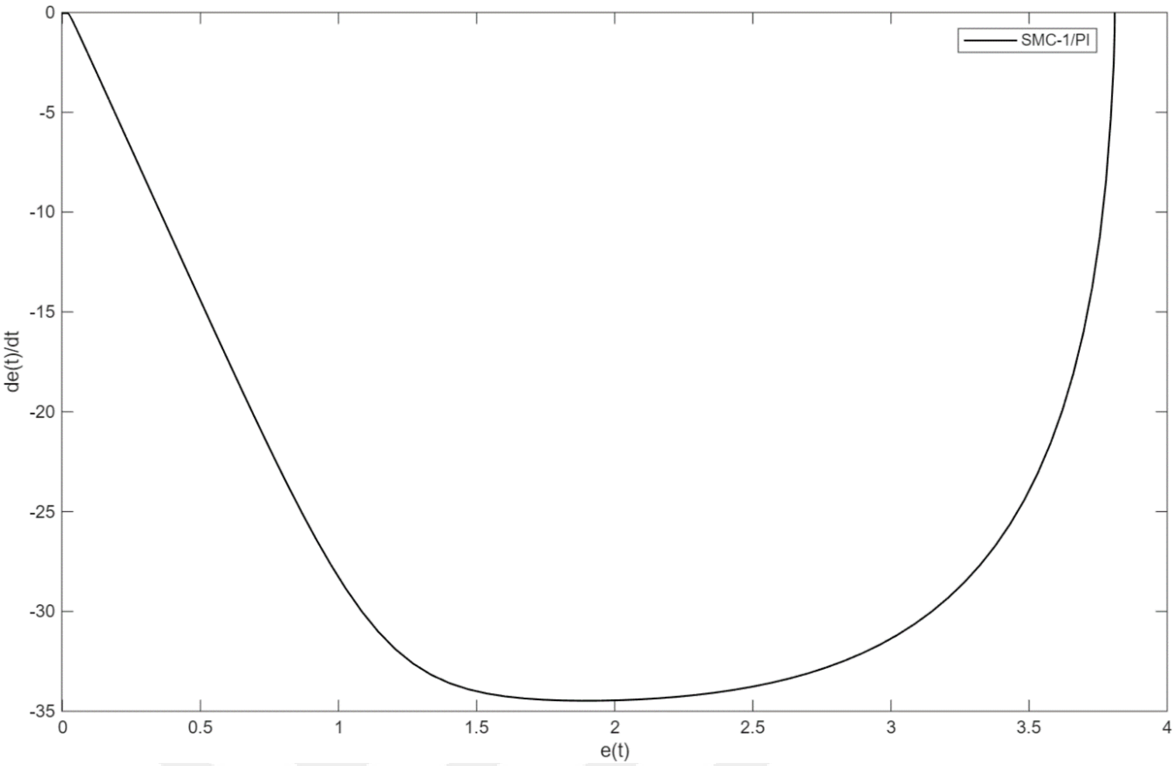

Figure 4.33. Phase plane of $e(t)$ and $de(t)/dt$ signal (SMC-1/PI)

As shown in Table 4.7, the cascade SMC-1/PI controller achieves a rise time of 0.1094 s and a settling time of 0.2002 s, providing a faster transient performance compared to several single-loop configurations. The controller also ensures 0% overshoot, which indicates that the system operates in a highly stable manner with oscillations eliminated. Furthermore, the delay time of 0.072 s demonstrates that the system responds promptly to input changes. From the performance indices in Table 4.8, it can be observed that the controller achieves relatively low values such as ITAE = 0.0192, IAE = 0.3008 and ISTE = 0.003 confirming its effectiveness in minimizing both the magnitude of errors and their long-term impact. However, the relatively higher values of ISE = 0.7546 and particularly ITSE = 0.2609 suggest that improvements in squared error–based measures are more limited. Overall, the cascade SMC-1/PI structure provides a stable and overshoot-free transient response while significantly reducing error indices, thereby enhancing the overall control performance.

Table 4.7. Time domain results (SMC-1/PI)

Controller	Rise Time (s)	Settling time (s)	Overshoot (%)	Delay time (s)
Cascade Outer-Loop SMC-1/Inner-Loop PI	0.1094	0.2002	0	0.0720

Table 4.8. Performance indices (SMC-1/PI)

Controller	ITAE	ISE	IAE	ITSE	ISCI	ISTE
Cascade Outer-Loop SMC-1/Inner-Loop PI	0.0192	0.7546	0.3008	0.2609	24.2	0.003

4.4.3. Cascade Sliding Mode Control: Outer-Loop SMC-1 /Inner-Loop PID (SMC-1/PID)

This subsection presents and analyzes the simulation results of the cascade structure composed of an outer-loop SMC-1 controller and an inner-loop PID controller, including the output speed signal (Figure 4.34), armature current signal (Figure 4.35), control input voltage signal (Figure 4.36), equivalent input signal (Figure 4.37), switching input signal (Figure 4.38), sliding surface signal (Figure 4.39), speed error signal (Figure 4.40), and the phase plane of the error and its derivative (Figure 4.41). The outer-loop parameters are selected as $k_d = 1.1,\ k_p = 65,\ k_i = 4,$ $k_s = 5,\ \ \Omega = 8.1$. The inner-loop PID controller is tuned with proportional, integral and derivative gains of PID = $3\left(1 + \frac{1}{6s} + 0.0033s\right)$, respectively. The results indicate that the SMC-1/PID structure enhances both transient and steady-state responses compared to SMC-1/P and SMC-1/PI controllers. The derivative term in the inner-loop accelerates the system's reaction to sudden changes, while the integral action effectively eliminates steady-state errors. This synergy leads to faster settling times, reduced oscillations and improved overall system accuracy.

The error plots, along with their derivatives, confirm that the reference signal is tracked with high precision. Furthermore, the sliding surface trajectories show that the system remains consistently close to the desired manifold, highlighting both stability and robustness against disturbances.

Overall, the simulation results validate that the SMC-1/PID hybrid controller provides a more comprehensive control performance, combining the robustness of sliding mode with the dynamic adaptability of the PID structure. This makes the approach more versatile and reliable for systems where both fast response and long-term accuracy are critical.

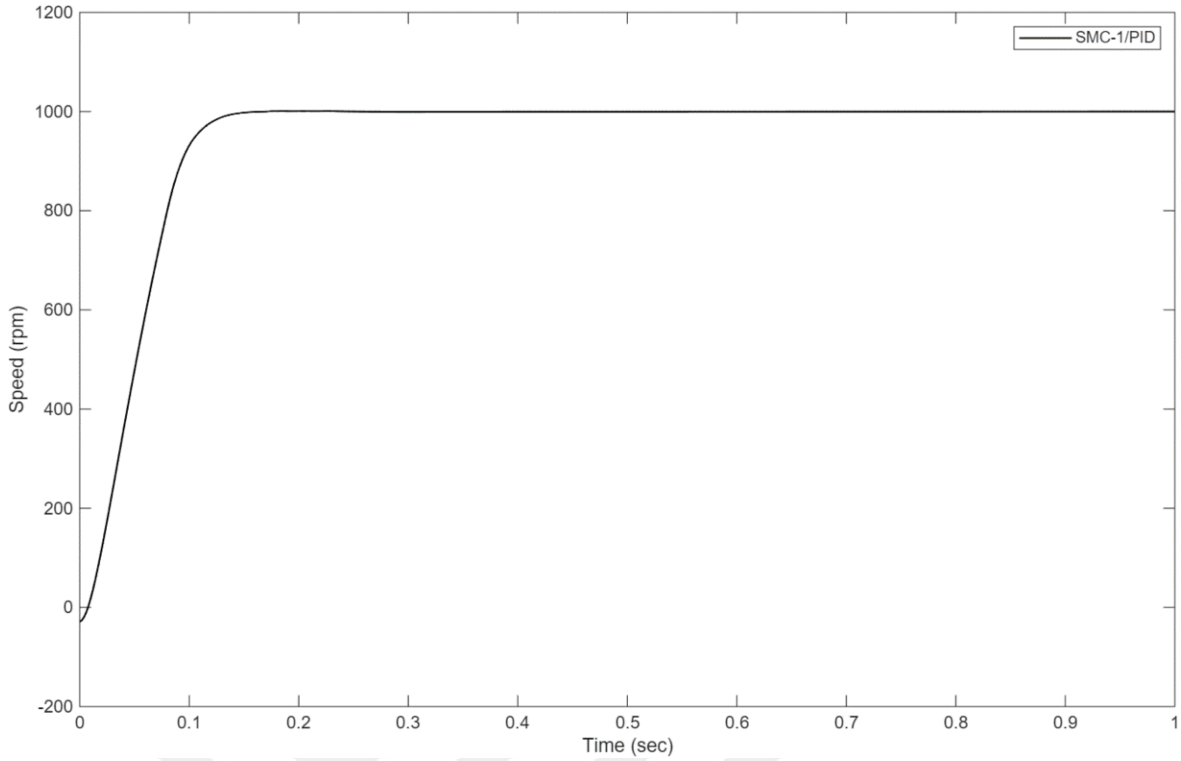

Figure 4.34. Output speed signal (rpm) (SMC-1/PID)

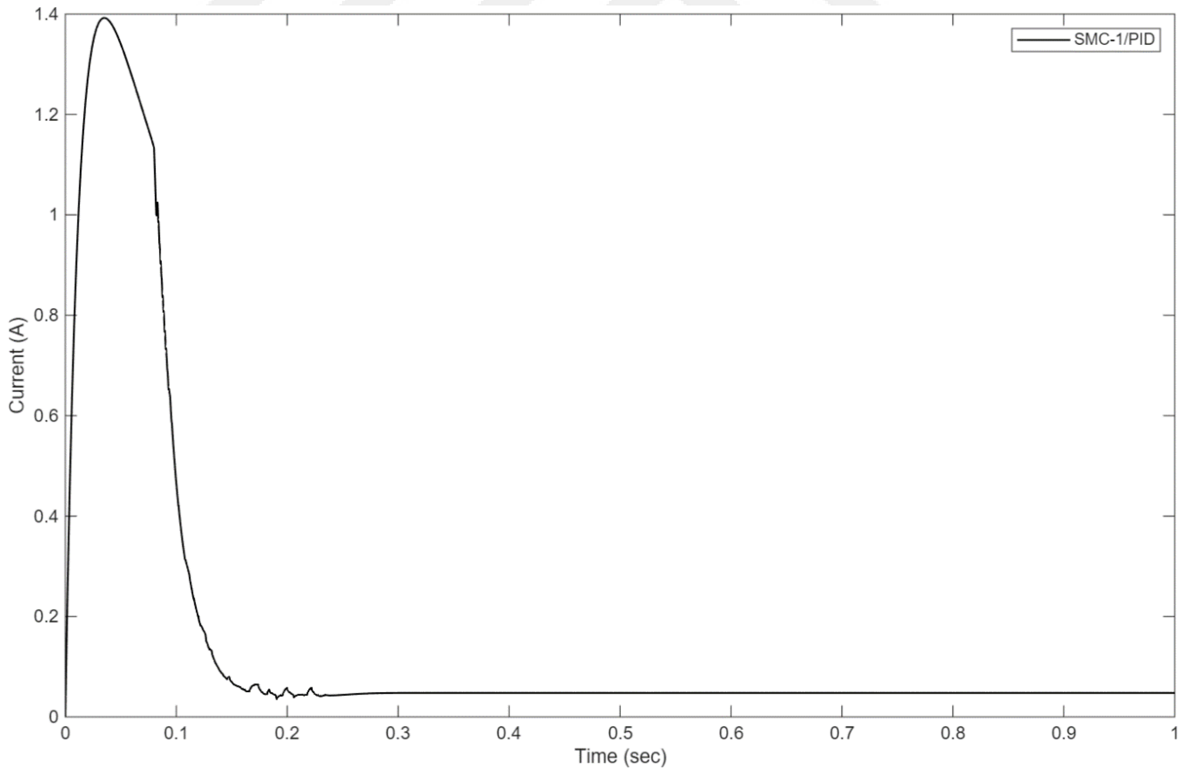

Figure 4.35. Armature current signal, $i_a(t)$ (SMC-1/PID)

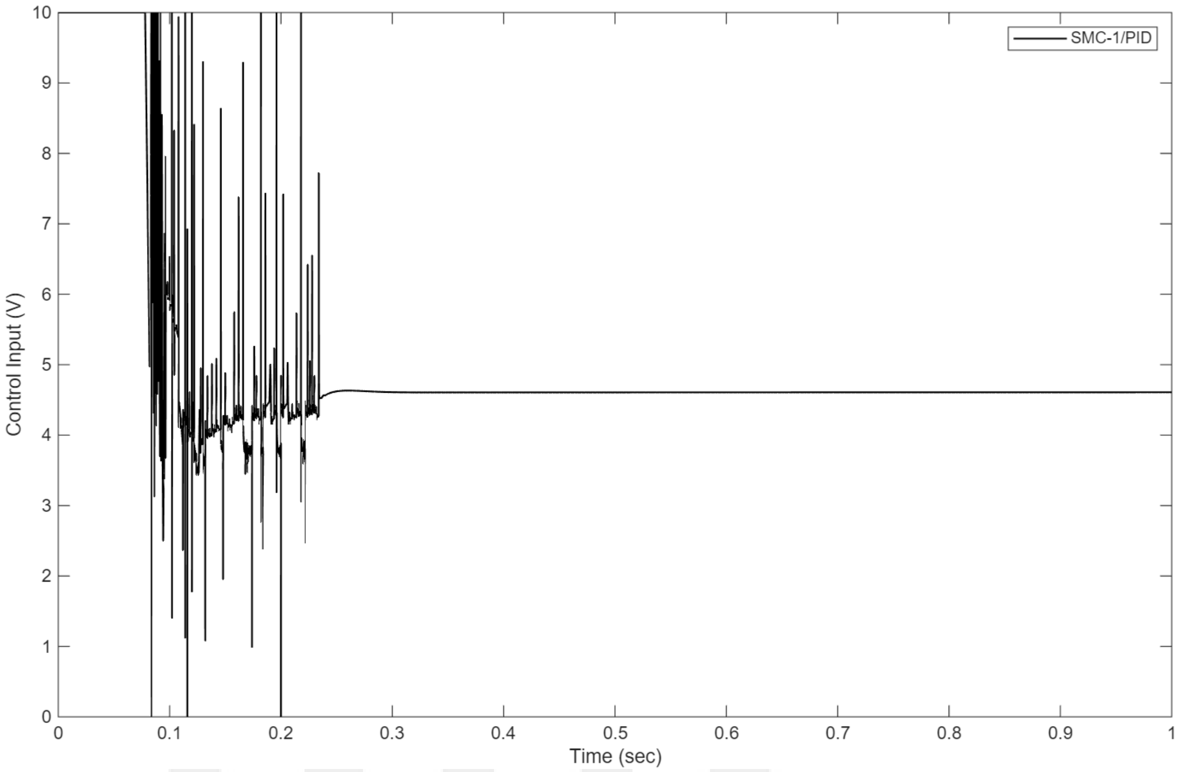

Figure 4.36. Control input voltage signal, $u(t)$ (SMC-1/PID)

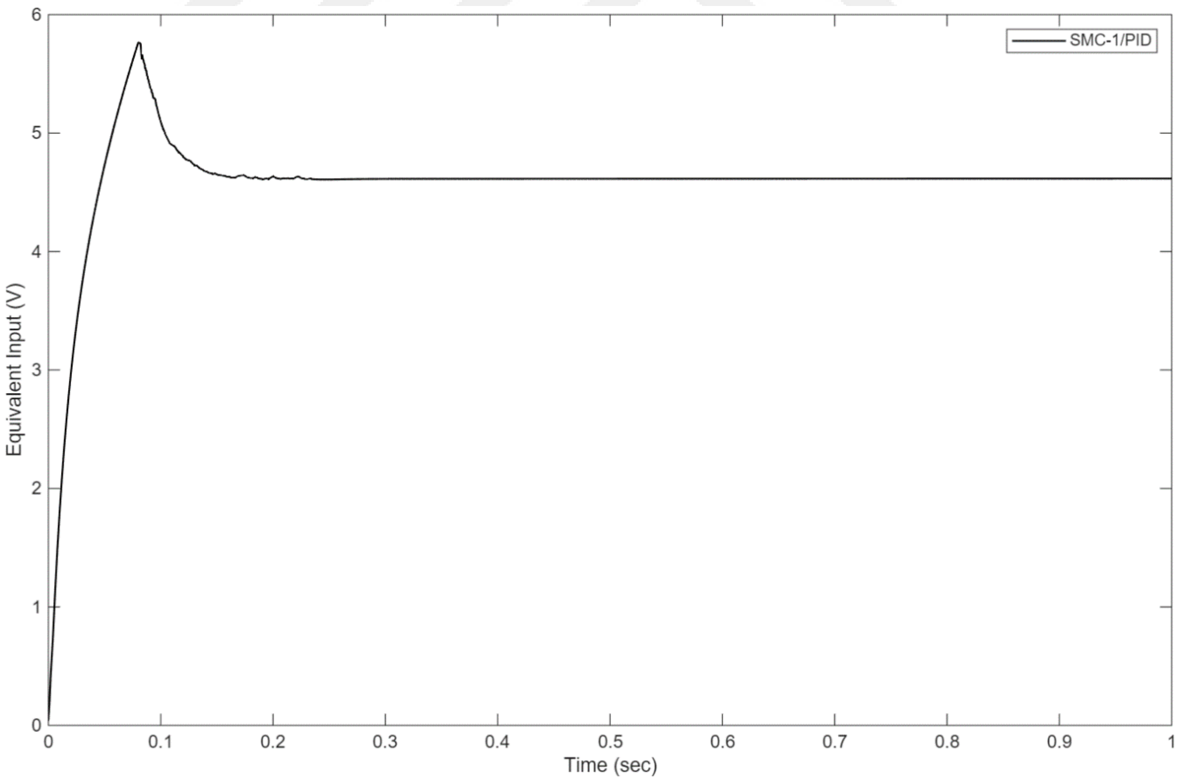

Figure 4.37. Equivalent input signal, $u_{eq}(t)$ (SMC-1/PID)

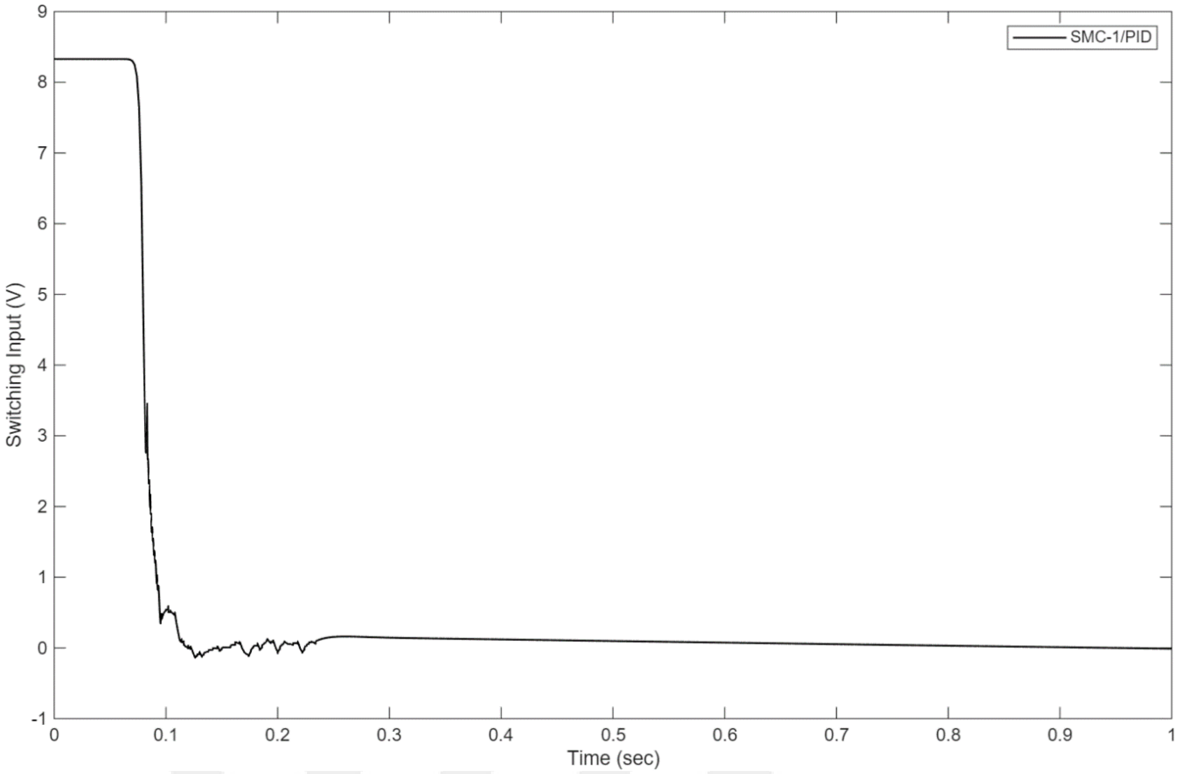

Figure 4.38. Switching input signal, $u_{sw}(t)$ (SMC-1/PID)

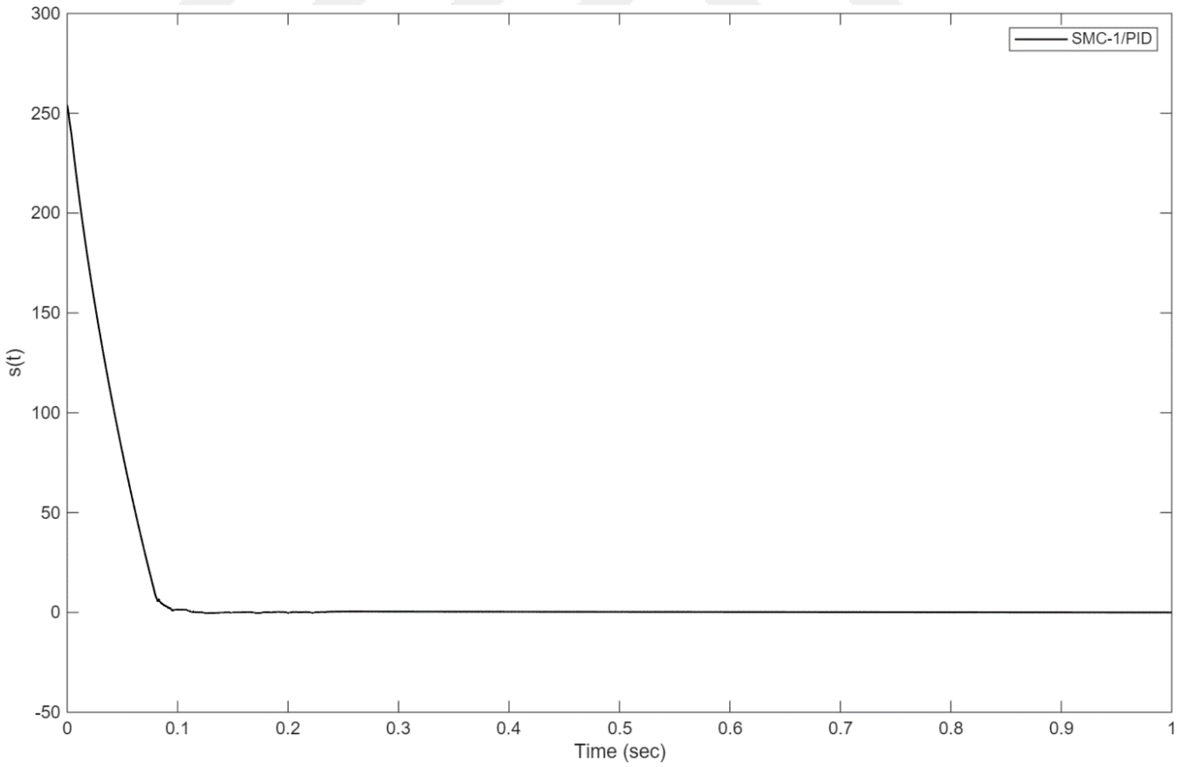

Figure 4.39. Sliding surface signal, $s(t)$ (SMC-1/PID)

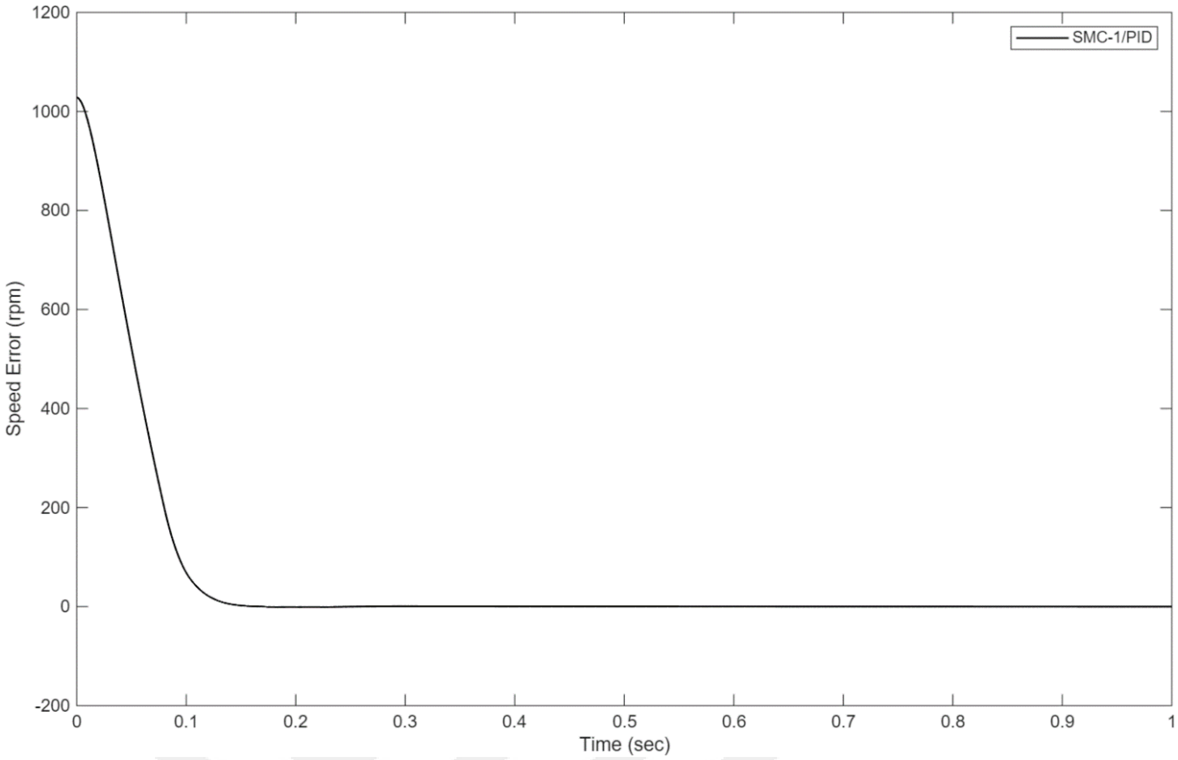

Figure 4.40. Speed error signal (rpm) (SMC-1/PID)

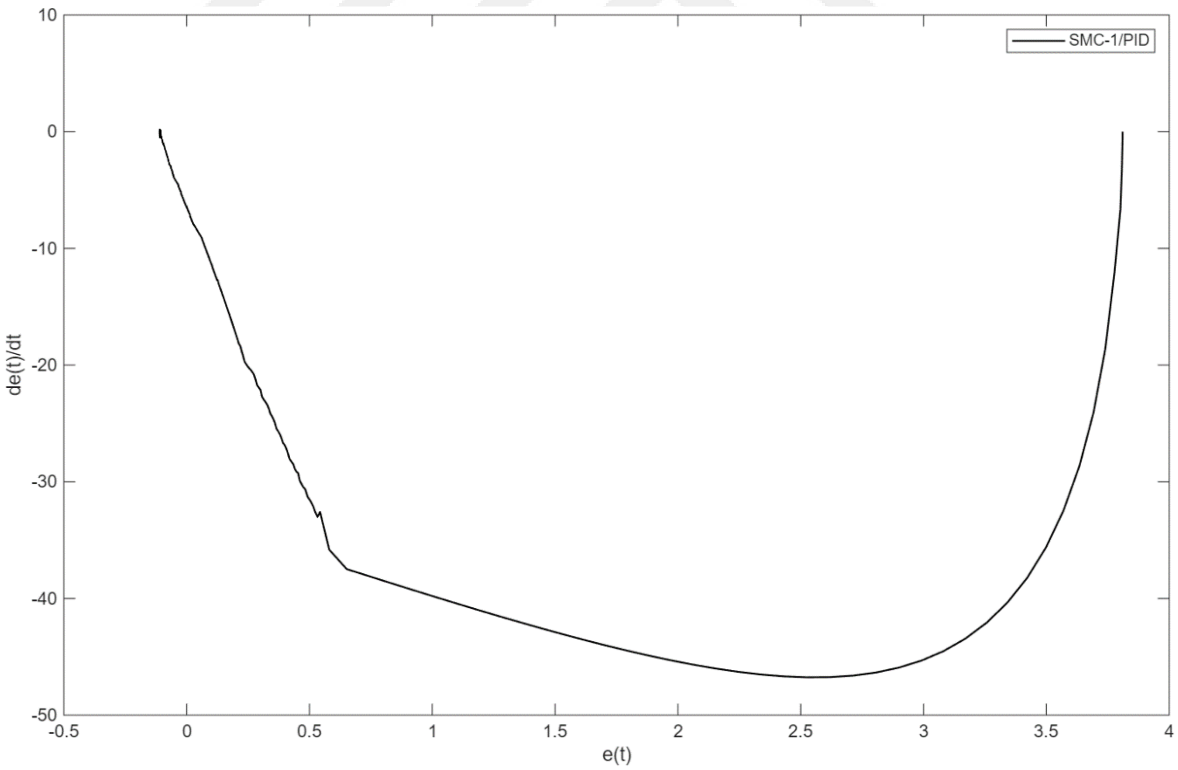

Figure 4.41. Phase plane of $e(t)$ and $de(t)/dt$ signal (SMC-1/PID)

According to the time domain results data presented in Table 4.9, the cascade SMC-1/PID controller exhibits a fast and stable transient response. The rise time is measured at 0.0766 s, the settling time at 0.1209 s, while the system delay is 0.0520 s and the overshoot is minimal at only 0.09%. These results indicate that the control structure provides a prompt response while effectively suppressing oscillations. From the performance indices listed in Table 4.10, the controller demonstrates its effectiveness in limiting error magnitude and time-weighted impact with ITAE = 0.0585, ISE = 0.5268, IAE = 0.2874 and ITSE = 0.0178. The control effort indicators, namely ISCI = 30.84 and ISTE = 0.034, further suggest a balanced control action without excessive actuator activity. Overall, the results indicate that the SMC-1 based PID controller achieves a fast, stable and efficient control performance.

Table 4.9. Time domain results (SMC-1/PID)

Controller	Rise Time (s)	Settling time (s)	Overshoot (%)	Delay time (s)
Cascade Outer-Loop SMC-1/Inner-Loop PID	0.0766	0.1209	0.09	0.0520

Table 4.10. Performance indices (SMC-1/PID)

Controller	ITAE	ISE	IAE	ITSE	ISCI	ISTE
Cascade Outer-Loop SMC-1/Inner-Loop PID	0.0585	0.5268	0.2874	0.0178	30.84	0.034

4.5. Simulation Results of Cascade Sliding Mode Controllers: (1) Outer-Loop SMC-2 /Inner-Loop P (SMC-2/P), (2) Outer-Loop SMC-2 /Inner-Loop PI (SMC-2/PI) and (3) Outer-Loop SMC-2 /Inner-Loop PID (SMC-2/PID)

In this subsection, the performance of the SMC-2 structure is evaluated by combining it with three different inner-loop controllers: P, PI and PID. The aim is to analyze how the outer-loop SMC interacts with each type of classical controller in the inner-loop and to determine which combination provides the most stable and efficient system response in terms of overshoot, steady-state error and settling time.

Simulation results indicate that when the inner-loop is controlled by a P controller, the response shows fast dynamics but suffers from higher steady-state error due to the lack of integral action. On the other hand the PI configuration significantly improves steady-state accuracy while maintaining a relatively fast response, although it introduces a moderate overshoot. Finally, the PID configuration provides the best overall performance by balancing overshoot, transient response and steady-state error reduction, thanks to the derivative component that improves system stability and damping.

The comparative evaluation demonstrates that the SMC-2/PID cascade structure is the most effective among the tested strategies, achieving both robustness against disturbances and precise reference tracking.

4.5.1. Cascade Sliding Mode Control: Outer-Loop SMC-2/Inner-Loop P (SMC-2/P)

This subsection presents and analyzes the simulation results of the cascade configuration with an outer SMC-2 controller and an inner-loop proportional controller, including the output speed signal (Figure 4.42), armature current signal (Figure 4.43), control input voltage signal (Figure 4.44), equivalent input signal (Figure 4.45), switching input signal (Figure 4.46), sliding surface signal (Figure 4.47), phase plane of the sliding surface and its derivative (Figure 4.48), speed error signal (Figure 4.49), and the phase plane of the error and its derivative (Figure 4.50). The SMC-2 controller is designed with the parameters $k_{sc} = 2,\ k_d = 1.5,\ k_p = 50,\ k_i = 2,\ \Omega_c = 10,\ \beta = 80,\ \lambda_1 = 50$. The inner-loop P controller is adjusted with a gain of $k_p = 1$. The simulated voltage and current responses indicate that the SMC-2/P structure ensures rapid transient behavior and stable steady-state performance. The proportional action in the inner-loop allows quick response, while the outer-loop SMC-2 improves robustness against parameter variations and external disturbances. The control signal shows reduced chattering compared with conventional SMC.

Error plots and their derivatives confirm precise trajectory tracking, while the sliding surface results demonstrate that the system states remain close to the desired manifold. These outcomes highlight that the SMC-2/P hybrid configuration offers improved speed and robustness compared to a simple proportional controller.

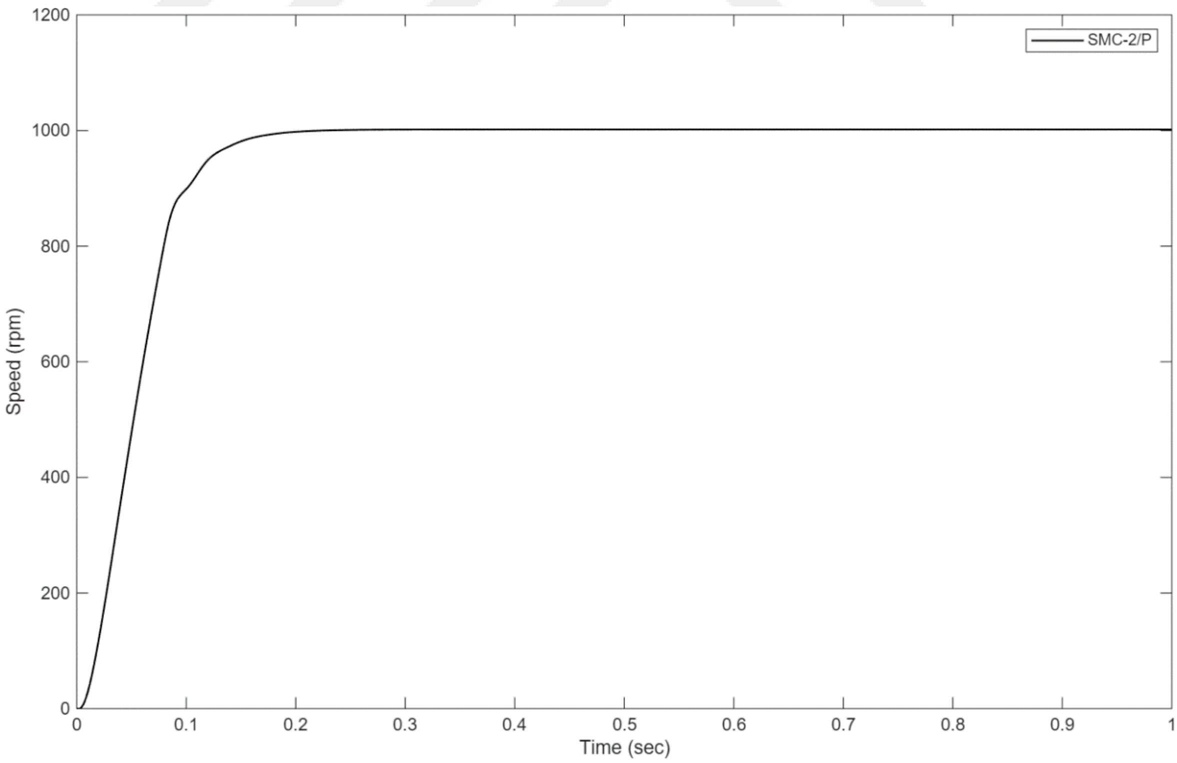

Figure 4.42. Output speed signal (rpm) (SMC-2/P)

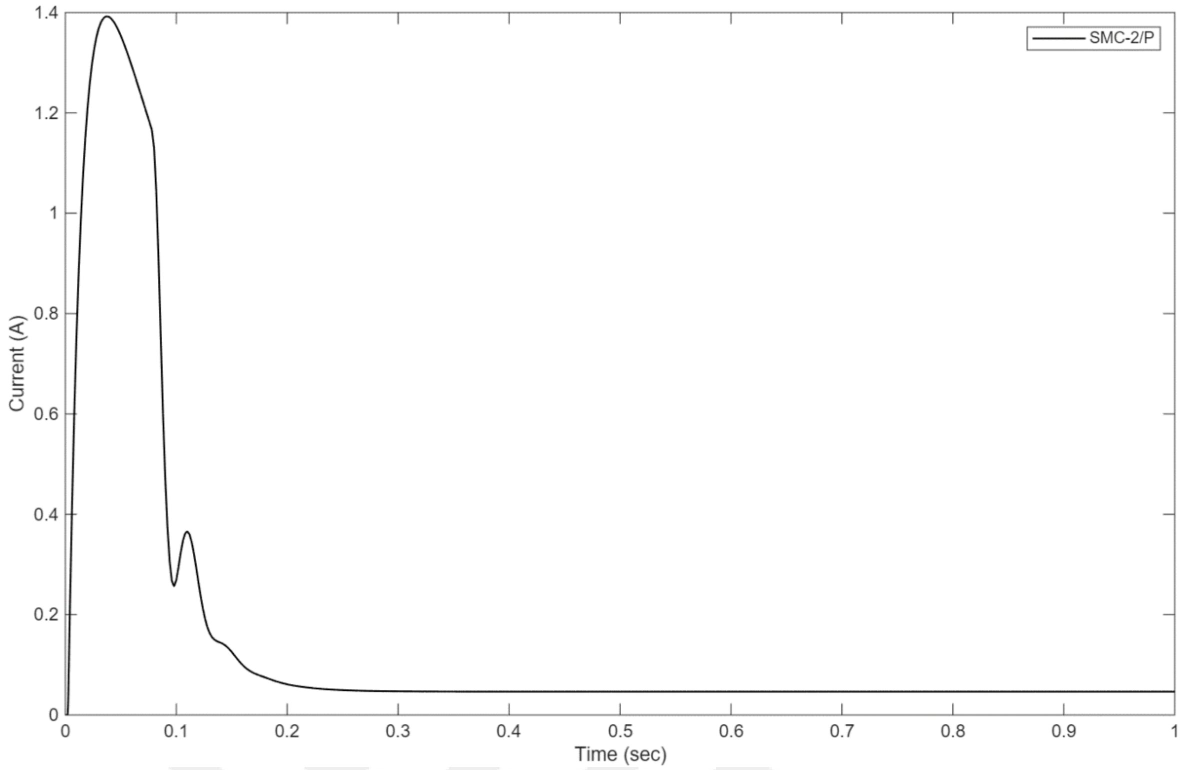

Figure 4.43. Armature current signal, $i_a(t)$ (SMC-2/P)

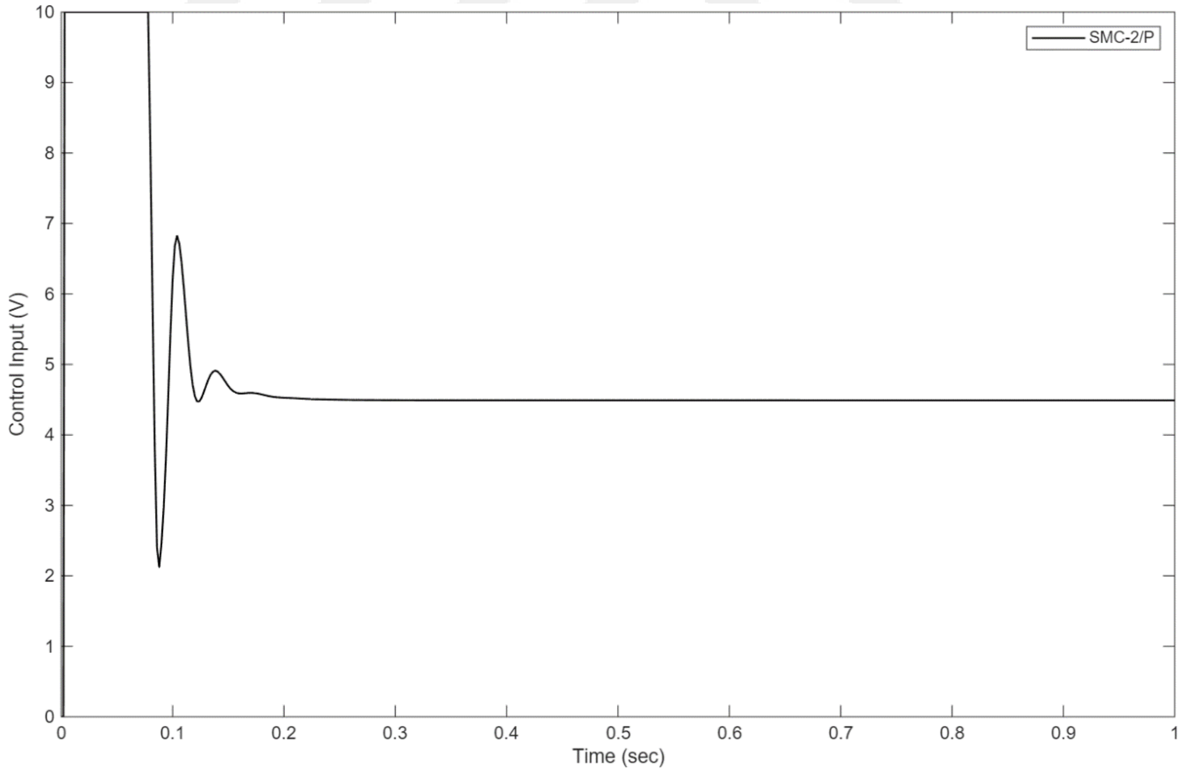

Figure 4.44. Control input voltage signal, $u(t)$ (SMC-2/P)

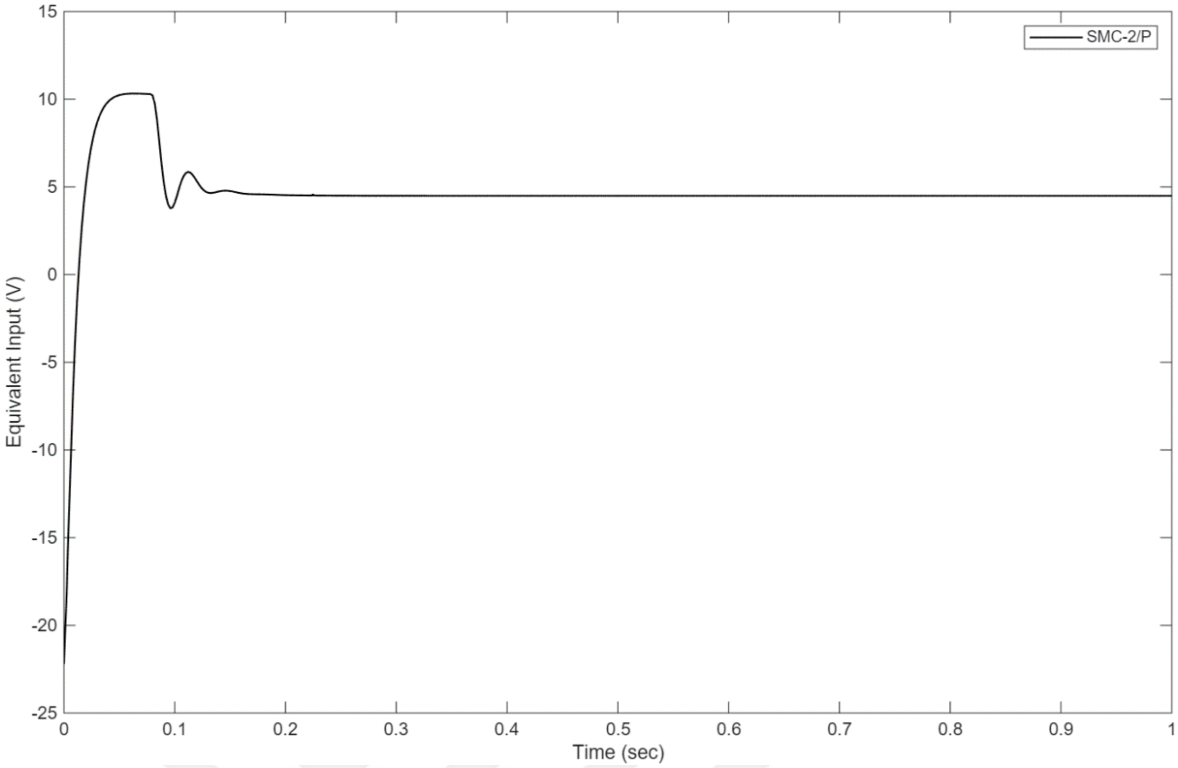

Figure 4.45. Equivalent input signal, $u_{eq}(t)$ (SMC-2/P)

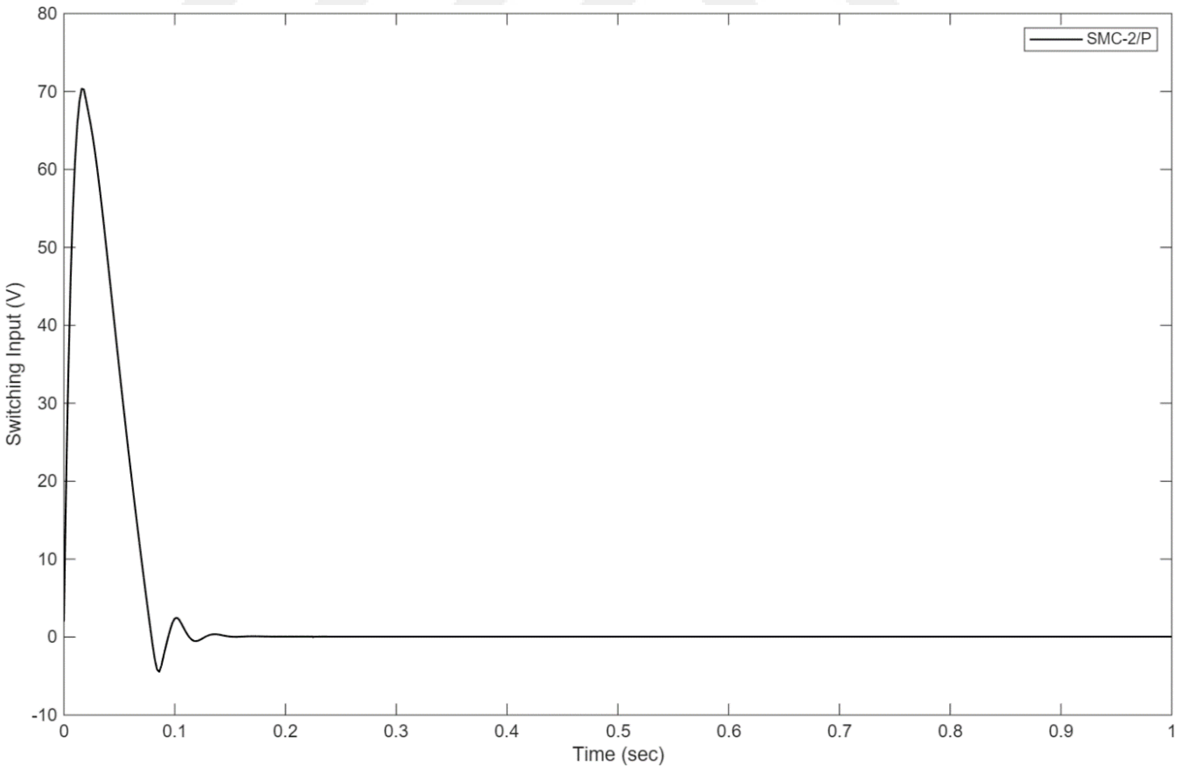

Figure 4.46. Switching input signal, $u_{sw}(t)$ (SMC-2/P)

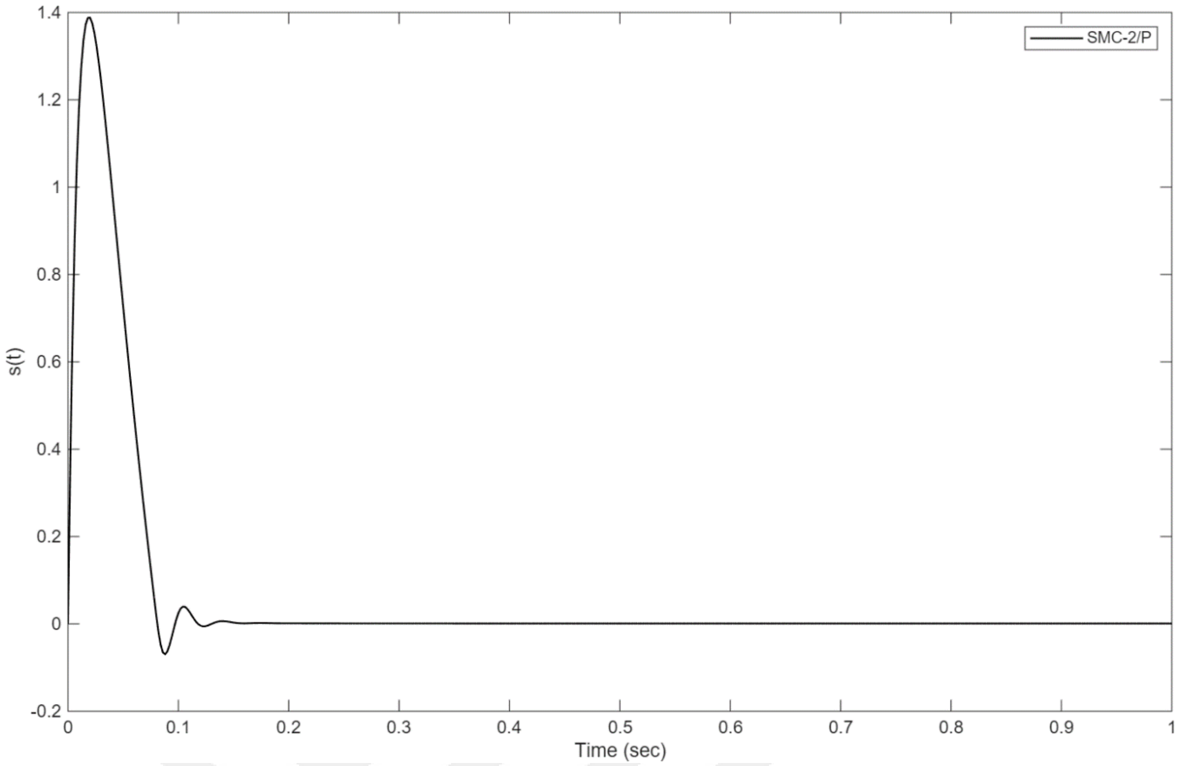

Figure 4.47. Sliding surface signal, $s(t)$ (SMC-2/P)

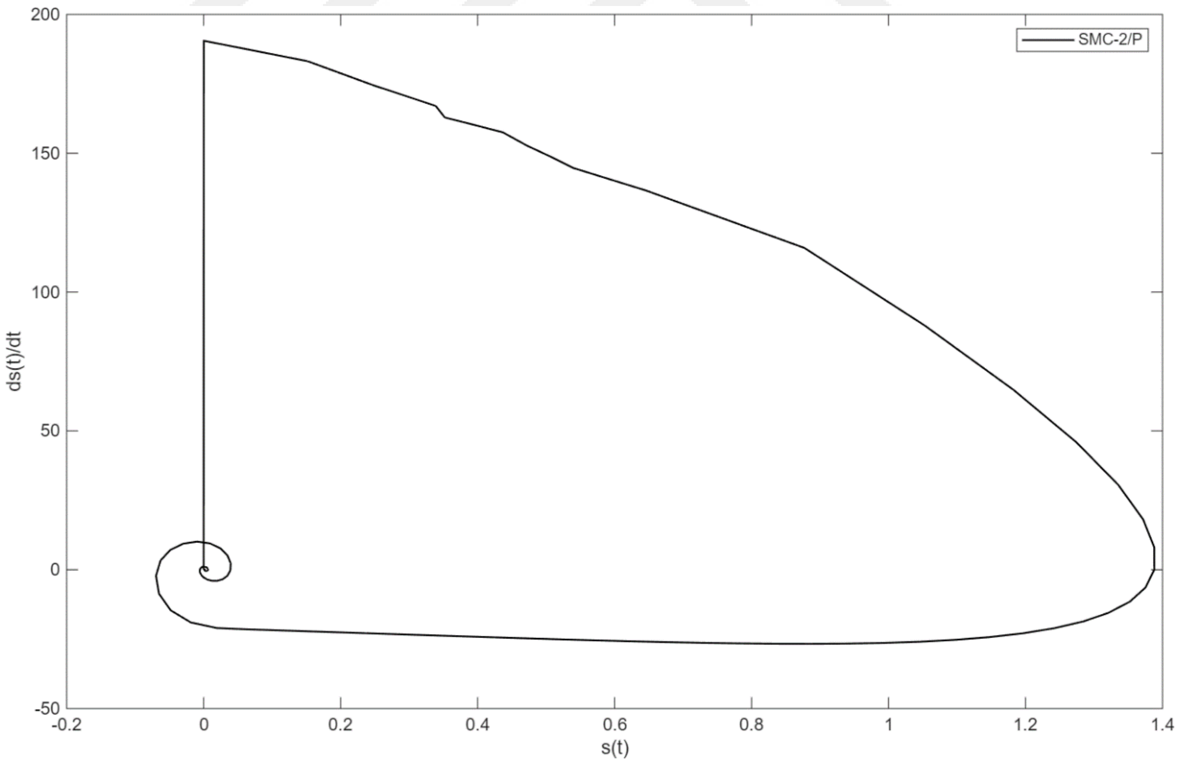

Figure 4.48. Phase plane of $s(t)$ and $ds(t)/dt$ signal (SMC-2/P)

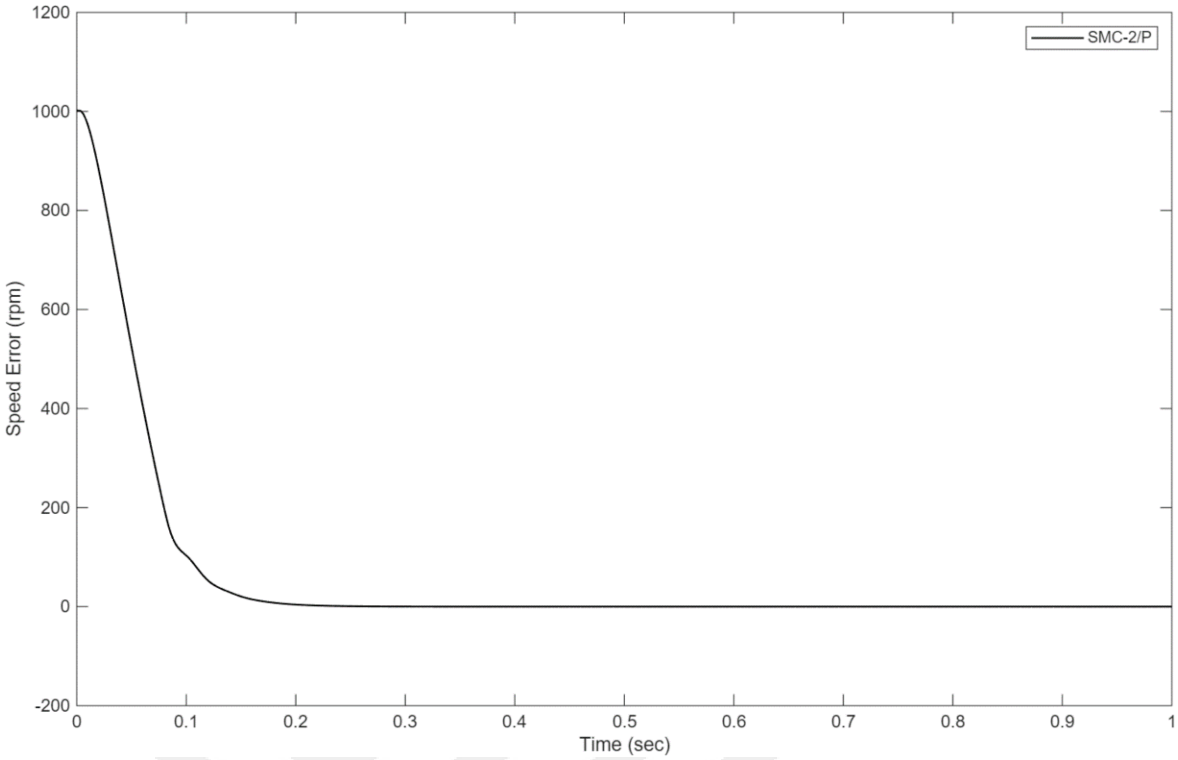

Figure 4.49. Speed error signal (rpm) (SMC-2/P)

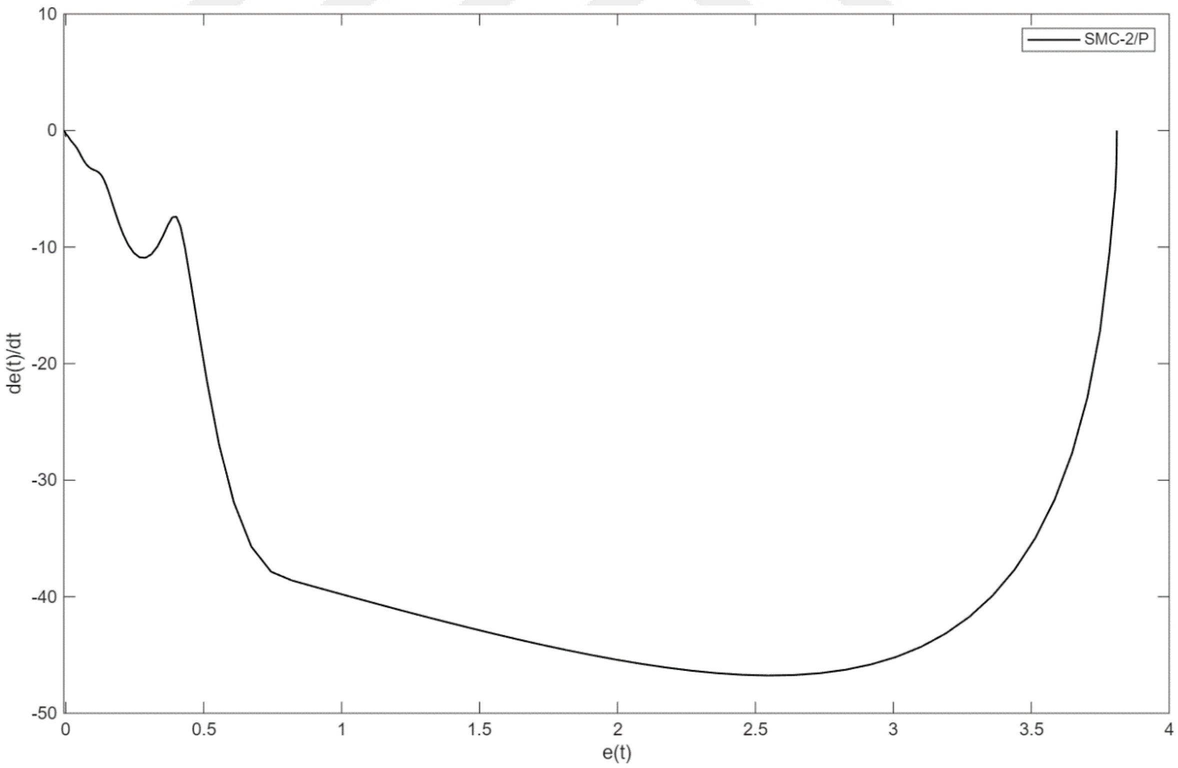

Figure 4.50. Phase plane of $e(t)$ and $de(t)/dt$ signal (SMC-2/P)

According to the time domain results data presented in Table 4.11 the cascade SMC-2/P controller demonstrates a fast and stable transient performance. The rise time is 0.0831 s and the settling time is 0.1508 s, while the overshoot is completely eliminated at 0%. The system delay of 0.0540 s indicates that the control structure responds promptly and effectively to input changes. Examining the performance indices in Table 4.12, the controller achieves ITAE = 0.0115, ISE = 0.5559, IAE = 0.2208 and ITSE = 0.0140 reflecting efficient limitation of both error magnitude and its time-weighted impact. Additionally, the control effort indicator ISCI = 26.64 and ISTE = 0.0017, suggest that the system maintains balanced control action while avoiding excessive actuator activity. Overall, these results demonstrate that the SMC-2 based P cascade controller provides fast, stable and effective performance.

Table 4.11. Time domain results (SMC-2/P)

Controller	Rise Time (s)	Settling time (s)	Overshoot (%)	Delay time (s)
Cascade Outer-Loop SMC-2/Inner-Loop P	0.0831	0.1508	0	0.0540

Table 4.12. Performance indices (SMC-2/P)

Controller	ITAE	ISE	IAE	ITSE	ISCI	ISTE
Cascade Outer-Loop SMC-2/Inner-Loop P	0.0115	0.5559	0.2208	0.0140	26.64	0.0017

4.5.2. Cascade Sliding Mode Control: Outer-Loop SMC-2/Inner-Loop PI (SMC-2/PI)

The simulation results are presented in Figure 4.60–Figure 4.68, including the output speed signal (Figure 4.60), armature current signal (Figure 4.61), control input voltage signal (Figure 4.62), equivalent input signal (Figure 4.63), switching input signal (Figure 4.64), sliding surface signal (Figure 4.65), phase plane of the sliding surface and its derivative (Figure 4.66), speed error signal (Figure 4.67), and the phase plane of the error and its derivative (Figure 4.68). In this part, the simulation results of the CSMC structure with an outer SMC-2 controller and an inner-loop PI controller are presented. The outer SMC-2 is configured with the parameters $k_{sc} = 3.2,\ k_d = 0.9,\ k_p = 28,\ k_i = 8.5,\ \Omega_c = 8,\ \beta = 170,\ \lambda_1 = 50$. The PI controller in the inner-loop is tuned with PI = $28\left(1 + \frac{1}{3.29s}\right)$. The simulation results show that the SMC-2/PI configuration provides smoother transient dynamics and higher steady-state accuracy than the SMC-2/P structure. The integral term in the PI controller eliminates steady-state error, while the SMC-2 controller maintains robustness and disturbance rejection. The control effort is shared effectively between the two controllers, leading to reduced oscillations and minimized chattering.

The error and derivative responses verify precise reference tracking, while the sliding surface and its derivative confirm that the system trajectory remains aligned with the predefined manifold. Overall, the findings demonstrate that the SMC-2/PI hybrid scheme delivers superior performance compared to first-order cascade designs.

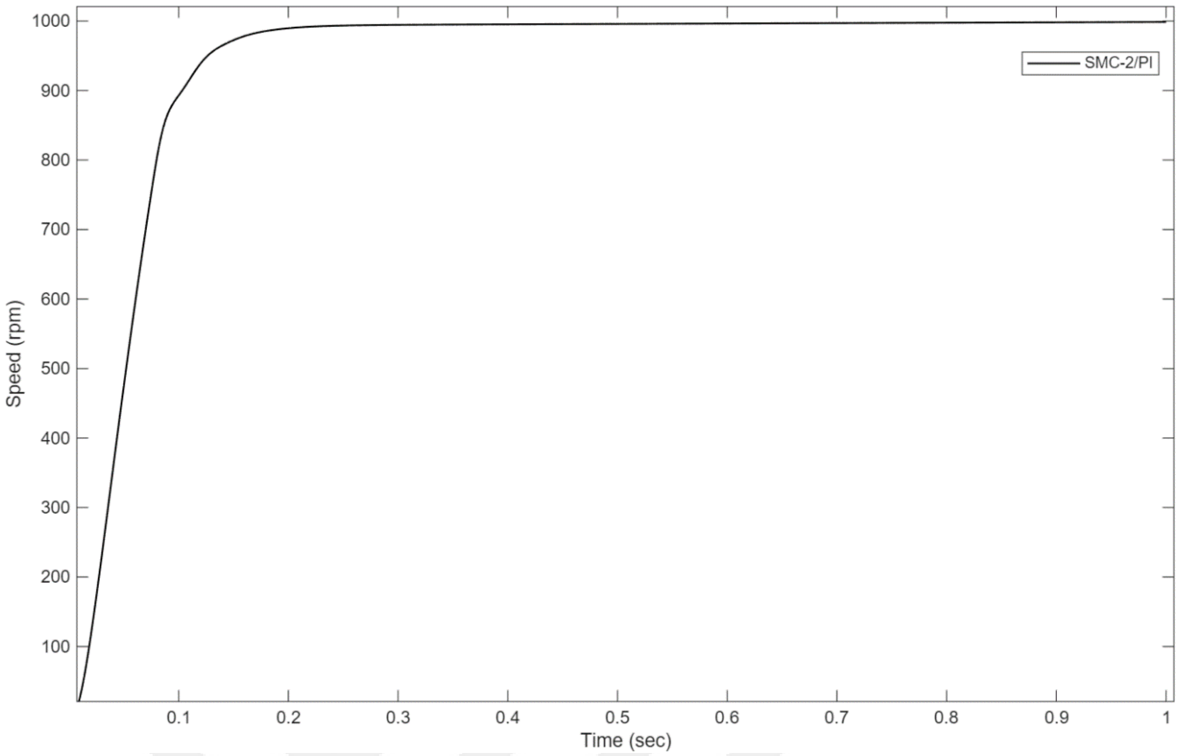

Figure 4.51. Output speed signal (rpm) (SMC-2/PI)

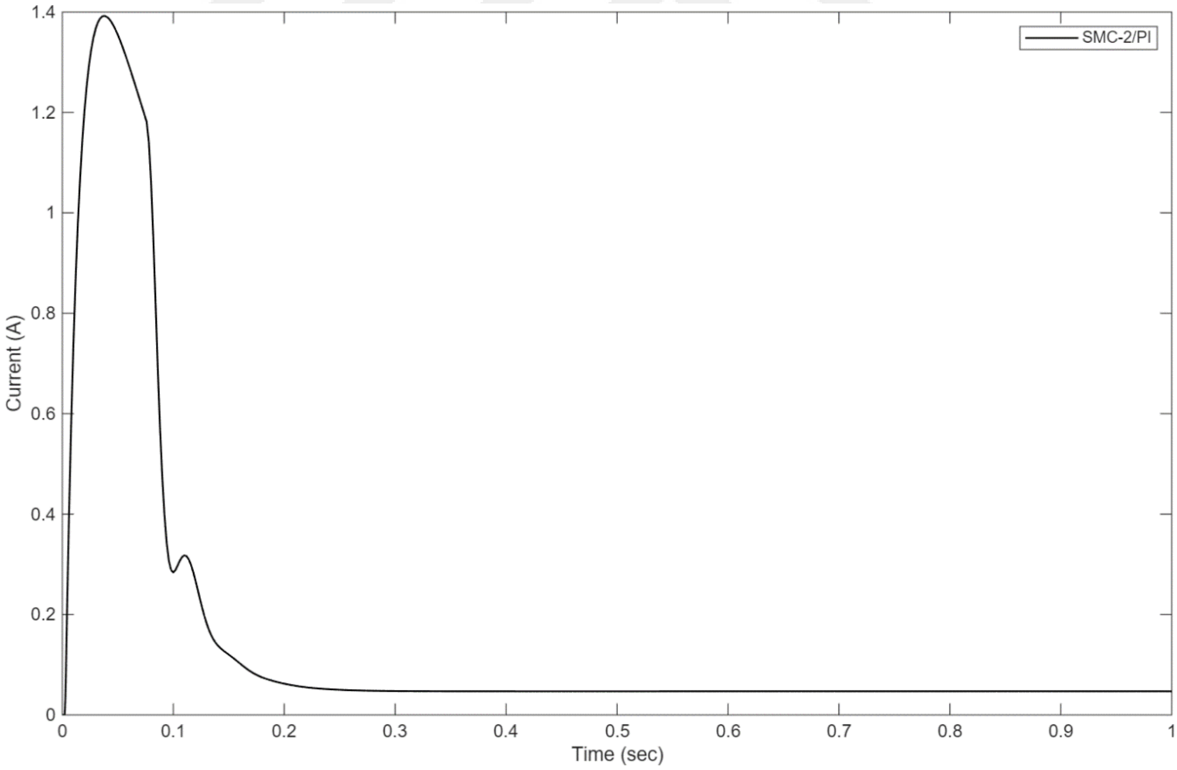

Figure 4.52. Armature current signal, $i_a(t)$ (SMC-2/PI)

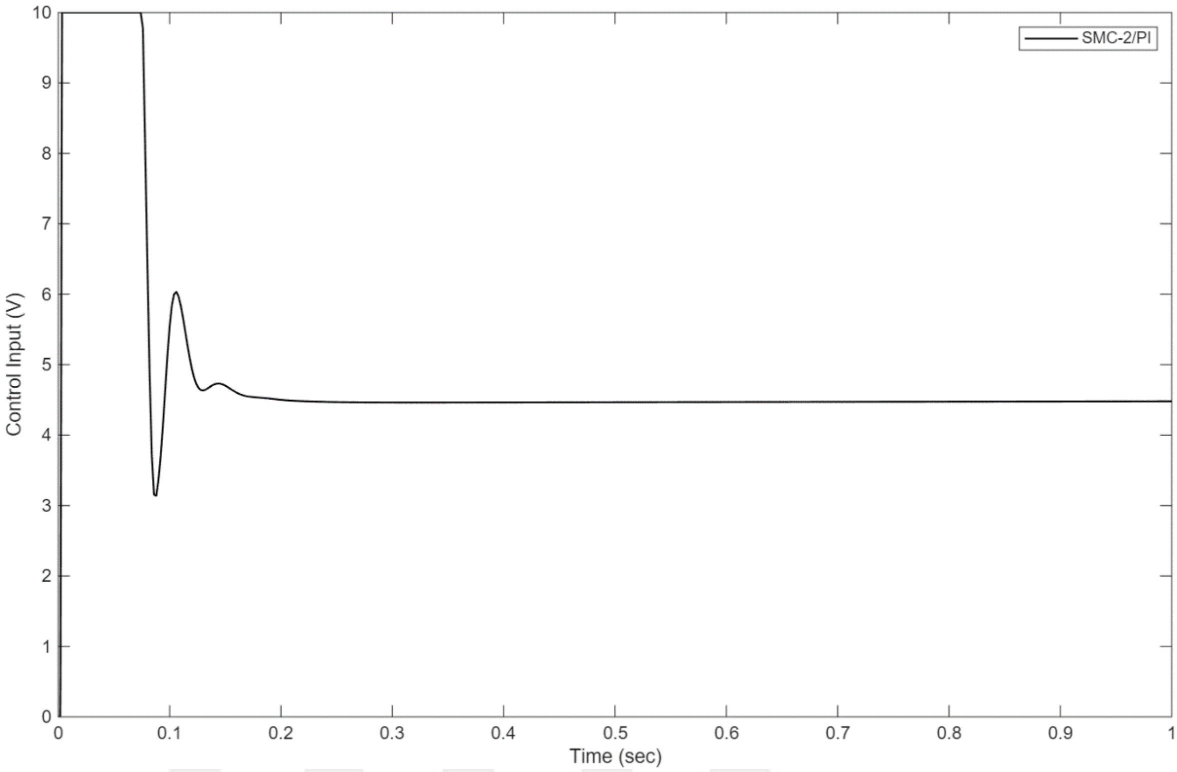

Figure 4.53. Control input voltage signal, $u(t)$ (SMC-2/PI)

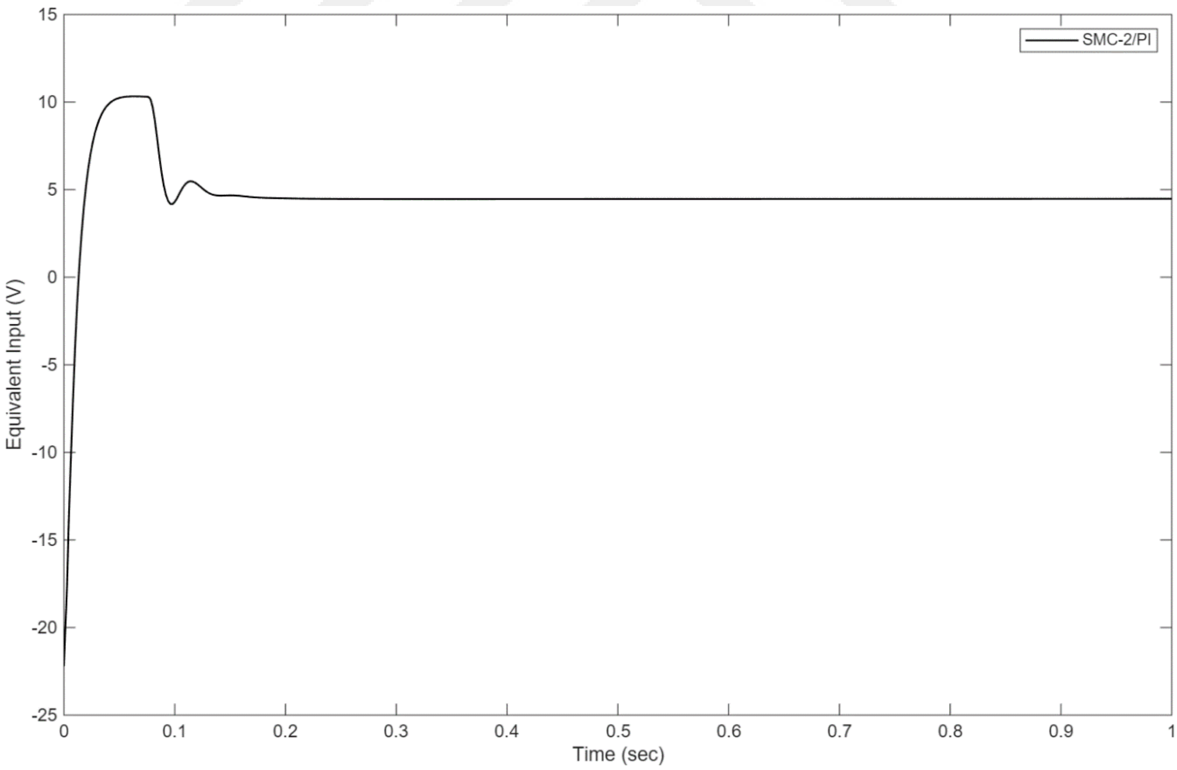

Figure 4.54. Equivalent input signal, $u_{eq}(t)$ (SMC-2/PI)

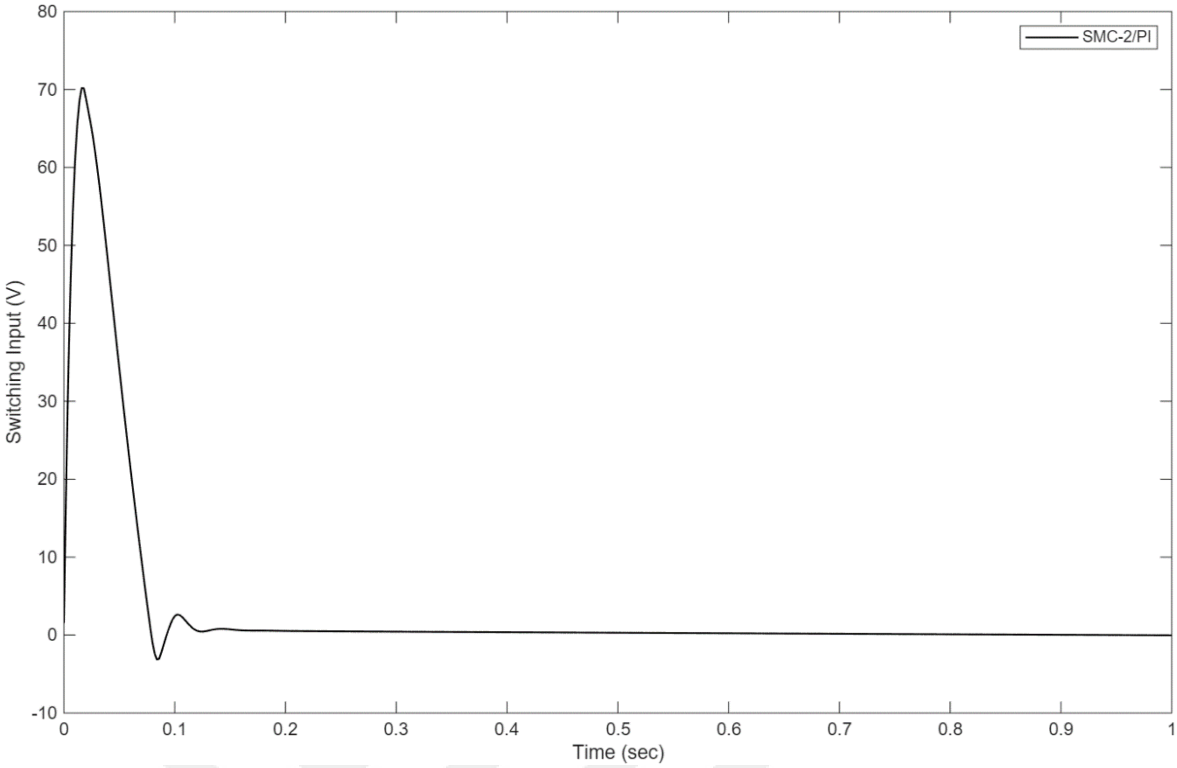

Figure 4.55. Switching input signal, $u_{sw}(t)$ (SMC-2/PI)

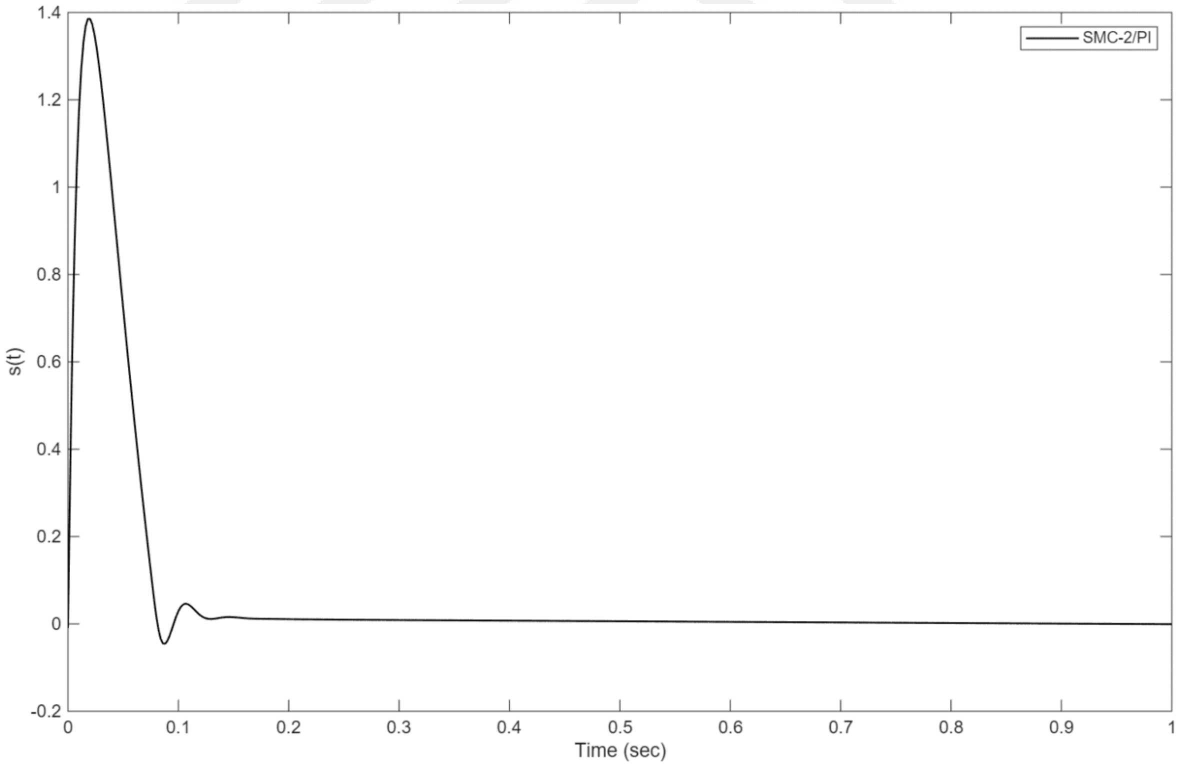

Figure 4.56. Siding surface signal, $s(t)$ (SMC-2/PI)

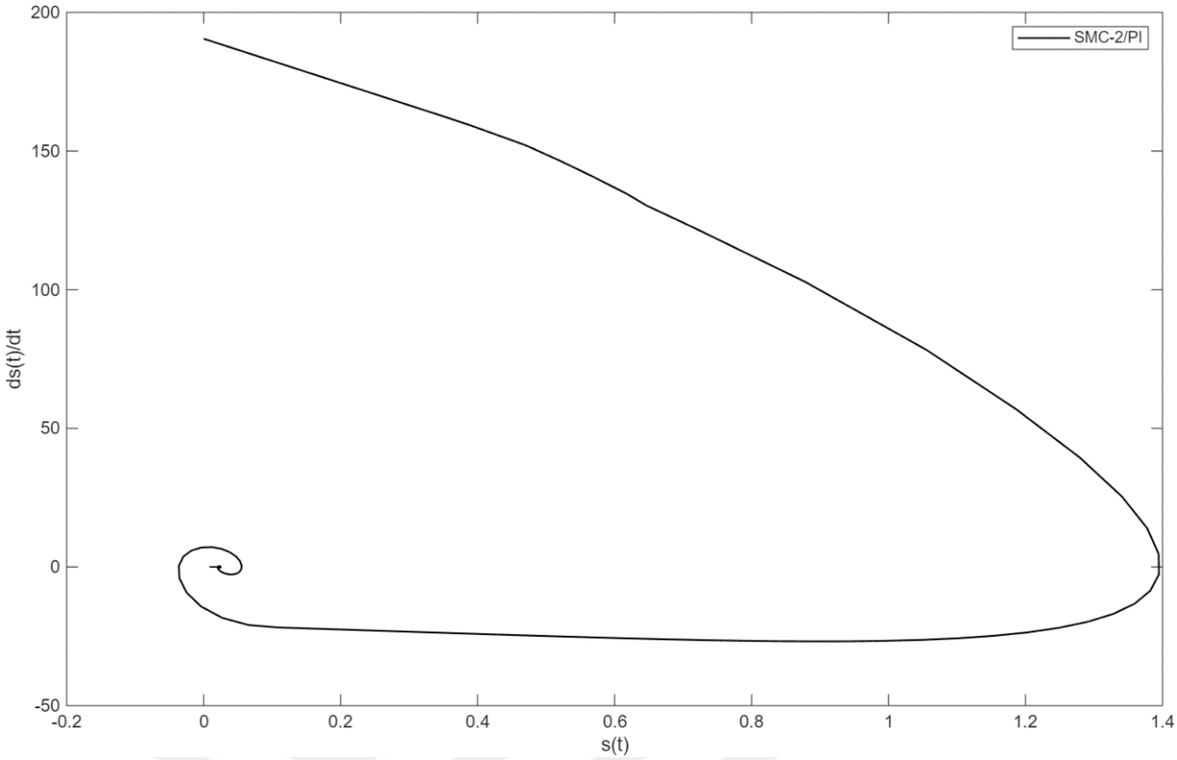

Figure 4.57. Phase plane of $s(t)$ and $ds(t)/dt$ signal (SMC-2/PI)

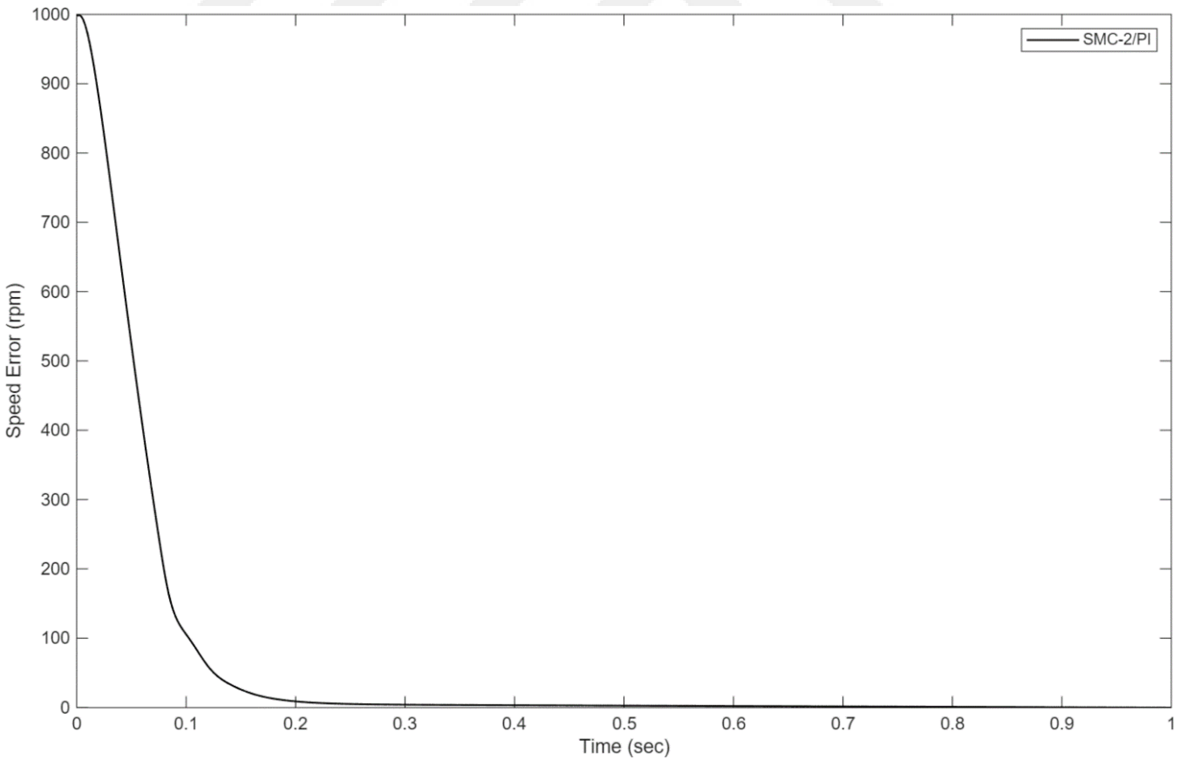

Figure 4.58. Speed error signal (rpm) (SMC-2/PI)

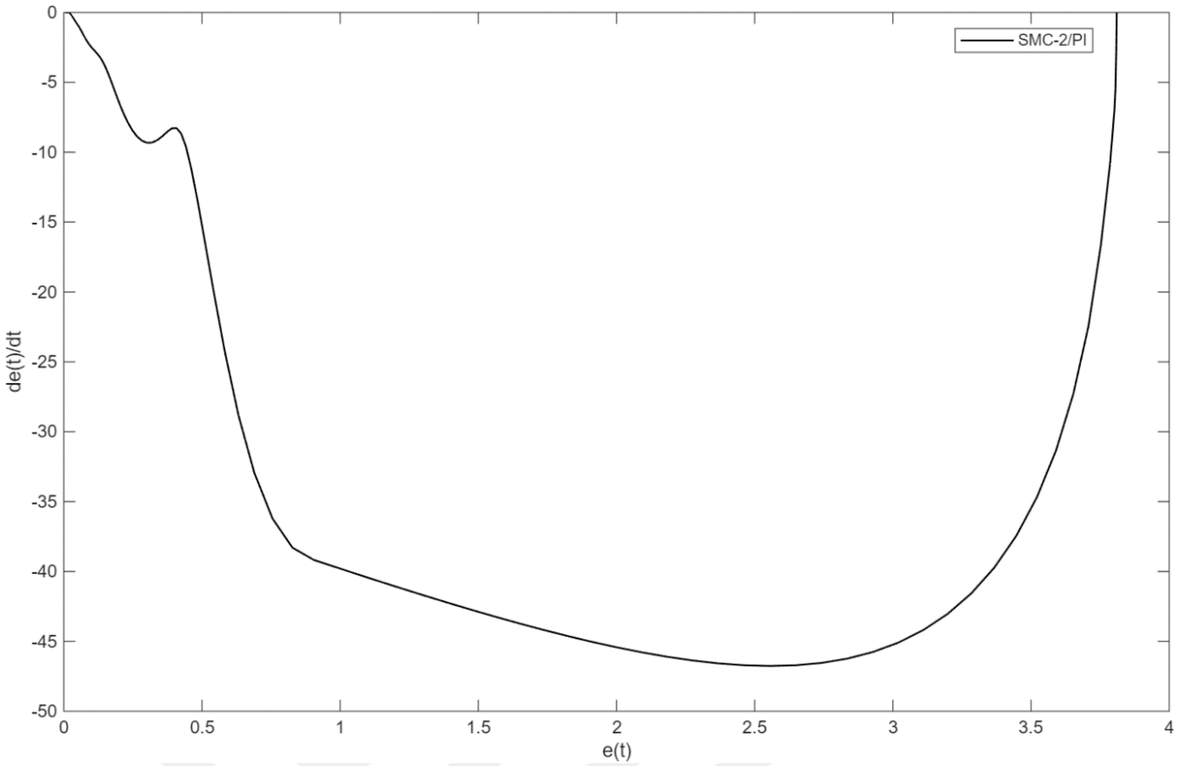

Figure 4.59. Phase plane of $e(t)$ and $de(t)/dt$ signal (SMC-2/PI)

According to the time domain results presented in Table 4.13, the cascade SMC-2/PI controller exhibits a fast and stable transient performance. The rise time is 0.0843 s, the settling time is 0.1607 s and with an overshoot of 0%, indicating a fully stable response. The system delay of 0.0540 s further demonstrates the controller's prompt and effective reaction to input changes. Examining the performance indices in Table 4.14, the controller achieves ITAE = 0.0145, ISE = 0.599, IAE = 0.2313 and ITSE = 0.0143 reflecting effective limitation of error magnitude and time-weighted impact. The control effort indicator ISCI = 26.26 and ISTE = 0.004 indicate a balanced control action while avoiding excessive actuator activity. Overall, these results demonstrate that the SMC-2/PI cascade controller provides a fast, stable and efficient control performance.

Table 4.13. Time domain results (SMC-2/PI)

Controller	Rise Time (s)	Settling time (s)	Overshoot (%)	Delay time (s)
Cascade Outer-Loop SMC-2/Inner-Loop PI	0.0843	0.1607	0	0.0540

Table 4.14. Performance indices (SMC-2/PI)

Controller	ITAE	ISE	IAE	ITSE	ISCI	ISTE
Cascade Outer-Loop SMC-2/Inner-Loop PI	0.0145	0.599	0.2313	0.0143	26.26	0.004

4.5.3. Cascade Sliding Mode Control: Outer-Loop SMC-2/Inner-Loop PID (SMC-2/PID)

The simulation results are presented in Figure 4.60–Figure 4.68, including the output speed signal (Figure 4.60), armature current signal (Figure 4.61), control input voltage signal (Figure 4.62), equivalent input signal (Figure 4.63), switching input signal (Figure 4.64), sliding surface signal (Figure 4.65), phase plane of the main sliding surface and its derivative (Figure 4.66), speed error signal (Figure 4.67), and the phase plane of the error and its derivative (Figure 4.68). This subsection reports the simulation outcomes of the cascade SMC-2/PID configuration. The outer SMC-2 controller is designed with the parameters $k_{sc} = 2,\ k_d = 1.6,\ k_p = 67,\ k_i = 5,\ \Omega_c = 10,\ \beta = 50,\ \lambda_1 = 150$. The inner-loop PID controller is tuned with PID = $15\left(1 + \frac{1}{15s} + 0.00067s\right)$. The voltage and current responses from the simulations demonstrate that the SMC-2/PID system achieves the fastest transient response with excellent steady-state accuracy. The derivative term in the PID controller improves responsiveness to rapid changes, while the integral term eliminates residual errors. Together, these effects lead to short settling times, reduced oscillations and accurate tracking.

The error and derivative responses verify precise reference tracking. Moreover, the sliding surface analysis shows that the system states remain close to the desired manifold even under disturbances. These results prove that the SMC-2/PID cascade control strategy offers the most versatile and efficient performance, combining the robustness of SMC-2 with the adaptability of PID control.

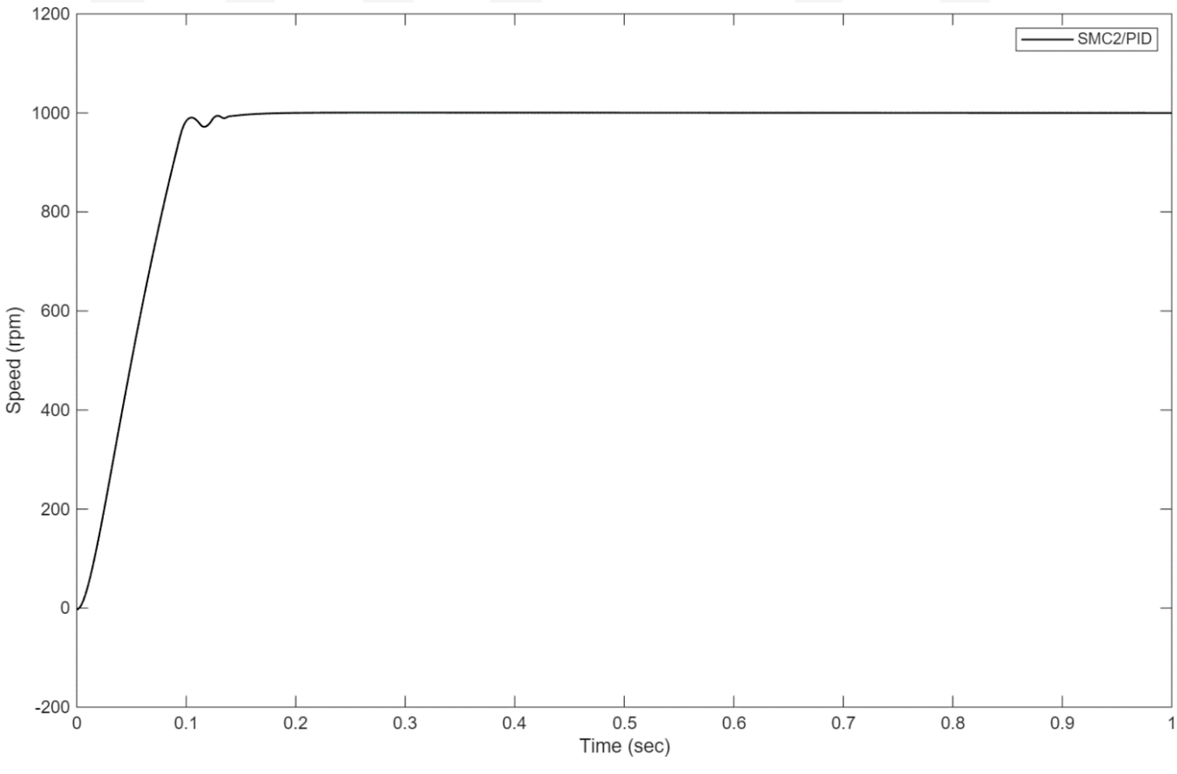

Figure 4.60. Output speed signal (rpm) (SMC-2/PID)

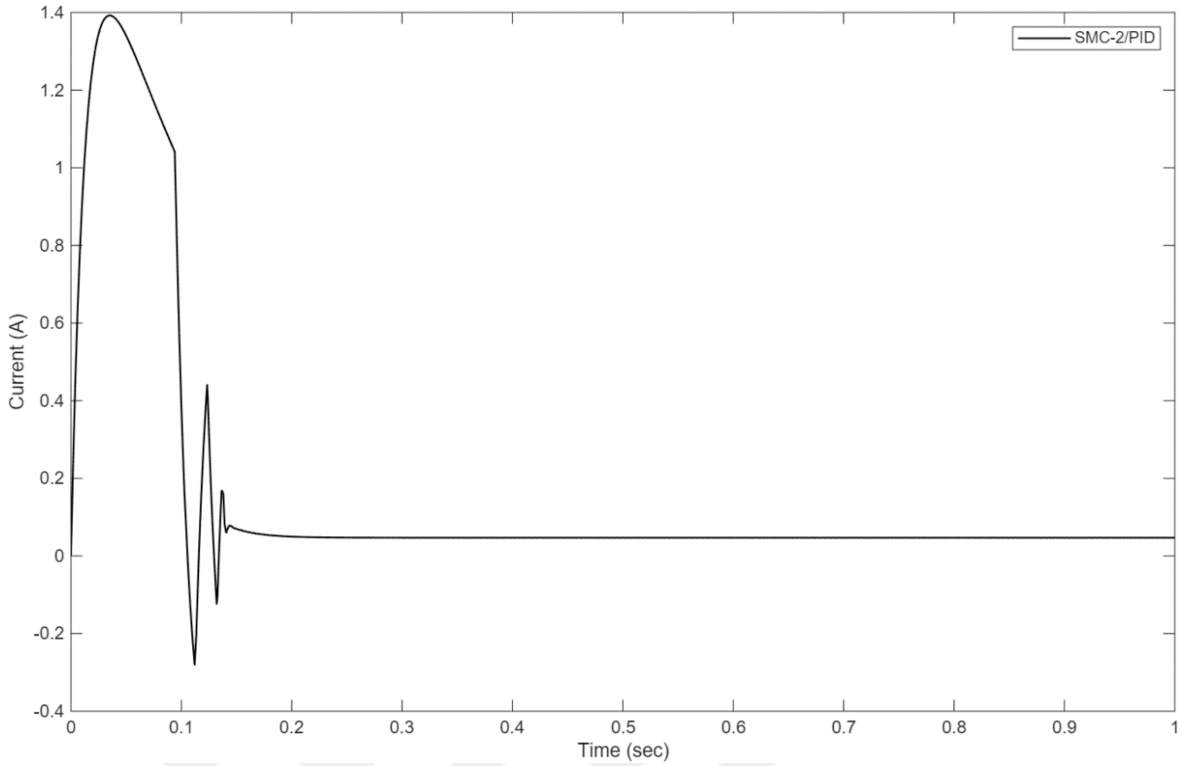

Figure 4.61. Armature current signal, $i_a(t)$ (SMC-2/PID)

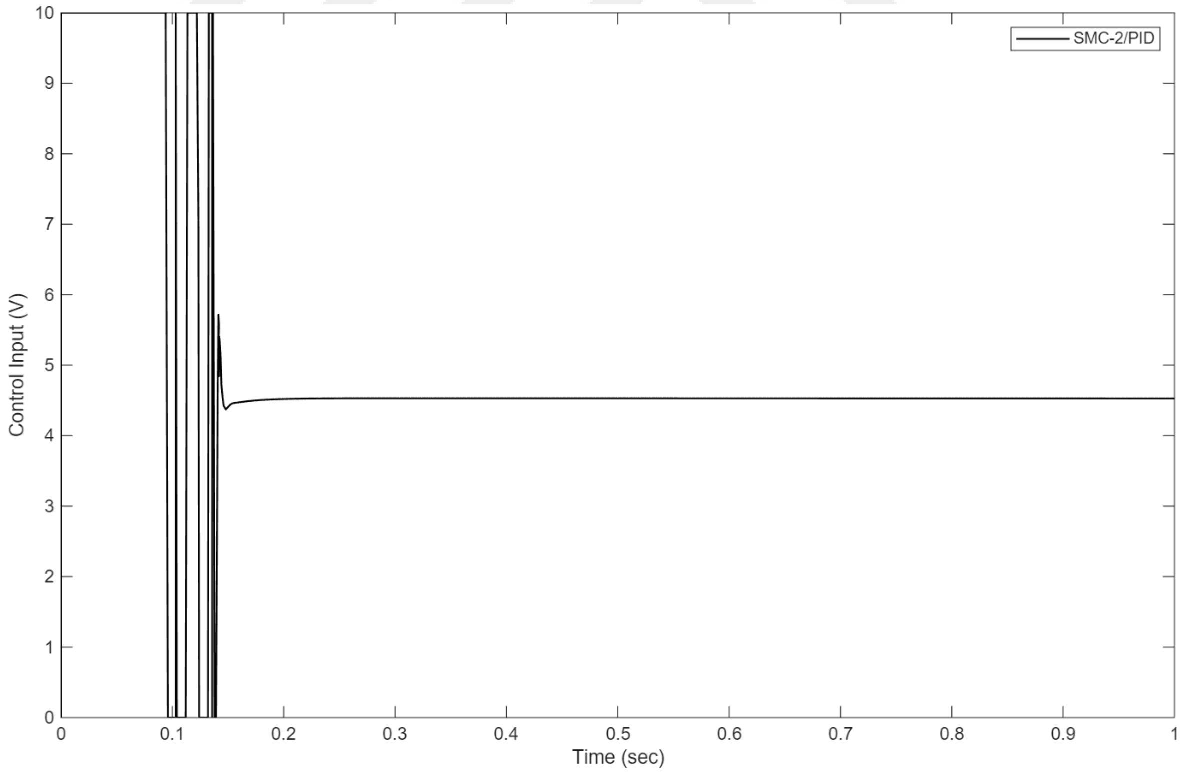

Figure 4.62. Control input voltage signal, $u(t)$ (SMC-2/PID)

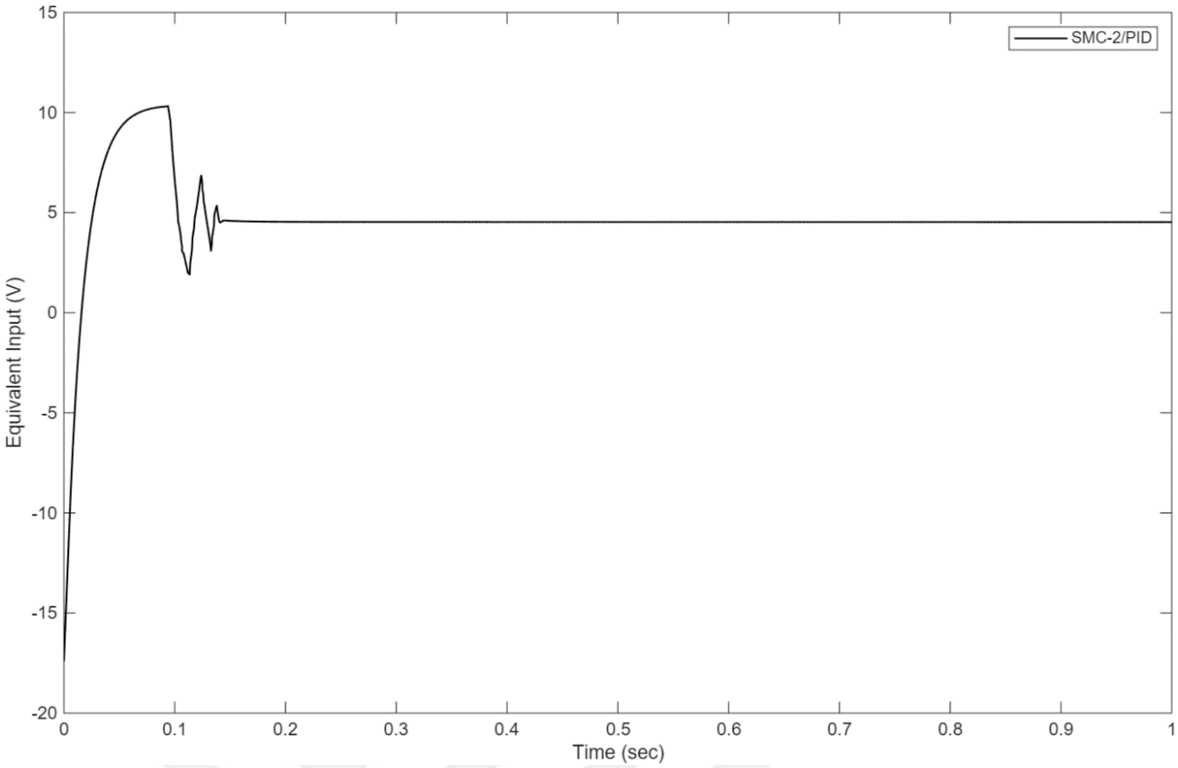

Figure 4.63. Equivalent input signal, $u_{eq}(t)$ (SMC-2/PID)

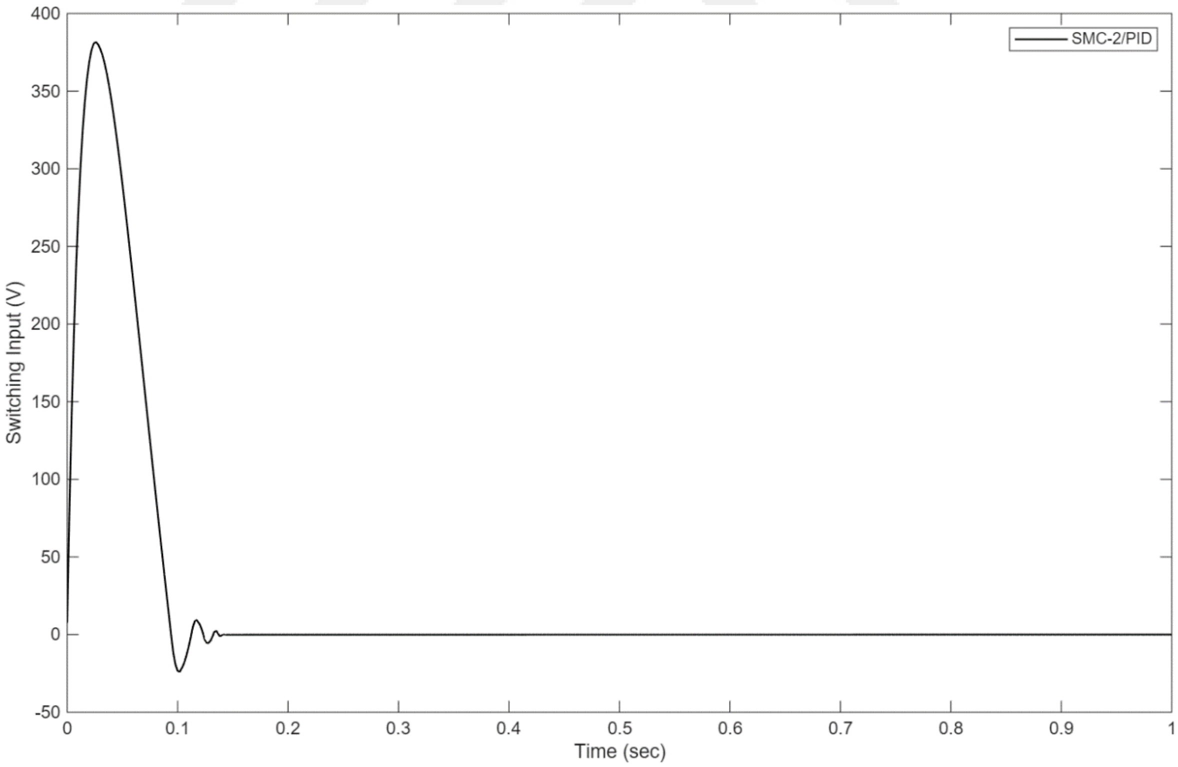

Figure 4.64. Switching input signal, $u_{sw}(t)$ (SMC-2/PID)

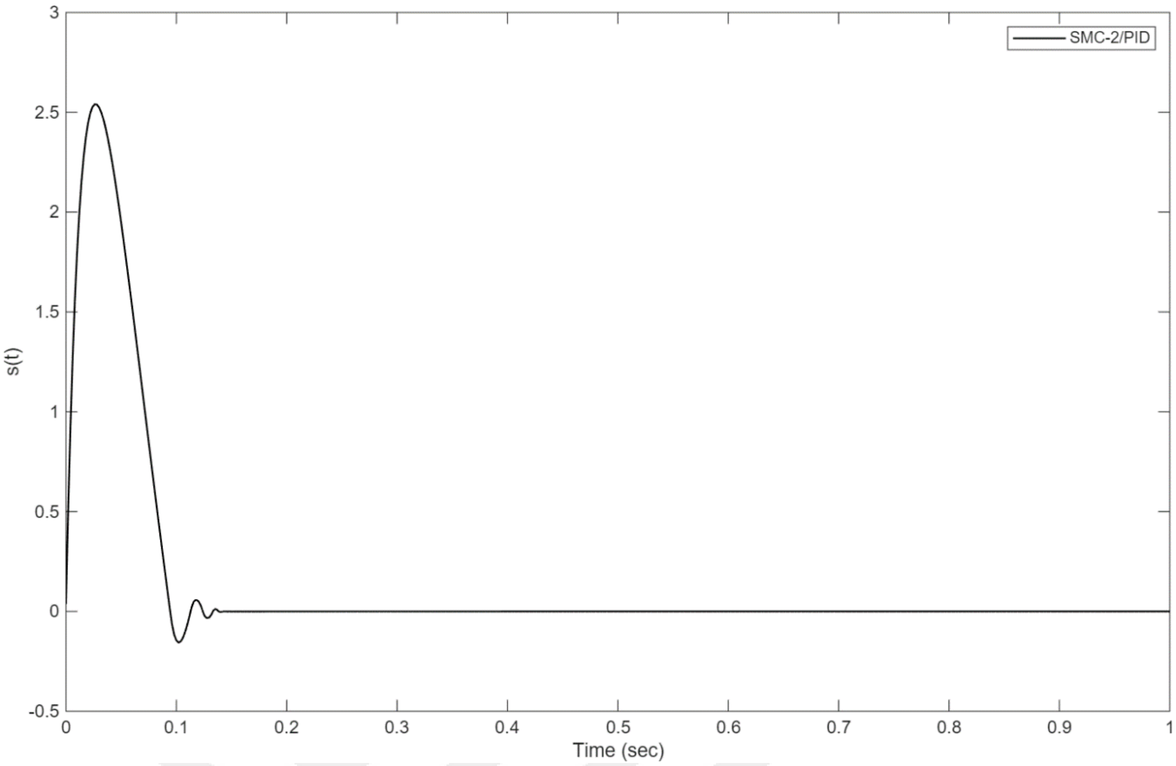

Figure 4.65. Sliding surface signal, $s(t)$ (SMC-2/PID)

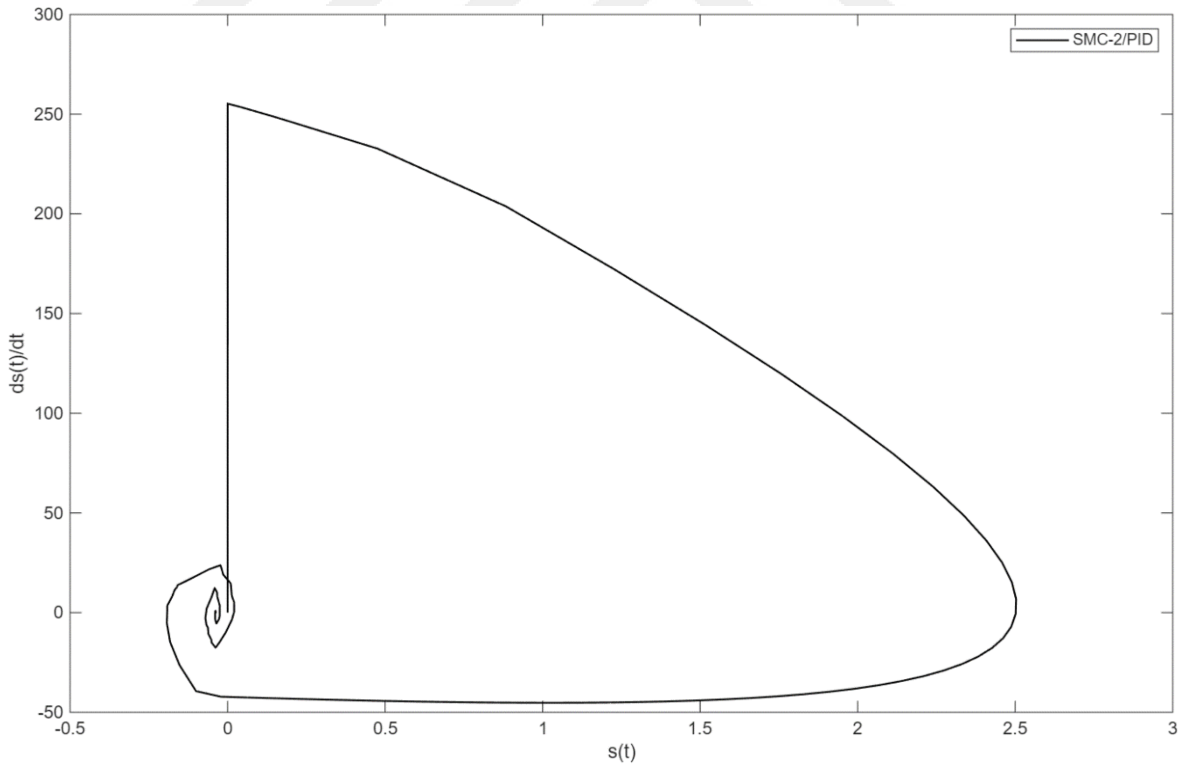

Figure 4.66. Phase plane of $s(t)$ and $ds(t)/dt$ signal (SMC-2/PID)

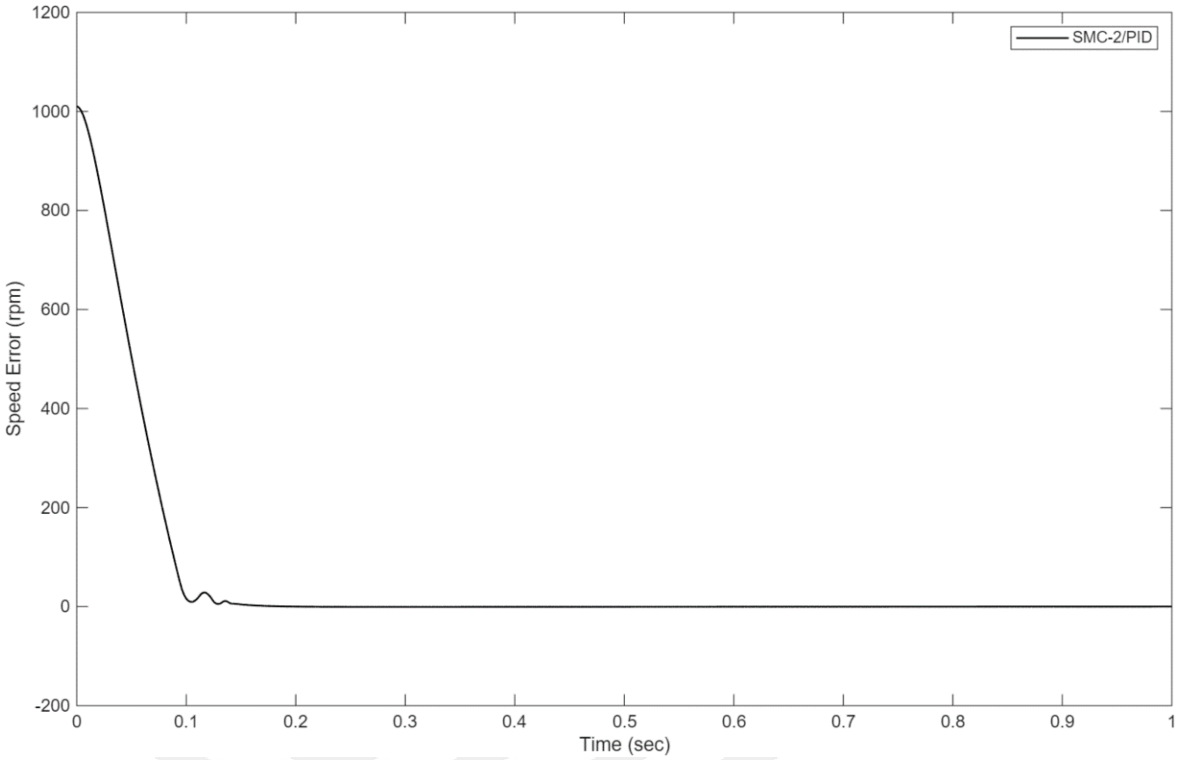

Figure 4.67. Speed error signal (rpm) (SMC-2/PID)

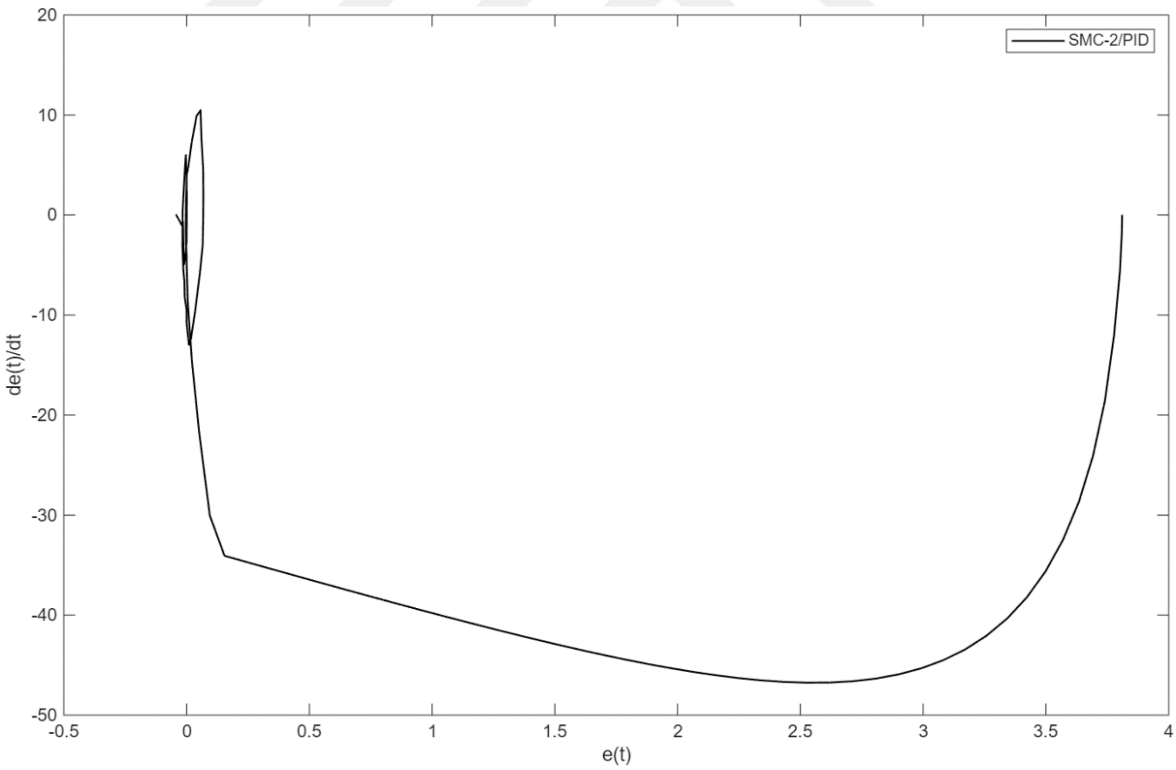

Figure 4.68. Phase plane of $e(t)$ and $de(t)/dt$ signal (SMC-2/PID)

According to the time domain results presented in Table 4.15, the cascade SMC-2/PID controller demonstrates a fast and stable transient performance. The rise time is 0.0726 s and the settling time is 0.1217 s, with an overshoot of only 0.06%, indicating a nearly ideal stable response. The system delay of 0.05 s further demonstrates that the control structure responds promptly to input changes. Examining the performance indices in Table 4.16, the controller achieves ITAE = 0.026, ISE = 0.5179, IAE = 0.2282 and ITSE = 0.013 reflecting effective limitation of error magnitude and time-weighted influence. The control effort indicator ISCI = 28.66 and ISTE = 0.0131 suggest a balanced control action without excessive actuator activity. Overall, these results indicate that the SMC-2/PID cascade controller provides a fast, stable and efficient control performance.

Table 4.15. Time domain results (SMC-2/PID)

Controller	Rise Time (s)	Settling time (s)	Overshoot (%)	Delay time (s)
Cascade Outer-Loop SMC-2/Inner-Loop PID	0.0726	0.1217	0.06	0.05

Table 4.16. Performance indices (SMC-2/PID)

Controller	ITAE	ISE	IAE	ITSE	ISCI	ISTE
Cascade Outer-Loop SMC-2/Inner-Loop PID	0.026	0.5179	0.2282	0.013	28.66	0.0131

4.6. Cascade Sliding Mode Controllers: (1) Outer-Loop SMC-1/Inner-Loop SMC-1 (SMC-1/SMC-1) and (2) Outer-Loop SMC-2/Inner-Loop SMC-1 (SMC-2/SMC-1)

In this section, the CSMC approach is investigated, focusing on two different configurations: the SMC-1/SMC-1 and the SMC-2/SMC-1. These designs were implemented to evaluate the effectiveness of cascade structures in improving dynamic response and reducing steady-state error compared to single-loop SMC. The proposed models were simulated in MATLAB/Simulink and system responses including output speed, current, control input signals, error signals and sliding surface dynamics were analyzed in detail. The results indicate that cascade control enhances the overall system performance by providing faster transient behavior, reduced oscillations and improved robustness under varying operating conditions. In particular, the configuration employing the outer-loop SMC-2 showed superior performance, achieving smoother control actions and more accurate tracking compared to the cascade structure with an outer-loop SMC-1.

4.6.1. Cascade Sliding Mode Control: Outer-Loop SMC-1/Inner-Loop SMC-1 (SMC-1/SMC-1)

Controller Design

This section includes the mathematical design of controllers used for the inner and outer-loops.

- **Outer-Loop SMC-1 Parameters:**

  Control coefficients: $k_d = 0.4,\ k_p = 32,\ k_i = 1,\ k_s = 16$

  Smoothing parameter: $\Omega = 3$

- **Inner-Loop SMC-1 Parameters:**
  Control coefficients: $k_d = 1,\ k_p = 20,\ k_i = 0.2,\ k_s = 6$
  Smoothing parameter: $\Omega = 4$

The CSMC configuration employing the SMC-1/SMC-1 is comprehensively modeled and analyzed. The dynamic behavior of this control scheme is thoroughly examined by evaluating multiple system signals. The output speed responses, depicted in Figure 4.69, reveal the system's capability to closely track the reference input with minimal transient deviations. Figure 4.70 presents the output current signal, highlighting the electrical characteristics and stability of the cascade-controlled system. The control effort required to maintain desired performance is shown in Figure 4.71, followed by the equivalent input in Figure 4.72, which characterizes the discrete switching behavior intrinsic to SMC. Further insight into the system's internal dynamics is provided by the switching input (Figure 4.73) and sliding surface signal (Figure 4.74), which reflect the controller's corrective actions and the system's proximity to the sliding manifold. Error signal (Figure 4.75), the error signal along with its derivative (Figure 4.76) offer detailed visualization of the transient response and control accuracy. Collectively, these figures substantiate the robustness and efficacy of the cascade SMC-1/SMC-1 control approach in delivering stable, precise and responsive control performance.

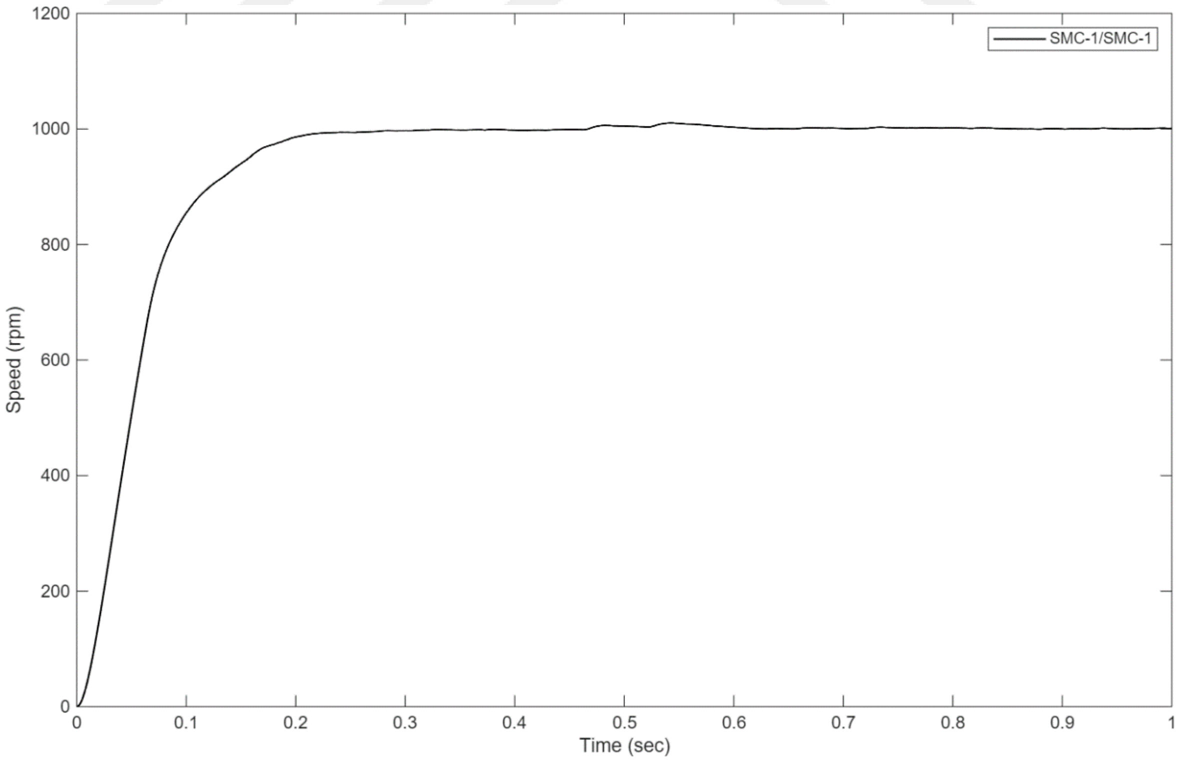

Figure 4.69. Output speed signal (rpm) (SMC-1/SMC-1)

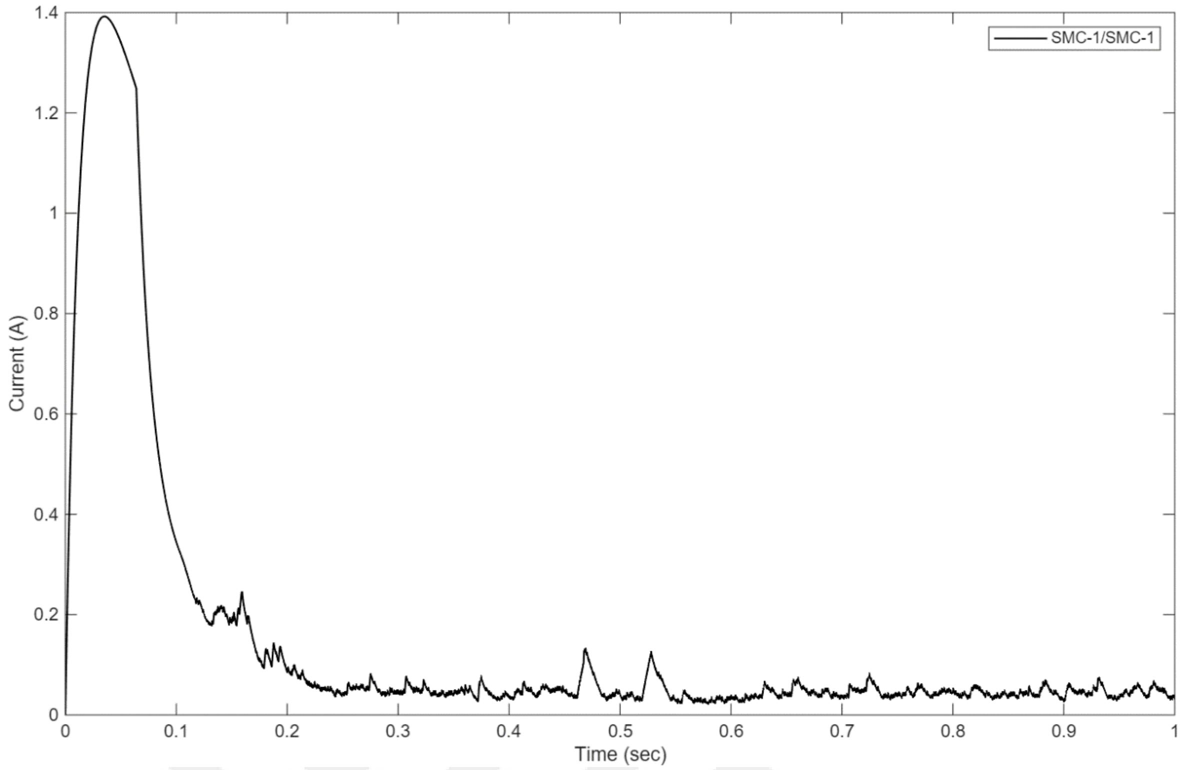

Figure 4.70. Armature current signal, $i_a(t)$ (SMC-1/SMC-1)

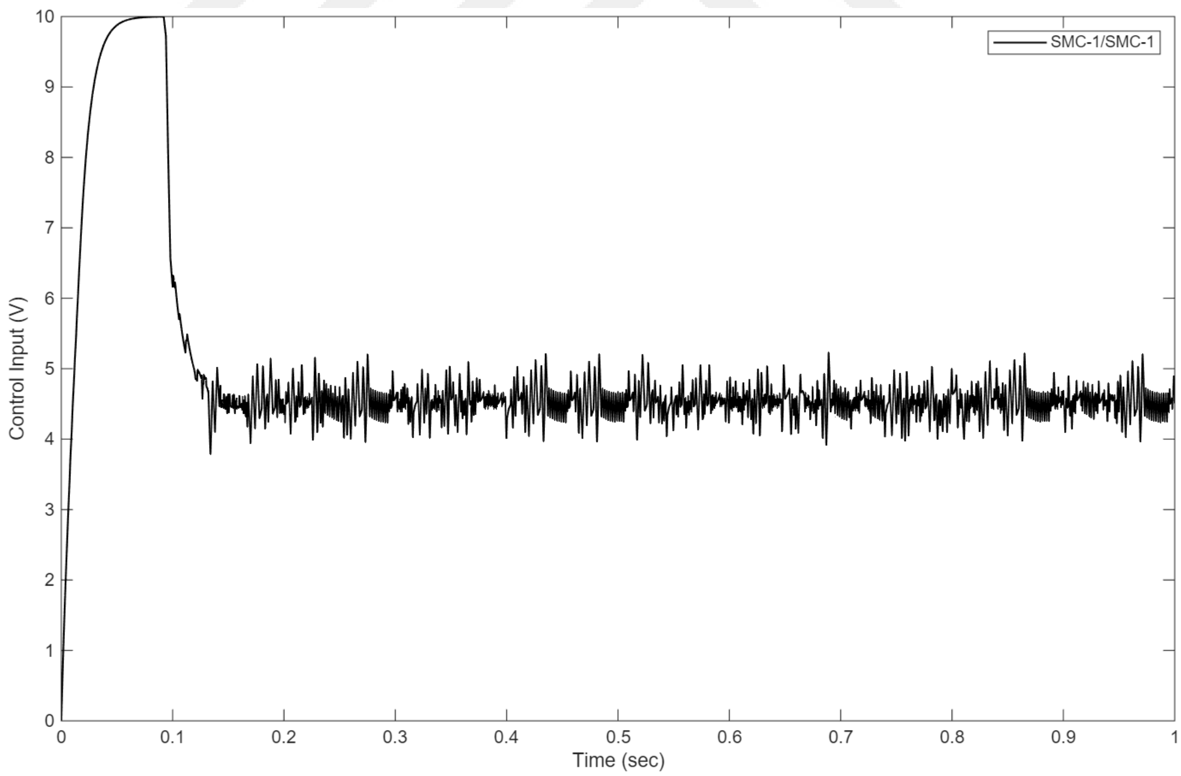

Figure 4.71. Control input voltage signal, $u(t)$ (SMC-1/SMC-1)

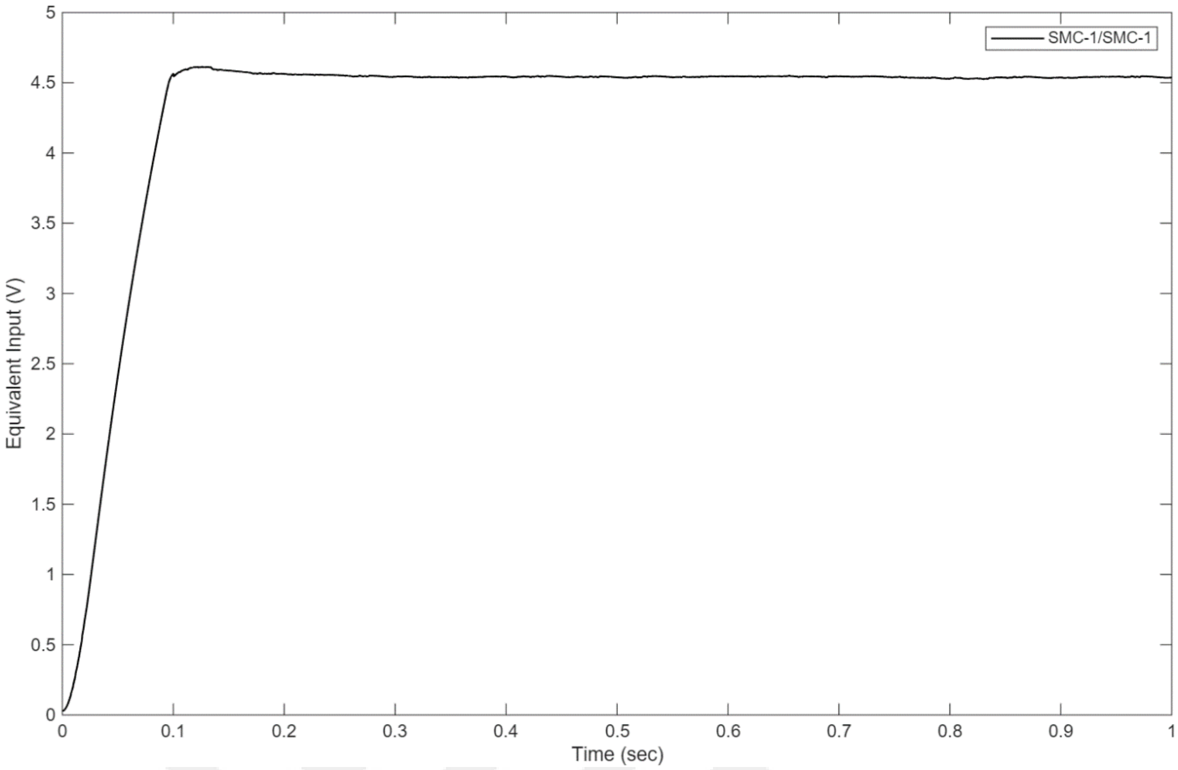

Figure 4.72. Equivalent input signal, $u_{eq}(t)$ (SMC-1/SMC-1)

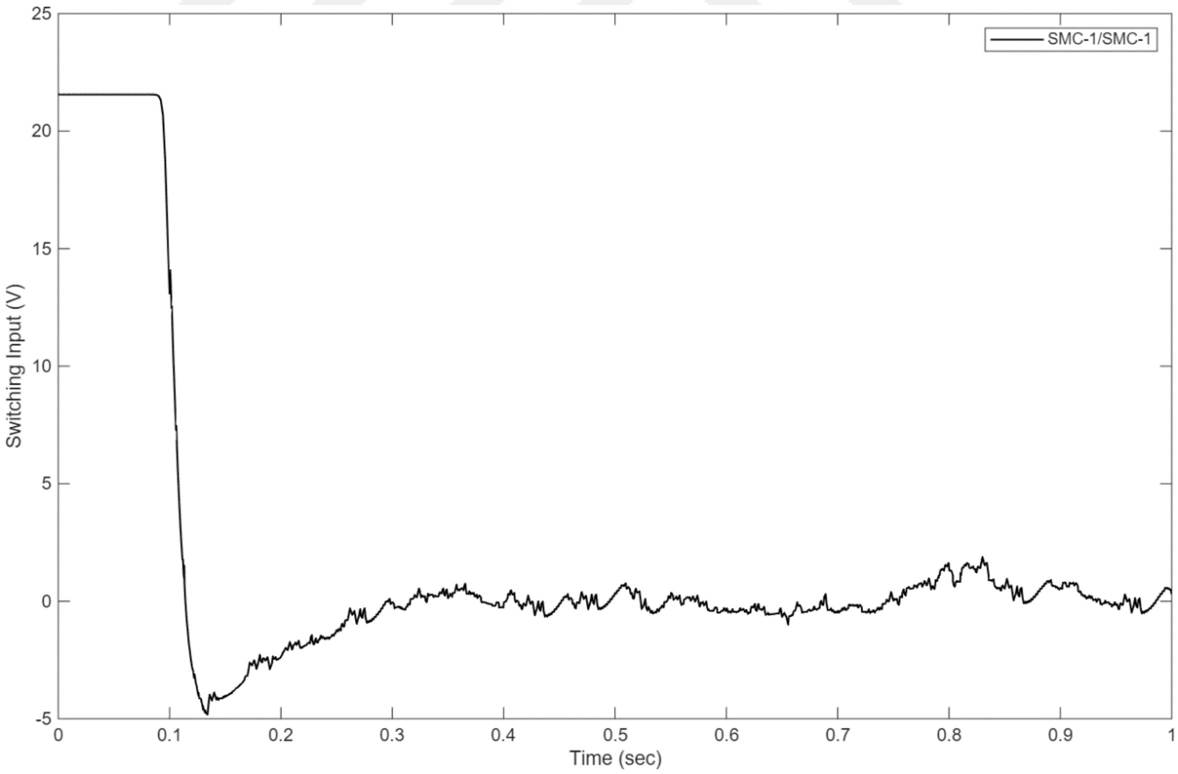

Figure 4.73. Switching input signal, $u_{sw}(t)$ (SMC-1/SMC-1)

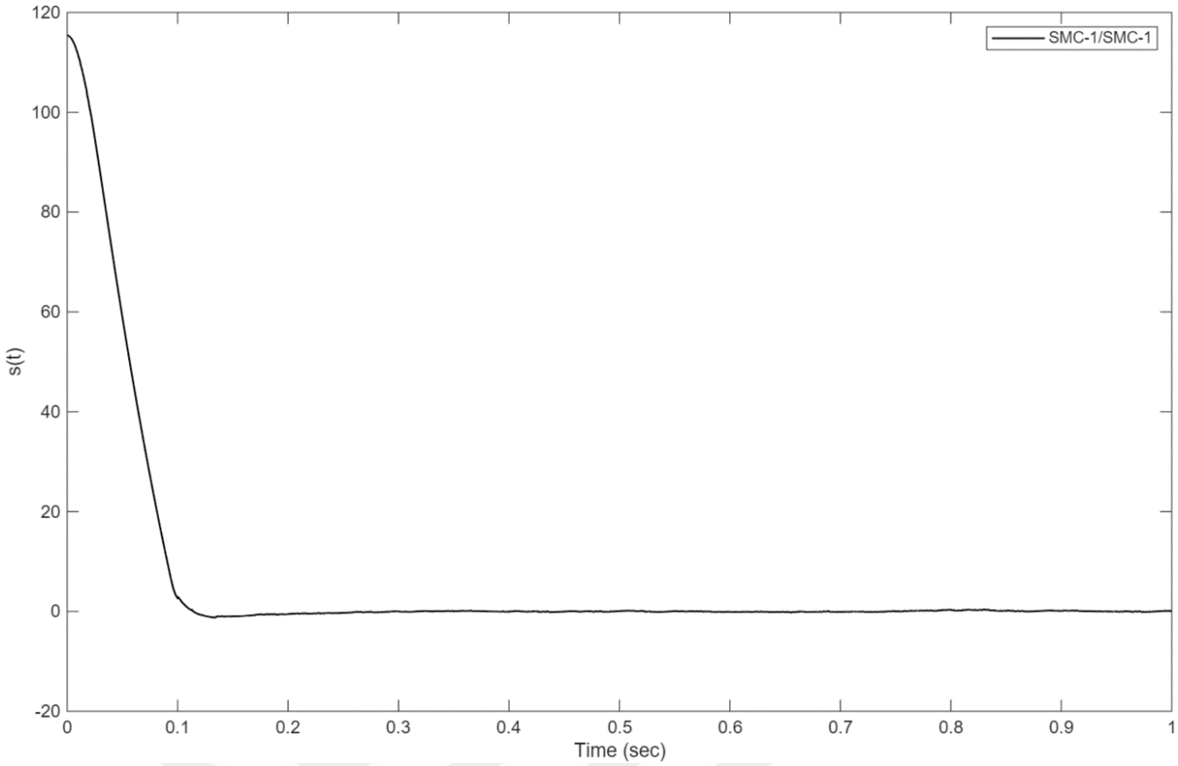

Figure 4.74. Sliding surface signal, $s(t)$ (SMC-1/SMC-1)

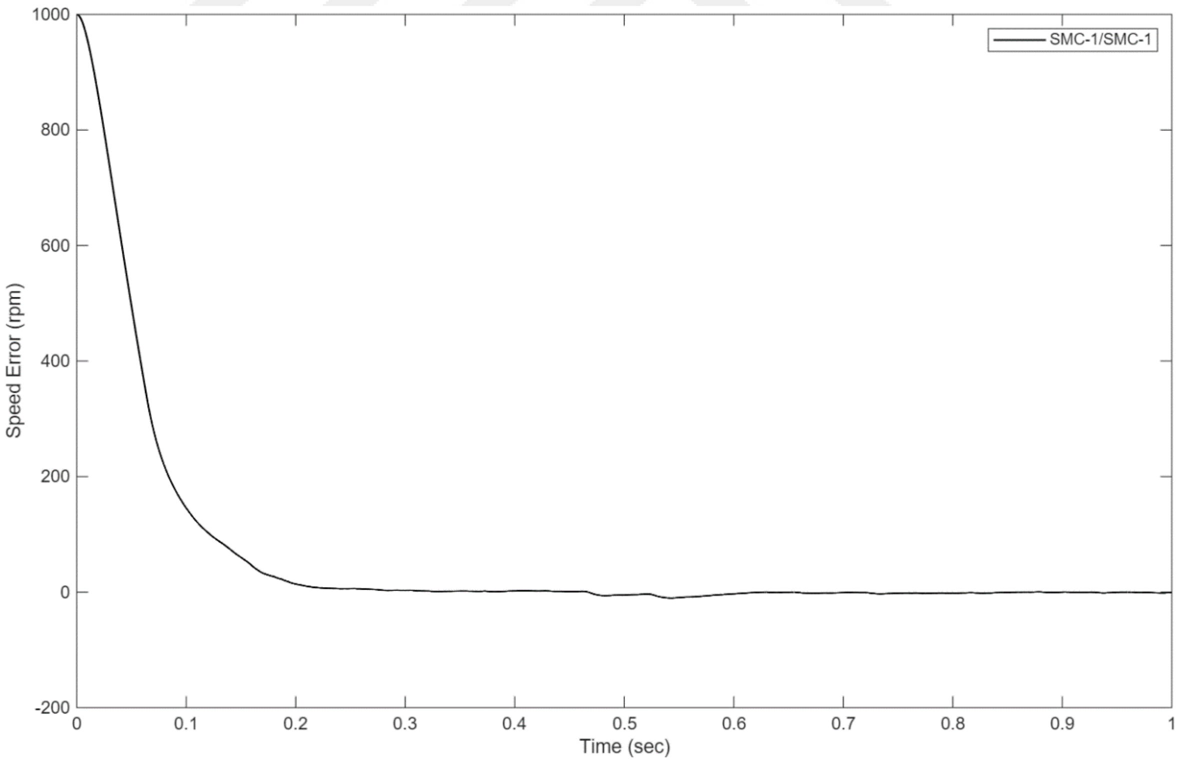

Figure 4.75. Speed error signal (rpm) (SMC-1/SMC-1)

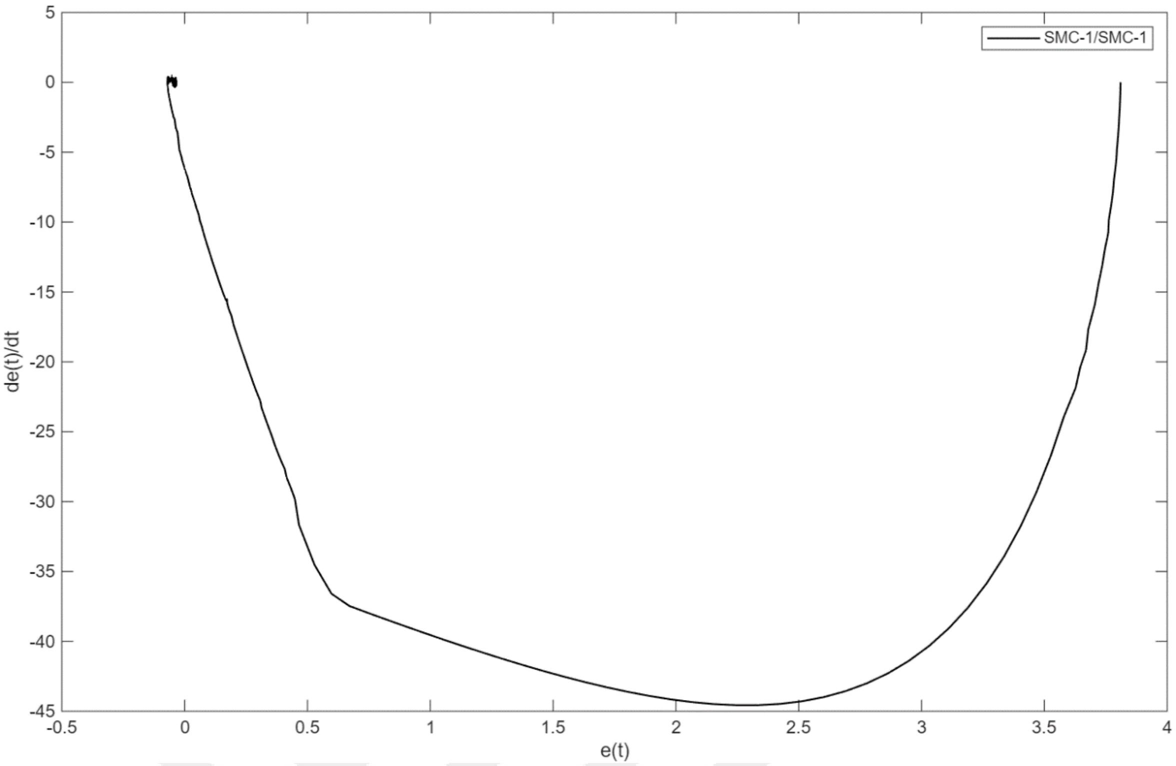

Figure 4.76. Phase plane of $e(t)$ and $de(t)/dt$ signal (SMC-1/SMC-1)

According to the time domain results presented in Table 4.17, the SMC-1/SMC-1 cascade controller demonstrates a fast and stable transient response. The rise time is 0.1062 s and the settling time is 0.1912 s, with an overshoot of 0.94% indicating a controlled and stable behavior. The system delay of 0.05 s further confirms the controller's prompt and effective response to input changes. Examining the performance indices in Table 4.18 the controller achieves ITAE = 0.0140, ISE = 0.534, IAE = 0.234 and ITSE = 0.014 demonstrating effective limitation of error magnitude and its time-weighted effects. The control effort indicator ISCI = 39.1 and ISTE = 0.0006 suggest that the system maintains balanced control action without excessive actuator activity. Overall, the results indicate that the SMC-based cascade controller provides a fast, stable and efficient control performance.

Table 4.17. Time domain results (SMC-1/SMC-1)

Controller	Rise Time (s)	Settling time (s)	Overshoot (%)	Delay time (s)
Cascade SMC Outer-Loop SMC-1/Inner-Loop SMC-1	0.1062	0.1912	0.94	0.05

Table 4.18. Performance indices (SMC-1/SMC-1)

Controller	ITAE	ISE	IAE	ITSE	ISCI	ISTE
Cascade SMC Outer-Loop SMC-1/Inner-Loop SMC-1	0.014	0.534	0.234	0.014	39.1	0.000

4.6.2. Cascade Sliding Mode Control: Outer-Loop SMC-2/Inner-Loop SMC-1 (SMC-2/SMC-1)

- **Outer-Loop SMC-2 Parameters:**
  Control coefficients: $k_d = 1.3,\ k_p = 55,\ k_i = 1.5,\ k_s = 3$
  Smoothing parameter: $\Omega = 16$
  Sliding surface parameters: $\lambda_1 = 150,\ \beta = 1$
- **Inner-Loop SMC-1 Parameters:**
  Control coefficients: $k_d = 0.4,\ k_p = 11,\ k_i = 5,\ k_{sc} = 6.5$
  Smoothing parameter: $\Omega = 10.5$

The CSMC system combining SMC-2/SMC-1 is modeled in detail. The output speed response demonstrates a highly accurate tracking capability with minimal transient deviations, surpassing the performance observed in the SMC-1/SMC-1 configuration. The output speed response illustrated in Figure 4.77, Figure 4.78 presents the armature current signal, which exhibits enhanced stability and reduced ripple, indicating a smoother electrical behavior under cascade control. The control effort required, displayed in Figure 4.79, reflects an efficient control strategy, while the switching input in Figure 4.80 shows reduced chattering compared to the previous configuration. Further insights into the system's internal dynamics are provided by the equivalent input (Figure 4.81) and sliding surface signal (Figure 4.82) which illustrate precise corrective actions and strong adherence to the sliding manifold. Error signal (Figure 4.83), the error signal and its derivative (Figure 4.84), clearly depict improved transient response and control accuracy. Collectively, these figures highlight the superior robustness, smoother control signals and enhanced overall performance of the SMC-2/SMC-1 cascade control system when compared to the SMC-1/SMC-1 architecture.

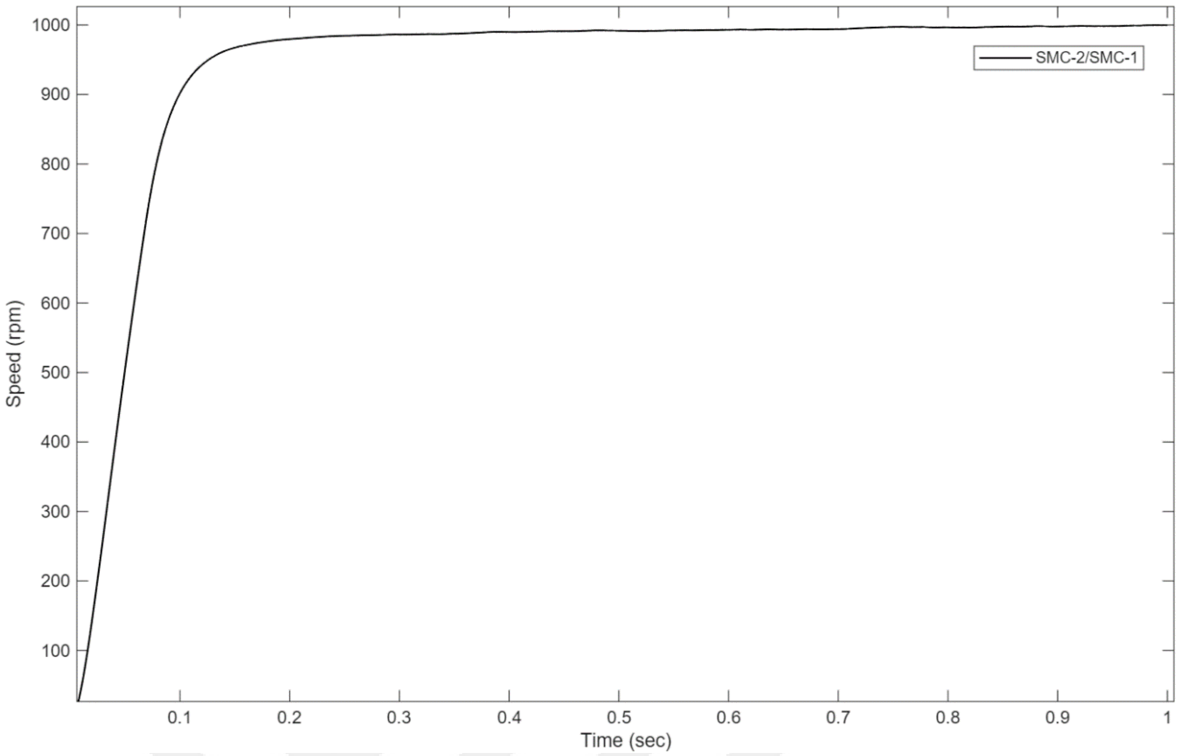

Figure 4.77. Output speed signal (rpm) (SMC-2/SMC-1)

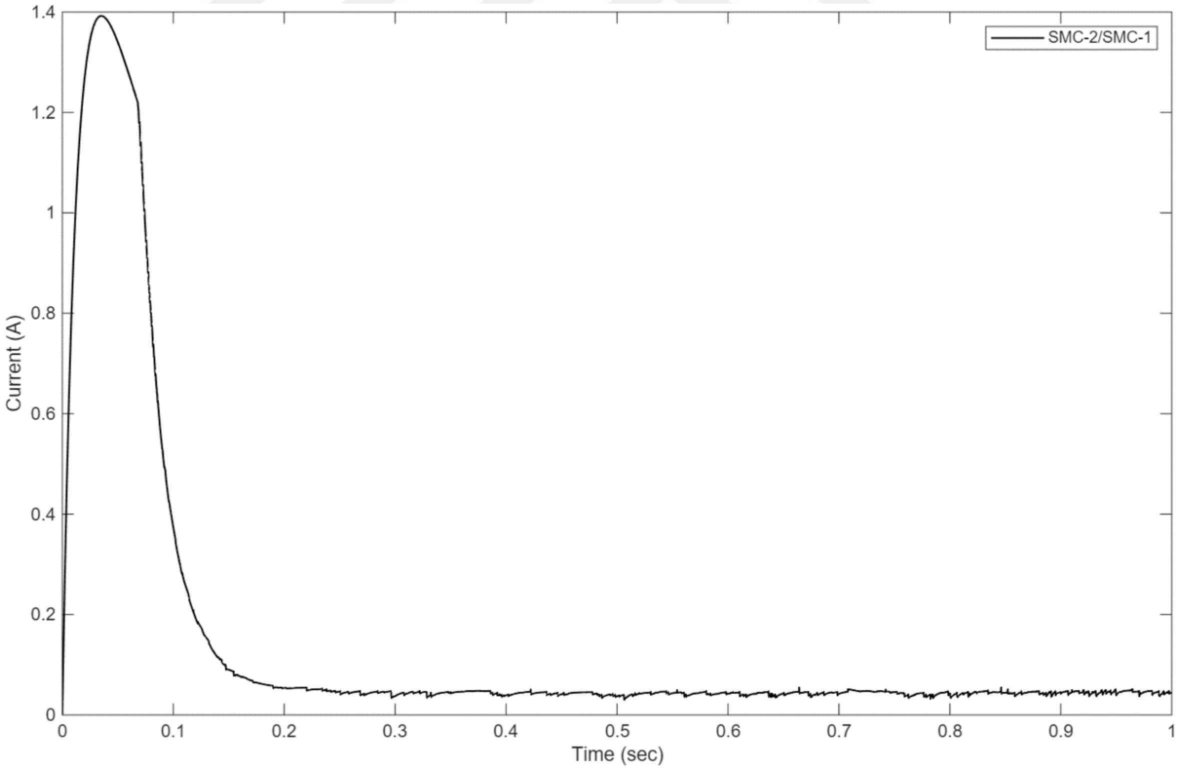

Figure 4.78. Armature current signal, $i_a(t)$ (SMC-2/SMC-1)

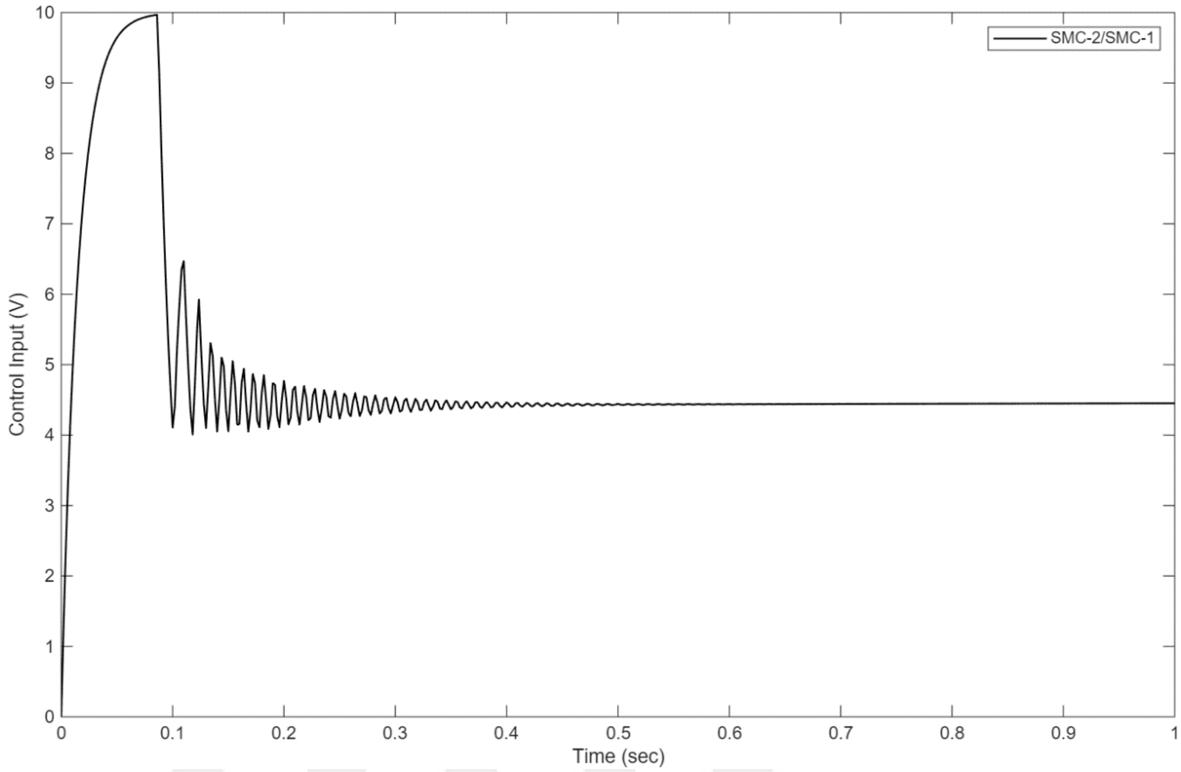

Figure 4.79. Control input voltage signal, $u(t)$ (SMC-2/SMC-1)

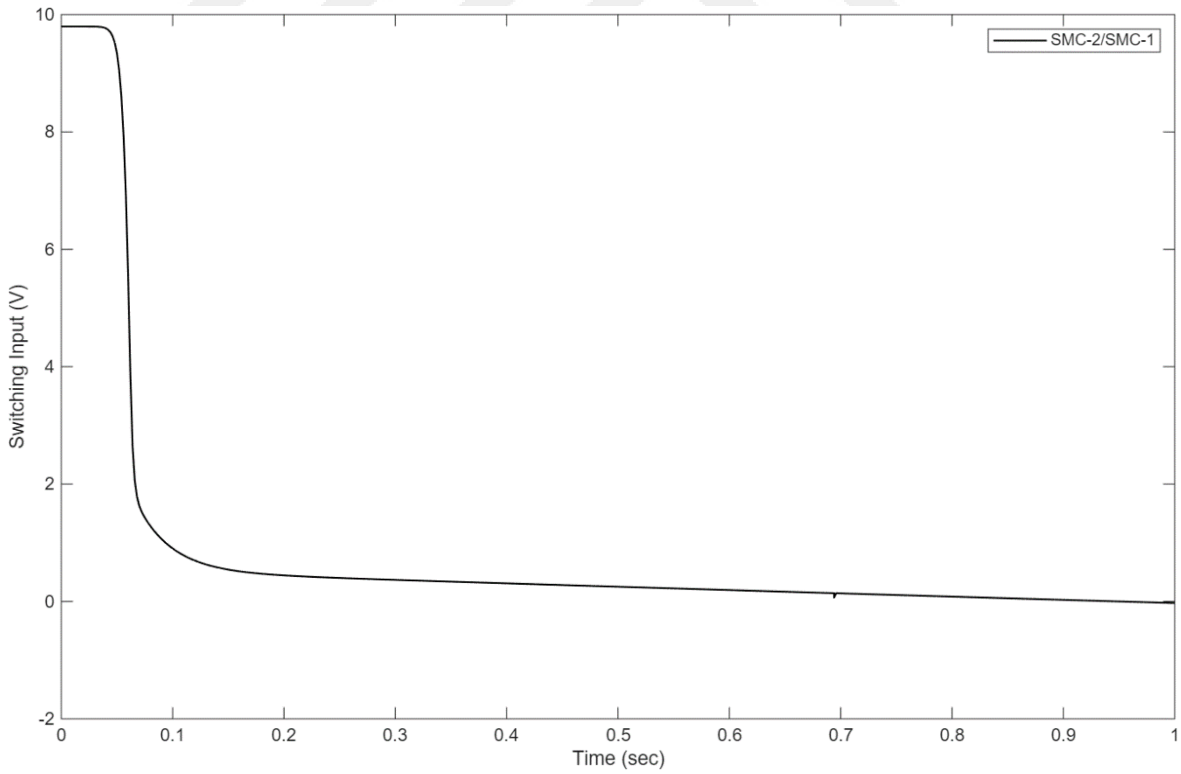

Figure 4.80. Switching input signal, $u_{sw}(t)$ (SMC-2/SMC-1)

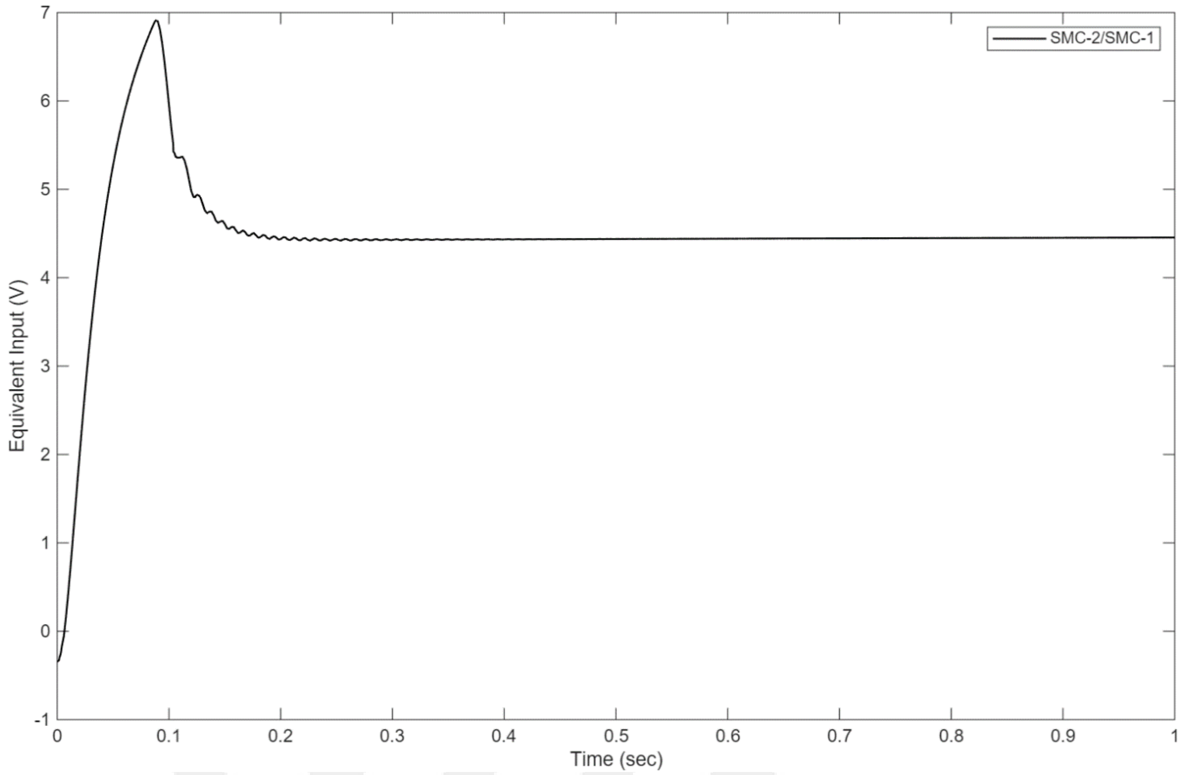

Figure 4.81. Equivalent input signal, $u_{eq}(t)$ (SMC-2/SMC-1)

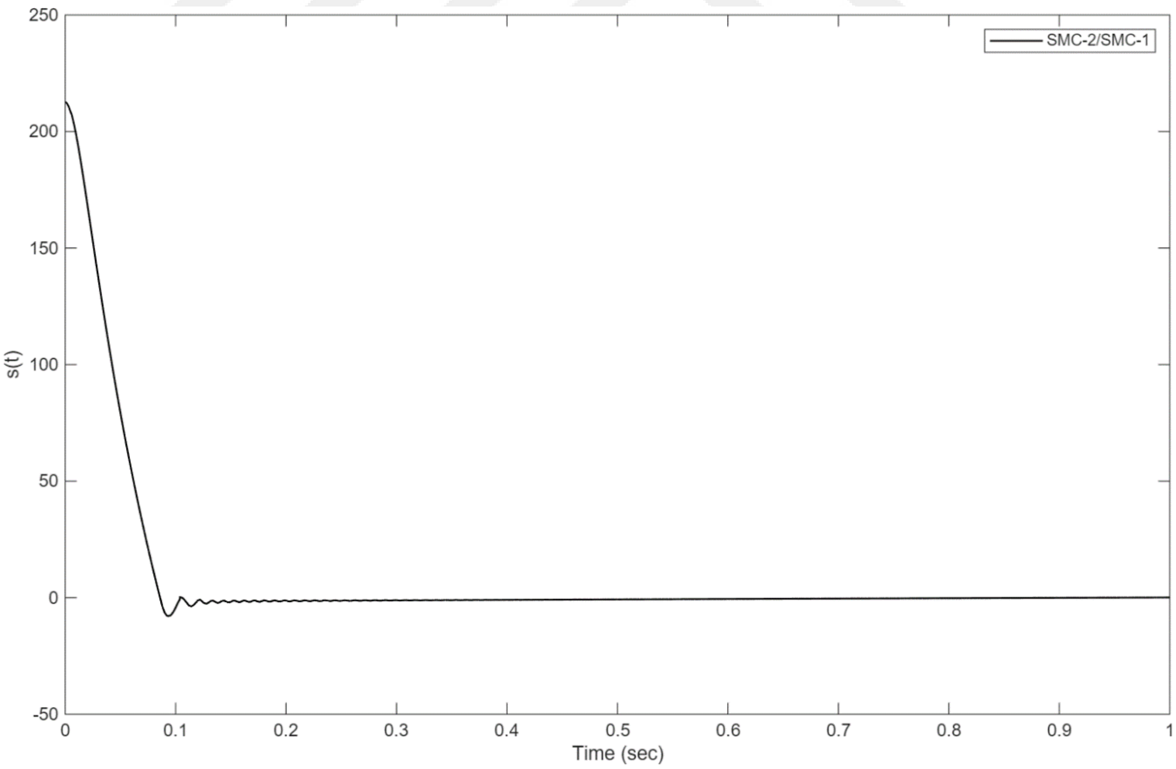

Figure 4.82. Sliding surface signal, $s(t)$ (SMC-2/SMC-1)

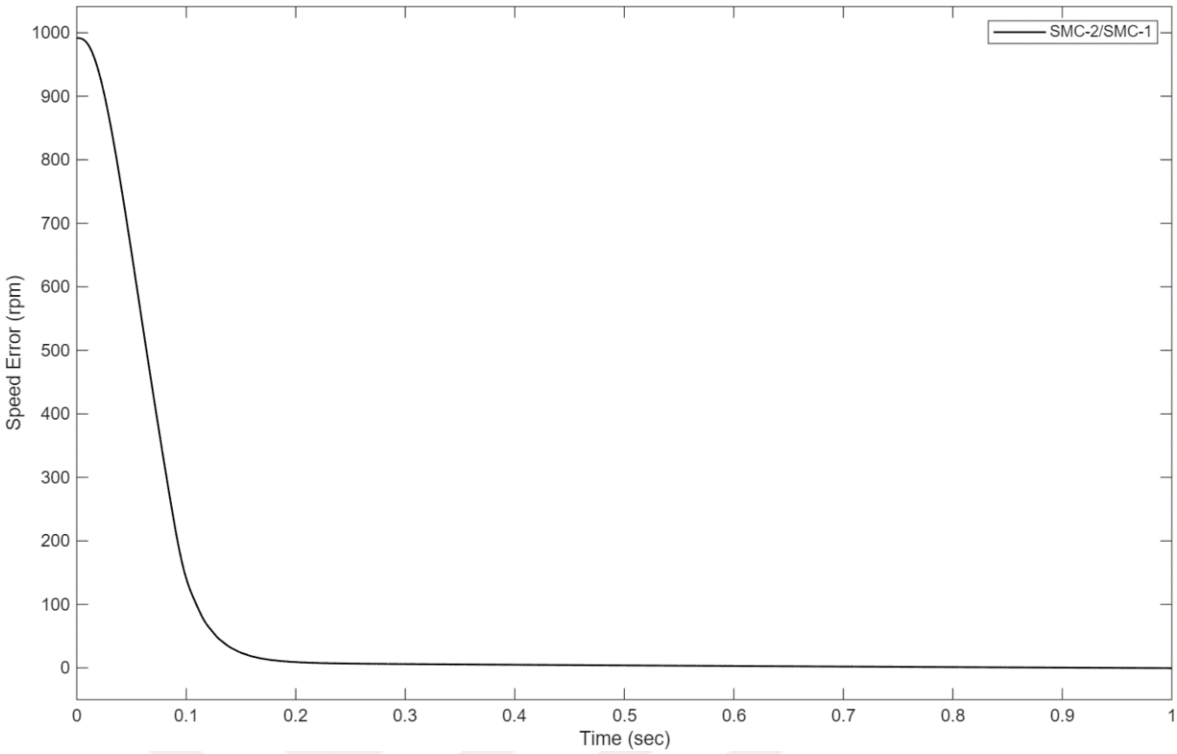

Figure 4.83. Speed error signal (rpm) (SMC-2/SMC-1)

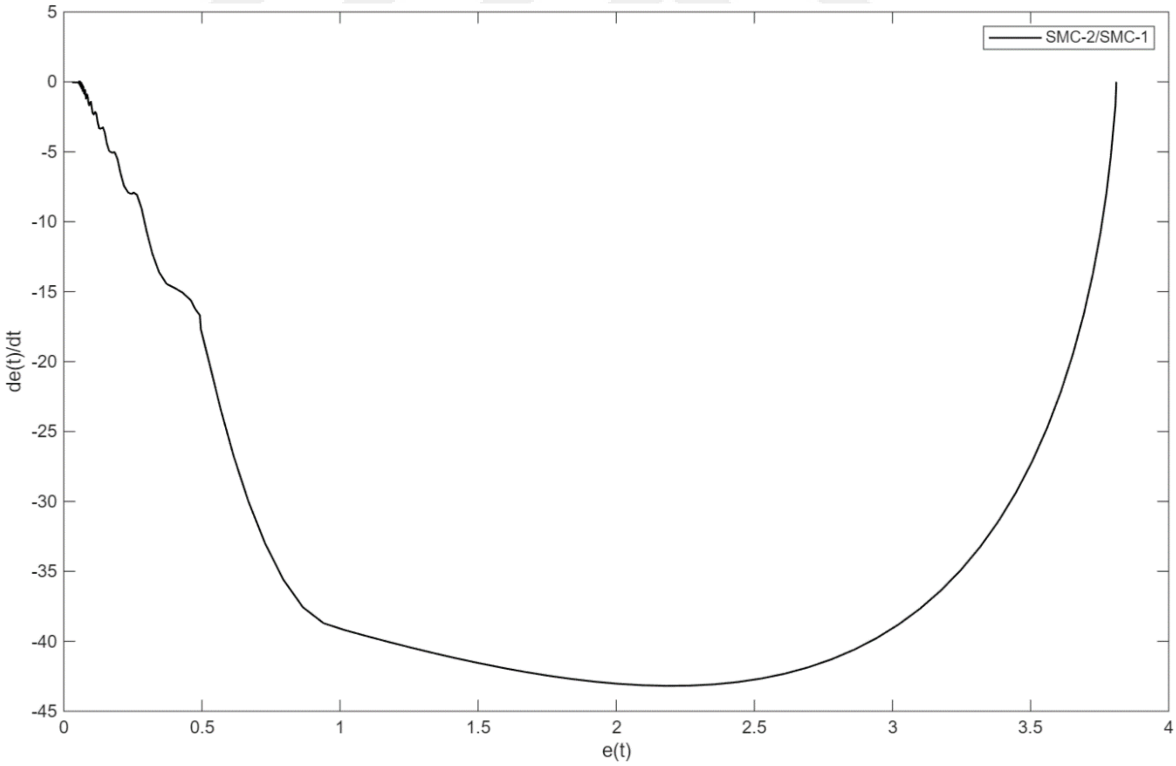

Figure 4.84. Phase plane of $e(t)$ and $de(t)/dt$ signal (SMC-2/SMC-1)

According to the time domain results presented in Table 4.19, the SMC-2/SMC-1 cascade controller demonstrates a fast and stable transient response. The rise time is 0.0835 s and the settling time is 0.18 s, with an overshoot of only 0.01%, indicating a highly stable response. The system delay of 0.05 s further confirms the controller's prompt and effective response to input changes. Examining the performance indices in Table 4.20 the controller achieves ITAE = 0.018, ISE = 0.523, IAE = 0.231 and ITSE = 0.013 reflecting effective limitation of error magnitude and its time-weighted effects. The control effort indicator ISCI = 47.95 and ISTE = 0.000 indicate that the system maintains a balanced control action without excessive actuator activity. Overall, these results demonstrate that the SMC-based cascade controller provides fast, stable and efficient control performance.

Table 4.19. Time domain results (SMC-2/SMC-1)

Controller	Rise Time (s)	Settling time (s)	Overshoot (%)	Delay time (s)
Cascade SMC Outer-Loop SMC-2/Inner-Loop SMC-1	0.0835	0.18	0.01	0.05

Table 4.20. Performance indices (SMC-2/SMC-1)

Controller	ITAE	ISE	IAE	ITSE	ISCI	ISTE
Cascade SMC Outer-Loop SMC-2/Inner-Loop SMC-1	0.018	0.523	0.231	0.013	47.95	0.000

4.7. Experimental Results of Single-Loop Controllers (P, PI, PID)

In this section, the experimental results obtained from the single-loop P, PI and PID controllers are presented and analyzed. The performance of each controller is evaluated based on real-time measurements of system response, including output speed, current, control signals and error dynamics. These experimental findings are compared with the simulation data to validate the accuracy and effectiveness of the implemented control strategies.

4.7.1. Experimental Results of Single-Loop P Controller

Figure 4.85 shows the experimental setup of the single-loop control system. In this subsection, the experimental results for the single-loop proportional (P) controller are presented. The proportional gain was set to $k_p = 50$, which was determined experimentally to achieve a satisfactory balance between response speed and steady-state accuracy. During the experiments, the system outputs—including speed (Figure 4.86), current signal (Figure 4.87), control signal (Figure 4.88), the error signal (Figure 4.89), and the error alongside its derivative (Figure 4.90)—were measured and analyzed. The findings demonstrate that the single-loop P controller is capable of regulating the DC motor speed with a relatively simple structure, although a noticeable steady-state error remains compared to more advanced control strategies.

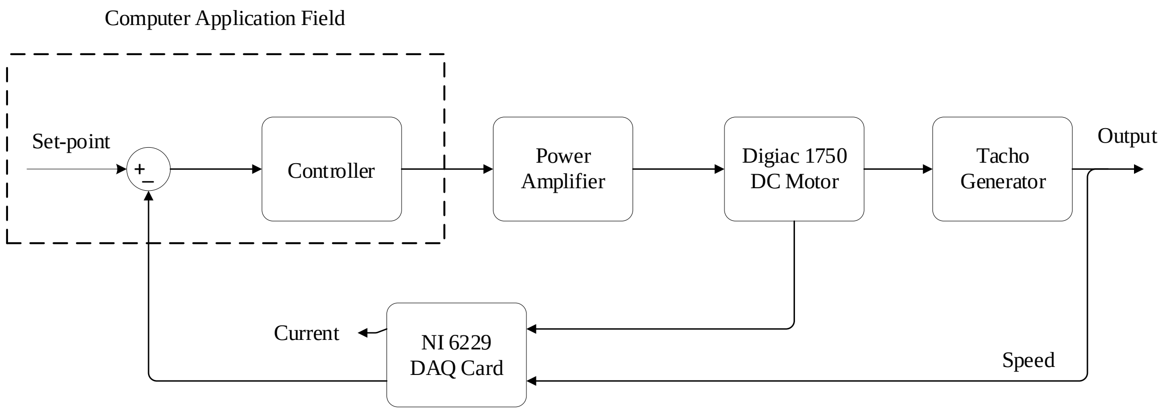

Figure 4.85. Experimental setup of the single-loop control system

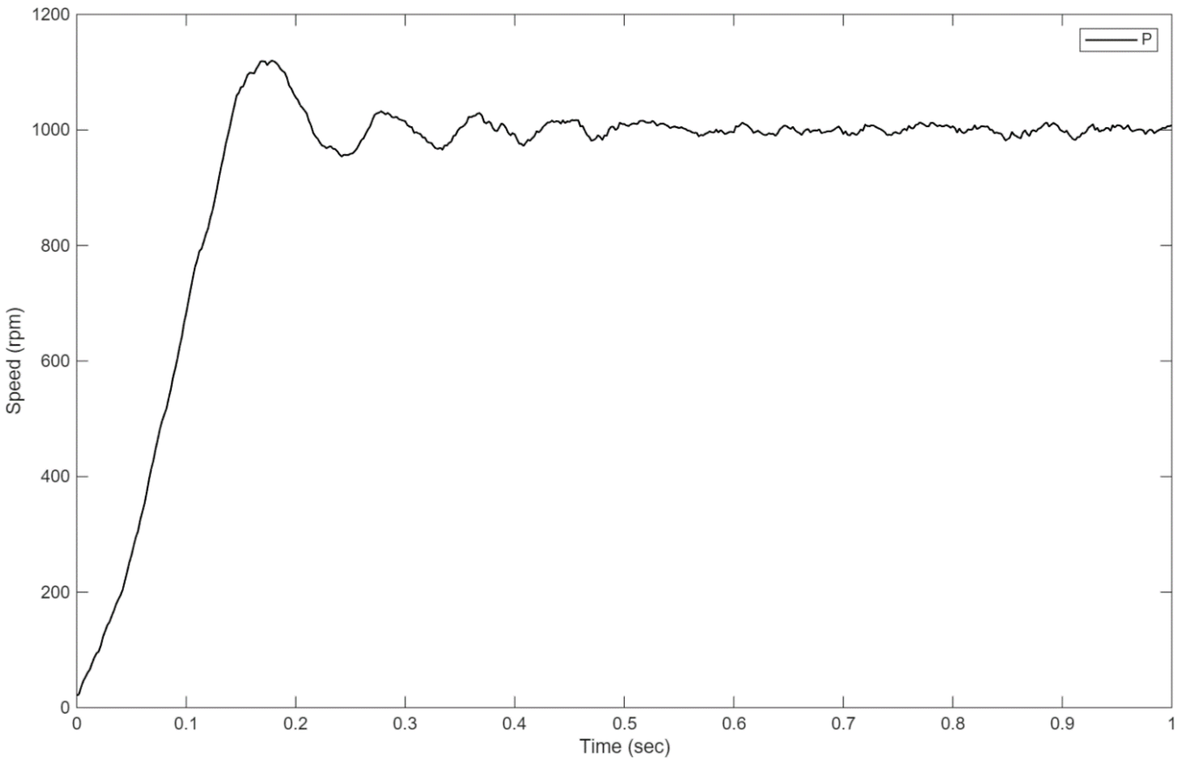

Figure 4.86. Output speed (rpm) (P)

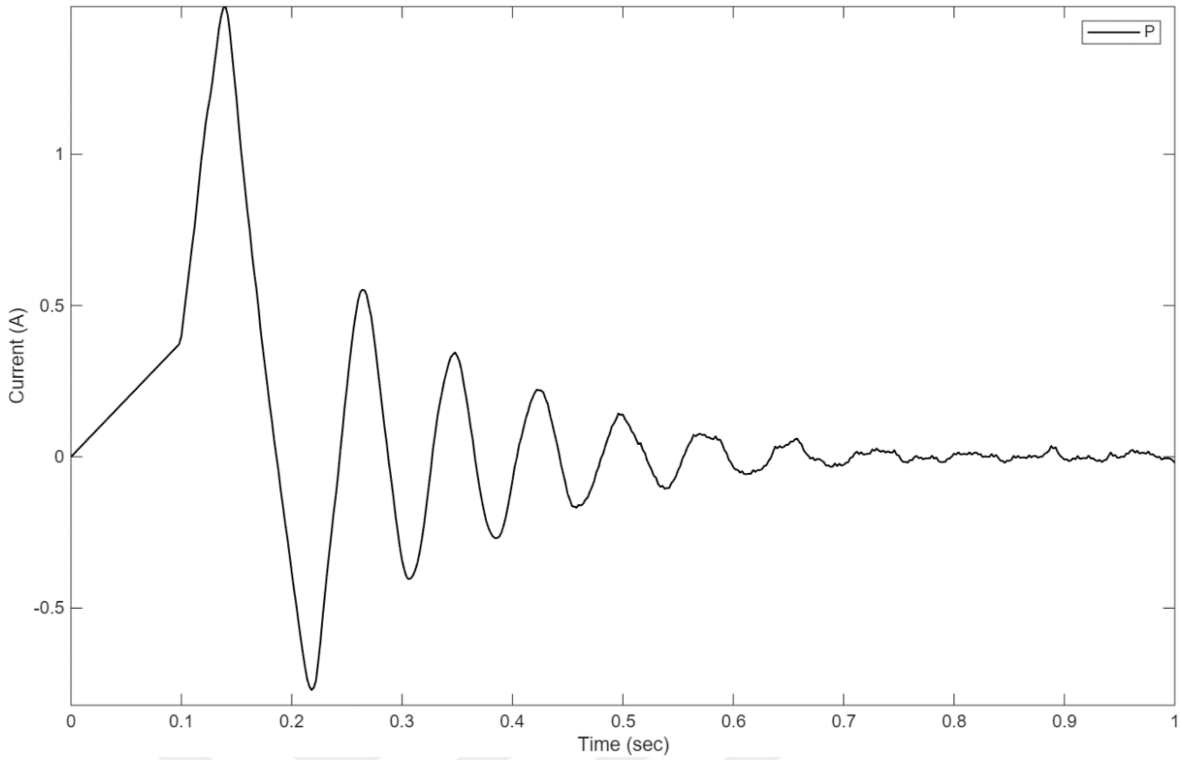

Figure 4.87. Armature current, $i_a(t)$ (P)

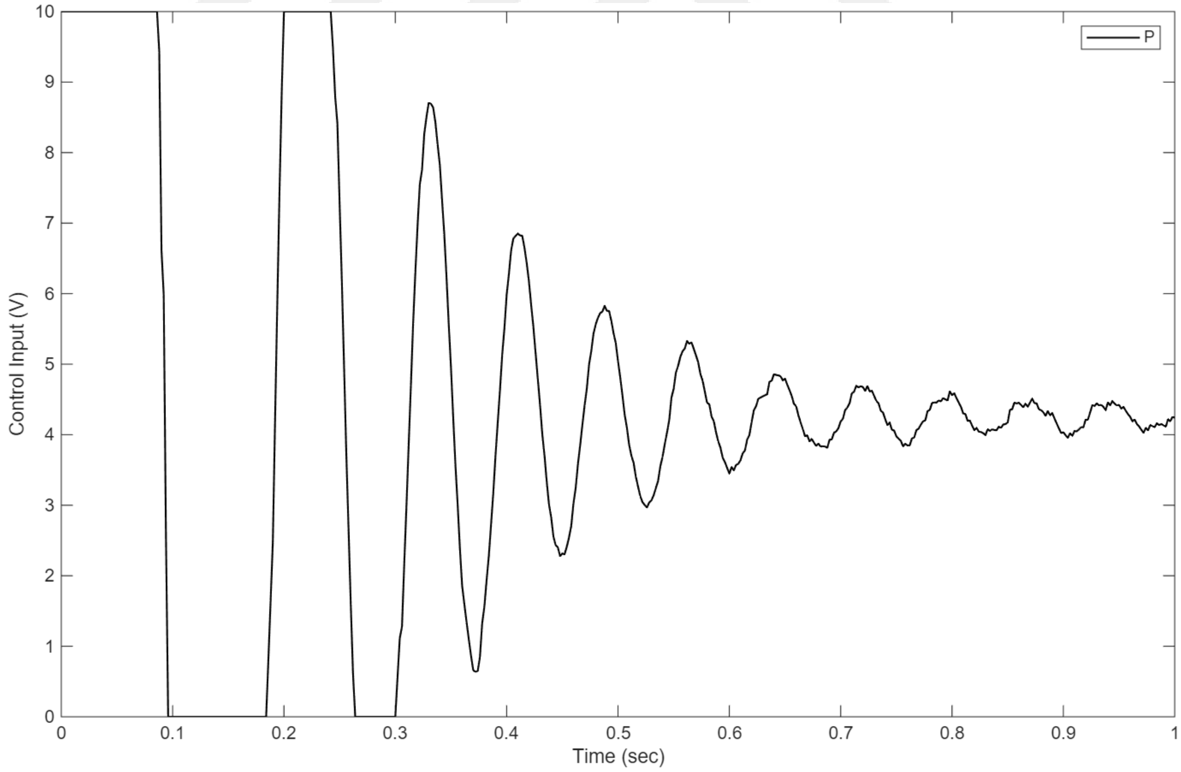

Figure 4.88. Control input voltage, $u(t)$ (P)

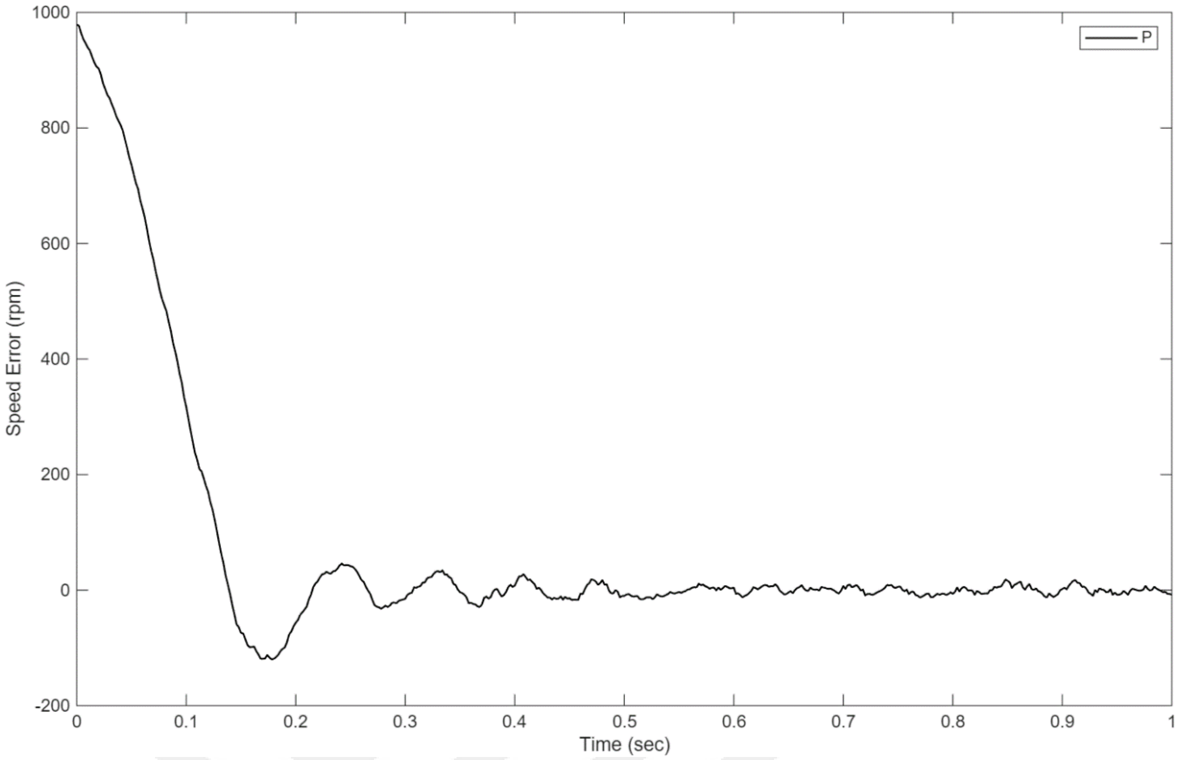

Figure 4.59. Speed error (rpm) (P)

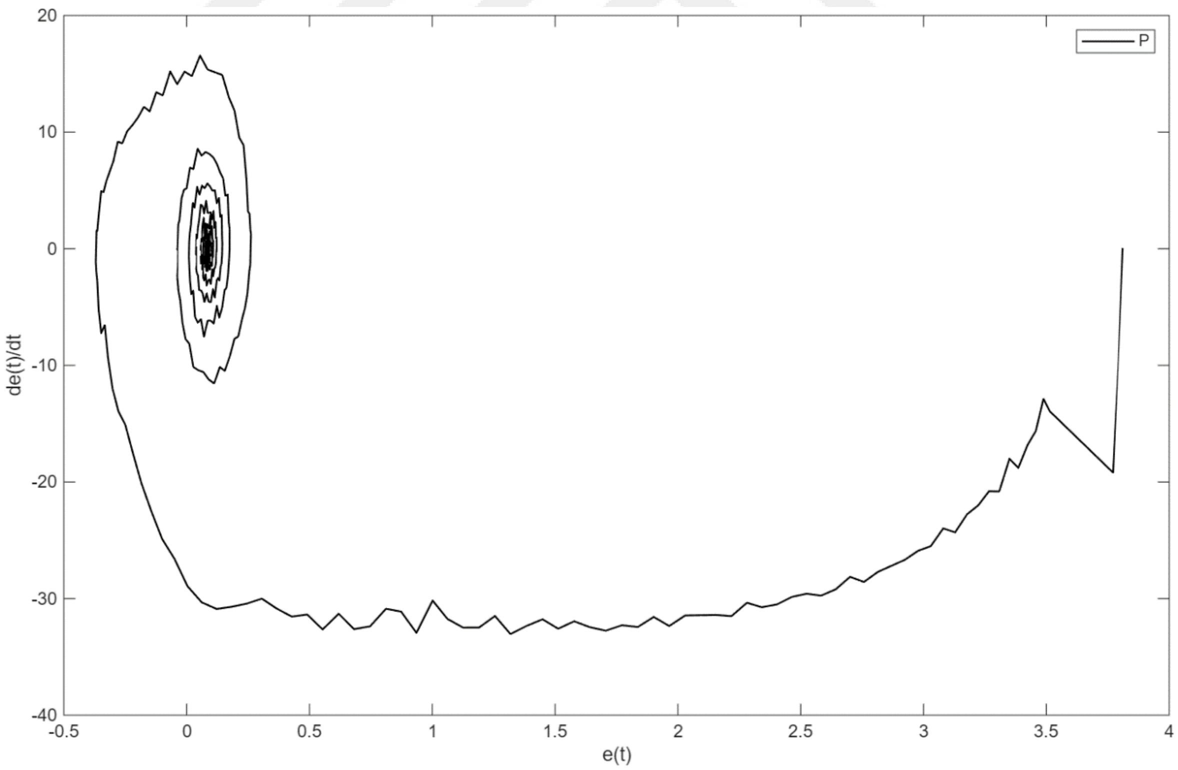

Figure 4.90. Phase plane of $e(t)$ and $de(t)/dt$ (P)

According to the time domain results presented in Table 4.21 the single-loop P controller exhibits a measurable transient response. The rise time is 0.0614 s and the settling time is 0.2842 s, with an overshoot of 14.9% indicating a significant overshoot behavior. The system delay is 0.0320 s, demonstrating that the controller responds promptly to input changes. Examining the performance indices in Table 4.22 the controller achieves ITAE = 0.0590, ISE = 0.8864, IAE = 0.397 and ITSE = 0.037 reflecting that error magnitudes and their time-weighted effects are moderately constrained. The control effort indicator ISCI = 31.95 and ISTE = 0.028, indicate a measurable control performance with a limited level of control effort. Overall, the results suggest that while the single-loop P controller provides a rapid rise, it exhibits noticeable overshoot and moderate stability.

Table 4.21. Time domain performance specifications (P)

Controller	Rise Time (s)	Settling time (s)	Overshoot (%)	Delay time (s)
P	0.0614	0.2842	14.9	0.0320

Table 4.22. Output performance indices (P)

Controller	ITAE	ISE	IAE	ITSE	ISCI	ISTE
P	0.0590	0.8864	0.397	0.037	31.95	0.028

4.7.2. Experimental Results of Single-Loop PI Controller

In this subsection, the experimental results of the single-loop proportional–integral (PI) controller are presented. The controller parameters were set as follows: proportional gain $k_p = 25$ and integral gain $t_i = 2.08$. PI = $25\left(1 + \frac{1}{2.08s}\right)$, these values were determined experimentally to achieve a desirable compromise between fast transient response and minimal steady-state error. During the experiments, the system responses–including output speed (Figure 4.91), armature current (Figure 4.92), control input signal (Figure 4.93), error signal (Figure 4.94), error-the derivative were measured and analyzed (Figure 4.95). The results indicate that the PI controller provides improved steady-state performance compared to the P controller, while maintaining an adequate transient response in the regulation of the DC motor speed.

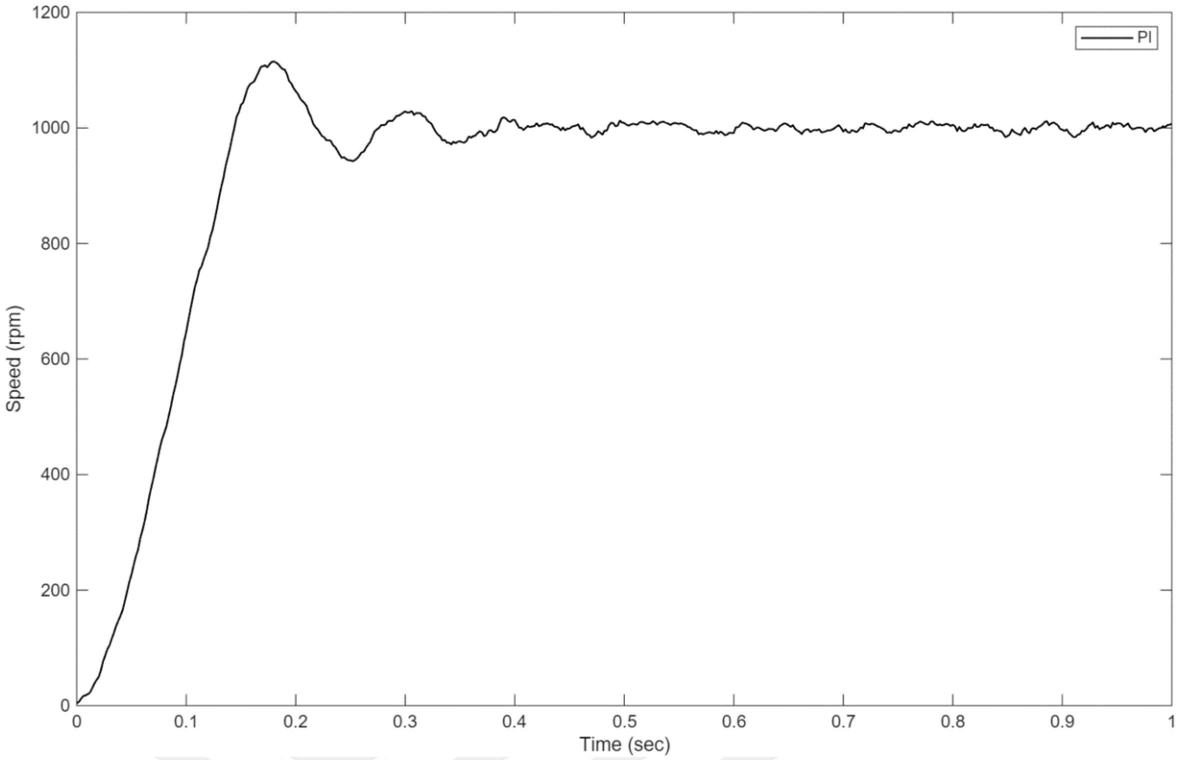

Figure 4.91. Output speed (rpm) (PI)

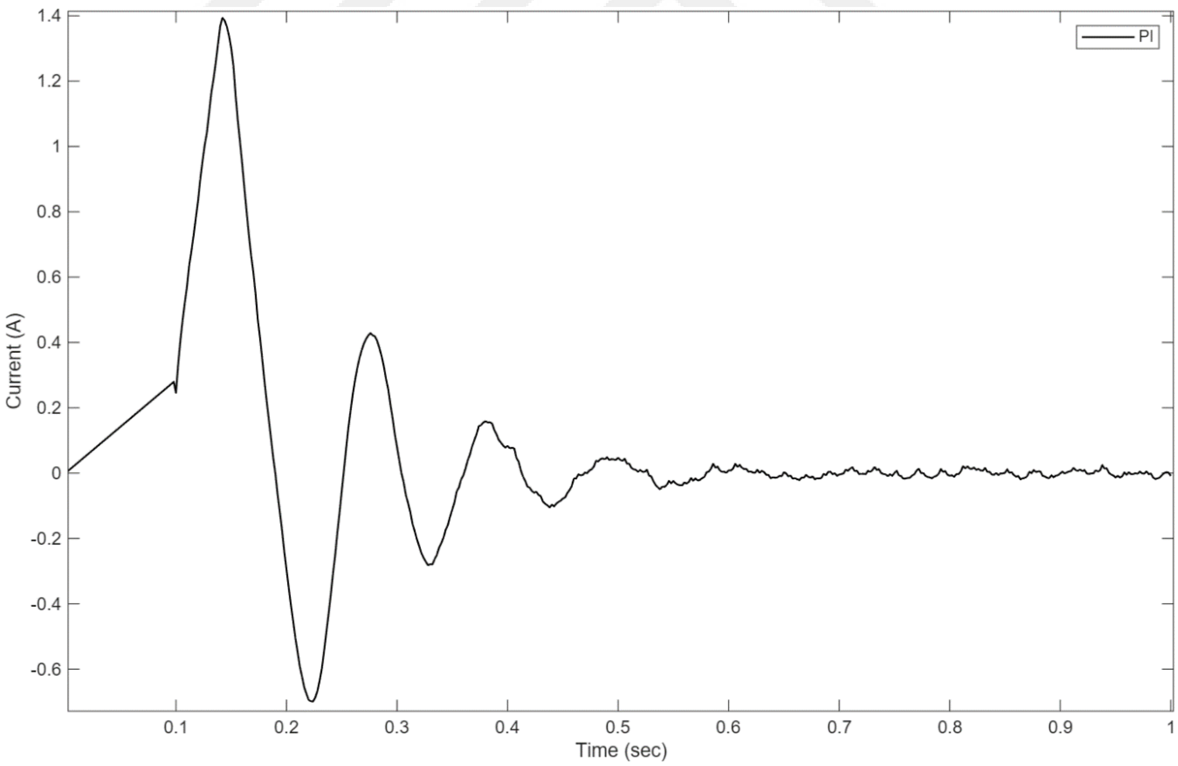

Figure 4.92. Armature current, $i_a(t)$ (PI)

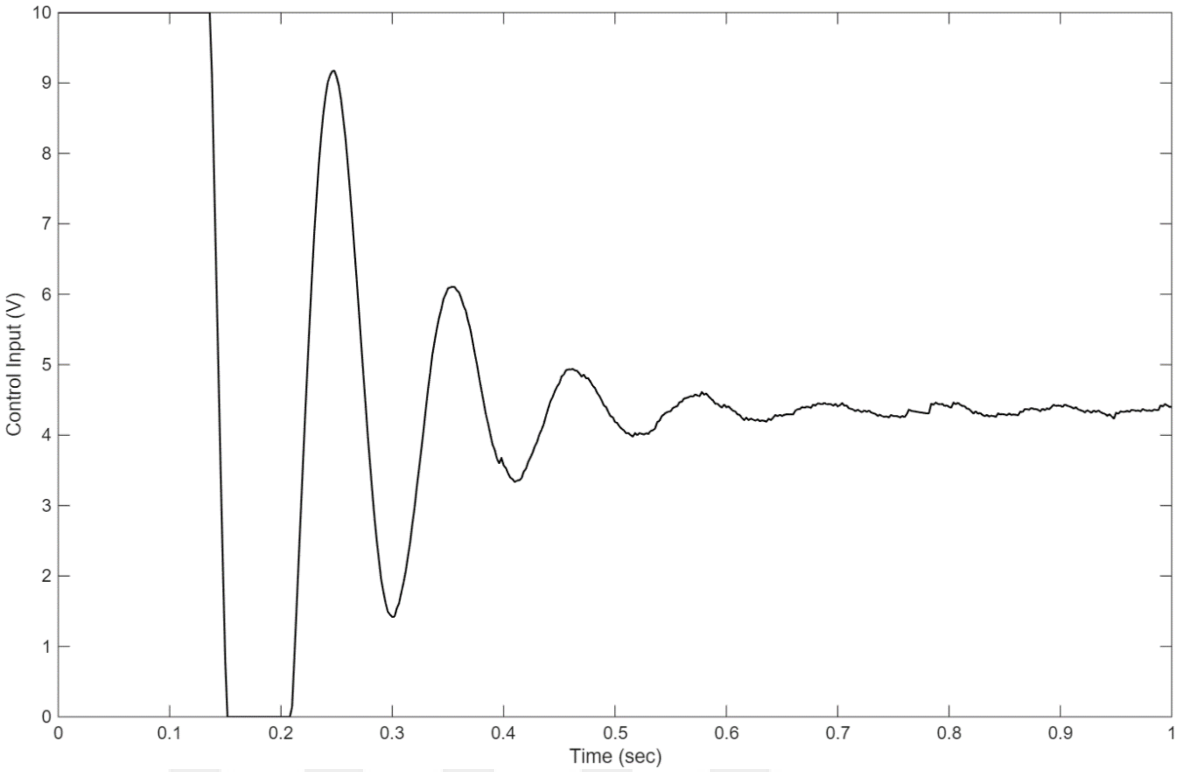

Figure 4.93. Control input voltage, $u(t)$ (PI)

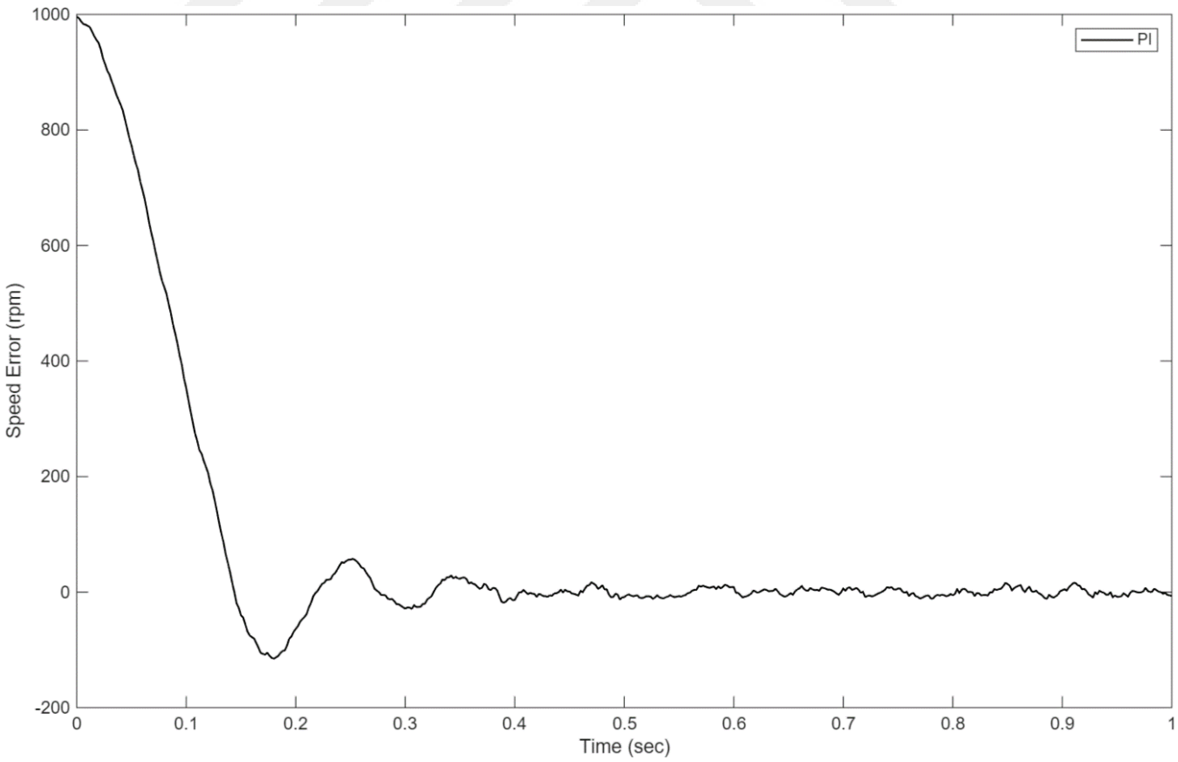

Figure 4.94. Speed error (rpm) (PI)

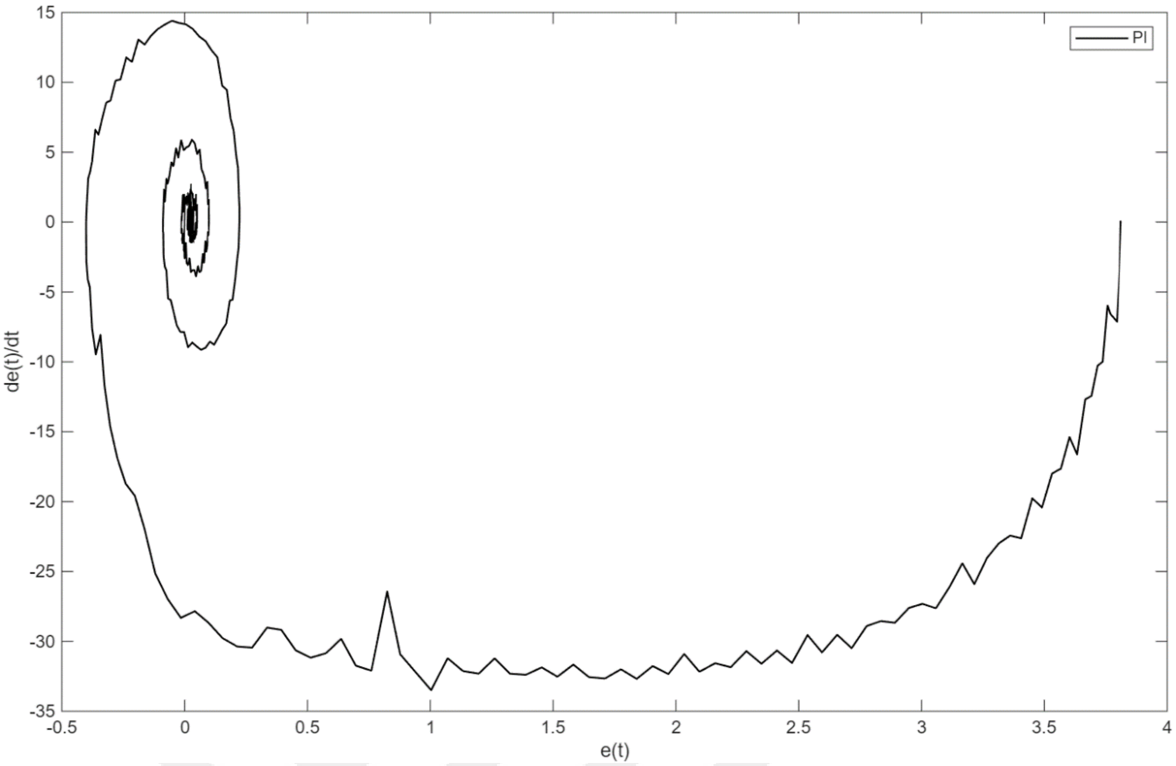

Figure 4.95. Phase plane of $e(t)$ and $de(t)/dt$ (PI)

According to the domain performance specifications presented in Table 4.23, the single-loop PI controller exhibits a measurable transient performance. The rise time is 0.098 s and the settling time is 0.3564 s, with an overshoot of 12.01%, indicating a moderate overshoot behavior. The system delay is 0.0820 s, demonstrating that the controller responds promptly yet in a controlled manner to input variations. Examining the performance indices in Table 4.24 the controller achieves ITAE = 0.0342, ISE = 0.865, IAE = 0.357 and ITSE = 0.034 reflecting that error magnitudes and their time-weighted effects are effectively constrained. The control effort indicator ISCI = 30.08 and ISTE = 0.0096 indicate balanced control action without excessive actuator effort. The results suggest that the single-loop PI controller provides a measurable rise and settling response, maintaining moderate overshoot and stable performance**.**

Table 4.23. Time domain performance specifications (PI)

Controller	Rise Time (s)	Settling time (s)	Overshoot (%)	Delay time (s)
PI	0.098	0.356	12.01	0.082

Table 4.24. Output performance indices (PI)

Controller	ITAE	ISE	IAE	ITSE	ISCI	ISTE
PI	0.034	0.865	0.357	0.034	30.08	0.009

4.7.3. Experimental Results of Single-Loop PID Controller

In this subsection, the experimental results of the single-loop PID controller are presented. The controller parameters were set as follows: PID = $30\left(1 + \frac{1}{0.333s} + 0.02s\right)$. These parameters were tuned to achieve optimal control performance during the experiments. The system responses, including output speed (Figure 4.96), armature current (Figure 4.97), control input signal (Figure 4.98), error (Figure 4.99) as well as error and the error's derivative were recorded and analyzed (Figure 4.100). The results demonstrate the effectiveness of the PID controller in regulating the DC motor speed and current with satisfactory transient and steady-state characteristics.

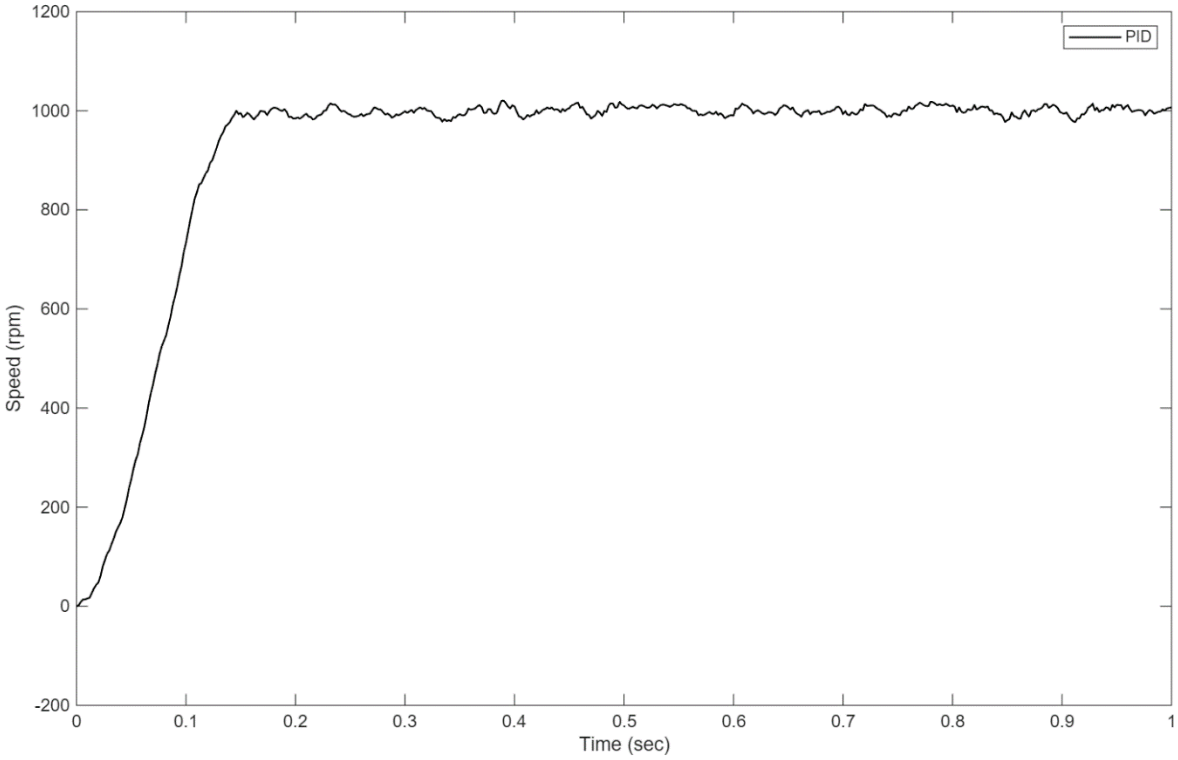

Figure 4.96. Output speed (rpm) (PID)

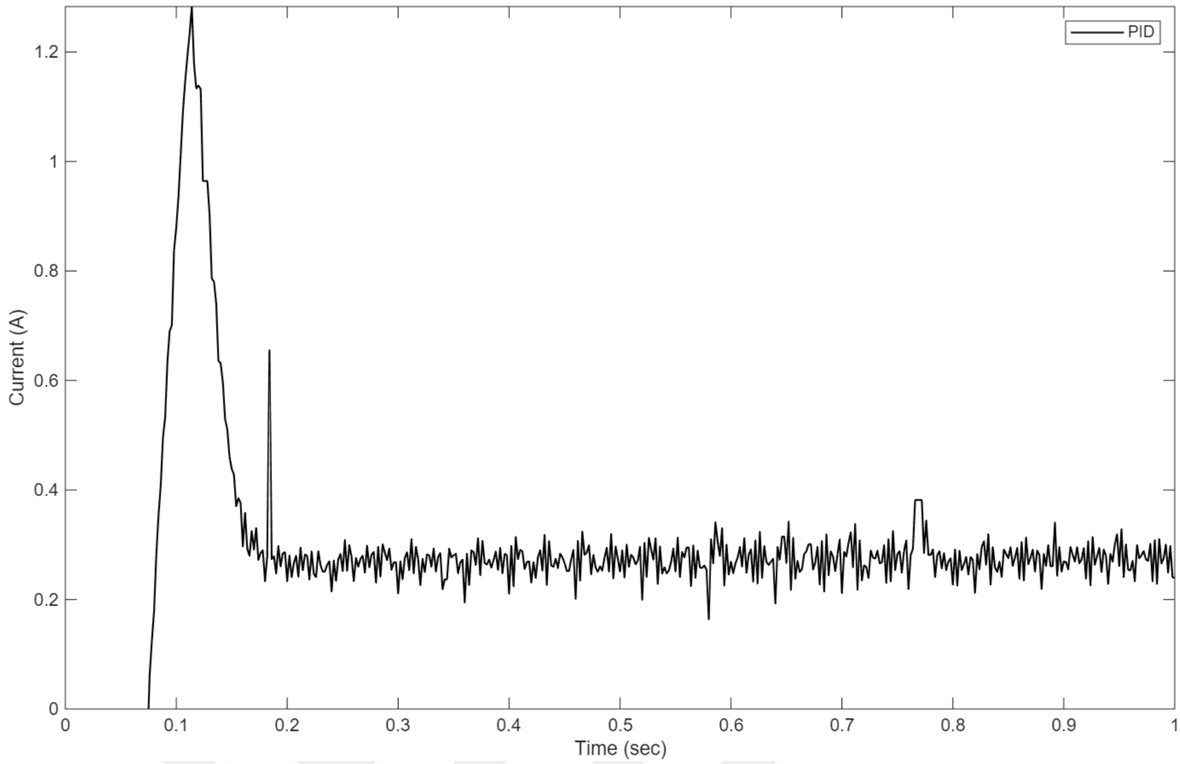

Figure 4.97. Armature current, $i_a(t)$ (PID)

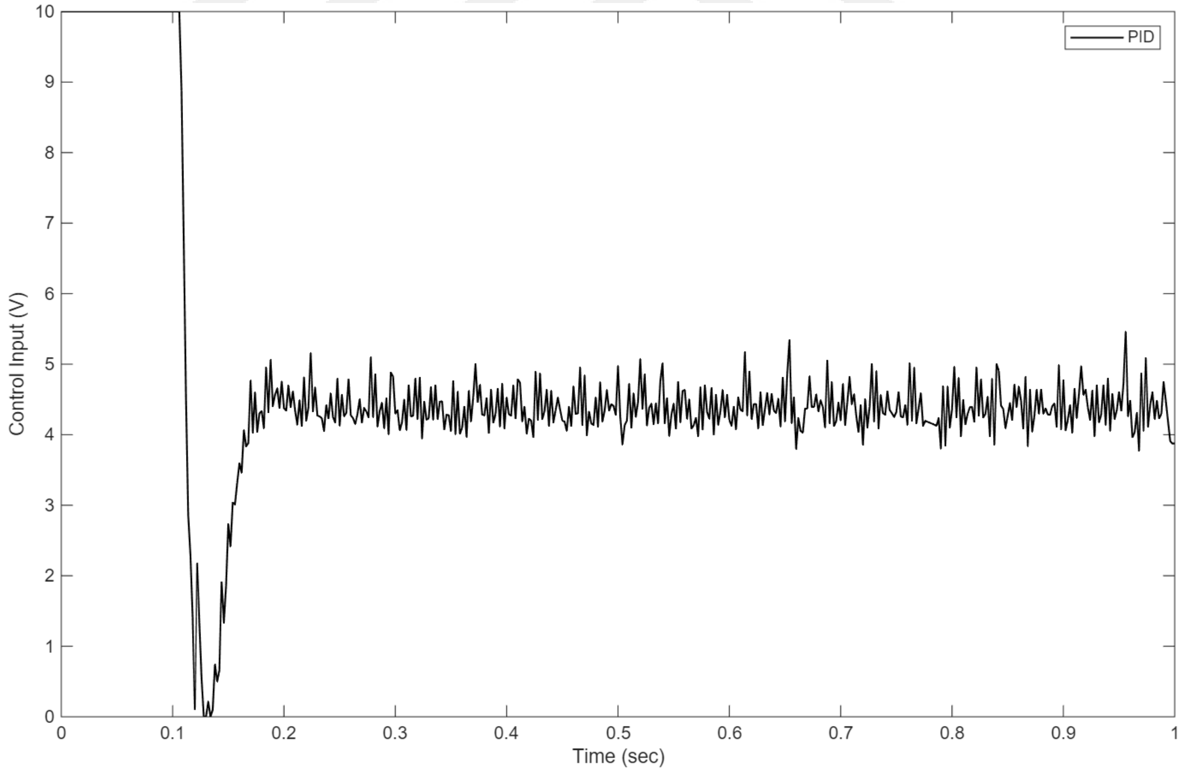

Figure 4.98. Control input voltage, $u(t)$ (PID)

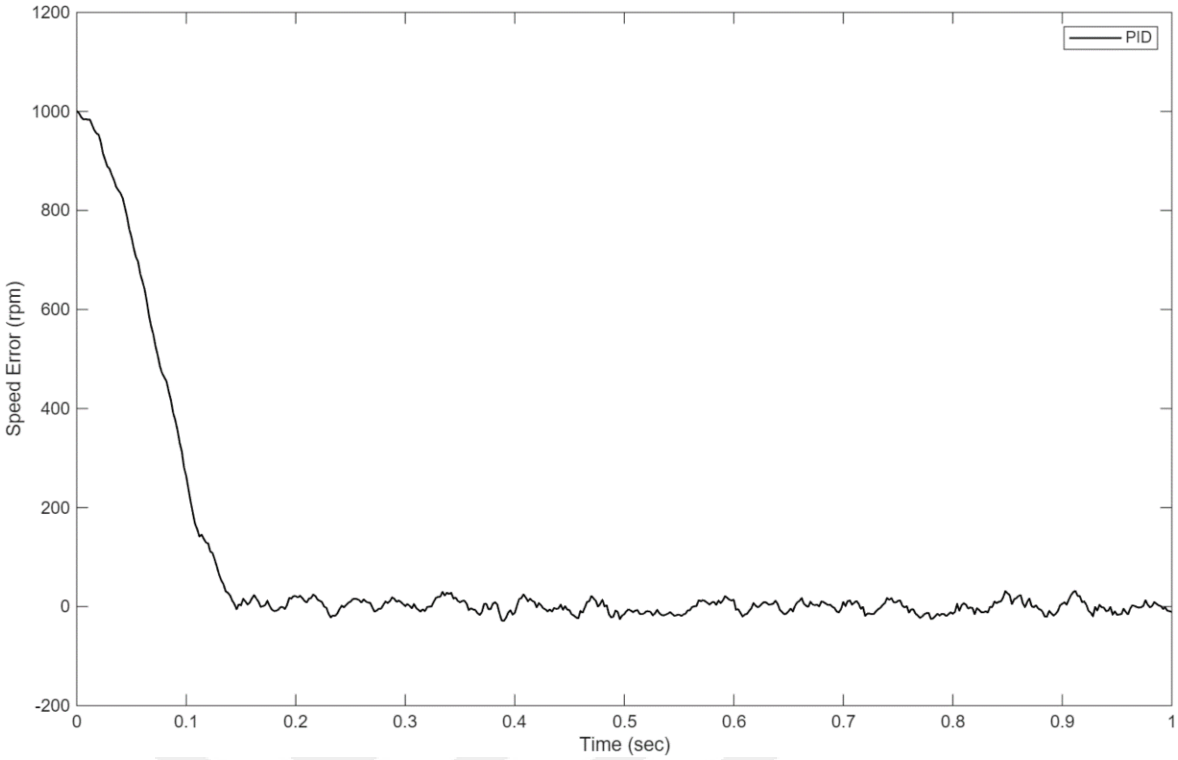

Figure 4.99. Speed error (rpm) (PID)

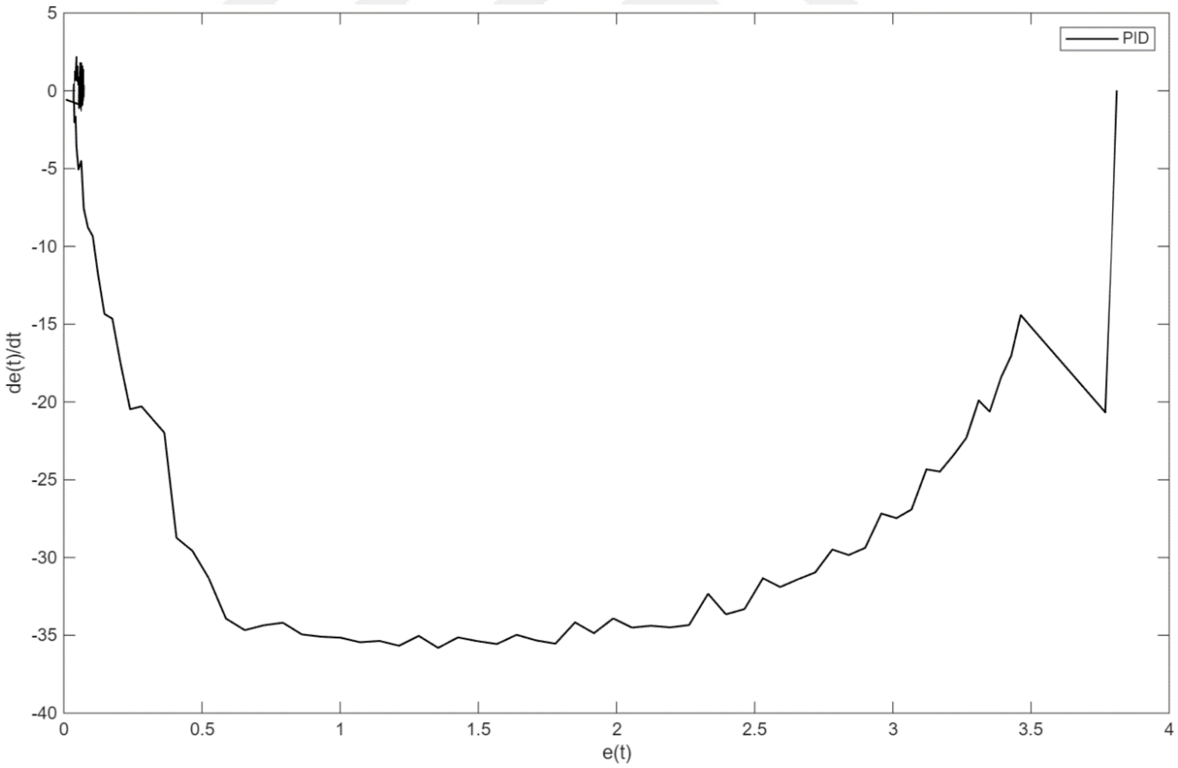

Figure 4.100. Phase plane of $e(t)$ and $de(t)/dt$ (PID)

According to the domain performance specifications presented in Table 4.25 the single-loop PID controller exhibits a fast and stable transient performance. The rise time is 0.0911 s and the settling time is 0.1403 s, with an overshoot of 0.63%, indicating a controlled and nearly ideal response. The system delay of 0.078 s further confirms the controller's prompt and balanced response to input changes. Examining the performance indices in Table 4.26 the controller achieves ITAE = 0.03, ISE = 0.82, IAE = 0.32 and ITSE = 0.02, reflecting effective limitation of error magnitude and time-weighted effects. The control effort indicator ISCI = 28.14 and ISTE = 0.014, indicate a balanced control action without excessive actuator activity. These results demonstrate that the single-loop PID controller provides a fast, stable and effective control performance.

Table 4.25. Time domain performance specifications (PID)

Controller	Rise Time (s)	Settling time (s)	Overshoot (%)	Delay time (s)
PID	0.0911	0.1403	0.63	0.078

Table 4.26. Output performance indices (PID)

Controller	ITAE	ISE	IAE	ITSE	ISCI	ISTE
PID	0.030	0.820	0.320	0.020	28.14	0.014

4.8. Experimental Results of Cascade Controllers: (1) Cascade Outer-Loop PI/Inner-Loop P (PI/P), (2) Cascade Outer-Loop PI /Inner-Loop PI (PI/PI) and (3) Cascade Outer-Loop PID/Inner-Loop PI (PID/PI)

In this section, the experimental results of various cascade controller configurations, including PID–PI, PI–PI and PI–P structures, are presented and comparatively evaluated. Each configuration consists of an outer-loop for speed regulation and an inner-loop for current control. The outer-loop controllers (PID or PI) aim to minimize the steady-state error and improve the transient performance in speed tracking, while the inner-loop controllers (PI or P) are designed to ensure fast and stable current regulation. Experimental measurements, including motor speed, armature current, control signals and error responses were recorded for each control strategy. The comparative analysis highlights the distinctive advantages and limitations of each configuration. Overall cascade control structures demonstrated superior performance over single-loop controllers by offering faster dynamic responses, better disturbance rejection and improved steady-state accuracy.

4.8.1. Experimental Results of Cascade Controller: Outer-Loop PI/Inner-Loop P (PI/P)

Figure 4.101 shows the experimental setup of the cascade-loop control system. In this subsection, the experimental results of the cascade controller configuration, consisting of an outer-loop PI and an inner-loop P, are presented. The controller parameters were set as PI = $10\left(1+\frac{1}{s}\right)$ for the outer-loop PI, while the inner-loop P was implemented with $k_p = 10$. The outer-loop PI controller was designed to achieve accurate speed tracking and minimize steady-state error, whereas the inner-loop P controller provided a fast current response by reacting directly to reference changes. During the experiments, system responses such as output speed (Figure 4.102), motor armature current (Figure 4.103), control input signal (Figure 4.104), error signal (Figure 4.105), and the error alongside its derivative (Figure 4.106) were recorded and examined. The analysis indicates that the PI–P cascade control structure enhances both transient performance and overall stability compared to single-loop implementations, resulting in faster dynamic behaviour and improved steady-state accuracy.

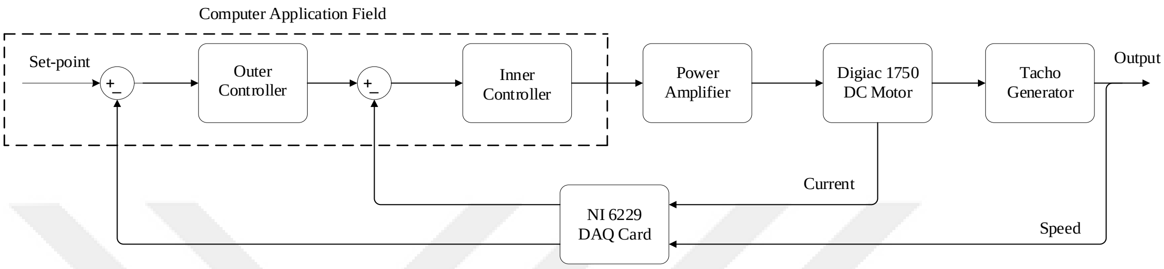

Figure 4.101. Experimental setup of the cascade-loop control system

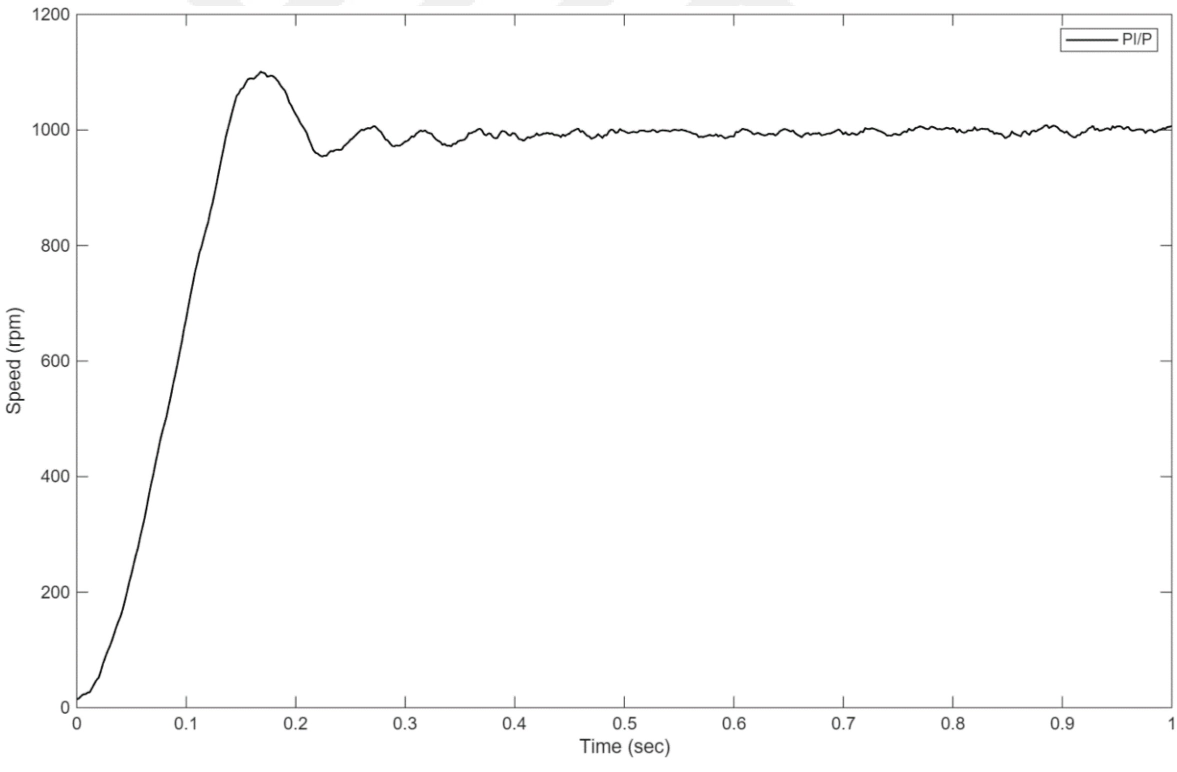

Figure 4.102. Output speed (rpm) (PI/P)

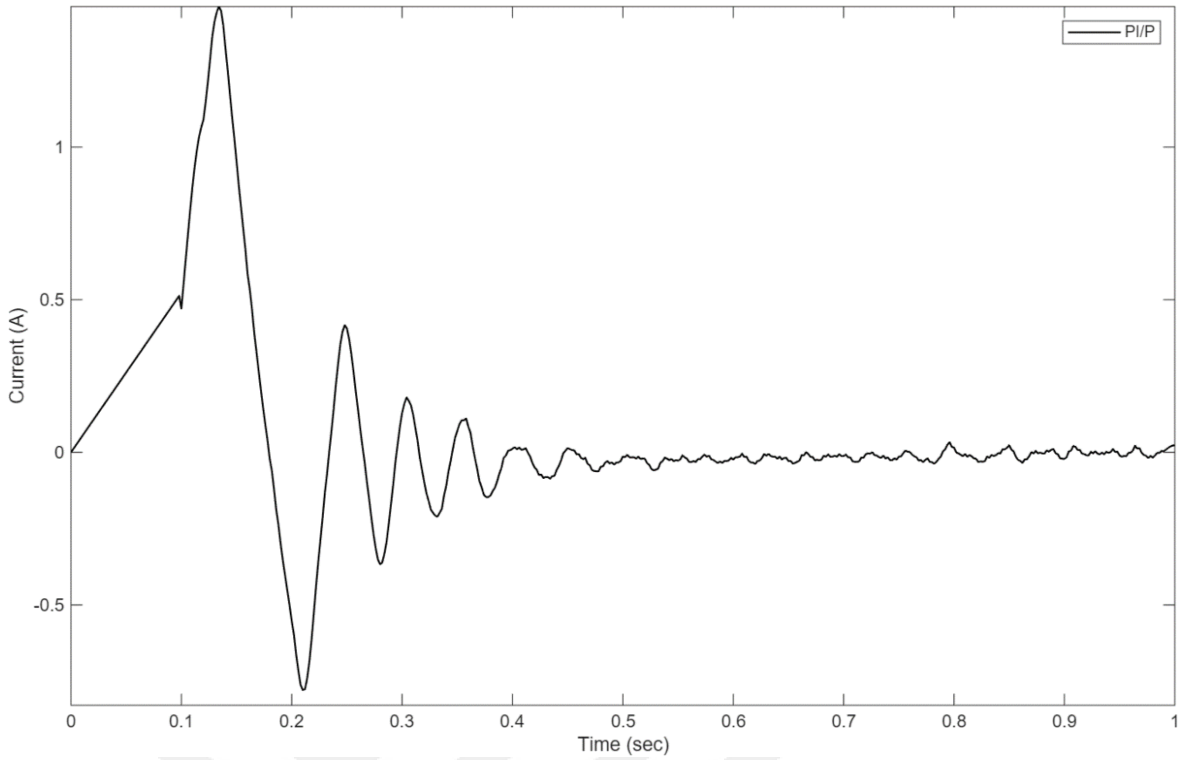

Figure 4.103. Armature current, $i_a(t)$ (PI/P)

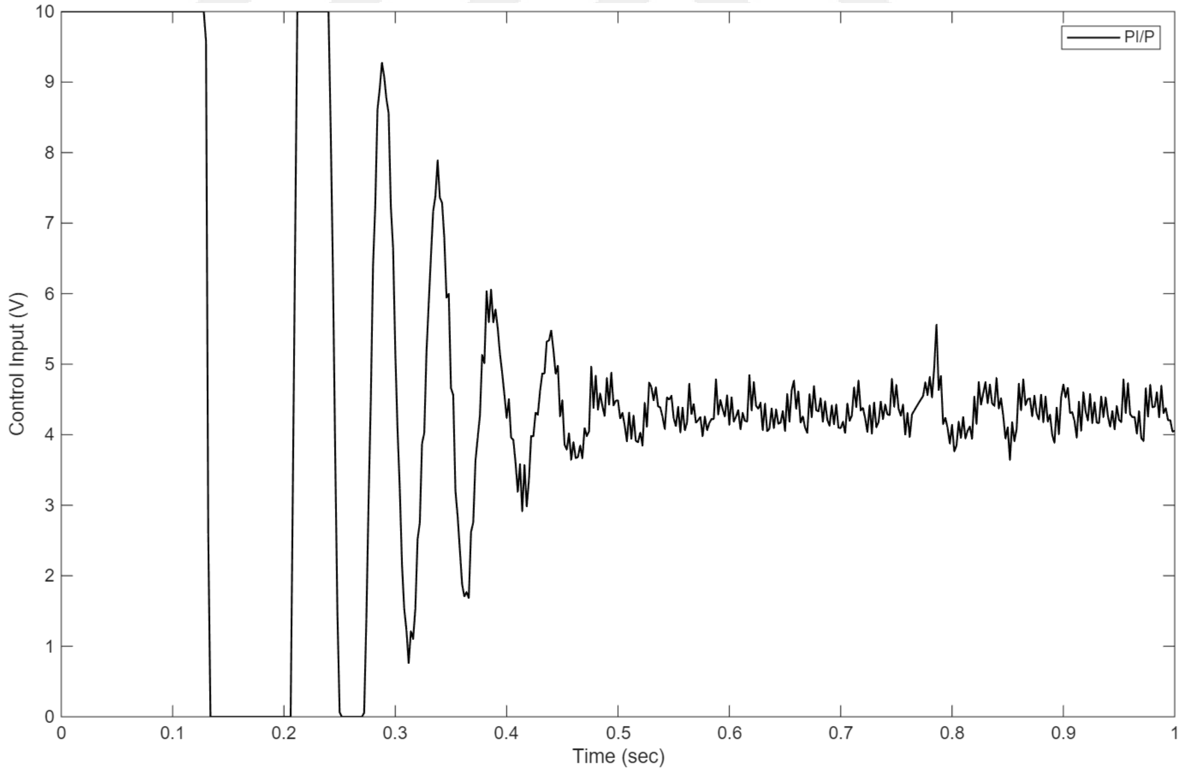

Figure 4.104. Control input voltage, $u(t)$ (PI/P)

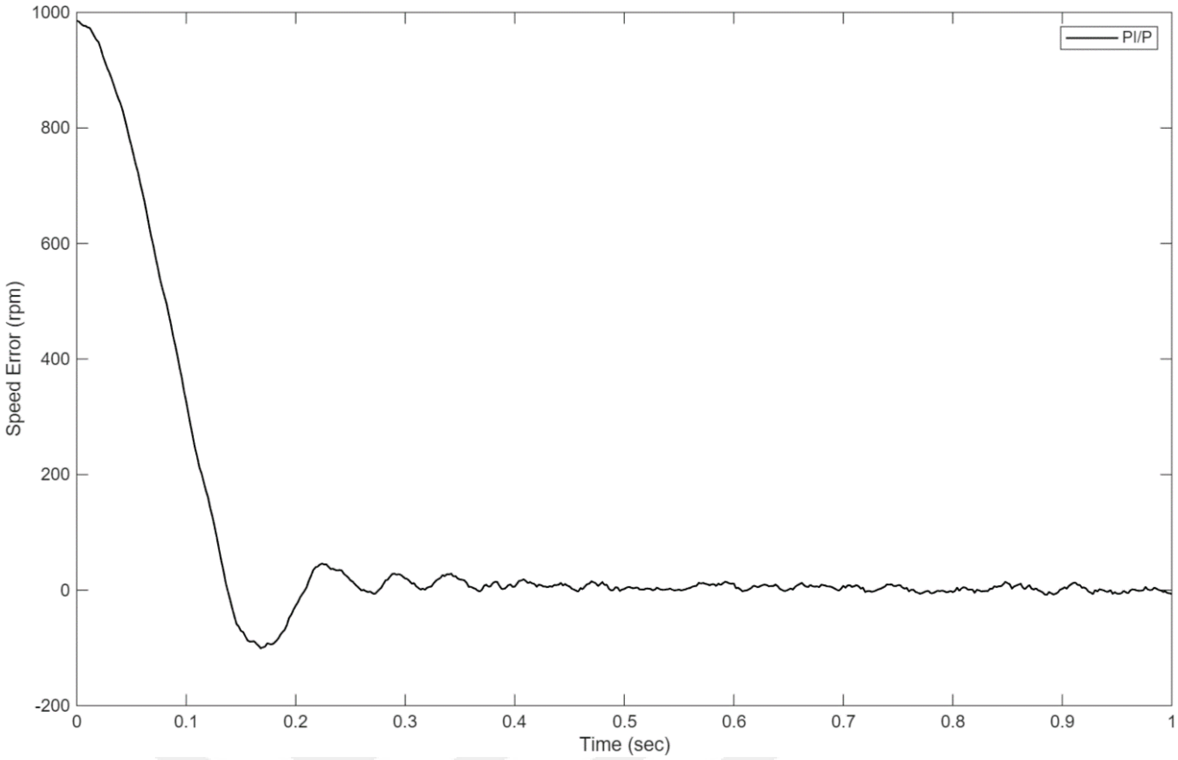

Figure 4.105. Speed error (rpm) (PI/P)

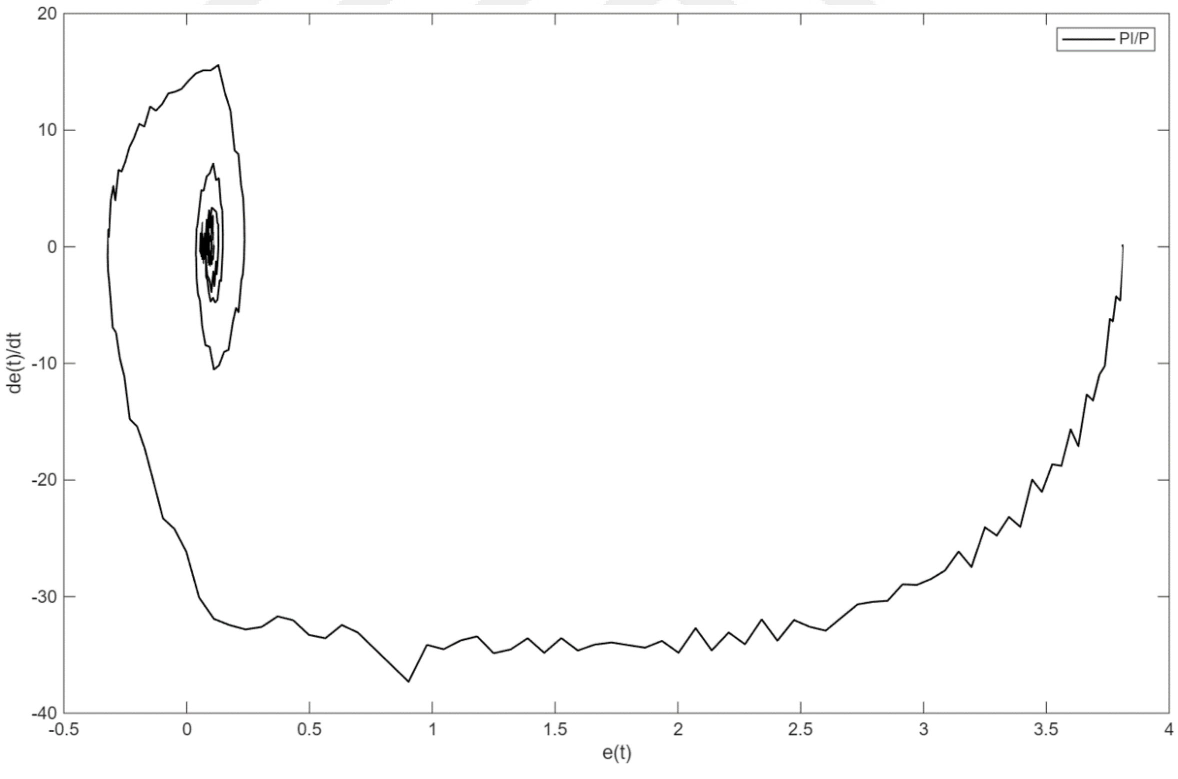

Figure 4.106. Phase plane of $e(t)$ and $de(t)/dt$ (PI/P)

The domain performance specifications presented in Table 4.27 indicate that the cascade PI/P controller exhibits a distinct transient behavior. The rise time is 0.1017 s, the settling time is

0.3005 s and the overshoot is 8.63%. The system delay of 0.0860 s demonstrates that the control structure responds effectively to input variations. Examining the performance indices in Table 4.28, the controller achieves ITAE = 0.0506, ISE = 0.917, IAE = 0.391 and ITSE = 0.038 reflecting controlled limitation of error magnitude and its time-weighted effects. The control effort indicator ISCI = 31.38 and ISTE = 0.0217, indicate balanced control action without excessive actuator activity. These results suggest that the cascade PI/P controller provides a rapid rise with limited overshoot and stable performance.

Table 4.27. Time domain performance specifications (PI/P)

Controller	Rise Time (s)	Settling time (s)	Overshoot (%)	Delay time (s)
Cascade Outer-Loop PI/Inner-Loop P	0.1017	0.3005	8.63	0.0860

Table 4.28. Output performance indices (PI/P)

Controller	ITAE	ISE	IAE	ITSE	ISCI	ISTE
Cascade Outer-Loop PI/Inner-Loop P	0.0506	0.917	0.391	0.038	31.38	0.0217

4.8.2. Experimental Results of Cascade Control: Outer-Loop PI/Inner-Loop PI (PI/PI)

In this subsection, the experimental results of the cascade controller structure, consisting of an PI/PI are presented. The controller parameters for the outer-loop PI were set PI = $10\left(1+\frac{1}{s}\right)$ to while the inner-loop PI was configured with PI = $10\left(1+\frac{1}{5s}\right)$. The outer-loop PI controller was designed to achieve precise speed regulation and minimize steady-state error, while the inner-loop PI controller ensured effective current control with smooth dynamic behavior. The experimental results include output speed (Figure 4.107), motor current (Figure 4.108), control signal (Figure 4.109), error (Figure 4.110), error and the error's derivative (Figure 4.111). Analysis of these results shows that the PI–PI cascade configuration enhances both transient and steady-state performance compared to single-loop controllers, resulting in faster response and improved system stability.

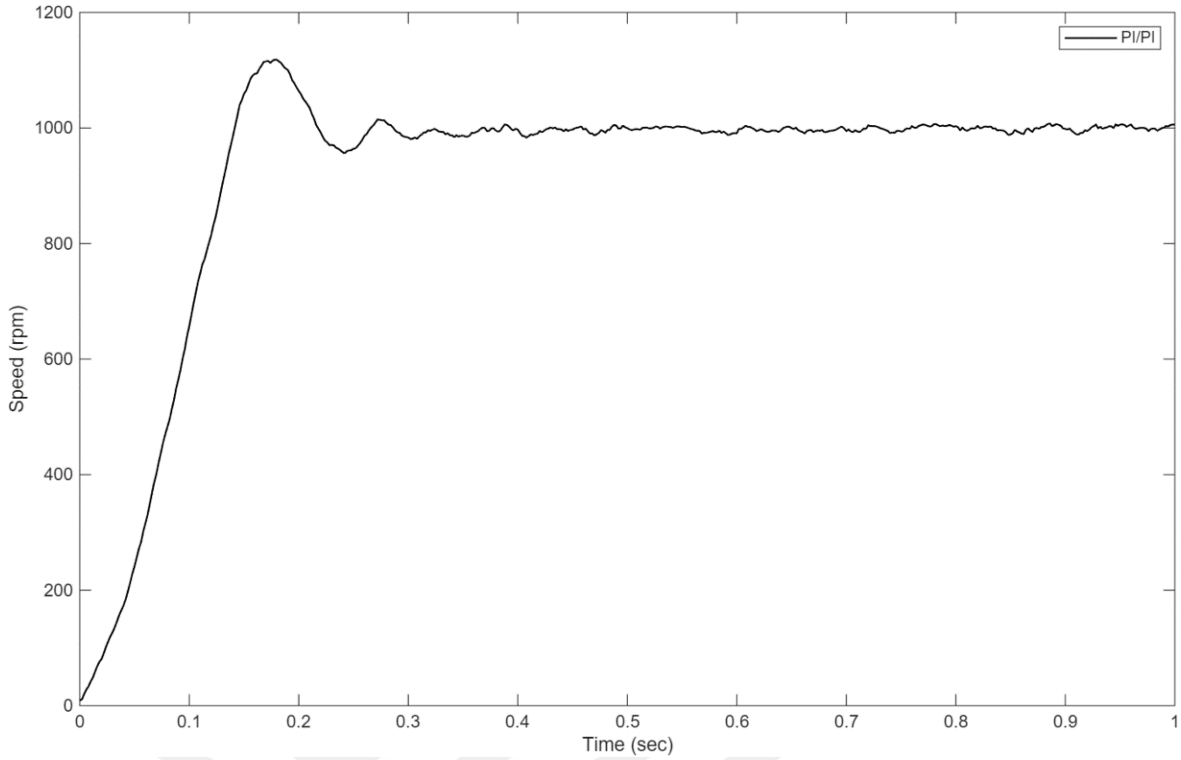

Figure 4.107. Output speed (rpm) (PI/PI)

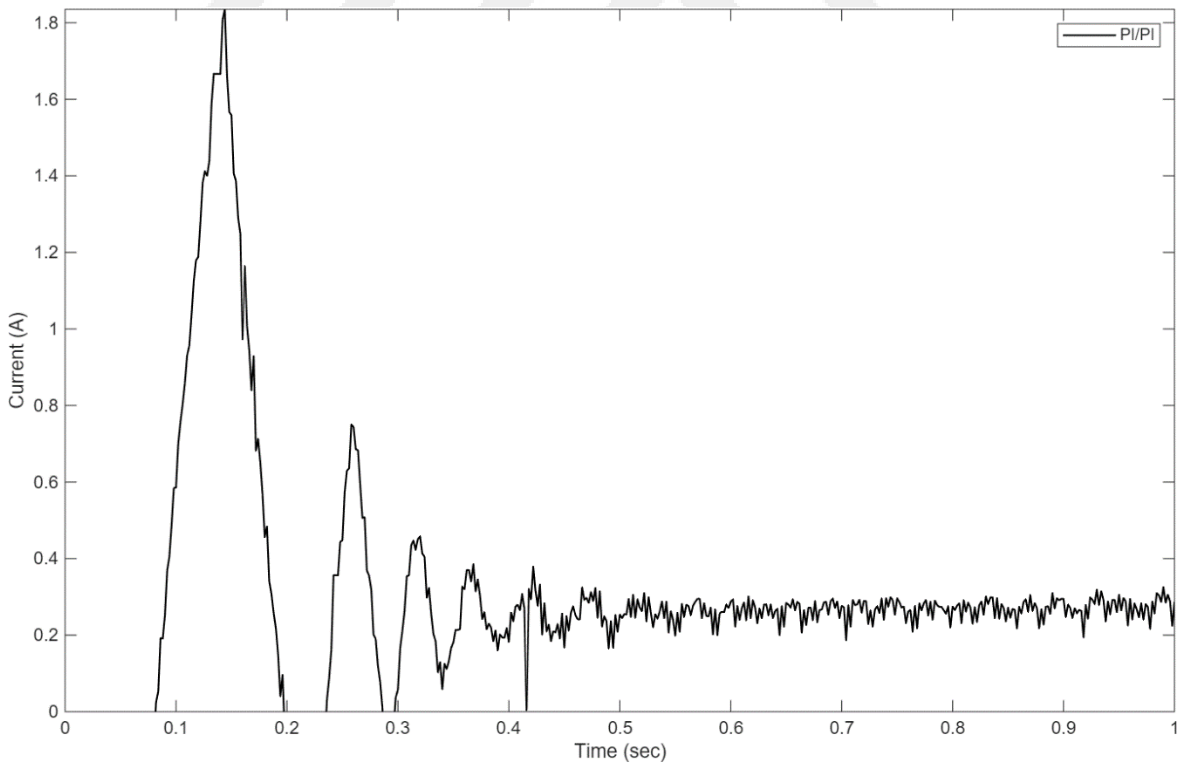

Figure 4.108. Armature current, $i_a(t)$ (PI/PI)

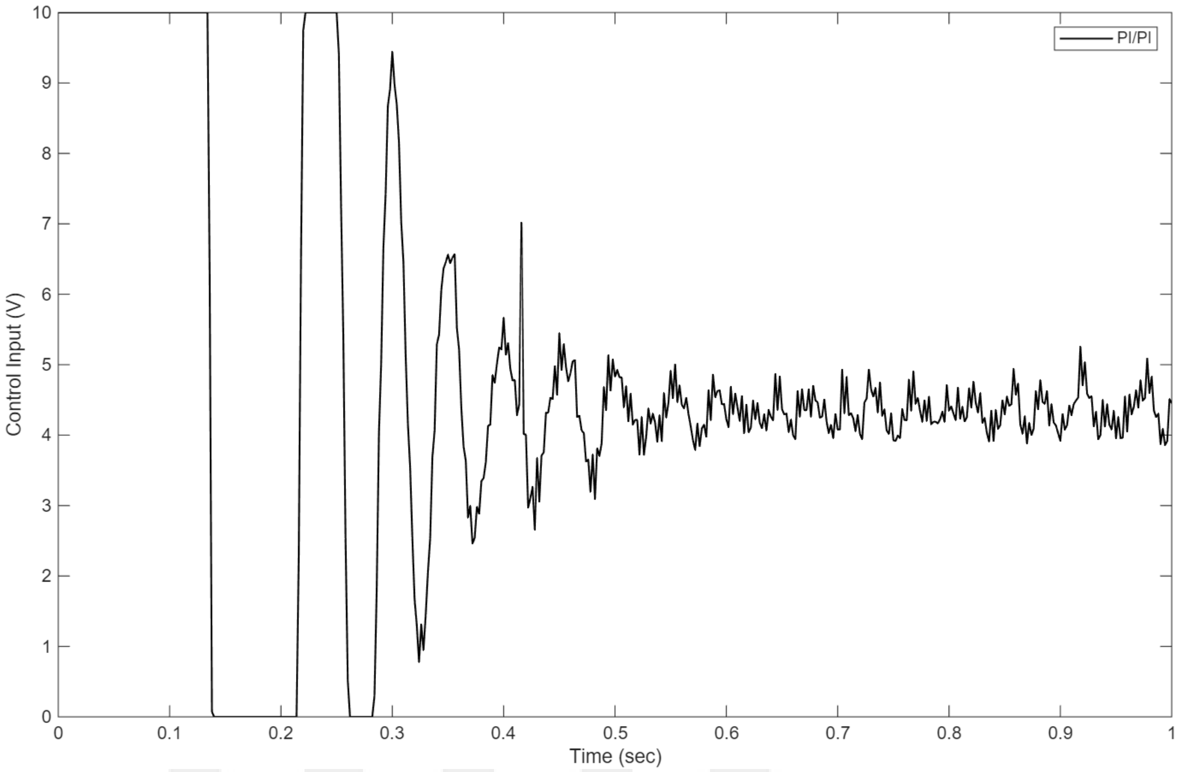

Figure 4.109. Control input voltage, $u(t)$ (PI/PI)

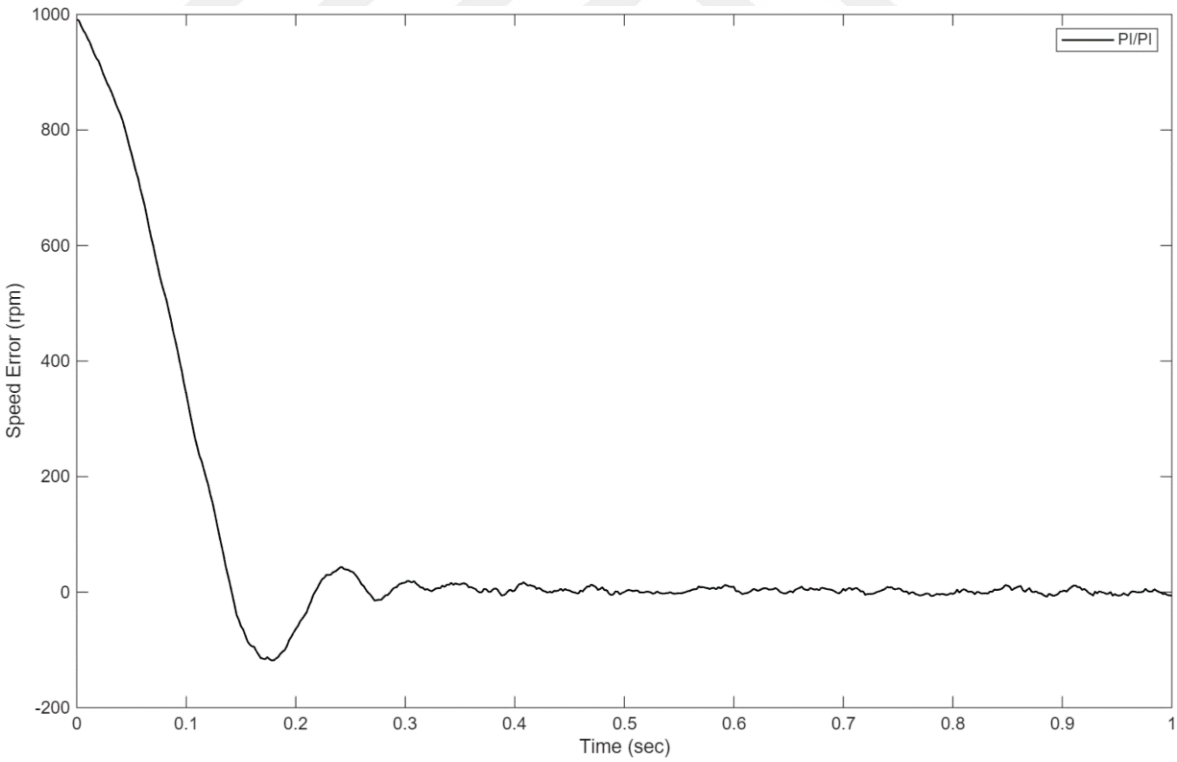

Figure 4.110. Speed error (rpm) (PI/PI)

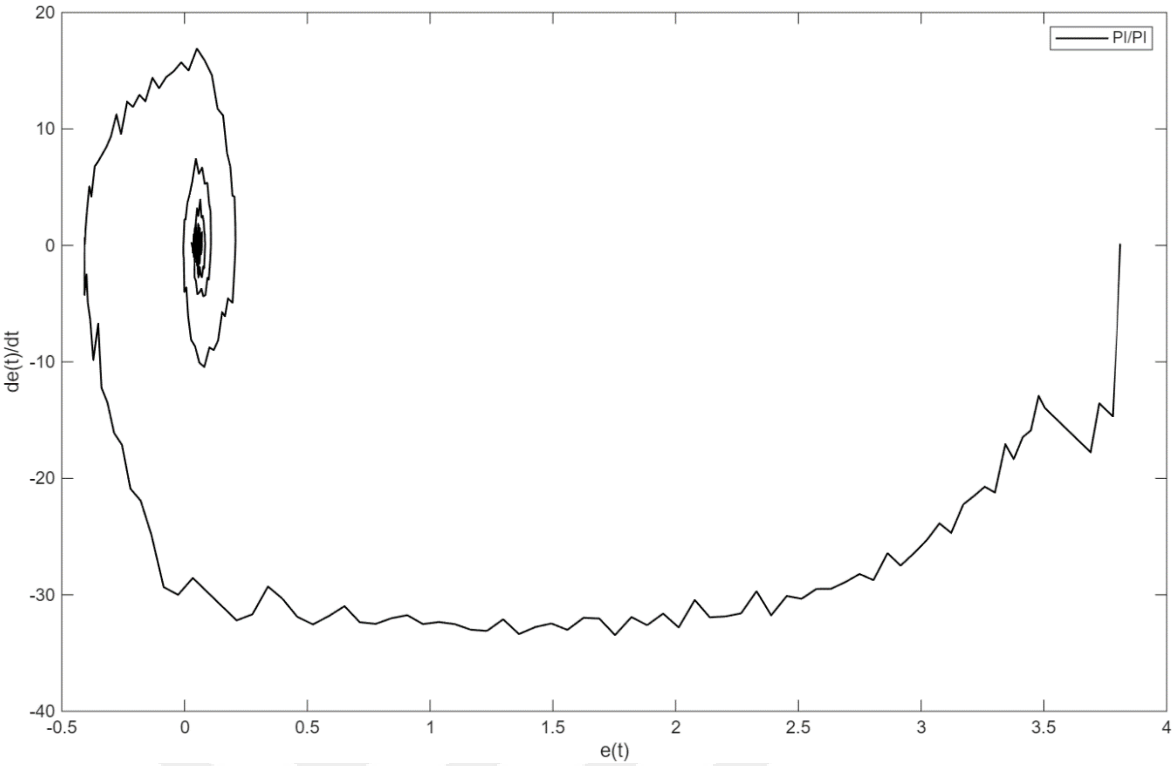

Figure 4.111. Phase plane of $e(t)$ and $de(t)/dt$ (PI/PI)

The domain performance specifications presented in Table 4.29 indicate that the cascade PI/PI controller demonstrates a fast and stable transient behavior. The rise time is 0.1023 s, the settling time is 0.2519 s and the overshoot is 9.26%. The system delay of 0.0880 s confirms that the control structure responds effectively to input variations. Examining the performance indices in Table 4.30, the controller achieves ITAE = 0.0352, ISE = 0.926, IAE = 0.365 and ITSE = 0.037 reflecting controlled limitation of error magnitude and its time-weighted effects. The control effort indicator ISCI = 31 and ISTE = 0.011 indicate balanced control action without excessive actuator activity. These results suggest that the cascade PI/PI controller provides a rapid rise with limited overshoot and stable performance.

Table 4.29. Time domain performance specifications (PI/PI)

Controller	Rise Time (s)	Settling time (s)	Overshoot (%)	Delay time (s)
Cascade Outer-Loop PI/Inner-Loop PI	0.1023	0.2519	9.26	0.0880

Table 4.30. Output performance indices (PI/PI)

Controller	ITAE	ISE	IAE	ITSE	ISCI	ISTE
Cascade Outer-Loop PI/Inner-Loop PI	0.0352	0.926	0.365	0.037	31	0.011

4.8.3. Experimental Results of Cascade Control: Outer-Loop PID/Inner-Loop PI (PID/PI)

In this subsection, the experimental results of the cascade controller structure with an outer-loop PID and an inner-loop PI are presented. The controller parameters were selected as PID = $0.3(1+\frac{1}{0.24s}+133.33s)$ for the outer-loop and PI = $1.65(1+\frac{1}{1.375s})$ for the inner-loop. The outer-loop PID controller was designed to provide precise speed regulation, while the inner-loop PI controller ensured effective current control. The experimental results include output speed (Figure 4.112), motor current (Figure 4.113), control signal (Figure 4.114), error signal (Figure 4.115), and the combined error-derivative behavior (Figure 4.116). Analysis of these results indicates that the PID-PI cascade configuration enhances transient response and overall system stability compared to single-loop controllers, resulting in reduced steady-state error and faster dynamic performance.

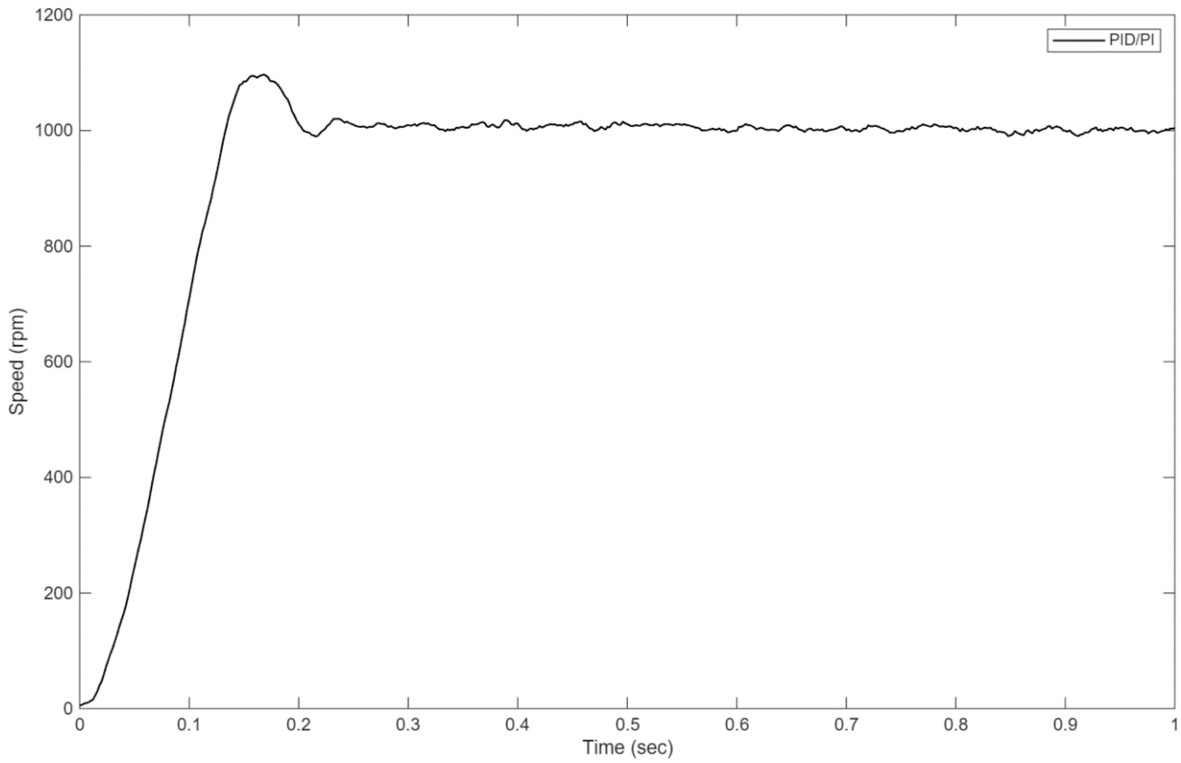

Figure 4.112. Output speed (rpm) (PID/PI)

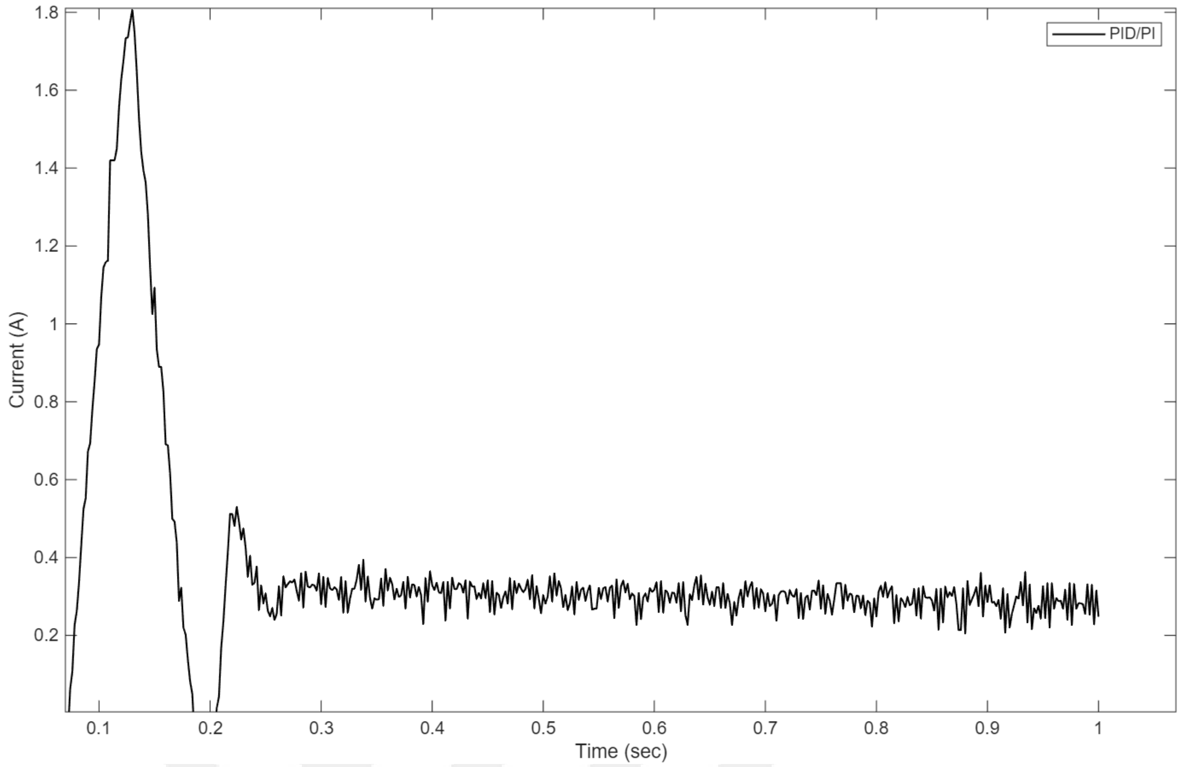

Figure 4.113. Armature current, $i_a(t)$ (PID/PI)

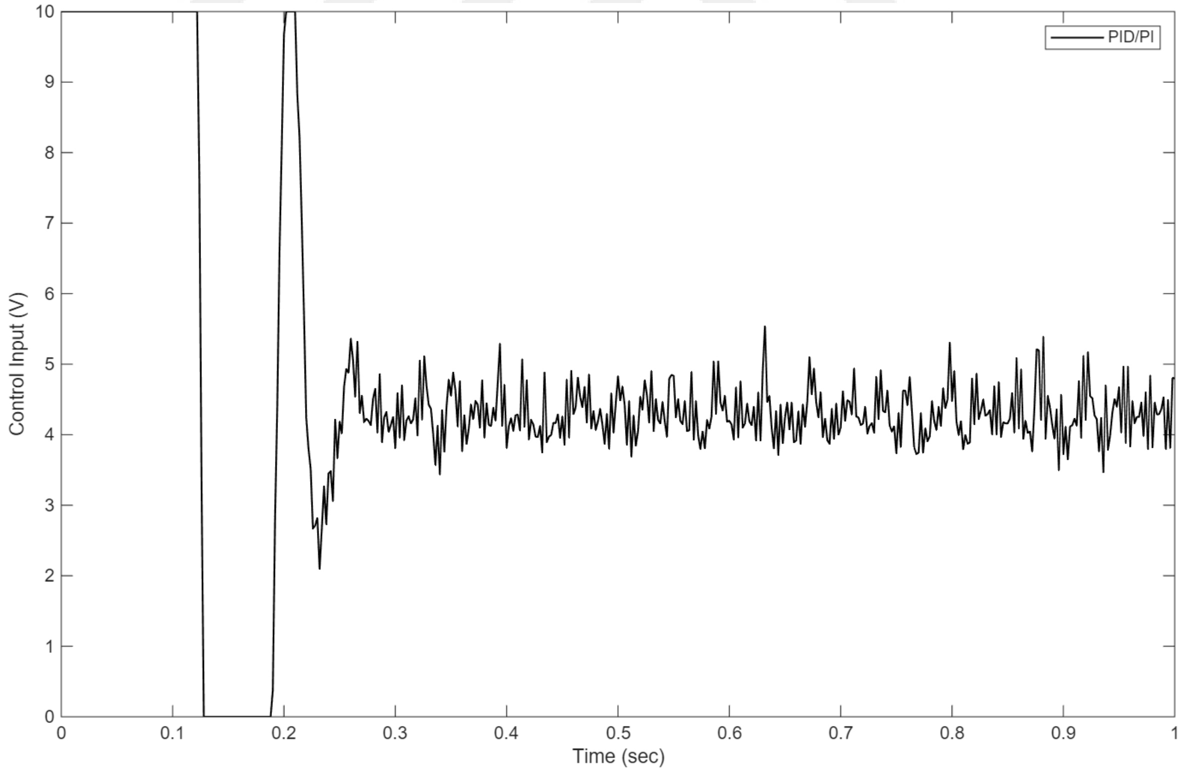

Figure 4.114. Control input voltage, $u(t)$ (PID/PI)

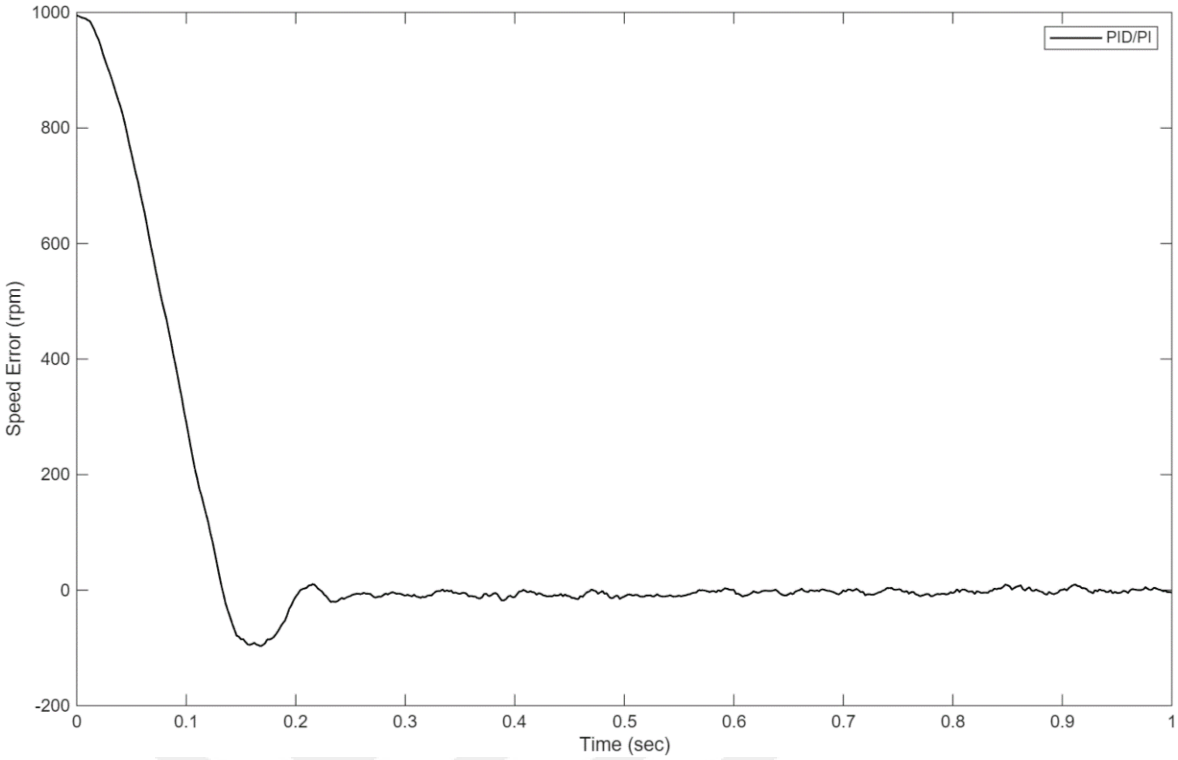

Figure 4.115. Speed error (rpm) (PID/PI)

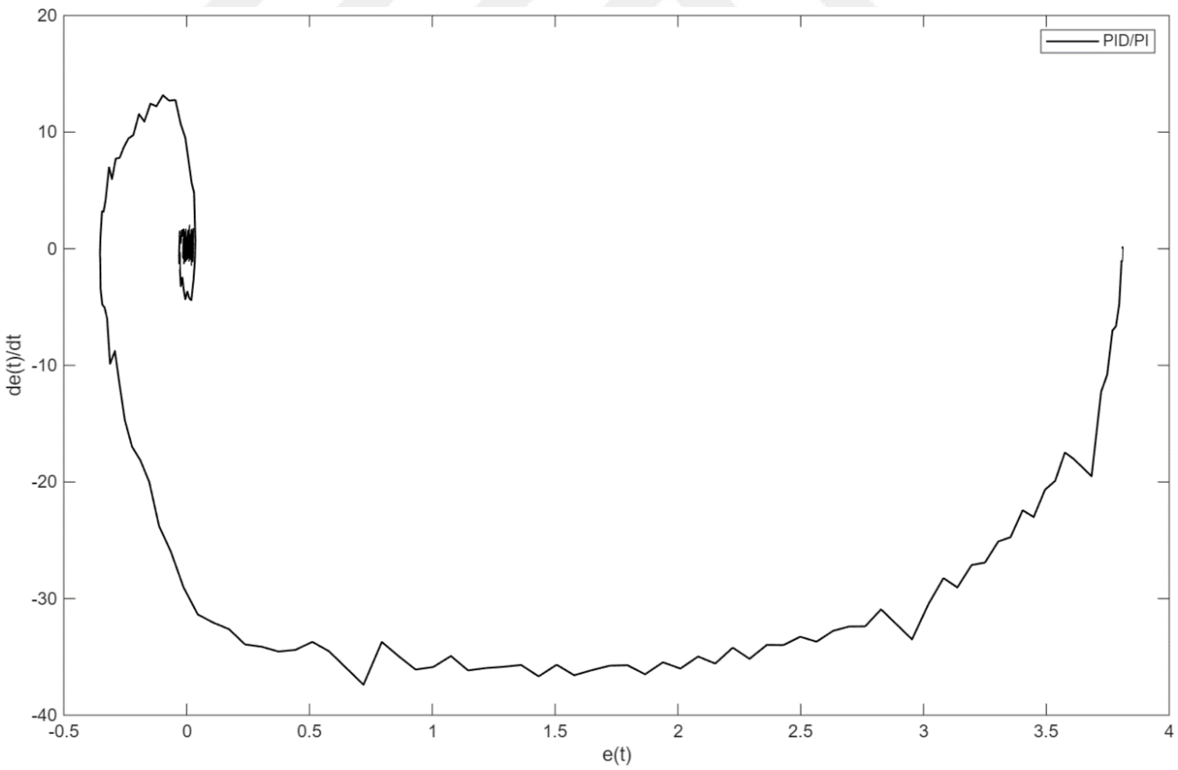

Figure 4.116. Phase plane of $e(t)$ and $de(t)/dt$ (PID/PI)

The time domain performance specifications presented in Table 4.31 indicate that the cascade PID/PI controller exhibits a fast and balanced transient behavior. The rise time is 0.0904 s, the settling time is 0.1996 s and the overshoot is 9.99%. The system delay of 0.084 s confirms that the control structure responds effectively to input variations. Examining the performance indices in Table 4.32 the controller achieves ITAE = 0.02, ISE = 0.85, IAE = 0.32 and ITSE = 0.03 reflecting controlled limitation of error magnitude and its time-weighted effects. The control effort indicator ISCI = 28.6 and ISTE = 0.0051 indicate balanced control action without excessive actuator activity. These results suggest that the cascade PID/PI controller provides a rapid rise with limited overshoot and stable performance.

Table 4.31. Time domain performance specifications (PID/PI)

Controller	Rise Time (s)	Settling time (s)	Overshoot (%)	Delay time (s)
Cascade Outer-Loop PID/Inner-Loop PI	0.0904	0.1996	9.99	0.084

Table 4.32. Output performance indices (PID/PI)

Controller	ITAE	ISE	IAE	ITSE	ISCI	ISTE
Cascade Outer-Loop PID/Inner-Loop PI	0.02	0.85	0.32	0.03	28.6	0.0051

4.9. Experimental Results of Single-Loop Sliding Mode Controllers: (1) SMC-1 and (2) SMC-2

This section presents and analyzes the experimental results of the single-loop SMC (SMC-1 and SMC-2). Both controllers were implemented on the experimental setup to assess their real-time performance in regulating motor speed and current under varying operating conditions. The results cover output speed, motor armature current, control input signal, error signal, and the combined error, its derivative characteristics. The findings confirm that both SMC strategies deliver robust and reliable performance, effectively compensating for disturbances and parameter variations. Moreover, the SMC-2 controller demonstrates improved dynamic behavior and reduced steady-state error compared to SMC-1, consistent with the simulation results.

4.9.1. Experimental Results of Single-Loop Sliding Mode Control (SMC-1)

In this subsection, the experimental results obtained from the single-loop SMC-1 controller designed with parameters $k_d = 0.5$, $k_p = 20$, $k_i = 2$, $k_s = 3.2$, $\Omega = 8$ are presented and analyzed. The output speed (Figure 4.117) response demonstrates the SMC-1 controller’s capability to regulate motor speed effectively. Motor current (Figure 4.118), the control input signal (Figure 4.119) represents the input effort necessary to maintain the desired operating point. The error signal (Figure 4.120), the combined plot of error and its derivative (Figure 4.121), the sliding surface signal (Figure 4.122), and the sliding surface with its derivative provide a comprehensive view of the system’s performance (Figure 4.123). The error signal illustrates the instantaneous deviation from the desired trajectory, while the combined plot of error and its derivative highlights how the controller compensates for both transient and steady-state errors. The sliding surface signal and its derivative demonstrate that the system trajectory remains close to the predefined manifold, ensuring robustness against disturbances and parameter variations. Furthermore, the equivalent (Figure 4.124) and switching input (Figure 4.125) signals illustrate the decomposition of the control input into continuous and discontinuous components, highlighting the inherent switching nature of SMC. Overall, the experimental results confirm that the SMC-1 controller provides robust and stable performance, albeit with slightly higher switching activity compared to the more advanced SMC-2 approach.

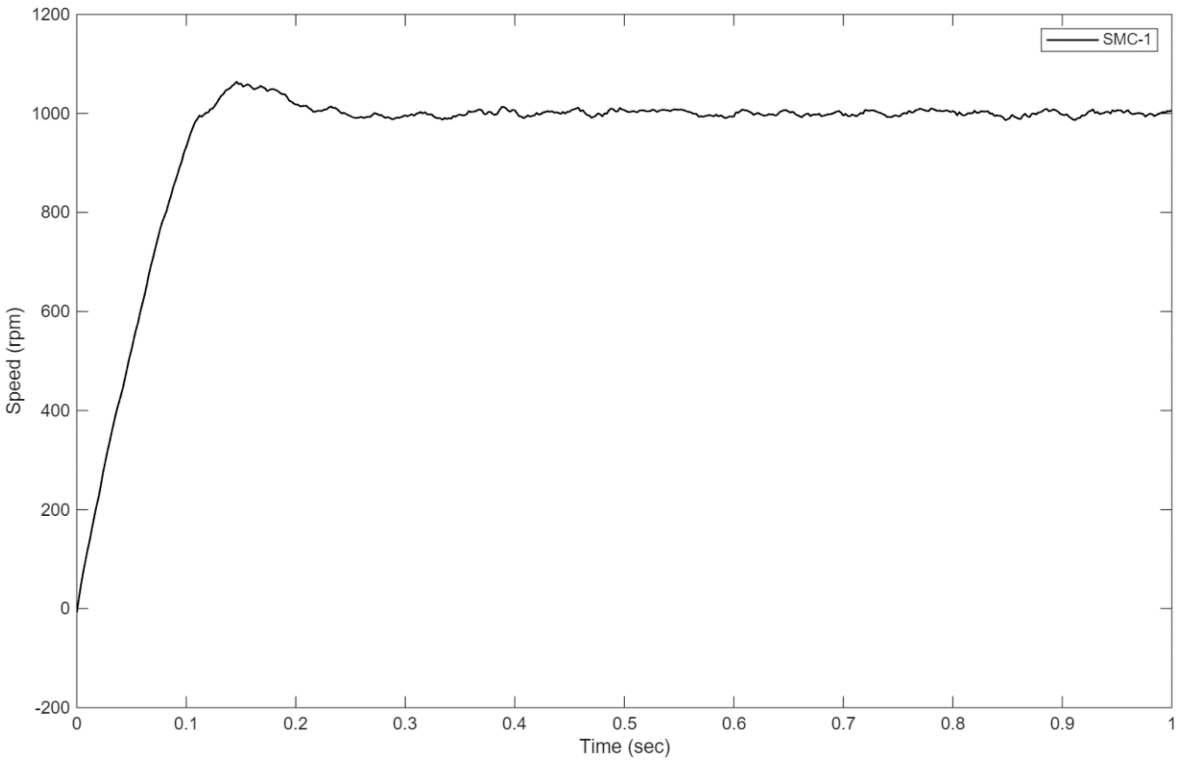

Figure 4.117. Output speed (rpm) (SMC-1)

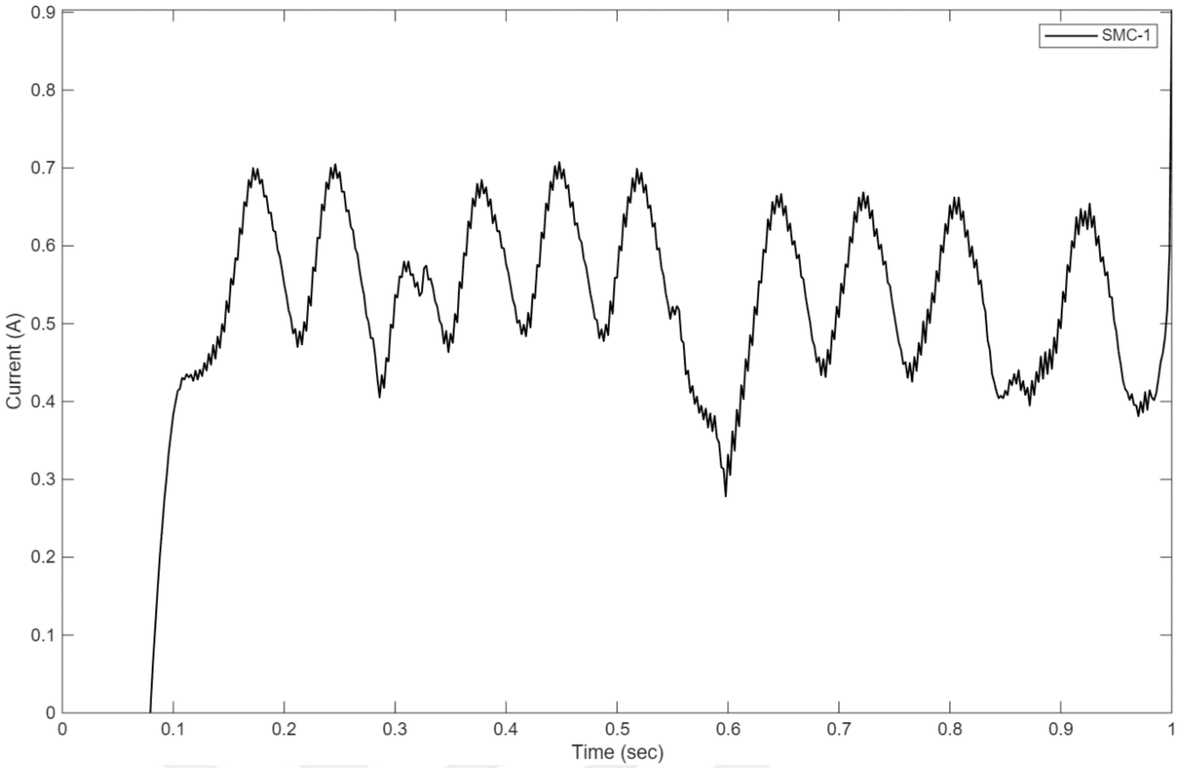

Figure 4.118. Armature current, $i_a(t)$ (SMC-1)

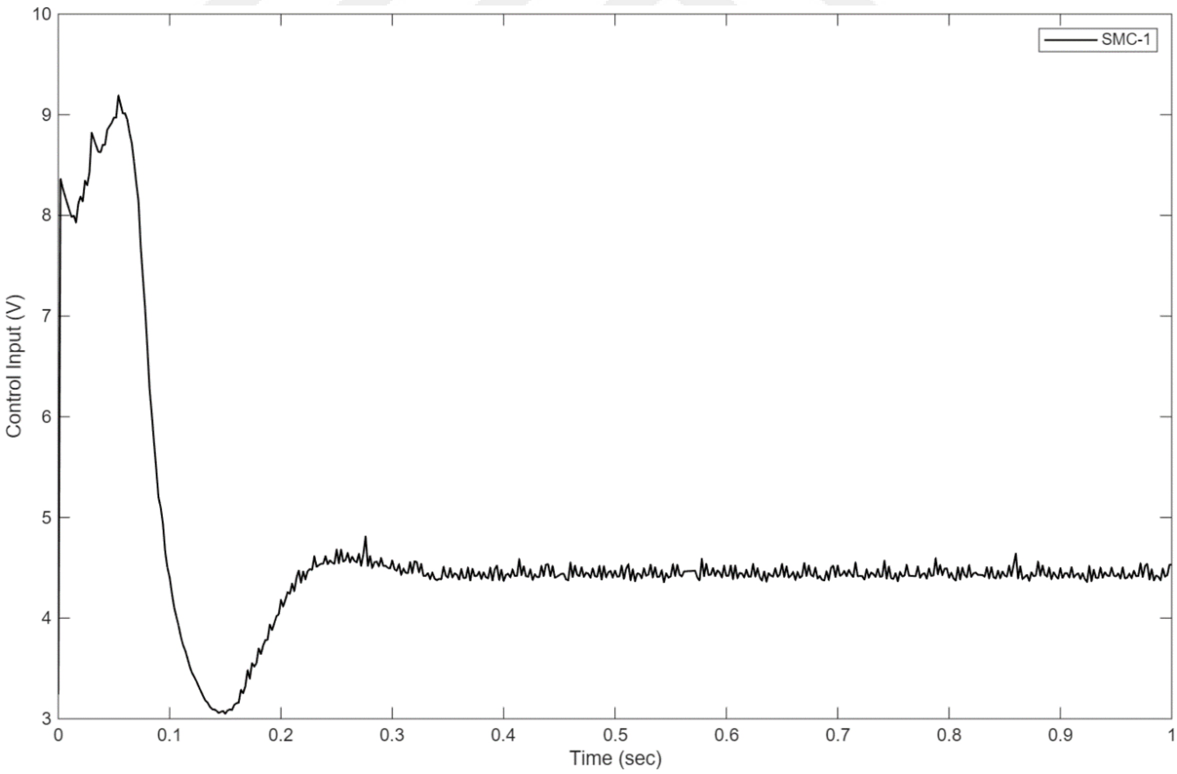

Figure 4.119. Control input voltage, $u(t)$ (SMC-1)

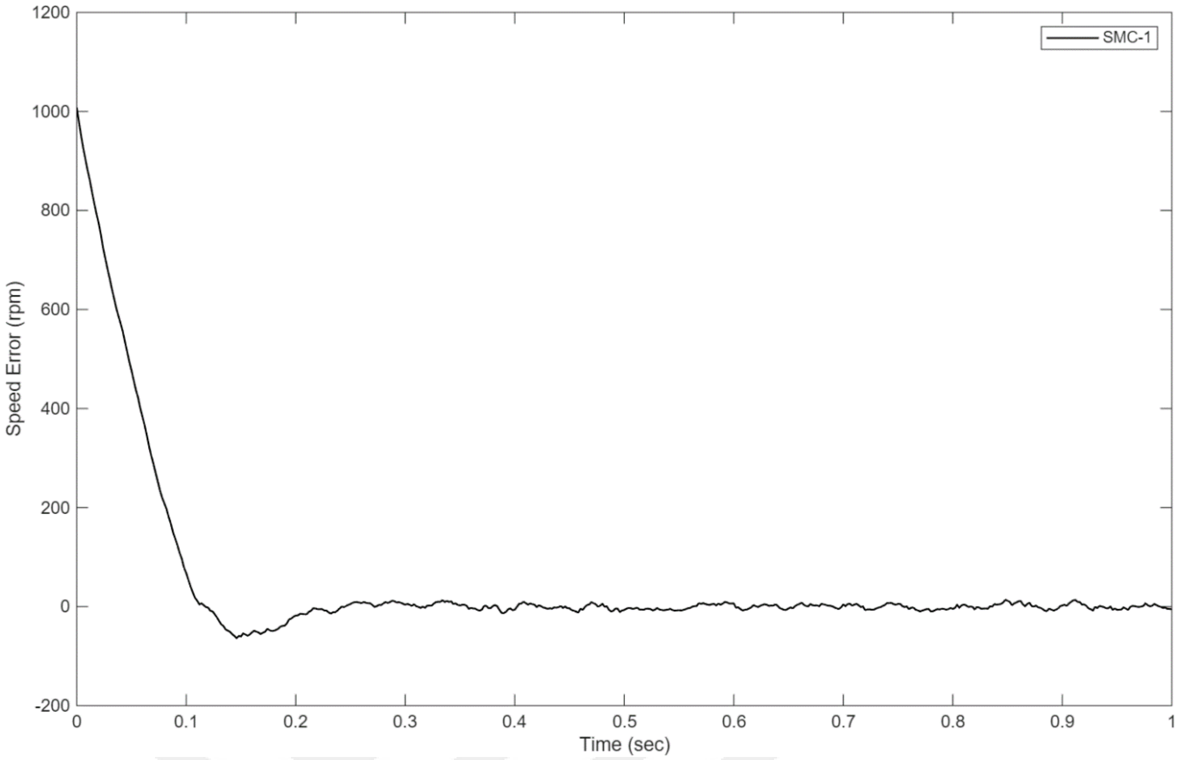

Figure 4.120. Speed error (rpm) (SMC-1)

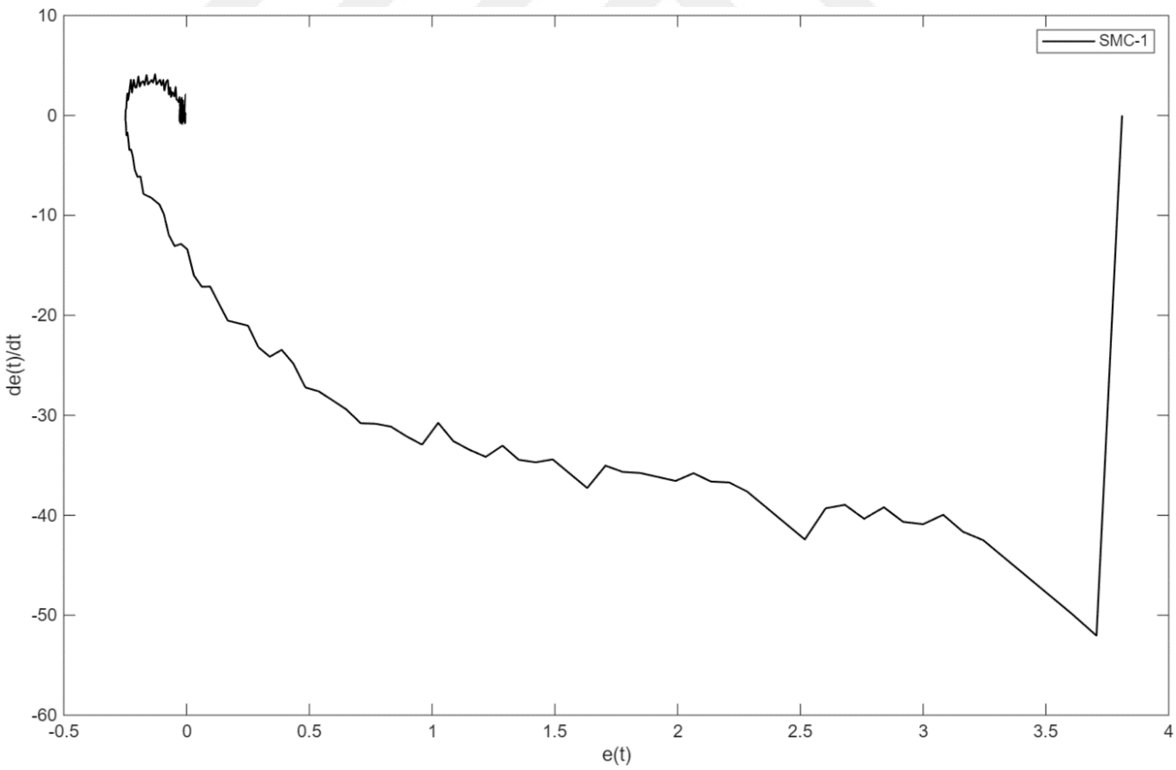

Figure 4.121. Phase plane of $e(t)$ and $de(t)/dt$ (SMC-1)

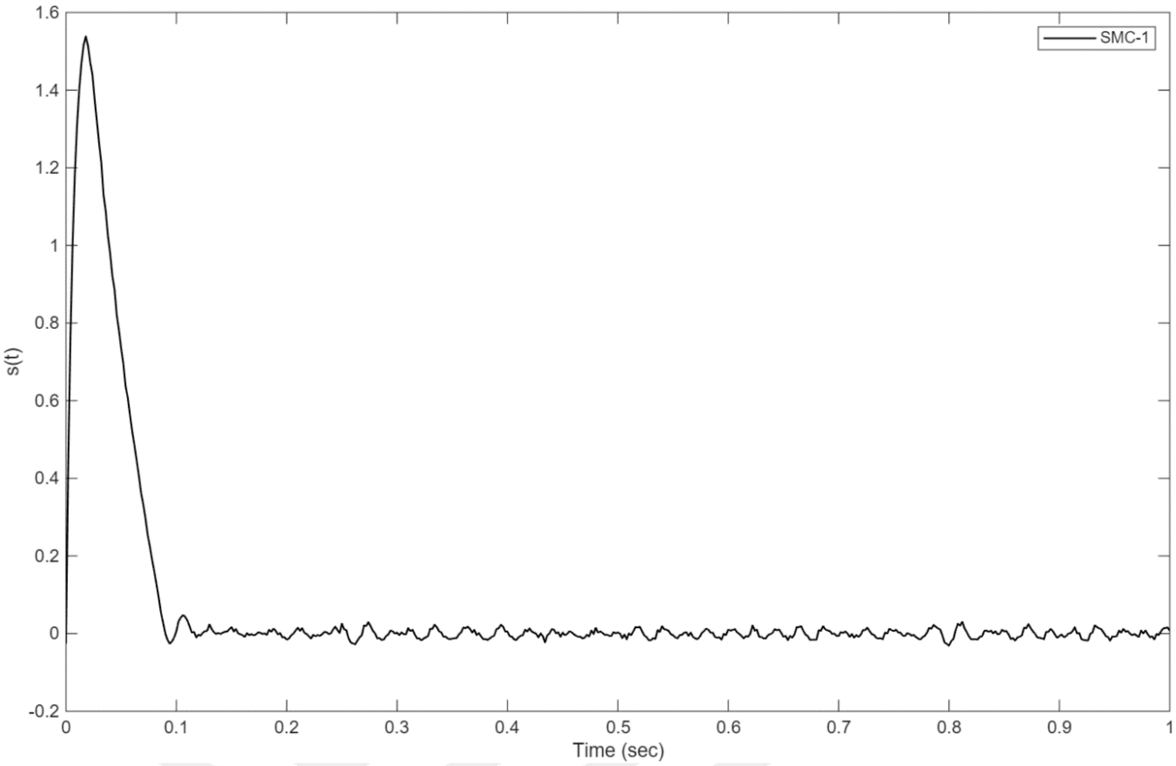

Figure 4.122. Sliding surface, $s(t)$ (SMC-1)

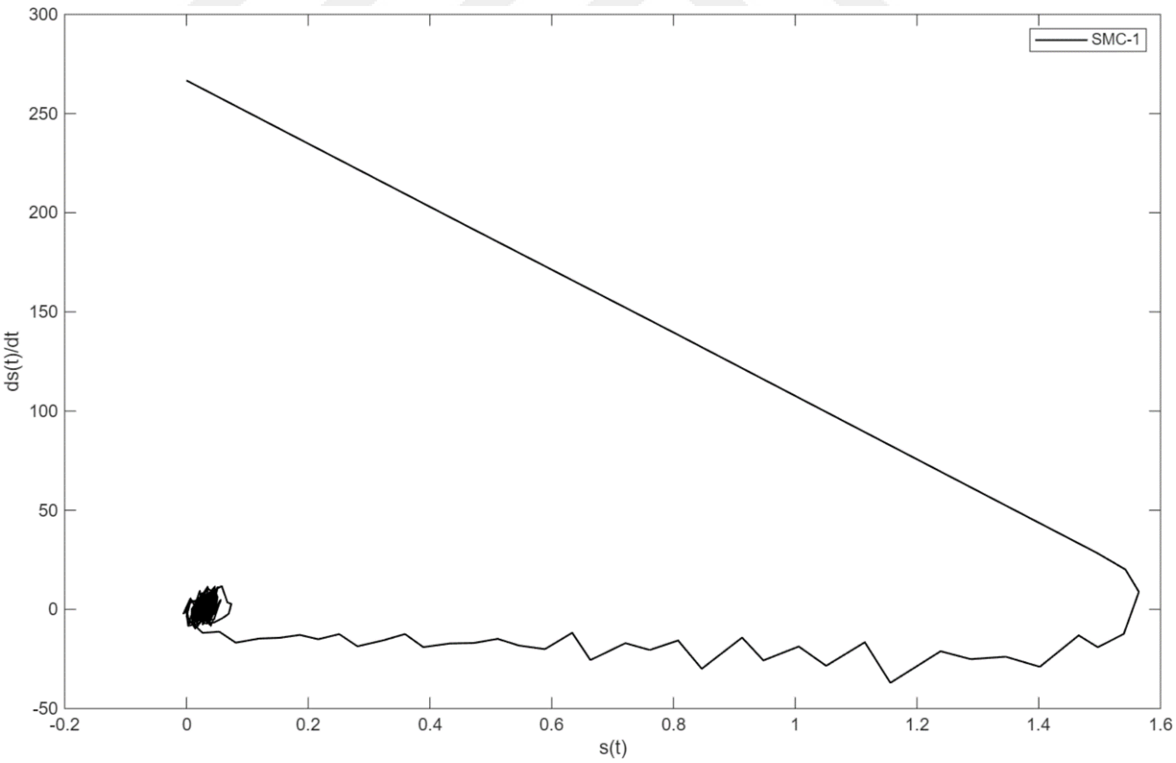

Figure 4.123. Phase plane of $s(t)$ and $ds(t)/dt$ (SMC-1)

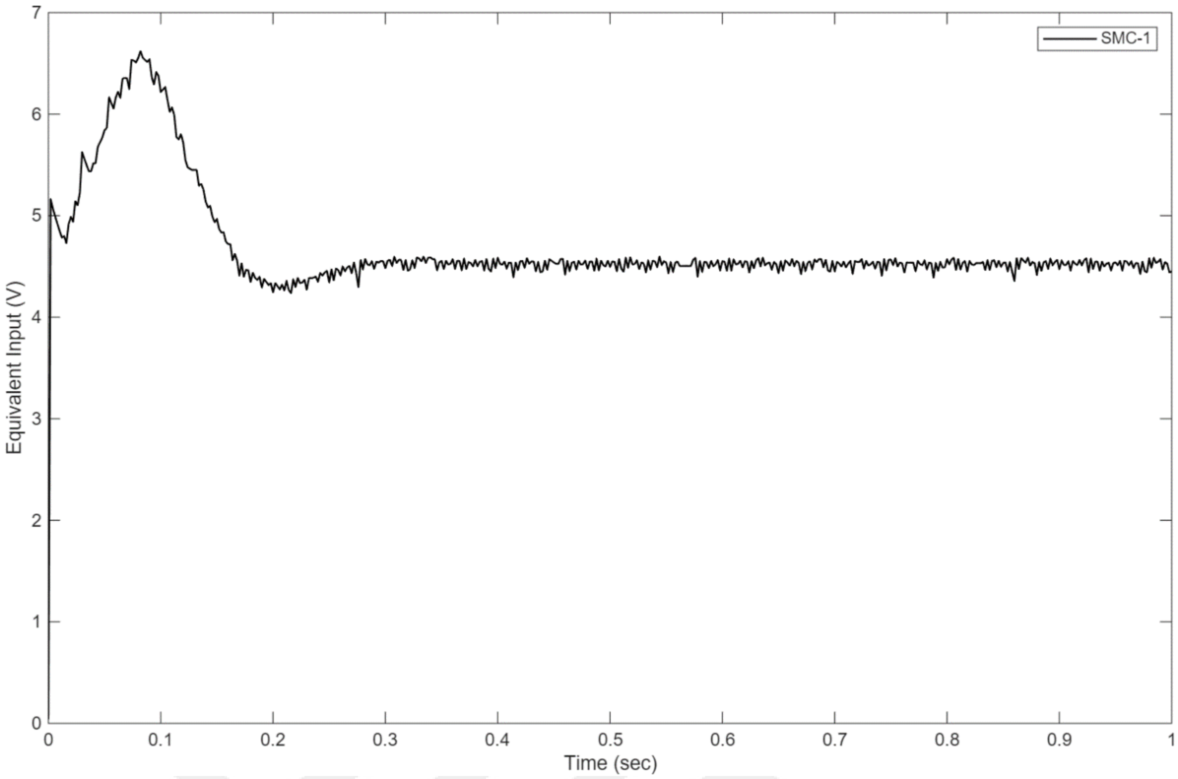

Figure 4.124. Equivalent input, $u_{eq}(t)$ (SMC-1)

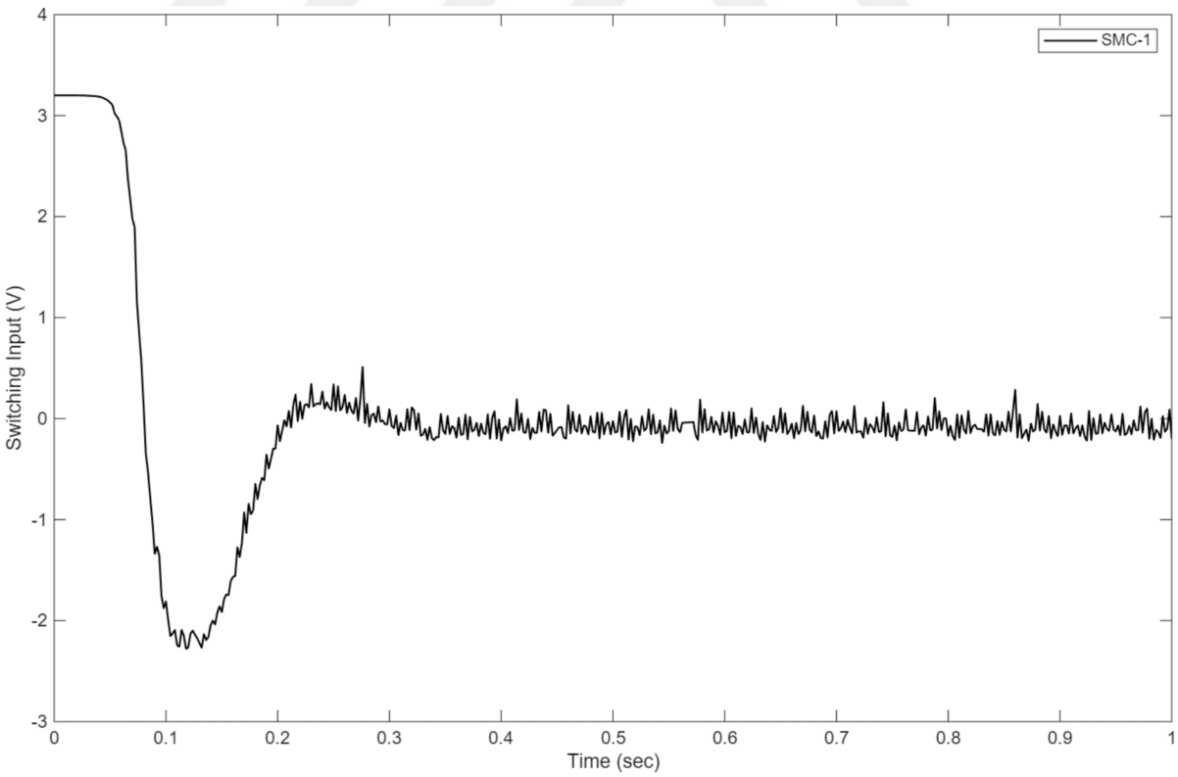

Figure 4.125. Switching input, $u_{sw}(t)$ (SMC-1)

The domain performance specifications presented in Table 4.33 demonstrate that the single-loop SMC-1 controller exhibits a balanced and effective transient performance. The rise time is 0.0874 s, the settling time is 0.2082 s and the overshoot is 5.85% indicating a controlled response. The system delay of 0.048 s shows that the controller responds quickly and reliably to input signals. Performance Indices Examining the performance indicators in Table 4.34 the controller achieves ITAE = 0.02, ISE = 0.45, IAE = 0.22 and ITSE = 0.01, reflecting effective limitation of system errors and their time-weighted effects. The control effort indicator ISCI = 23.37 and ISTE = 0.0080, indicate that the system maintains balanced control without excessive actuator activity. These results demonstrate that the single-loop SMC-1 controller provides a fast, balanced and effective control performance.

Table 4.33. Time domain performance specifications (SMC-1)

Controller	Rise Time (s)	Settling time (s)	Overshoot (%)	Delay time (s)
SMC-1	0.0874	0.2082	5.85	0.048

Table 4.34. Output performance indices (SMC-1)

Controller	ITAE	ISE	IAE	ITSE	ISCI	ISTE
SMC-1	0.02	0.45	0.22	0.01	23.37	0.0080

4.9.2. Experimental Results of Single-Loop Sliding Mode Controller (SMC-2)

In this subsection, the experimental results obtained from the single-loop SMC-2 controller with parameters $k_c = 3.4,\ k_d = 1.6,\ k_p = 70,\ k_i = 10,\ \Omega_c = 8,\ \beta = 160,\ \lambda_1 = 60$ are presented in detail. The output speed response (Figure 4.126) confirms that the system remains stable and accurately regulated under the SMC-2 control law. Motor current signal (Figure 4.127), the control input signal (Figure 4.128) represents the effort applied to achieve the desired dynamic behavior. The error signal (Figure 4.129), the combined plot of error and its derivative (Figure 4.130), the sliding surface signal (Figure 4.131), and the sliding surface with its derivative (Figure 4.132) provide a comprehensive view of the system's performance. In addition, the equivalent (Figure 4.133) and switching input (Figure 4.134) signals clearly separate the control input into its continuous and discontinuous components, highlighting the fast response and inherent robustness of the SMC. Overall, the experimental outcomes verify the efficiency and reliability of the SMC-2 controller in practical implementation.

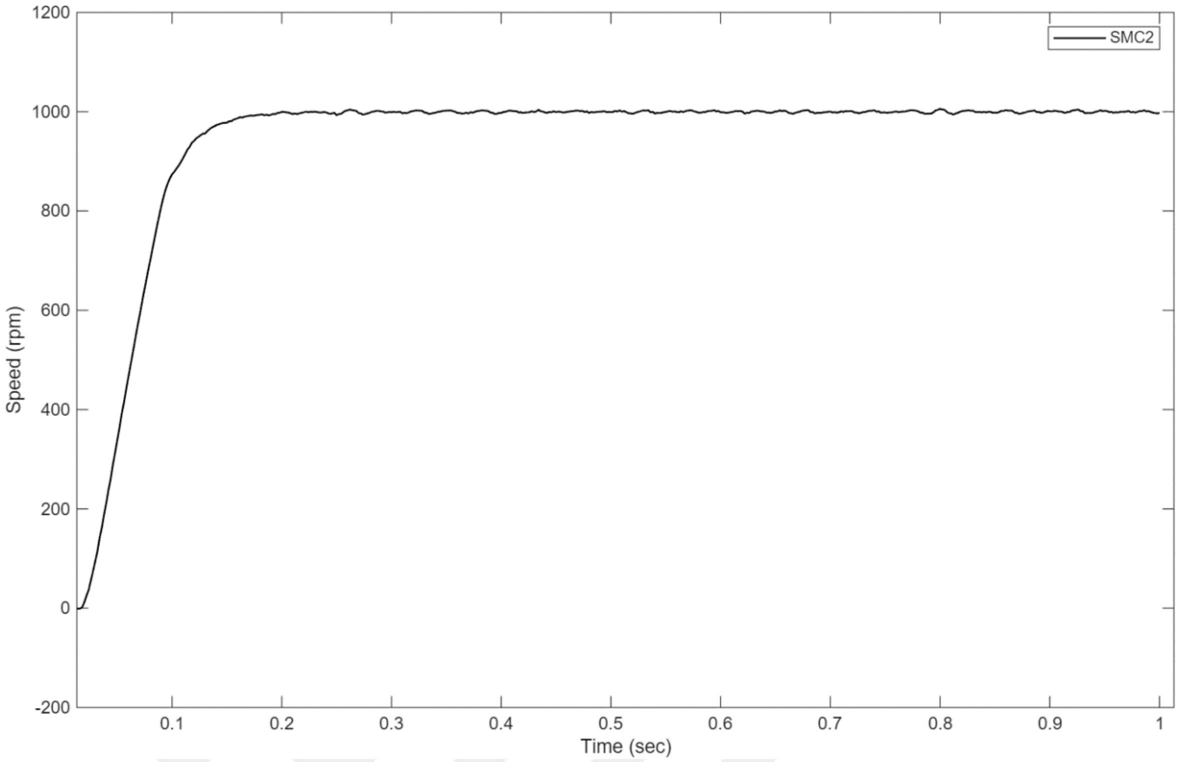

Figure 4.126. Output speed (rpm) (SMC-2)

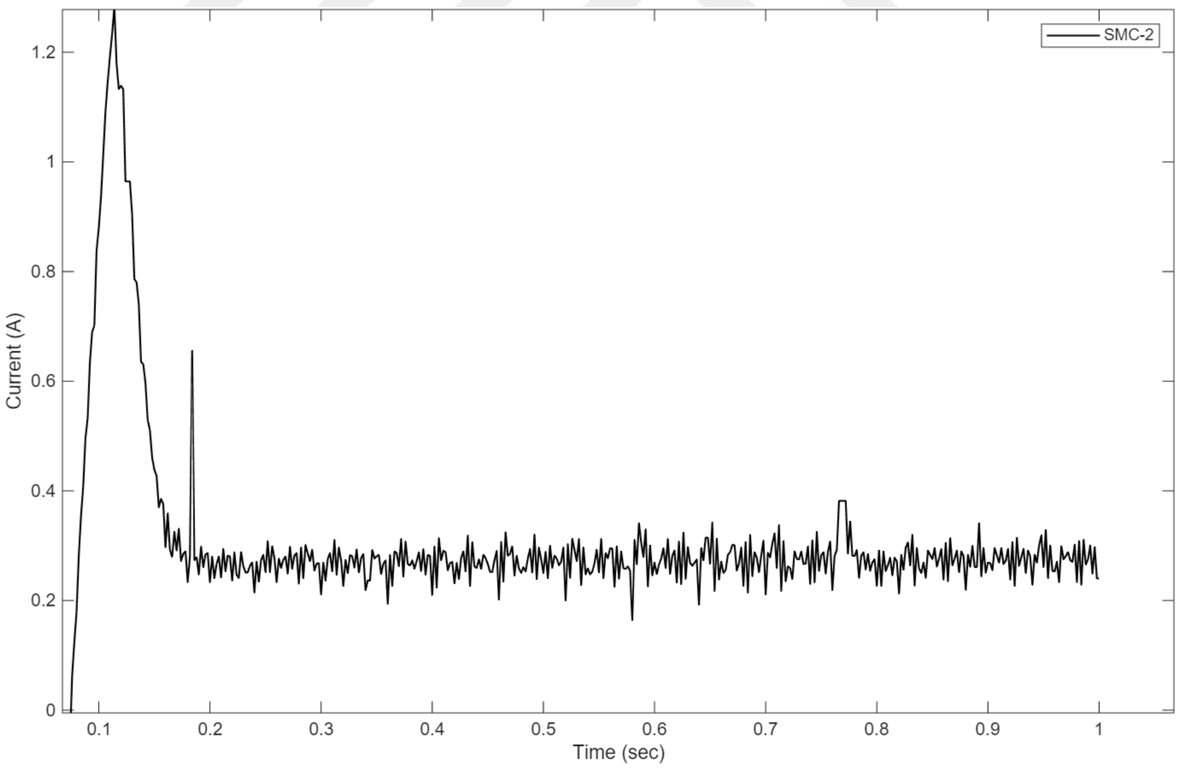

Figure 4.127. Armature current, $i_a(t)$ (SMC-2)

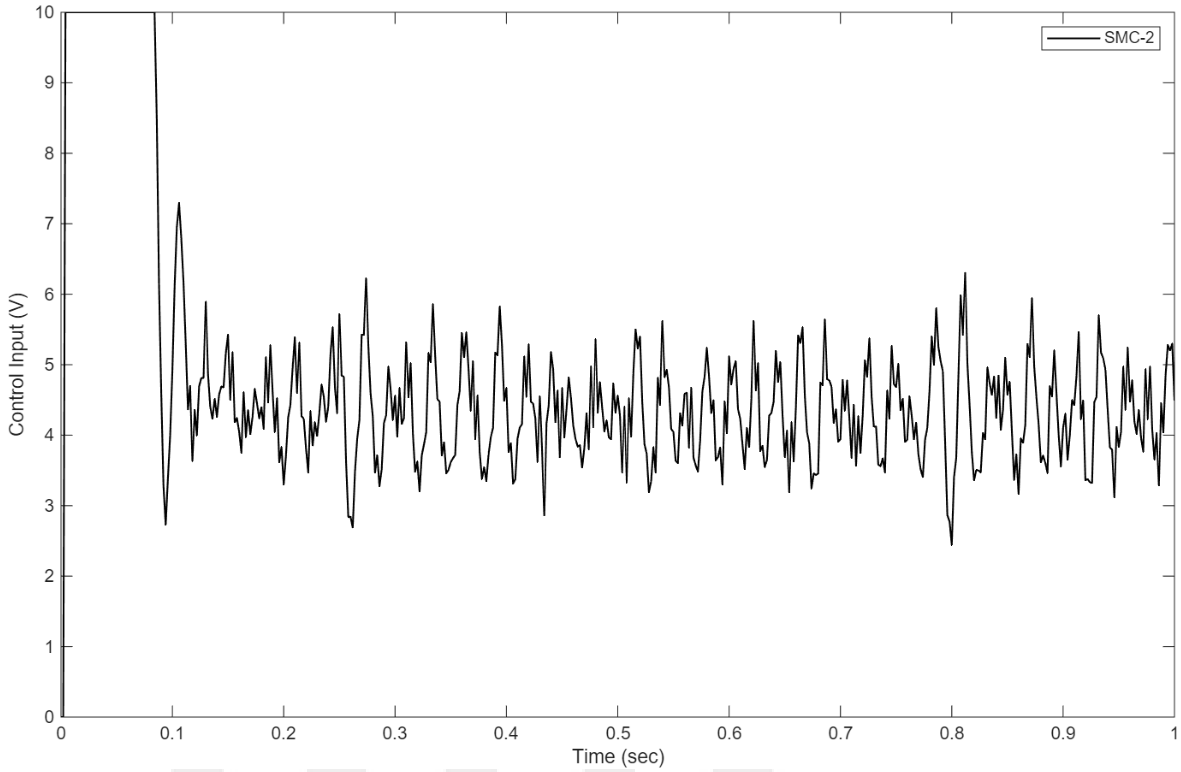

Figure 4.128. Control input voltage, $u(t)$ (SMC-2)

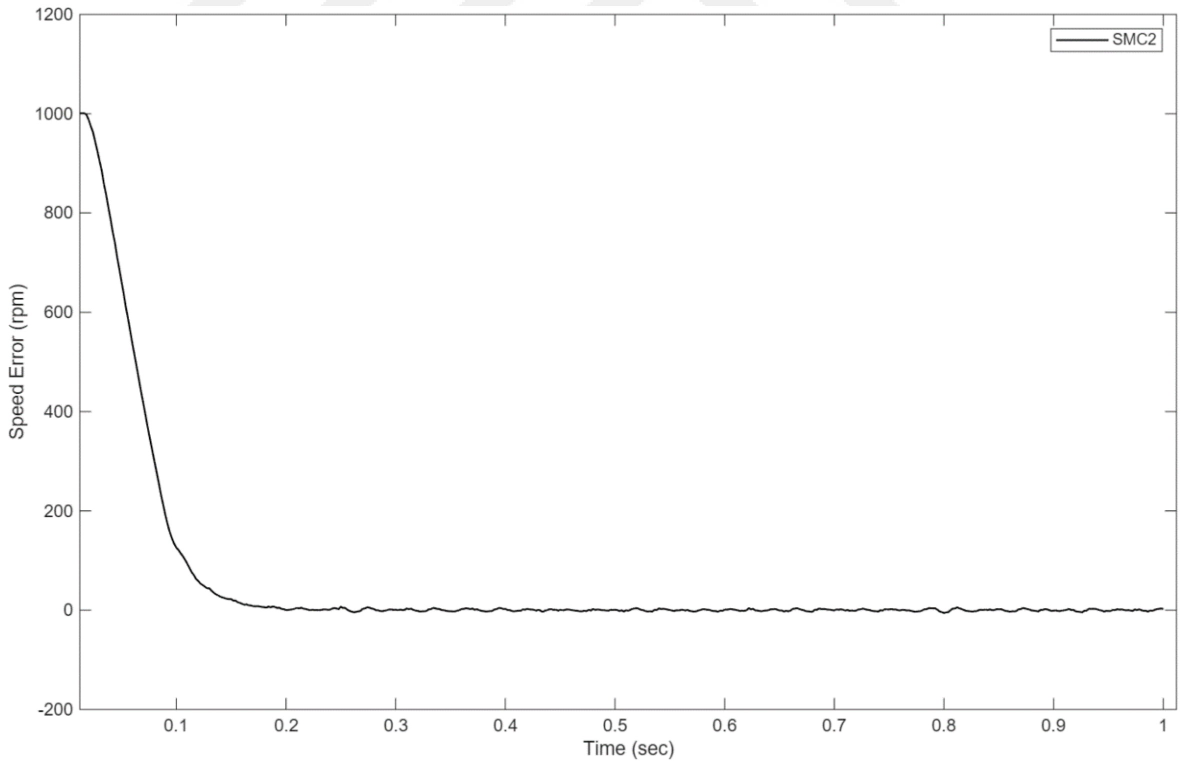

Figure 4.129. Speed error (rpm) (SMC-2)

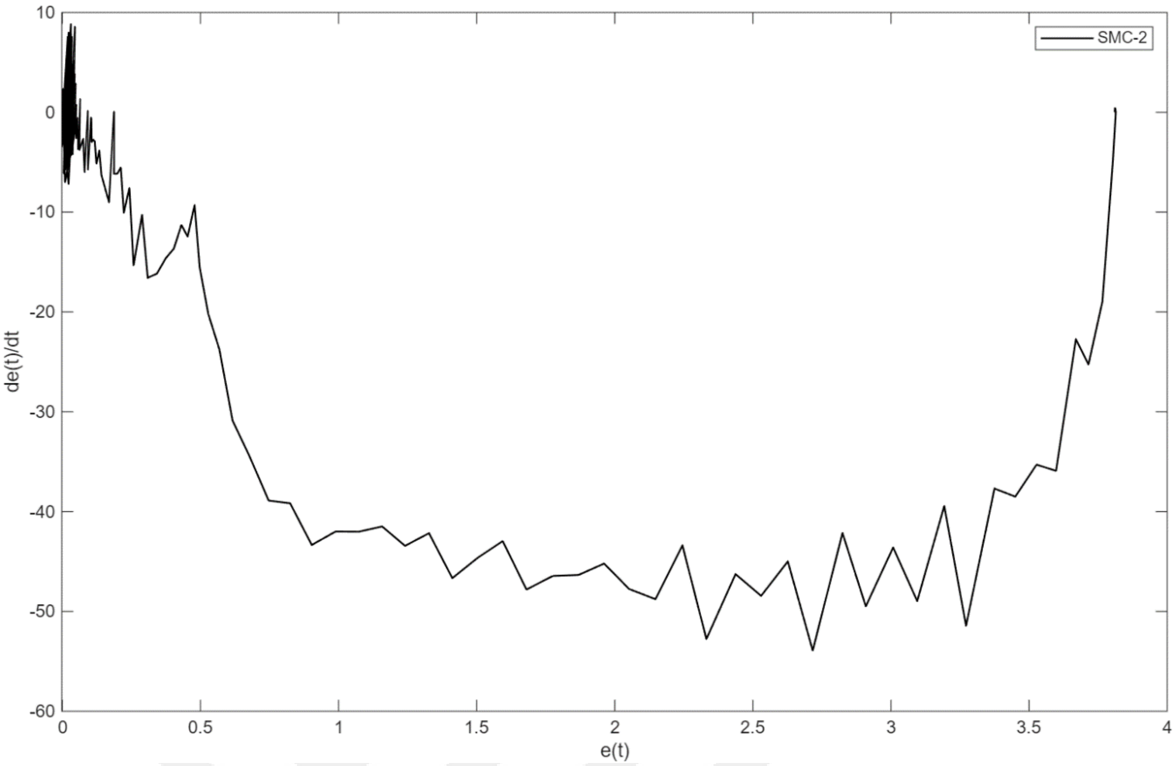

Figure 4.130. Phase plane of $e(t)$ and $de(t)/dt$ (SMC-2)

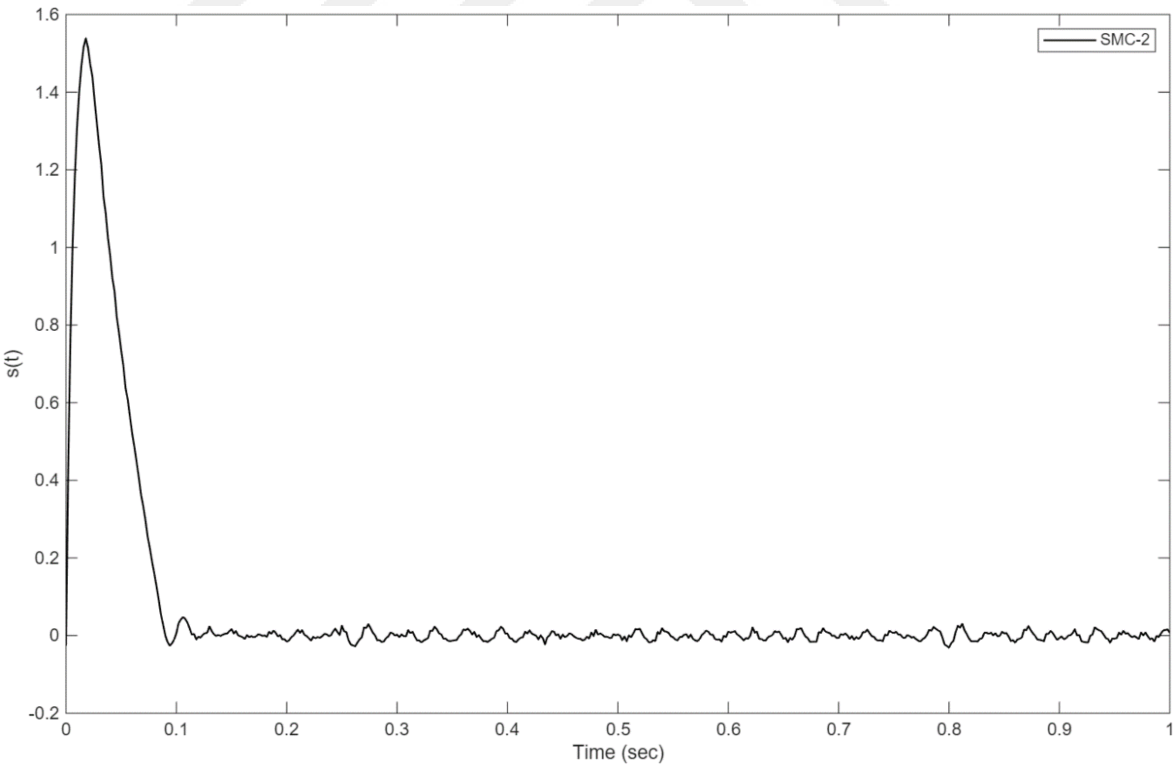

Figure 4.131. Sliding surface, $s(t)$ (SMC-2)

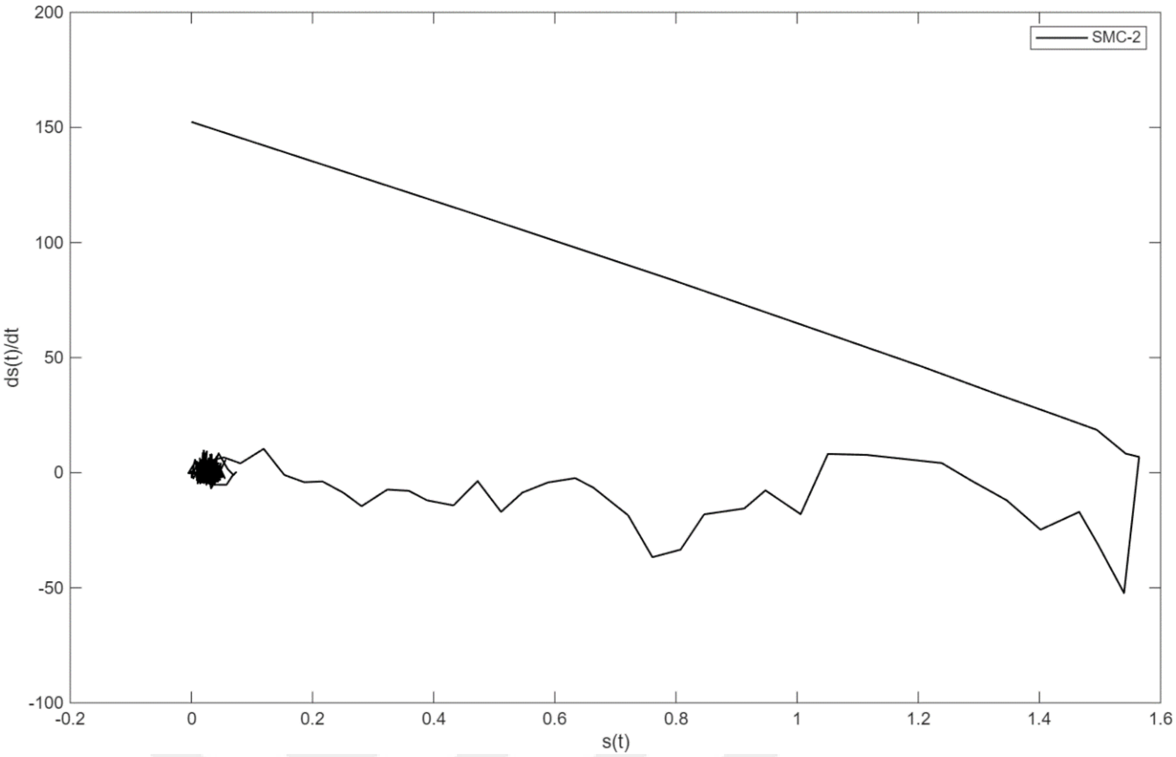

Figure 4.132. Phase plane of $s(t)$ and $ds(t)/dt$ (SMC-2)

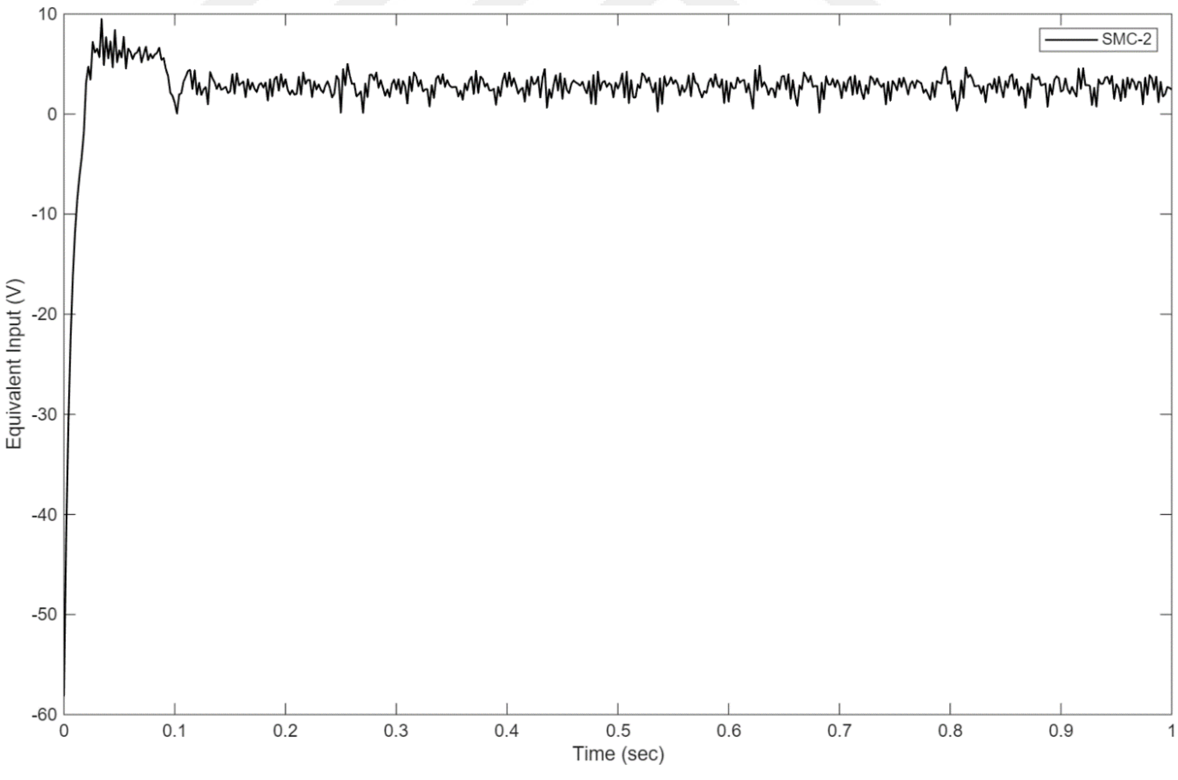

Figure 4.133. Equivalent input, $u_{eq}(t)$ (SMC-2)

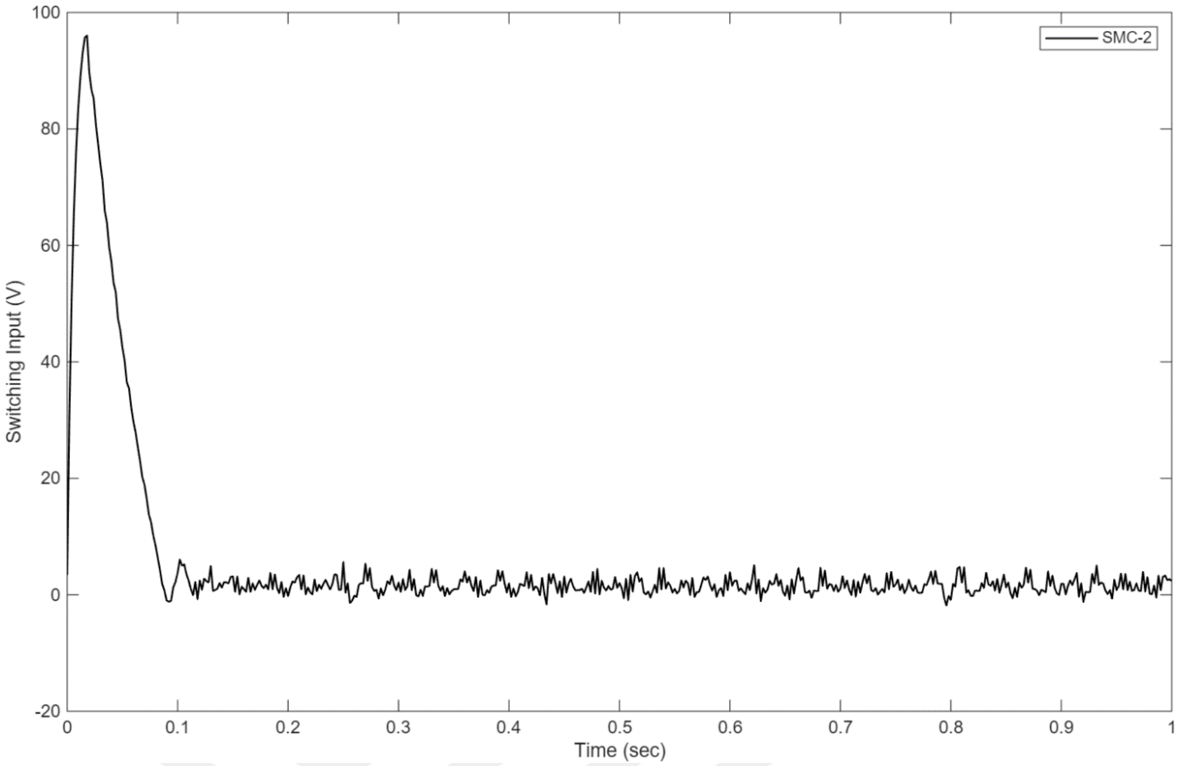

Figure 4.134. Switching input, $u_{sw}(t)$ (SMC-2)

The domain performance specifications presented in Table 4.35 indicate that the single-loop SMC-2 controller demonstrates a rapid, precise and stable dynamic performance in the transient regime. The rise time is 0.0770 s, the settling time is 0.1491 s and the overshoot is 0.81% indicating a highly controlled response. The system delay of 0.064 s demonstrates that the controller responds efficiently and sensitively to input variations. Performance Indices Examining the performance indicators in Table 4.36 the controller achieves ITAE = 0.02, ISE = 0.72, IAE = 0.27 and ITSE = 0.01 reflecting that error magnitudes and their time-weighted effects are maintained at minimal levels. The control effort indicator ISCI = 22.87 and ISTE = 0.0074, suggest that the system provides optimized control while avoiding excessive actuator activity. Overall the findings validate that the single-loop SMC-2 controller delivers a rapid, precise and stable control performance.

Table 4.35. Time domain performance specifications (SMC-2)

Controller	Rise Time (s)	Settling time (s)	Overshoot (%)	Delay time (s)
SMC-2	0.0770	0.1491	0.81	0.064

Table 4.36. Output performance indices (SMC-2)

Controller	ITAE	ISE	IAE	ITSE	ISCI	ISTE
SMC-2	0.02	0.72	0.27	0.01	22.87	0.0074

4.10. Experimental Results of Cascade Sliding Mode Controllers: (1) Outer-Loop SMC-1/Inner-Loop P (SMC-1/P), (2) Outer-Loop SMC-1/Inner-Loop PI (SMC-1/PI), (3) Outer-Loop SMC-1/Inner-Loop PID (SMC-1/PID), (4) Outer-Loop SMC-2/Inner-Loop P (SMC-2/P), (5) Outer-Loop SMC-2/Inner-Loop PI (SMC-2/PI), (6) Outer-Loop SMC-2/Inner-Loop PID (SMC-2/PID)

This section presents the experimental step responses and performance indices of the CSMC. The evaluated controller structures consist of outer-loop SMC-1 with inner-loop P, PI, and PID controllers, as well as outer-loop SMC-2 combined with P, PI, and PID controllers. The obtained results reveal the main dynamic characteristics of each configuration, including rise time, settling time, overshoot, and system delay. Moreover, performance indices such as ITAE, ISE, IAE, ITSE, ISCI and ISTE are examined to comprehensively assess the error behavior and control signal quality. Overall, the findings confirm that CSMC configurations achieve fast, stable, and accurate control performance under real-time operating conditions.

4.10.1. Experimental Results of Cascade Sliding Mode Control: Outer-Loop SMC-1/Inner-Loop P (SMC-1/P)

In this subsection, the experimental findings of the CSMC strategy, consisting of an outer-loop SMC-1 controller and an inner-loop P controller, are presented. The outer-loop SMC-1 controller is designed with parameters $k_d = 0.5,\ k_p = 35,\ k_i = 2,\ k_s = 3.2,\ \Omega = 15$, while the inner-loop P controller is tuned with $k_p = 4$. The output speed (Figure 4.135) and armature current (Figure 4.136) responses indicate that the SMC-1/P cascade configuration achieves fast transient behavior and satisfactory steady-state performance. The control signal (Figure 4.137) demonstrates a balanced interaction between the robust characteristics of the outer SMC-1 controller and the quick response of the inner-loop P controller, resulting in reduced overshoot, limited oscillations, and a noticeable reduction in the chattering effect typically observed in SMC.

Furthermore, the error signal (Figure 4.138) and its derivative verify accurate reference tracking, while the combined plots of error (Figure 4.139), its derivative (from the outer-loop) illustrate stable system operation and improved disturbance rejection capability. The analysis of the sliding surface (Figure 4.140) and the sliding surface with its derivative (Figure 4.141) confirms that the system trajectory remains close to the predefined manifold, highlighting the stability and robustness of the SMC-1/P design. The equivalent signal (Figure 4.142) and the switching signal (Figure 4.143).

Overall, the experimental results confirm that the SMC-1/P hybrid control approach enhances system performance compared to a standalone P controller by merging the robustness of SMC with the simplicity and speed of proportional control.

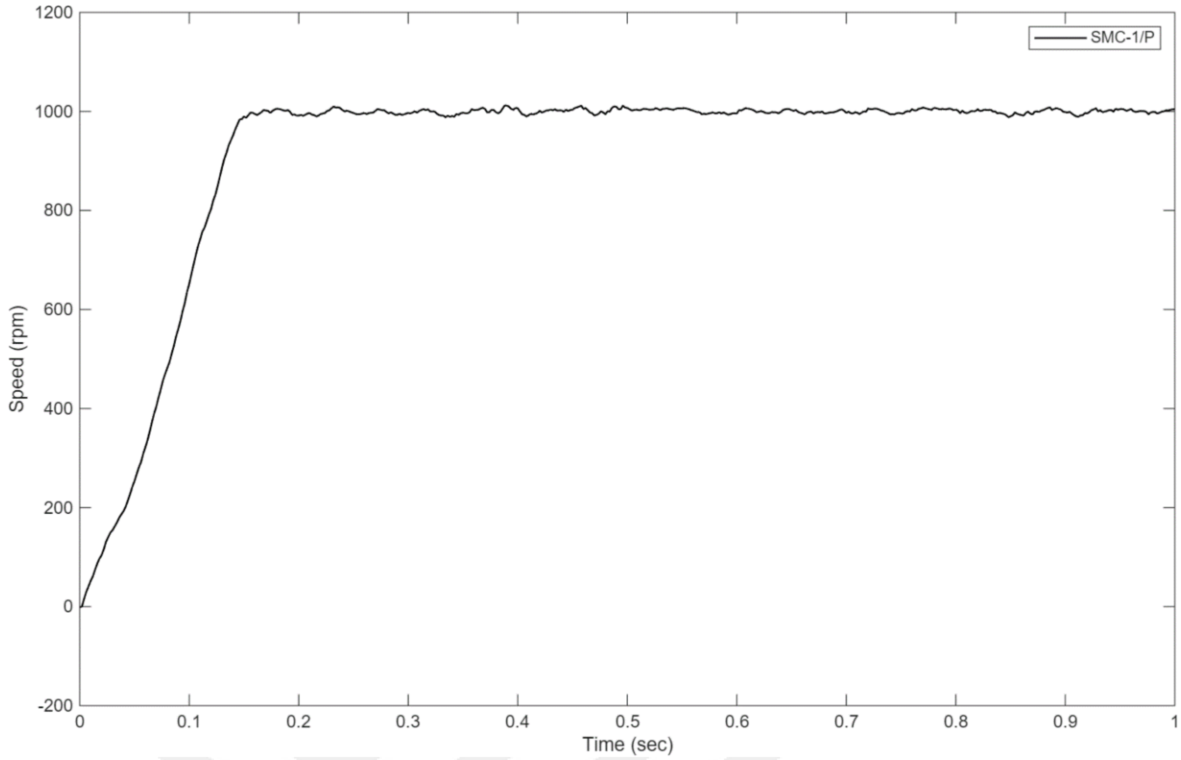

Figure 4.135. Output speed (rpm) (SMC-1/P)

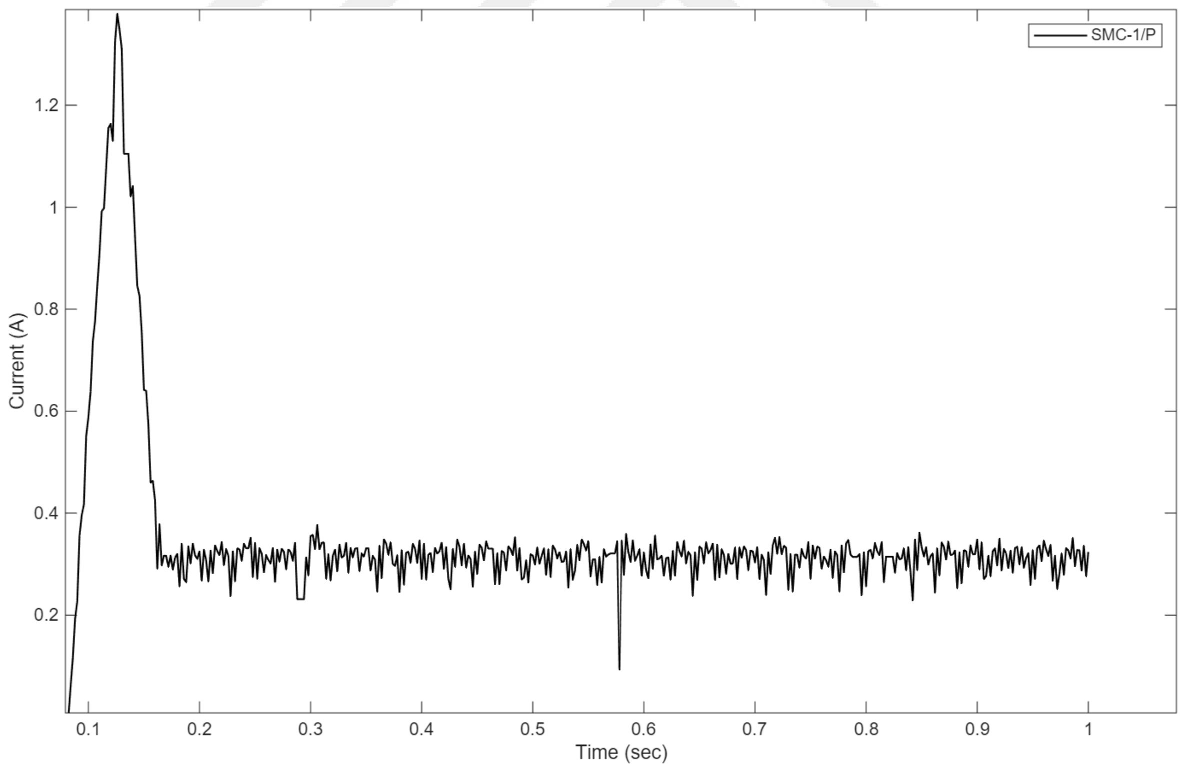

Figure 4.136. Armature current, $i_a(t)$ (SMC-1/P)

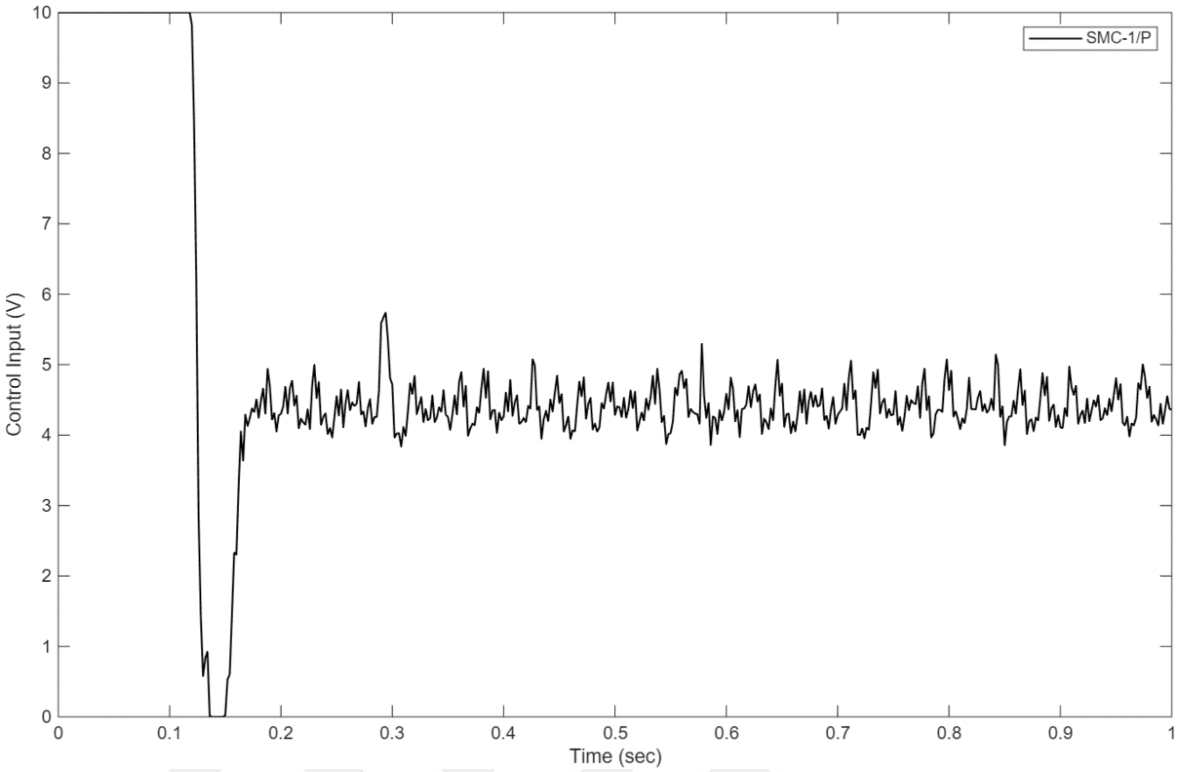

Figure 4.137. Control input voltage, $u(t)$ (SMC-1/P)

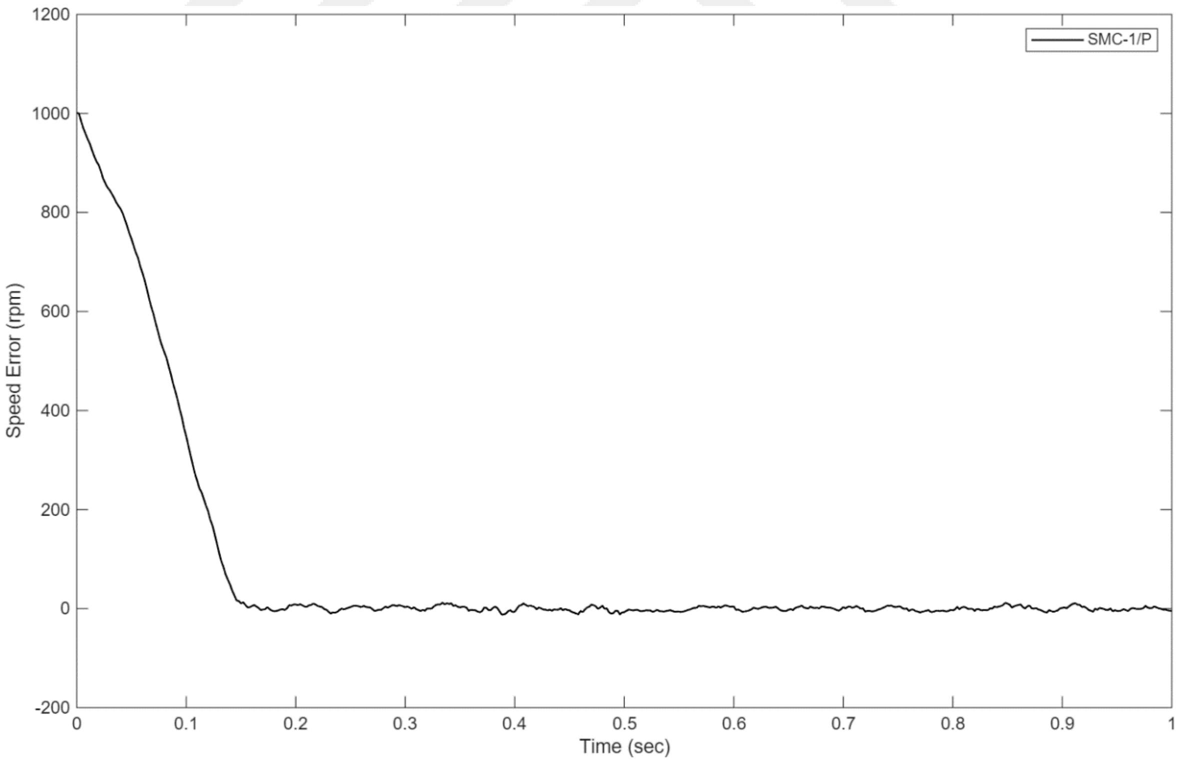

Figure 4.138. Speed error (rpm) (SMC-1/P)

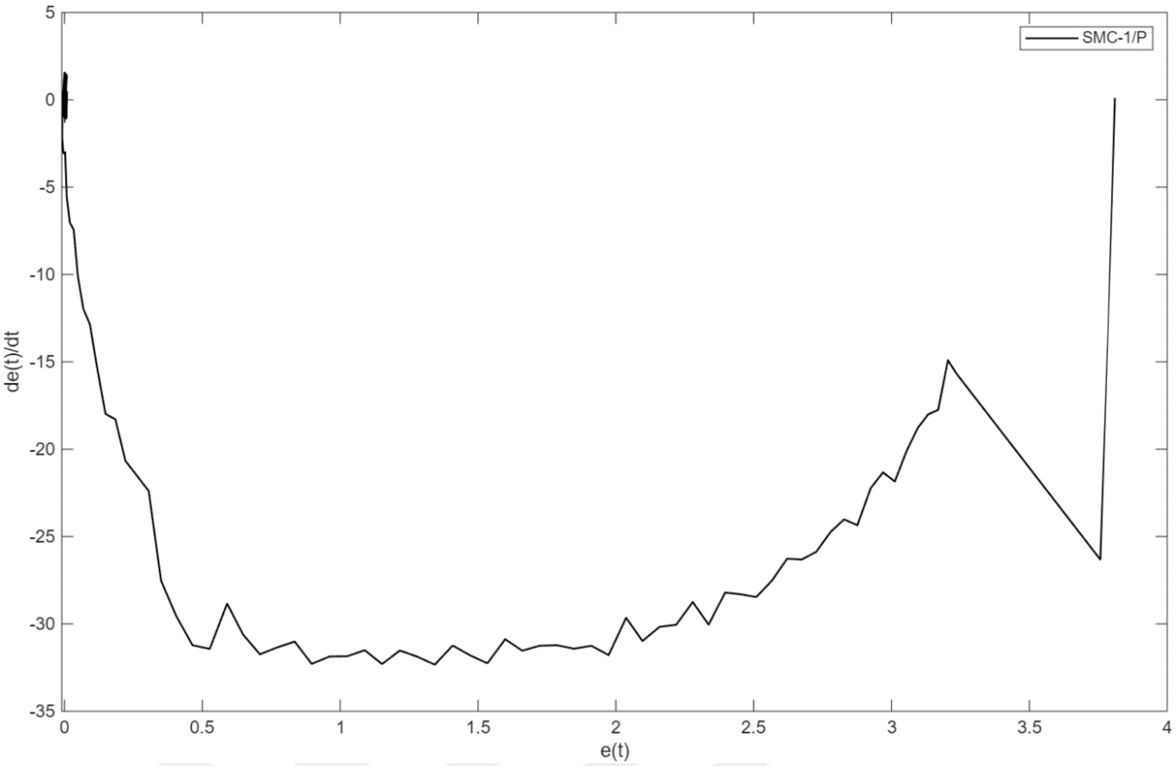

Figure 4.139. Phase plane of $e(t)$ and $de(t)/dt$ (SMC-1/P)

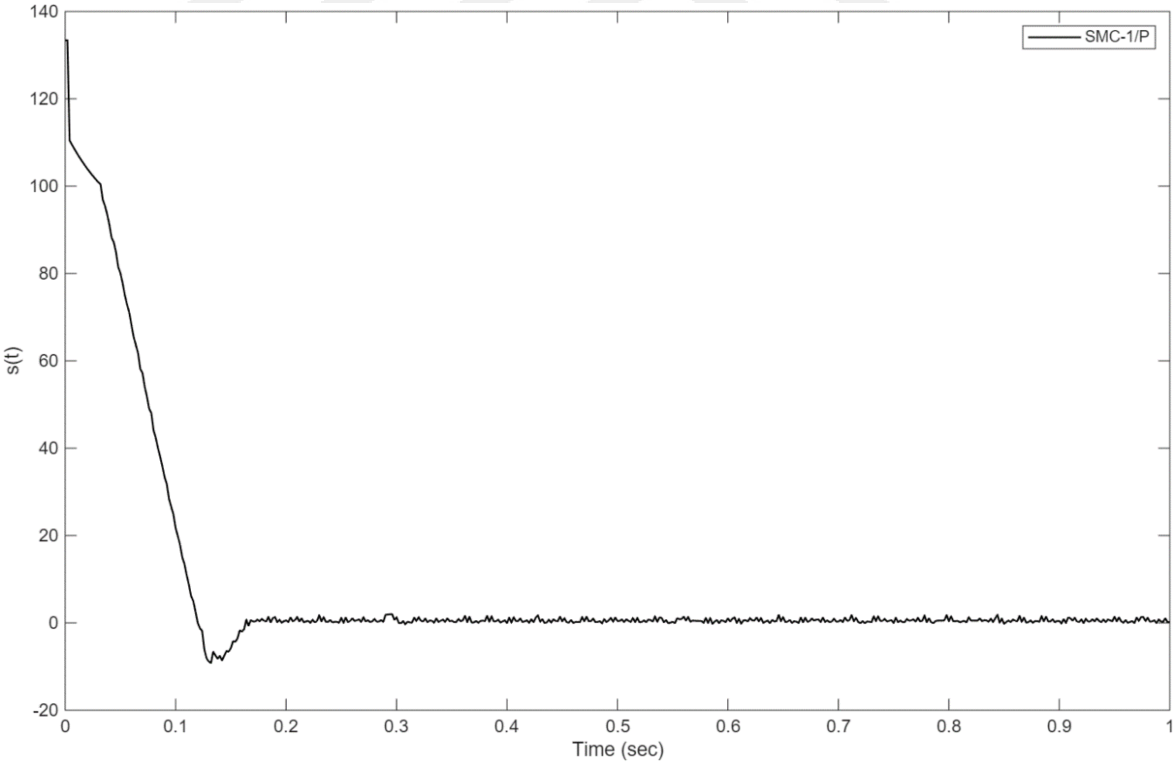

Figure 4.140. Sliding surface, $s(t)$ (SMC-1/P)

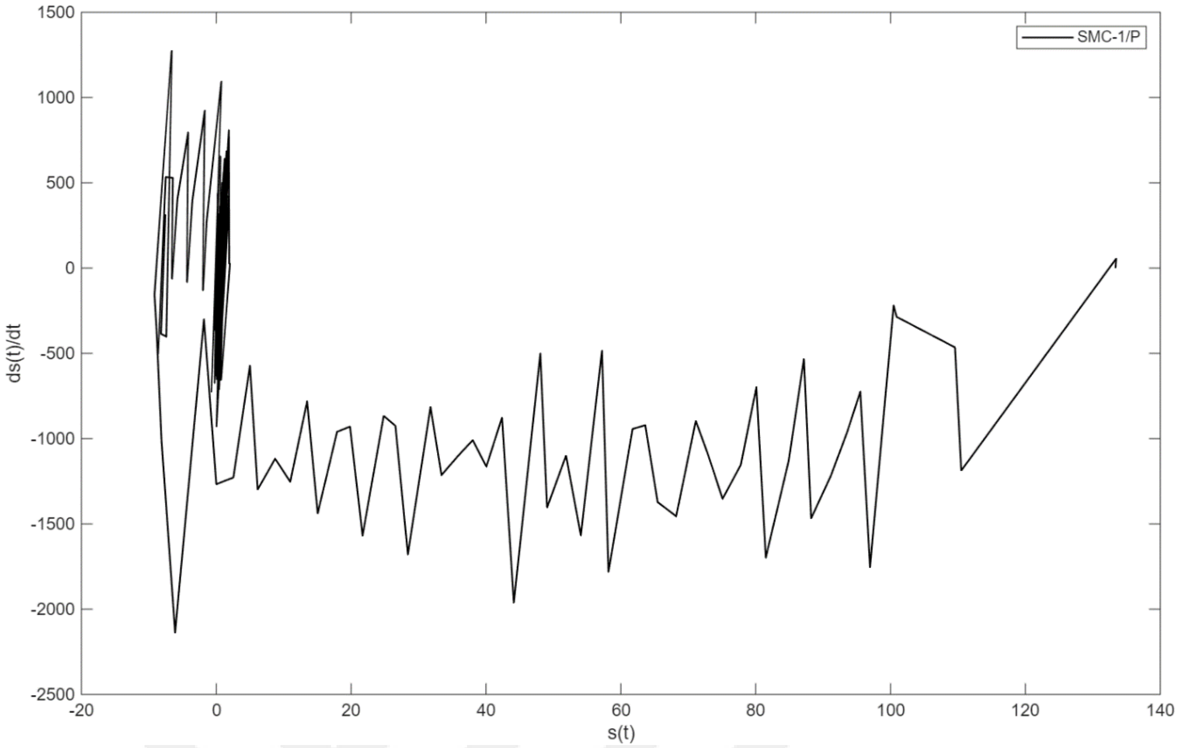

Figure 4.141. Phase plane of $s(t)$ and $ds(t)/dt$ (SMC-1/P)

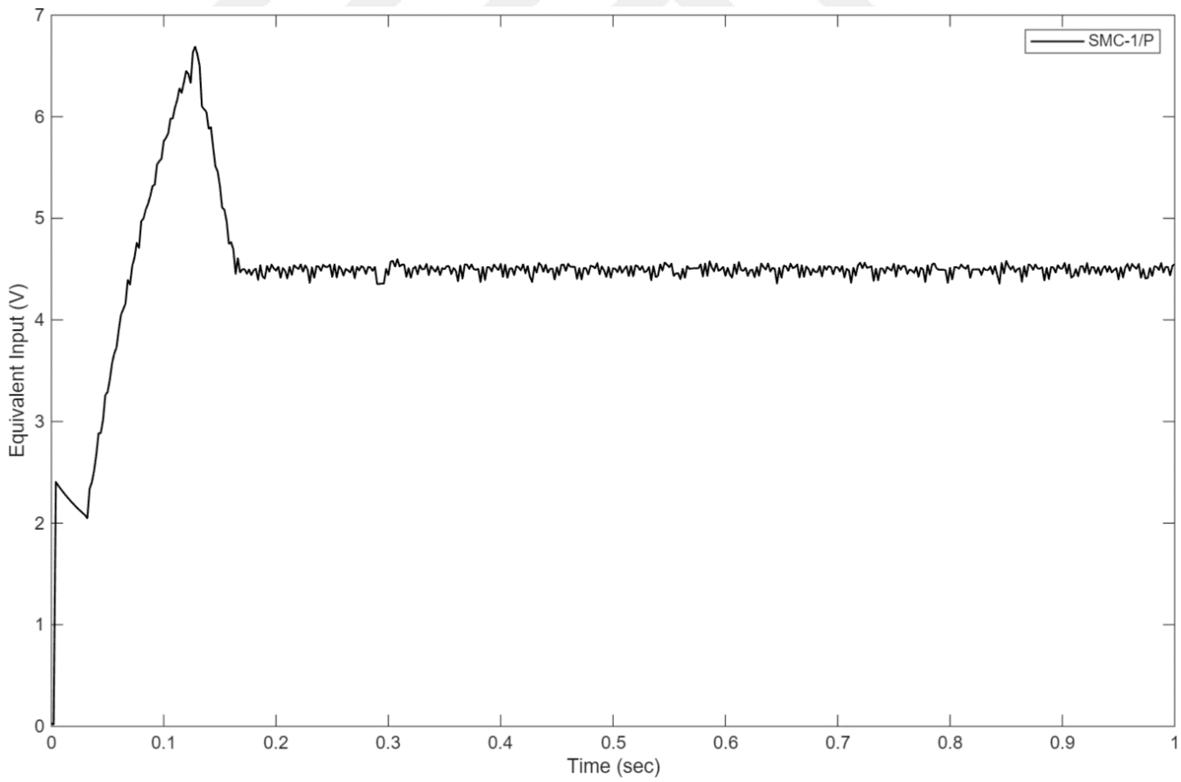

Figure 4.142. Equivalent input, $u_{eq}(t)$ (SMC-1/P)

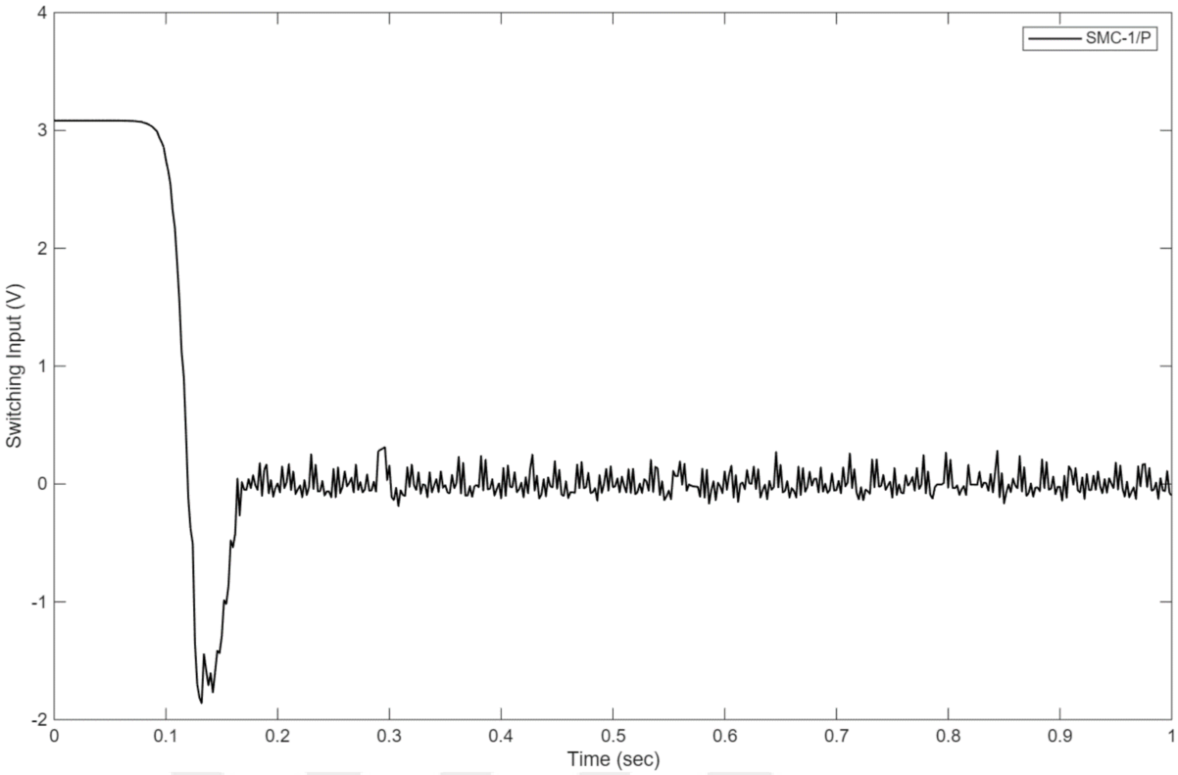

Figure 4.143. Switching input, $u_{sw}(t)$ (SMC-1/P)

The time domain performance specifications presented in Table 4.37 indicate that the cascade SMC-1/P controller exhibits rapid and stable dynamic performance. The rise time is calculated to be 0.1122 seconds, the settling time is 0.1474 seconds, and the overshoot is 0.24%, which collectively indicates a transient response that is highly controlled. The system delay of 0.0840 s indicates that the control structure responds promptly and sensitively to input variations. Performance indices an examination of the performance indicators presented in Table 4.38 reveals that the controller attains ITAE = 0.015, ISE = 0.816, IAE = 0.3039 and ITSE = 0.0316. This indicates that the magnitude of errors and their time-weighted effects are sustained at minimal levels. The control effort indicator ISCI = 28.78 and ISTE = 0.0007 suggest that the system provides optimised control while avoiding excessive actuator activity. The findings corroborate the hypothesis that the cascade SMC-1/P controller delivers fast, precise and stable control performance.

Table 4.37. Time domain performance specifications (SMC-1/P)

Controller	Rise Time (s)	Settling time (s)	Overshoot (%)	Delay time (s)
Cascade Outer-Loop SMC-1/Inner-Loop P	0.1122	0.1474	0.24	0.0840

Table 4.38. Output performance indices (SMC-1/P)

Controller	ITAE	ISE	IAE	ITSE	ISCI	ISTE
Cascade Outer-Loop SMC-1/Inner-Loop P	0.015	0.816	0.3039	0.0316	28.78	0.0007

4.10.2. Experimental Results of Cascade Sliding Mode Control: Outer-Loop SMC-1/Inner-Loop PI (SMC-1/PI)

In this subsection, the experimental findings of the CSMC strategy, consisting of an outer-loop SMC-1 controller and an inner-loop PI controller, are presented. The outer-loop SMC-1 controller is designed with parameters $k_d = 0.5,\ k_p = 35,\ k_i = 2,\ k_s = 3.2,\ \Omega = 15$ while the inner-loop PI controller is tuned with PI = $4\left(1 + \frac{1}{10s}\right)$. The output speed (Figure 4.144) and armature current response (Figure 4.145) graphs demonstrate that the cascade configuration ensures a rapid transient response and improved steady-state performance. The control input signal (Figure 4.146) demonstrates the equilibrium between the robustness of the SMC and the precision of the inner-loop PI controller, thereby leading to a reduction in oscillations and a minimisation of the chattering effect. In addition the error signal (Figure 4.147), the combined plot of error and its derivative (Figure 4.148), have been shown to demonstrate efficient tracking of the reference input. Furthermore, the combined error and derivative graphs confirm stable operation and enhanced disturbance rejection. The sliding surface signal (Figure 4.149), the sliding surface with its derivative (Figure 4.150) indicate that the system trajectory remains close to the designed sliding manifold, validating the robustness of the SMC-PI configuration. In addition to the equivalent signal (Figure 4.151) and the switching signal (Figure 4.152) provide a comprehensive view of the system's performance. The experimental results obtained from the present study confirm that this hybrid control approach in comparison with a standalone PI controller, by effectively combining robustness and accuracy.

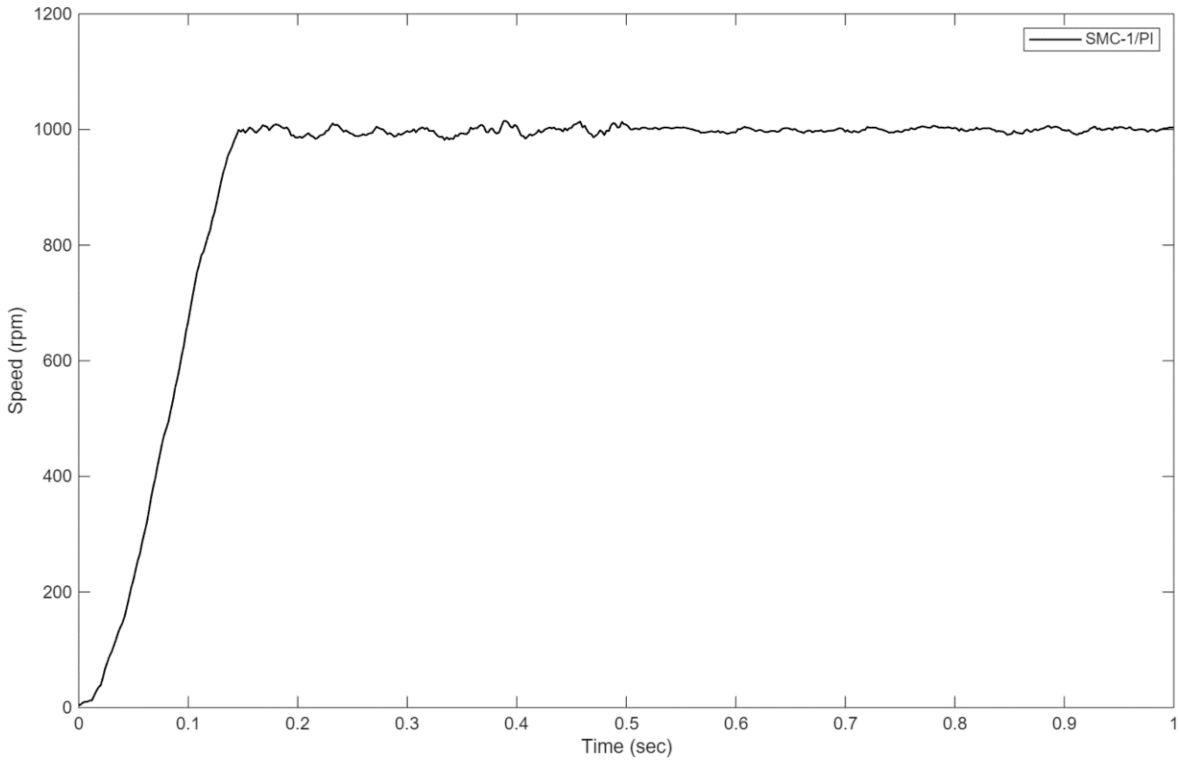

Figure 4.144. Output speed (rpm) (SMC-1/PI)

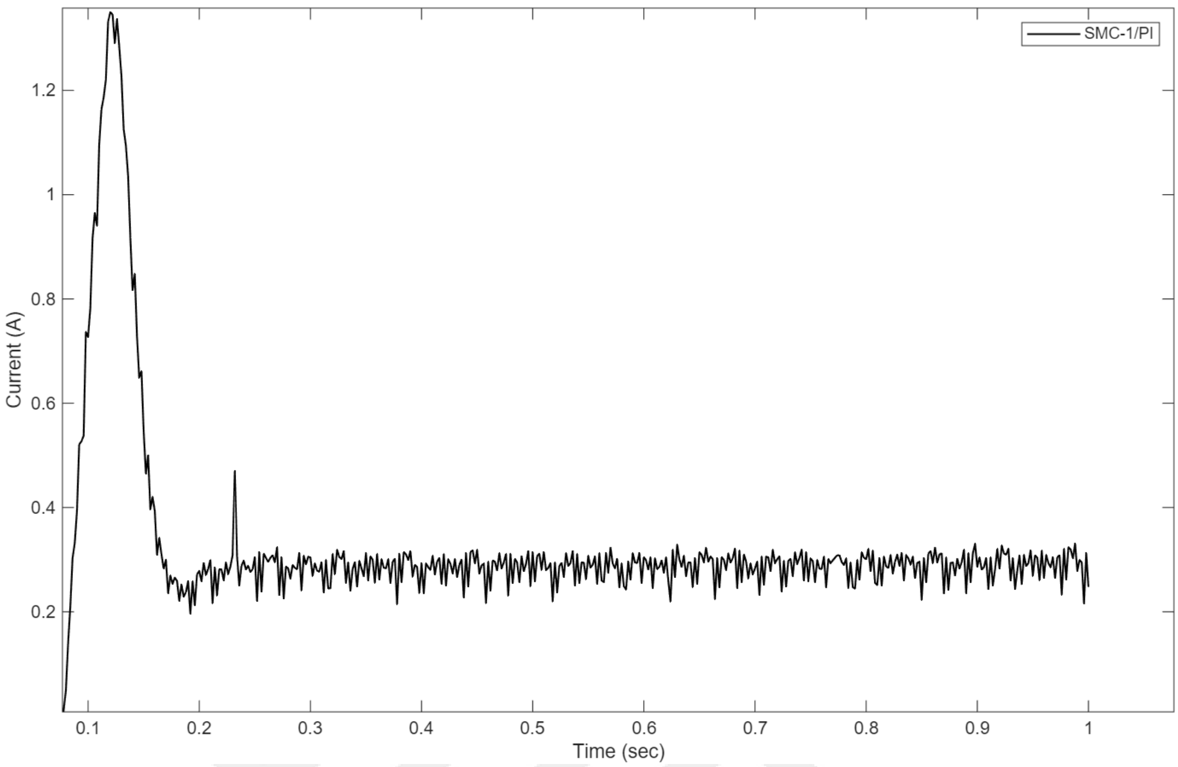

Figure 4.145. Armature current, $i_a(t)$ (SMC-1/PI)

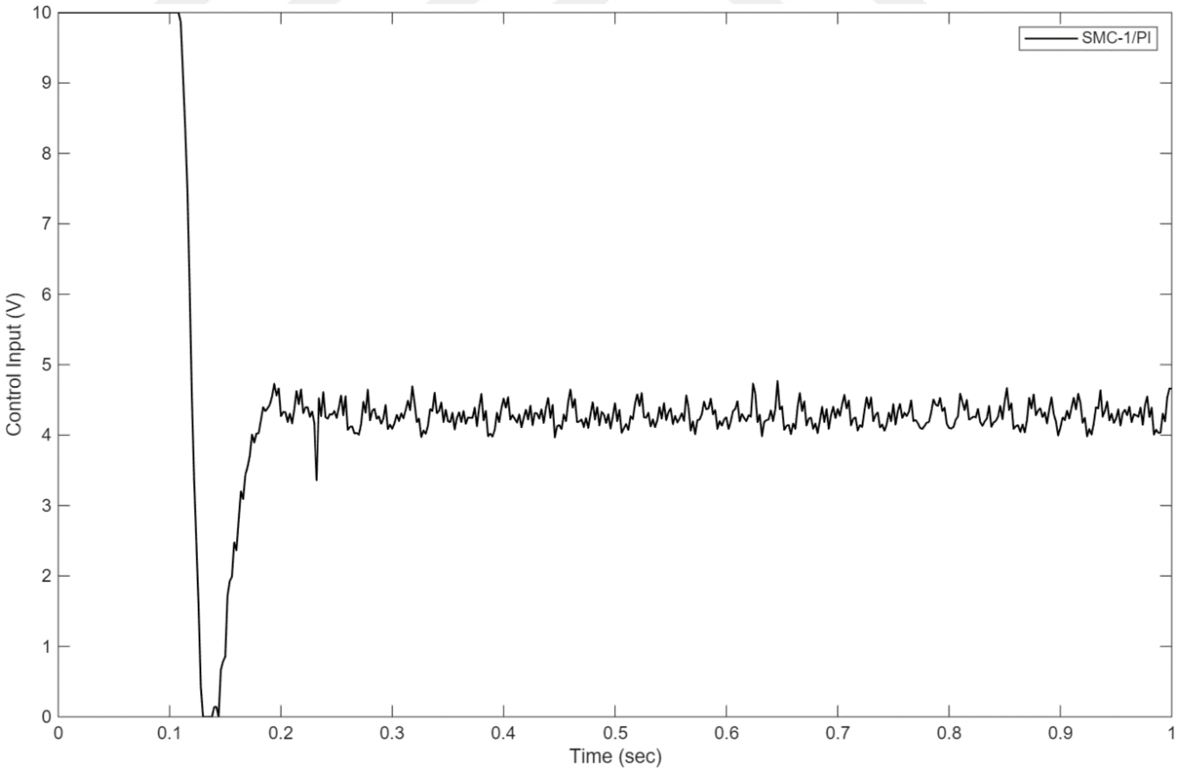

Figure 4.146. Control input voltage, $u(t)$ (SMC-1/PI)

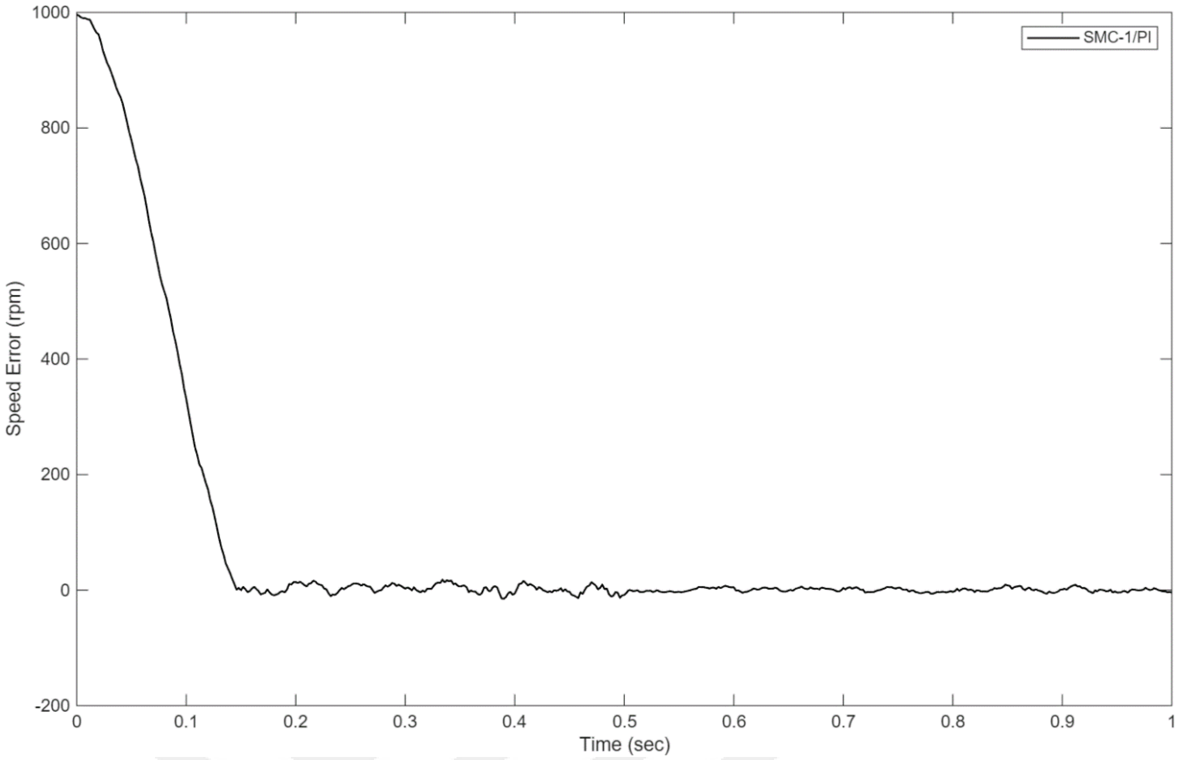

Figure 4.147. Speed error (rpm) (SMC-1/PI)

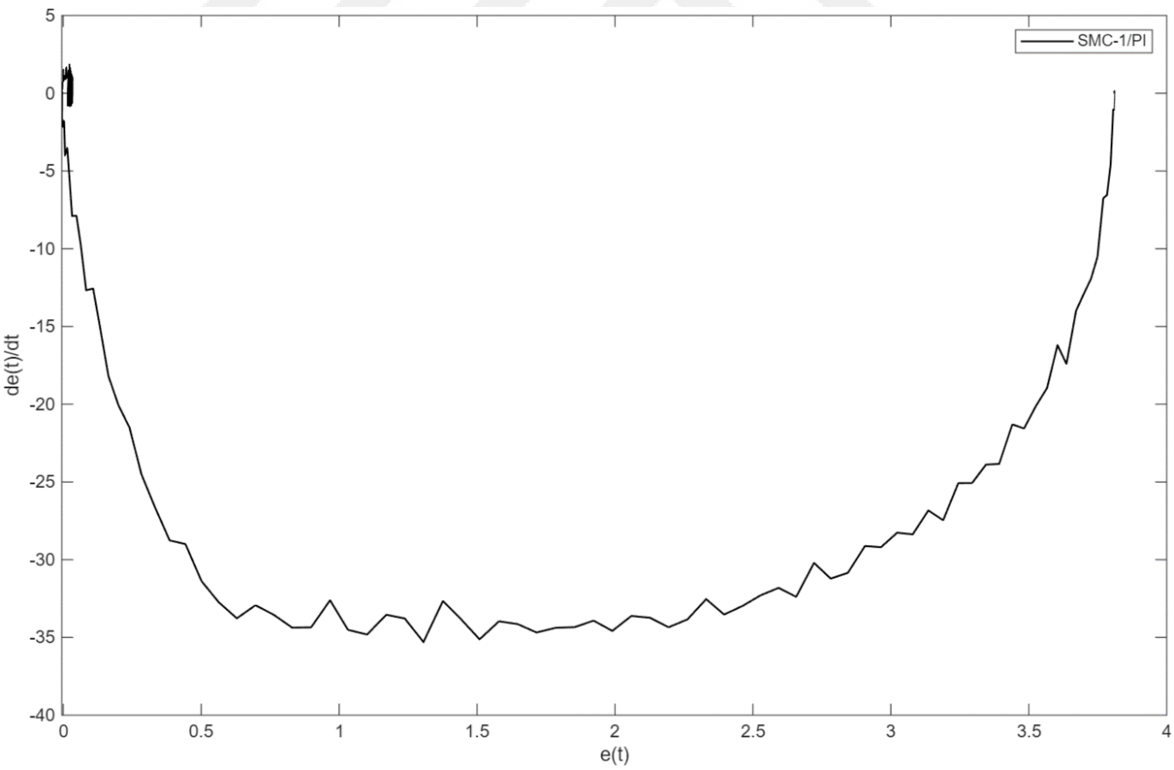

Figure 4.148. Phase plane of $e(t)$ and $de(t)/dt$ (SMC-1/PI)

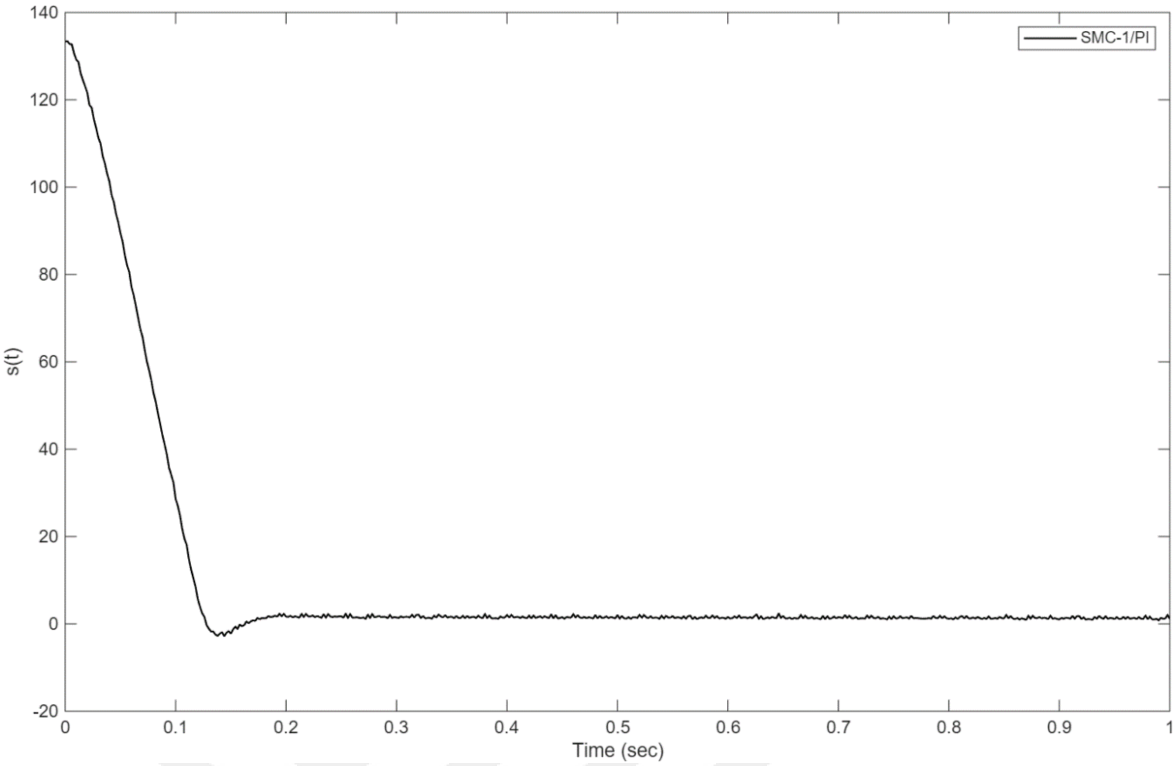

Figure 4.149. Sliding surface, $s(t)$ (SMC-1/PI)

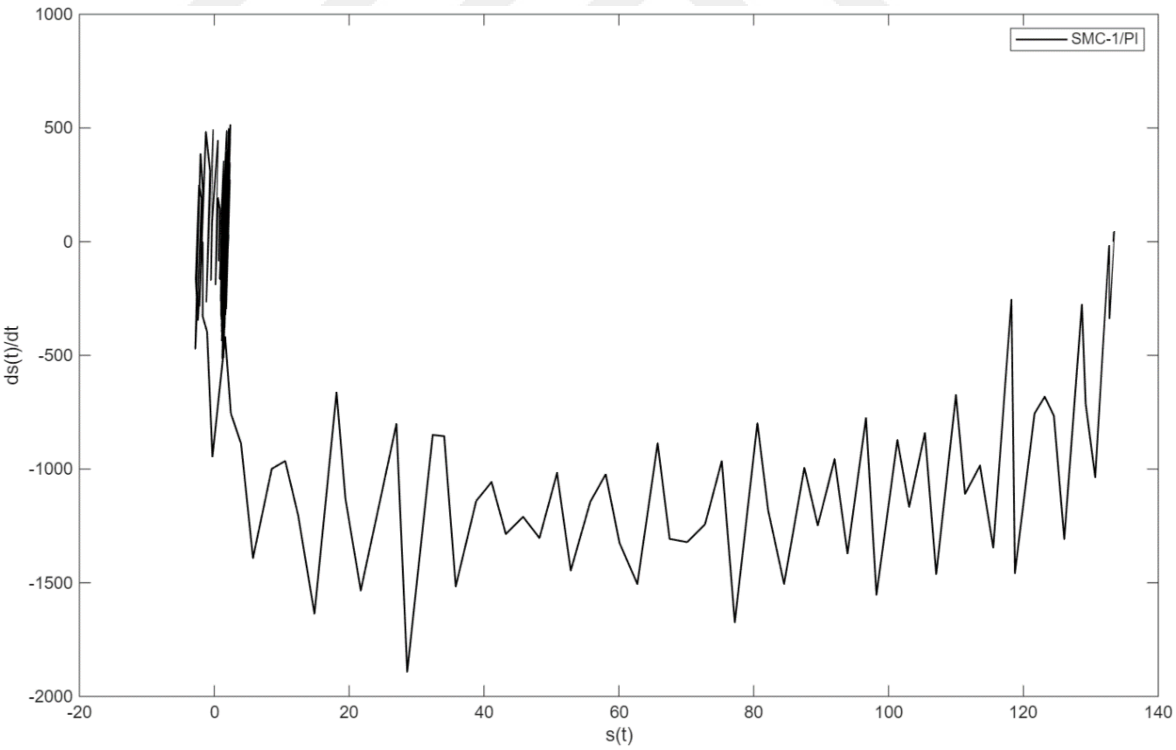

Figure 4.150. Phase plane of $s(t)$ and $ds(t)/dt$ (SMC-1/PI)

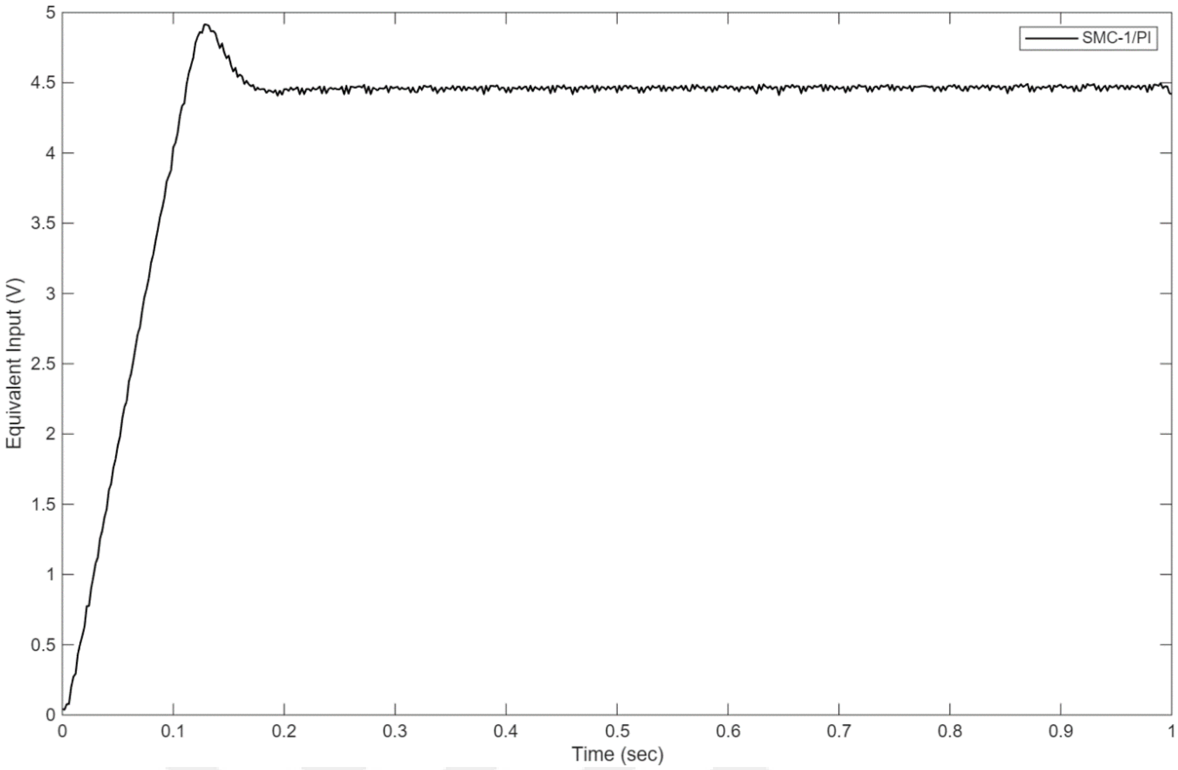

Figure 4.151. Equivalent input, $u_{eq}(t)$ (SMC-1/PI)

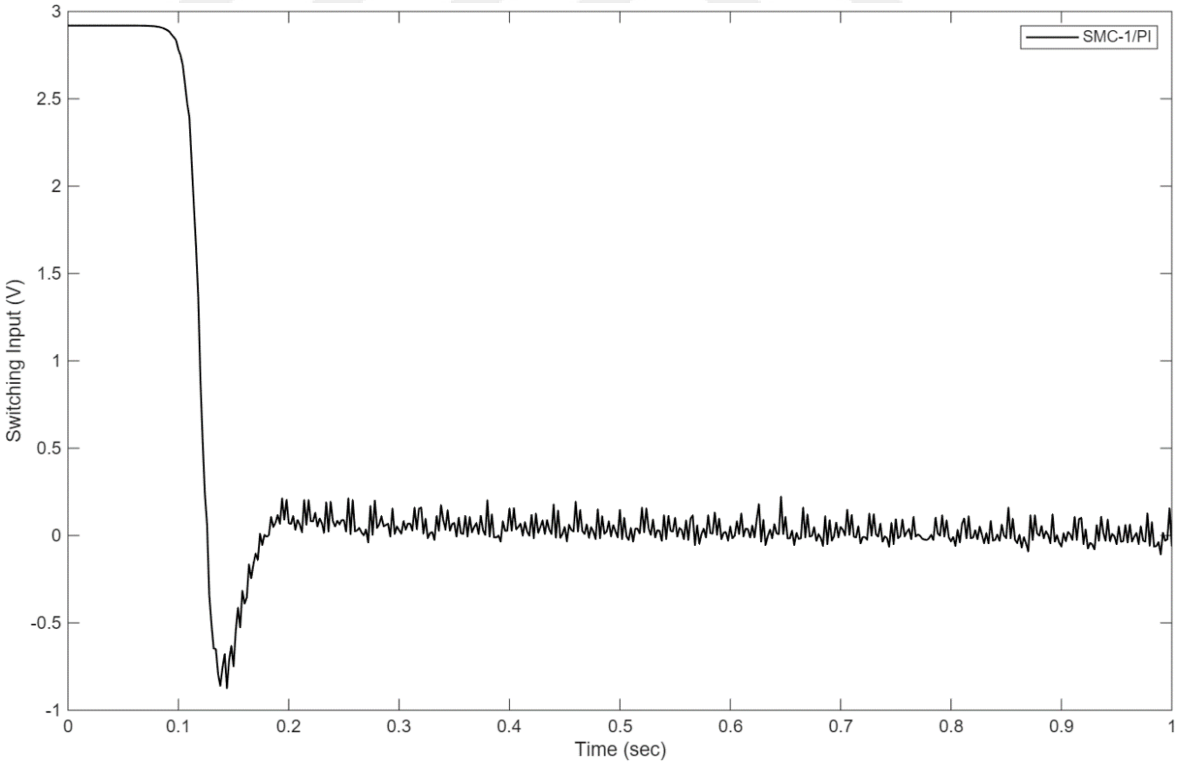

Figure 4.152. Switching input, $u_{sw}(t)$ (SMC-1/PI)

The time domain performance specifications presented in Table 4.39 indicate that the cascade SMC-1/PI controller provides a fast and stable transient response. The rise time is measured at 0.0952 seconds, the settling time at 0.1431 seconds, and the overshoot at 0.64%, indicative of a highly controlled transient behaviour. The system delay of 0.084 s indicates that the control structure responds effectively and sensitively to input variations. Performance Indices

An examination of the performance indicators presented in Table 4.40 reveals that the controller attains ITAE = 0.09, ISE = 1.10, IAE = 0.53 and ITSE = 0.05. This suggests that the magnitude of errors and their time-weighted effects are effectively constrained. The control effort indicator ISCI = 27.28 and ISTE = 0.4280, suggest that the system maintains balanced control without excessive actuator activity. The findings demonstrate that the cascade SMC-1/PI controller provides rapid, precise and stable control performance.

Table 4.39. Time domain performance specifications (SMC-1/PI)

Controller	Rise Time (s)	Settling time (s)	Overshoot (%)	Delay time (s)
Cascade Outer-Loop SMC-1/Inner-Loop PI	0.0952	0.1431	0.64	0.084

Table 4.40. Output performance indices (SMC-1/PI)

Controller	ITAE	ISE	IAE	ITSE	ISCI	ISTE
Cascade Outer-Loop SMC-1/Inner-Loop PI	0.09	1.10	0.53	0.05	27.28	0.4280

4.10.3. Experimental Results of Cascade Sliding Mode Control: Outer-Loop SMC-1/Inner-Loop PID (SMC-1/PID)

In this subsection, the experimental findings of the CSMC strategy consisting of an outer-loop SMC-1 controller and an inner-loop PID controller, are presented. The outer-loop SMC-1 controller is designed with parameters $k_d = 0.5,\ k_p = 35,\ k_i = 2,\ k_s = 3.2,\ \Omega = 15$ while the inner-loop PID controller is tuned with PID = $10\left(1 + \frac{1}{20s} + 0.1s\right)$. The output speed (Figure 4.153) and current response (Figure 4.154) graphs demonstrate that the cascade configuration ensures a rapid transient response and improved steady-state performance. The control signal (Figure 4.155) demonstrates the equilibrium between the robustness of the SMC and the precision of the inner-loop PID controller, thereby leading to a reduction in oscillations and a minimisation of the chattering effect. Furthermore the error signal (Figure 4.156), error and its derivative (Figure 4.157) demonstrate efficient tracking of the reference input, while the combined error and derivative graphs confirm stable operation and enhanced disturbance rejection. The trajectory of the system, the sliding surface (Figure 4.158), as indicated by the sliding surface and its derivative (Figure 4.159), remains in close proximity to the designed sliding manifold. The equivalent signal (Figure 4.160), and the switching signal (Figure 4.161), further indicate how the SMC maintains the desired system behavior by compensating for uncertainties and enforcing the sliding condition**.**

This observation validates the robustness of the SMC-PID configuration. The experimental results obtained from the present study confirm that this hybrid control approach improves overall performance in comparison with a standalone PID controller, by effectively combining robustness and accuracy.

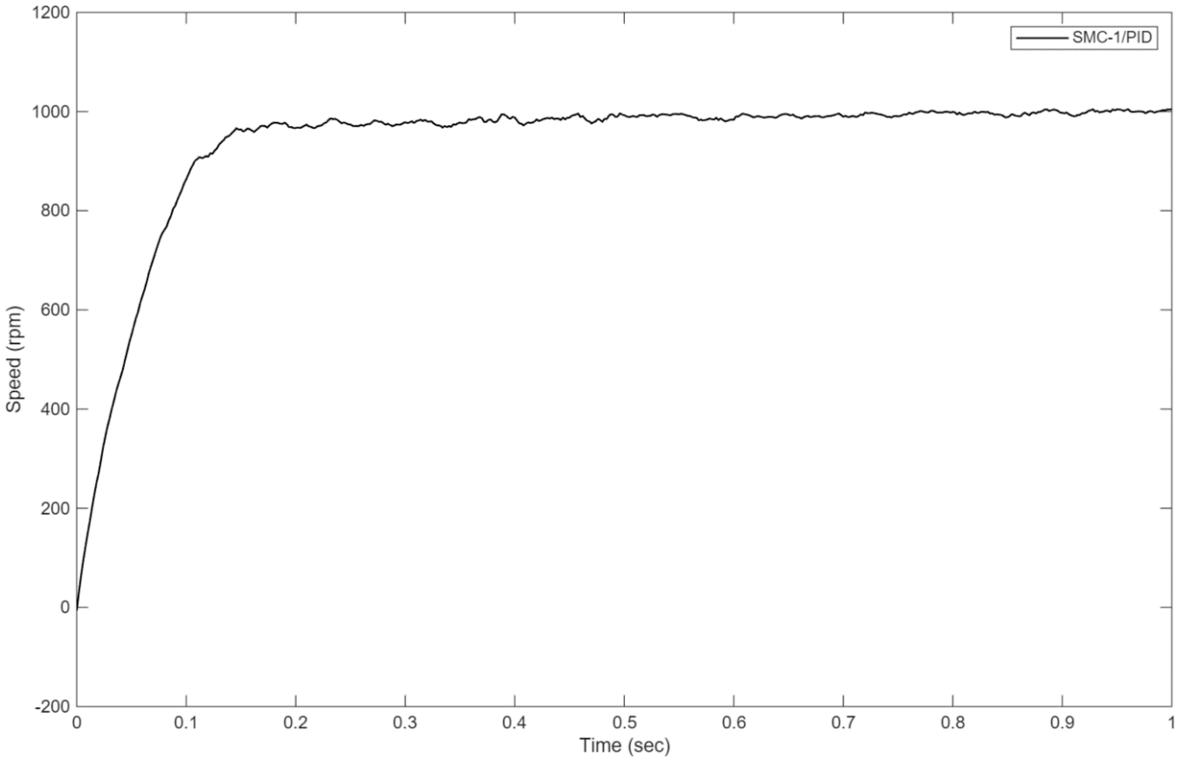

Figure 4.153. Output speed (rpm) (SMC-1/PID)

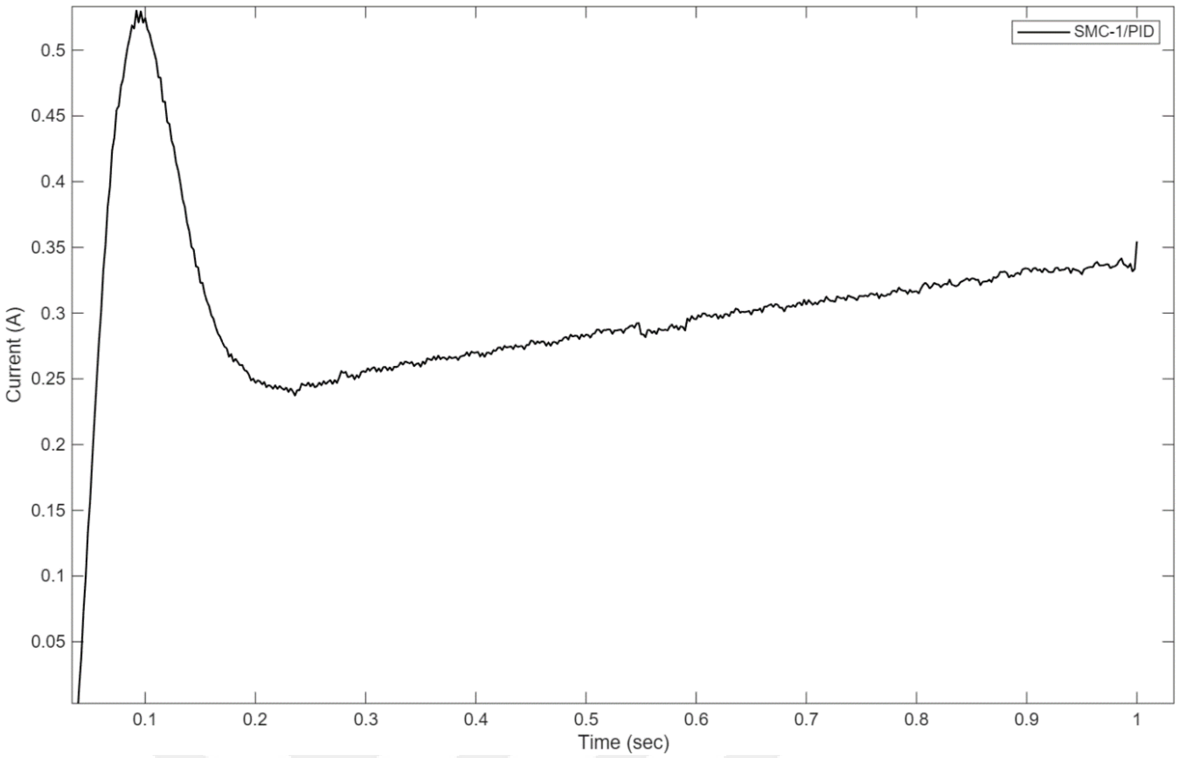

Figure 4.154. Armature current, $i_a(t)$ (SMC-1/PID)

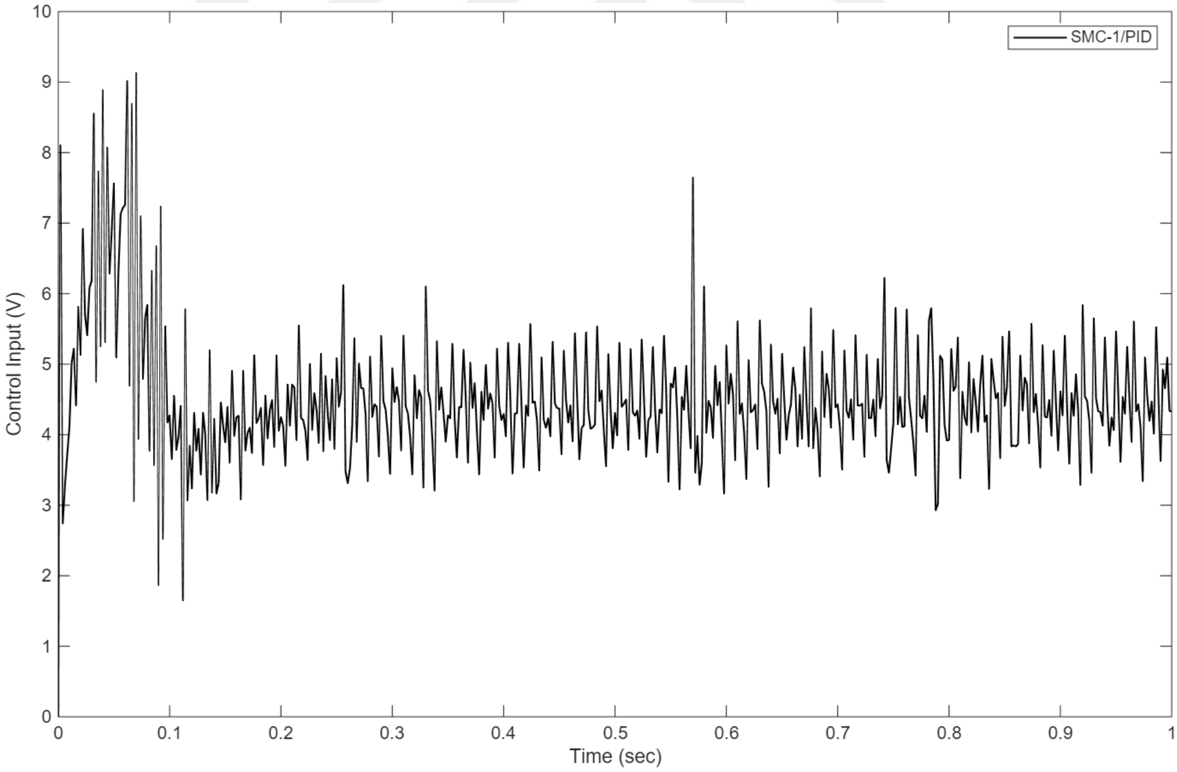

Figure 4.155. Control input voltage, $u(t)$ (SMC-1/PID)

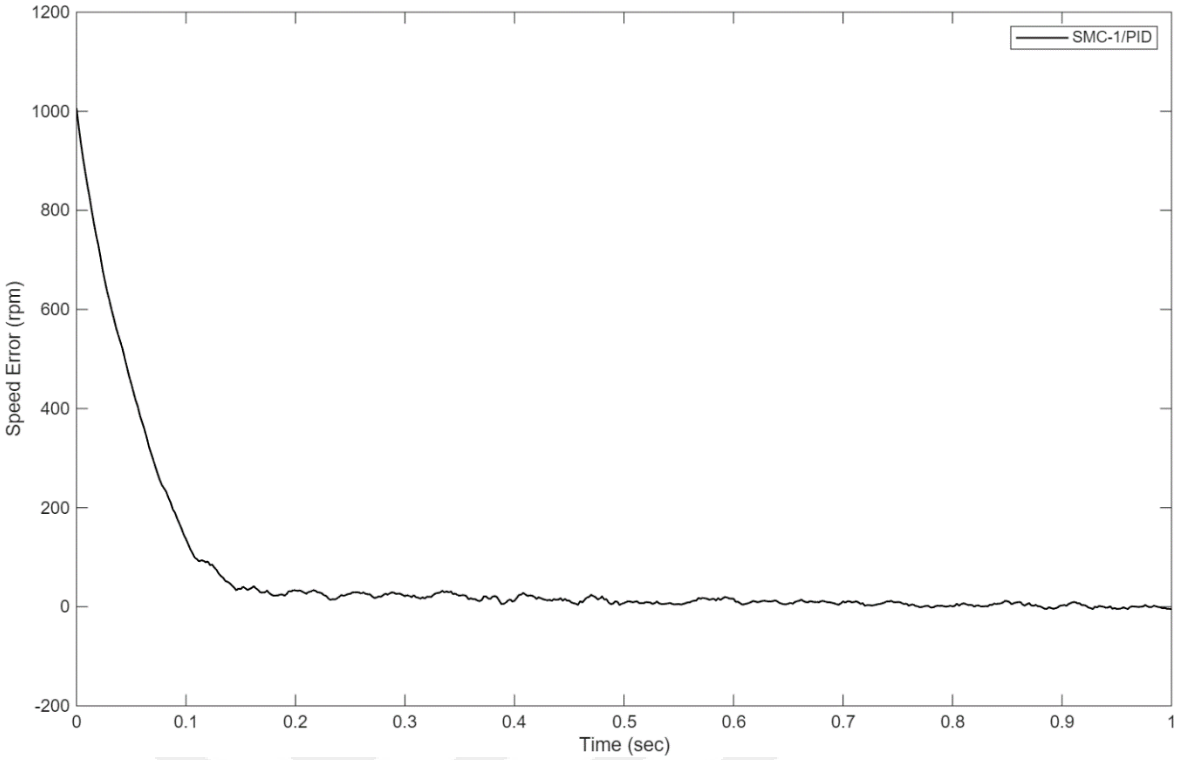

Figure 4.156. Speed error (rpm) (SMC-1/PID)

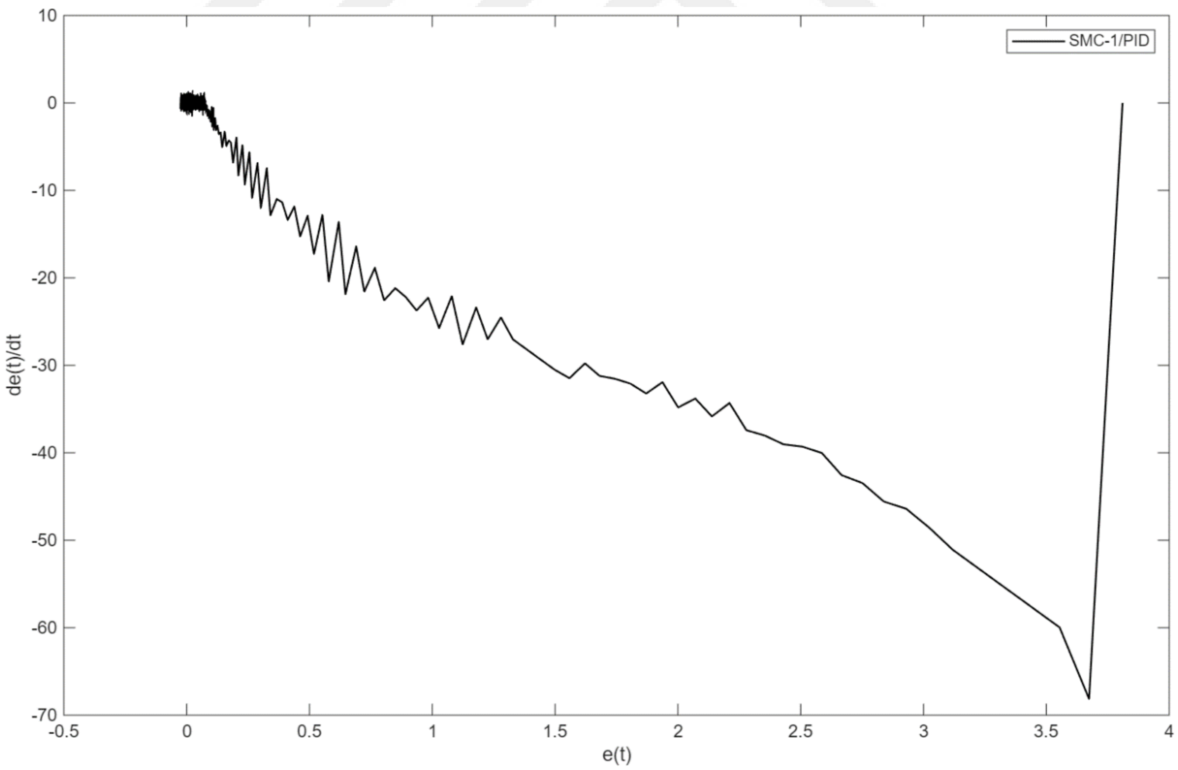

Figure 4.157. Phase plane of $e(t)$ and $de(t)/dt$ (SMC-1/PID)

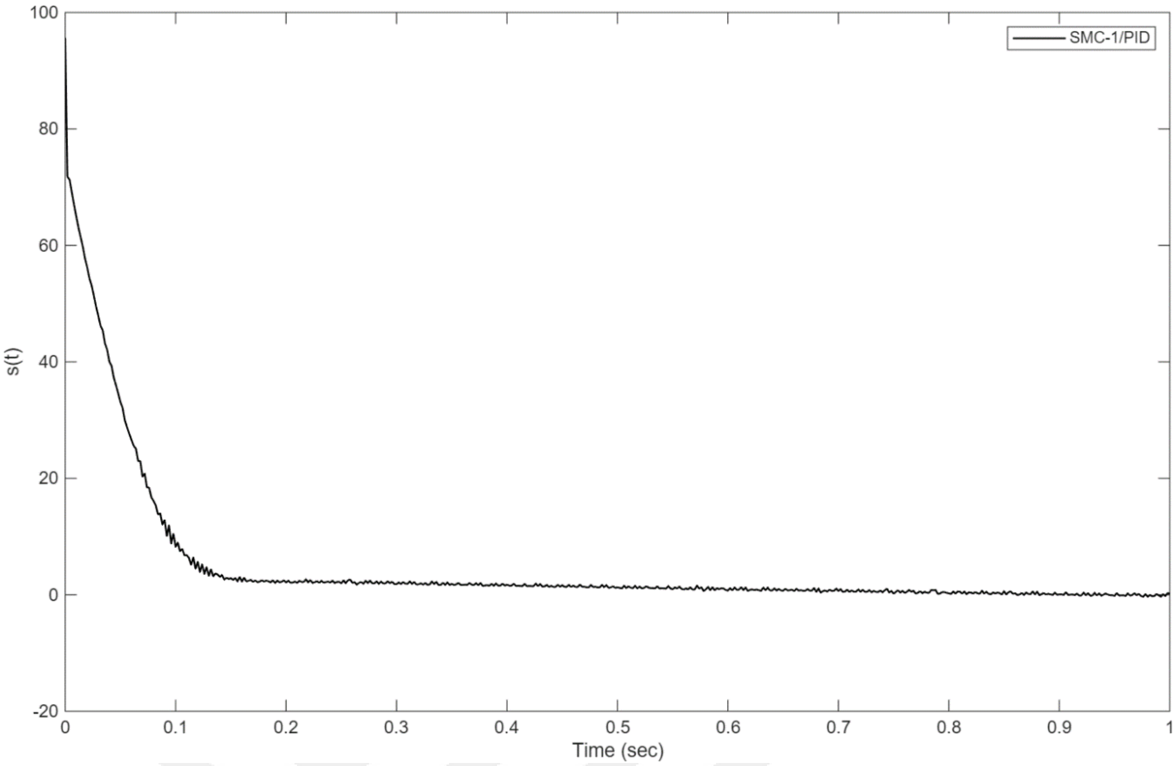

Figure 4.158. Sliding surface, $s(t)$ (SMC-1/PID)

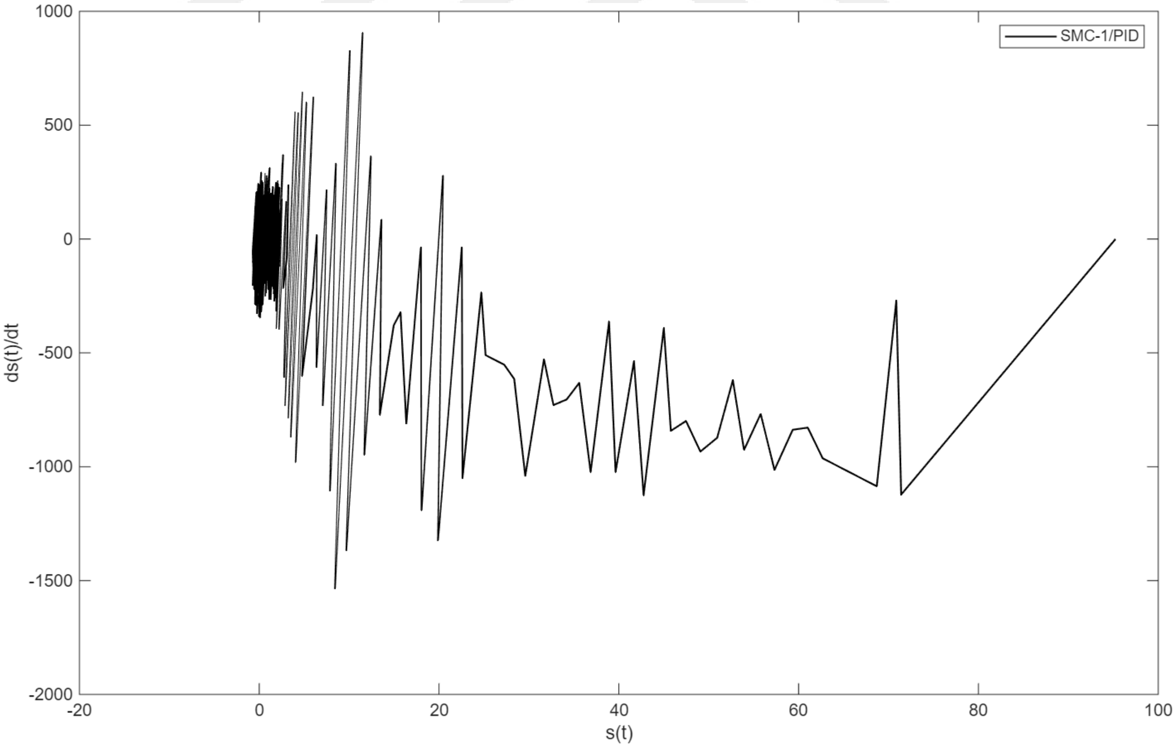

Figure 4.159. Phase plane of $s(t)$ and $ds(t)/dt$ (SMC-1/PID)

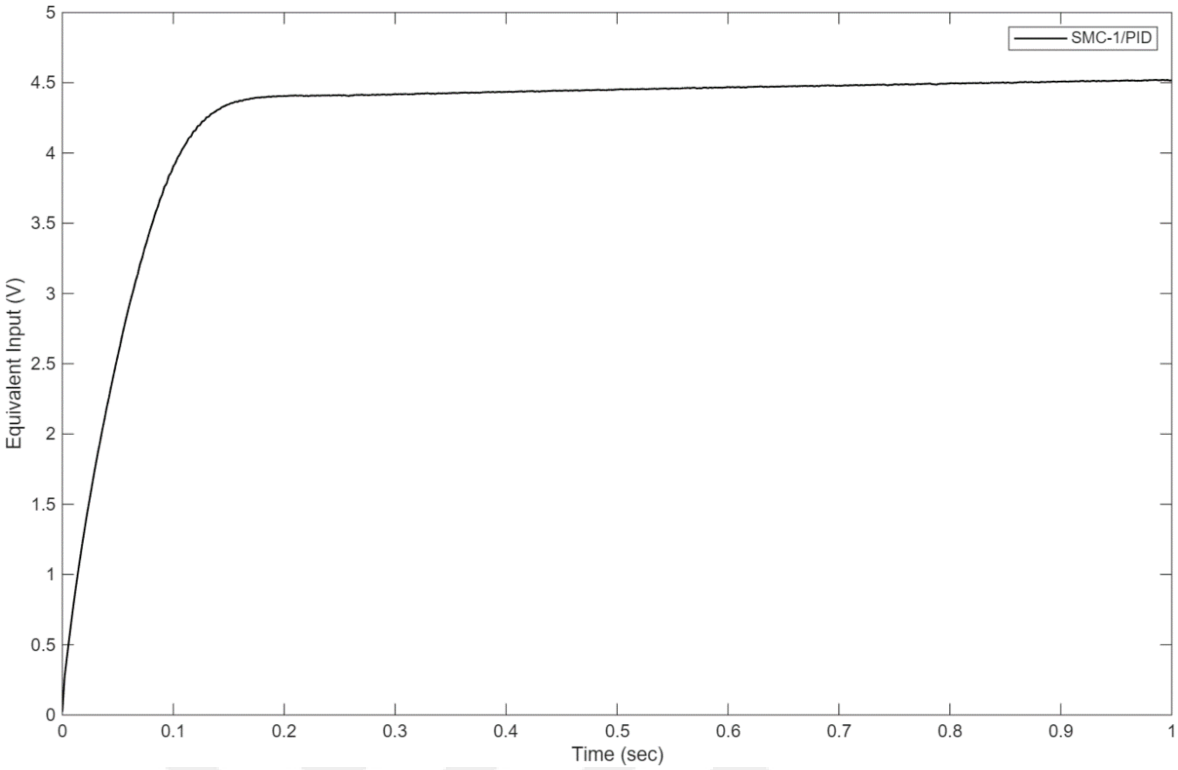

Figure 4.160. Equivalent input, $u_{eq}(t)$ (SMC-1/PID)

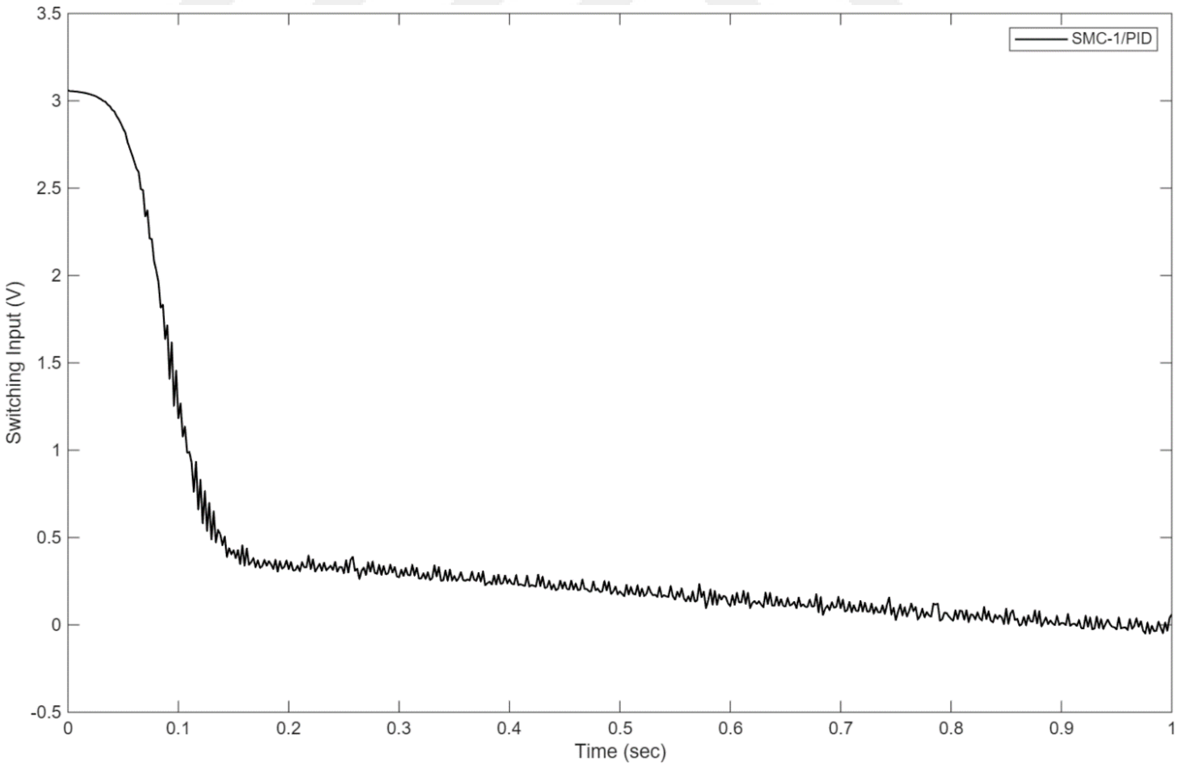

Figure 4.161. Switching input, $u_{sw}(t)$ (SMC-1/PID)

The time domain performance specifications presented in Table 4.41 indicate that the cascade SMC-1/PID controller exhibits high precision and stability in the transient regime. The rise time is calculated to be 0.1063 s, the settling time is 0.3762 s, and the overshoot is 0.03%, demonstrating an extremely controlled transient response. The system delay of 0.0440 s indicates that the control structure responds promptly and sensitively to input variations. Performance Indices

An examination of the performance indicators presented in Table 4.42 reveals that the controller attains ITAE = 0.0196, ISE = 0.4233, IAE = 0.2241 and ITSE = 0.0115. This indicates that the magnitude of errors and their time-weighted effects are sustained at minimal levels. The control effort indicator ISCI = 22.95 and ISTE = 0.0017, suggest that the system provides balanced control without excessive actuator activity. The findings demonstrate that the cascade SMC-1/PID controller provides control performance that is high in precision, rapid and stable.

Table 4.41. Time domain performance specifications (SMC-1/PID)

Controller	Rise Time (s)	Settling time (s)	Overshoot (%)	Delay time (s)
Cascade Outer-Loop SMC-1/Inner-Loop PID	0.1063	0.3762	0.03	0.0440

Table 4.42. Output performance indices (SMC-1/PID)

Controller	ITAE	ISE	IAE	ITSE	ISCI	ISTE
Cascade Outer-Loop SMC-1/Inner-Loop PID	0.0196	0.4233	0.2241	0.0115	22.95	0.001

4.10.4. Experimental Results of Cascade Sliding Mode Control: Outer-Loop SMC-2/Inner-Loop P (SMC-2/P)

This subsection presents the experimental results of the CSMC configuration, consisting of an outer-loop SMC-2 controller and an inner-loop P controller. The outer-loop SMC-2 controller is tuned with parameters $k_c = 3,\ k_d = 0.85,\ k_p = 40,\ k_i = 5,\ \Omega_c = 10,\ \beta = 150,\ \lambda_1 = 50$ while the inner-loop P controller is designed with gains $k_p = 2$. The experimental speed (Figure 4.162), and current response (Figure 4.163), graphs demonstrate a highly stable transient behaviour and improved steady-state accuracy compared to conventional control structures. The control input signal (Figure 4.164), indicates an efficient distribution of control effort between the sliding mode and P actions, significantly reducing chattering and ensuring smooth operation. The error signal (Figure 4.165), error and derivative signals (Figure 4.166), demonstrate rapid convergence towards the reference trajectory, while the combined error and derivative signals validate the robustness of this hybrid configuration. Furthermore the sliding surface signal (Figure 4.167), the sliding surface with its derivative (Figure 4.168), the equivalent signal (Figure 4.169), and the switching signal (Figure 4.170) provide a comprehensive view of the system’s performance.

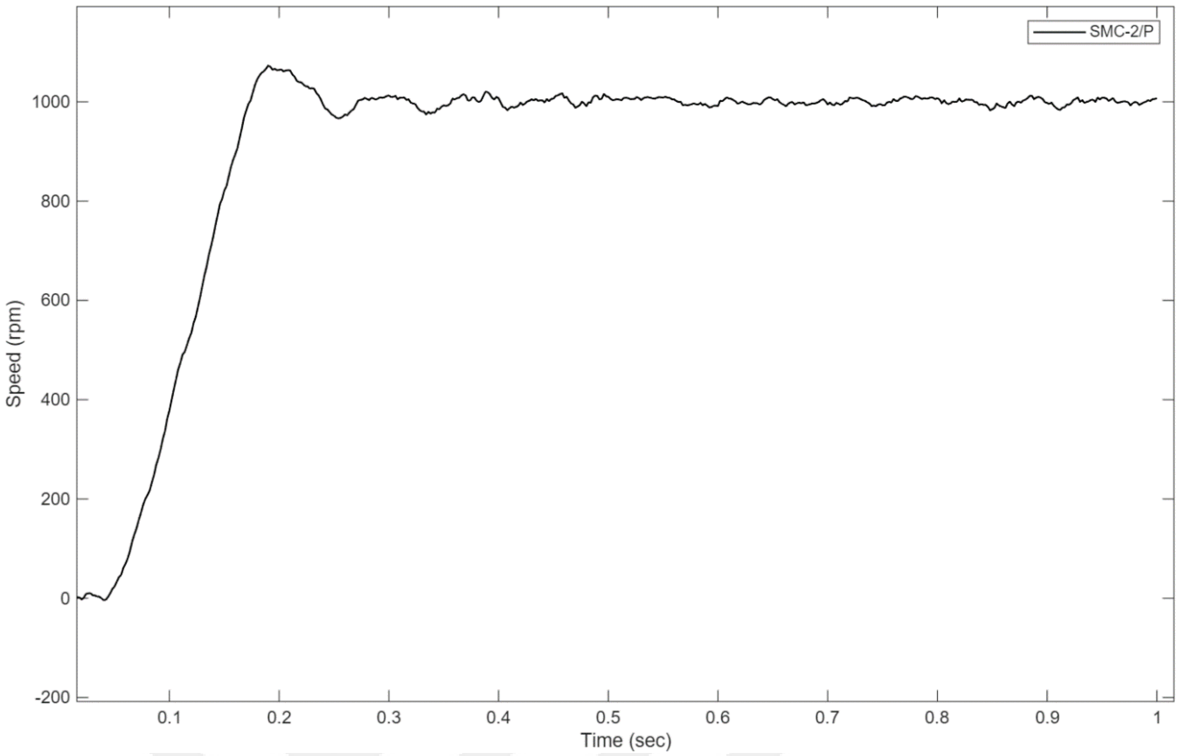

Figure 4.162. Output speed (rpm) (SMC-2/P)

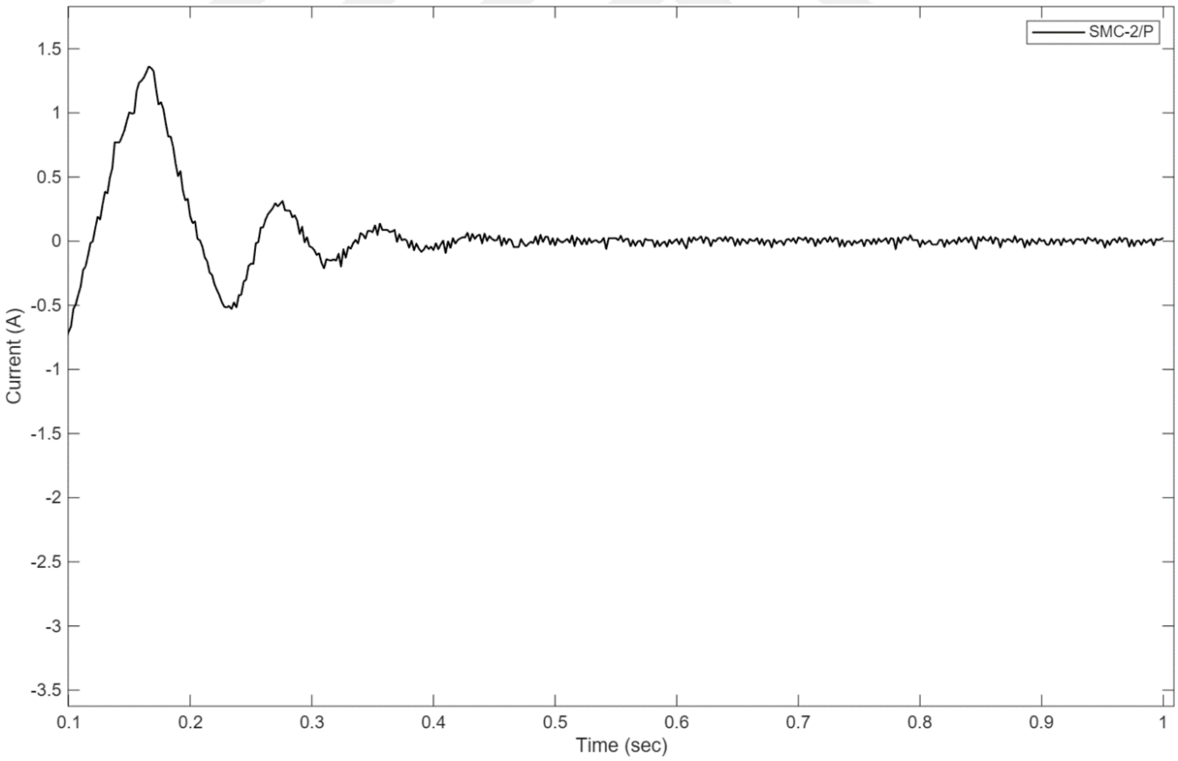

Figure 4.163. Armature current, $i_a(t)$ (SMC-2/P)

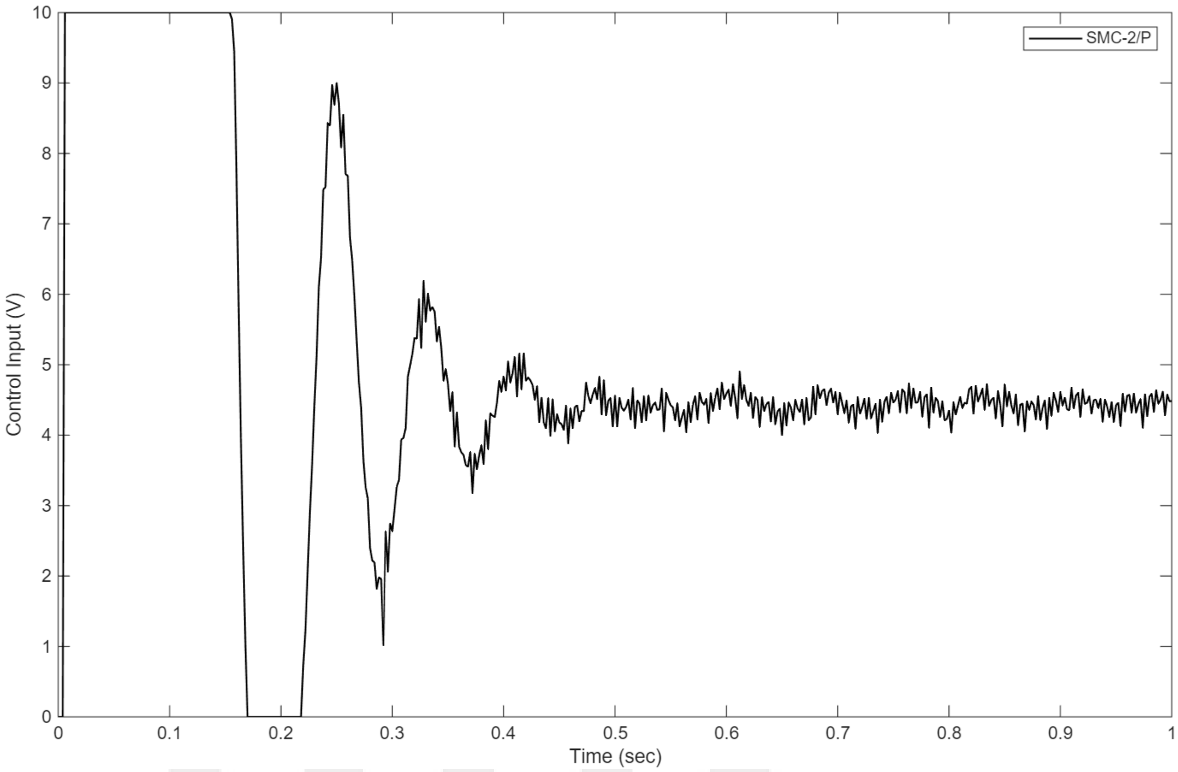

Figure 4.164. Control input voltage, $u(t)$ (SMC-2/P)

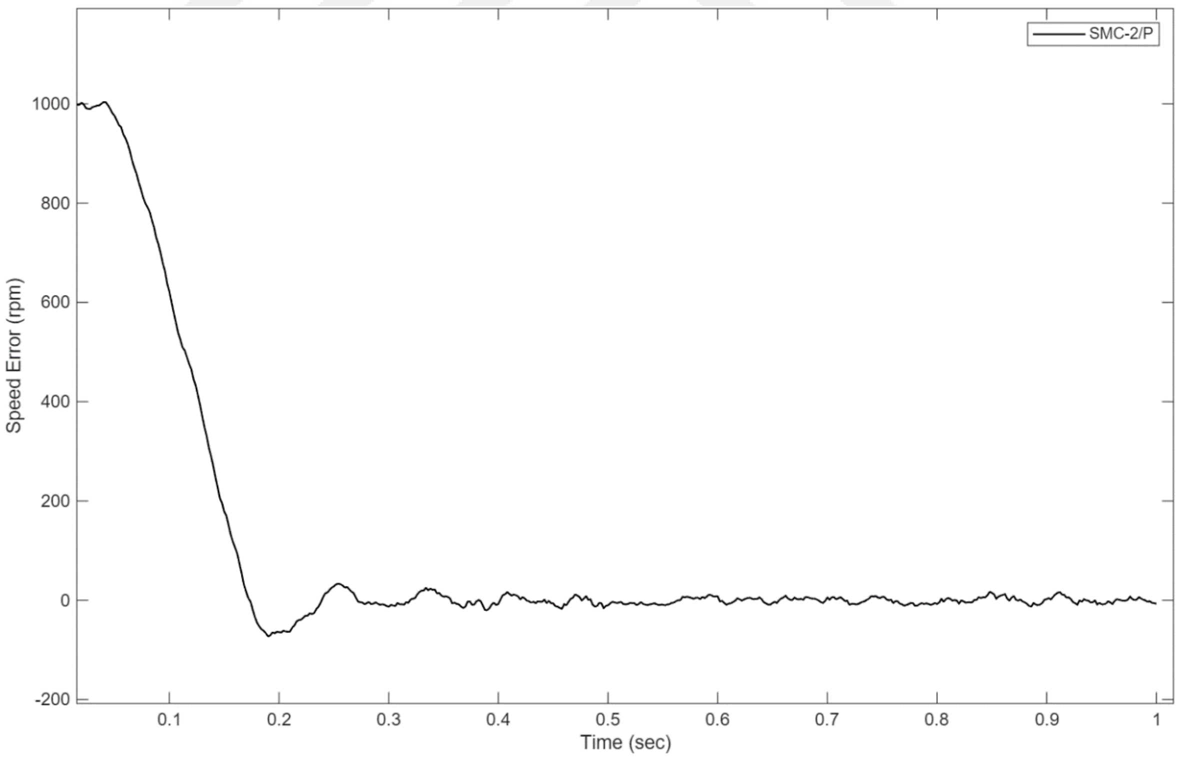

Figure 4.165. Speed error (rpm) (SMC-2/P)

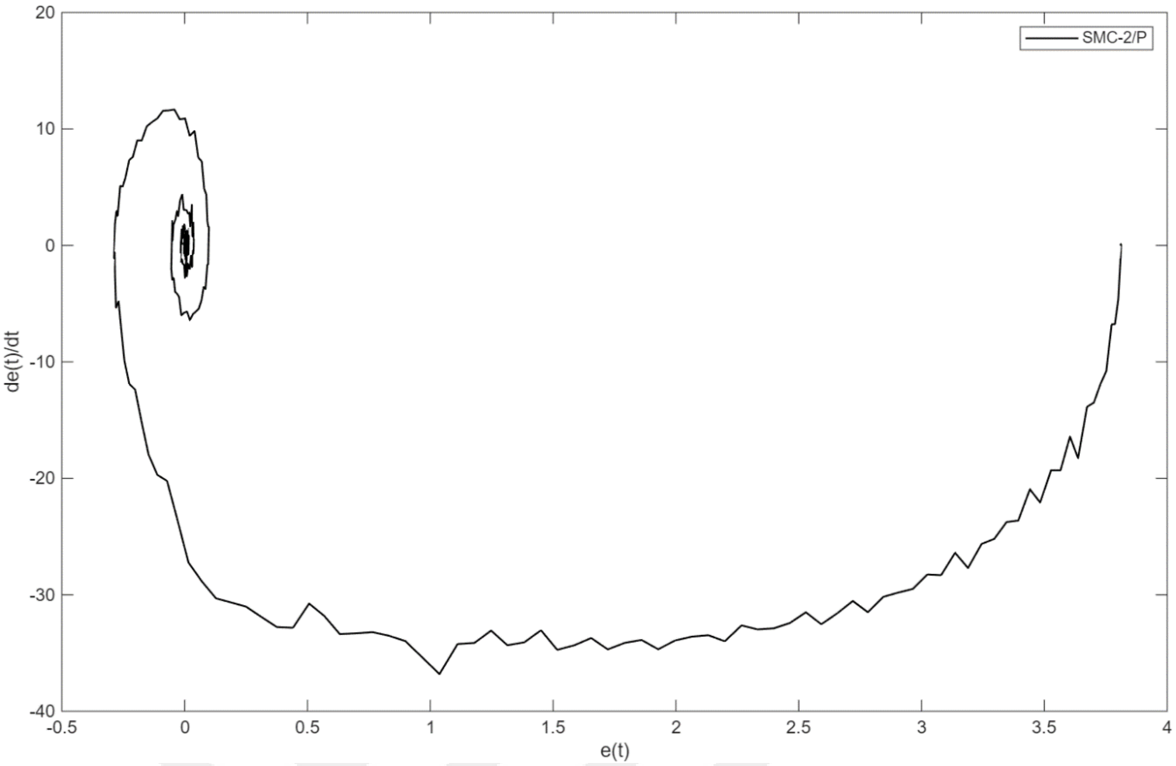

Figure 4.166. Phase plane of $e(t)$ and $de(t)/dt$ (SMC-2/P)

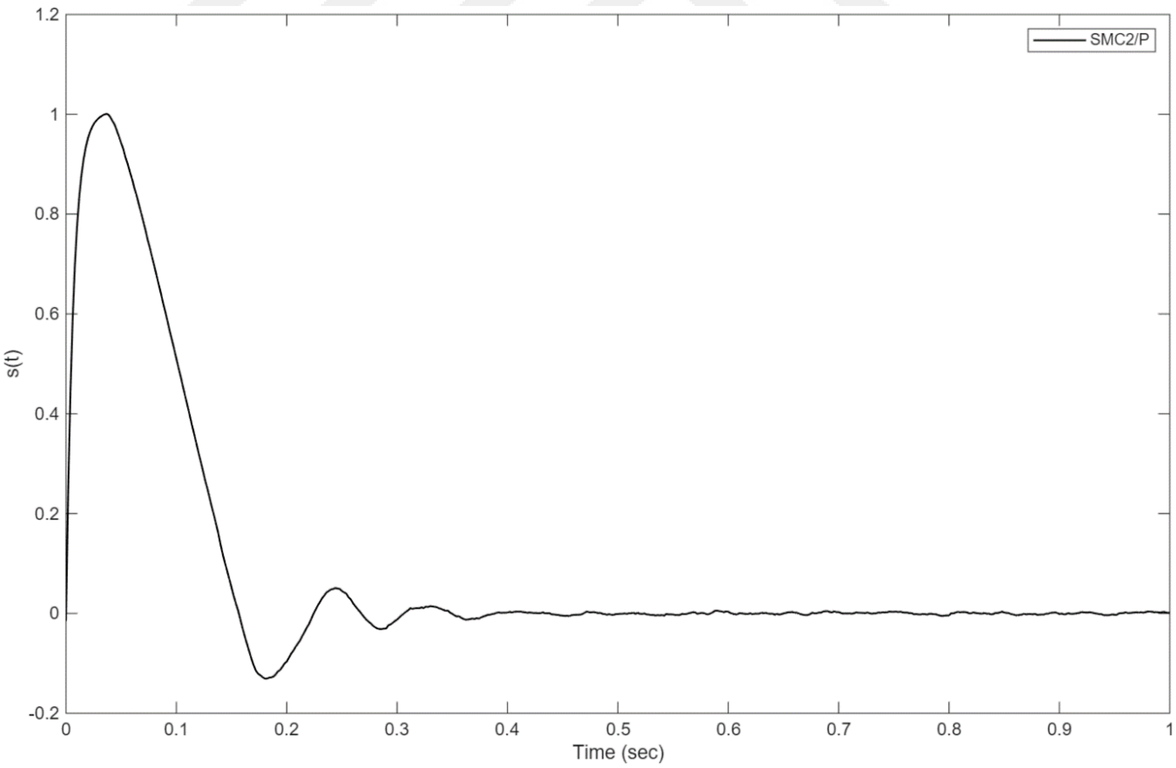

Figure 4.167. Sliding surface, $s(t)$ (SMC-2/P)

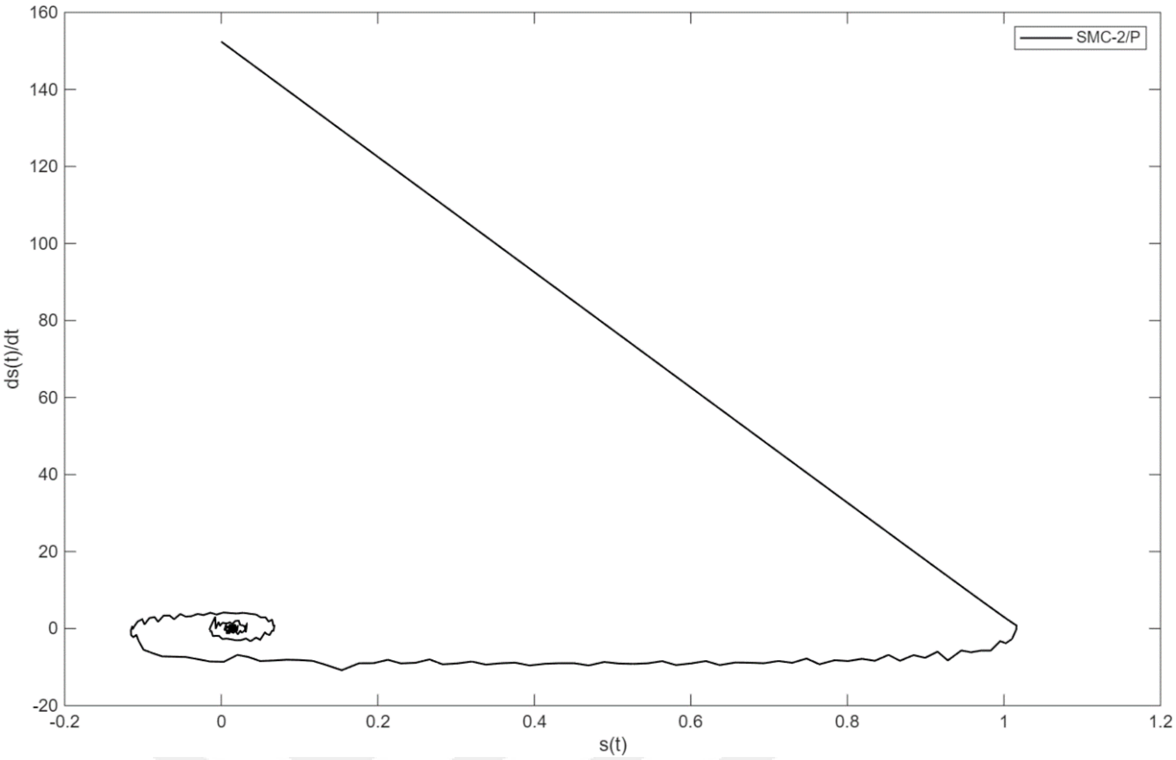

Figure 4.168. Phase plane of $s(t)$ and $ds(t)/dt$ (SMC-2/P)

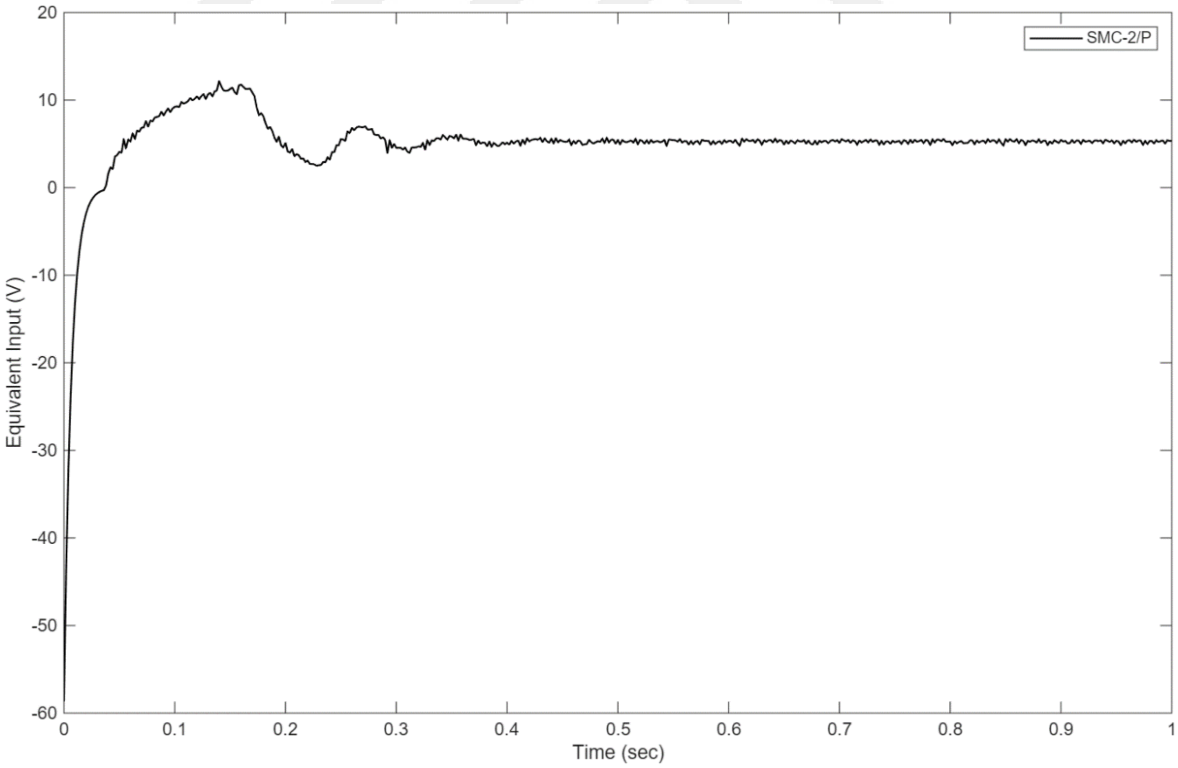

Figure 4.169. Equivalent input, $u_{eq}(t)$ (SMC-2/P)

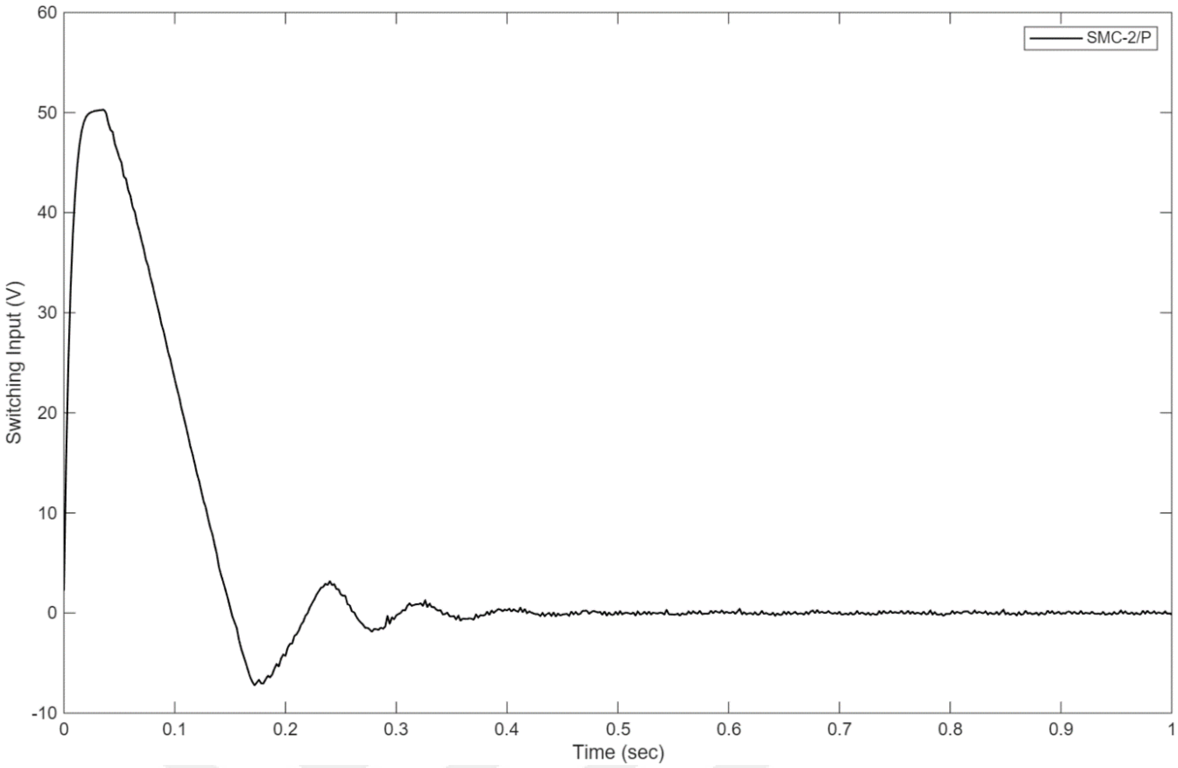

Figure 4.170. Switching input, $u_{sw}(t)$ (SMC-2/P)

The time domain performance data presented in Table 4.43 demonstrate that the cascade - SMC-2/P controller provides effective and stable transient performance under real system conditions. The rise time is calculated to be 0.0952 seconds, the settling time is 0.2612 seconds, and the overshoot is 7.67%, indicating a controlled transient response. The system delay of 0.1160 s indicates that the controller responds sensitively and promptly to input variations. Performance Indices

An examination of the performance indicators presented in Table 4.44 reveals that the controller attains ITAE = 0.032, ISE = 1.357, IAE = 0.4512 and ITSE = 0.07. This observation signifies that the magnitude of errors and their time-weighted effects are effectively constrained. The control effort indicator ISCI = 32 and ISTE = 0.0033, suggest that the system maintains balanced control without excessive actuator activity. The experimental findings demonstrate that the cascade SMC-2/P controller delivers rapid, stable and effective performance under real operational conditions.

Table 4.43. Time domain performance specifications (SMC-2/P)

Controller	Rise Time (s)	Settling time (s)	Overshoot (%)	Delay time (s)
Cascade Outer-Loop SMC-2/Inner-Loop P	0.0952	0.2612	7.67	0.1160

Table 4.44. Output performance indices (SMC-2/P)

Controller	ITAE	ISE	IAE	ITSE	ISCI	ISTE
Cascade Outer-Loop SMC-2/Inner-Loop P	0.032	1.357	0.4512	0.07	32	0.0033

4.10.5. Experimental Results of Cascade Sliding Mode Control: Outer-Loop SMC-2/Inner-Loop PI (SMC-2/PI)

This subsection presents the experimental results of the CSMC configuration, consisting of an outer-loop SMC-2 controller and an inner-loop PI controller. The outer-loop SMC-2 controller is tuned with parameters $k_c = 3.2,\ k_d = 0.9,\ k_p = 28,\ k_i = 8.5,\ \Omega_c = 8,\ \beta = 170,\ \lambda_1 = 50$ while the inner-loop PI controller is designed with gains PI = $1.6\left(1 + \frac{1}{2.66s}\right)$. The experimental output speed (Figure 4.171) and current response (Figure 4.172) graphs demonstrate a highly stable transient behaviour and improved steady-state accuracy compared to conventional control structures. The control signal (Figure 4.173) indicates an efficient distribution of control effort between the sliding mode and PI actions, significantly reducing chattering and ensuring smooth operation. The error (Figure 4.174), error and its derivative signals (Figure 4.175) demonstrate rapid convergence towards the reference trajectory, validate the robustness of this hybrid configuration. The sliding surface (Figure 4.176), and the sliding surface with its derivative (Figure 4.177), serve to confirm that the system trajectory remains well-aligned with the designed sliding manifold. Furthermore the equivalent signal (Figure 4.178) and the switching signal (Figure 4.179) provide a comprehensive view of the system's performance. The experimental findings demonstrate that the SMC-2/PI cascade configuration provides enhanced robustness, faster convergence and lower steady-state error compared to the SMC-1/PI combination. This confirms the superiority of SMC-2 in hybrid architectures.

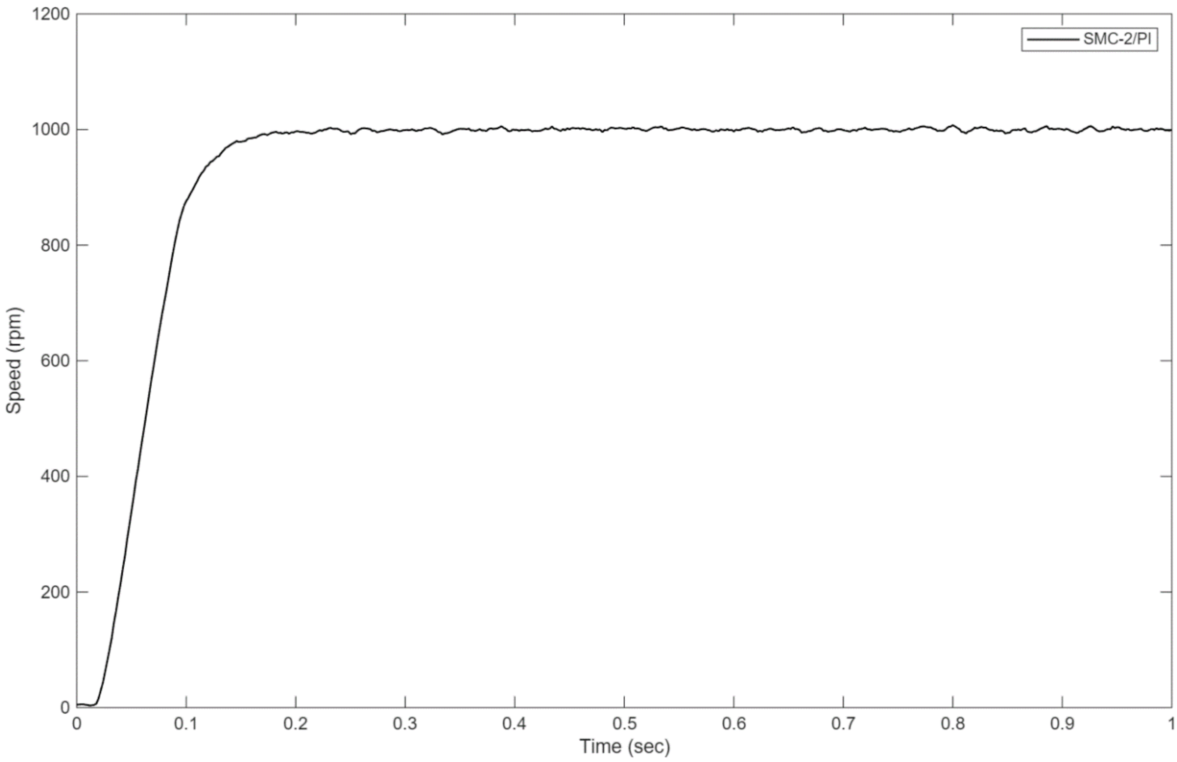

Figure 4.171. Output speed (rpm) (SMC-2/PI)

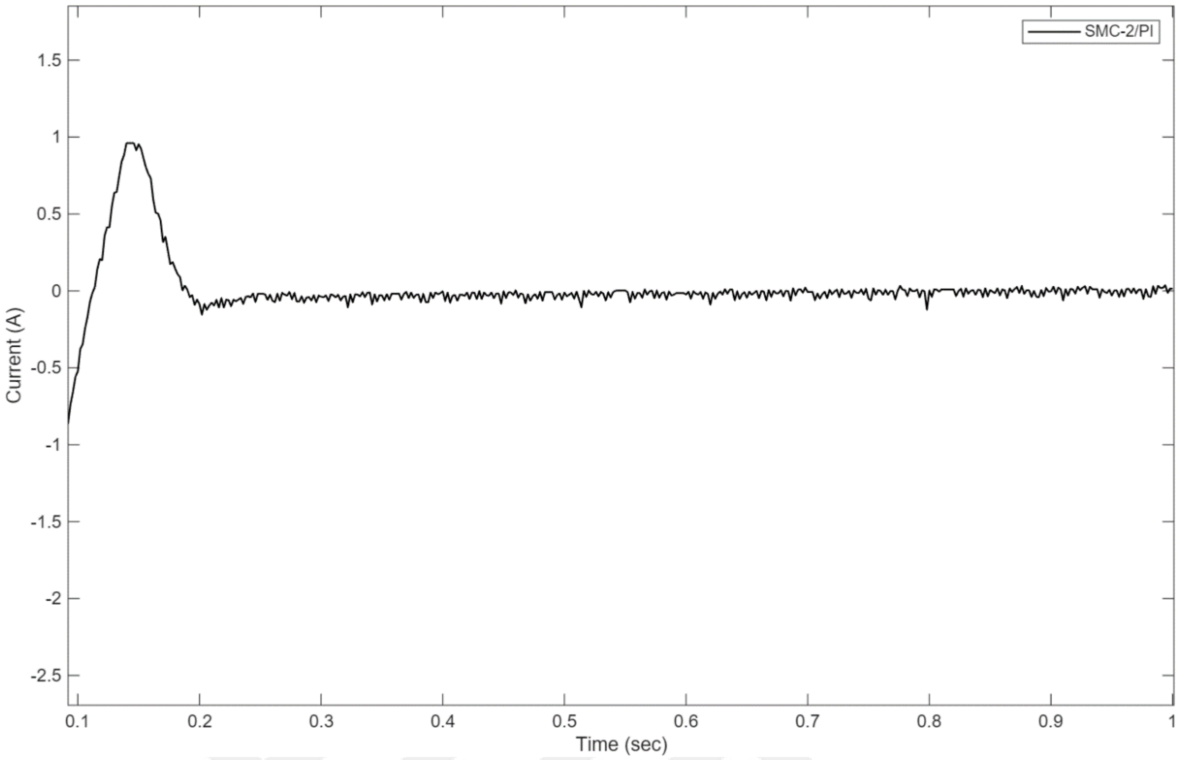

Figure 4.172. Armature current, $i_a(t)$ (SMC-2/PI)

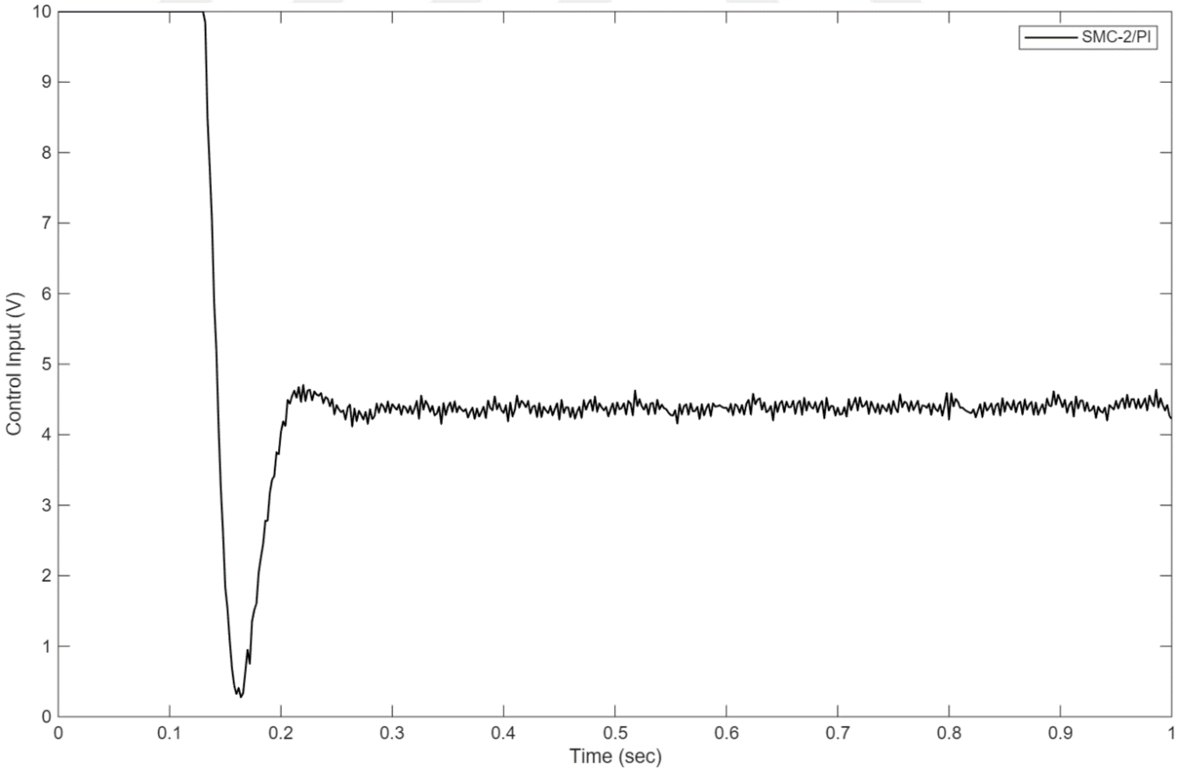

Figure 4.173. Control input voltage, $u(t)$ (SMC-2/PI)

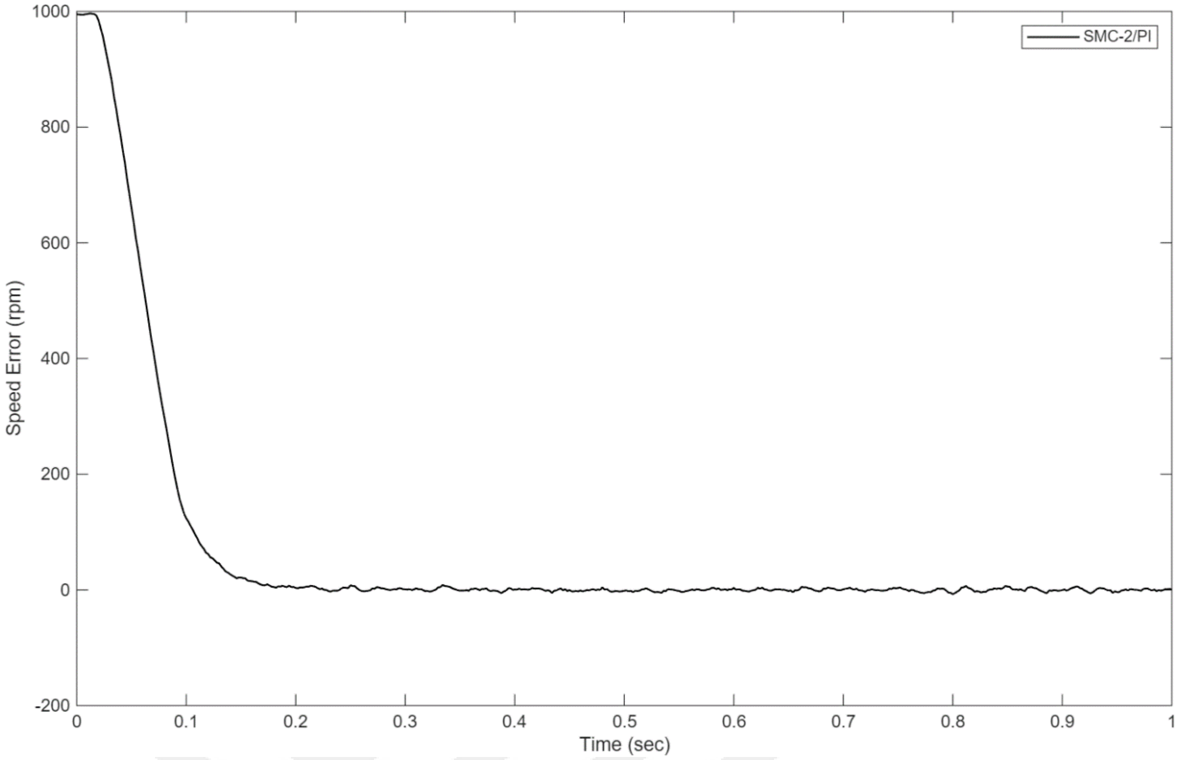

Figure 4.174. Speed error (rpm) (SMC-2/PI)

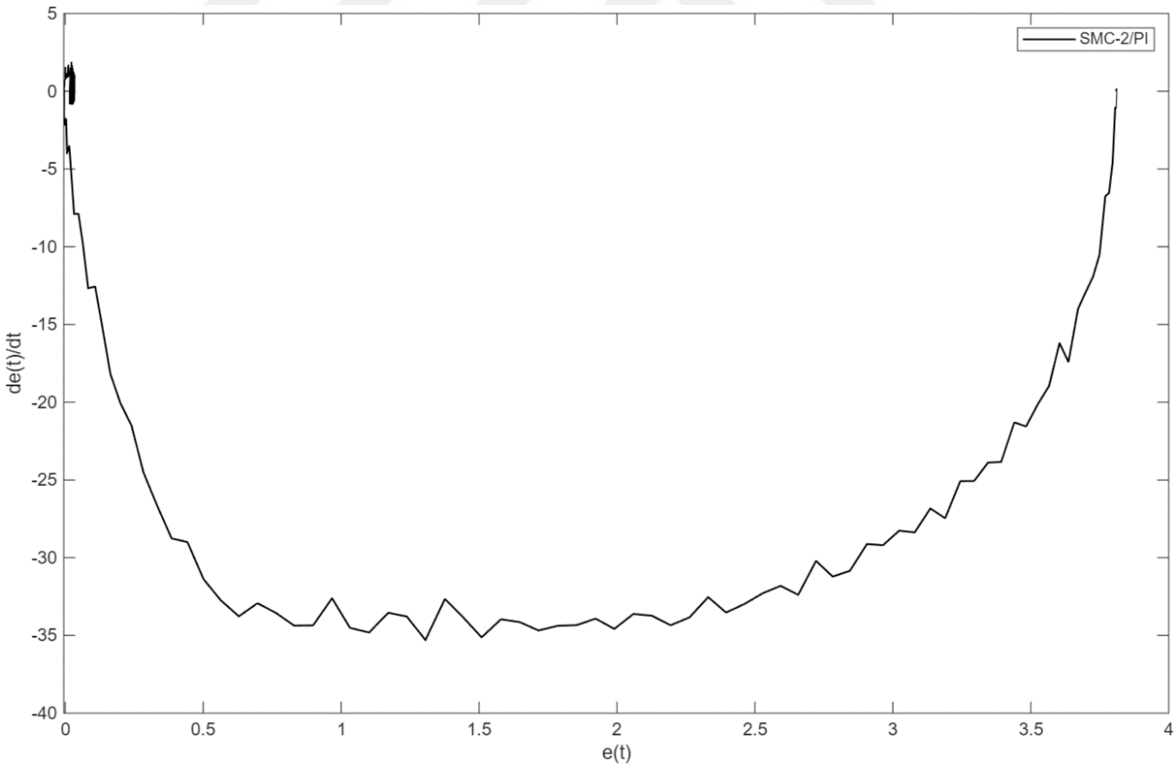

Figure 4.175. Phase plane of $e(t)$ and $de(t)/dt$ (SMC-2/PI)

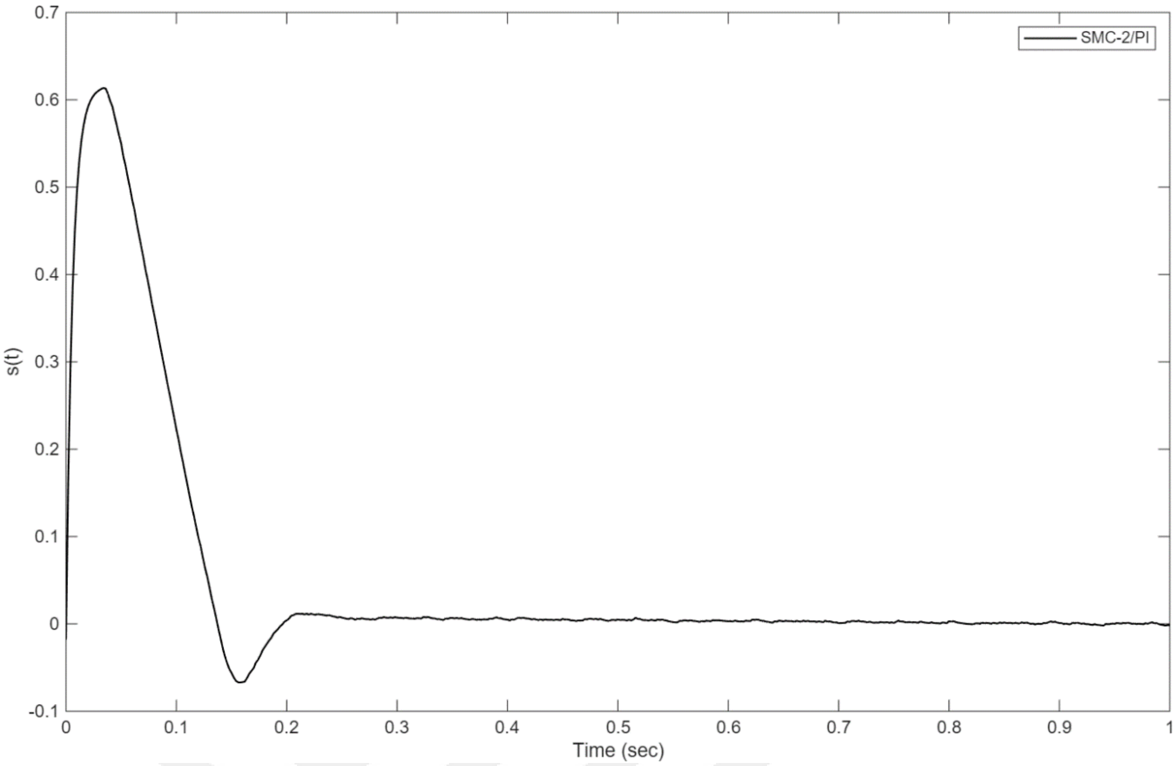

Figure 4.176. Sliding surface, $s(t)$ (SMC-2/PI)

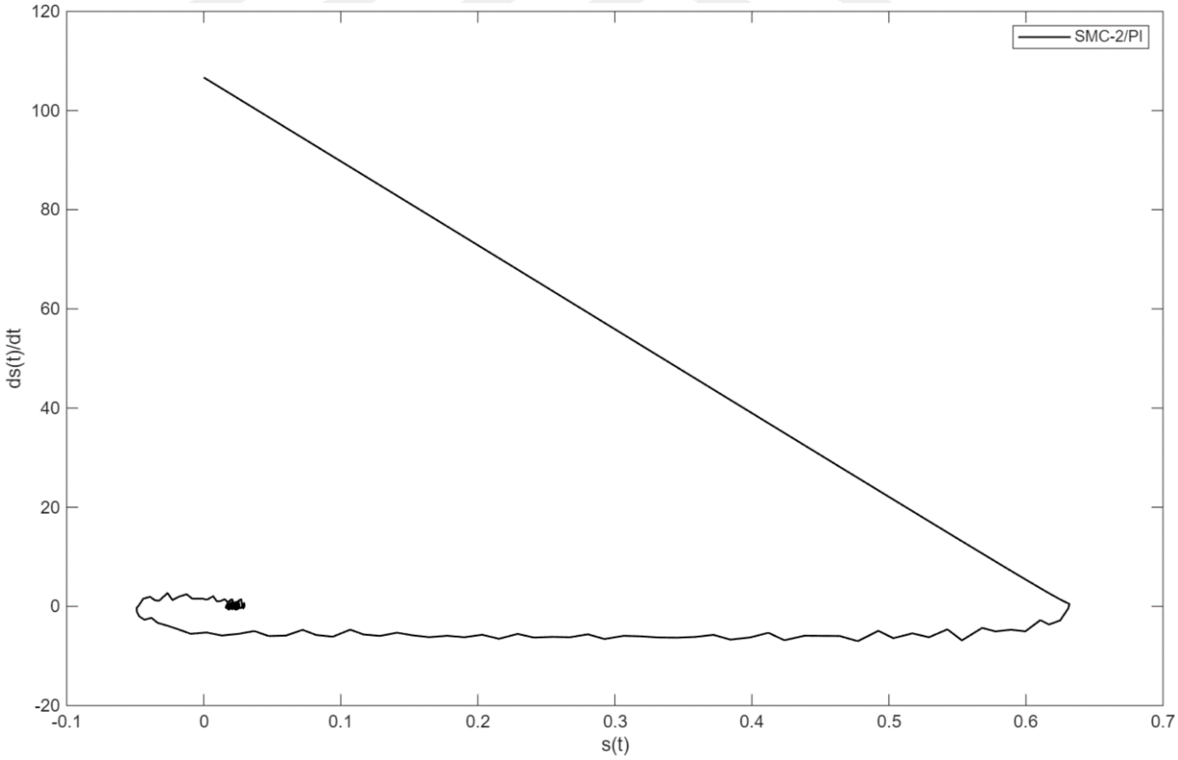

Figure 4.177. Phase plane of $s(t)$ and $ds(t)/dt$ (SMC-2/PI)

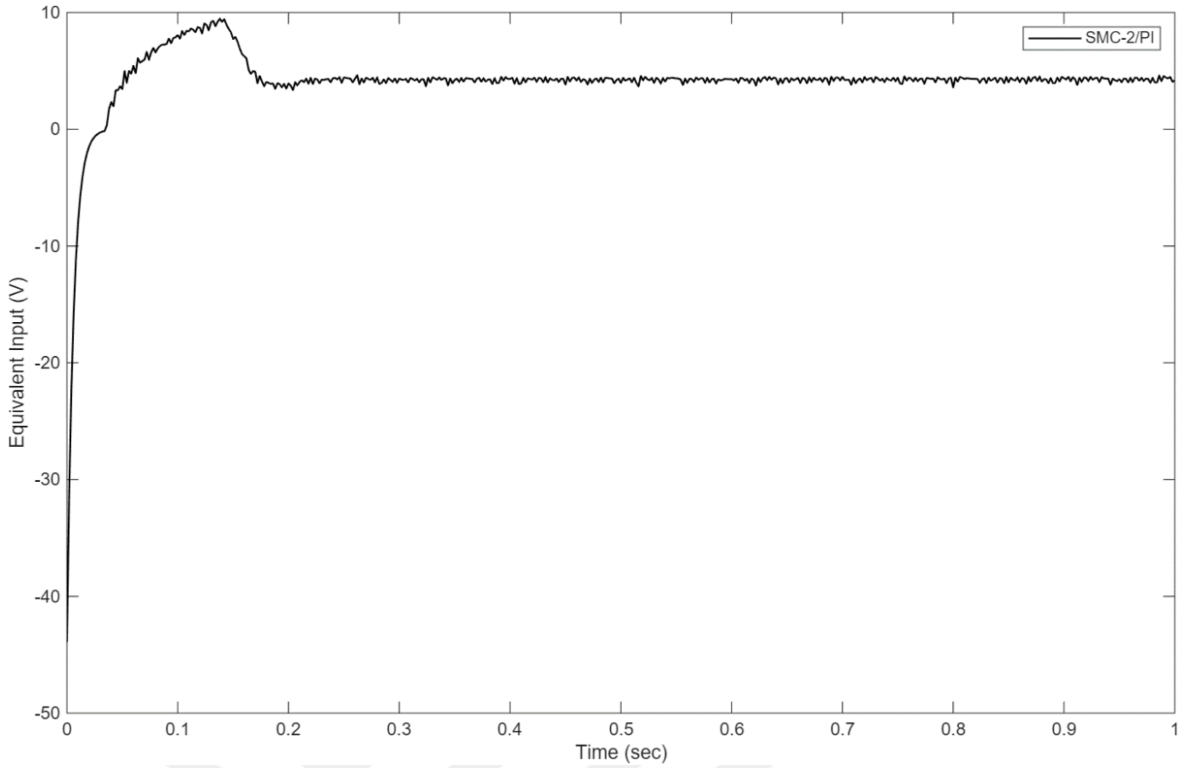

Figure 4.178. Equivalent input, $u_{eq}(t)$ (SMC-2/PI)

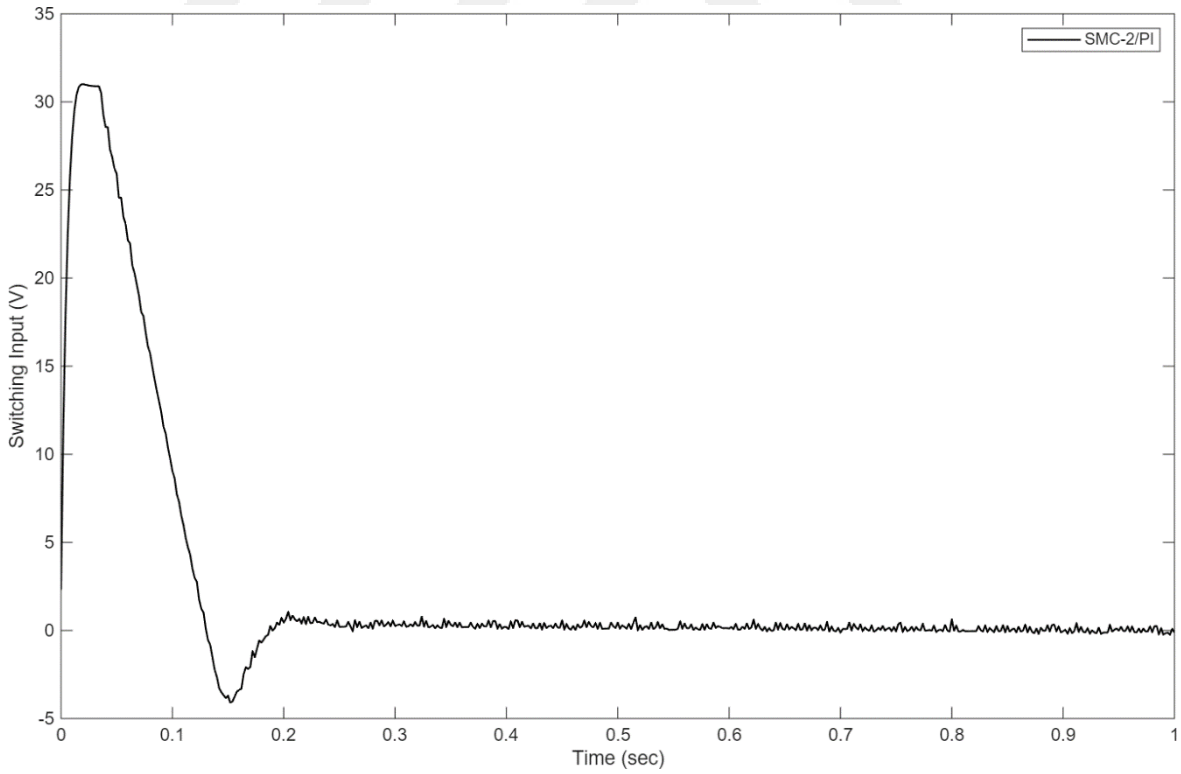

Figure 4.179. Switching input, $u_{sw}(t)$ (SMC-2/PI)

The experimental time domain performance specifications data presented in Table 4.45 indicate that the cascade SMC-2/PI provides an extremely stable and rapid transient response. The rise time is 0.0910 s, the settling time is 0.1307 s and the overshoot is 0.00%, reflecting a highly controlled behavior. The system delay of 0.070 s indicates that the controller responds promptly and efficiently to input variations. Performance Indices

An examination of the performance indicators presented in Table 4.46 reveals that the controller attains ITAE = 0.02, ISE = 0.94, IAE = 0.37 and ITSE = 0.03. This suggests that the magnitude of errors and their time-weighted effects are sustained at minimal levels. The control effort indicator ISCI = 21.21 and ISTE = 0.0100, suggest that the system maintains balanced and effective control without requiring excessive actuator activity. The experimental findings demonstrate that the cascade SMC-2/PI controller provides a rapid, stable and effortless control performance.

Table 4.45. Time domain performance specifications (SMC-2/PI)

Controller	Rise Time (s)	Settling time (s)	Overshoot (%)	Delay time (s)
Cascade Outer-Loop SMC-2/Inner-Loop PI	0.0910	0.1307	0.00	0.070

Table 4.46. Output performance indices (SMC-2/PI)

Controller	ITAE	ISE	IAE	ITSE	ISCI	ISTE
Cascade Outer-Loop SMC-2/Inner-Loop PI	0.02	0.94	0.37	0.03	21.21	0.0100

4.10.6. Experimental Results of Cascade Sliding Mode Control: Outer-Loop SMC-2/Inner-Loop PID (SMC-2/PID)

This subsection presents the experimental results of the CSMC configuration, consisting of an outer-loop SMC-2 controller and an inner-loop PID controller. The outer-loop SMC-2 controller is tuned with parameters $k_c = 3.2,\ k_d = 0.2,\ k_p = 45,\ k_i = 5,\ \Omega_c = 8,\ \beta = 170,\ \lambda_1 = 60$ while the inner-loop PID controller is designed with gains PID = $1\left(1 + \frac{1}{2s} + 0.01s\right)$. The experimental output speed (Figure 4.180) and current response (Figure 4.181) graphs demonstrate a highly stable transient behaviour and improved steady-state accuracy compared to conventional control structures. The control signal (Figure 4.182) indicates an efficient distribution of control effort between the sliding mode and PID actions, significantly reducing chattering and ensuring smooth operation. The error (Figure 4.183), error and its derivative signals (Figure 4.184) demonstrate rapid convergence towards the reference trajectory and validate the robustness of this hybrid configuration. The sliding surface (Figure 4.185), sliding surface and its derivative (Figure 4.186) serve to confirm that the system trajectory remains well-aligned with the designed sliding manifold. Furthermore the equivalent signal (Figure 4.187) and the switching signal (Figure 4.188). The experimental findings demonstrate unequivocally that the SMC-2/PID cascade configuration provides enhanced robustness, faster convergence and lower steady-state error in comparison with the SMC-1/PI combination. This confirms the superiority of SMC-2 in hybrid architectures.

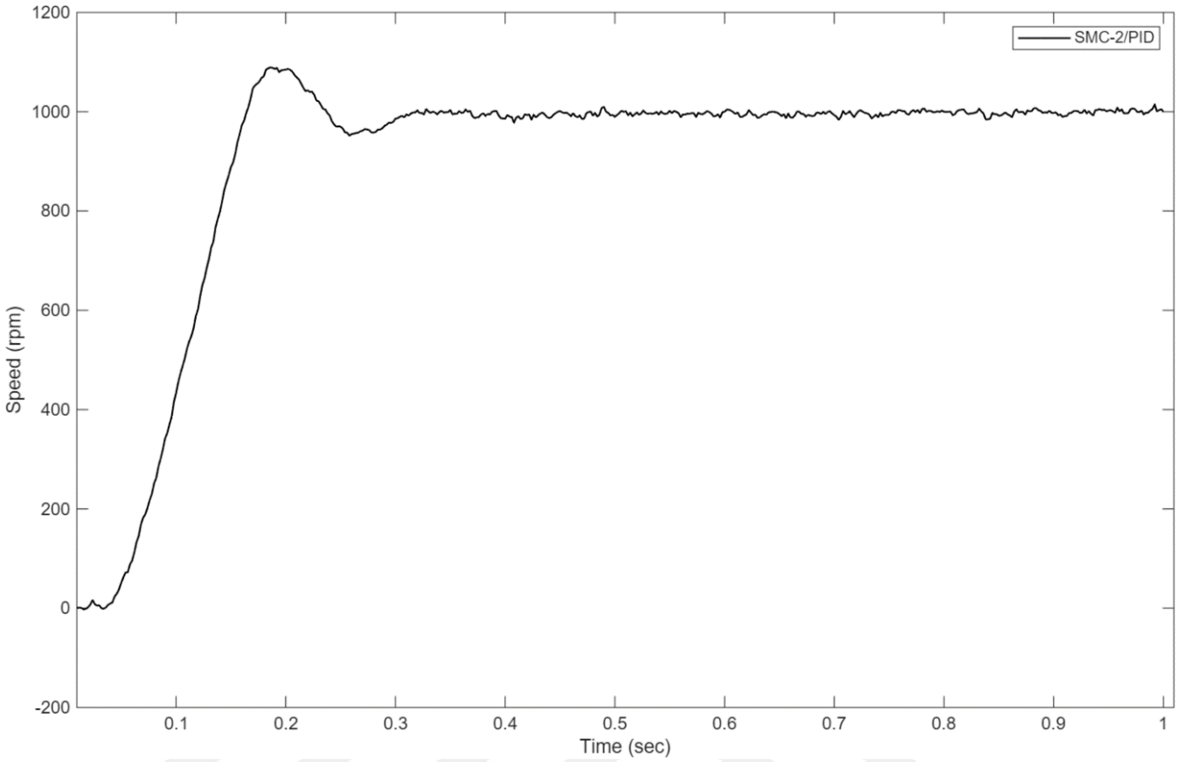

Figure 4.180. Output speed (rpm) (SMC-2/PID)

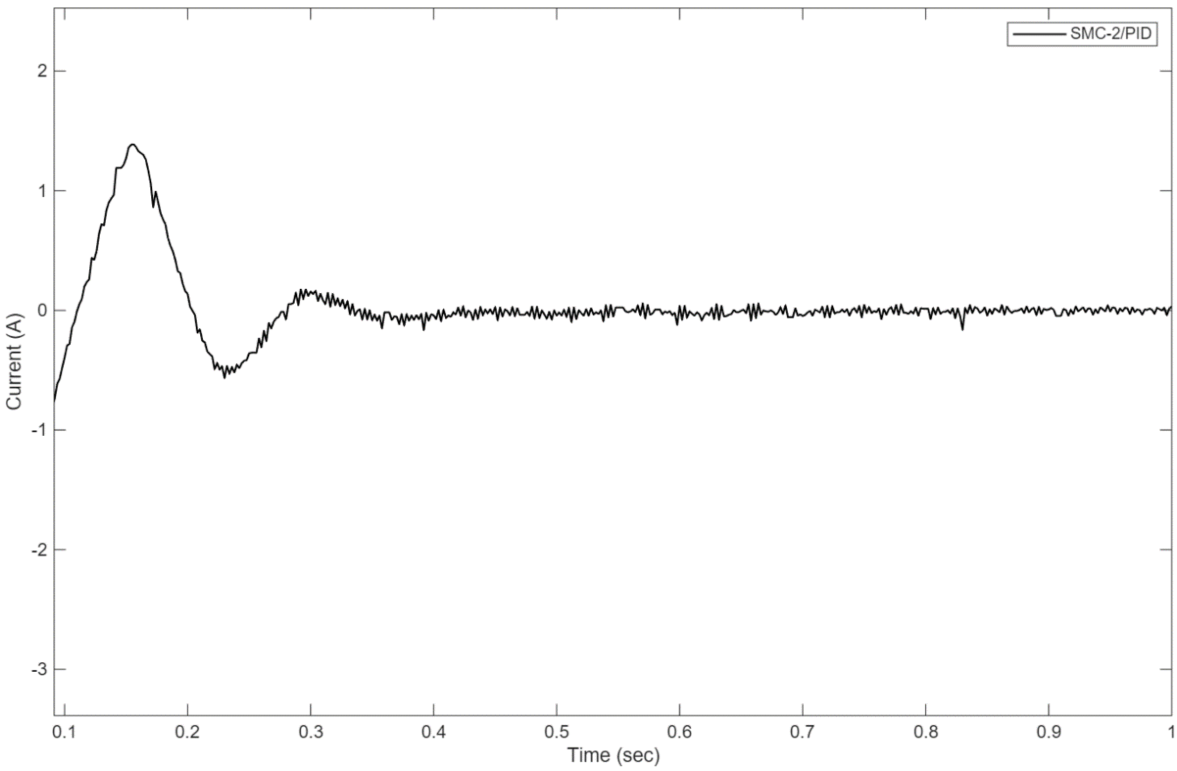

Figure 4.181. Armature current, $i_a(t)$ (SMC-2/PID)

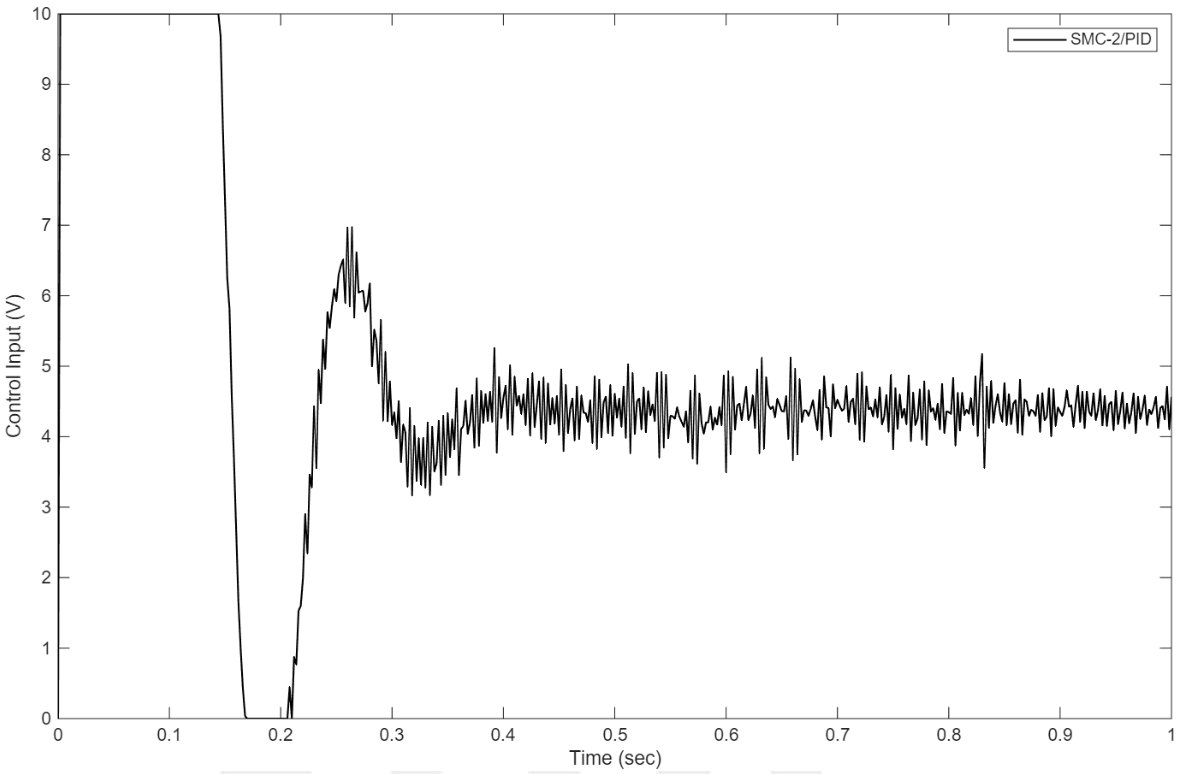

Figure 4.182. Control input voltage, $u(t)$ (SMC-2/PID)

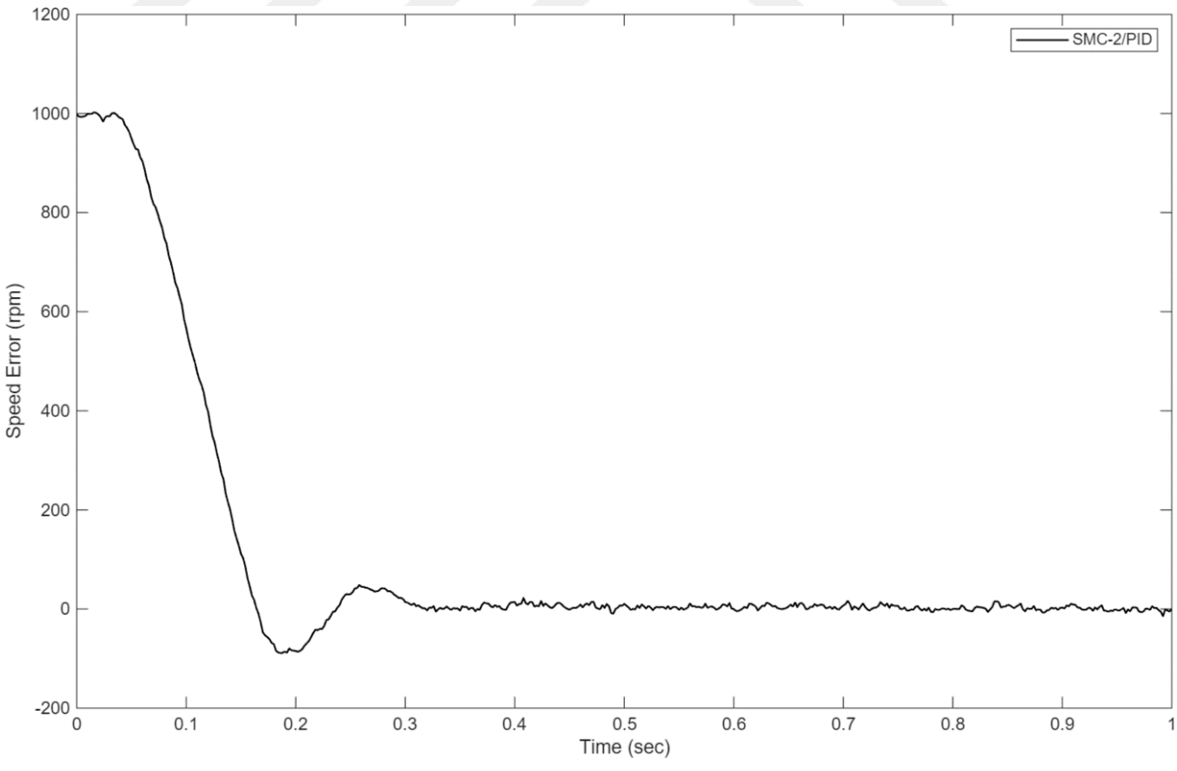

Figure 4.183. Speed error (rpm) (SMC-2/PID)

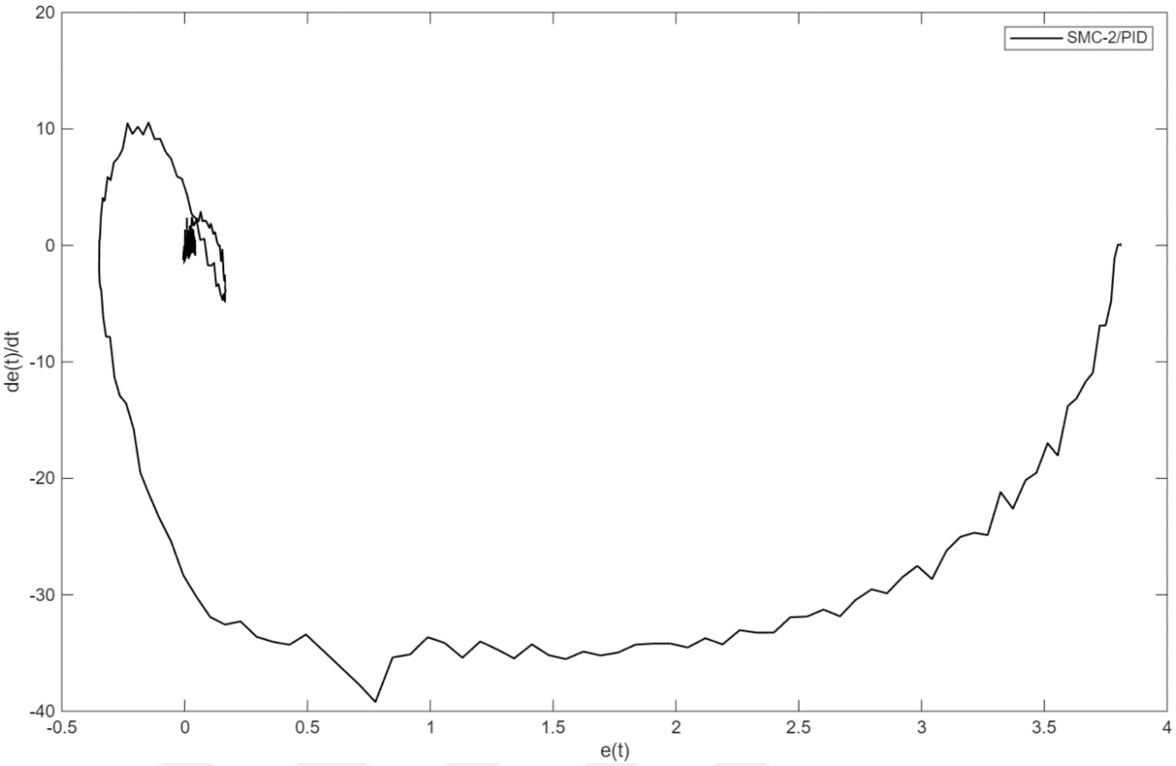

Figure 4.184. Phase plane of $e(t)$ and $de(t)/dt$ (SMC-2/PID)

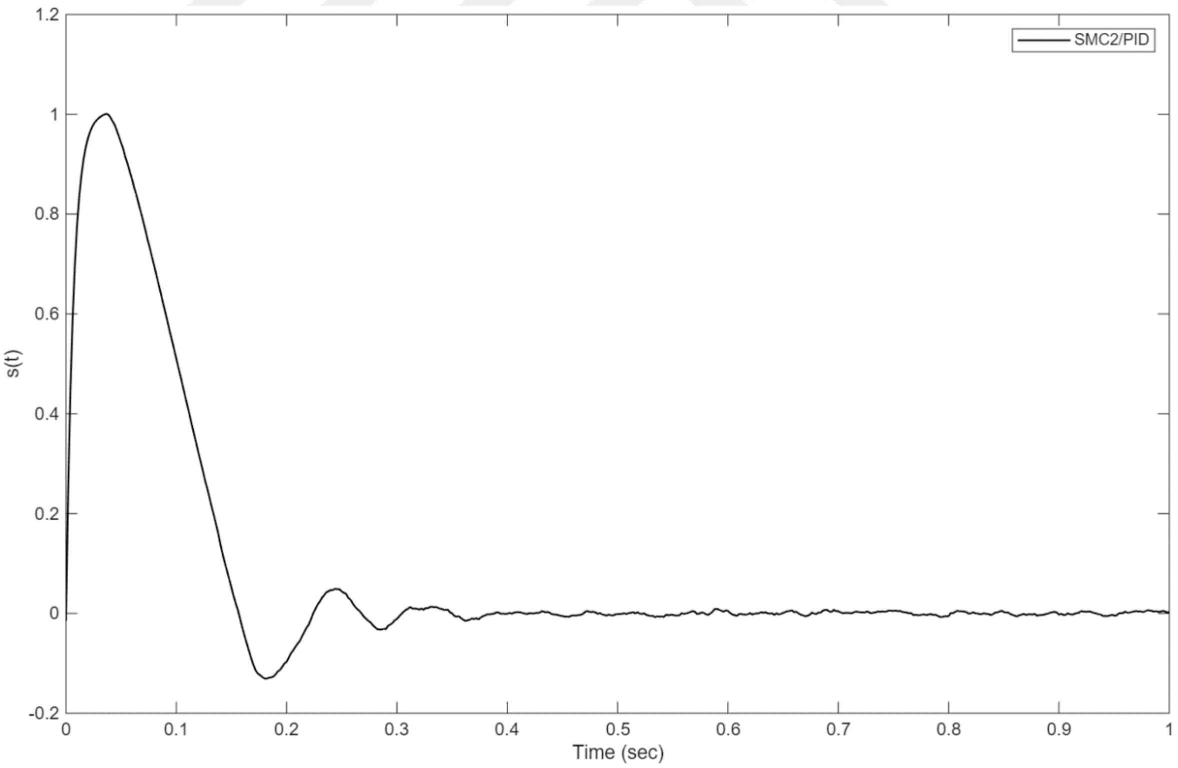

Figure 4.185. Sliding surface, $s(t)$ (SMC-2/PID)

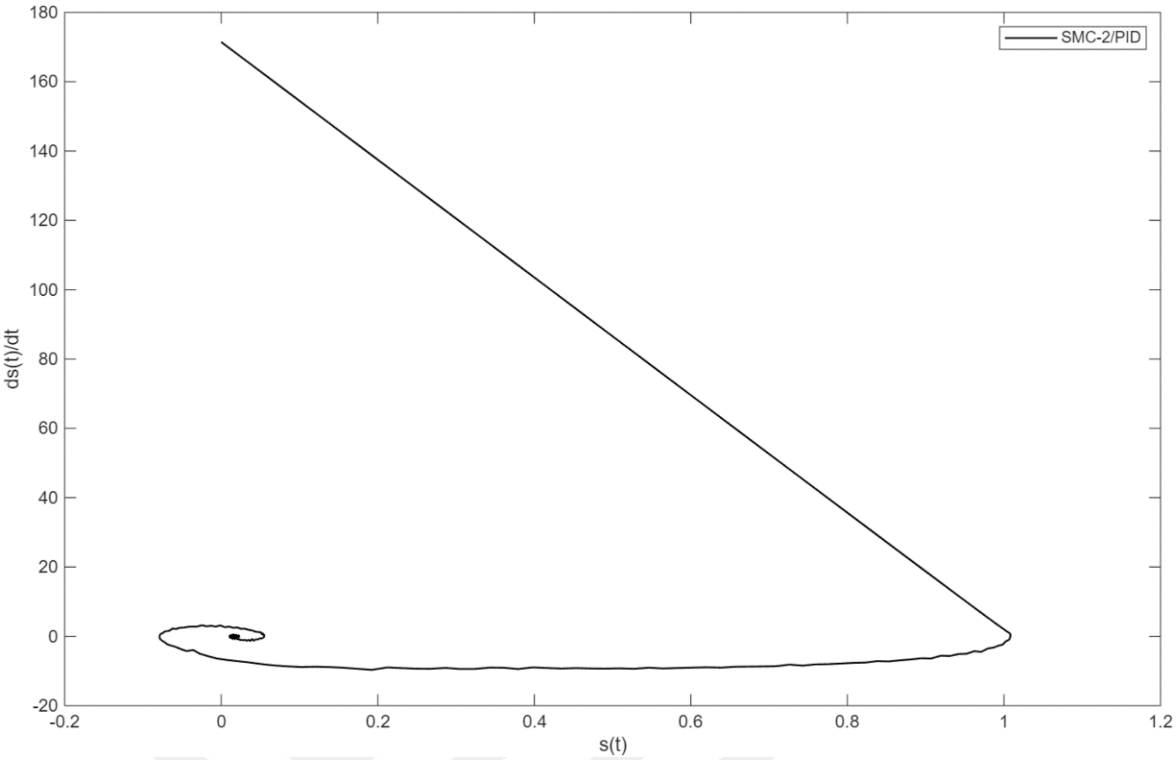

Figure 4.186. Phase plane of $s(t)$ and $ds(t)/dt$ (SMC-2/PID)

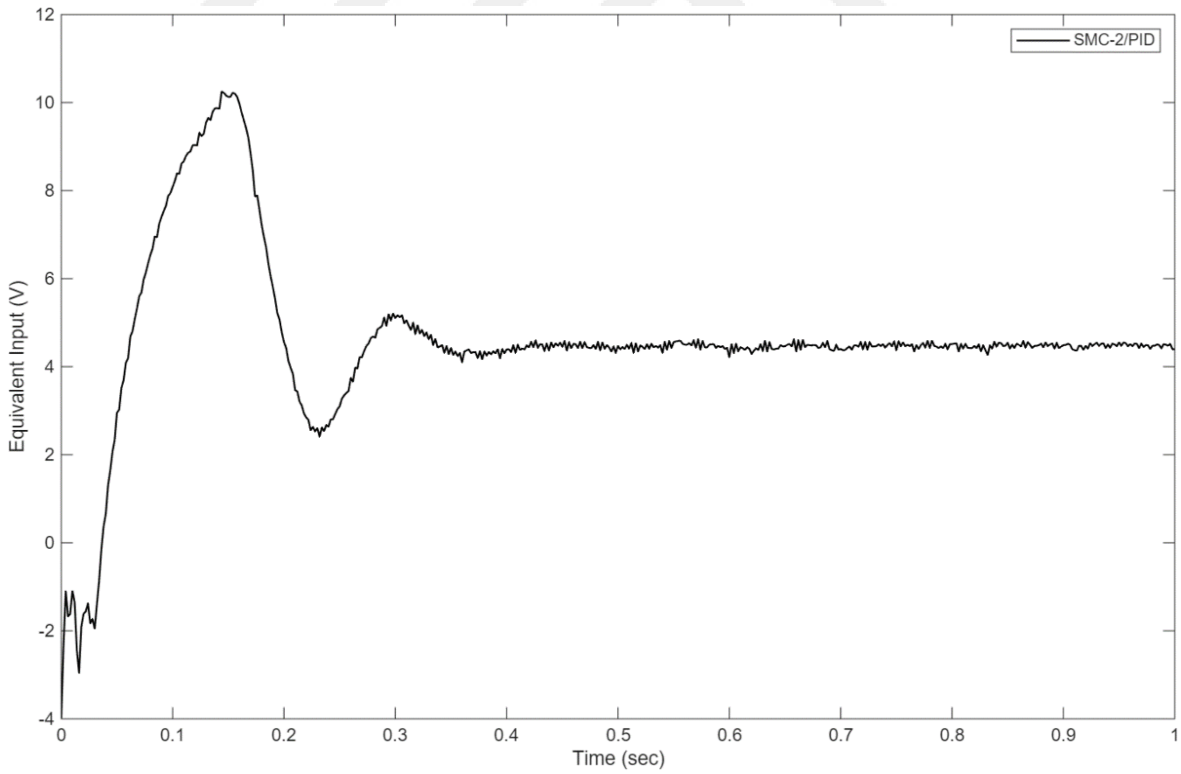

Figure 4.187. Equivalent input, $u_{eq}(t)$ (SMC-2/PID)

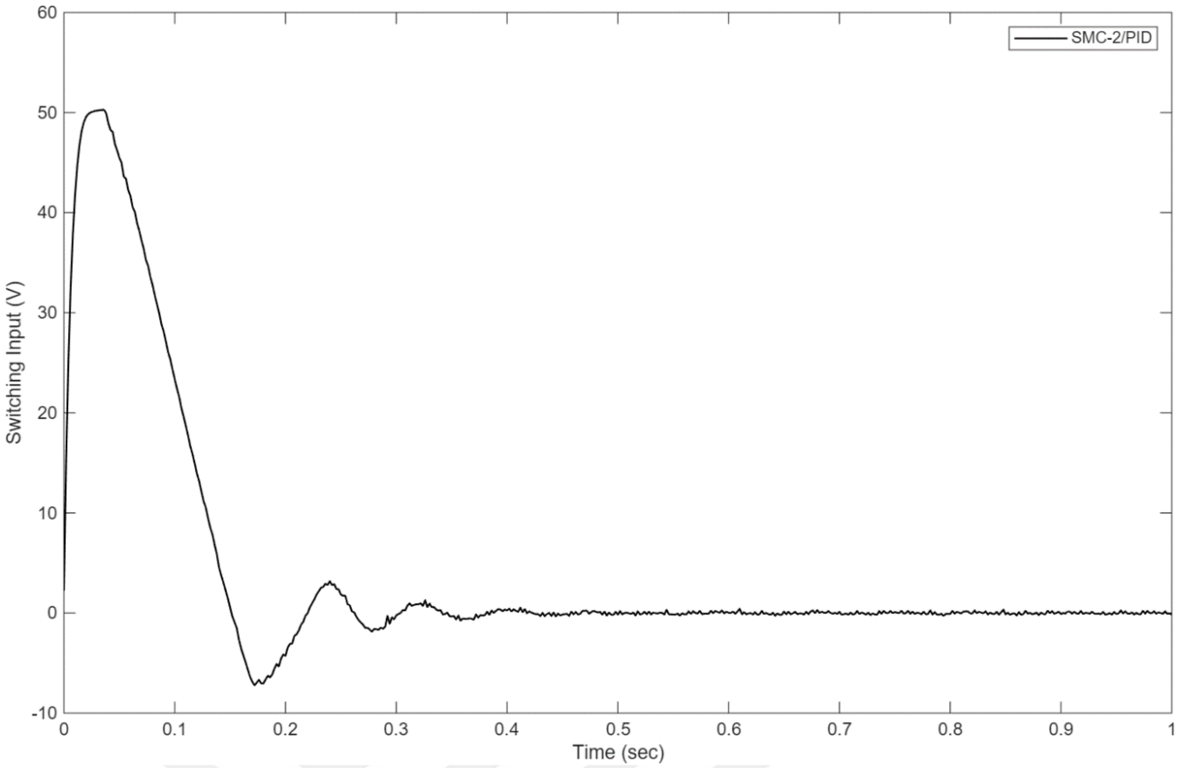

Figure 4.188. Switching input, $u_{sw}(t)$ (SMC-2/PID)

The experimental time domain performance data presented in Table 4.47 indicate that the cascade SMC-2/PID controller demonstrates effective and stable transient performance. The rise time is 0.0916 s, the settling time is 0.2969 s and the overshoot is 9.20%, reflecting well-controlled transient behaviour. The system delay of 0.11 s indicates that the controller responds sensitively and promptly to input variations. Performance Indices

An examination of the performance indicators presented in Table 4.48 reveals that the controller attains ITAE = 0.036, ISE = 1.275, IAE = 0.442 and ITSE = 0.0625. This outcome indicates that the magnitude of errors and their time-weighted effects are effectively constrained. The control effort indicator ISCI = 29.73 and ISTE = 0.0063, suggest that the system maintains balanced control without requiring excessive actuator effort. The experimental findings demonstrate that the cascade SMC-2/PID controller provides rapid, stable and effective transient performance.

Table 4.47. Time domain performance specifications (SMC-2/PID)

Controller	Rise Time (s)	Settling time (s)	Overshoot (%)	Delay time (s)
Cascade Outer-Loop SMC-2/Inner-Loop PID	0.0916	0.2969	9.20	0.11

Table 4.48. Output performance indices (SMC-2/PID)

Controller	ITAE	ISE	IAE	ITSE	ISCI	ISTE
Cascade Outer-Loop SMC-2/Inner-Loop PID	0.036	1.275	0.442	0.0625	29.73	0.0063

4.11. Experimental Results of Cascade Sliding Mode Controllers: (1) Outer-Loop SMC-1/Inner-Loop SMC-1 (SMC-1/SMC-1) and (2) Outer-Loop SMC-2/Inner-Loop SMC-1 (SMC-2/SMC-1)

4.11.1. Experimental Results of Cascade Sliding Mode Control: Outer-Loop SMC-1/Inner-Loop SMC-1 (SMC-1/SMC-1)

In this subsection, the experimental results of the CSMC scheme, composed of an SMC-1/SMC-1 controller, are presented. The outer SMC-1 controller is designed with parameters $k_d = 0.2,\ k_p = 12,\ k_i = 1,\ k_s = 3,\ \Omega = 8$. The inner-loop SMC-1 controller is tuned with parameters $k_d = 0.8,\ k_p = 8,\ k_i = 5,\ k_s = 2.4,\ \Omega = 6$. The measured speed (Figure 4.189) and current responses (Figure 4.190) indicate that the SMC-1/SMC-1 cascade configuration achieves a rapid transient response while maintaining satisfactory steady-state performance. The control signal (Figure 4.191) demonstrates the cooperative interaction between the robust outer-loop and the responsive inner-loop, resulting in reduced overshoot, minimised oscillations, and a significant reduction of the chattering commonly observed in SMC.

The error signal (Figure 4.192) demonstrates the instantaneous deviation from the reference, while the combined plot of error and its derivative (Figure 4.193) illustrates the system's precise tracking of the reference and the maintenance of stable closed-loop behaviour with enhanced disturbance rejection. The sliding surface signal (Figure 4.194) illustrates the system's adherence to the sliding manifold, and the sliding surface together with its derivative (Figure 4.195) further confirms that the system trajectory remains close to the intended manifold, ensuring robust performance. Furthermore, the equivalent signal (Figure 4.196) and the switching signal (Figure 4.197) illustrate how the SMC maintains the desired system behaviour by compensating for uncertainties and enforcing the sliding condition. Collectively, these results validate the robustness and effectiveness of the SMC-1/SMC-1 cascade control strategy.

The experimental findings demonstrate that the proposed SMC-1/SMC-1 cascade approach significantly outperforms single-loop control structures by effectively combining the advantages of SMC in both inner and outer loops.

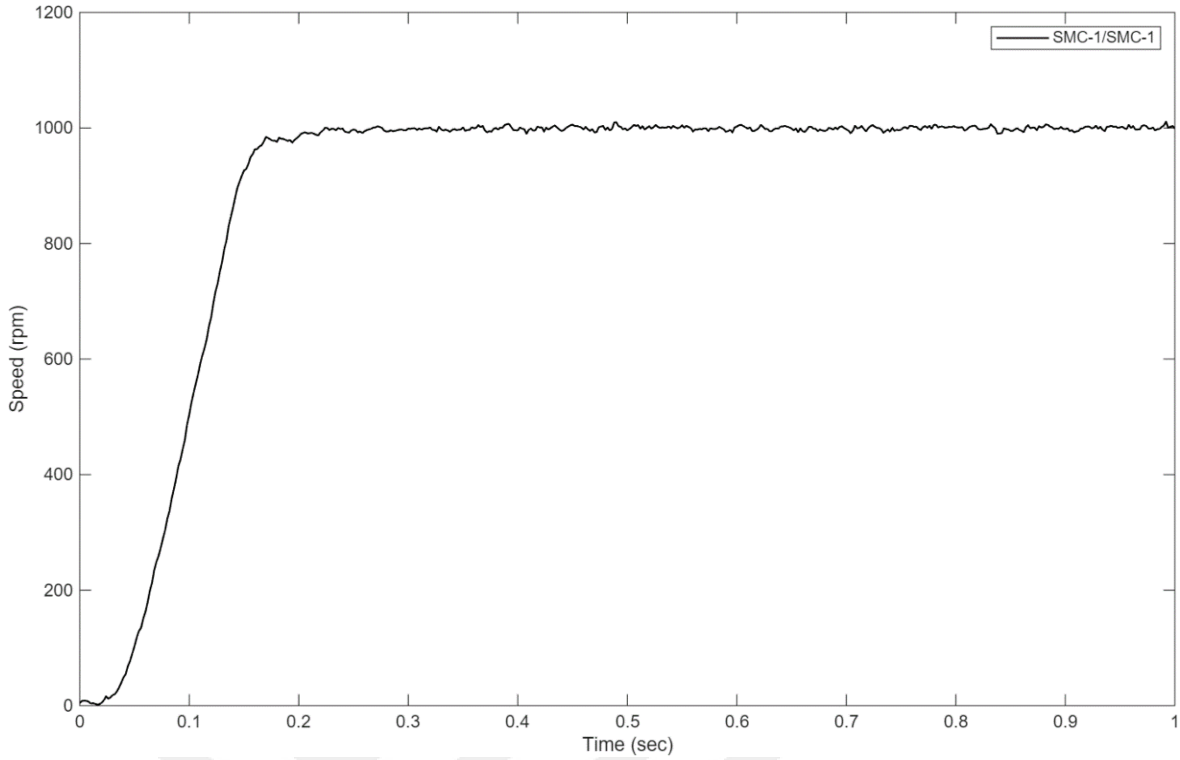

Figure 4.189. Output speed (rpm) (SMC-1/SMC-1)

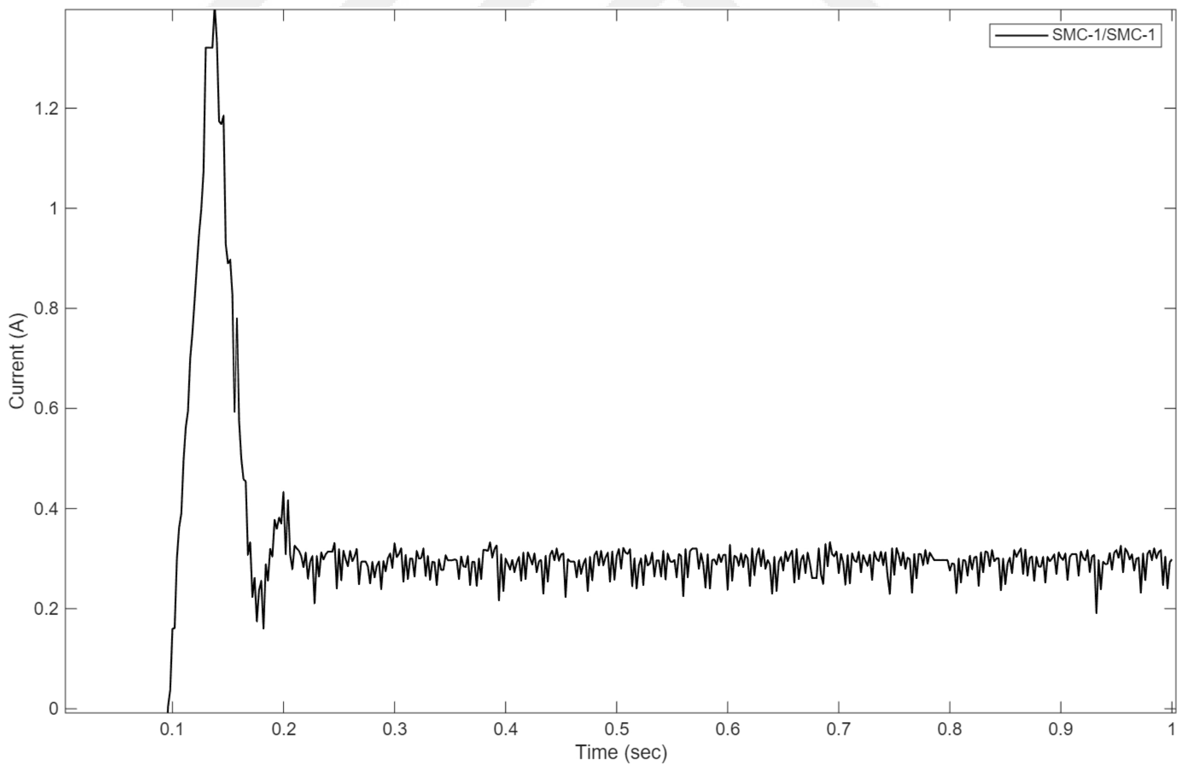

Figure 4.190. Armature current, $i_a(t)$ (SMC-1/SMC-1)

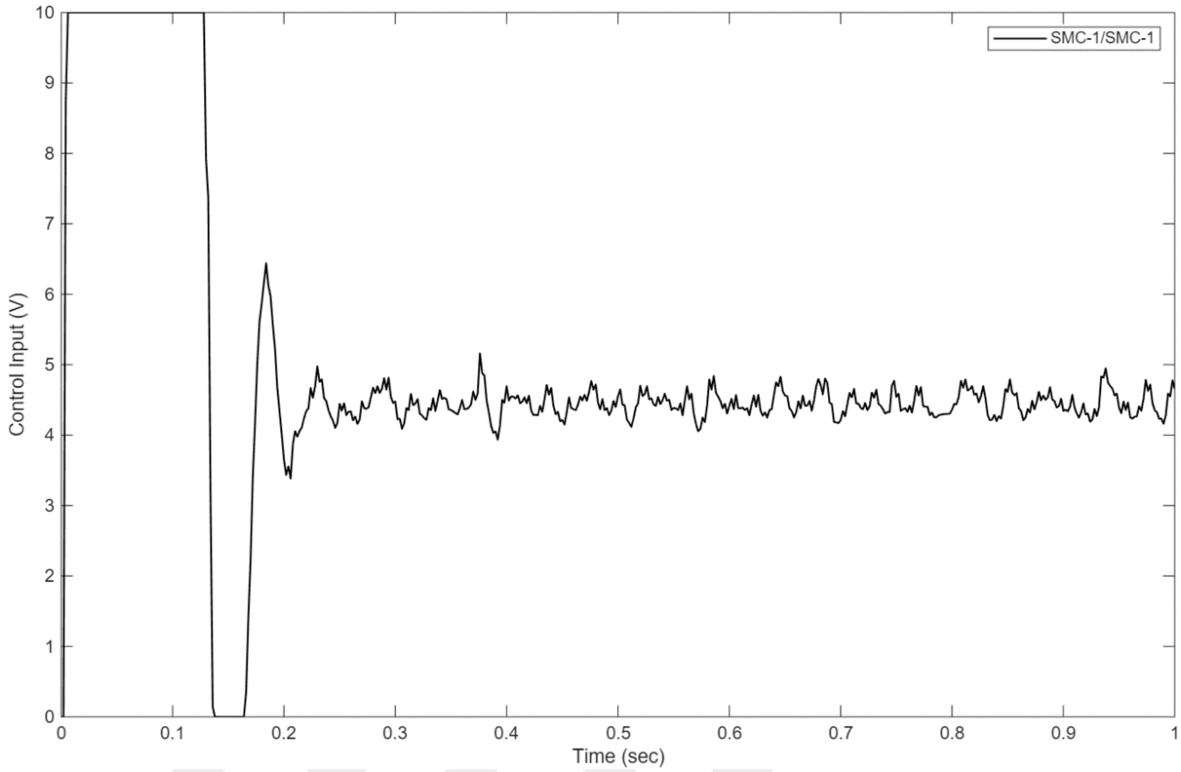

Figure 4.191. Control input voltage, $u(t)$ (SMC-1/SMC-1)

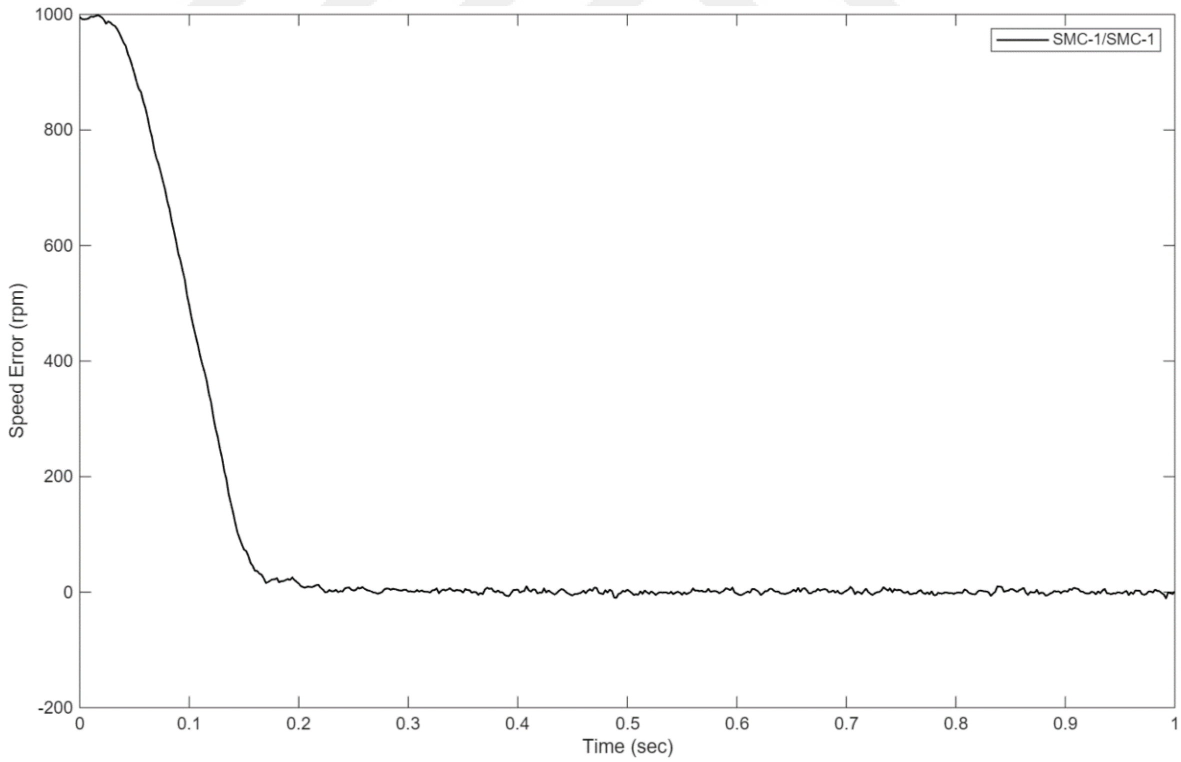

Figure 4.192. Speed error (rpm) (SMC-1/SMC-1)

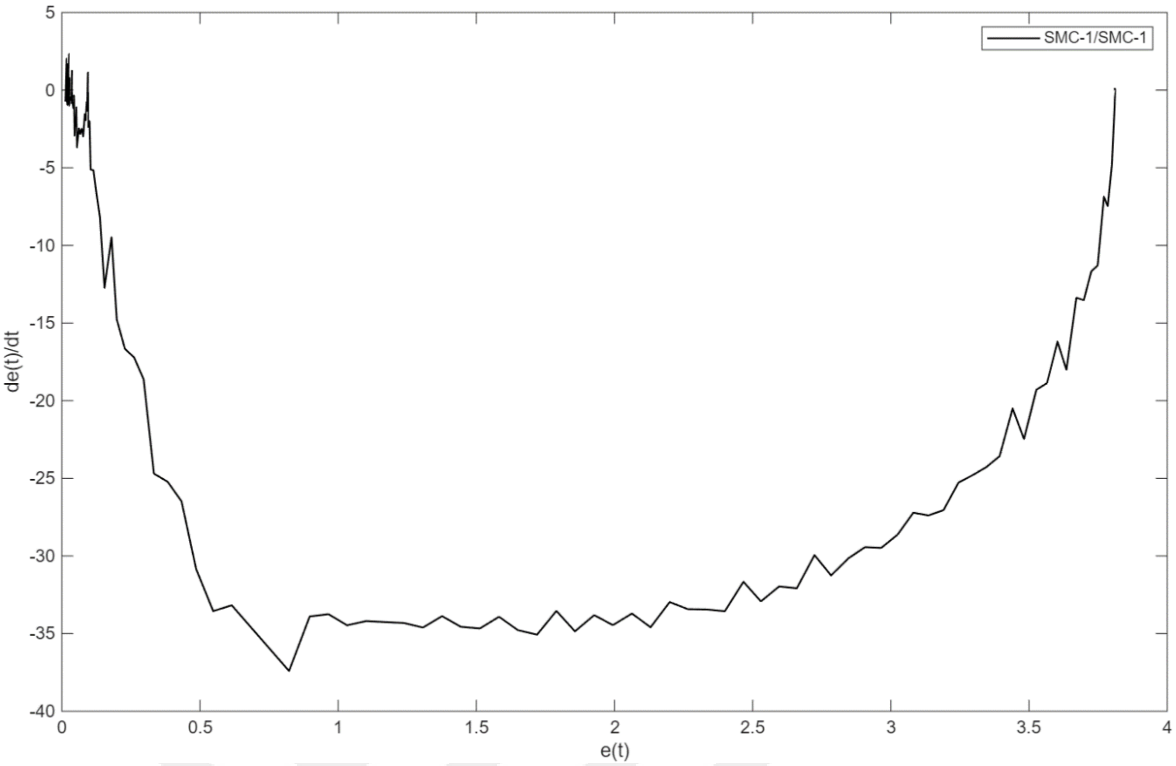

Figure 4.193. Phase plane of $e(t)$ and $de(t)/dt$ (SMC-1/SMC-1)

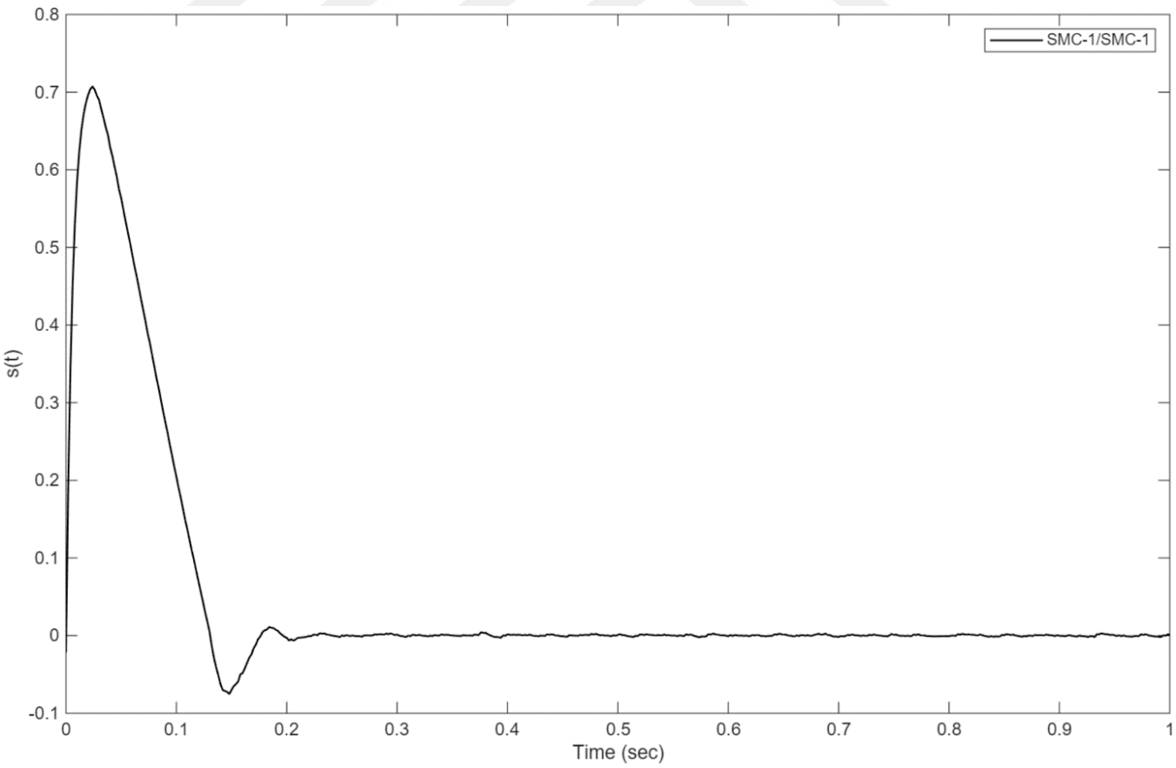

Figure 4.194. Sliding surface, $s(t)$ (SMC-1/SMC-1)

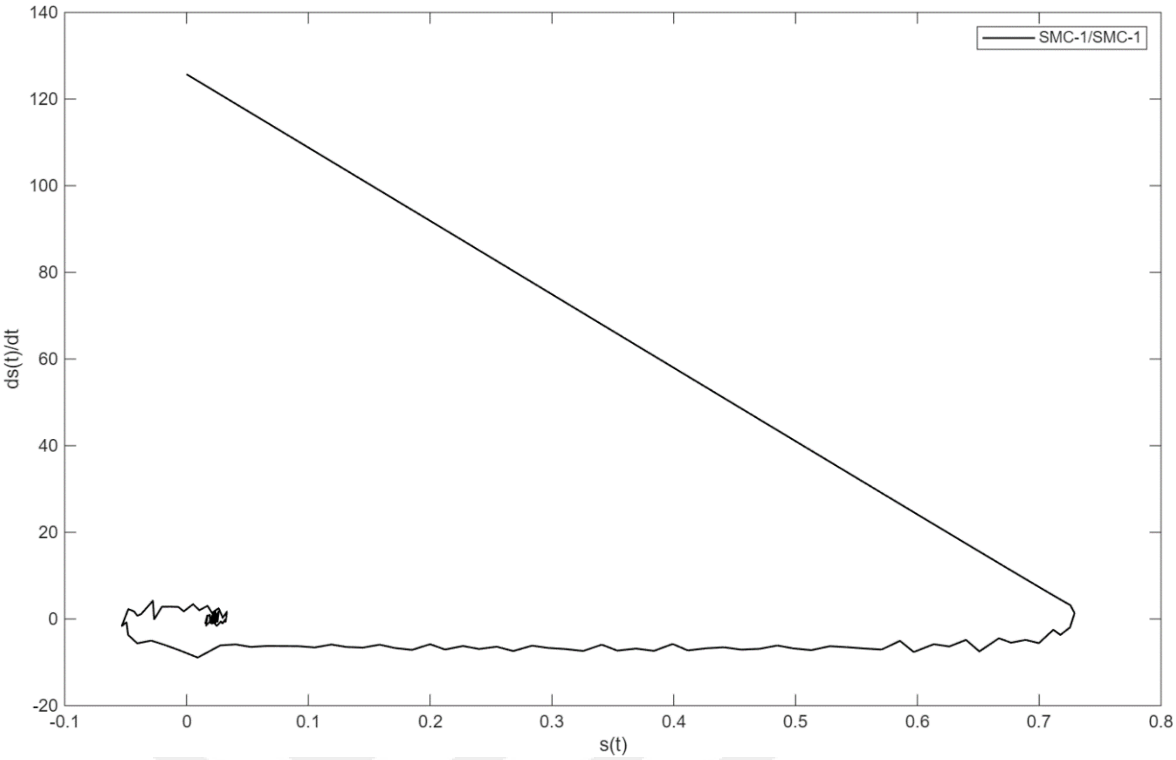

Figure 4.195. Phase plane of $s(t)$ and $ds(t)/dt$ (SMC-1/SMC-1)

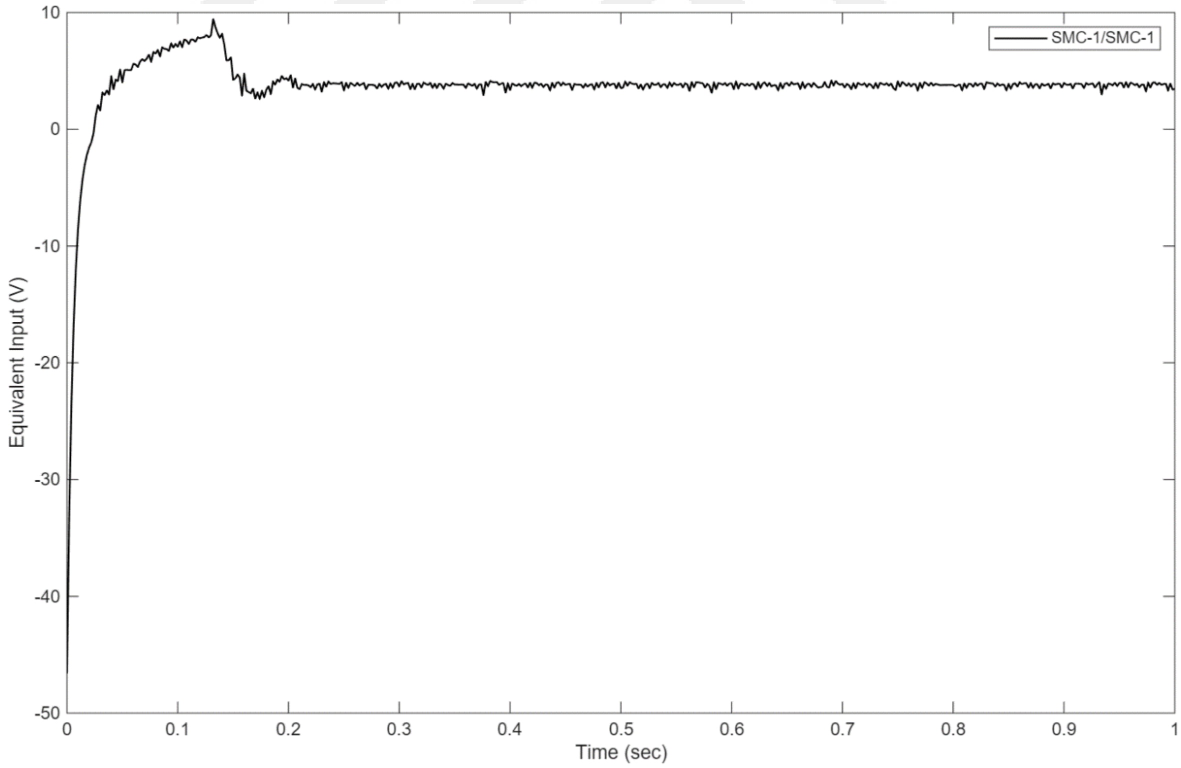

Figure 4.196. Equivalent input, $u_{eq}(t)$ (SMC-1/SMC-1)

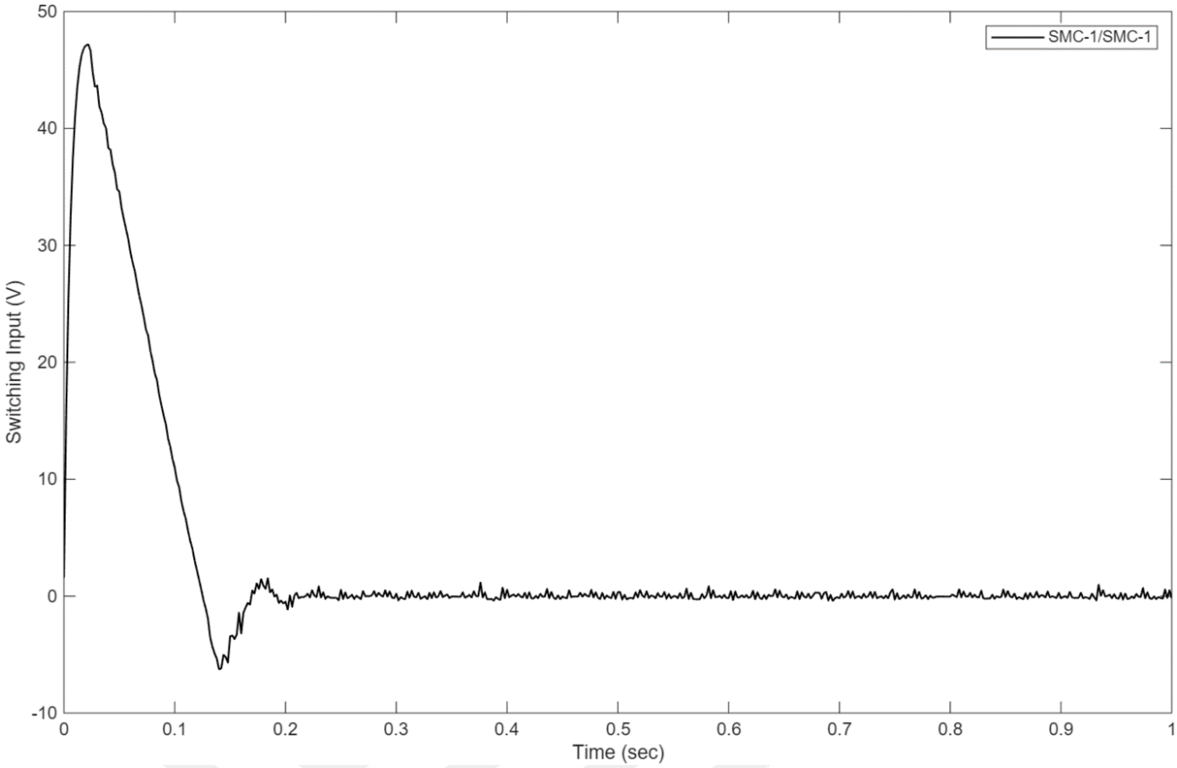

Figure 4.197. Switching input, $u_{sw}(t)$ (SMC-1/SMC-1)

As demonstrated in Table 4.49, the experimental time domain performance data indicate that the SMC-1/SMC-1 controller demonstrates stable and precise transient performance. The rise time is 0.0916 s, the settling time is 0.1742 s and the overshoot is 0.11%, reflecting a highly controlled transient behaviour. The system delay of 0.102 s indicates that the controller responds promptly and efficiently to input variations. Performance Indices

An examination of the performance indicators presented in Table 4.50 reveals that the controller attains ITAE = 0.031, ISE = 1.150, IAE = 0.397 and ITSE = 0.052. This finding indicates that the magnitude of errors and their time-weighted effects are effectively constrained. The control effort indicator ISCI = 29.3 and ISTE = 0.008, suggest that the system maintains balanced and efficient control. The experimental findings demonstrate that the cascade SMC-1/SMC-1 controller delivers rapid, precise and stable transient performance.

Table 4.49. Time domain performance specifications (SMC-1/SMC-1)

Controller	Rise Time (s)	Settling time (s)	Overshoot (%)	Delay time (s)
Cascade SMC Outer-Loop SMC-1/Inner-Loop SMC-1	0.0916	0.1742	0.11	0.102

Table 4.50. Output performance indices (SMC-1/SMC-1)

Controller	ITAE	ISE	IAE	ITSE	ISCI	ISTE
Cascade SMC Outer-Loop SMC-1/Inner-Loop SMC-1	0.031	1.150	0.397	0.052	29.3	0.008

4.11.2. Experimental Results of Cascade Sliding Mode Control: Outer-Loop SMC-2/Inner-Loop SMC-1 (SMC-2/SMC-1)

In this subsection, the experimental results of the CSMC configuration, consisting of SMC-2/SMC-1 controller, are presented. The outer SMC-2 controller is designed with parameters $k_c = 2.5,\ k_d = 0.05,\ k_p = 40,\ k_i = 5,\ \Omega_c = 15,\ \beta = 35,\ \lambda_1 = 15$. The inner-loop SMC-1 controller is tuned with parameters $k_d = 0.8,\ k_p = 5,\ k_i = 8,\ k_s = 2.8,\ \Omega = 6$. The experimental output speed (Figure 4.198) and current responses (Figure 4.199) indicate that the SMC-2/SMC-1 cascade structure achieves both a fast transient response and satisfactory steady-state performance. The control signal (Figure 4.200) illustrates the combined effect of the robust outer-loop SMC-2 and the responsive inner-loop SMC-1, which collectively mitigate overshoot, minimise oscillations, and suppress the chattering phenomenon that is often observed in SMC.

The error signal (Figure 4.201) and the combined plot of error and its derivative (Figure 4.202) confirm accurate tracking of the reference input, while also demonstrating stable closed-loop behaviour and effective disturbance rejection. The sliding surface signal (Figure 4.203) and its derivative (Figure 4.204) illustrate that the system states remain close to the predefined sliding manifold, thereby ensuring robust performance. Furthermore, the equivalent signal (Figure 4.205) and the switching signal (Figure 4.206) demonstrate the manner in which the SMC upholds the desired system behaviour by compensating for uncertainties and enforcing the sliding condition. A comparative evaluation of transient and steady-state characteristics demonstrates that the SMC-2/SMC-1 cascade configuration outperforms single-loop SMC implementations, providing faster settling times, reduced steady-state error, and smooth control action without excessive control effort. The experimental results verify that the distribution of control responsibilities across the inner and outer loops achieves an effective balance between robustness and response smoothness.

In conclusion, the proposed SMC-2/SMC-1 cascade control structure is shown to be a reliable and efficient solution for systems subject to parameter uncertainties and external disturbances. The combination of the robustness of the SMC in both loops with carefully tuned parameters has been demonstrated to result in the enhancement of the dynamic response of the system, the minimisation of chattering, and the rejection of disturbances.

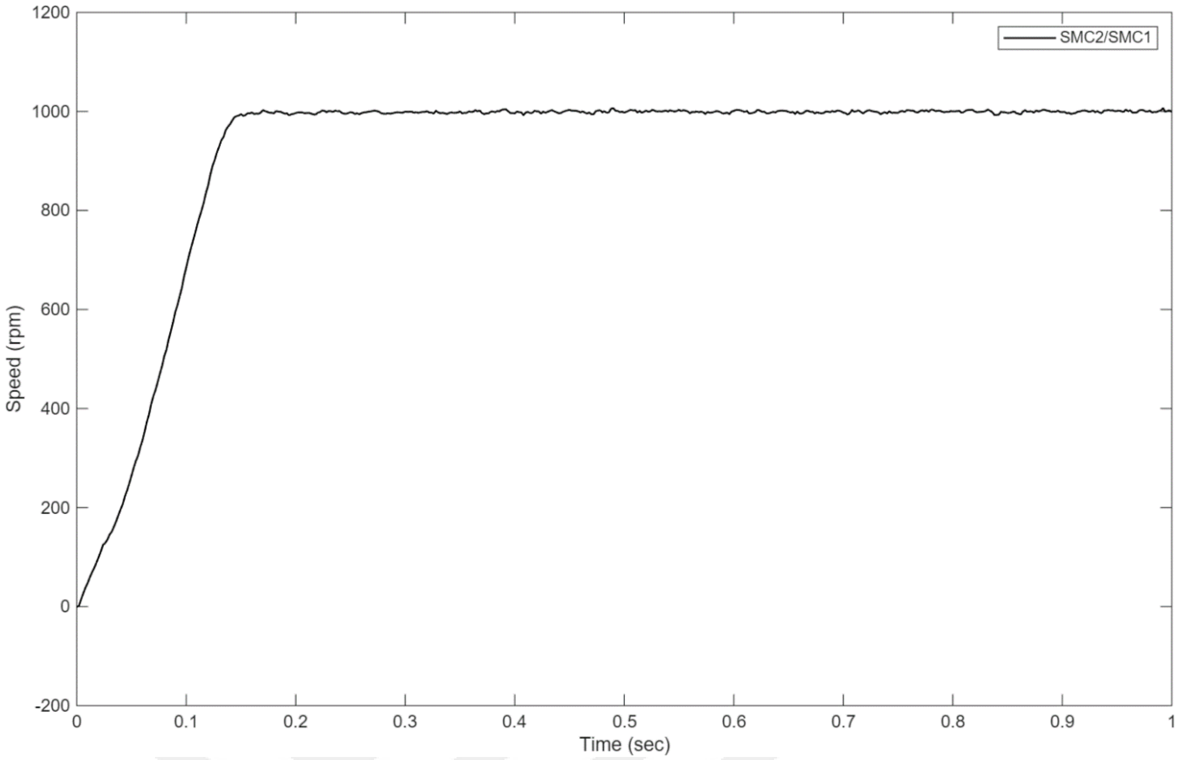

Figure 4.198. Output speed (rpm) (SMC-2/SMC-1)

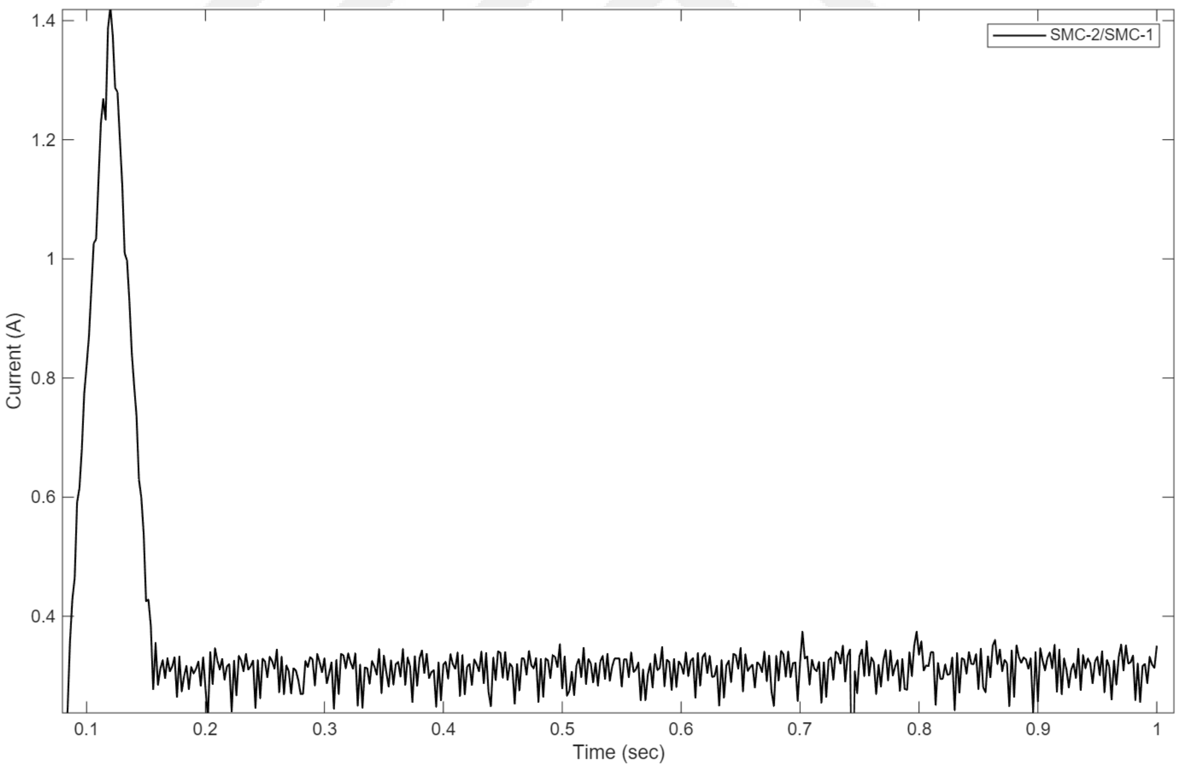

Figure 4.199. Armature current, $i_a(t)$ (SMC-2/SMC-1)

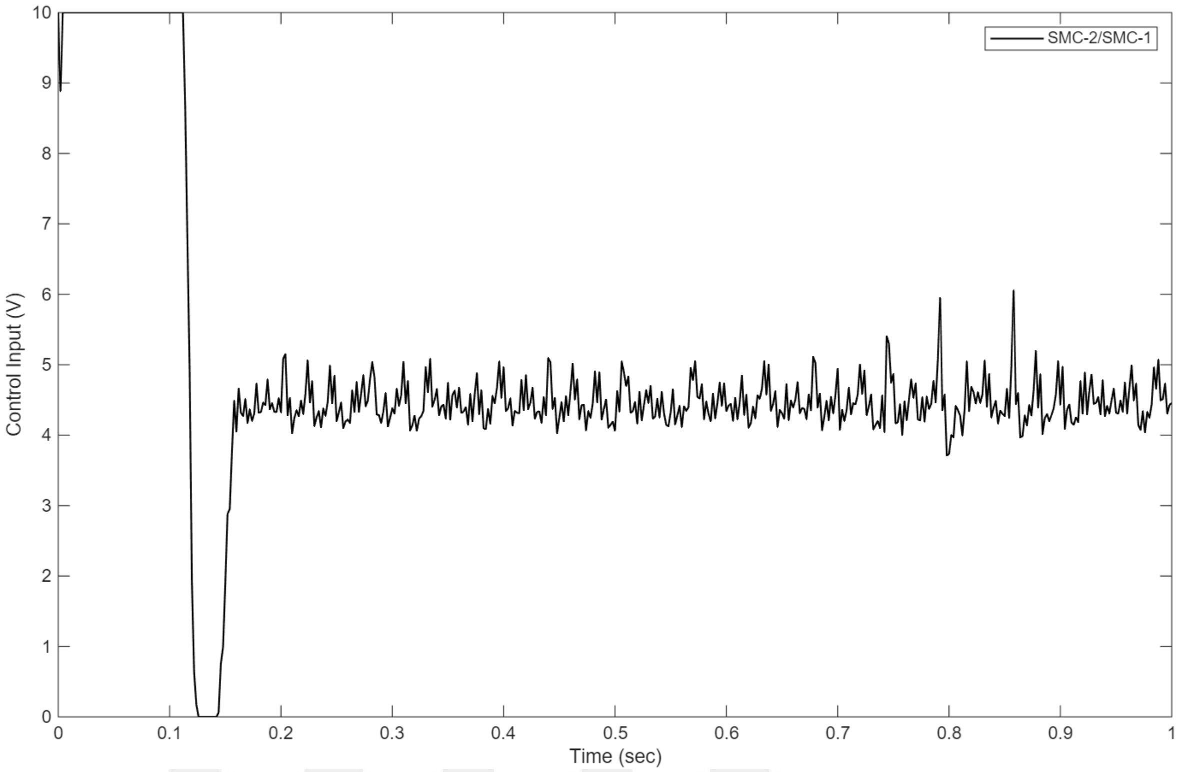

Figure 4.200. Control input voltage, $u(t)$ (SMC-2/SMC-1)

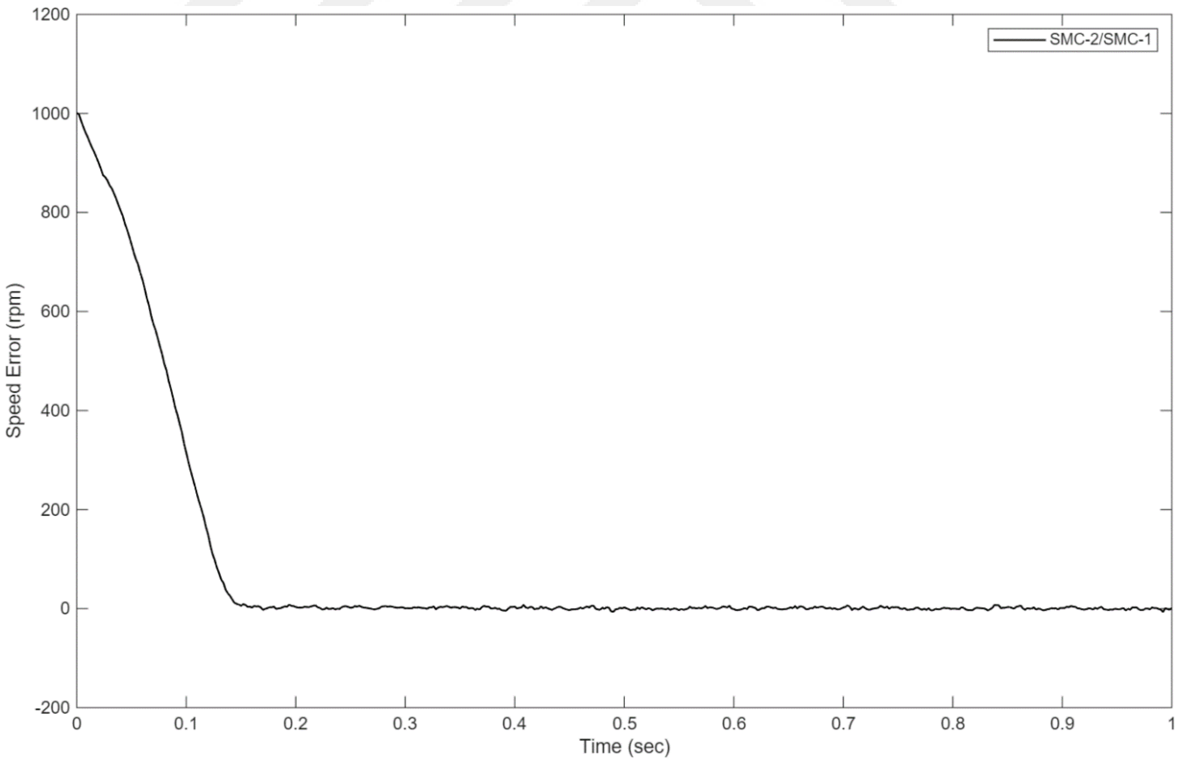

Figure 4.201. Speed error (rpm) (SMC-2/SMC-1)

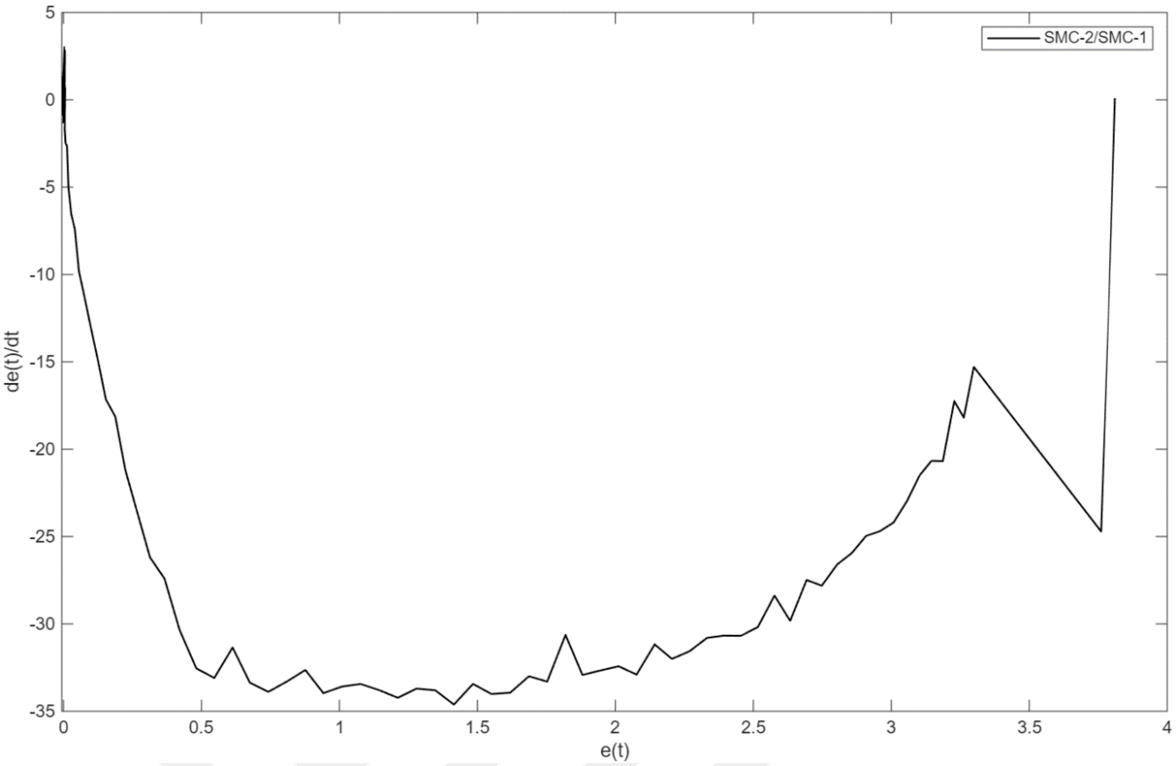

Figure 4.202. Phase plane of $e(t)$ and $de(t)/dt$ (SMC-2/SMC-1)

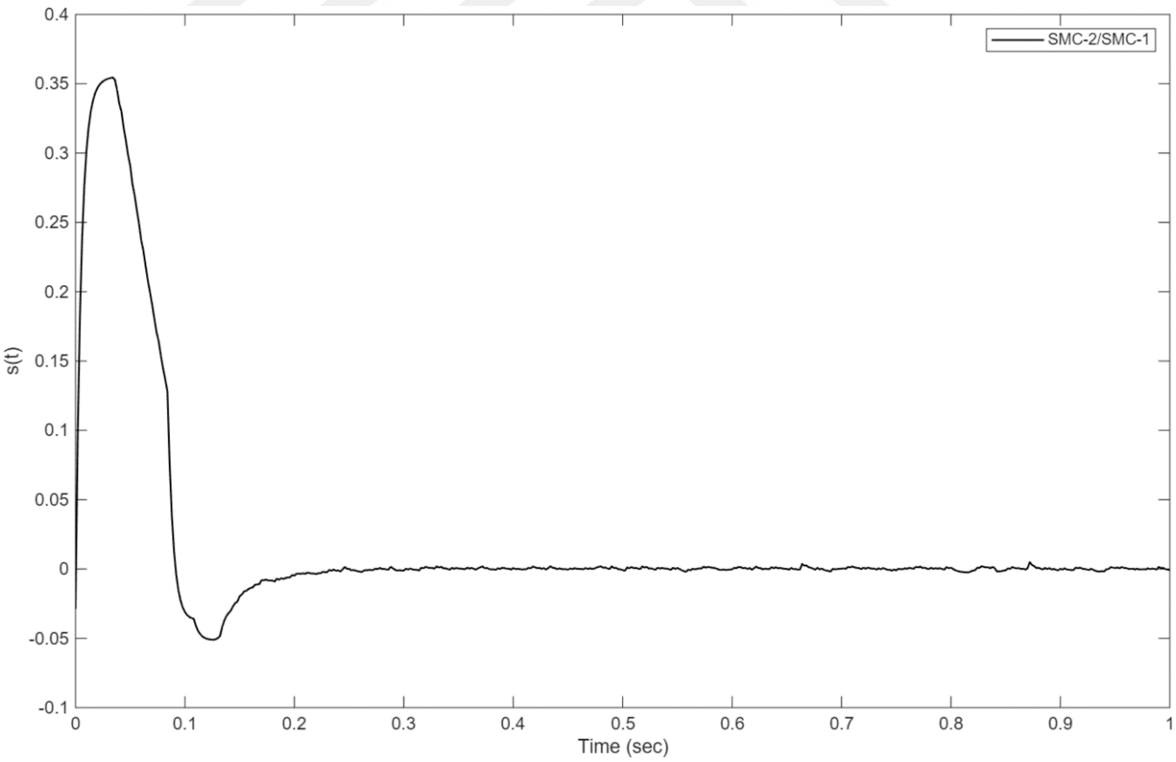

Figure 4.203. Sliding surface, $s(t)$ (SMC-2/SMC-1)

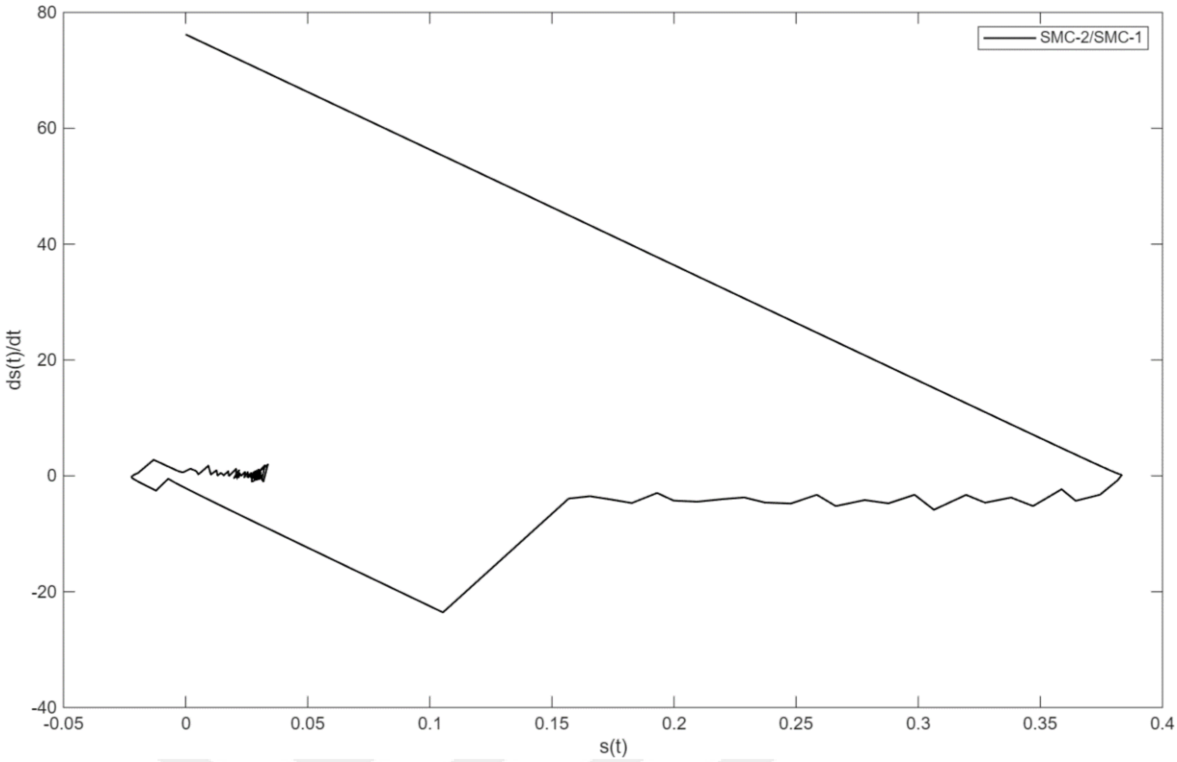

Figure 4.204. Phase plane of $s(t)$ and $ds(t)/dt$ (SMC-2/SMC-1)

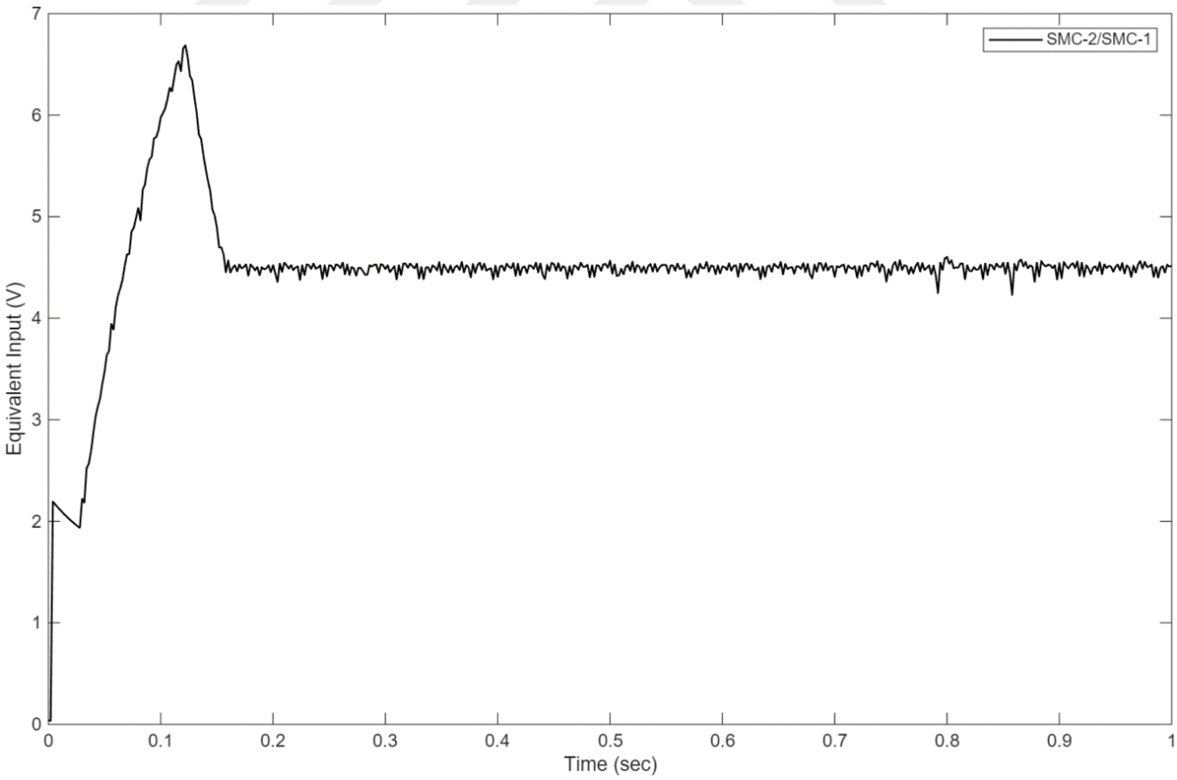

Figure 4.205. Equivalent input, $u_{eq}(t)$ (SMC-2/SMC-1)

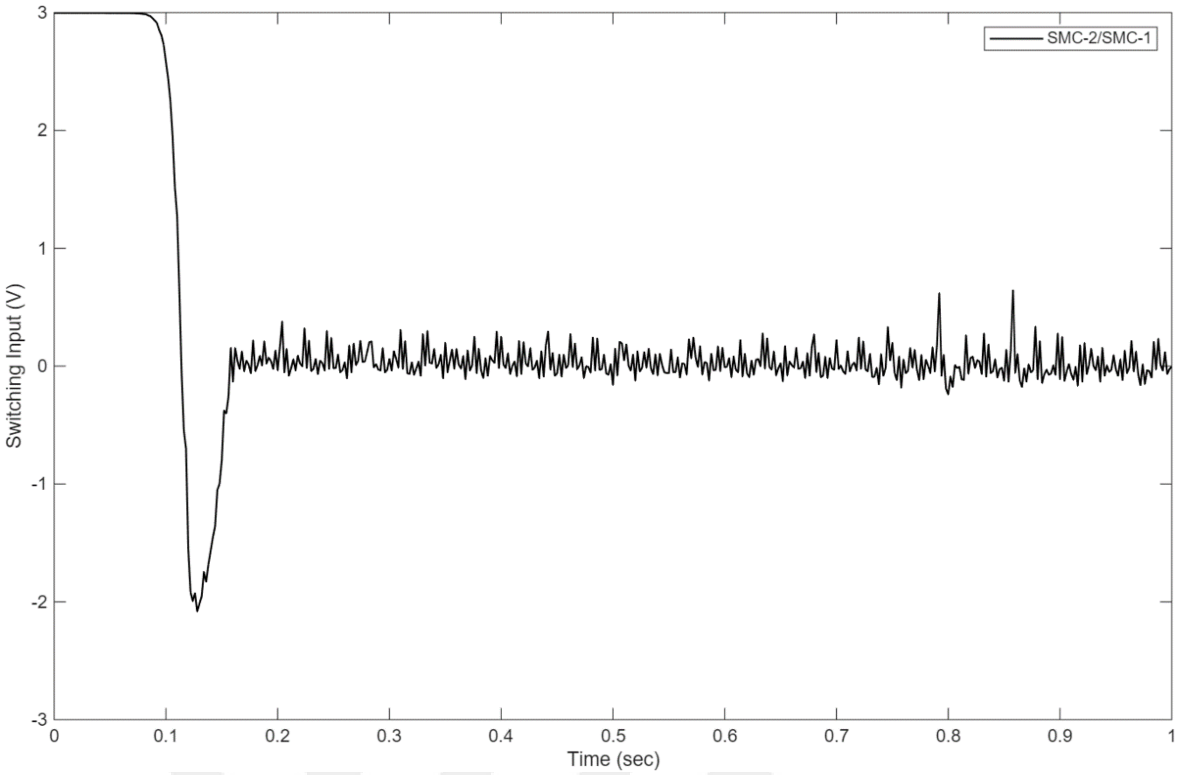

Figure 4.206. Switching input, $u_{sw}(t)$ (SMC-2/SMC-1)

The experimental time domain performance data presented in Table 4.51 indicate that the cascade SMC-2/SMC-1 controller delivers rapid and stable transient performance. The rise time is measured at 0.1055 s, the settling time at 0.14 s, and the overshoot at 0%, indicative of a highly controlled response. The system delay of 0.068 s confirms that the controller responds effectively and promptly to input variations. Performance indices an examination of the performance indicators presented in Table 4.52 reveals that the controller attains ITAE = 0.014, ISE = 0.797, IAE = 0.294 and ITSE = 0.029. This outcome demonstrates that the magnitude of errors and their time-weighted effects are effectively constrained. The control effort indicator ISCI = 28.59 and ISTE = 0.0005, suggest that the system maintains balanced and efficient control. The experimental findings demonstrate that the cascade SMC-2/SMC-1 controller provides fast, stable and precise transient performance.

Table 4.51. Time domain performance specifications (SMC-2/SMC-1)

Controller	Rise Time (s)	Settling time (s)	Overshoot (%)	Delay time (s)
Cascade SMC Outer-Loop SMC-2/Inner-Loop SMC-1	0.1055	0.14	0	0.068

Table 4.52. Output performance indices (SMC-2/SMC-1)

Controller	ITAE	ISE	IAE	ITSE	ISCI	ISTE
Cascade SMC Outer-Loop SMC-2/Inner-Loop SMC-1	0.014	0.797	0.294	0.029	28.59	0.0005

5. RESULTS AND DISCUSSIONS

The experimental and simulation results for all controllers are clearly summarised in Tables 5.1, 5.2, 5.3 and 5.4, as demonstrated in the following section. The tables provide a detailed comparison of each controller's performance, including transient and steady-state characteristics, to evaluate their effectiveness under different operating conditions.

Table 5.1. Simulation results of time domain performance specifications

Controller	Rise Time (s)	Settling time (s)	Overshoot (%)	Delay time (s)	Output deviation (rpm)
P-Ziegler Nichols	0.0646	0.1220	3.70	0.0160	±8
PI-Ziegler Nichols	0.0644	0.1205	3.20	0.0160	±7
PID-Ziegler Nichols	0.0665	0.0982	0.00	0.0160	±6
Single-Loop P	0.0710	0.1165	3.71	0.0500	±8
Single-Loop PI	0.0710	0.1157	3.37	0.0500	±7
Single-Loop PID	0.1244	0.2328	0.00	0.0520	±6
Single-Loop SMC-1	0.0998	0.1516	0.19	0.0740	±10
Single-Loop SMC-2	0.0944	0.1744	0.05	0.0540	±8
Cascade Outer-Loop PI/ Inner-Loop P	0.0712	0.0958	2.35	0.0050	±7
Cascade Outer-Loop PI/ Inner-Loop PI	0.0727	0.0985	0.60	0.0520	±6
Cascade Outer-Loop PID/ Inner-Loop PI	0.0725	0.0982	0.26	0.0500	±12
Cascade Outer-Loop SMC-1/ Inner-Loop P	0.1645	0.2350	0.00	0.1060	±6
Cascade Outer-Loop SMC-1/ Inner-Loop PI	0.1094	0.2002	0.00	0.0720	±6
Cascade Outer-Loop SMC-1/ Inner-Loop PID	0.0766	0.1209	0.09	0.0520	±5
Cascade Outer-Loop SMC-2/ Inner-Loop P	0.0831	0.1508	0.00	0.0540	±5
Cascade Outer-Loop SMC-2/ Inner-Loop PI	0.0843	0.1607	0.00	0.0540	±3
Cascade Outer-Loop SMC-2/ Inner-Loop PID	0.0726	0.1217	0.06	0.05	±4
Cascade SMC Outer-Loop SMC-1/Inner-Loop SMC-1	0.1062	0.1912	0.94	0.050	±6
Cascade SMC Outer-Loop SMC-2/Inner-Loop SMC-1	0.0835	0.1800	0.01	0.050	±4

Table 5.2. Simulation results of output performance indices

Controllers	ITAE	ISE	IAE	ITSE	ISCI	ISTE
P-Ziegler Nichols	0.1613	0.606	0.476	0.0615	0.606	0.1041
PI-Ziegler Nichols	0.1697	0.617	0.493	0.0670	0.617	0.1094
PID-Ziegler Nichols	0.1338	0.580	0.430	0.0456	0.580	0.0850
Single-Loop P	0.0209	0.517	0.220	0.0127	27.83	0.0101
Single-Loop PI	0.0221	0.517	0.223	0.0128	27.23	0.0106
Single-Loop PID	0.0256	0.573	0.278	0.0178	24.80	0.0088
Single-Loop SMC-1	0.0373	1.067	0.417	0.0534	22.89	0.0048
Single-Loop SMC-2	0.0400	0.805	0.333	0.0286	25.52	0.0173
Cascade Outer-Loop PI/Inner-Loop P	0.0150	0.516	0.209	0.0120	27.32	0.0060
Cascade Outer-Loop PI/Inner-Loop PI	0.0320	0.519	0.242	0.0130	27.86	0.0168
Cascade Outer-Loop PID/ Inner-Loop PI	0.0250	0.517	0.229	0.0130	27.81	0.0120
Cascade Inner-Loop P/Outer-Loop SMC-1	0.0305	1.077	0.418	0.0560	22.27	0.0030
Cascade Outer-Loop SMC-1/Inner-Loop PI	0.0192	0.754	0.300	0.2609	24.20	0.0034
Cascade Outer-Loop SMC-1/Inner-Loop PID	0.0585	0.526	0.287	0.0178	30.84	0.0340
Cascade Outer-Loop SMC-2/Inner-Loop P	0.0115	0.555	0.220	0.0140	26.64	0.0017
Cascade Outer-Loop SMC-2/Inner-Loop PI	0.0145	0.599	0.231	0.0143	26.26	0.0040
Cascade Outer-Loop SMC-2/Inner-Loop PID	0.0260	0.517	0.228	0.0130	28.66	0.0131
Cascade SMC Outer-Loop SMC-1/Inner-Loop SMC-1	0.0140	0.534	0.234	0.0140	39.10	0.0006
Cascade SMC Outer-Loop SMC-2/Inner-Loop SMC-1	0.0189	0.523	0.231	0.0130	47.95	0.0006

Table 5.3. Experimental results of time domain performance specifications

Controllers	Rise Time (s)	Settling time (s)	Overshoot (%)	Delay time (s)	Output deviation (rpm)
Single-Loop P	0.0614	0.2842	14.90	0.032	± 12
Single-Loop PI	0.0981	0.3564	12.01	0.082	± 10
Single-Loop PID	0.0911	0.1403	0.630	0.078	± 7
Single-Loop SMC-1	0.0874	0.2082	5.850	0.048	± 12
Single-Loop SMC-2	0.0770	0.1491	0.810	0.064	± 10
Cascade Outer-Loop PI/ Inner-Loop P	0.1017	0.3005	8.630	0.086	± 10
Cascade Outer-Loop PI/ Inner-Loop PI	0.1023	0.2519	9.260	0.088	± 9
Cascade Outer-Loop PID/Inner-Loop PI	0.0904	0.1996	9.990	0.084	± 15
Cascade Outer-Loop SMC-1/Inner-Loop P	0.1122	0.1474	0.240	0.084	± 7
Cascade Outer-Loop SMC-1/Inner-Loop PI	0.0952	0.1431	0.640	0.084	± 8
Cascade Outer-Loop SMC-1/Inner-Loop PID	0.1063	0.3762	0.030	0.044	± 6
Cascade Outer-Loop SMC-2/Inner-Loop P	0.0952	0.2612	7.670	0.116	± 8
Cascade Outer-Loop SMC-2/Inner-Loop PI	0.0910	0.1307	0.000	0.070	± 5
Cascade Outer-Loop SMC-2/Inner-Loop PID	0.0916	0.2969	9.200	0.110	± 7
Cascade SMC Outer-Loop SMC-1/Inner-Loop SMC-1	0.0916	0.1742	0.110	0.102	± 6
Cascade SMC Outer-Loop SMC-2/Inner-Loop SMC-1	0.1055	0.1400	0.000	0.068	± 5

Table 5.4. Experimental results of output performance indices

Controllers	ITAE	ISE	IAE	ITSE	ISCI	ISTE
Single-Loop P	0.0590	0.886	0.397	0.037	31.95	0.0280
Single-Loop PI	0.0342	0.865	0.357	0.034	30.08	0.0096
Single-Loop PID	0.0300	0.820	0.320	0.020	28.14	0.0140
Single-Loop SMC-1	0.0220	0.450	0.220	0.010	23.37	0.0080
Single-Loop SMC-2	0.0200	0.720	0.270	0.010	22.87	0.0074
Cascade Outer-Loop PI/ Inner-Loop P	0.0506	0.917	0.391	0.038	31.38	0.0217
Cascade Outer-Loop PI/ Inner-Loop PI	0.0352	0.926	0.365	0.037	31.00	0.0110
Cascade Outer-Loop PID/Inner-Loop PI	0.0200	0.850	0.320	0.030	28.60	0.0051
Cascade Outer-Loop SMC-1/Inner-Loop P	0.0158	0.816	0.303	0.031	28.78	0.0007
Cascade Outer-Loop SMC-1/Inner-Loop PI	0.0900	1.100	0.530	0.050	27.28	0.4280
Cascade Outer-Loop SMC-1/Inner-Loop PID	0.0196	0.423	0.224	0.011	22.95	0.0017
Cascade Outer-Loop SMC-2/Inner-Loop P	0.0320	1.357	0.451	0.070	32.00	0.0033
Cascade Outer-Loop SMC-2/Inner-Loop PI	0.0200	0.940	0.370	0.030	21.21	0.0100
Cascade Outer-Loop SMC-2/Inner-Loop PID	0.0360	1.275	0.442	0.062	29.73	0.0063
Cascade SMC Outer-Loop SMC-1/Inner-Loop SMC-1	0.0310	1.150	0.397	0.052	29.30	0.0080
Cascade SMC Outer-Loop SMC-2/Inner-Loop SMC-1	0.0140	0.797	0.294	0.029	28.59	0.0005

5.1. Simulation of Step Response Analyses

As illustrated in Table 5.1, the domain performance specifications of various classical and SMC-based controllers are presented. When the rise time, settling time, overshoot and steady-state deviation values are evaluated collectively, the superiority of SMC-based cascade controllers becomes evident. The primary observations can be summarised as follows:

Classical controllers (P, PI, PID - Ziegler–Nichols):

- t is imperative that fast rise times (approximately 0.064–0.066 s) and moderate settling times (approximately 0.1 s) are provided.

- Nevertheless, steady-state deviations of ±6–8 rpm and noticeable overshoot (up to 3.7%) result in limited steady-state precision.

The control performance of the system is satisfactory for basic tracking purposes; however, its robustness and disturbance rejection remain inadequate.

Single-loop SMC controllers (SMC-1 and SMC-2):

- It is evident that there is negligible overshoot (0.19% and 0.05%), thereby demonstrating the inherent stability and robustness of the SMC.
- The settling times of the system (0.1516–0.1744 s) were found to be marginally prolonged in comparison to classical methodologies. The output deviations (±8–10 rpm) indicated that single-loop SMC was not capable of employing its full disturbance rejection capacity.

Cascade SMC-based controllers:

It is evident that the provision of significant enhancement in both transient and steady-state performance is of paramount importance.

i) SMC-2/PI: The controller demonstrates no overshoot (0%) and attains the lowest steady-state deviation (±3 rpm) among all controllers. As demonstrated in Figure 1, the proposed system demonstrates a superior settling time when compared to the single-loop SMC-2 (0.1607 s vs. 0.1744 s).
ii) SMC-2/PID: This system has been demonstrated to offer an optimal balance between response speed and accuracy. It exhibits a rise time of 0.0726 s, negligible overshoot (0.06%) and low deviation (±4 rpm).
iii) SMC-2/SMC-1: This configuration is characterised by its ability to deliver the most stable behaviour, with no occurrence of overshoot (0.01%) and a steady-state deviation of ±4 rpm. This evidence substantiates the robustness of the CSMC configuration.

Overall evaluation:

- It is evident that SMC-based cascades demonstrate superior performance in comparison to classical and normally loop controllers with regard to overshoot suppression, stability and steady-state accuracy.
- It has been demonstrated that the optimal overall performance is attained when SMC-2 is utilised in the outer-loop, thereby ensuring expeditious, seamless and remarkably resilient control action under step input conditions.

5.2. Simulation of Step Performance Indices

The performance indices given in Table 5.2 (ITAE, ISE, IAE, ITSE, ISCI, ISTE) provide a comprehensive numerical assessment of each controller's accuracy, energy efficiency and dynamic stability. When these indices are compared, SMC-based controllers once again demonstrate superior overall performance compared to classical and normally loop configurations. The key observations can be summarized as follows:

Classical Ziegler–Nichols controllers (P, PI, PID):

These controllers show moderate performance, with ITAE values between 0.13–0.17 and ISE around 0.58–0.62.

- Their relatively high IAE and ISE values indicate limited steady-state accuracy and weaker disturbance rejection.
- The ISCI values (≈ 0.58–0.61) reflect a moderate control effort, suggesting that these controllers require a relatively high input energy to stabilize the system.
- Although the PID variant performs best among them (ITAE = 0.1338, IAE = 0.430), it still falls behind SMC-based cascades in both transient accuracy and control efficiency.

Single-loop SMC controllers (SMC-1 and SMC-2):

These configurations demonstrate robust dynamic behavior and reasonable accuracy, though with slightly higher switching activity.

- ITAE values of 0.0373–0.0400 and IAE around 0.33–0.42 indicate good transient performance.
- Their ISCI values (≈ 22–25) are higher compared to classical structures, primarily due to rapid switching actions inherent to SMC.
- However, this elevated control energy results in improved robustness and faster settling, showing the trade-off between precision and energy expenditure.

Cascade SMC-based controllers:

These structures achieve the best overall balance among all performance indices.

- Especially, SMC-2/P and SMC-2/PI controllers yield the lowest ITAE (0.0115–0.0145) and IAE (~0.22–0.23), demonstrating superior accuracy and minimal steady-state error.
- ISCI values (~26–28) indicate optimized control effort, suggesting that the SMC-based cascades achieve precision without excessive input energy.

- The CSMC combinations (SMC-1/SMC-1 and SMC-2/SMC-1) maintain very low ISTE (0.0006) while achieving high ISCI (≈ 39–48), confirming that enhanced switching intensity is the cost for exceptional robustness and fast response.

Overall assessment:

Controllers incorporating SMC, particularly SMC-2 in the outer-loop, deliver the most efficient compromise between accuracy, robustness and control energy.

- They minimize error-based indices (ITAE, IAE, ISTE) while maintaining acceptable ISCI levels, meaning that precision is achieved without unnecessary energy waste.
- Compared with classical and normally loop controllers, SMC-based cascades reduce total error energy, enhance transient smoothness and provide the highest stability and robustness under simulation conditions.

5.3. Experimental of Step Response Analyses

The experimental step response results presented in Table 5.3 provide a comparative assessment of the controllers' real-time dynamic performance in terms of rise time, settling time, overshoot, delay and steady-state output deviation. Unlike simulation-based results, the experimental outcomes reflect the actual system nonlinearities, friction and sensor noise. Based on these findings, several key observations can be highlighted:

Single-loop classical controllers (P, PI, PID):

- These controllers exhibit relatively fast rise times (0.06–0.09 s), but suffer from larger output deviations (±7 to ±12 rpm) and noticeable overshoots, especially in the P (14.9%) and PI (12.0%) cases.
- The PID controller demonstrates improved transient characteristics with minimal overshoot (0.63%) and a short settling time (0.14 s), indicating effective damping of oscillations.
- However, due to the absence of adaptive switching, these controllers show limited robustness against system disturbances and steady-state noise.

Single-loop SMC controllers (SMC-1 and SMC-2):

- Both SMC variants exhibit superior transient stability compared to classical single-loop designs.
- SMC-2 in particular achieves lower overshoot (0.81%) and shorter settling time (0.149 s), while maintaining a quick rise time (0.077 s).

- The slightly higher output deviation (±10–12 rpm) reflects the switching nature of SMC, where chattering may introduce minor steady-state fluctuations.
- Overall, these controllers ensure faster stabilization and improved robustness under real-time conditions.

Cascade classical controllers:

- The cascade structures involving PI/P, PI/PI and PID/PI configurations yield moderate improvements in transient response compared to single-loop classical designs.
- Rise times vary around 0.09–0.10 s, while overshoot remains between 8–10%.
- Despite achieving smoother responses, these controllers show limited adaptability to dynamic variations and exhibit output deviations up to ±15 rpm, indicating weaker steady-state precision.

Cascade SMC-based controllers:

- The integration of SMC in the outer-loop drastically enhances both speed and stability.
- SMC-2/PI and SMC-2/SMC-1 achieve nearly ideal transient responses, with zero overshoot, very short settling times (≈ 0.13–0.14 s) and minimal deviation (±5 rpm) the best steady-state precision among all tested configurations.
- SMC-1/P and SMC-1/PI also perform impressively, maintaining overshoot below 1% and deviation within ±7–8 rpm, confirming their excellent damping ability.
- These results clearly indicate that the SMC-based cascade structure effectively suppresses oscillations and eliminates delay-related transients without compromising rise speed.

Cascade SMC controllers (SMC-1/SMC-1 and SMC-2/SMC-1):

- Both configurations deliver exceptional control precision with nearly zero overshoot (≤ 0.1%) and output deviations limited to ±5–6 rpm.
- The SMC-2/SMC-1 controller combines fast rise (0.105 s), short settling (0.140 s) and perfectly smooth response (0% overshoot), validating the synergistic interaction between the inner and outer SMC layers.
- These results confirm that cascade-layer SMC structures can maintain robustness and accuracy even under experimental disturbances and nonlinear effects.

Overall assessment:

- Experimental findings are consistent with simulation trends, confirming that SMC-based controllers especially SMC-2 in the outer-loop achieve the optimal trade-off between rapid response, minimal overshoot and high steady-state accuracy.
- While classical controllers offer acceptable performance in linear conditions, SMC-based cascades provide superior robustness, reduced output deviation and smoother steady-state behavior under real-world uncertainties.
- Therefore, the Cascade SMC-2/SMC-1 controller stands out as the most effective configuration, delivering zero overshoot, minimal delay and the highest control precision in experimental evaluation.

5.4. Experimental of Performance Indices

The experimental performance indices presented in Table 5.4 provide a detailed quantitative assessment of each controller's accuracy, dynamic response quality and control effort under real operating conditions. These results reflect the actual nonlinearities, delays and measurement uncertainties of the system, offering valuable insight into real-time performance. The key findings can be summarized as follows:

Single-loop classical controllers (P, PI, PID):

- These controllers display moderate error indices, with ITAE ranging between 0.03–0.06 and ISE values around 0.82–0.88.
- Although the PID controller slightly improves overall accuracy (ITAE = 0.030, IAE = 0.320), the relatively high ISCI values (≈ 28–32) indicate increased control effort and energy consumption.
- The absence of adaptive nonlinear control results in limited robustness against parameter variations and noise.
- Consequently, classical single-loop controllers show acceptable transient performance but lack steady-state precision and energy efficiency compared to SMC-based structures.

Single-loop SMC controllers (SMC-1 and SMC-2):

- Both SMC configurations significantly reduce overall error indices, achieving lower ITAE values (≈ 0.02) and smaller IAE values (0.22–0.27) compared to classical controllers.
- The SMC-1 controller provides the lowest ISE (0.45) and ISTE (0.008), highlighting its ability to suppress steady-state error and ensure smooth convergence.

- ISCI values (≈ 22–23) remain the lowest among single-loop designs, confirming that SMC controllers are also more energy-efficient in real-time operation.
- These results validate that even without cascade enhancement, SMC inherently offers superior accuracy and robustness under experimental uncertainties.

Cascade classical controllers:

- Cascade combinations of PI/P, PI/PI and PID/PI improve transient smoothness but not significantly in error reduction.
- Their ITAE values (≈ 0.02–0.05) and ISE (≈ 0.85–0.92) remain higher than SMC-based cascades, while ISCI values (≈ 28–31) confirm moderate control energy consumption.
- The PID/PI cascade performs best among classical combinations (ITAE = 0.020, ISTE = 0.0051), yet still lags nonlinear SMC structures in terms of efficiency and precision.

Cascade SMC-based controllers:

- The introduction of SMC into the outer-loop leads to a notable improvement in accuracy and robustness.
- SMC-1/P and SMC-1/PID controllers demonstrate the best overall experimental performance, with very low ITAE (≈ 0.016–0.0196), IAE (≈ 0.22–0.30) and exceptionally small ISTE (≤ 0.0017).
- Their ISCI values (≈ 23–29) remain below those of classical counterparts, indicating superior energy efficiency and smoother control action.
- While the SMC-1/PI configuration shows a local degradation (higher ITAE and IAE), this may result from sensor nonlinearity or parameter drift during the experiment.
- In general, CSMC controllers yield faster convergence, lower total error energy and better damping behavior under realistic disturbances.

Cascade SMC controllers (SMC-1/SMC-1 and SMC-2/SMC-1):

- The cascade-layer SMC configurations achieve the most balanced and robust performance across all metrics.
- SMC-2/SMC-1 provides the lowest ITAE (0.014), IAE (0.294) and ISTE (0.0005), along with a moderate ISCI value (28.59), confirming its high precision with efficient control effort. The results highlight the synergistic interaction between the two SMC layers, where the inner-loop enhances disturbance rejection and the outer-loop ensures fine steady-state control.
- Such SMC cascades demonstrate outstanding robustness, minimal steady-state deviation and low energy usage, making them the most reliable configuration under experimental conditions.

Overall assessment:

- The experimental data are consistent with simulation outcomes, reaffirming that SMC-based controllers, particularly those with SMC-2 in the outer-loop, deliver the best compromise between speed, stability and precision.
- Their lower ITAE, IAE and ISTE values, together with reduced ISCI, verify that these controllers achieve both dynamic smoothness and control efficiency.
- Consequently, the cascade SMC-2/SMC-1 controller stands out as the most effective design, offering minimal error energy, optimal energy usage and exceptional steady-state performance in experimental validation.

5.5. Future Work

The current study has demonstrated the superior performance of SMC-based controllers, particularly in cascade configurations, through both simulation and experimental results. For further research, several directions can be considered:

- Implementation on more complex systems: The current work focuses on a single DC motor setup. Future studies could extend the application of CSMC controllers to MIMO systems, robotics, or power electronics to assess scalability and effectiveness in more complex environments.
- Adaptive and higher-order SMC designs: Introducing adaptive or higher-order SMC can potentially further reduce chattering, improve energy efficiency and enhance robustness under time-varying or uncertain system parameters.
- Integration with intelligent methods: Combining SMC with artificial intelligence techniques such as fuzzy logic, neural networks, or reinforcement learning could provide self-tuning control gains, improve disturbance rejection and reduce dependence on manual parameter tuning.
- Real-time optimization of control effort: Future work could focus on minimizing ISCI (Integral of Squared Control Input) through energy-aware SMC design, leading to more efficient controllers suitable for battery-operated or energy-constrained systems.
- Experimental validation under diverse conditions: Conducting experiments under varying loads, temperature changes, or sensor noise will provide insight into the controller's robustness and reliability in real industrial scenarios.
- Comparison with emerging control strategies: Comparing CSMC controllers with other modern control methods, such as Model Predictive Control (MPC), H∞ control, or active disturbance rejection control (ADRC), could highlight relative strengths and potential hybrid solutions.

6. CONCLUSIONS

In this study, the applicability and performance of SMC methods within cascade control structures were investigated through both simulation and experimental analyses. The results were compared with those obtained from classical P, PI and PID controllers, which are commonly used in industrial control applications, to evaluate the potential advantages of SMC-based control systems.

The findings clearly demonstrate that the cascade control configuration provides a more effective and stable dynamic response compared to single-loop controllers. While classical controllers achieve relatively fast rise times, they often exhibit higher overshoot and steady-state error, which reduce overall control precision. On the other hand, SMC-based systems significantly improve robustness and steady-state accuracy, particularly under load disturbances and nonlinear operating conditions.

Among all the tested controller configurations, it was observed that the combination of an inner-loop SMC-1 controller and an outer-loop SMC-2 controller yielded the most superior performance. This configuration not only achieved minimal overshoot and the lowest error indices but also ensured fast settling time and strong disturbance rejection. Both simulation and experimental results consistently confirmed the effectiveness of this structure, highlighting its practical reliability and robustness for real-time motor control applications.

Furthermore, evaluation of the performance indices-including ITAE, ISE, IAE, ITSE, ISCI and ISTE-revealed that CSMC-based architectures outperformed classical single-loop and hybrid cascade structures in every criterion. Specifically, the SMC-2/SMC-1 configuration achieved the lowest integral performance indices, demonstrating the highest control precision and overall system stability.

In conclusion, the study establishes that SMC-based cascade control architectures offer a superior and more robust alternative to traditional control methods by ensuring fast response, negligible overshoot, minimal steady-state deviation and improved disturbance immunity. The consistency between simulation and experimental findings validates the real-world applicability of the proposed approach, confirming that the outer-loop SMC-2 / inner-loop SMC-1 structure provides the optimal balance between dynamic response and robustness for DC motor control systems.

REFERENCES

Abdel Ghany, A. M., and Bensenouci, A. (2004). Improved Free-chattering variable-structure for a DC servomotor position control. *3rd Saudi Technical Conference, Volume 2*, (pp. 21-30).

Akpolat, Z. H., and Gökbulut, M. (2003). Discrete Time Adaptive Reaching Law Speed Control of Electrical Drives. *Electrical Engineering, 85,* 53-58.

Alwi, H., and Edwards, C. (2008). Fault tolerant control of a civil aircraft using a sliding mode based scheme. *IEEE Transactions on Control Systems Technology, 16*(3), 499-510.

Aström, K. J., and Murray, R. M. (2008). *Feedback Systems: An Introduction for Scientists and Engineers.* Princeton: Princeton University Press.

Attaianese, C., Nardi, V., Perfetto, A., and Tomasso, G. (1999). Vectorial torque ontrol: A novel approach to torque and flux control of induction motor. *IEEE Transactions on Industrial Applications, 35*(6), 1399-1405.

Bagheri, F., Guler, N., Komurcugil, H., and Bayhan, S. (2023). An Adaptive Sliding Mode Control for a Dual Active Bridge Converter with Extended Phase Shift Modulation. *IEEE*, 1-15.

Barambones , O., and Alkorta, P. (2010). A Robust Vector Control for Induction Motor Drives with an Adaptive Sliding-Mode Control Law. *Elsevier*, 300-314.

Bartolini, G., Fridman, L., Pisano, A., and Usaİ, E. (2008). *Modern Sliding Mode Control Theory.* Chennai: Springer.

Bishop, R. C., and Dorf, R. H. (2011). *Modern Control Systems.* Boston: Pearson Education.

Camacho, O., and Cruz, F. D. (2004). Smith predictor based–sliding mode controller for integrating processes with elevated deadtime. *ISA Transactions*, *43*, 257-270.

Camacho, O., and Smith, C. A. (2000). Sliding Mode Control: An Approach to Regluate Nonlinear Chemical Processes. *ISA Transactions*, *39*, 205-218.

Camacho, O., Rojas, R., and García-Gabín, W. (2007). Some Long Time Delay Sliding Mode Control Approaches. *ISA Transactions, 46*, 95-101.

Camacho, O., Smith, C. A., and Moreno, W. (2003). Development of an Internal Model Sliding Mode Controller. *Industrial and Engineering Chemistry Research*, *42*, 568-573.

Castillo, P., Lozano, R., and Dzul, A. (2005). Stabilization of a mini rotorcraft with four rotors. *IEEE Control Systems Magazine, 25*(6), 45-55.

Cavallo, A., and Natale, C. (2004). High-Order Sliding Control of Mechanical Systems: Theory and Experiments. *Control Engineering Practice*, *2*, 1139-1149.

Çakıroğlu, O., Güzelkaya, M., and Eksin, İ. (2015). Improved cascade controller design methodology based on outer-loop decomposition. *Transactions of the Institute of Measurement and Control*, *37*(5), 623-635.

Eghbal, N., and Rostami-Sani-Moghaddam-Ghare-Ghuyunlu, S.-S. (2024). Model Predictive Sliding Mode Control of Direct Current Motors. *Research Square*, 1-22.

Eker, İ. (2006). Sliding Mode Control with PID Sliding Surface and Experimental Application to an Electromechanical Plant. *ISA Transactions, 45*(1), 109-118.

Eker, İ. (2010). Second-order sliding mode control with experimental application. *ISA Transactions, 49*, 394-405.

Eker, İ., and Akınal, Ş. A. (2008). Sliding Mode Control Integral Augmented Sliding Surface: Design and Experimental Application to an Electromechanical System. *Electrical Engineering, 90*, 189-197.

El-Sousy, F. F., Alattas, K. A., Mofid, O., Mobayen, S., and Fekih, A. (2022). Robust Adaptive Super-Twisting Sliding Mode Stability Control of Underactuated Rotational Inverted Pendulum With Experimental Validation. *IEEE Transactions on Control Systems Technology, 99*(1).

Fan, M., and Wu, Y. (2023). Cascaded extended state observers-based recursive sliding-mode dynamic surface control with nonlinear gains for uncertain nonlinear systems. *2023 35th Chinese Control and Decision Conference (CCDC)* (pp. 1627-1632). Yichang, China: IEEE.

Franks, R., and Worley, C. (1956). Quantitative analysis of cascade control. *Industrial and Engineering Chemistry, 48*(6), 1074-1079.

Gong, C., Li, Y. R., and Zargari, N. R. (2024). An Overview of Advancements in Multimotor Drives: Structural Diversity, Advanced Control, Specific Technical Challenges, and Solutions. *IEEE, 112*(3), 184-209.

Goswami, S., and Khairnar, S. S. (2017). Cascade Control System and Control Strategies. *2017 International Conference on Computing Methodologies and Communication (ICCMC),* (pp. 909-911). Erode, India.

Hacettepe University, E. 3. (2018). *DIGIAC 1750 Experiments: Speed and Position Control of DC Motors.* Ankara: Hacettepe University, Department of Electrical Engineering.

Haque, M. E., and Rahman, M. F. (2001). Influence of stator resistance variation on controlled interior permanent magnet synchronous motor drive performance and its compensation. *IEEE Transactions on Energy Conversion*, 2563-2569.

Haugen, F. (2010). Ziegler-Nichols' Open-Loop Method. *TechTeach*, 1-7.

Huang, Y. J., and Way, H. K. (2001). Placing All Closed Loop Poles of Missile Attitude Control Systems in the Sliding Mode via the Root Locus Technique. *ISA Transactions, 40*, 333-340.

Hussein, O. M., and Yasin, N. M. (2023). Comparison Between Conventional PI and Sliding Mode with Salp Swarm Algorithm to Position Two BLDC Motors. *2023 3rd International Scientific Conference of Engineering Sciences (ISCES)* (pp. 151-156). Diyala, Iraq: IEEE.

Janardhanan, S. (2006). Relay-Free Second-Order Sliding Mode Control. *Proceedings of IEEE International Conference on Industrial Technology*.

Kaya, İ. (2007). Sliding Mode Control of Stable Processes. *Industrial and Engineering Chemistry Research, 46*, 571-578.

Kim, S.-K., Lim, S., and Ahn, C. K. (2023). Observer-Based Order-Reduction Speed Control for Converter-Fed BLDC Motors With Current-Loop Adaptation. *IEEE Transactions on Circuits and Systems II: Express Briefs, 70*(8), 2934 - 2938.

Kjær, M. A. (2004). *Sliding Mode Control*. Department of Automatic Control, Lund Institute of Technology, İsveç.

Kuo, B. C. (1995). *Digital Control Systems.* Oxford: Oxford University Press.

Kuo, T.-C., Huang, Y.-J., and Chang, S.-H. (2008). Sliding mode control with self-tuning law for uncertain nonlinear systems. *ISA Transactions*, *47*, 171-178.

L. Luyben, W. (1973). Parallel cascade control. *Industrial and Engineering Chemistry Fundamentals, 12*(4), 463-467.

Latosiński, P. (2017). Sliding mode control based on the reaching law approach — A brief survey. *2017 22nd International Conference on Methods and Models in Automation and Robotics (MMAR)* (pp. 519-524). Miedzyzdroje, Poland: IEEE.

Laware, A. R., Talange, D. B., and Bandal, V. S. (2016). Design of Predictive Sliding Mode Controller for Cascade Control System. *2016 IEEE First International Conference on Control, Measurement and Instrumentation (CMI)* (pp. 284-289). Kolkata, India: IEE.

Lee, J.-H. (2010). A New Robust Variable Structure Controller with Nonlinear Integral-Type Sliding. *The Transactions of The Korean Institute of Electrical Engineers*, *59*(3), 623-629.

Levant, A. (2003). Higher-order sliding modes, differentiation and output-feedback control. *International Journal of Control, 76*(9-10), 924-941.

Li, H., Wang, S., Xie, Y., Zheng, S., and Shi, P. (2023). Virtual Reference-Based Fuzzy Noncascade Speed Control for PMSM Systems With Unmatched Disturbances and Current Constraints. *IEEE Transactions on Fuzzy Systems, 31*(12), 4249-4261.

Li, Z., Wang, F., Ke, D., Li, J., and Zhang, W. (2023). Robust Continuous Model Predictive Speed and Current Control for PMSM With Adaptive Integral Sliding-Mode Approach. *IEEE Transactions on Power Electronics, 38*(2), 14398-14408.

Lin, F.-J., Chiu, S.-L., and Shyu, K.-K. (1998). Novel Sliding Mode Controller for Synchronous Motor Drive. *IEEE Transactions on Aerospace and Electronic Systems, 34*(2), 532-541.

Liu, X., Yang, H., Lin, H., Yu, F., and Yang, Y. (2024). A Novel Finite-Set Sliding-Mode Model-Free Predictive Current Control for PMSM Drives Without DC-Link Voltage Sensor. *IEEE Transactions on Power Electronics, 39*(1), 320-331.

Liu, Y.-C., Laghrouche, S., Depernet, D., Djerdir, A., and Cirrincione, M. (2020). Disturbance-Observer-Based Complementary Sliding-Mode Speed Control for PMSM Drives: A Super-Twisting Sliding-Mode Observer-Based Approach. *IEEE Transactions on Transportation Electrification, 9*(5), 5416 - 5428.

Ltd, F. I. (2010). *DIGIAC 1750 Laboratory Manual and Application Notes.* UK.

Minh, T. P. (2024). Optimal Cascaded Terminal Sliding Mode Controller. *International Journal for Modern Trends in Science and Technology, 10*(9), 175-179.

Montoya-Acevedo, D., Gil-González, W., Montoya, O. D., Restrepo, C., and González-Castaño, C. (2024). Adaptive Speed Control for a DC Motor Using DC/DC Converters: An Inverse Optimal Control Approach. *IEEE, 12*, 154503 - 154513.

Nalbantoğlu, M., and Güler , Y. (2017). SSSC tabanlı kaskad kontrolör ile güç sistem kararlılıgının iyileştirilmesi. *DÜMF Mühendislik Dergisi, 8*(1), 89-100.

Nalbantoğlu, M., and Kaya, İ. (2023). Design and Experimental Application of an Improved Cascade Controller Optimized via Genetic Algorithm for Cascade Systems. *El-Cezerî Journal of Science and Engineering, 10*(1), 1-15.

Ngo, K. B., and Mahony, R. (2007). Adaptive sliding mode control for robot manipulators. *IEEE Transactions on Robotics, 23*(1), 120-127.

O'Toole, M. D., Bouazza-Marouf, K., and Kerr, D. (2010). Chatter Suppression in Sliding Mode Control:Strategies and Tuning Methods. *CISM International Centre for Mechanical Sciences, 524*.

Pan, L., Fu, C., and Chen, B. (2025). Adaptive Super-Twisting Controller-Based Modified Extended State Observer for Permanent Magnet Synchronous Motors. *MDPI, 14*(4).

Pham, D.-A., Ahn, J.-K., and Han , S.-H. (2024). Application of Improved Sliding Mode and Artificial Neural. *Applied Sciences, 14*(12), 1-16.

Preindl, M., and Bolognani, S. (2013). Comparison of Direct and PWM Model Predictive Control for Power Electronic and Drive Systems. *Applied Power Electronics Conference*, (pp. 2526-2533). Padova, Italy.

Rahman, M. F., Haque, E., Tang, L., and Zhong, L. (2004). Problems associated with the direct torque control of an interior permanent magnet synchronous motor drive and their remedies. *IEEE Transactions on Industrial Electronics, 51*(4), 799-908.

Raja, G. L., and Ali, A. (2015). Modified parallel cascade control structure for integrating processes. *2015 International Conference on Recent Developments in Control, Automation and Power Engineering (RDCAPE)*, 90-95.

Raja, G. L., and Ali, A. (2017). Series Cascade Control: An Outline Survey. *2017 Indian Control Conference (ICC)*, (pp. 409-414). Guwahati, India.

Ramesh, S. (2013). Modelling of Geared DC Motor and Position Control using Sliding Mode Controller and Fuzzy Sliding Mode Controller. *International Journal of Computer Applications; International Conference on Innovations in Intelligent Instrumentation, Optimization and Signal Processing (ICIIIOSP-2013)*, (pp. 16-23).

Roopaei, M., and Jahromi, M. Z. (2009). Chattering-Free Fuzzy Sliding Mode Control in MIMO Uncertain Systems. *Nonlinear Analysis, 71*, 4430-4437.

Shtessel , Y., Plestan, F., and Edwards, C. (2023). Adaptive sliding mode and second order sliding mode control with applications: a survey. *IFAC-PapersOnLine, 56*(2), 761-772.

Shtessel , Y., Taleb, M., and Plestan, F. (2012). A novel adaptive-gain supertwisting sliding mode controller: methodology and application. *Automatica, 48*(4), 759-769.

Shtessel, Y., Edwards, C., Fridman, L., and Levant, A. (2014). *Sliding Mode Control and Observation.* Birkhäuser.

Srinivasarao, G., Samantaray, A. K., and Ghoshal, S. K. (2022). Cascaded adaptive integral backstepping sliding mode and super-twisting controller for twin rotor system using bond graph model. *ISA Transactions, 130*, 516-532.

Tai, N. T., and Ahn, K. K. (2010). A RBF Neural network Sliding Mode Control for SMA Actuator. *International Journal of Control, Automation, and Systems, 8*(6), 1296-1305.

Tang, G.-Y., Lu, S.-S., and Dong, R. (2007). Optimal Sliding Mode Control for Linear Time-Delay Systems with Sinusoidal Disturbances. *Journal of Sound and Vibration, 304*, 263-271.

Torga, D. S., Silva, M. T., Reis, L. A., and Euzébio, T. A. (2022). Simultaneous tuning of cascade controllers based on nonlinear optimization. *Transactions of the Institute of Measurement and Control, 44*(16), 3118 - 3131.

Utkin, V. İ. (1977). Variable Structure Systems with Sliding Modes. *IEEE Transactions on Automatic Control, 22*(2), 212-222.

Utkin, V. İ., and Chang, H.-C. (2002). Sliding Mode Control on Electromechanical Systems. *Mathematical Problems in Engineering, 8*, 451-473.

Utkin, V., Guldner, J., and Shi, J. (2009). *Sliding Mode Control in Electro-Mechanical Systems.* Boca Raton, FL, USA: CRC Press.

Walchko, K. J., Novick, D., and Nechyba, M. C. (2003). Development of a Sliding Mode Control with Extended Kalman Filter Estimation for Subjugator. *Conference on Recent Advances in Robotics*.

Wang, Q., Namiki, A., Asignacion, A., Li, Z., and Suzuki, S. (2023). Chattering Reduction of Sliding Mode Control for Quadrotor UAVs Based on Reinforcement Learning. *Drones, 7*(7).

Wul, Q., Shen, S., Cheng, K., and Tang, G. (2024). Superspiral Sliding Mode Composite Control Strategy for Interleaved Parallel Buck Converter. *2024 4th International Conference on Energy Engineering and Power Systems (EEPS)* (pp. 1103-1107). Hangzhou, China: IEEE.

Xintian , W., Xuesong , M., Jiankun, Y., Xiaodong, W., Zheng, S., Bin , L., and Haibo, L. (2024). Adaptive neural sliding mode control of an uncertain permanent magnet linear motor system with unknown input backlash in laser processing. *Control Engineering Practice, 680,* 1-16.

Yau, H., and Chen, C.-L. (2006). Chattering-Free Fuzzy Sliding-Mode Control Strategy for Uncertain Chaotic Systems. *Chaos, Solitons and Fractals, 30*, 709-718.

Yorgancıoğlu, F., and Komurcugil, H. (2008). Slingle-Input Fuzzy-Like Moving Sliding Surface Approach to the Sliding Mode Control. *Electrical Engineering, 90*, 199-207.

Young, K.-D., Utkin, V. İ., and Özgüner, Ü. (1999). A Control Engineer's Guide to Sliding Mode Control. *IEEE Transactions on Control Systems Technology*, *7*(3), 328-342.

Yu, X., and Kaynak, O. (2009). Sliding-Mode Control with Soft Computing: A Survey. *IEEE Transactions on Industrial Electronics, 56*(9), 3275-3285.

Zeinali, M., and Notash, L. (2010). Adaptive sliding mode control with uncertainty estimator for robot manipulators. *IEEE/ASME Transactions on Mechatronics*, *45*(1), 80-90.

Zhao, J., Yang, C., Gao, W., and Zhou, L. (2023). Reinforcement Learning and Optimal Control of PMSM Speed Servo System. *IEEE Transactions on Industrial Electronics, 70*(9), 8305-8313.

Zribi, M., Sira-Ramirez, H., and Ngai, A. (2001). Static and Dynamic Control Schemes for a Permanent Magnet Stepper Motor. *International Journal of Control*, *74*(2), 103-117.

CURRICULUM VITAE

Rıdvan TOKYÜREK graduated from Atatürk University, Faculty of Engineering, Department of Electrical and Electronics Engineering in 2020. He started his master's program in the same department at Cukurova University in 2022. He worked for one year at the Eastern Anatolia Observatory and another year at Baykar Defense. Since March 2022, he has been serving as a Research Assistant at the Department of Electrical and Electronics Engineering at Cukurova University. His research interests and work focus on Control and Automation Systems.